

ISSN 1980-9743
ISSN-e 2675-5475



Soils and Rocks



AB
MS 70



Soils and Rocks

Volume 43, N. 3

2020

SOILS and ROCKS

An International Journal of Geotechnical and Geoenvironmental Engineering

Editor Renato Pinto da Cunha - University of Brasília, Brazil

Co-editor José Couto Marques - University of Porto, Portugal

Executive Board

Paulo J. R. Albuquerque
Campinas State University, Brazil

Nuno Cristelo
University of Trás-dos-Montes and Alto Douro, Portugal

Leandro Neves Duarte
Federal University of São João Del-Rei, Brazil

Teresa M. Bodas Freitas
Technical University of Lisbon, Portugal

Gilson de F. N. Gitirana Jr. (*Secretary*)
Federal University of Goiás, Brazil

Sara Rios
University of Porto, Portugal

Paulo Scarano Hemsí
Aeronautics Institute of Technology, Brazil

José A. Schiavon
Aeronautics Institute of Technology, Brazil

Ana Vieira
National Laboratory for Civil Engineering, Portugal

Advisory Panel

H. Einstein
MIT, USA

Roger Frank
ENPC-Cermes, France

John A. Hudson
Imperial College, UK

Kenji Ishihara
University of Tokyo, Japan

Michele Jamiolkowski
Studio Geotecnico Italiano, Italy

Willy A. Lacerda
COPPE-UFRJ, Brazil

E. Maranha das Neves
Lisbon Technical University, Portugal

Paul Marinos
NTUA, Greece

Nielen van der Merve
University of Pretoria, South Africa

James K. Mitchell
Virginia Tech., USA

Lars Persson
SGU, Sweden

Harry G. Poulos
University of Sidney, Australia

Nick Rengers
ITC, The Netherlands

Fumio Tatsuoka
Tokyo University of Science, Japan

Luiz Gonzalles de Vallejo
UCM, Spain

Soils and Rocks publishes papers in English in the broad fields of Geotechnical Engineering, Engineering Geology, and Geoenvironmental Engineering. The Journal is published quarterly in March, June, September and December. The first issue was released in 1978, under the name *Solos e Rochas*, being originally published by the Graduate School of Engineering of the Federal University of Rio de Janeiro. In 1980, the Brazilian Association for Soil Mechanics and Geotechnical Engineering took over the editorial and publishing responsibilities of *Solos e Rochas*, increasing its reach. In 2007, the journal was renamed Soils and Rocks and acquired the status of an international journal, being published jointly by the Brazilian Association for Soil Mechanics and Geotechnical Engineering, by the Portuguese Geotechnical Society, and until 2010 by the Brazilian Association for Engineering Geology and the Environment.

Soils and Rocks

1978,	1 (1, 2)
1979,	1 (3), 2 (1,2)
1980-1983,	3-6 (1, 2, 3)
1984,	7 (single number)
1985-1987,	8-10 (1, 2, 3)
1988-1990,	11-13 (single number)
1991-1992,	14-15 (1, 2)
1993,	16 (1, 2, 3, 4)
1994-2010,	17-33 (1, 2, 3)
2011,	34 (1, 2, 3, 4)
2012-2019,	35-42 (1, 2, 3)
2020,	43 (1, 2, 3,

ISSN 1980-9743
ISSN-e 2675-5475

CDU 624.131.1

SOILS and ROCKS

An International Journal of Geotechnical and Geoenvironmental Engineering

Publication of

ABMS - Brazilian Association for Soil Mechanics and Geotechnical Engineering

SPG - Portuguese Geotechnical Society

Volume 43, N. 3, July-September 2020

Invited Editor: Waldemar C. Hachich

Table of Contents

EDITORIAL

A Journal is born...

Willy A. Lacerda

i

A message from the President of the SPG

Manuel de Matos Fernandes

ii

A message from the Editorial Board

Renato P. da Cunha, Gilson de F. N. Gitirana Jr., José Schiavon

iii

Preface from the invited editor

Waldemar C. Hachich

iv

LECTURE

Risk management for geotechnical structures: consolidating theory into practice

Andre P. Assis

311

ARTICLES

Spread Footings Bearing on Circular and Square Cement-Stabilized Sand Layers Above Weakly Bonded Residual Soil

Nilo Cesar Consoli, Eclesielter Batista Moreira, Lucas Festugato, Gustavo Dias Miguel

339

A review on some factors influencing the behaviour of nonwoven geotextile filters

Ennio M. Palmeira

351

Guidelines and recommendations on minimum factors of safety for slope stability of tailings dams

Fernando Schnaid, Luiz Guilherme F.S. de Mello, Bruno S. Dzialoszynski

369

Stabilization of major soil masses using drainage tunnels

Werner Bilfinger, Luiz Guilherme F.S. de Mello, Claudio Michael Wolle

397

Experimental, numerical, and analytical investigation of the effect of compaction-induced stress on the behavior of reinforced soil walls

Seyed H. Mirmoradi, Maurício Ehrlich, Gabriel Nascimento

419

Foundation-structure interaction on high-rise buildings

Alexandre Duarte Gusmão, Augusto Costa Silva, Maurício Martines Sales

441

Some topics of current practical relevance in environmental geotechnics

Maria Eugenia Gimenez Boscov, Paulo Scarano Hems

461

Requiem for risk classification matrices

Waldemar C. Hachich

497

A Journal is born...

In 1975, a large delegation of professors and students from COPPE attended the V Pan American Congress of Soil Mechanics and Foundation Engineering, in Buenos Aires, Argentina. Jacques de Medina, Dirceu de Alencar Velloso, Willy Lacerda, and Francisco de Rezende Lopes were part of this “entourage”. It became evident during the conference that the amount of Brazilian papers outnumbered those presented by any other Association.

At the Conference’s banquet, during a conversation, Prof. Norbert Morgenstern, who was one of the invited speakers at that conference, directed himself to the four of us and made an interesting remark that was going to persist in our minds for the next year: “Brazil has produced many research papers. It is time for you to have your own journal”. We contemplated that idea until one day, in 1976, during a meeting at Dirceu Velloso’s office, when we decided to create the magazine. The name *Solos e Rochas* was an unanimity.

Then came the practical questions. Who the editor would be? How to financially support the journal? How would we select the articles for the first issues? And so on. It was decided that Dirceu Velloso would be the first Editor of *Solos e Rochas*, Francisco Lopes would be responsible for the production of issues, and Medina and I would be associates, starting as the first reviewers. COPPE’s Director at the time was Professor Paulo Alcântara Gomes. When approached, he immediately agreed to fund the journal.

And so it was. The first articles were written by invited authors. The article by Prof. Marcio M. Soares was ready for publication by the end of 1976. The paper had to wait, until the journal found the required funding for the first issue. Soon, the first paper was followed by the manuscripts written by Paulo Cruz and Willy Lacerda, delivered for production by the end of 1977.

With COPPE’s support and the delivery of these two additional articles, the first issue was published in January, 1978. That would be the only issue of that year. A second issue followed, in 1979. By the end of 1979, COPPE could no longer afford to support the journal. To find a new source of funding, we reached out for help from Prof. Carlos de Souza Pinto, president of ABMS, proposing that the association should take over the direction of *Solos e Rochas*. He immediately accepted the idea, with a new chapter of the journal starting in 1980, now publishing three issues per year. From this point, we switched from publishing invited paper to a regular peer-review process, supported by numerous specialists. In 2007, during my term as President of ABMS, the journal became an international publication, with a brand-new name: *Soils and Rocks*. It has been a great satisfaction for me to follow the development of the journal to this day, and its commitment to excellence in the field of Soil Mechanics and Geotechnical Engineering, thanks recently to the efforts of its latest editors, starting with Waldemar Hachich.

On August 25, 2020

Willy A. Lacerda 
COPPE/UFRJ, Brazil

A message from the President of the SPG

It is with great pleasure that I write this brief Editorial, on behalf of the Portuguese Geotechnical Society (SPG), at the invitation of the President of the Brazilian Association for Soil Mechanics and Geotechnical Engineering (ABMS), Alexandre Gusmão, and of the President of the Commemorative Committee of the ABMS 70th anniversary, Waldemar Hachich.

The commemorative program of the 70 years of ABMS has been wide ranging and ambitious and now it includes this special issue of Soils and Rocks, with a number of papers by distinguished academics and professionals.

This “celebration” of the 70th anniversary is in alignment with previous commemorations of special dates that past leaders of ABMS have carefully organized. This respect, I should even say this loving care, for its History and for their most honorable, reveals the great self-esteem of ABMS, and this is undoubtedly inherent to the great institutions.

The involvement of young people in setting up this “celebration” is also in due correspondence with the events promoted by ABMS, and in particular the COBRAMSEG, congresses with enormous impact, where the strength and youth of the Brazilian geotechnical community can be felt.

From their inception, ABMS and SPG have developed collaboration links, which have attained a degree and produced results that I consider outstanding, amidst the diverse technical and scientific associations of our two countries.

We owe this to our “founding fathers”, Milton Vargas, Manuel Rocha, António José da Costa Nunes, Victor de Mello and many others (to name but a few). But in the two past decades these links have been further strengthened by the joint organization of our congresses, of the Victor de Mello Lesson and with the joint management of the Geotecnia and Soils and Rocks journals. For such intense collaboration were determinant the Presidents of ABMS Waldemar Hachich and Alberto Sayão, to whom I express my heartfelt recognition and homage.

In the person of Alexandre Gusmão, I affectionately salute the whole Brazilian geotechnical community, in this very special and emotional date!

Porto, 28th of August 2020

Manuel de Matos Fernandes 
President of SPG

A message from the Editorial Board


Soils and Rocks is going through significant changes in 2020. The Editorial Board has been renewed and our new Advisory Committee is now being selected and invited. We have a team of board members that is actively engaged and motivated, contributing to our plans for the journal. We have set several goals, based on feedback received from the technical and scientific community. In terms of editorial peer-review procedures, we are significantly reducing the time between paper submission and final decision. This has been achieved thanks to the assistance of our expert reviewers, who diligently observe our rigorous deadlines. We are implementing a revamped guide for authors, to help with the preparation of manuscripts that strictly adhere to the formatting rules of the journal. We are also establishing an author's checklist, to ensure that submissions fulfill the journal's requirements.


Another important new goal for 2020 was to increase the quantity of published papers and to decrease the time between article acceptance and its availability online. To achieve that target, we have changed the number of annual issues, from three to four. This goal is also closely related to the demand for the more frequent publications of special issues, offering opportunities to have sets of manuscripts on domain-specific fields within Geotechnical Engineering. The journal currently has special issues planned for 2021 and 2022, aimed to present expanded papers and lectures to be given in the next Luso-Brazilian Geotechnical Conference and in the Third Pan-American Conference on Unsaturated Soils.

We know that paper visibility influences the number and quality of submissions. Therefore, the Editorial Board is constantly working on improving and expanding the indexation of the journal. *Soils and Rocks* is currently indexed by Scopus, Web of Science, and Google Scholar, among other major citation databases. While our present citation metrics are lower than our set goals, we have an encouraging positive trend that we intend to maintain, gradually reaching a wider international recognition and interest.

We are pleased to announce that the current issue of *Soils and Rocks* introduces a new paper format. This format was designed to offer a fresh look, to include a machine-readable Creative Commons licensing information, to adopt a more streamlined method of identification of authors and corresponding affiliations, among several other modifications. This change is accompanied by a new and modern website.

Finally, it is important to emphasize that the changes and advancements that *Soils and Rocks* started to experience in 2020 wouldn't be possible without the steadfast support from the Brazilian Association for Soils Mechanics and Geotechnical Engineering and from the Portuguese Geotechnical Society, for which we are deeply grateful.

Renato P. da Cunha 
University of Brasília, Brazil

Gilson de F. N. Gitirana Jr. 
Federal University of Goiás, Brazil

José Schiavon 
Aeronautics Institute of Technology, Brazil

Preface from the invited editor

Seventy years is indeed a milestone to be celebrated, and certainly not just because it is a large round number. Those 70 years have been the stage for dozens and dozens of workshops, lectures, congresses, international conferences, thematic conferences, technical meetings, courses, and many more ABMS-promoted activities, including the most recent lives and webinars.

On the occasion of the celebration of fifty and sixty years, two magnificent books have been edited by ABMS: the first one focused mainly on the history of the Association, the second emphasizing its countless contributions to the qualification of the geotechnical engineers who have decisively contributed to turn major engineering projects into reality, both in Brazil and abroad.

The trend has certainly continued over the last decade, and the organizing committee considered that those new achievements could be better presented in the "ABMS Talks", a series of live interviews with nine former presidents, which took place in June and July, always coordinated by Alexandre Gusmão, the current president.

Both books and some presidents mentioned "Solos e Rochas", the journal created by our geotechnical colleagues in COPPE-UFRJ in 1978. This scientific journal went through several different phases, in Portuguese, before reaching its current status, in which it is co-edited in English by ABMS and the Portuguese Geotechnical Society (SPG). As a matter of fact, Soils and Rocks is just one of the many joint initiatives that strengthen the links between ABMS and SPG.

The seventieth anniversary of ABMS means also that Soils and Rocks is just over forty, and continuously publishing papers of recognized scientific value. This looked like the ideal occasion to commemorate Soils and Rocks as well, by publishing a special issue with invited authors whose papers would certainly bear witness to the quality of the journal. It was a difficult choice, and I must apologize for the many omissions. On the other hand, I enjoyed being editor some four years ago, but am even prouder of having somewhat influenced the choice of my two successors, both of whom are raising Soils and Rocks up to new levels of recognition and international visibility.

I wish them, Soils and Rocks, and especially ABMS, many continued decades of success.

Waldemar C. Hachich 

President of the Commemorative Commission of the 70 years of ABMS
and invited editor for this special issue of Soils and Rocks.

Pacheco Silva Lecture



The Pacheco Silva Lecture is delivered each two years by an important geotechnical professional from Brazil or abroad to honour the memory of the distinguished Brazilian geotechnical engineer Francisco Pacheco Silva (1918-1974). Pacheco Silva was a researcher of the Technological Research Institute (IPT/SP) for 33 years and consultant in geotechnical engineering in several occasions. In 1947 he obtained his MSc. degree from Harvard University, where he was a student of Karl Terzaghi and Arthur Casagrande. He worked in practically all fields of geotechnical engineering, but his main research interests were on soil behaviour, laboratory testing and geotechnical instrumentation. He was also one of the founders and past presidents of the Brazilian Association for Soil Mechanics and Geotechnical Engineering - ABMS.



Prof. André Assis

The 2018 Pacheco Silva lecturer is André Assis, 59 years old. Full Professor of the Department of Civil & Environmental Engineering at the University of Brasilia (UnB), Brazil. He graduated at the UnB (1980), worked as geotechnical engineer (1980-1984) and got his PhD from the University of Alberta, Canada (1990). In 1996-1997, he spent his sabbatical leave at the Mackay School of Mines, Univ. of Nevada at Reno, USA, and in 2005-2006 he was visiting professor at the EPFL (Swiss Federal Institute of Technology Lausanne), in Switzerland. His research interests and consulting are on tunnelling, rock mechanics, rock-fill dams and geotechnical risk management. He has already supervised more than 100 MSc and PhD theses, and published around 300 papers in international and national journals, congresses and symposia. He was president of the Brazilian Tunnelling Committee, CBT (1998-2002), of the International Tunnelling and Underground Space Association, ITA (2001-2004), and of the Brazilian Society for Soil Mechanics and Geotechnical Engineering, ABMS (2012-2016). He is one of the authors of the books *Tunnels in Brazil* and *Risk Management in Complex Structures*.

Soils and Rocks
v. 43, n. 3

Risk management for geotechnical structures: consolidating theory into practice

Andre P. Assis^{1, #} 

Lecture

Keywords

Curves of risk acceptance and tolerance
Failure probability
Geotechnical structures
Impact and consequences
Probabilistic methods
Risk management

Abstract

This paper intends to consolidate the theory of risk management into practical applications in geotechnical engineering, presenting concepts, clarifying procedures and discussing openly its difficulties and trends. It brings the evolution of the risk concept and its application to engineering, worldwide and in Brazil, showing the trend of risk management as a decision-making tool in engineering with fair acceptance by the society. The probabilistic approach is discussed and compared to the deterministic one, focusing on the obtaining of reliability indexes and failure probabilities for engineering structures. For this, quantitative methods, such as event and fault tree analyses and probabilistic methods, are reviewed, discussing their applications and comparing their advantages and disadvantages. Risk metrics and the evaluation of its two components, failure probability and consequences due to failure, are presented, focusing on the need to quantify and monetise consequences, and, consequently, the engineering risks. From this derives the concept of overall cost, which is the structure cost or value added to its risk value, providing an efficient tool to compare engineering alternatives and solutions. Finally, the risk management scheme is discussed, focusing on the need to establish an intelligent risk management system, which incorporates an automatic and intelligent communication tool, to disseminate among professionals, company hierarchy and outside stakeholders, the structure risks, according to their levels in the Risk Diagram and guided by the company Risk Policy. This is illustrated by examples of applications in two geotechnical structures (a dam and an urban tunnel), showing its enormous potential as a decision-making tool in engineering, using risk-based or risk-informed approach.

1. Introduction

This paper presents the contents of the Pacheco Silva Conference, awarded by the Brazilian Society for Soil Mechanics and Geotechnical Engineering (ABMS), and delivered during the XIX COBRAMSEG (Brazilian Congress on Soil Mechanics and Geotechnical Engineering) in Salvador, August 2018. The theme of the conference was agreed between the ABMS and the author, considering the growing demand for geotechnical risk analysis and management in Brazil and worldwide. This paper aims to present the basic concepts related to the probabilistic approach and risk management, including probabilistic methods to evaluate the probability of failure modes of geotechnical structures, estimation of consequences, in case of failure occurrence, risk calculation and evaluation considering the acceptance and tolerance curves, taking into account a ro-

bust theoretical background applied to practical examples, using the simplest language and manner as possible. From that it comes the proposed target of consolidating theory into practice of risk management applied to geotechnical structures.

Ground property variability has been recognised for a long time (Lumb, 1966) and concepts of risk and reliability applied to geotechnical engineering (Ang & Tang, 1975, 1984; Harr, 1987) have been available for the last four decades. However, the consideration of this knowledge to analyse and design geotechnical structures is still not fully widely applied, struggling with a deterministic culture established and dominant for a long time. In addition to the deterministic culture, several factors may have been contributing to the difficulties of applying risk management currently in geotechnical engineering, such as: i) poor background in statistics and probability of the professionals

[#]Corresponding author. E-mail address: aassis.p@gmail.com.

¹University of Brasilia, Brasilia, DF, Brazil.

Submitted on July 14, 2020; Final Acceptance on August 3, 2020; Discussion open until December 31, 2020.

DOI: <https://doi.org/10.28927/SR.433311>



This is an Open Access article distributed under the terms of the Creative Commons Attribution License, which permits unrestricted use, distribution, and reproduction in any medium, provided the original work is properly cited.

involved; ii) difficulties to establish the probability distribution of geotechnical properties and loadings due to lack or few number of data; iii) feeling that risk calculation is too complicated, complex, time consuming or not accurate enough; and iv) no familiarity with risk acceptance concepts contrarily to safety factors (or similar concepts), whose recommended values are well defined in standards and guidelines.

The fact that traditional engineering has always considered the concept of exactitude has led professionals and society to believe in accurate and precise calculations, with no chances for errors and potential failures. This concept has implied calculations following the deterministic approach, where in any engineering calculation, defined by an empirical, analytical or numerical formulation, material properties and loadings are deterministically defined by specific values, giving a unique result for the engineering calculation. However, it is well known by engineering professionals that some properties and loadings are variable or present uncertainties and should not be defined as a unique value. For this reason, concepts of safety margins or factors have been proposed, which means that the engineering result calculated by the deterministic approach has to obey a safety margin in relation to its critical value that defines a potential failure for that particular structure. In other words, the recognised variability and uncertainties of some engineering properties and loadings have been dealt by safety margins or similar concepts.

In the 1950s, the nuclear energy engineering had to deal with uncertainties for the first time in a clear, simple and objective way to share information with society. The Brookhaven Report (USAEC, 1957) analysed the consequences of an eventual failure of a nuclear powerplant reactor and estimated potential losses and impacts. Despite some fatalities and economic losses were estimated, no methodology for evaluating the failure probability was presented. This report can be considered the first to clearly tackle risks of engineering structures using qualitative estimation. Later, the Rasmussen Report (USNRC, 1975) presented a review of the Brookhaven Report, incorporating quantitative methodologies for estimating risk, in terms of both failure probability and potential consequences. These reports played an important role in promoting the probabilistic approach and risk analysis to deal with uncertainties and variabilities, clearly opposite to the deterministic approach commonly adopted in traditional engineering. In the 1990s, the concepts of risk analysis and management became more common and widely applied to several types of structures, turning into a decision-making tool in engineering (risk-based or risk-informed approach), which means that the calculated risk is taken as one of the key aspects for selecting the best engineering alternative, which has been called the New Engineering.

In Brazil, the pioneers of risk management applied to geotechnical engineering introduced these concepts in the

1980s and 1990s, in particular Fernando Franciss, Hachich (Hachich, 1981; Hachich & Vanmarcke, 1983), Pacheco (1990) and Aoki (Aoki & Cintra, 1996). In 1995, a graduate course dedicated to probabilistic approach and risk management applied to geotechnical engineering was created at the University of Brasilia (Assis *et al.*, 2018), which has motivated applied research on this topic and several M.Sc. and Ph.D. theses have been completed (Espósito, 1995, 2000; Lauro, 2001; Maia, 2003, 2007; Perini, 2009; Hidalgo, 2013; Alarcón-Guerrero, 2014; Charbel, 2015; Mendes, 2017; Franco, 2019; Mendes, 2019; Yokozawa, 2019). Other institutions in Brazil have also contributed actively to risk management in geotechnical structures, such as the Federal University of Ouro Preto (UFOP), Pontifical University of Rio de Janeiro (PUC-Rio) and University of São Paulo (USP), to cite a few. Lately, this topic has been gaining importance in the Brazilian geotechnical community and widely disseminated by the ABMS, contemplating risk aspects, analysis and management in three Milton Vargas Lectures (Coutinho, 2010; Aoki, 2011; Hachich, 2018), two Pacheco Silva Conferences (this paper; Aoki, 2016) and two Victor de Mello Lectures (Mitchell, 2014; Morgenstern, 2018).

Once assuming that engineering calculations incorporate uncertainties and sharing this concept with society, this has brought a dilemma between engineering and society. In general, engineering professionals attempt to focus only in the failure probability of their structures, which it usually quite low. On the other hand, the society only considers the consequences of an eventual failure of these engineering structures, which in some cases can be quite considerable or even catastrophic. Both views are realistic, but antagonistic. Then, the concept of risk, which incorporates both the failure probability and its potential consequences, is the only one able to consider the demands of both sides. In other words, the risk concept is the common denominator between engineering and society, therefore able to be the promising key parameter for decision of acceptable engineering solutions for the society.

It is worth recalling the evolution of engineering approaches during the last decades. In the past, the engineering approach focused basically on the technical benefits and costs of structures, which means that the dimensional view of engineers was only the engineering structure itself. Later, the environmental impacts caused by the implantation and operation of engineering structures have jointed the aspects of benefits and costs. One can say that the engineering view widened to two dimensions, focusing on the structures and their environmental impacts. More recently, the evolution of the current engineering approach has included engineering risks, which consider its failure probability and all dimensions of consequences due to its eventual failure. This means that the best engineering alternative nowadays has to take into account aspects of technical benefits and costs of the structure, its environmental impacts for implantation and during operation, and its potential con-

sequences to the society in case an eventual failure occurs, which is the risks of the engineering structure.

Since risk analysis and management is an essential aspect of the New Engineering, it is desirable to present the important components of risk theory and its practical application to geotechnical structures. As risk is based on uncertainties and variabilities, the first step is to discuss how to incorporate them in engineering calculations, which is done using the probabilistic approach in opposition to the deterministic one, commonly used in traditional engineering up to now.

2. Probabilistic approach

Before discussing the probabilistic approach, it is worth recalling the concept of failure criterion usually adopted for engineering structures. Among all engineering calculations, some are of interest for analysing the behaviour or checking the safety of structures. They are called performance indicators and examples in geotechnical engineering can be the flow rate of a dam, settlements of a foundation, safety factor of a slope, construction schedule, costs and so on. Each of these performance indicators is calculated by an engineering formulation, which can be empirical, analytical or numerical, and is generally expressed as:

$$y = f(x_1, x_2, \dots, x_n) \quad (1)$$

where y is the performance indicator, x_i are the input parameters (material properties, loadings etc.) and f is the function that defines the engineering formulation for this performance indicator.

For each performance indicator, a failure criterion can be defined. The concept of failure here has a very broad meaning, indicating deficient or total loss of the engineering structure performance (structural, functional, schedule overtime, over costs etc.). A critical value (y_{crit}) for the performance indicator is defined, which means that the structure would not perform satisfactorily if the performance indicator calculated value exceeds its critical value. Failure criteria can be expressed as:

$$\begin{aligned} y = f(x_1, x_2, \dots, x_n) &> y_{crit} \\ \text{or} \\ y = f(x_1, x_2, \dots, x_n) &< y_{crit} \end{aligned} \quad (2)$$

This concept is quite common in traditional engineering, which adopts the deterministic approach, calculating the performance indicator using constant values for all input parameters. The assumed values for input parameters are a choice of the engineer and commonly are taken as the mean, most likely or any other value according to his or her experience and common sense. As all input parameters are taken as constant values, the calculated value of the performance indicator is unique. In some occasions, to better understand how input parameters may affect the calculated value of the performance indicator, parametric or sensitive

analyses can be done to complement the deterministic calculation. Safety margins are defined between the performance-indicator calculated value and its critical value to cover eventual uncertainties and variabilities of input parameters and engineering processes (assumptions, modelling adequacy and so on). The concept of safety margins is very consolidated and well-accepted in traditional engineering and typical values are commonly suggested or prescribed by guidelines and standards.

On the other hand, the probabilistic approach can be taken as an alternative to the deterministic one, where uncertainties and variabilities of input parameters are considered in the evaluation of the performance-indicator engineering formulation (Eq. 1), using probabilistic methods. As some input parameters are taken as variables, and not constant values, the calculated value of the performance indicator is also a variable and can be described as a probabilistic distribution function. Besides the probabilistic function statistics (mean, standard deviation, etc.), this permits an additional and very important information, which is the failure probability (p_f), defined as the probability of the performance-indicator probabilistic function exceeding its critical value prescribed by the failure criterion. The statistics of the performance-indicator probabilistic function allow the evaluation of the reliability index β (Christian *et al.*, 1992, 1994) and the failure probability, expressed as:

$$\beta = \frac{(y_m - y_{crit})}{\sigma_y} \quad (3)$$

$$p_f = p(y > y_{crit}) \quad \text{or} \quad p_f = p(y < y_{crit}) \quad (4)$$

where β is the reliability index; y_m is the mean value of the performance indicator; y_{crit} is the critical value of the performance indicator as prescribed by the failure criterion; σ_y is the standard deviation of the performance indicator; and p_f is the failure probability.

It can be noted that the reliability index (β) has a similar concept of the safety margin, defined by the difference between the mean and critical values, normalised by the standard deviation. In other words, it is the number of standard deviations from the mean to the critical values of that performance indicator. Its main advantage is that it is independent of the performance-indicator probabilistic function, which is helpful for suggested or prescribed values in guidelines. On the contrary, the failure probability (p_f) can be only calculated for a certain probabilistic function. The main aspects and comparison between the deterministic and probabilistic approaches are shown on Table 1.

Figure 1 illustrates the schematic process of the probabilistic approach. Some input parameters assumed as variable (x_i) can be described by a probabilistic function that best fits its variability distribution. Input-parameter probabilistic functions are considered in the calculations of the performance-indicator engineering formulation using probabilistic methods. The result is the performance-in-

Table 1. Comparison between engineering approaches.

Engineering approach	Deterministic	Probabilistic
Input parameters of the engineering formulation (x_i independent variables)	Values of input parameter are assumed constant	Some input parameters are assumed as variables
Dependent variable y (performance indicator)	Result is a unique or a range of values for parametric or sensitivity analyses	Result is a probabilistic function or a mean value and its standard deviation
Failure criterion	Comparison between the calculated and critical values of the performance indicator y and check with the prescribed safety margin	The reliability index and failure probability of the performance indicator y are calculated and used in risk analyses

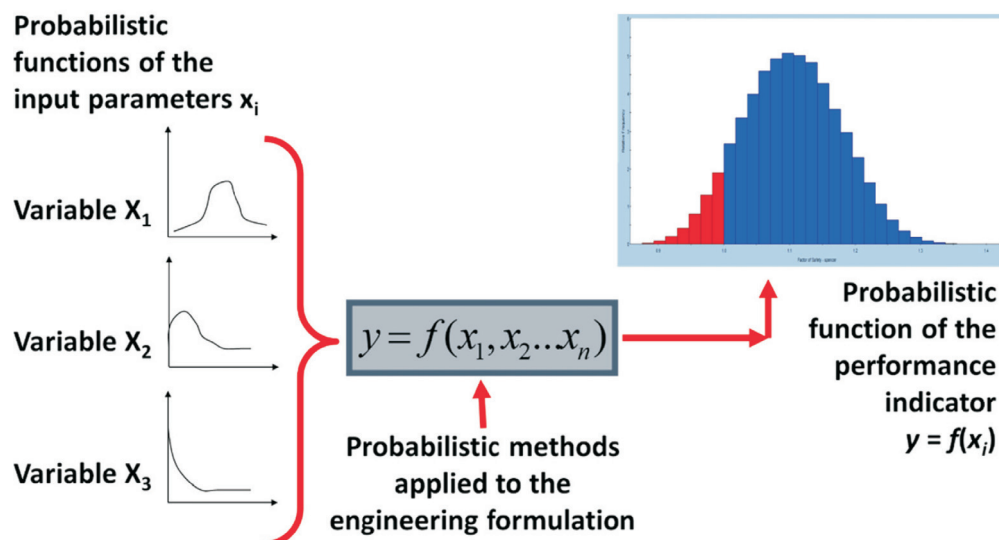
indicator probabilistic function and its statistics, which permits to calculate its mean value, standard deviation, reliability index, failure probability and so on.

As mentioned, one of the main advantages of the probabilistic approach is the evaluation of the failure probability or reliability index of the performance indicator, in addition to its mean value. Traditional engineering based only on deterministic approach usually takes decisions founded on the mean value or similar. When also taking into account the failure probability or reliability index, besides the mean value of the performance indicator, the input parameter variabilities (standard deviations and type of probability functions) are also considered. Figure 2 depicts this concept considering two slopes, with different mean and standard deviation values of the Factor of Safety (FS). Slope B has a greater FS mean value ($FS = 2.0$) than Slope A ($FS = 1.5$), but due to the greater scatter of its input parameters (standard deviation of 0.85 for Slope B against 0.25 for Slope A), Slope B also presents a higher value of the failure probability. Considering only the FS mean values, which is commonly the practice in traditional engineering, one may erroneously decide that Slope B is safer than Slope A. This reinforces that any attempt to establish

correlations for different structures between the mean value of performance indicators and their probabilities of failure may lead to misjudgements, because it misses an important information, which is the input data scatter, as depicted in Fig. 3.

Despite the advantages of the probabilistic approach applied to engineering, there are several challenges to be overcome in order to ensure reasonable and reliable results from it. The estimation or calculation of the failure probability can be done by different methods, ranging from the simplest to more complex ones, such as:

- Qualitative analyses are the simplest methods, where the failure probability is qualified by adjectives (for instance, ranging from practically impossible to very likely).
- Numerical values, where the adjectives qualifying the failure probability are replaced by a range of numbers (for instance, number 1 means practically impossible, increasing to number 5, which means very likely).
- Event-tree and fault-tree analyses describe the logical path of events leading to failure and allow to attribute probabilities to each event, finally quantifying the failure probability according to the relation among all participating events.

**Figure 1.** Schematic process of the probabilistic approach applied to engineering.

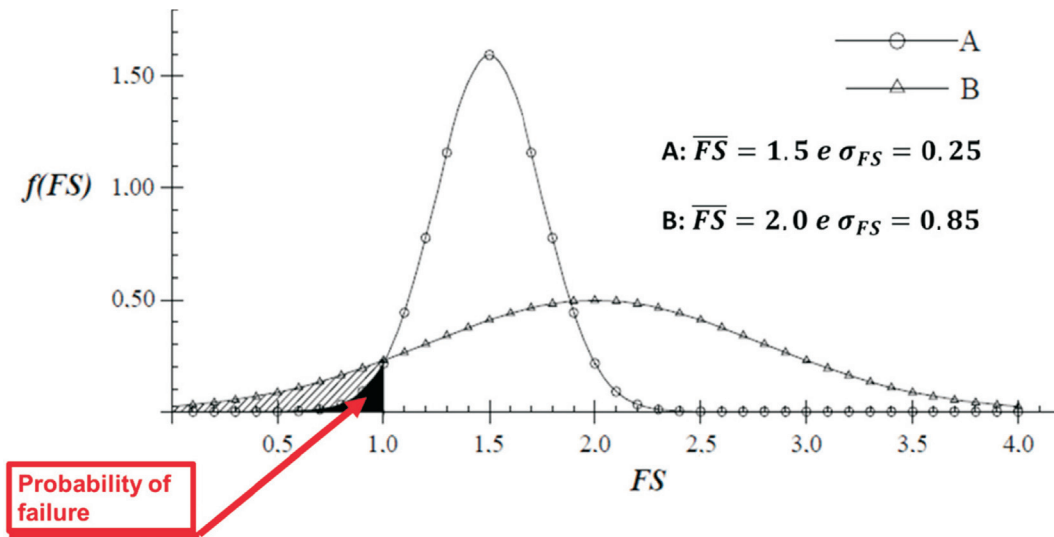


Figure 2. Comparison of the factor of safety of two slopes.

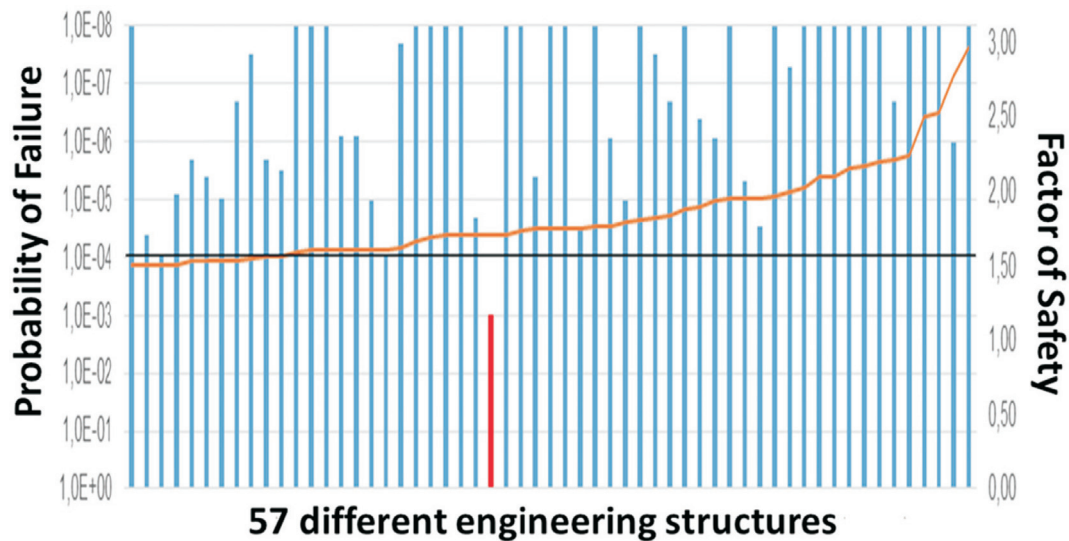


Figure 3. Comparison between factors of safety and failure probabilities of 57 different engineering structures, showing no correlation between these two variables.

- Probabilistic methods are the most complex ones, using the scheme depicted in Fig. 1.

The first challenge of applying probabilistic approach in engineering is the selection of the type of method to estimate or calculate the failure probability of structures. This depends on the availability and quality of input data, importance and complexity of the structure (dimensions and potential impacts in case of an eventual failure), level of engineering studies and knowledge and maturity of professionals and companies involved. At a first trial, the main point is to use the probabilistic approach, no matter how simple the chosen method is. However, there are many gains moving to quantitative methods (Assis *et al.*, 2019; Oboni & Oboni, 2020), which are the focus of this paper, more precisely the use of probabilistic methods to evaluate

the failure probability. As shown in Fig. 1, the quantification of the reliability index and failure probability of a certain performance indicator requires:

- Selection of a performance indicator, its engineering formulation and critical value (defined by the adopted failure criterion), what is also a common practice in traditional engineering.
- Definition of the probabilistic functions or statistics (mean and standard deviation) of input parameters (material properties), loadings, etc., which are taken as variables for the calculation of the performance indicator.
- Choice of the most adequate probabilistic method to obtain the probabilistic function or statistics of the performance indicator, and, consequently, its reliability index and failure probability.

- Interpretation of the probabilistic analysis results by the evaluation of the reliability index and failure probability, and, consequently, the risk management of the engineering structure.

Before discussing probabilistic methods, a word on event-tree and fault-tree analyses. These tools are quite important when the failure probability has to be quantified, but there is no well-defined engineering formulation to evaluate that performance indicator, so that probabilistic methods cannot be applied. In addition, event and fault trees are excellent engineering exercises, helping establish the logical sequence of events towards the final failure event (event tree) or backwards from the failure event, identifying the previous events necessary to cause the failure (fault tree). Once the event or the fault tree is set, these tools are useful and effective to understand the whole engineering process that may lead to the final failure event. Then, probabilities can be attributed to each event, using expert experience and perception or any other calculation tool. At the end, the probability of the failure event may be calculated using logical operators, following probability rules for events that may occur alternatively, simultaneously, in series and so on. Figure 4 shows an example of event tree for calculating the failure probability due to piping in a dam. Two aspects are of particular interest in this example: i) firstly, piping is a phenomenon that hardly is defined by a precise engineering formulation, so that the event tree analysis is required; ii) secondly, some probabilities of the branches of this event tree have been calculated using fault tree analysis. So, this example combines both event and fault tree techniques and, finally, the failure probability due to piping is quantitatively calculated. More detailed discus-

sions on event and fault tree analyses applied to piping in dams are presented by Fell *et al.* (2015) and Caldeira (2018).

Contrarily, when the performance indicator is well-defined by an engineering formulation (empirical or analytical expressions, or numerical calculations), the use of probabilistic methods is recommended and presents reliable results. Probabilistic methods can be defined as those able to determine the probabilistic distribution function or its statistics of a dependent variable (performance indicator), which is defined by an engineering formulation, based on the probabilistic distribution functions or their statistics of input variables (material properties, loadings, etc.). There are many probabilistic methods available and the most commonly used in geotechnical engineering are the Monte Carlo Method – MCM (Harr, 1987; Baecher & Christian, 2003; Fenton & Griffiths, 2008), First Order Second Moment – FOSM (Harr, 1987; Baecher & Christian, 2003), Point Estimate Method – PEM (Rosenblueth, 1975, 1981; Harr, 1987; Baecher & Christian, 2003), Hybrid Point Estimate Method – HPEM (Gitirana, 2005; Franco, 2019; Franco *et al.*, 2019; Yokozawa, 2019), First Order Reliability Method – FORM (Baecher & Christian, 2003; Fenton & Griffiths, 2008) and so on. All of them require the variability data (probabilistic distribution functions or statistics) of the input parameters, which is the second challenge of the probabilistic approach applied to engineering to be discussed in this paper.

The problem is how to obtain the probabilistic distribution functions of input parameters and loadings assumed as variable, considering that usually engineering input parameters and loadings are quite limited in values due to test-

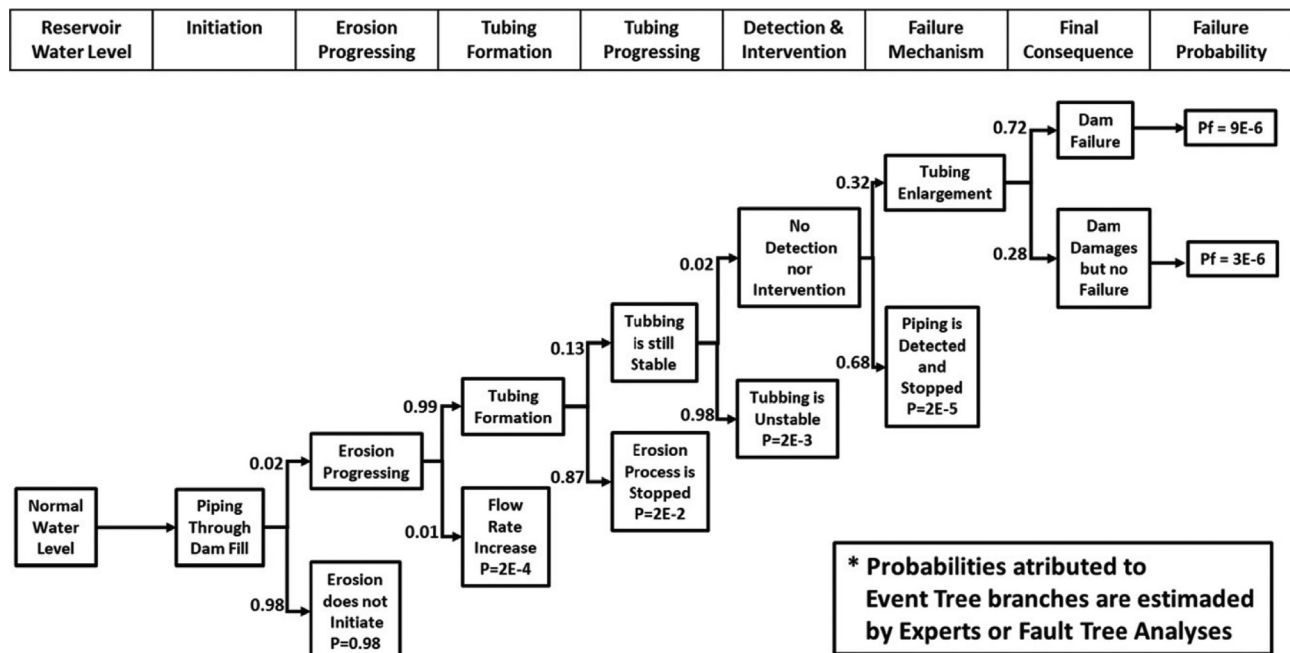


Figure 4. Example of an event tree for estimating the failure probability due to piping of a dam.

ing complexity, time and costs. There are some options to cope with this challenge. Firstly, consider that there are plenty of data for a certain input parameter, which is a sample statistically representative of that variable. In this case, data are treated by descriptive statistics, following these stages: i) Calculate the mean, standard deviation and any other moments of the sample data; ii) Organise the data in a histogram; iii) Fit any probabilistic distribution function; iv) Use any type of fitting test (minimum square of errors, Chi-square, Kolmogorov-Smirnov, etc.) to check which function better represents the sample data; v) Choose the probabilistic distribution function and its statistics for that particular input variable. More commonly, there is lack of enough data to obtain the probabilistic distribution functions of some input variables. In this case, the options to represent the variability of the input parameters are the following:

- The few existing data of a certain variable are used to estimate the mean value and the standard deviation is obtained by the coefficient of variation (CoV), as suggested in the literature and listed in Table A1 (several authors have reported typical or a range of CoV values for different geotechnical properties, as CoV values present much less scatter than the mean and standard deviation themselves); considering the obtained mean and standard deviation values, a probabilistic distribution function can be adopted for that variable (some authors have suggested the type of probabilistic functions that better fits some geotechnical properties, as shown in Table A2).
- In case of no suggested CoV value for a certain variable and, consequently, its standard deviation cannot be estimated, some simplified probabilistic functions can be adopted such as Constant or Triangular functions, which requires the minimum and maximum values of the variable (these limit values might be defined by expert and experienced engineers).

Some comments now follow on the above options to overcome the lack of enough data to describe the variability of input parameters taken as variables. The CoV values and their ranges suggested in Table A1 are the best option to overcome the lack of data. However, it is highly recommended that the chosen value be the result of a critical analysis from experienced engineers, considering their expectation of the variability of that parameters. For instance, the CoV range for the cohesion varies from 20 to 80 %, and 40 % is commonly taken for most cases; however, if the target is the cohesion CoV for a compacted soil, the lower values of the range can be considered, such as 20-25 %, but on the contrary, if the target is the cohesion CoV for a natural saprolitic soil, maybe the higher values of the range are more adequate, such as 60 % or more due to its enormous variability. Other important point to consider is that the simplified probabilistic functions (constant or triangular) do not require a defined standard deviation value, however, some probabilistic methods require this value even so. A

common approximation to estimate the standard deviation for these functions is to assume its value equal to 1/6 of the difference between the maximum and minimum limit values of that variable (this concept comes from the fact that variables described by the normal distribution present almost all its variability within the limits of three standard deviations around the mean value, totalling six standard deviations for the whole range).

Other important point to consider for representing the input variables by probabilistic distribution functions is the truncation of their value ranges. This is needed because some probabilistic functions are unbounded on both sides or on one side, requiring that limits are imposed on unbounded sides to avoid variable values outsider their realistic possible range. Two types of truncations are possible, the statistical and the engineering ones. The statistical truncation is usually done considering a number of standard deviations around the mean value (mean value minus m standard deviations and mean value plus n standard deviations, where commonly m is equal to n). As already mentioned, three standard deviations around the mean value for variables well-described by the Gaussian distribution represent almost the totality of the possible range (99.7 %) of that variable, so that this is a very commonly adopted truncation. Statistical truncations using smaller numbers of standard deviations around the mean values have to be taken with care, because, if the range of values for input variables are made narrower, the standard deviation of the dependent variable (performance indicator) evaluated by probabilistic methods may be done artificially smaller, leading to lower failure probabilities than the realistic ones (Hammah *et al.*, 2010). On the other hand, sometimes the statistically truncations define a range of values for a particular input variable that is not realistic, which means that the possible values of that variable are not physically acceptable. In this case, it is highly recommended to apply engineering truncation, defining the minimum and/or maximum acceptable limit values of the variable. It is helpful to have the expertise of experienced geotechnical engineers to define these limit values for the geotechnical properties to be represented by probabilistic distribution functions. In summary, the good practice is to firstly define the statistical truncation (three standard deviations around the mean value is recommended) and then, check if its range of values does not violate the possible engineering range of values for that input variable; if so, the range of values defined by the statistical truncation has to be corrected by the engineering truncation.

Once all input variables have their probabilistic distribution functions or their statistics (mean value and standard deviation) defined, probabilistic methods can be applied to obtain the probabilistic distribution function or its statistics of the dependent variable (performance indicator). Several probabilistic methods are available with their advantages and disadvantages and comments are made on the three

most popular methods applied to geotechnical engineering, which are the Monte Carlo Method (MCM), the First Order Second Moment Method (FOSM) and the Point Estimate Method (PEM).

The MCM is a probabilistic method that may be considered exact in obtaining the probabilistic distribution function of the dependent variable, since it solves randomly the engineering formulation for the dependent variable (performance indicator) N times, generating a sample of results, and when N is a number large enough, the statistics of the resulting sample do not change any more, achieving its stability, indicating that the results are final and considered exact. The aspects and steps for running the MCM (Fig. 5) can be summarised as follows:

- The MCM aims to obtain an approximate numerical simulation of the probabilistic distribution function of the dependent variable y (performance indicator), which is defined by an engineering formulation (empirical, analytical or numerical).
- The MCM requires the probabilistic distribution functions of all input variables.
- Independent and random values for each input variable x_i are obtained and an evaluation of the engineering formulation of the dependent variable y is done; for each input variable selection, its probabilistic distribution function is taken in its accumulative probability form, and a random number between 0 and 1 is obtained, applied to the accumulative probability curve, obtaining the value of the input variable x_i , which is used in that particular MCM simulation.
- Repeating this procedure N times, a sample of N discrete values of the dependent variable y is obtained; this process may require considerable computational effort, depending on the complexity of the engineering formulation.

- Taken this sample with N values of the dependent variable (performance indicator), a histogram can be plotted and the statistics (mean, standard deviation and other moments) calculated, as well the best-fit probabilistic distribution function found and the failure probability evaluated.
- Increment the number of MCM simulations until the resulting statistics is stabilised (they do not change compared to immediate previously ones as shown in Fig. 6); when that happens, the MCM results can be considered final and exact.

As soon as a sample of N results of the dependent variable (performance indicator) is obtained, the sample statistics can be calculated using descriptive statistics of discrete variables, as expressed below for the mean value, standard deviation and failure probability:

$$E(y) = \bar{y} = \frac{\sum (y_i)}{N} \quad (5)$$

$$\sigma_y = \sqrt{\frac{\sum (y_i - E(y))^2}{N}} \quad (6)$$

$$p_f = \frac{N_f}{N} \quad (7)$$

where: $E(y)$ is the mean value of the dependent variable y ; y_i are the discrete values obtained by MCM simulations; N is the total number of MCM simulations; σ_y is the standard deviation of the dependent variable; p_f is the failure probability of the dependent variable; N_f is the number of MCM simulations that indicates failure ($y_i < y_{crit}$ or $y_i > y_{crit}$).

A key point is to know when the number N of MCM simulations is large enough and the results can be considered already stabilised. Statistically speaking there is a for-

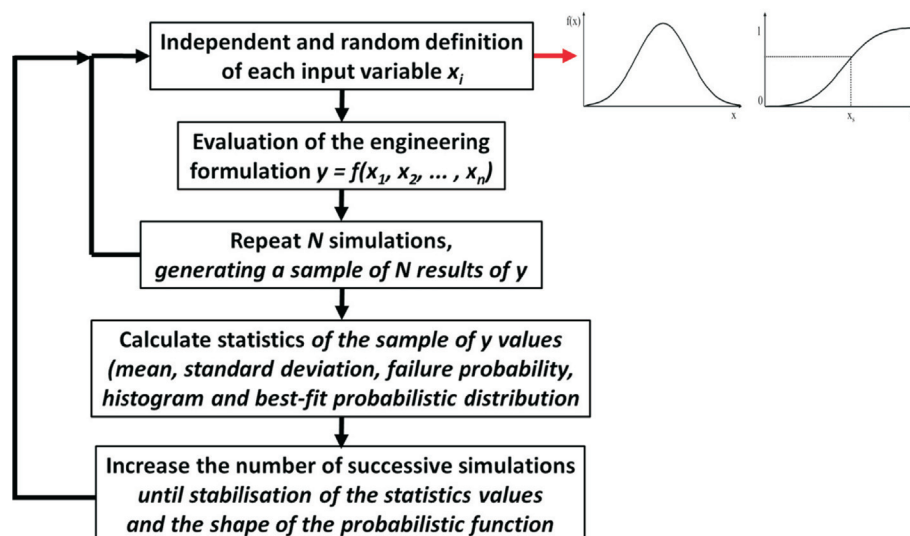


Figure 5. Main steps of the MCM simulations.

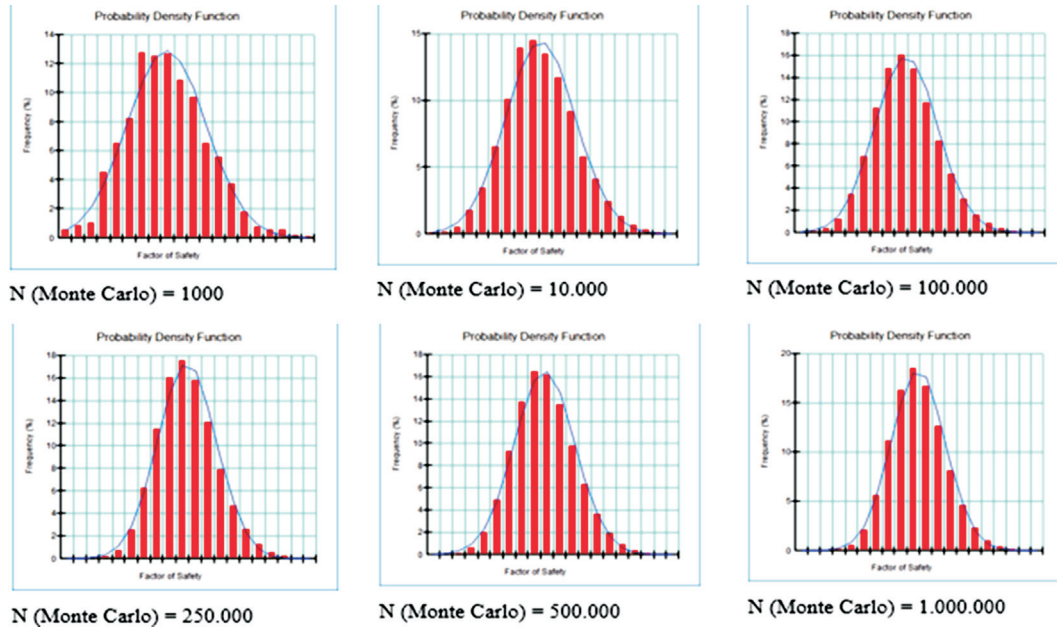


Figure 6. MCM results with different N simulations, showing that increasing N the results tend to stabilize, which can be considered final and exact.

mulation to estimate the number of MCM simulations, assuming that an error α may occur, which is expressed by:

$$N = \left(\frac{Z_{\alpha/2}^2}{4\alpha^2} \right)^n \quad (8)$$

where N is the desirable number of MCM simulations assuming that an error α in the results may occur; $Z_{\alpha/2}$ is the number of standard deviations around the mean value to reach an error $\alpha/2$ at each distribution tail; n is the number of input variables.

This statistical formulation usually yields an enormous number of MCM simulations N . For example, if an error α of 5 % is intended, Z is 2 standard deviations and assuming four input variables ($n = 4$), the number N of MCM simulations estimated is over 25 billion. Therefore, commonly the criterion to verify the stabilisation of the MCM statistics is observational, as shown in Fig. 7. In this case, one can notice that 200,000 simulations are enough to stabilise all statistics resulting from the MCM simulations.

Some important aspects related to the MCM results, in particular to the failure probability calculated by the frequentist formulation presented by Eq. 7, are worth some comments. It is recommended that the failure probability calculated from Eq. 7 should only be accepted if the number N of MCM simulations is at least one order of magnitude (10 times) greater than the inverse of the failure probability calculated. For example, if p_f is calculated as 10^{-4} , it requires at least 10^5 MCM simulations. Other common mistake in reporting the failure probability calculated by the MCM is to take it as zero, when after a certain number of simulations N , no failure case is found. This does not guarantee

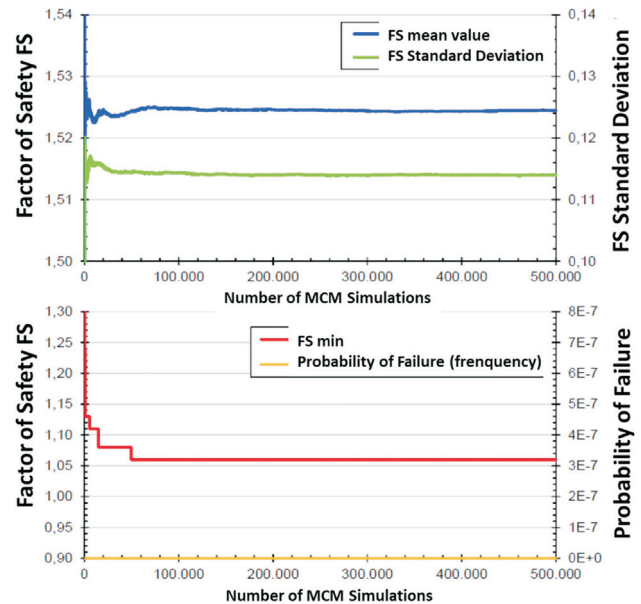


Figure 7. Observational criterion to verify the MCM simulation results stabilisation.

that p_f is zero but, simply, that within the number of simulations carried out, no failure event could be discovered by that particular MCM simulation process. The best form to report this result is that the failure probability is simply smaller than $1/N$ ($p_f < 1/N$). This recalls another problem related to the acceptance of the failure probability calculated by the frequentist formulation (Eq. 7), when the number of MCM simulations N is not large enough. This is quite common due to the enormous computational efforts required by the MCM to evaluate many engineering formulations. In

this case a sample of N results is obtained, but the results are not stabilised and are not enough to evaluate the failure probability. For this reason, a good alternative to evaluate the failure probability is to assume that the best-fit probabilistic distribution function derived from the sample histogram is the best estimator for the real one, and calculate the failure probability using this distribution. The best-fit technique can be done using the statistics calculated by Eqs. 5 and 6 from the sample of MCM results and applying them to different probabilistic distribution functions, choosing the one that best-fits the histogram of MCM results (best-fit by moments). Alternatively, the best-fit of the MCM results can be done by minimising the square of the errors between the histogram and different probabilistic functions, selecting the best-fit probabilistic function as the one with the minimum square of errors (maximum likelihood estimator), and, then, calculating its statistics, as described by Van Gelder (2000). This best-fit technique is the most used in commercial software. Other question commonly raised is that if the best-fit technique should focus on the overall histogram or on the tail of the histogram where the failure probability is calculated, as illustrated in Fig. 8. There are no simple answers to these questions, but a best-fit technique of the overall histogram is preferred over the best-fit of the histogram tail, simply because it fits the whole variability phenomenon and not a part of it.

In summary, the MCM is demanding, requiring the complete definition of the probabilistic functions of input variables and may need computational efforts to reach acceptable results, in function of the complexity of the engineering formulation to be solved. In doing so, the outcome results are also complete (statistics and definition of the probabilistic function of the dependent variable) and can be considered final and exact. However, in many cases, the necessary computational efforts may be excessive or even not acceptable for a realistic schedule of engineering tasks.

The alternative to overcome this problem is to use approximate probabilistic methods in place of the MCM, being the most popular in geotechnical engineering the FOSM and PEM.

The FOSM is a method that considers the first-order approximation of the Taylor Series expansion applied to the equation of the second statistical moment (variance). It requires only the mean and standard deviation values of input variables, but also returns only the mean and standard deviation values of the dependent variable (performance indicator). Considering some assumptions, such as the probabilistic distribution functions of the input variables are symmetric and these variables are independent among themselves, the FOSM equations for the performance-indicator mean and standard deviation values can be expressed as:

$$E(y) = \bar{y} = f(\bar{x}_1, \bar{x}_2, \dots, \bar{x}_n) \quad (9)$$

$$V(y) = \sum_{i=1}^n \left(\frac{\partial y}{\partial x_i} \right)^2 V(x_i) \quad (10)$$

where $E(y)$ is the mean value of the dependent variable y (performance indicator); f is the engineering formulation to calculate the dependent variable y as a function of the independent input variable x_i ; \bar{x}_i are the mean values of the independent input variables; $V(y)$ is the variance value of the dependent variable y ; $V(x_i)$ are the variance values of the independent input variables x_i ; and $(\partial y / \partial x_i)$ are the partial derivatives of the dependent variable y in relation to each independent input variable x_i .

The mean value of the dependent variable y is given by Eq. 9, inputting the mean values of the independent variables into the engineering formulation defined to calculate the performance indicator. In other words, the method assumes that the best estimator of the mean value of y is given

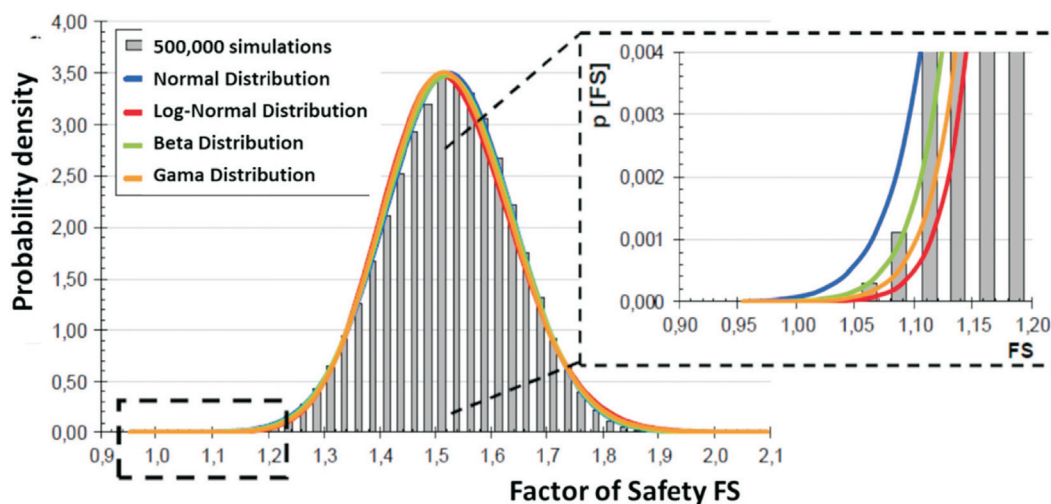


Figure 8. Possible alternatives of the best-fit technique of the probabilistic distribution function, focusing on the overall histogram or the histogram tail.

by the function f evaluated using the mean values of the input variables \bar{x}_i . In fact, this is a similar procedure when the deterministic approach is adopted, calculating the performance indicator using the mean values of input parameters and loadings. The FOSM major difficulty is to obtain the partial derivatives ($\partial y / \partial x_i$) of the engineering formulation used to calculate y as a function of each independent input variable (Eq. 10). In many cases, these partial derivatives may be not easily determined or are even not possibly defined. The problem was solved replacing the partial derivatives by a numerical approximation (Christian *et al.*, 1992, 1994; Christian, 1999, 2004; Baecher & Christian, 2003). The partial derivatives intend to evaluate how the engineering function of y is affected by each input parameter; in other words, they evaluate the mathematical weight of each input parameter in the engineering formulation used to calculate the performance-indicator variance. To do so, the numerical approximation proposes to increase by a small increment the value of each input parameter, independently, keeping the other input parameters at their mean values, and calculate a new value of the y_i . The numerical approximation of a certain partial derivative is given by:

$$\frac{\partial y}{\partial x_i} = \frac{y_i - \bar{y}}{\Delta x_i} = \frac{\Delta y_i}{\Delta x_i} \quad (11)$$

where y_i is the new value of the y -function calculated with the incremental value of a certain input parameter ($x_i = \bar{x}_i + \Delta x_i$); \bar{y} is the mean value of the dependent variable, given by Eq. 9; and Δx_i is a small increment added to the mean value of each input parameter.

In the literature, this small increment given for each input variable is usually reported as 10 % of its mean value. In fact, the exact value of this increment is not relevant because it is only used to calculate the new value of the y -function, and, then, to estimate the value of the partial derivative around the mean value of dependent variable \bar{y} , taking the increment of the y -value and dividing it by the increment of the input variable x_i , yielding the dependence of the dependent variable y per unit of that particular input parameter. Farias & Assis (1998) analysed the effect of the increment size and concluded that the value of 10 % is appropriate, but it could be any other value, except extremely small values, which could induce numerical errors in evaluating Eq. 11, or very large values, which could erroneously evaluate the derivative when its shape departs to far from a linear dependency between the y -function and that particular input variable. In this case, the evaluation of the partial derivatives by numerical approximation using two points around the mean value of the dependent variable \bar{y} is highly recommended, and given by:

$$\frac{\partial y}{\partial x_i} = \frac{y_i^+ - y_i^-}{\Delta x_i} = \frac{\Delta y_i}{\Delta x_i} \quad (12)$$

where y_i^+ is the new value of the y -function evaluated with an incremental value of a certain input parameter ($x_i = \bar{x}_i + \Delta x_i / 2$); y_i^- is the new value of the y -function evaluated with a decremental value of a certain input parameter ($x_i = \bar{x}_i - \Delta x_i / 2$).

Figure 9 illustrates how the two-point evaluation of the numerical approximation of the partial derivatives fits much better for any shape of the derivative function of the dependent variable y in relation to a particular input variable x_i . Duncan (2000) suggested the two-point numerical approximation of the partial derivatives, using the increment and decrement of each input variable equal to one standard deviation. The two-point numerical approximation technique requires a larger computational effort, since the single-point numerical calculation implies $N = n + 1$ calculations of the y -function, where n is the number of independent input variables, and the two-point numerical approximation needs $N = 2n + 1$.

At the final evaluation of Eq. 10, the variance of the dependent variable $V(y)$ (performance indicator) is calculated by the summation of the product between the partial derivatives and variances of input parameters, which means that the y -variance is given by the sum of the mathematical weight (partial derivative) multiplied by the statistical weight of each input variable (its individual variance). This type of calculation allows to estimate the individual weight of each input-variable variance to the total y -variance, simply dividing them, usually reported in percentage (%), as depicted in Fig. 10. This result helps understand the effect of each input-variable variance in the total variance, allowing to focus on those input variables that play a more important role in the process. The final outcome of the FOSM is only the mean and standard deviation values of the dependent variable, but it also only requires these statistics of input variables. The computational effort is very low, requiring only $N = n + 1$ calculations for the one-point numerical approximation of the partial derivatives or $N = 2n + 1$ for the two-point alternative numerical approximation. The main disadvantage is that the method does not return any information on the type of the probabilistic function of the dependent variable, which has to be assumed, and this is required to calculate the failure probability for that performance indicator.

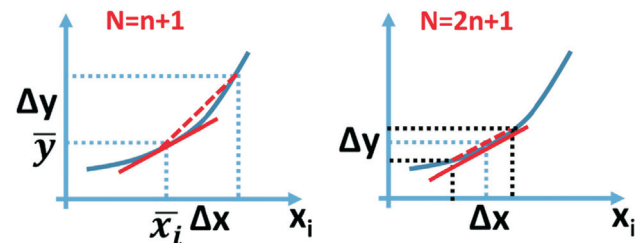


Figure 9. Numerical approximation schemes (one-point and two-points), illustrating the better fitting of the two-point technique for derivative functions departing from linear dependency.

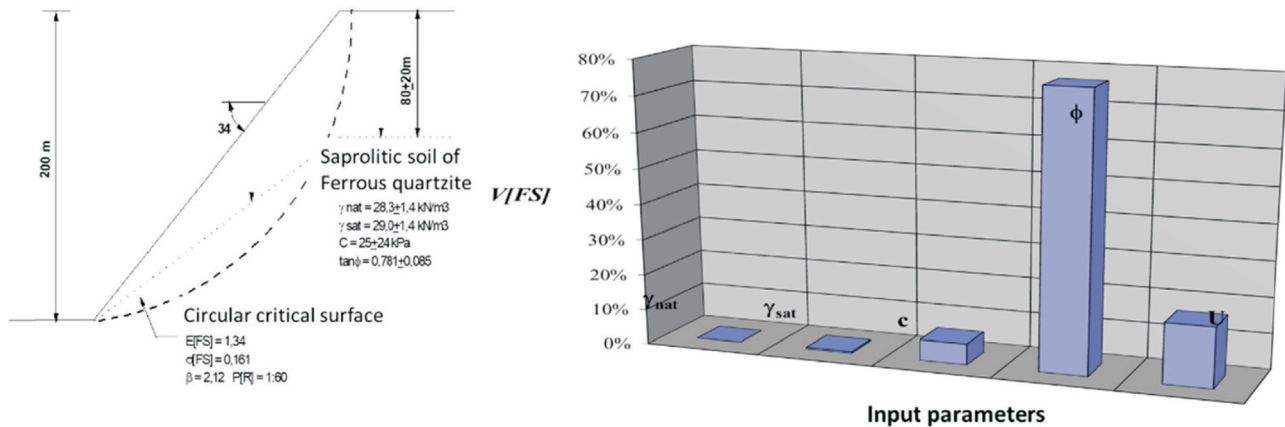


Figure 10. Influence of the variances of each input variable (unit weight, cohesion, friction angle and pore pressure) on the final variance of the dependent variable (factor of safety) (modified from Sandroni & Sayão, 1993).

The other alternative probabilistic method is the Point Estimate Method (PEM), derived by Rosenblueth (1975; 1981). The PEM is based on the Gaussian quadrature (Christian & Baecher, 1999; Baecher & Christian, 2003) to numerically calculate the moments of the probabilistic distribution function of the dependent variable y , based on all possible combinations of two estimate points of the input variables. For each input variable x_i , two estimate points are defined, being its mean value plus and minus one standard deviation value, such as $x_i^+ = \bar{x}_i + \sigma x_i$ and $x_i^- = \bar{x}_i - \sigma x_i$. So that, the PEM also only requires the mean and standard deviation values of all input variables. Once the two estimate points are defined for all input variables, the engineering function for the dependent variable y is solved N times, considering all possible combinations among the estimate points of all input variables, what gives $N = 2^n$ calculations (where n is the number of input variables). This means that the PEM generates a sample of N results of the dependent variable y . Then, the statistical moments of the dependent variable are calculated using descriptive statistics for discrete values, as given by Eq. 5 for the mean value and Eq. 6 for the standard deviation value, simply replacing N by 2^n . Moments $M3$ (symmetry) e $M4$ (kurtosis) can also be calculated using similar equations. These expressions are for independent input variables and corrections based on the correlation coefficients may be applied when these variables are dependent among themselves. The PEM also only returns the mean and standard deviation values, and other statistical moments, as it only requires similar data of the input variables. As the FOSM, the PEM does not yield any information on the type of the probabilistic function of the dependent variable (performance indicator), which has to be assumed to calculate the failure probability.

Table 2 presents a comparison of these probabilistic methods. The MCM and PEM generate a sample of results of the performance indicator y (dependent variable), allowing each individual calculation to explore the most critical response for that set of input parameters, including possible

changes in the failure mechanism, which means that multiple mechanisms may be considered. The final variance of the dependent variable is calculated from all their individual results in relation to its mean value. In this aspect, the FOSM is more limited, since it calculated a unique failure mechanism for the mean values of input parameters and the final variance is evaluated only in relation to this mean-value failure mechanism of the dependent variable. There are several publications in the literature (for instance, Griffiths & Fenton, 2007), comparing these methods and their applicability in geotechnical engineering. In general, the FOSM results indicate a lower failure probability than the other two methods, exactly because it explores less the scatter of input data and potential failure mechanisms. The HPEM presents the advantages of the FOSM in terms of the low number of required simulations and the influence of each input parameter in the final result, and explores all variability of parameters and mechanisms as done in the PEM, yielding similar reliable results as the PEM (Gitirana, 2005; Franco, 2019; Franco *et al.*, 2019; Yokozawa, 2019).

In summary, probabilistic approach and quantitative evaluation allow obtaining the failure probability value of a certain performance indicator. This can be done by Event and Fault Tree Analyses, when the performance indicator is not well-defined by an engineering formulation (empirical or analytical formula, or numerical solutions), or, on the contrary, by probabilistic methods, when the engineering formulation is well set for that performance indicator. As it can be noticed, the whole probabilistic approach and methods are not perfectly defined and some assumptions might be needed. However, estimations of the variabilities of input parameters yield better and more complete engineering results than the assumptions that input parameters and loadings are taken as constant values and the final result is unique, as commonly done in the deterministic approach. Paraphrasing Warren Buffett and adapting his thought, it is preferable to have an approximate probabilistic result than a precise deterministic one that is certainly wrong. This re-

Table 2. Comparison of the most common used probabilistic methods in geotechnical engineering (Assis *et al.*, 2018, 2019).

Probabilistic method	Advantages	Disadvantages
Monte Carlo (MCM)	Final results may be exact Obtains all statistics and the probabilistic function of the dependent variable	Requires complete probabilistic functions of all input variables May imply considerable computational effort
First Order Second Moment (FOSM)	Very fast computations Requires only the mean and standard deviation values of input variables Obtains the influence of each input variable on the final variance of the dependent variable	Requires the assumption of a probabilistic function for the dependent variable to evaluate its failure probability Final variance is limited to the influence of the variances of input variables around the mean value (does not change the failure mechanism for each set of input parameters)
Point Estimate (PEM)	Computational efforts are reasonable Requires only the mean and standard deviation values of input variables	Requires the assumption of a probabilistic function for the dependent variable to evaluate its failure probability

inforces that probabilistic results in terms of failure probabilities should not be taken as exact numbers, but as an indication of their magnitude, mainly focusing firstly on their order of magnitude (power of 10, for instance 10^{-4} or 10^{-5}) and, then, on their decimal digits, avoiding to report non-significant digits (5×10^{-5} is preferred to 5.15×10^{-5}). Following similar logic, very small calculated probabilities may not have enough accuracy, so that it is recommended to report 10^{-7} or 10^{-8} as the lowest possible failure probability for geotechnical structures (this means that if any lower failure probability than those values is calculated, it is reported at the suggested lowest limit), as suggested by Mitchell (2014).

Once the reliability index or failure probability for a certain performance indicator is determined, the question is how to consider their values within the scope of engineering decision making. A first and easy attempt is to correlate the results of the probabilistic approach to the conventional concepts of safety margins and factors, commonly used in conventional engineering (deterministic approach). This leads to erroneous findings, simply because the variabilities of input data are not considered in this correlation. The only and truly alternative is to integrate the results of the probabilistic approach, in particular the reliability index or failure probability, into the concept of risk, as defined and applied to engineering.

3. Risk metrics and analyses

The risk concept, as defined in engineering, comes from an uncertain event that, if it happens, may lead to a structure behaviour different from that forecasted and expected, generating consequences from this unexpected behaviour, which can be better or worse than those forecasted. Uncertain events that may lead to better consequences are

called opportunities and those causing worse and undesirable consequences are hazards. This risk concept implies two main variables that are taken together, the probability of occurrence of the uncertain event and the potential consequences caused, if the uncertain event occurs (damage, impacts and so on). It is very important to understand and consider this engineering risk concept clearly, to ease the communication among all stakeholders and the society about a certain structure. This reminder is even more important considering that colloquial language usually takes the word *risk* as synonymous of chance, likelihood, probability (for instant, what is the risk to have a storm today?). The engineering concept of risk has to take, both, the probability of occurrence and potential consequences. This concept is well accepted implicitly in our mind. For instance, when deciding to take a plane, the consequences of a crash is disastrous (loss of all lives on board), but it is usually accepted because the probability of a crash (failure) is very small (taken as 10^{-6} to 10^{-7}). The same should apply to all engineering structure. There is no engineering structure with risk equal to zero, there is always a failure probability to all structures. In the same manner as the decision making to take the plane, the failure probability has to be analysed in conjunction with the potential consequences of an engineering structure failure, in case it occurs, and to be accepted by engineers and society if the failure probability and consequences are within certain limits (acceptance and tolerance curves).

A first and easy approach to carry out a risk analysis is by qualitative methods, where the failure probability and consequences are described by adjectives, according to their susceptibility and severities. An example of this qualitative method is the risk index, which results from the multiplication of the probability and consequence factors

(Table 3). This is the method currently adopted by the dam safety legislation in Brazil. Several characteristics of the dam are considered using a point summation system to classify its susceptibility to failure in three categories (high, moderate and low). Similarly, the potential consequences sum points considering the presence of people and environment downstream, size of the reservoir and so on, also classifying it in three categories (high, moderate and low). Table 4 presents the risk categories (A, B and C) that consider the susceptibility to failure of the dam and its potential damage (consequences). It is important to note that, in the dam safety legislation in Brazil, the term risk unfortunately is erroneously applied only to the failure probability of the dam, and not to the joint product of failure probability and its consequences, which must be corrected for ensuring precise risk communication among all.

The evolution from qualitative to quantitative analyses of risk requires a risk metrics that could be applied to all type of engineering structures, including the different types of consequences. The expected outcome from the engineering risk concepts yields to:

$$R = p_f \cdot C \quad (13)$$

where R is the engineering risk; p_f is the failure probability of the engineering structure; and C are the potential consequences due to its failure, if it occurs.

Equation 13 can be expanded to include cases where the failure is given by a sequence of independent events, as

defined in Event Tree Analyses, leading to the final failure probability as a result of the product of individual event probabilities towards the structure failure. Also, the consequences due to a failure of complex engineering structures involve different types of impacts, which are usually categorised in spheres of consequences, such as those related to:

- The structure itself - all costs due to the physical loss of the structure (works for cleaning the failure and rebuilding the structure) and the outgoing profit during the period of time that the structure is not operating;
- Health and Safety of People – costs due to medical treatments of injuries and compensations for life losses of workers and outsiders;
- Public and private properties – indemnity costs for partial or total losses of vehicles, housing, commercial, business, educational, industrial and agribusiness facilities, and all types of infrastructure (roads, bridges, water supply, sewage treatment plants, etc.);
- The environment – indemnity and recovery costs of environmental protected areas and parks, woods and forests, rivers and lakes, and so on.
- Reputational Damages – this is usually related to the losses of the company value, for instance in the stock markets, and future legal difficulties and constraints, such as obtaining of permits to engage new projects, or to enlarge, update or keep operation of on-going facilities.

Table 3. Example of Risk Index to qualitatively carry out risk analyses.

Risk Index		Consequence Factor			
Probability and Consequence Matrix	Insignificant		Low	Moderate	High
	1	2	3	4	
Probability Factor	Insignificant	1	2	3	4
	1				
	Low	2	4	6	8
	2				
	Moderate	3	6	9	12
	3				
	High	4	8	12	16
	4				

Table 4. Example of qualitative risk analysis for evaluating dam safety in Brazil.

Risk Category	Potential associated damage (consequences)		
Failure probability	High	Moderate	Low
High	A	B	C
Moderate	A	C	D
Low	A	C	E

All these consequences may happen and have to be summed, considering that each type of consequence has its own vulnerability (ability of a particular consequence to occur due to the structure failure). One point that commonly arises is how to sum different types of consequences. The best and most efficient alternative is the monetisation of the consequences and sum their values. For this, it is necessary to establish methodologies on how to monetise each type of consequence, which is not a complicated issue, except when dealing with life losses of people. Despite all aspects related to social, culture, religion, economic income, age and so on, it is highly recommended to not define a value for people lives, but simply take the value paid for compensation of life loss, with no difference among people, no matter how different they might be. In other words, each life loss will be compensated by the same amount, despite age, gender, education, social or professional position, and so on. As people life losses bring an enormous impact in the society, it is recommended to assume the highest compensation value possible, in order to make people lives the one most important or one of the most important consequences in the risk calculation. In doing so, the engineering risk expression becomes:

$$R(\$) = p_f \cdot C(\$) = \prod p_{fi} \cdot \sum p_j \cdot C_j(\$) \quad (14)$$

where $R(\$)$ is the monetised value of the engineering risk; p_{fi} are the individual failure probabilities of serial events leading to the final failure of the engineering structure, which are multiplied; p_j are the vulnerabilities (value from zero to 1) for each type of consequence (when equal to 1 means that that consequence will happen, if the failure occurs); $C_j(\$)$ are the monetised value for each type of consequence.

As examples of consequence monetisation, Oboni & Oboni (2020) reported that the Fundão Dam failure, occurred in Mariana, Brazil, in 2015, may cost over US\$ 40 billion to the owners (BHP and Vale mining companies) to cover all spheres of consequences and the oil spill that happened in the Gulf of Mexico, in 2010, where 5 million barrels leaked into the ocean, has costed to BP company around US\$ 65 billion in controlling, cleaning and recovery measures, and penalties.

The major advantage of risk monetisation is that the risk value of a certain engineering structure can be added to its own construction cost or value, leading to the concept of overall cost, given by:

$$OC(\$) = CC(\$) + R(\$) \quad (15)$$

where $OC(\$)$ is the overall cost of a certain engineering structure or alternative; $CC(\$)$ is the construction cost or value of the structure or alternative; and $R(\$)$ is the monetised risk value for that particular structure or alternative.

The overall cost is a very powerful concept, because by integrating the risk for each engineering alternative, it allows a better analysis of all engineering alternatives. This

certainly avoids the common mistake in simply selecting the lowest price offer, which probably presents higher risks (quality, maintenance, durability, contractor bankruptcy and so on). On the other hand, a more expensive offer for the structure could indicate better engineering data, design and construction, leading to lower risks. And an easy solution to solve this dispute is to analyse the overall cost (Eq. 15) and take it as a decision-making tool, as done in the bidding for the contractors of a subway line in Copenhagen, Denmark, as shown in Fig. 11.

4. Risk management applied to geotechnical structures

As risks can be qualified or quantified, the following task is to implement a risk management system. Figure 12 presents a scheme of sequence tasks for risk management (ABNT, 2018) that goes from the identification of the risk event (uncertain event that may cause risk), to risk calculation and evaluation, to the measures for risk elimination or mitigation, if necessary. This is a cyclic scheme, indicating that risks have to be re-evaluated from time to time, and when any changes in circumstances occur.

The first task of the risk management scheme (Fig. 12) is the Identification of Risk Events. This can be done initially by all involved professionals (owners, designer, contractors, operational teams) or with the help of a board of expert and experienced engineers, using provocative methodologies, such as SWOT (Strengths, Weaknesses, Opportunities and Treats), Delphi or Brainstorming. Examples of risk events are slope instability, piping, overtopping and liquefaction for an earth or tailings dam. Each type of geotechnical structure presents characteristic risk events. When risk events have been identified and listed, it is recommended that they are organised in order from the highest to the lowest potential risks. Then, each risk event identified has to be qualified in terms of causes, likelihood of occurrence, potential impacts and possible solutions, and then it has to be recorded in the Risk Register. The most important annotation for each risk in the Risk Register is the nomination of its technical responsible and its owner. The Risk Responsible is usually a technical and competent pro-

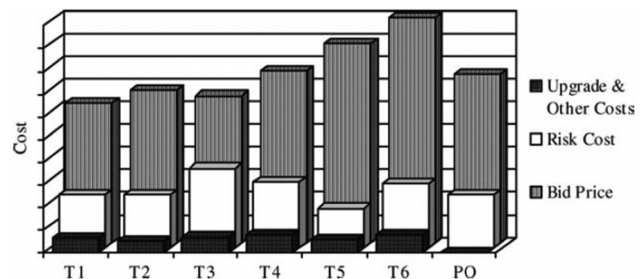


Figure 11. Concept of overall cost for deciding the bidding of a subway line (Eskesen *et al.*, 2004).

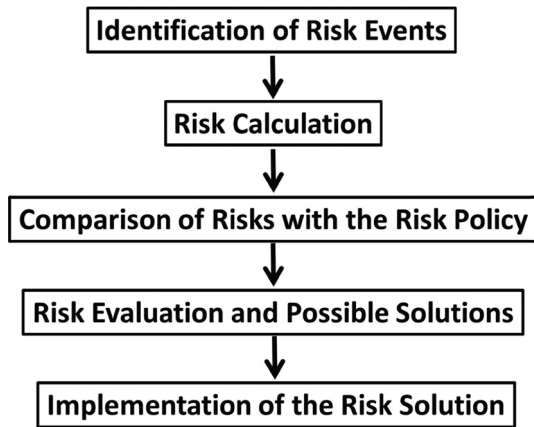


Figure 12. Risk management scheme.

professional in charge of taking care and following the risk for all its existence, contracting and implementing risk solutions, and monitoring them. The Risk Responsible has to do or follow the risk calculation and evaluation as described in Fig. 12 and report the risk status to the Risk Owner. The Risk Owner is a professional who has the power in the company hierarchy to authorise budget for implementing the necessary risk solutions as demanded by the Risk Responsible. The Risk Owner is the ultimate professional in charge of the risk management. Despite these nominations being essential for an efficient risk management in any company, unfortunately, in many cases, the whole process failed because some people may not feel comfortable with this transparency required for the risk management process. The most common mistake is the attempt of higher hierarchy officials to impose the risk ownership to technical professionals that do not have power to decide on budget issues.

The next step of the risk management process is the Risk Calculation, which has already been discussed in this paper, in terms of, both, the quantification of the failure probability by event and fault tree analyses or probabilistic methods, and the monetisation of all different types of consequences. Once the risk components are calculated, they are usually plotted in the Risk Diagram, also called Farmer's diagram, which is a bi-log graphic, with the value of the consequences in the x -axis and the failure probability in the y -axis (Fig. 13). As engineering risk is defined by Eq. 13 or 14, in a bi-log graphic, the product between failure probability and consequences becomes a sum of the logs of these variables; then, any diagonal line represents a certain risk value. For instance, taken the same diagonal with a certain risk value, this risk value can be achieved by a higher failure probability and lower consequence value, or vice versa. One can also note that risk mitigations, moving from a higher risk value (upper diagonal) to a lower one, can be done using active engineering solutions, which decrease the failure probability of the structure (vertical arrow), or by passive solutions, which decrease the consequence value (horizontal arrow).

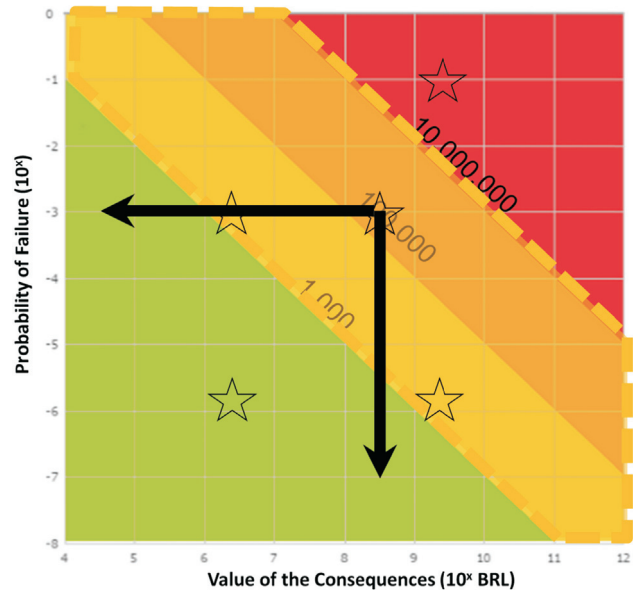


Figure 13. Risk (Farmer's) diagram used to plot risk values.

For instance, considering a slope stability problem with high risk, the solution could be any stabilisation measure (active solution), such as drainage or anchors, that increases the safety factor and, consequently, reduces the failure probability of that slope, or the installation of barriers that does not affect the safety of the slope, but minimises the consequences in case the slope fails.

When plotting risk values in the Risk Diagram, one immediate question is raised, which is the level of acceptable risks. This is defined by the Risk Policy that establishes the acceptance zone (usually painted in green colour), the intolerable zone (red colour) and the attention zone (yellow colour), also referred as ALARP, which stands for *as low as reasonably practical*. Originally this denomination was established in the United Kingdom for risks whose engineering complexity, time and cost for reducing them were not worth or unreasonably high. All efforts should be done to reduce these risks to a level as low as possible, considering reasonable engineering solutions, time and costs. If they still remain at a level considered high, but no more engineering solutions are reasonably practical, these risks have to be closely monitored and potentially affected consequences, especially people, trained to follow safe protocols if warned previously to any major problem. In practice, the zone between the acceptance diagonal line (upper limit of the accepted or insignificant risks) and the tolerance diagonal line (lower limit of the intolerable risks) is preferably named as attention zone, despite the concepts of ALARP being still valid.

There is no consensus for the limits of these zones, but considerable advances have been achieved in the last decades and years, mainly led by the Anglo-Saxon countries (UK, Australia, USA, The Netherlands and so on). The first application of the Farmer's diagram showing limits of

tolerable risks for geotechnical structures was presented by Whitman (1984). Since then, acceptance and tolerance curves have been proposed, and more recently they became stricter, more severe, indicating lower risk acceptance by the society. Presently, most risk criteria limit the acceptance zone of one potential life loss (consequence) to a probability of 10^{-4} to 10^{-5} (FEMA, 2015; Morgenstern, 2018), as shown in Fig. 13, assuming a life loss compensation of R\$ 10 million (Brazilian Real - BRL). Some Risk Diagrams show explicitly an additional x -axis with the number of potential life losses, due to its importance and concern to society, so that one can see the total consequence value, but, separately, also the number of potential life losses. The tolerance curve is usually assumed one or two orders of magnitude above the acceptance diagonal line, depending on the Risk Policy of the company, guidelines or standards (of professional societies) or legislation. In Brazil, there are no guidelines, standards or legislation prescribing acceptance and tolerance limits, which recalls the necessary and important role to be taken by professional societies and regulatory agencies. More recently, two complementary concepts have been applied to the definition of acceptance and intolerance zones, which is a truncation of the maximum failure probability accepted for each type of engineering structures and a truncation of the maximum consequence value accepted by the company owning the engineering structures. The first truncation is a horizontal line in the Risk Diagram that limits the maximum failure probability. In practice, the diagonal line that defines the acceptable risk limit cannot continue its trend and failure probabilities higher than that value indicated by the truncation line for maximum probability are not acceptable. The second truncation is a vertical line in the Risk Diagram that limits the maximum consequence value accepted by the company, otherwise, in case that failure occurs, the company could not deal with that loss amount, indicating higher chances of bankruptcy. This truncation for consequence value is usually calculated based on the company annual profit or as a percentage of its total value. Oboni & Oboni (2020) present a very complete discussion on all types of acceptance and tolerance risk criteria. Figure 14 shows an example of risk zones with complementary truncation lines.

In addition to the acceptance and tolerance limits, the Risk Policy, which is defined by the highest hierarchy of the company, has to establish how the risk information is communicated among the company hierarchy, according to risk levels, and to all stakeholders and authorities. It has to be revised periodically, taking into consideration the past experience of risk management and new demands from the society.

Having the risk policy defined and the structural risks calculated, the Risk Responsible and Owner have all elements for risk evaluation and making decisions of the most suitable treatment solutions for the risks. However, in com-

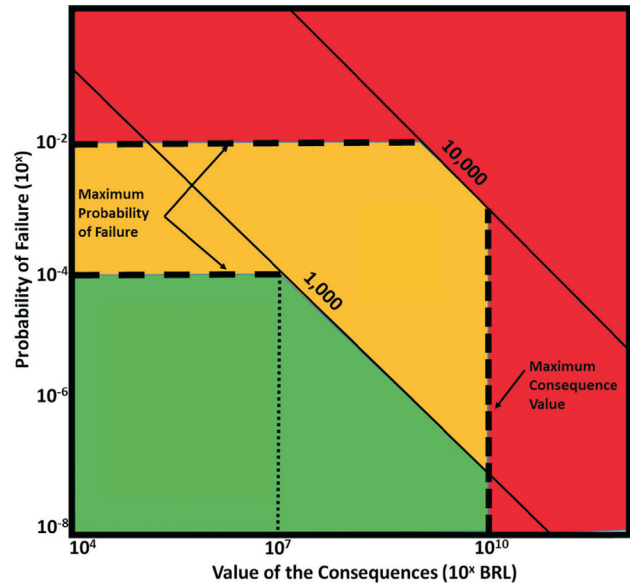


Figure 14. Risk Diagram showing an example of acceptance and intolerance zones using complementary truncations for maximum failure probability and consequence value.

plex structures or large enterprises with several structures, which demand a large number of people involved in the risk management, there are chances of lack or miscommunications among professionals, stakeholders and the society that may jeopardise the whole process. In this case, it is highly recommended an intelligent risk management process, as depicted in Fig. 15.

An intelligent risk management system is guided by the Risk Policy defined by the highest hierarchy of the company, or by guidelines or standards prescribed by professional associations or legislation. The Risk Management Office is in charge of executing the Risk Policy inside the company, providing personnel training and methodologies for all processes related to risk management. It should supervise all risk management processes done by company

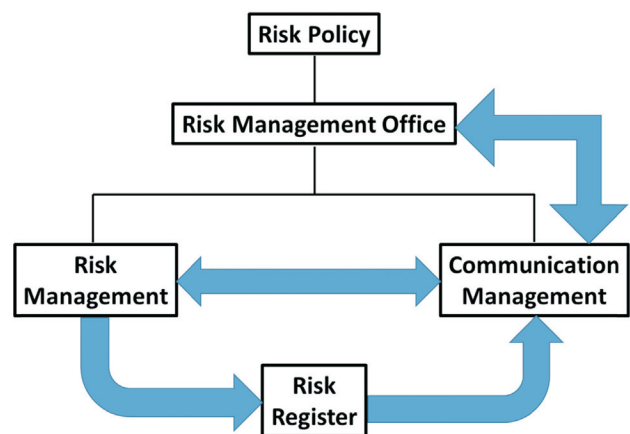


Figure 15 Example of the structure of an intelligent risk management system (Assis *et al.*, 2019).

staff or contracted from outside companies (in this case, it has to specify the terms of reference for these works done by consultant companies). It is important that the Risk Management Office be directly linked to the highest hierarchy of the company, in order to be independent of any intermediate control or inappropriate censorship. The Risk Management involves all steps of risk identification, calculation and evaluation, as already described in this paper and illustrated in Fig. 12. Each risk identified and calculated has to be annotated in the Risk Register, including the nomination of the Risk Responsible and Risk Owner. Any change in the risk is written in the Risk Register, which works as an actual register of the risks for all their existence. When the risk is in the Risk Register, the Communication Management reads it and disseminates its information to all professionals involved and company hierarchy officials, according to its level and zone in the Risk Diagram (Figs. 13 and 14). This communication is done automatically by an IT software, which is programmed according to the definitions of the Risk Policy. It is important to note the need for an automatic communication to avoid any personnel interference, provoking lack or miscommunications. In some cases, risk communication should go outside the company, reaching stakeholders and the society (for instance, civil defence and state authorities). More details on an intelligent risk management system can be found in Assis *et al.* (2019).

5. Examples of risk management applied to geotechnical structures

The first example presented in this paper is a tailings dam, where the Event Risk Identification stage recognises four potential failure modes: i) slope instability; ii) piping; iii) overtopping; and iv) liquefaction. All of them, if they happen, could lead to severe damage to the structure and, consequently, to downstream population, facilities and environment. For each possible failure mode, a performance indicator and a failure criterion have to be selected. For instance, the factor of safety (FS) is taken as performance indicator for the slope stability and liquefaction and its critical value indicating failure (failure criterion) is set to FS smaller than 1. For overtopping, the water level on the dam reservoir could be chosen as performance indicator and its critical value could be set as the topographic level of the dam crest (in this case, it is assumed that if overtopping

occurs, the downstream slope is eroded, leading to the whole structure failure). All these three failure modes have engineering formulations to evaluate their performance indicators, so that probabilistic methods are applied to calculate their failure probabilities. For piping, the performance indicator is not so evident and there is no clear engineering formulation to evaluate the whole process, considering the hydraulic gradient, characteristics of the soil to be eroded and to progressively evolve to piping formation, until leading to dam failure. Therefore, event and fault tree analyses are used to estimate the failure probability due to piping, as exemplified by Figure 4 and described in detail by Fell *et al.* (2015) and Caldeira (2018). The failure probabilities for these four possible failure modes are presented in Table 5.

It is worth a word on the FS statistics and its failure probability obtainment. The engineering formulation chosen to evaluate the FS was the Spencer Method and the probabilistic method was the Monte Carlo (MCM was preferred to be potentially exact and with a computational effort for this type of analyses considered acceptable; it takes about 2 days in a standard configuration computer for running the full analysis). For each set of input parameters, taken for consolidated and drained conditions, a critical failure mechanism was searched and its FS calculated. Many commercial software set as default a fixed failure mechanism obtained by the mean values of input parameters and, then, do all dispersion analyses using this failure mechanism, only varying the values of input parameters. This is not appropriate since, in geotechnical engineering, many failure mechanisms are dependent on geotechnical parameters, and may be changing their shape and position inside the ground mass. Therefore, careful setting of the software is mandatory in order to make sure that the MCM is fully exploring all possibilities of parameter variabilities and failure mechanism options. Nowadays, there is a trend, with promising advances, for searching for alternative methods to the MCM, which are faster, require much less computational effort, and provide similar reliability of the results.

Other important aspect to mention is related to the evaluation of the FS and its failure probability due to liquefaction. The condition for liquefaction to occur assumes that actions happened, called liquefaction triggers, which can be static or dynamic, that changed soil conditions from drained to undrained behaviour. Then, the stability analy-

Table 5. Example of risk analysis applied to a tailings dam.

Failure mode	Failure probability (p_f)	Consequences (BRL(\$) $\times 10^6$)	Risk (BRL(\$) $\times 10^6$)
Slope instability	10^{-5}	3,000-4,000	0.03-0.04
Piping	5×10^{-4}	3,000-4,000	1.5-2
Liquefaction	10^{-3}	4,000	4
Overtopping	10^{-4}	3,000-4,000	0.3-0.4

ses are executed using undrained strength parameters for submerged materials that are potentially susceptible to liquefaction. As described, the liquefaction instability may only occur if a series of independent events happens successively: first the trigger event has to happen, followed by the undrained failure of the structure at its peak-undrained strength values, and, finally, the structure failure overcoming its liquefied undrained strength. So, the failure probability due to liquefaction is given by a product of three failure probabilities (the occurrence probability of the trigger event, the failure probability using peak and undrained-strength parameters and the failure probability using the liquefied strength; $p_{f_liquefaction} = p_{trigger} \times p_{f_peak_undrained} \times p_{f_liquefied}$). The evaluation of failure probabilities using peak undrained and liquefied strengths is similar to the procedure used for any slope stability analysis. The main unknown in this calculation is the definition of the trigger event and estimation of its occurrence probability. For dynamic events, the most common trigger is related to earthquakes and, in this case, it is possible to study or measure their magnitudes and frequencies, determining a certain magnitude for a specific time frequency, which is taken as its occurrence probability. For static trigger events, this evaluation is much more complicated or unknown. Commonly, its occurrence probability is estimated based on the frequency of accidents already registered for the same type of geotechnical structure.

For evaluating the consequences due to a dam failure, dam break analyses, which are hydraulic studies, have to be carried out, implying in the following considerations:

- The amount of reservoir mass that will outflow due to the dam breach has to be assumed or estimated; in case of water reservoir, 100 % of the total mass is usually taken, but in case of tailings reservoir, more complex assumptions or studies are necessary, and common values range from 33 to 100 %.
- The hydraulic breach formation in the dam, due to slope instability, piping, liquefaction or overtopping, requires assumptions of its geometry (shape, width and depth) and evolution time; this is important to evaluate how much and how fast the reservoir mass flows.
- As the reservoir mass flows downstream, its propagation is extremely influenced by fluid parameters, which could be water or slurry (mix of water and solids), topography, which requires a precise digital model of the terrain, and roughness characteristics of the terrain surface, which is related to the type of vegetation or soil use, such as green field, pasture for cattle raising, paved surfaces, water bodies, building structures and so on.
- The results of dam break analysis provide information on the likely flooded area, including, for each geographical position, the flood depth and velocity, and the flood arrival time; the product of flood depth and velocity gives an estimation of the energy of the flow mass, called hydrodynamic risk or flood hazard factor, which is related

to potential damage (Fig. 16), and the flood arrival time is extremely helpful for preparing emergency plans, including establishing evacuation routes and training people.

- These results are overlapped with all information related to population, housing, educational, commercial, industrial and agribusiness facilities, environmental protected areas and parks, and so on, using databases available in governmental agencies (for instance, the database of the Brazilian Institute for Geography and Statistics – IBGE, or similar ones).
- To verify potential damage, the hydrodynamic risk (flood hazard) factor for each geographical position is checked against the occupation and use of that area; for each type of occupation and use, there are threshold limits or vulnerability curves of hydrodynamic risk (flood hazard) factors that indicate partial or total loss, or failure, applied to people, vehicles, different types of buildings, and so on (Fig. 16). Flood hazard criteria and vulnerability curves are discussed in detail by AIDR (2012) and Oboni & Oboni (2020).
- The final result is the inventory of all potential losses and damages, which are monetised using the social and economic values registered in the governmental databases; an important point to discuss is the possibility to have or not any warning prior to structure failure, which may affect enormously the number of life losses; this depends on the type of failure mode and on the efficiency of the emergency plans, including training, drills and full transparency of the risk information.

The consequence values of this dam failure example are shown in Table 5. All failure modes, except liquefaction, present two values, the first one, considering a warning at least 4 h before the dam failure, and the second one, assuming warning at the failure moment. For the liquefaction failure mode, as it happens suddenly, the only option is the warning at the failure moment. As one can conclude from Table 5, the highest risk in this example is due to liquefaction and this highest risk value should be the one plotted in the Risk Diagram for that particular structure.

The second example is derived from the feasibility studies of an urban tunnel for a metro system presented by Alarcón-Guerrero (2016). Other researchers have studied risk analysis and management applied to tunnelling as Einstein (1996), Sturk *et al.* (1996), Shahriar *et al.* (2008), Meng *et al.* (2010), Sousa (2010), Mollon *et al.* (2013), Jarek (2016) and Napa-Garcia *et al.* (2017). The performance indicator chosen by Alarcón-Guerrero (2016) was the distortion angle, defined by the difference of settlements estimated for two locations divided by their distance. The failure criteria prescribed, in general, a limit value of 1:300 for partial structural damages and a critical value of 1:100 to total structural damages. However, these limit values could change depending on the type and age of the structures, since the metro line runs through different nei-

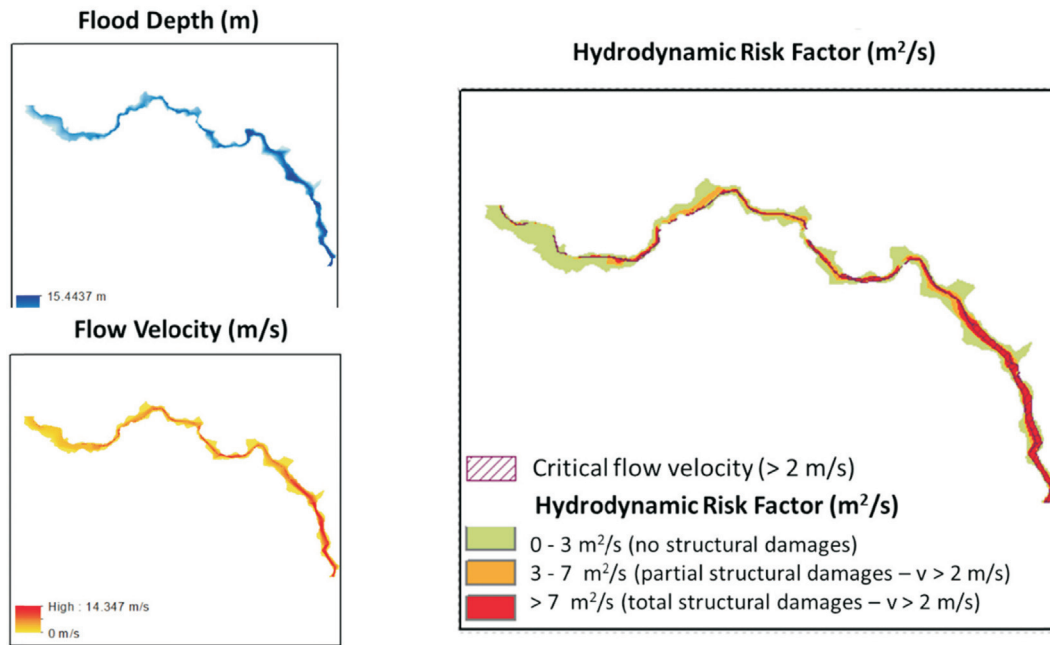


Figure 16. Results from dam break analyses in terms of flood height and flow velocity, resulting in hydrodynamic risk factors and damage criteria.

ghbourhoods, ranging from historical and old buildings to very modern skyscrapers. The engineering formulation was the tunnelling-induced settlement calculation by 3D numerical simulations, using the Finite Element Method. Input variables include deformability and strength parameters for all geologic lithotypes, water table, tunnel geometry and position inside the ground, and tunnelling and support system parameters related to conventional and mechanised methods. As the 3D numerical simulations impose enormous computational efforts, the use of the MCM was not feasible, leading to the adoption of approximate probabilistic methods. Also, the number of input parameters was initially tremendous, which could cause computational problems even to some approximate methods. So, as a first step, the FOSM was applied to identify the most relevant input variables to the performance indicator (settlement and consequently the distortion angle) variance. Then, with the number of input variables limited according to the FOSM findings, the PEM was carried out to calculate the statistics of the performance indicator. Finally, the failure probability was estimated assuming a Gaussian distribution for the dependent variable.

The estimation of the consequence values considered the tunnelling-induced damages to all structures and according to their failure criteria (historical and cultural buildings, conventional housing, low-height buildings and modern skyscrapers), consequences were estimated and monetised. Vulnerability probabilities (ability to suffer damage) were applied to people according to their age and position inside buildings, and to the type of structure and foundation. The final result is a risk-zone map indicating

risk acceptance and intolerance for the chosen tunnelling method, as shown in Fig. 17. Indeed, risk management is a powerful tool for decision making.

6. Closing remarks

This paper intends to bring the theory of risk management to practical applications in geotechnical engineering, consolidating concepts, clarifying procedures and discussing openly its difficulties and trends. Most comments, recommendations and conclusions have been already written along the text, so that only the most relevant ones are listed here.

Probabilistic approach and risk analyses and management bring additional and helpful information, challenging the conventional decision making in engineering, breaking paradigms, but requiring training, culture and setting new acceptance and tolerance criteria.

Risk management in complex structures and in enterprises with different types of structures requires risk quantification and monetisation. In doing so, the concepts of monetised risk and overall costs become a powerful decision tool for evaluating different alternatives of engineering solutions or structures.

Preliminary qualitative risk analyses can play an important role in qualifying risk events and organising them in a priority list, recommending those to be submitted to a more detailed risk evaluation, using quantification and monetisation methodologies.

Monetised risks are efficient tools for decision making, because a common language is used and understood by

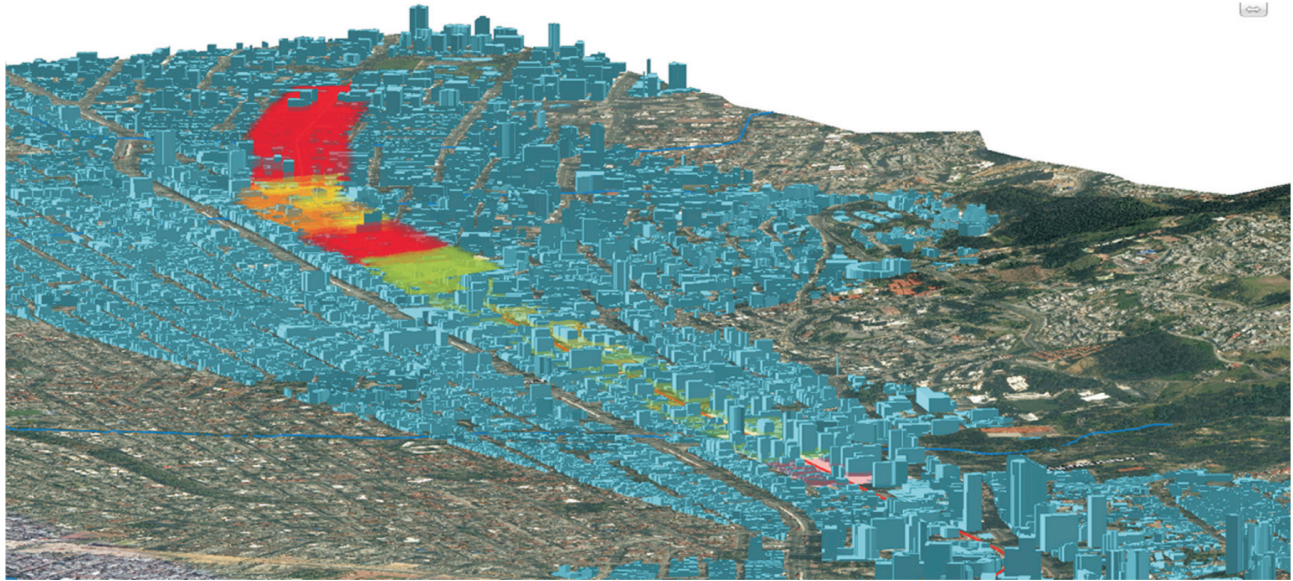


Figure 17. Risk acceptance and intolerance zones for an urban tunnel of a metro system (Alarcón-Guerrero, 2014).

all stakeholders, and may be used as metrics for contingencies, insurances and security deposits.

Monetised risks allow to aggregate all corporate risks (Assis *et al.*, 2019), despite their types and structure differences, leading to a unique risk value for the whole company.

Risks, that are evaluated for a period of time (for instance, annually) and may be recurrent along time, have to be estimated for the life span of that engineering structure, which yields the chance to have a failure during the entire structure lifetime.

Risk management is not a protection shield against all accidents, it does not avoid all failures, but it is an efficient tool that helps control and diminish them, and minimise consequences, if they occur.

Risk management is a tool towards a better engineering and, when done correctly and communicated transparently to all professional and stakeholders, it is essential to discuss new projects, their benefits and risks, leading engineering to regain its paramount role for the needs of modern societies.

Acknowledgments

Firstly, the author would like to express his gratitude to the Brazilian Society for Soil Mechanics and Geotechnical Engineering (ABMS) for the honourable distinction to present this Pacheco Silva Conference. To all my students, whose enthusiasm and dedication in their research, contribute significantly to this theme. To the São Paulo Metro Company and Vale for the support and confidence given for the development and implementation of a risk management system applied to their geotechnical structures. And finally, to Fernando Olavo Franciss, pioneer of risk management in geotechnical structures in Brazil, with

whom we learned, discussed and developed much of what is consolidated in this paper; to Franciss, my deepest gratitude and dedication of this conference and paper.

References

- ABNT (2018). Risk Management – Guidelines: NBR ISO 31000. Brazilian Association for Technical Standards (ABNT), São Paulo, Brazil, 17 p. (in Portuguese).
- AIDR (2012). Technical Flood Risk Management Guideline 7-3: Flood Hazard. Australian Institute for Disaster Resilience, Melbourne, Australia, 27 p.
- Alarcón-Guerrero, J.E. (2014). Geomechanical Risk Management due to Urban Tunnelling: Application to the Bogota Metro. Ph.D. Thesis, University of Brasília, Brasília, 342 p. (in Portuguese).
- Ang, A.H-S. & Tang, W.H. (1975). Probability Concepts in Engineering Planning and Design: Basic Principles. John Wiley & Sons, New York, v. 1, 409 p.
- Ang, A.H-S. & Tang, W.H. (1984). Probability Concepts in Engineering Planning and Design: Decision, Risk and Reliability. John Wiley & Sons, New York, v. 2, 561 p.
- Aoki, N. & Cintra, J.C.A. (1996). Influence of the soil mass variabilities on the pile lengths (in Portuguese). Proc. 3rd Seminar of Special Foundation Engineering, ABEF/ABMS, São Paulo, v. 1, pp. 173-184.
- Aoki, N. (2011). Failure probability and safety factors in foundations. Milton Vargas Lecture (PPT presentation). Brazilian Society for Soil Mechanics and Geotechnical Engineering (ABMS), São Paulo (in Portuguese).
- Aoki, N. (2016). Paradigms of the Safety Factors. Pacheco Silva Conference (PPT presentation), Brazilian Society for Soil Mechanics and Geotechnical Engineering (ABMS), São Paulo (in Portuguese).

- Assis, A.P.; Esposito, T.J.; Gardoni, M.G. & Maia, J.A.C. (2018). *Statistic and Probabilistic Methods Applied to Geotechnics*. Course Notes, Graduate Programme on Geotechnical Engineering, University of Brasilia, Brasilia, 291 p. (in Portuguese).
- Assis, A.P.; Franciss, F.O. & Rabechini Jr., R. (2019). *Risk Management: Complex Structures*. CRV, Curitiba, 342 p. (in Portuguese).
- Baecher, G.B. & Christian, J.T. (2003). *Reliability and Statistics in Geotechnical Engineering*. John Wiley & Sons, West Sussex, 605 p.
- Caldeira, L. (2018). Internal erosion in dams. XXXV Manuel Rocha Lecture, *Soils & Rocks*, 41(3):237-263. <https://doi.org/10.28927/SR.413237>
- Charbel, P.A. (2015). *Risk Management Applied to Mine Ore Dilution*. Ph.D. Thesis, University of Brasilia, Brasilia, 403 p. (in Portuguese).
- Christian, J.T. (1999). Factors affecting the calculated reliability of slopes. Proc. XI Pan-American Conference on Soil Mechanics and Geotechnical Engineering, ISSMGE / ABMS / SAMS / SPG, Iguassu Falls, v. 3, pp. 1225-1231.
- Christian, J.T. (2004). Geotechnical engineering reability: How well do we know what we are doing?. *Journal of Geotechnical and Geoenvironmental Engineering*, 130(10):985-1003. [https://doi.org/10.1061/\(ASCE\)1090-0241\(2004\)130:10\(985\)](https://doi.org/10.1061/(ASCE)1090-0241(2004)130:10(985))
- Christian, J.T. & Baecher, G.B. (1999). Point-estimate method as numerical quadrature. *Journal of Geotechnical and Geoenvironmental Engineering*, 125(9):779-786. [https://doi.org/10.1061/\(ASCE\)GT.1943-5606.0000509](https://doi.org/10.1061/(ASCE)GT.1943-5606.0000509)
- Christian, J.T.; Ladd, C.C. & Baecher, G.B. (1992). Reliability and probability in stability analysis. *Stability and Performance of Slopes and Embankments II*, Geotechnical Special Publication No. 31, ASCE, New York, 2: 1071-1111.
- Christian, J.T.; Ladd, C.C. & Baecher, G.B. (1994). Reliability applied to slope stability analysis. *Journal of Geotechnical Engineering*, 120(12):2180-2207. [https://doi.org/10.1061/\(ASCE\)0733-9410\(1994\)120:12\(2180\)](https://doi.org/10.1061/(ASCE)0733-9410(1994)120:12(2180))
- Coutinho, R.Q. (2010). *Risk management applied to landslides for planning the soil use*. Milton Vargas Lecture (PPT presentation), Brazilian Society for Soil Mechanics and Geotechnical Engineering (ABMS), São Paulo (in Portuguese).
- Duncan, M. (2000). Factors of safety and reliability in geotechnical engineering. *Journal of Geotechnical and Geoenvironmental Engineering*, 126(4):307-316. [https://doi.org/10.1061/\(ASCE\)GT.1943-5606.0000509](https://doi.org/10.1061/(ASCE)GT.1943-5606.0000509)
- Einstein, H.H. (1996). Risk and risk analysis in rock engineering. *Tunnelling and Underground Space Technology*, 11(2):141-155. [https://doi.org/10.1016/0886-7798\(6\)00014-4](https://doi.org/10.1016/0886-7798(6)00014-4)
- Eskesen, S.D.; Tengborg, P.; Kampmann, J. & Veicherts, T.H. (2004). Guidelines for tunnelling risk management: Working Group 2 of the international tunnelling and underground space association (ITA). *Tunnelling and Underground Space Technology*, 19(3):217-237. <https://doi.org/10.1016/j.tust.2004.01.001>
- Espósito, T.J. (1995). *Geotechnical Control of the Construction of Tailings Dams – Slope Stability Analyses and Seepage Studies*. M.Sc. Dissertation, University of Brasilia, Brasilia, 159 p. (in Portuguese).
- Espósito, T.J. (2000). *Probabilistic and Observational Methodology Applied to Tailings Dams Built by Hydraulic Fill*. Ph.D. Thesis, University of Brasilia, Brasilia, 363 p. (in Portuguese).
- Farias, M.M. & Assis, A.P. (1998). Comparison among probabilistic methods applied to slope stability. Proc. XI COBRAMSEG, Brazilian Society for Soil Mechanics and Geotechnical Engineering (ABMS), Brasilia, v. 2, pp. 1305-1314 (in Portuguese).
- Fell, R.; MacGregor, P.; Stapledon, D.; Bell, G. & Foster, M. (2015). *Geotechnical Engineering of Dams*. CRC Press, Boca Raton, 1338 p.
- FEMA (2015). *Federal Guidelines for Dam Safety Risk Management*. FEMA, Washington, 39 p.
- Fenton, G.A., Griffiths, D.V. (2008). *Risk Assessment in Geotechnical Engineering*. John Wiley & Sons, New York, 480 p.
- Franco, V.H. (2019). *Mathematical and Probabilistic Modelling Approach for Estimation of Surface Settlements due to TBM Tunnelling*. Ph.D. Thesis, University of Brasilia, Brasilia, 153 p.
- Franco, V.H.; Gitirana Jr, G.F.N. & Assis, A.P. (2019). Probabilistic assessment of tunneling-induced building damage. *Computers and Geotechnics*, 113(9):1-15. <https://doi.org/10.1016/j.compgeo.2019.103097>
- Gitirana Jr., G.F.N. (2005). *Weather-Related Geo-Hazard Assessment Model for Railway Embankment Stability*. Ph.D. Thesis, University of Saskatchewan, Saskatoon, 403 p.
- Griffiths, D. & Fenton, G. (2007). *Probabilistic Methods in Geotechnical Engineering*. International Centre for Mechanical Science (CISM), Springer, Vienna, 340 p.
- Hachich, W.C. (1981). *Seepage-Related Reliability of Embankment Dams*. Ph.D. Thesis, Massachusetts Institute of Technology, Cambridge, 173 p.
- Hachich, W. & Vanmarcke, E. (1983). Probabilistic updating of pore pressure fields. *Journal of Geotechnical Engineering*, ASCE, 109(3):373-385.
- Hachich, W. (2018). *Safety, reliability and risks in geotechnical structures*. Milton Vargas Lecture (PPT presentation). Brazilian Society for Soil Mechanics and Geotechnical Engineering (ABMS), São Paulo.

- Hammah, R.; Yacoub, T. & Curran, J. (2010). The influence of correlation and distribution truncation on slope stability analysis results. *RocScience* (www.rocsience.com), 6 p.
- Harr, M.E. (1987). *Reliability-Based Design in Civil Engineering*. McGraw-Hill, New York, 291 p.
- Hidalgo, C.A.M. (2013). *Uncertainties, Vulnerabilities and Risk Evaluation due to Slope Instabilities in Roads*. Ph.D. Thesis, University of Brasilia, Brasilia, 250 p. (in Portuguese).
- Jarek, A. (2016). *Application of the Boundary Element Method in the Analysis of Tunnel Stability in Discontinuous Media: A Probabilistic Approach*. Ph.D. Thesis, Federal University of Paraná, Curitiba, 151 p. (in Portuguese).
- Kulhawy, F.H. (1992). On the evaluation of static soil properties. *Stability and Performance of Slopes and Embankments II*, Geotechnical Special Publication No. 31, ASCE, v. 1, pp. 95-115.
- Lacasse, S. & Nadim, F. (1977). *Uncertainties in characterizing soil properties*. Publ. No. 201, Norwegian Geotechnical Institute, Oslo, Norway, 49-75.
- Lauro, C.A. (2001). *Probabilistic Modelling of the 3D Discontinuity Distribution in Fractured Rockmass*. Ph.D. Thesis, University of Brasilia, Brasilia, 253 p. (in Portuguese).
- Lumb, P. (1966). The variability of natural soils. *Canadian Geotechnical Journal*, 3(2):74-97. <https://doi.org/10.1139/t66-009>
- Maia, J.A.C. (2003). *Probabilistic Methods Applied to the Stability of Rock Slopes and Openings*. M.Sc. Dissertation, University of Brasilia, Brasilia, 192 p. (in Portuguese).
- Maia, J.A.C. (2007). *Probabilistic Modelling of the Plastic Zone of Underground Structures in Rock*. Ph.D. Thesis, University of Brasilia, Brasilia, 161 p. (in Portuguese).
- Mendes, L.O. (2019). *Probabilistic Analysis of the Potential Failure of Static and Dynamic Liquefaction in Dams*. M.Sc. Dissertation, University of Brasilia, Brasilia, 147 p. (in Portuguese).
- Mendes, L.T.G. (2017). *Probabilistic Analysis of Rock Tunnel Behaviour*. M.Sc. Dissertation, University of Brasilia, Brasilia, 142 p. (in Portuguese).
- Meng, Q.; Qu, X.; Wang, X.; Yuanita, V. & Wong, S.C. (2010). Quantitative risk assessment modelling for non-homogeneous urban road tunnels. *Risk Analysis*, 31(3):382-403, <https://doi.org/10.1111/j.1539-6924.2010.01503.x>
- Mitchell, J.K. (2014). Lessons from the lives of two dams. IV Victor de Mello Lecture, ABMS/SPG. *Soils & Rocks*, 37(2):99-109. <https://doi.org/10.28927/SR>
- Mollon, G.; Dias, D. & Soubra, A.H. (2013). Probabilistic analyses of tunnelling-induced ground movements. *Acta Geotechnica*, 8(2):181-199. <https://doi.org/10.1007/s11440>
- Morgenstern, N.R. (2018). Geotechnical risk, regulation and public policy. VI Victor de Mello Lecture, ABMS/SPG. *Soils and Rocks*, 41(2):107-129. <https://doi.org/10.28927/SR.412107>
- Napa-Garcia, G.; Beck, A. & Celestino, T.B. (2017). Reliability analyses of underground openings with Point Estimate Method. *Tunnelling and Underground Space Technology*, 64(1):154-163. <https://doi.org/10.1016/j.tust.2016.12.010>
- Oboni, F. & Oboni, C. (2020). *Tailings Dam Management for the Twenty-First Century: What Mining Companies Need to Know and Do to Thrive in Our Complex World*. Springer, Cham, 278 p.
- Pacheco, M. (1990). Probability and risk analysis concepts applied to geotechnical studies and design. *Proc. IX COBRAMSEF, Brazilian Society for Soil Mechanics and Geotechnical Engineering (ABMS)*, Salvador, pp. 35-56. (in Portuguese).
- Perini, D.S. (2009). *Study of the Processes Applied to Risk Analysis of Earth Dams*. M.Sc. Dissertation, University of Brasilia, Brasilia, 128 p. (in Portuguese).
- Phoon, K.K. & Kulhawy, F.H. (1999a). Characterization of geotechnical variability. *Canadian Geotechnical Journal*, 36(4):612-624. <https://doi.org/10.1139/t99-038>
- Phoon, K.K. & Kulhawy, F.H. (1999b). Evaluation of geotechnical property variability. *Canadian Geotechnical Journal*, 36(4):625-639. <https://doi.org/10.1139/t99-039>
- Rosenblueth, E. (1975). Point estimates for probability moments. *Proceedings of the National Academy of Sciences*, 72(10):3812-3814. <https://doi.org/10.1073/pnas.72.10.3812>
- Rosenblueth, E. (1981). Two-point estimates in probabilities. *Applied Mathematical Modelling*, 5(5):329-335. [https://doi.org/10.1016/S0307-904X\(81\)80054-6](https://doi.org/10.1016/S0307-904X(81)80054-6)
- Sandroni, S.S. & Sayão, A.S. (1993). The use of relative failure probability in the design of open pit mine slopes. *Innovative Mine Design for the 21st Century*, Balkema, Rotterdam, pp. 21-24.
- Shahriar, K.; Sharifzadeh, M. & Hamidi, J.K. (2008). Geotechnical risk assessment-based approach for rock TBM selection in difficult ground conditions. *Tunnelling and Underground Space Technology*, 23(2008):318-325. <https://doi.org/10.1016/j.tust.2007.06.012>
- Sousa, R.L. (2010). *Risk Analysis for Tunnelling Projects*. Ph.D. Thesis, Massachusetts Institute of Technology, Cambridge, 589 p.
- Sturk, R.; Olsson, L. & Johansson, J. (1996). Risk and decision analysis for large underground projects, as applied to the Stockholm ring road tunnels. *Tunnelling and Underground Space Technology*, 11(2):157-164. [https://doi.org/10.1016/0886-7798\(96\)00019-3](https://doi.org/10.1016/0886-7798(96)00019-3)
- USAEC (1957). *Theoretical Possibilities and Consequences of Major Accidents in Large Nuclear Power Plants*.

- The Brookhaven Report (WASH-740), US Atomic Energy Commission, Washington, 105 p.
- USNRC (1975). Reactor Safety Study: An Assessment of Accident Risks in US Commercial Nuclear Power Plants. The Rasmussen Report (WASH-1400), US Nuclear Regulatory Commission, Washington, 142 p.
- Uzielli, M.; Lacasse, S.; Nadim, F. & Phoon, K. (2007). Soil variability analysis for geotechnical practice. 2nd International Workshop on Characterization and Engineering Properties of Natural Soils, Singapore, vol. 3, pp. 1653-1752.
<https://doi.org/10.1201/NOE0415426916.ch3>
- Van Gelder, P.H.A.J.M. (2000). Statistical Methods for the Risk-Based Design of Civil Structures. PrintPartners Ipskamp B.V., Enschede, 249 p.
- Whitman, R.V. (1984). Evaluating calculated risk in geotechnical engineering. *Journal of Geotechnical Engineering*, 110(2):145-189.
[https://doi.org/10.1061/\(ASCE\)0733-9410\(1984\)110:2\(143\)](https://doi.org/10.1061/(ASCE)0733-9410(1984)110:2(143))
- Yokozawa, S.Y. (2019). Evaluation of Probabilistic Methods Applied in the Risk Analysis due to Slope Instability of Dams. M.Sc. Dissertation, University of Brasília, Brasília, 113 p. (in Portuguese).

Appendix

Table A1. Suggested values of Coefficients of Variation (CoV) to some geotechnical properties.

Geotechnical properties	Range of CoV (%) and most likely value	References
Unit weight γ	3-7; < 10 5	Harr (1987); Kulhawy (1992); Uzielli <i>et al.</i> (2007)
Moisture content w	8-30 20	Uzielli <i>et al.</i> (2007)
Atterberg limits w_L, w_p	6-30 20	Phoon & Kulhawy (1999a and 1999b); Uzielli <i>et al.</i> (2007)
Void ratio e and Porosity n	7-30 20	Uzielli <i>et al.</i> (2007)
Cohesion c	20-80 40	Baecher & Christian (2003)
Undrained strength S_u	13-40 Triaxial UU \rightarrow 10-30 Triaxial CU \rightarrow 20-55 Triaxial CIU \rightarrow 20-40 25	Harr (1987); Kulhawy (1992); Lacasse & Nadim (1997); Phoon & Kulhawy (1999); Duncan (2000); Uzielli <i>et al.</i> (2007)
Undrained strength ratio S_u/σ_v'	5-15 10	Harr (1987); Kulhawy (1992); Duncan (2000)
Friction angle ϕ	2-13; 5-15 10	Harr (1987); Kulhawy (1992); Baecher & Christian (2003); Uzielli <i>et al.</i> (2007)
Deformability modulus E_0	10-30 20	Baecher & Christian (2003); Mollon <i>et al.</i> (2012)
Coefficient of consolidation c_v	33-68 50	Duncan (2000); Uzielli <i>et al.</i> (2007)
Index of compression C_c	10-37 25	Harr (1987); Kulhawy (1992); Duncan (2000); Uzielli <i>et al.</i> (2007)
Overconsolidation ratio OCR	10-35 20	Harr (1987); Lacasse & Nadim (1997); Duncan (2000); Baecher & Christian (2003); Uzielli <i>et al.</i> (2007)
Coefficient of earth pressure at rest K_0	40-75 50	Phoon & Kulhawy (1999)
Coefficient of permeability K	68-90; 130-240; 200-300 200	Harr (1987); Benson <i>et al.</i> (1999); Duncan (2000); Baecher & Christian (2003); Uzielli <i>et al.</i> (2007)
SPT blowing count N_{SPT}	15-45; 25-50 30	Harr (1987); Kulhawy (1992); Uzielli <i>et al.</i> (2007)
CPT mechanical q_c	15-37	Harr (1987); Kulhawy (1992); Uzielli <i>et al.</i> (2007)

Geotechnical properties	Range of CoV (%) and most likely value	References
	Clay 20-40 30	
	Sand 20-60 40	
CPT q_t	Clay < 20 10	Harr (1987); Kulhawy (1992); Uzielli <i>et al.</i> (2007)
CPT electrical q_c	5-15 10	Harr (1987); Kulhawy (1992); Uzielli <i>et al.</i> (2007)
DMT (resistência de ponta) q_{DMT}	5-15 10	Kulhawy (1992)
Vane Test VST S_v	10-20 Clay 10-40 25	Kulhawy (1992); Uzielli <i>et al.</i> (2007)
Pressuremeter PMT P_L	Clay 10-35 25	Uzielli <i>et al.</i> (2007)
	Sand 20-50 35	
Pressuremeter PMT E_{PMT}	Sand 15-65 40	Uzielli <i>et al.</i> (2007)

Obs. The Most Likely Values of CoV reported in bold are those more frequently assumed in geotechnical engineering design and reports.

Table A2. Types of probabilistic functions commonly suggested to some geotechnical properties (modified from Uzielli *et al.*, 2017).

Geotechnical property	Soil type	Probabilistic distribution function
Water content	All	Normal/Log-normal
Liquidity limit	All	Normal/Log-normal
Plasticity limit	Sand/Silt	Normal/Log-normal
Void ratio	All	Normal
Porosity	All	Normal
Consolidation coefficient c_v	All	Normal/Log-normal
CPT strength	Sand	Log-normal
Undrained strength	Clay	Normal/Log-normal
Ratio between undrained strength and effective principal stress	Clay	Normal/Log-normal
Cohesion	Clay	Normal/Log-normal
Unit weight	All	Normal
Friction angle	Sand	Normal

Articles

Soils and Rocks
v. 43, n. 3

Spread footings bearing on circular and square cement-stabilized sand layers above weakly bonded residual soil

Nilo Cesar Consoli^{1, #} , Eclesielter Batista Moreira¹ , Lucas Festugato¹ ,
Gustavo Dias Miguel¹ 

Article

Keywords

Artificially cemented layer
Ground improvement
Lightly bonded residual soil
Spread footings

Abstract

The practice of soil-cement reinforced layers to bear shallow foundations is a feasible option in low bearing capacity soils. This paper addresses the interpretation of plate load tests bearing on compacted artificially cemented sand layers of distinct sizes and shapes (cylindrical and prismatic) overlaying a weakly bonded residual soil stratum. Static load tests were carried out on a rigid circular steel plate (diameter of 300-mm) resting on sand-cement reinforced layers with distinct areas (diameters/widths of 450, 600, and 900-mm) and constant thickness of 300-mm. The results have shown two distinct failure modes that rely on the cemented layer's diameter/width: (a) the steel plate and the artificially cemented layer punch together into the weakly bonded residual soil, without the failure of the cemented layer, and (b) the artificially cemented layer fails. The combination of two traditional methods for predicting bearing capacity in soils was successfully applied considering the shape (and geometry) of the improved layer and the existence (or not) of interaction of the lateral of the cemented layers and the residual soil. Finally, this study highlights the importance of considering the shapes and sizes of soil-cement layers in the bearing capacity estimation (combining analytical solutions) of spread footings resting on treated layers above weakly bonded residual soils.

1. Introduction

In Southern Brazil, urban and industrial developments often take place in terrain where the underlying soils are highly drainable weakly bonded residual soils with high void ratios. These residual soils are usually partly saturated (degree of saturation of about 80 %) and even when saturated, any generated pore pressure is rapidly dissipated. Hence, immediate settlements are more relevant than consolidation settlements in these soils. Such type of material can suffer a high reduction in volume when the bonds are broken. The solution adopted to support significant building loads is usually a deep foundation. However, for some projects, a deep foundation may not be economically feasible. An example is the construction of low-rise, low-cost housing or commercial buildings, where piling costs can represent an unacceptably large proportion of the total investment. The present research studied an alternative to deep foundations: shallow spread footings are placed on an

upper layer that has been mechanically improved by incorporation of an engineered cementing material. The approach produces a double-layer foundation system, in which the upper layer has been artificially cemented through mixing, compaction, and curing.

There have been many studies of shallow foundations on layered systems, most of them concentrating on cases in which a sand layer overlies a soft clay stratum (*e.g.*, Meyerhof, 1974; Burd & Frydman, 1997; Kenny & Andrawes, 1997). Only a few (*e.g.*, Vesic, 1975) dealt with cohesive-frictional soils. The accuracy of the Vesic (1975) solution in predicting the ultimate bearing capacity of a footing resting on an artificially cemented upper layer, overlying a weakly bonded residual soil with a high void ratio, is unknown. The stress-strain-strength behavior of artificially cemented soils has been studied in the past by several investigators (*e.g.*, Clough *et al.*, 1981; Coop & Atkinson, 1993; Huang & Airey, 1998; Consoli *et al.*, 2000, 2006,

[#]Corresponding author. E-mail address: consoli@ufrgs.br.

¹Programa de Pós-Graduação em Engenharia Civil, Universidade Federal do Rio Grande do Sul, Porto Alegre, RS, Brazil.

Submitted on May 28, 2020; Final Acceptance on July 6, 2020; Discussion open until December 31, 2020.

DOI: <https://doi.org/10.28927/SR.433339>



This is an Open Access article distributed under the terms of the Creative Commons Attribution License, which permits unrestricted use, distribution, and reproduction in any medium, provided the original work is properly cited.

2008, 2009, 2010, 2011, 2012, 2013, 2014, 2015, 2016, 2017, 2018, 2019, 2020a, b, c; Dalla Rosa *et al.*, 2008).

Foppa *et al.* (2020) and Caballero (2019) observed, in small scale load tests of footings resting on a soil-cement reinforced layer over a loose sand, two distinct types of failure: in the first, the reinforcement layer is punched through the soil, without showing any fissuring, up to a settlement corresponding to the natural soil bearing capacity. In the second, after an initial settlement, the reinforced layer breaks, showing a fissure that may be located near the edge or at the footing's center axis, which propagates upwards as the settlement continues.

The main purpose of the present research is to investigate the response of compacted soil-cement layers, with distinct geometries and resting on a weak cohesive frictional soil, to field plate loads. The system failure modes, load-displacement characteristics and bearing capacity prediction are also addressed.

2. Experimental program

The experimental program was carried out in three stages. Firstly, the materials characterization was performed. Then, mechanical properties of molded specimens were determined through consolidated drained triaxial tests, including the stress-strain behavior of the natural soil and the cemented mixture. Finally, plate load tests were performed directly on the residual soil and on the improved layers, considering distinct layer diameters (D_r) and edges (L_r), with and without side friction and with the same thicknesses (H_r), which allowed the assessment of the influence of the reinforcement layer area and side friction (adhesion) on the load capacity, as well as the failure modes of the foundation system.

2.1 Weakly bonded (cohesive-frictional) residual soil site

The features of the residual soil at the experimental site have been determined by *in situ* cone penetration tests (CPT). The CPT soil profile, to a depth of 7 m, is portrayed in Fig. 1. The CPT data shows a soil crust with less than 1 m, with tip resistance (q_c) reaching 4.8 MPa, overlaying a 3 m layer with q_c of approximately 1.0 MPa, and a 3 m layer with a maximum q_c of 1.7 MPa. The side friction (f_s) follows a similar pattern.

From a sample retrieved from a depth of 2.0 m, it was possible to determine the particle size distribution, showing 2.0 % medium sand (0.425 mm and 2.0 mm), 20.0 % fine sand (0.075 mm and 0.425 mm), 22.0 % silt (0.002 mm and 0.075 mm) and 56.0 % of clay (≤ 0.002 mm). The liquid limit and plasticity index were determined to be 42 % and 11 %, respectively, with the natural moisture content at 33 %. According to the USCS (ASTM 2017) the soil was classified as a lean clay with sand - CL. The unit weight of the solid grains is 26.7 kN/m³, while the average bulk unit weight and the dry unit weight were determined to be 16.1 kN/m³ and 12.1 kN/m³, respectively. Finally, a void ra-

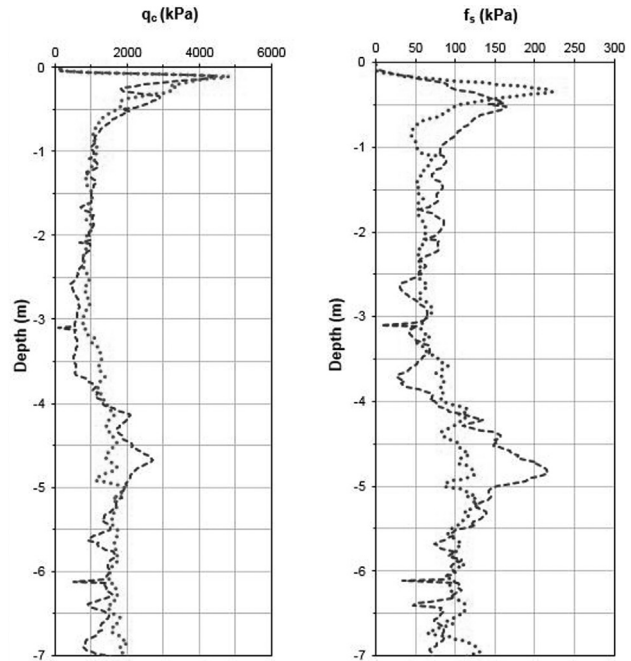


Figure 1. CPT soil profiles to a depth of 7-m.

tio 1.21 and a degree of saturation 73 % were also determined. The unconfined compressive strength, determined after the specimens were immersed in water for 24 h, was 89 kPa (average value), varying between 84 kPa (minimum value) and 92 kPa (maximum value). The hydraulic conductivity is relatively high at 1.1×10^{-5} m/s.

Stress-strain curves obtained from drained triaxial tests of fully saturated undisturbed specimens, under confining pressures of 20, 60 and 100 kPa, are shown in Fig. 2. The 20 kPa confining pressure test revealed a small strain stiffness of 49 MPa and a Poisson coefficient (ν) of 0.15 (after a strain of 0.01 %, measured with Hall effect sensors). The reduction in soil stiffness for the higher confining pressures - 60 and 100 kPa - is not surprising in such lightly bonded soils, due to the changes in fabrics produced by the elimination of the cementation at the particles' contact points, caused by the increased confining pressures (Leroueil & Vaughan, 1990; Consoli *et al.*, 1998, 2000, 2006). All the axial strain-volumetric strain curves present contractive behavior (Fig. 2b). The failure envelope presents an effective peak friction angle (ϕ') of 31.8° and an effective cohesion intercept (c') of 23.8 kPa.

In addition, as the naturally bonded soil in the field is partly saturated ($S_r = 73$ %), the matric suction was assessed through the filter paper technique described by the ASTM D5298 standard (ASTM, 2003) using a Whatman grade 42 filter paper (Chandler *et al.*, 1992, Marinho & Oliveira, 2006). Considering the field conditions (moisture content and degree of saturation), the average matric suction was estimated at 8.8 kPa (varying between 4 and 10 kPa), which corresponds to less than 10 % of the unconfined compressive strength of the natural soil.

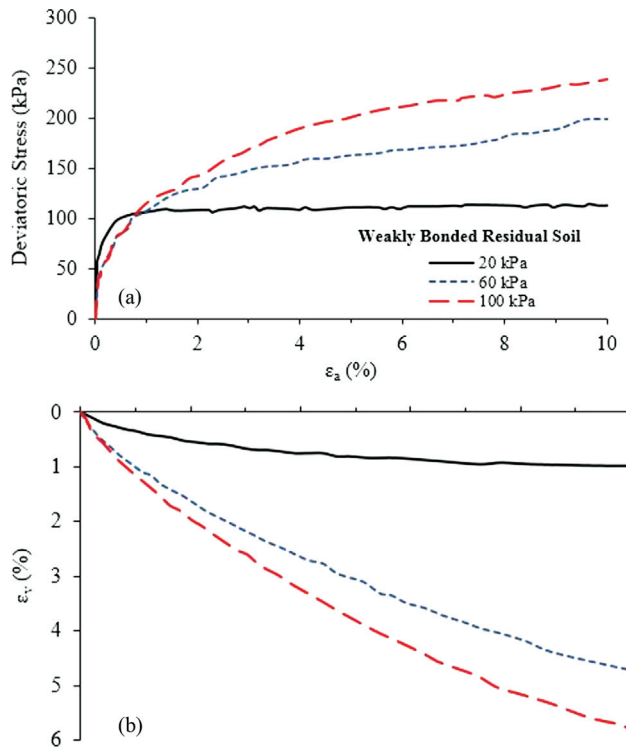


Figure 2. Saturated drained conventional triaxial tests at confining stresses of 20, 60 and 100-kPa for bonded residual soil: (a) deviator stress vs. ϵ_a and (b) ϵ_v vs. ϵ_a .

2.2 Artificially cemented field layers

The artificially cemented field layers prepared in the present research were composed of Osório sand blended with 5 % Portland cement (in percentage of the dry sand). The percentage of Portland cement was chosen considering the international and Brazilian experience with soil-cement (*e.g.*, Ingles & Metcalf, 1972, Mitchell, 1981, Consoli *et al.*, 2009) in experimental and practical works. Water was added to the mixtures to obtain overall water content of 10 % (Consoli *et al.*, 2010) and the mixing continued until a homogeneous paste was acquired. The sand used is eolic, quartzitic, free of organic matter, non-plastic, and obtained from the Osório region in the province of Rio Grande do Sul, Brazil. The sand properties are listed in Table 1. According to ASTM (2017), the soil is classified as poorly graded sand (SP). Early high strength Portland cement [Type III - ASTM (2019)] was used as a cementation agent. Its fast gain of strength allowed a curing period of 28 days for the field trials (as well as the samples collected in the field for laboratory trials). The specific gravity of cement grains is 3.05. Tap water was employed all over this study.

Six circular and three square artificially cemented Osório sand layers were built on the surface of the residual soil site. The circular layers were built with diameters (D) of 450, 600, and 900 mm and a thickness (H) of 300 mm, while square layers were built with widths (L) of 450, 600,

Table 1. Physical properties of the studied soils.

Properties	Residual soil	Osório sand
Specific gravity	2.67	2.63
Medium sand (0.425 mm < diameter < 2.0 mm): %	2.0	0.3
Fine sand (0.075 mm < diameter < 0.425 mm): %	20.0	97.6
Silt (0.002 mm < diameter < 0.075 mm): %	22.0	1.6
Clay (diameter < 0.002 mm): %	56.0	0.5
Liquid limit	42.0	-
Plastic index	11.0	Non-plastic
Soil classification (ASTM, 2017)	CL	SP

and 900 mm, also with a thickness of 300 mm. The typical test configuration describing the improved soil layers is presented in Fig. 3. Before mixing and compaction of the upper-cemented layers, a 500 mm thick layer, of local residual soil, was removed from the test area and the pit was dug according to the specified dimensions of each circular and square layer (see Table 2). Each cemented layer was compacted in several sub-layers, by manual compaction, until the specified 300 mm thickness was achieved. The final layer had a pre-determined dry unit weight of 15.4 kN/m³ (void ratio of 0.70), and was left to cure for 28 days, prior to the field loading tests.

After curing, and immediately before the test, the natural residual soil in contact with the lateral of the treated layers, coded D₄₅₀H₃₀₀, D₆₀₀H₃₀₀ and D₉₀₀H₃₀₀, was removed, so that these results could be compared with those obtained by the layers which were left in contact with the lateral soil. The mechanical parameters of the artificially cemented layers were acquired through conventional saturated drained triaxial tests, isotropically consolidated under effective confining pressures of 20, 40 and 100 kPa (Fig. 4), performed on undisturbed specimens directly collected from the stabilized slabs, after the 28-days curing period. The 20 kPa confining pressure triaxial result presents a small strain Young modulus of 3,430 MPa and a Poisson coefficient (ν) of about 0.2 (measured after 0.01 % strains, using Hall effect sensors). The stress-strain response of all tests, regardless of the confining stress, shows a linear response, up to peak, followed by a brittle and strain softening behavior (Fig. 4a). The results led to a peak friction angle (ϕ') of 36.4° and a cohesion intercept (c') of 145.5 kPa.

2.3 Spread footing testing program

The field tests were performed based on the contents of ABNT NBR 6489 (2019). The load (Q) was applied by a hydraulic jack reacting on a structural loaded beam and was measured by a calibrated 500 kN load cell. To measure the

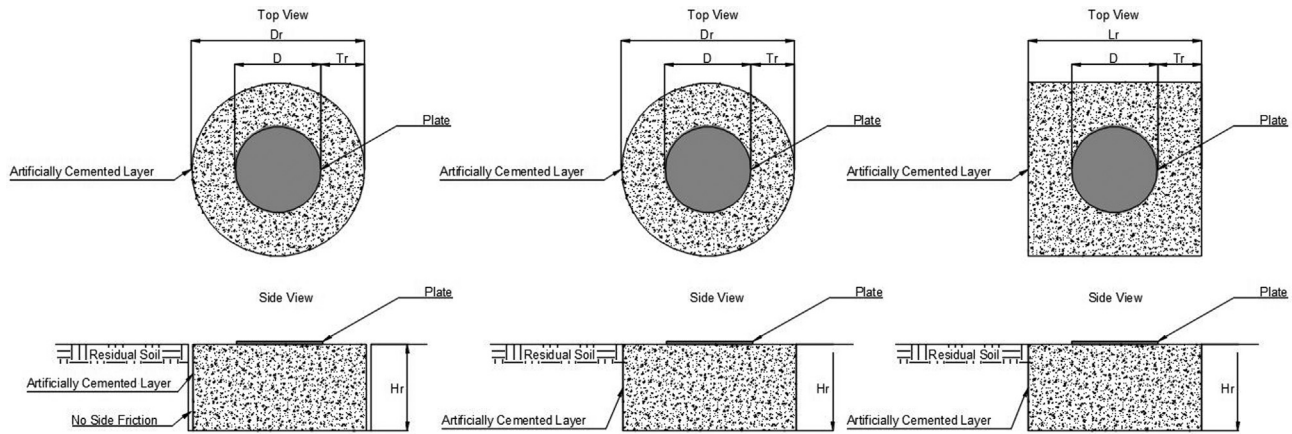


Figure 3. Tests setup depicting the improved soil layers: (a) improved soil circular layers without side friction; (b) improved soil circular layers with side friction; (c) improved soil square layers with side friction.

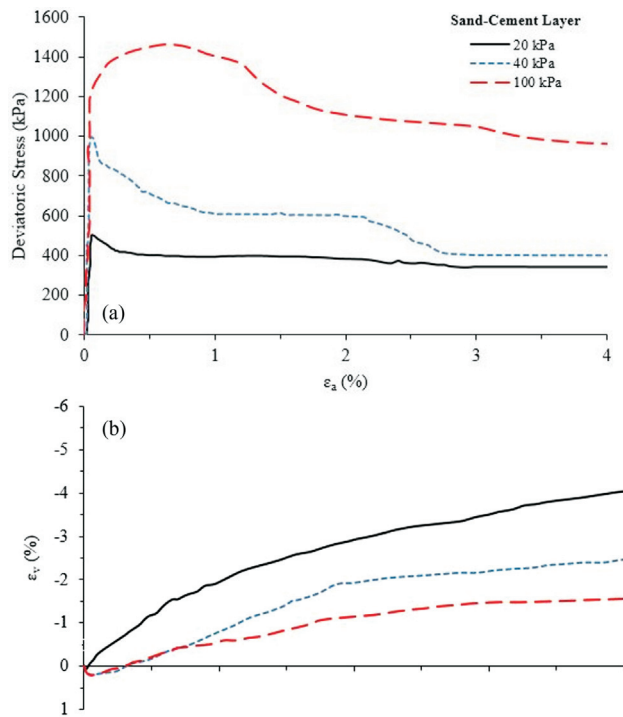


Figure 4. Artificially cemented layers CID tests at confining stresses of 20, 40 and 100-kPa: (a) deviator stress vs. axial strain (ϵ_a) and, (b) volumetric strain (ϵ_v) vs. axial strain (ϵ_a).

vertical displacement, three dial gauges, with a 0.01 mm resolution and 50 mm course, were installed at the top of the plate, on an equilateral triangle pattern. The devices were installed on a supporting beam and fixated by peripheral rods. The load was applied in similar increments of less than one tenth of the expected bearing capacity. The failure load (Q_u) was assumed to be that corresponding to a relative displacement (δ/D) of 3.0 %. Such failure criterion was suggested by Consoli *et al.* (2009), based on previous stud-

ies of more than 200 spread footings carried out by Berardi & Lancellotta (1991).

The spread footing testing program comprises twelve spread footing tests (see Table 2). Three spread footing tests were carried out using 300, 600, and 900 mm diameter rigid steel footings, directly on the residual soil, after the removal of the 500 mm upper layer of the local crust. Nine further spread footing tests were carried out using 300 mm diameter rigid footings, on the sand-cement layers (Table 2).

3. Spread footing testing results and analysis

Figure 5 presents results of applied load vs. vertical displacements of the twelve spread footing tests carried out in the present research. Looking first at the results of the three footing tests [300-mm diameter (coded D300), 600-mm diameter (coded D600) and 900-mm diameter (coded D900)] bearing directly on the weakly bonded residual soil, it can be observed that at a given settlement, higher loads are related to larger footing diameter (and consequently larger areas of the footings). Punching failure of the residual soil at the edge of the circular steel footings was observed in all three tests carried out, regardless of the footing diameter. Looking now to the results of the three 300-mm diameter steel footing tests bearing on sand-Portland cement field circular and square layers [with diameters of 450, 600 and 900-mm both with and no side friction, coded D₄₅₀H₃₀₀, D₆₀₀H₃₀₀, D₉₀₀H₃₀₀ (for circular layers without side friction), coded D₄₅₀H₃₀₀ - SF, D₆₀₀H₃₀₀ - SF, D₉₀₀H₃₀₀ SF (for circular layers with side friction) and coded L₄₅₀H₃₀₀, L₆₀₀H₃₀₀, L₉₀₀H₃₀₀ (for square layers with side friction) - see Table 2] over the weakly bonded residual soil, it can be observed that for a given settlement higher loads were observed for larger artificially cemented sand field layers. However, there are distinct failure mechanisms according to the diameter/width of the sand-Portland cement layers.

Table 2. Artificially cemented layer field dimensions, strength of cemented layer field specimens.

Test	Code	Diameter of the circular steel plate - D (mm)	Geometric form	Treated layer		H/D	Note
				Diameter or width - D_r or L_r (mm)	Thickness - H_r (mm)		
1	D300	300	-	-	-	-	Natural Soil
2	D600	600	-	-	-	-	Natural Soil
3	D900	900	-	-	-	-	Natural Soil
4	D _r 450H _r 300	300	Circular	450	300	1	No side friction
5	D _r 600H _r 300	300	Circular	600	300	1	No side friction
6	D _r 900H _r 300	300	Circular	900	300	1	No side friction
7	D _r 450H _r 300 - SF	300	Circular	450	300	1	Side Friction
8	D _r 600H _r 300 - SF	300	Circular	600	300	1	Side Friction
9	D _r 900H _r 300 - SF	300	Circular	900	300	1	Side Friction
10	L _r 450H _r 300 - SF	300	Square	450	300	1	Side Friction
11	L _r 600H _r 300 - SF	300	Square	600	300	1	Side Friction
12	L _r 900H _r 300 - SF	300	Square	900	300	1	Side Friction

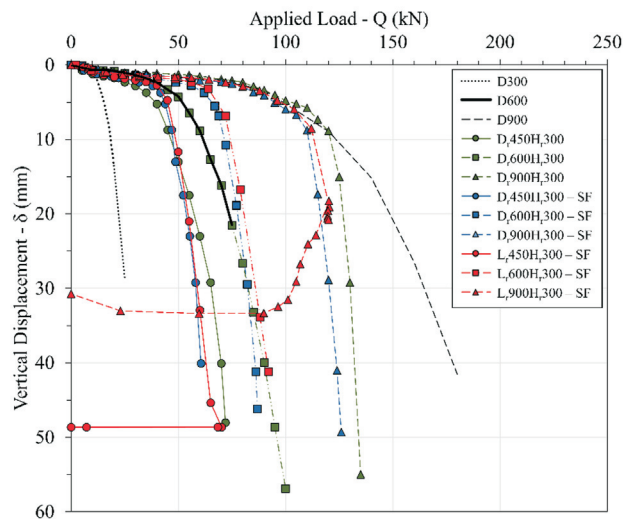


Figure 5. Load-settlement curves of 300-mm diameter (coded D300), 600-mm diameter (coded D600) and 900-mm diameter (coded D900) circular steel footing bearing on weakly bonded residual soil, and 300-mm diameter circular steel footing bearing on 450, 600 and 900-mm diameter treated layer without side friction (coded D_r450H_r300, D_r600H_r300 and D_r900H_r300), 450, 600 and 900-mm diameter treated layer with side friction (coded D_r450H_r300 - SF, D_r600H_r300 - SF and D_r900H_r300 - SF) and, 450, 600 and 900-mm widths treated layer with side friction (coded L_r450H_r300, L_r600H_r300 and L_r900H_r300) of artificially cemented sand layers over weakly bonded residual soil.

Punching failure of the residual soil was observed at the edge of the sand-cement field layers with 450 mm in diameter and a 450 mm side (coded D_r450H_r300, coded D_r450H_r300 - SF and L_r450H_r300 - SF) and 600 mm in diameter and 600 mm square (coded D_r600H_r300, coded

D_r600H_r300 - SF and L_r600H_r300 - SF), as if these six treated layers were part of the shallow foundation structure. This failure mechanism was corroborated by the field analysis of the treated layers after the end of the test, since no cracks or fractures were observed in such layers (see photo of the intact treated circular and square layer with 450 mm diameter and width, respectively and, 300 mm thick retrieved from the field in Fig 6).

For punching failure, as the load increases, there is breakage of the bonds of the weakly bonded residual soil below the spread footing structure, and vertical continuous penetration of the footing structure, with virtually no lateral soil movement. On the other hand, after a certain vertical load (Q) was applied to the 300 mm diameter rigid circular steel plate bearing on the sand-cement layers of 900 mm diameter (D_r900H_r300), 900 mm diameter with side friction (D_r900H_r300 - SF) and 900 mm square (L_r900H_r300 - SF), there was a failure of such artificially cemented layers after reaching certain Q . This mode of failure (fracturing of the layers) was attested by the cracks found in the cylindrical and prismatic volume that was cut vertically after completion of the load test [see photos of the failed layer of 900 mm diameter (D_r900H_r300) in Fig. 7 and of 900 mm width (L_r900H_r300 - SF) in Fig. 8]. Consoli *et al.* (2009) observed similar failures for the infinite cemented layers. These authors also verified, by means of finite element method simulations, that tensile cracks start at the bottom of the cemented soil layer, below the circular plates.

Looking back to Fig. 5, it is possible to observe that applied load (Q) vs. vertical displacement (δ) curves of the tests D600 and D_r600H_r300 are identical. Such similarity is not a coincidence, since D600 (a circular steel footing of

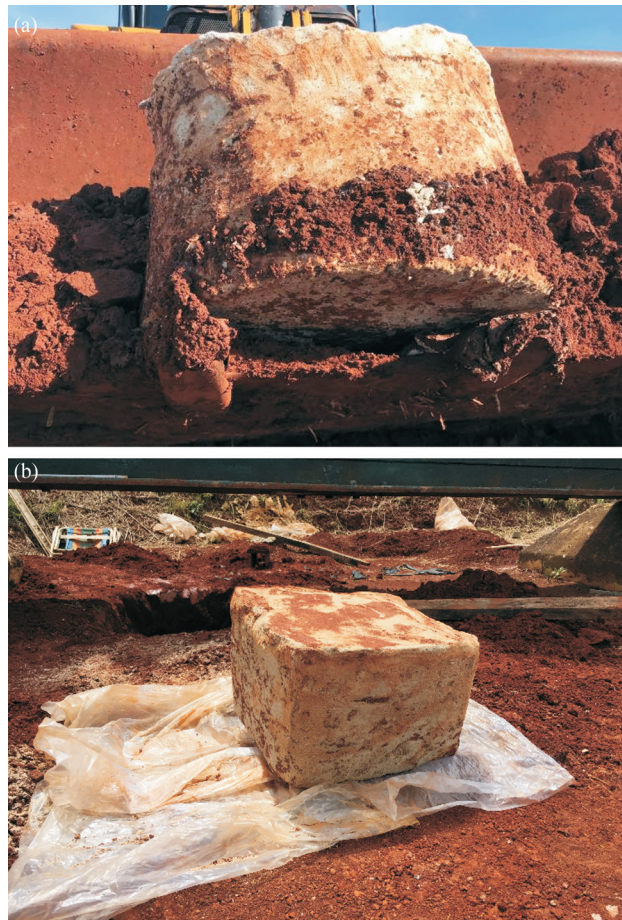


Figure 6. Improved sand-Portland cement retrieved from the field: (a) Cylindrical shape of the 450-mm diameter and 300-mm thick (coded $D_{r450H,300}$); and (b) Prismatic shape of the 450-mm square and 300-mm thick (coded $L_{r450H,300} - SF$).

600 mm diameter) is distributing its load through the same area of the base of the $D_{r600H,300}$ test, with a circular footing of 300 mm diameter, bearing on a sand-cement field layer with 600 mm diameter and 300 mm thick, that is kept intact until the end of the test. In other words, the sand-cement field layer with 600 mm diameter and 300 mm thick is acting as if it is part of the shallow foundation structure of a circular footing of 600 mm diameter. So, in reality, D_{r600} and $D_{r600H,300}$ spread footing tests have a similar base regarding the transfer of the vertical stresses to the residual soil. However, the same does not happen for the sand-cement circular and square layers coded $D_{r600H,300} - SF$ and $L_{r600H,300} - SF$, because the side friction (and adhesion) increases their bearing capacity. It can also be noticed that the bearing capacity of the sand-cement square layer ($L_{r600H,300} - SF$) is slightly larger than the sand-cement circular layer ($D_{r600H,300} - SF$) due to the area and perimeter of the square layer being larger than the circular layer. Also, in Fig. 5, it can be observed that the applied load (Q) vs. vertical displacement (δ) curves of spread footing tests D_{r900} and $D_{r900H,300}$



Figure 7. Photos of the (a) general view and (b) vertical cut in the middle of the 900-mm diameter and 300-mm thick Portland cement improved sand layer (coded $D_{r900H,300}$) to check failure mechanism below the steel plate vertically loaded.

are coincident only up to a certain load. Such situation is also not a coincidence, since D_{r900} (a circular steel footing of 900 mm diameter) is distributing its load through to the same area of the $D_{r900H,300}$, up to a point of fracturing the artificially cemented layer. After the failure of the sand-cement field layer starts to occur, the two Q vs. δ curves separate from each other.

Based on studies by Consoli *et al.* (1998), the applied load (Q) vs. vertical displacements (δ) curves are normalized by dividing Q by the foundation-residual soil contact area [named equivalent stress (σ_{eq})] and δ by the diameter of the foundation-residual soil contact area (D_r), named relative displacement (δ/D_r). Fig. 9 presents the normalized results of the three circular steel footing tests bearing directly on the weakly bonded residual soil (coded D_{r300} , D_{r600} and D_{r900}), which ends up in a unique curve. Normalized σ_{eq} vs. δ/D_r results for the two shallow foundation tests bearing on improved layers that failed by punching (coded $D_{r450H,300}$ and $D_{r600H,300}$, in which the steel footing plus the Portland cement improved layers behaved as a sin-



Figure 8. Photos of (a) the top view and (b) vertical cut in the middle of the 900-mm square and 300-mm thick Portland cement improved sand layer (coded L_{900H300} - SF) to check failure mechanism below the steel plate vertically loaded.

gle shallow foundation resting on the bonded residual soil, also maintained their behavior similar to the tests performed directly on the natural bonded residual soil. However, the same does not happen for the normalized σ_{eq} vs. δ/D_r results of the sand-cement field circular layers (coded D_r450H_r300 - SF and D_r600H_r300 - SF) and square layers (coded L_r450H_r300 - SF and L_r600H_r300 - SF), once the side friction (and adhesion) further enhances their behavior at

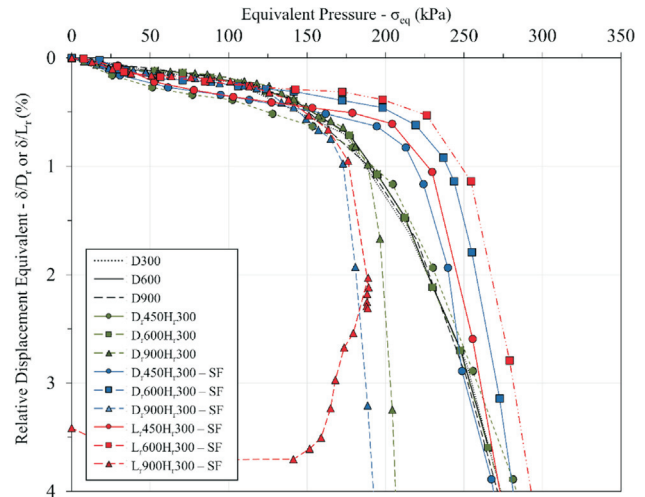


Figure 9. Equivalent pressure (σ_{eq}) vs. relative displacement (δ/D_r or δ/L_r) curves of 300 mm, 600 mm and 900 mm diameter circular steel footing bearing on weakly bonded residual soil, and 300 mm diameter circular steel footing bearing on 450, 600 and 900-mm diameter treated layer without side friction (coded D_r450H_r300, D_r600H_r300 and D_r900H_r300), 450, 600 and 900 diameter treated layer with side friction (coded D_r450H_r300 - SF, D_r600H_r300 - SF and D_r900H_r300 - SF) and 450, 600 and 900 widths treated layer with side friction (coded L_r450H_r300 - SF, L_r600H_r300 - SF and L_r900H_r300 - SF) of artificially cemented sand layers over weakly bonded residual soil.

small relative displacements. The normalized σ_{eq} vs. δ/D_r curve of D_r900H_r300 shallow foundation test is also similar (practically the same “unique” curve based on the previous normalized results) up to the occurrence of the extensive cracking of the improved layer, whose macroscopic sequel clearly starts at a relative displacement (δ/D_r) of about 1.0 % (see Fig. 9). After such point, the normalized σ_{eq} vs. δ/D_r curve of D_r900H_r300 shallow foundation test diverge from the “unique” general normalized curve. Related behavior is followed by tests coded D_r900H_r300 - SF and L_r900H_r300 - SF.

Figure 10 and Table 3 show the field failure load (Q_u) results (in a space diameter of the cement treated sand layer vs. failure load) and analytical solutions based on the Hansen (1961) and Vesic (1975) theories in a unique graph. It is expected that the results where soil punching occurred could be determined using standard analytical bearing capacity theory of Hansen (1961), while that in the three cases [900 mm diameter and square (coded D_r900H_r300, D_r900H_r300 - SF and L_r900H_r300 - SF)] where the failure mode prediction is the occurrence of failure of the artificially cemented layer, the Vesic (1975) bearing capacity theory of double layer is expected to give good results up to $H/D = 1.0$ (Consoli *et al.*, 2008). The Hansen (1961) method [Eq. (1)] was applied as if the structural foundation was a single element (steel footing plus cement improved sand layer) resting on weakly bonded residual soil. The

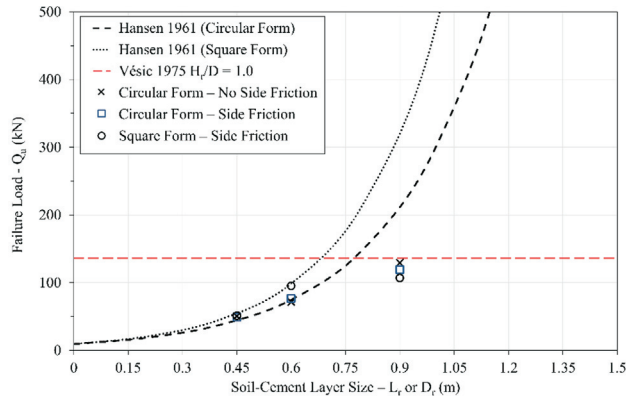


Figure 10. Bearing capacity of square and circular shallow foundations prediction considering soil cement layer as a part of the foundation (Hansen, 1961) and considering it as an infinite treated layer with $H/D = 1.0$ (Vesic, 1975).

strength parameters of the weakly bonded residual soil were reduced to a lower limit value of $2/3$ in order to agree with Terzaghi (1943) recommendations for punching failure mechanisms (Consoli *et al.*, 1998).

$$\frac{Q_u}{A_c} = c'N_c S_c + \frac{D_r}{2} \gamma N_\gamma S_\gamma \quad (1)$$

where A_c is the area of the cemented layer, D_r is the diameter of the improved layer, γ is the unit weight of the residual soil; N_c , N_γ are the bearing capacity factors; and S_c , S_γ are the shape factors for circular and square foundations, given by

$$N_c = \left[e^{\pi \tan \phi'} \tan^2 \left(45^\circ + \frac{\phi'}{2} \right) - 1 \right] \cot \phi' \quad (2)$$

$$N_\gamma = 2 \left[e^{\pi \tan \phi'} \tan^2 \left(45^\circ + \frac{\phi'}{2} \right) + 1 \right] \tan \phi' \quad (3)$$

$$S_c = 1 + \frac{e^{\pi \tan \phi'} \tan^2 \left(45^\circ + \frac{\phi'}{2} \right)}{\left(e^{\pi \tan \phi'} \tan^2 \left(45^\circ + \frac{\phi'}{2} \right) - 1 \right) \cot \phi'} \quad (4)$$

$$S_\gamma = 0.6 \quad (5)$$

The Vesic (1975) solution [Eq. (6)] establishes the bearing capacity of a footing resting on an infinite upper cement-sand layer with strength parameters c_1' and ϕ_1' superposed to a lower (bonded residual soil) weak layer with strength parameters c_2' and ϕ_2' (involving both cohesion and friction strength parameters) as:

Table 3. Field and analytical failure loads (Q_u) and failure modes of shallow foundations bearing on cement treated layers.

D_r or L_r (m)	Q_u (kN) - at $\delta/D = 3\%$				$Q_{u(n)}$ (kN) - Hansen (1961)	$Q_{u(n)}$ (kN) - Vésic (1975)	Prevision	Field result
	Circular		Square					
	No side friction	Side friction	Side friction	Square				
0.45	50.6	49.1	51.0	57.1	-	Punching	Punching	
0.60	71.7	76.6	95.3	103.2	-	Punching	Punching	
0.90	129.2	119.2	106.9	-	136.2	Cemented layer generalized failure	Cemented layer generalized failure	

$$\frac{Q_u}{A_c} = \left[q_0 + \left(\frac{1}{\frac{1 - (\sin \phi'_1)^2}{1 + (\sin \phi'_1)^2}} \right) c'_1 \cot \phi'_1 \right] \times e^{\frac{4}{1 + (\sin \phi'_1)^2} \tan \phi'_1 \left(\frac{H_r}{D_r} \right) - \left(\frac{1}{\frac{1 - (\sin \phi'_1)^2}{1 + (\sin \phi'_1)^2}} \right) c'_1 \cot \phi'_1} \quad (6)$$

where A_s is the area of the steel plate, q_0 is the bearing capacity as if the spread footing was resting on the top of the natural soil, considering the reduction in the strength parameters for punching the failure mechanism.

From Fig. 10, it is possible to notice that the bearing capacity prediction considering the cement treated sand layer is a fine analytical solution when considering as a part of the shallow foundation. Such solution threshold is given by the cement treated layer (Vesic, 1975) solution, for specific H/D . The composition of the two analytical solutions described above has shown to be a useful tool to predict the failure behavior of cement treated sand layers resting above the weakly bonded residual soil.

4. Conclusions

This study evaluated the behavior of circular steel plates bearing on distinct diameters and widths cement treated sand layers, maintaining the same thicknesses, on weakly bonded residual soil site. From the data gathered from the present study, the following conclusions can be portrayed:

- Two distinct modes of rupture were observed in the present field study, depending on the diameter or widths of sand-Portland cement blend. For the sand-Portland cement layers diameters and widths up to 600 mm, the limit load was successfully evaluated as if the improved layers worked in association with the circular steel foundation, as a foundation transferring its load directly to the weakly bonded residual soil (which fails due to punching), once no cracking or fissuring were observed in the artificially cemented layer. The reinforced layers of diameter (or width) of 900 mm broke due to the excessive tensile stresses that were developed in the bottom of the cemented layer. Therefore, the carrying capacity of the circular plate supported in this layer can be evaluated as if this layer were “infinite” or continuous;
- A single curve in σ_{eq} vs. δ/D_r space is achieved when plotting the spread footing field tests performed, with and without improved layer, up to the rupture of the treated layer (when applicable);
- The combined use of Hansen (1961) and Vesic (1975) analytical solutions proved to be a useful way to predict the failure behavior and the bearing capacity of cement

treated layers of distinct shapes bearing on weakly bonded residual soil site.

Acknowledgments

The authors wish to explicit their appreciation to MCT-CNPq (Editais INCT, Universal & Produtividade em Pesquisa), FAPERGS/CNPq 12/2014 - PRONEX (Project # 16/2551-0000469-2), and MEC-CAPES (PROEX) for the support to the research group.

References

- ABNT (2019). Soil - Static Load Test on Shallow Foundation - NBR 6489. Associação Brasileira de Normas Técnicas, São Paulo, Brazil.
- ASTM (2003). Standard Test Method for Measurement of Soil Potential (Suction) Using Filter Paper - ASTM D5298. ASTM International, West Conshohocken, Philadelphia, USA.
- ASTM (2017). Standard Practice for Classification of Soils for Engineering Purposes (Unified Soil Classification System) - ASTM D2487. ASTM International, West Conshohocken, Philadelphia, USA.
- ASTM (2019). Standard Specification for Portland Cement - ASTM C150. ASTM International, West Conshohocken, Philadelphia, USA.
- Berardi, R. & Lancellotta, R. (1991). Stiffness of granular soil from field performance. *Géotechnique*, 41(1):149-157. <https://doi.org/10.1680/geot.1991.41.1.149>
- Burd, J. & Frydman, S. (1997). Bearing capacity of plane-strain footings on layered soil. *Canadian Geotechnical Journal*, 34(2):241-253. <https://doi.org/10.1139/t96-106>
- Caballero, R.D. (2019). Desenvolvimento de uma Metodologia de Projeto de Fundações Superficiais Circulares Assentes Sobre Camada de Solo-Cimento. M.Sc. Dissertation, Programa de Pós-Graduação em Engenharia Civil, Universidade Federal do Rio Grande do Sul, Porto Alegre, Brasil, 198 p. (in Portuguese). <https://lume.ufrgs.br/handle/10183/194594>.
- Chandler, R.J.; Crilly, M.S. & Montgomery-Smith, G. (1992). A low-cost method of assessing clay desiccation for low-rise buildings. *Proceedings of the Institution of Civil Engineers - Civil Engineering*, 92(2):82-89. <https://doi.org/10.1680/icien.1995.27840>
- Clough, G.W.; Sitar, N.; Bachus, R.C. & Rad, N.S. (1981). Cemented sands under static loading. *Journal of Geotechnical Engineering Division*, 107(6):799-817.
- Consoli, N.C.; Schnaid, F. & Milititsky, J. (1998). Interpretation of plate load tests on residual soil site. *Journal of Geotechnical and Geoenvironmental Engineering*, 124(9):857-867. [https://doi.org/10.1061/\(ASCE\)1090-0241\(1998\)124:9\(857\)](https://doi.org/10.1061/(ASCE)1090-0241(1998)124:9(857))
- Consoli, N.C.; Rotta, G.V. & Prietto, P.D.M. (2000). Influence of curing under stress on the triaxial response of

- cemented soils. *Géotechnique*, 50(1):99-105. <https://doi.org/10.1680/geot.2000.50.1.99>
- Consoli, N.C.; Rotta, G.V. & Prietto, P.D.M. (2006). Yielding-compressibility-strength relationship for an artificially cemented soil cured under stress. *Géotechnique*, 56(1):69-72. <https://doi.org/10.1680/geot.2006.56.1.69>
- Consoli, N.C.; Thomé, A.; Donato, M. & Graham, J. (2008). Loading tests on compacted soil, bottom-ash and lime layers. *Proceedings of the Institution of Civil Engineers - Geotechnical Engineering*, 161(1):29-38. <https://doi.org/10.1680/geng.2008.161.1.29>
- Consoli, N.C.; Dalla Rosa, F. & Fonini, A. (2009). Plate load tests on cemented soil layers overlying weaker soil. *Journal of Geotechnical and Geoenvironmental Engineering*, 135(12):1846-1856. [https://doi.org/10.1061/\(ASCE\)GT.1943-5606.0000158](https://doi.org/10.1061/(ASCE)GT.1943-5606.0000158)
- Consoli, N.C.; Cruz, R.C.; Floss, M.F. & Festugato, L. (2010). Parameters controlling tensile and compressive strength of artificially cemented sand. *Journal of Geotechnical and Geoenvironmental Engineering*, 136(5):759-763. [https://doi.org/10.1061/\(ASCE\)GT.1943-5606.0000278](https://doi.org/10.1061/(ASCE)GT.1943-5606.0000278)
- Consoli, N.C.; Cruz, R.C. & Floss, M.F. (2011). Variables controlling strength of artificially cemented sand: Influence of curing time. *Journal of Materials in Civil Engineering*, 23(5):692-696. [https://doi.org/10.1061/\(ASCE\)MT.1943-5533.0000205](https://doi.org/10.1061/(ASCE)MT.1943-5533.0000205)
- Consoli, N.C.; Cruz, R.C.; Viana da Fonseca, A. & Coop, M.R. (2012). Influence of cement-voids ratio on stress-dilatancy behavior of artificially cemented sand. *Journal of Geotechnical and Geoenvironmental Engineering*, 138(1):100-109. [https://doi.org/10.1061/\(ASCE\)GT.1943-5606.0000565](https://doi.org/10.1061/(ASCE)GT.1943-5606.0000565)
- Consoli, N.C.; Festugato, L.; Da Rocha, C.G. & Cruz, R.C. (2013). Key parameters for strength control of rammed sand-cement mixtures: Influence of types of Portland cement. *Construction and Building Materials*, 49:591-597. <https://doi.org/10.1016/j.conbuildmat.2013.08.062>
- Consoli, N.C.; Lopes Jr., L.S.; Consoli, B.S. & Festugato, L. (2014). Mohr-Coulomb failure envelopes of lime-treated soils. *Géotechnique*, 64(2):165-170. <https://doi.org/10.1680/geot.12.P.168>
- Consoli, N.C.; Festugato, L.; Consoli, B.S. & Lopes Jr., L.S. (2015). Assessing failure envelopes of soil-fly ash-lime blends. *Journal of Materials in Civil Engineering*, 26(9):04014174. [https://doi.org/10.1061/\(ASCE\)MT.1943-5533.0001134](https://doi.org/10.1061/(ASCE)MT.1943-5533.0001134)
- Consoli, N.C.; Quiñónez Samaniego, R.A.; Marques, S.F.V.; Venson, G.I.; Pasche, E. & González Velázquez, L.E. (2016). A single model establishing strength of dispersive clay treated with distinctive binders. *Canadian Geotechnical Journal*, 53(12):2072-2079. <https://doi.org/10.1139/cgj-2015-0606>
- Consoli, N.C.; Marques, S.F.V.; Floss, M.F. & Festugato, L. (2017). Broad-spectrum empirical correlation determining tensile and compressive strength of cement-bonded clean granular soils. *Journal of Materials in Civil Engineering*, 29(6):06017004. [https://doi.org/10.1061/\(ASCE\)MT.1943-5533.0001858](https://doi.org/10.1061/(ASCE)MT.1943-5533.0001858)
- Consoli, N.C.; da Silva, A.P.; Nierwinski, H.P. & Sosnoski, J. (2018). Durability, strength, and stiffness of compacted gold tailings - cement mixes. *Canadian Geotechnical Journal*, 55(4):486-494. <https://doi.org/10.1139/cgj-2016-0391>
- Consoli, N.C.; Leon, H.B.; Carretta, M.S.; Daronco, J.V.L. & Lourenço, D.E. (2019). The effects of curing time and temperature on stiffness, strength and durability of sand environment friendly binder blends. *Soils and Foundations*, 59(2):1428-1439. <https://doi.org/10.1016/j.sandf.2019.06.007>
- Consoli, N.C.; Festugato, L.; Scheuermann Filho, H.C.; Miguel, G.D.; Tebechrani Neto, A. & Andreghetto, D. (2020a). Durability assessment of soil-pozzolan-lime blends through ultrasonic pulse velocity test. *Journal of Materials in Civil Engineering*, 32(8):04020223. [https://doi.org/10.1061/\(ASCE\)MT.1943-5533.0003298](https://doi.org/10.1061/(ASCE)MT.1943-5533.0003298)
- Consoli, N.C.; Bittar Marin, E.J.; Quiñónez Samaniego, R.A.; Scheuermann Filho, H.C. & Cristelo, N.M.C. (2020b). Field and laboratory behaviour of fine-grained soil stabilized with lime. *Canadian Geotechnical Journal*, 57(6):933-938. <https://doi.org/10.1139/cgj-2019-0271>
- Consoli, N.C.; Carretta, M.S.; Festugato, L.; Leon, H.B.; Tomasi, L.F. & Heineck, K.S. (2020c). Ground waste glass-carbide lime as a sustainable binder stabilising three different silica sands. *Géotechnique*, *in press*. <https://doi.org/10.1680/jgeot.18.P.099>
- Coop, M.R. & Atkinson, J.H. (1993). The mechanics of cemented carbonate sands. *Géotechnique*, 43(1):53-67. <https://doi.org/10.1680/geot.1993.43.1.53>
- Dalla Rosa, F.; Consoli, N.C. & Baudet, B.A. (2008). An experimental investigation of the behaviour of artificially cemented soil cured under stress. *Géotechnique*, 58(8):675-679. <https://doi.org/10.1680/geot.2008.58.8.675>
- Foppa, D.; Sacco, R.L. & Consoli, N.C. (2020). Bearing capacity of footings on an artificially cemented layer above weak foundation layer. *Proceedings of the Institution of Civil Engineers - Ground Improvement*, *in press*. <https://doi.org/10.1680/jgrim.18.00089>
- Hansen, J.B. (1961). A general formula for bearing capacity. *Bulletin No. 11*, pp. 38-46. Copenhagen, Denmark: Danish Geotechnical Institute.
- Huang, J.T. & Airey, D. (1998). Properties of artificially cemented carbonate sand. *Journal of Geotechnical and Geoenvironmental Engineering*, 124(6):492-499. [https://doi.org/10.1061/\(ASCE\)1090-0241\(1998\)124:6\(492\)](https://doi.org/10.1061/(ASCE)1090-0241(1998)124:6(492))
- Ingles, O.G. & Metcalf, J.B. (1972). *Soil Stabilization: Principles and Practice*. Butterworths, Sydney.

- Kenny, M.J. & Andrawes, K.Z. (1997). The bearing capacity of footing on sand layer overlying soft clay. *Géotechnique*, 47(2):339-345. <https://doi.org/10.1680/geot.1997.47.2.339>
- Leroueil, S. & Vaughan, P.R. (1990). The general and congruent effects of structure in natural soils and weak rocks. *Géotechnique*, 40(3):467-488. <https://doi.org/10.1680/geot.1990.40.3.467>
- Marinho, F.A.M. & Oliveira, O.M. (2006). The filter paper method revisited. *Geotechnical Testing Journal*, 29(3):250-258. <https://doi.org/10.1520/GTJ14125>
- Meyerhof, G.G. (1974). Ultimate bearing capacity of footings on sand layer overlying clay. *Canadian Geotechnical Journal*, 11(2):223-229. <https://doi.org/10.1139/t74-018>
- Mitchell, J.K. (1981). Soil improvement - State of the art report. Proc. 10th Int. Conf. on Soil Mechanics and Foundation Engineering, A.A. Balkema, Rotterdam, pp. 509-565.
- Vesic, A.S. (1975). Bearing Capacity of Shallow Foundations. Winterkorn, H.F. & Fang, H.Y. (eds) *Foundation Engineering Handbook*, Van Nostrand Reinhold, New York, pp. 121-147.

List of Symbols

- A : area of footing
 A_c : area of the cemented layer
 A_s : area of the steel plate
 c' : effective cohesion intercept
 D : diameter of the circular steel shallow foundation
 D_r : diameter of the circular sand-Portland cement field layers
 f_s : CPT sleeve friction
 H_r : thickness of the sand-Portland cement field layers
 L_r : width of the square sand-Portland cement field layers
 q_c : CPT tip strength
 q_0 : bearing capacity of spread footing was resting on soil
 N_c , N_q and N_γ : bearing capacity factors
 Q : applied load
 Q_u : failure load
 S_c , S_q and S_γ : shape factors
 δ : vertical displacement
 δ/D or δ/D_r : relative displacement
 ε_a : axial strain
 ε_v : volumetric strain
 σ_{eq} : equivalent pressure at the base of the cemented layer
 ϕ' : effective friction angle

A review on some factors influencing the behaviour of nonwoven geotextile filters

Ennio M. Palmeira^{1,*} 

Article

Keywords

Filters
Geosynthetics
Geotextiles
Nonwovens

Abstract

Geotextiles have been extensively used as filters in geotechnical engineering for over 5 decades. The main reasons for this widespread utilization are that they are manufactured products with repeatable properties, are easy to install and to transport to distant working sites and can substitute natural filter materials where they are scarce or their use is prohibited by environmental regulations. Despite their technical and commercial success, the behaviour of geotextile filters can be quite complex, particularly in the case of nonwoven geotextiles, some reasons being that they are thin and compressible materials, with a complex micropore structure. This paper reviews and discusses some factors that can influence nonwoven needle-punched geotextile filter behaviour. The influences of confinement and partial clogging on filter pore dimensions are discussed based on results from special laboratory tests and theoretical approaches. Limitations of such approaches in simulating actual field conditions are also discussed. The study highlights the relevance of the factors presented and identifies procedures to quantify their influences and to reduce the possibility of filter poor performance.

1. Introduction

Geotextiles have been used for over 5 decades as filters in geotechnical and geoenvironmental engineering works. Some of the reasons for such widespread use are that they are simple and quick to install, easy to transport to the working site, can provide a cost-effective solution in comparison to traditional granular filters and can substitute natural filter materials in regions where they are scarce or their exploitation is prohibited by environmental regulations. An additional important advantage of the use of geotextile filters in civil engineering works, and of geosynthetics in general for that matter, is that they are capable of producing a more environmentally friendly engineering solution in comparison with conventional granular filters. Benefits such as less emissions of harmful gases to the atmosphere, less consumption of water and of renewable and non-renewable fuels can be achieved with the use of geosynthetics, among other environmental benefits. Examples of these benefits can be found in Stucki *et al.* (2011), Frischknecht *et al.* (2012), Heerten (2012) and Damians *et al.* (2017).

Despite filtration being the most traditional function of geotextiles, the behaviour of these filters in geotechnical and geoenvironmental works is still quite complex (Koer-

ner & Koerner, 2015). This is also so for traditional granular filters. However, geotextiles add further difficulties to filter behaviour understanding, such as low thickness, high compressibility, complex microstructure, possibility of mechanical damage and durability. The latter two can be properly avoided or may not be of concern for the expected conventional life of most of geotechnical engineering works, since in non-aggressive environments the life expectancy of plastics is expected to be sufficiently long.

Considering the characteristics of geotextiles, several filter criteria have been proposed throughout the years (Giroud, 1982, Heerten, 1982, Carrol, 1983, Mlynarek, 1985, Lawson, 1986, Fischer *et al.*, 1990, Luettich *et al.*, 1992, Giroud, 1996, Holtz *et al.*, 1997, for instance). Some of the basis for these criteria are similar to those for granular filters. The geotextile has to fulfil requirements such as capability of retaining the base soil particles (retention criterion), must be more (in some cases, over one order of magnitude) permeable than the soil (permeability criterion), must not clog (anti-clogging criterion) and must be durable enough (durability/endurance criterion).

Geotextile retention capacity has been assessed by laboratory tests and analytical and probabilistic solutions. Examples of retention criteria are presented in Wilson-

*Corresponding author. E-mail address: palmeira@unb.br.

¹Departamento de Engenharia Civil e Ambiental, Universidade de Brasília, Brasília DF, Brasil.

Submitted on May 29, 2020; Final Acceptance on June 23, 2020; Discussion open until December 31, 2020.

DOI: <https://doi.org/10.28927/SR.433351>



This is an Open Access article distributed under the terms of the Creative Commons Attribution License, which permits unrestricted use, distribution, and reproduction in any medium, provided the original work is properly cited.

Fahmy *et al.* (1996), Fisher *et al.* (1990), Palmeira & Gardoni (2000a) and Palmeira (2018). Basically, the following condition must be fulfilled:

$$FOS < aD_n \quad (1)$$

where FOS is the geotextile filtration opening size, D_n is a reference soil particle size (commonly D_{85} , which is the diameter for which 85 % of the remaining soil particles have diameters smaller than that value) and a is a number which depends on the criterion considered, geotextile type (woven or nonwoven), soil type, soil porosity, soil density, flow conditions etc.

The geotextile filtration opening size (FOS) is assumed as the equivalent diameter of the largest soil particle capable of passing through the geotextile. Experimentally, it can be determined by sieving tests, capillary flow tests and image analysis. Figure 1 shows schematically each of these testing techniques. Despite its simplicity and low cost, dry sieving (Fig. 1a) may lead to inaccurate results because electrostatic forces generated during sieving may retain particles attached to the geotextile fibres that otherwise would pass. Wet sieving and hydrodynamic sieving (Figs. 1b and 1c) eliminate the action of such forces. The wet sieving test has been adopted as a standard test in many countries due to its simplicity and low cost. Pore intrusion methods (Fig. 1d) require a rather sophisticated equipment, but testing is quicker and repeatable. Image analysis (Fig. 1e) employs microscopy, testing is complex and time consuming, which has restricted its use to research. Discussions on the advantages and limitations of these different methods for FOS measurement can be found in Bhatia and Smith (1996a and b) and Blond *et al.* (2015).

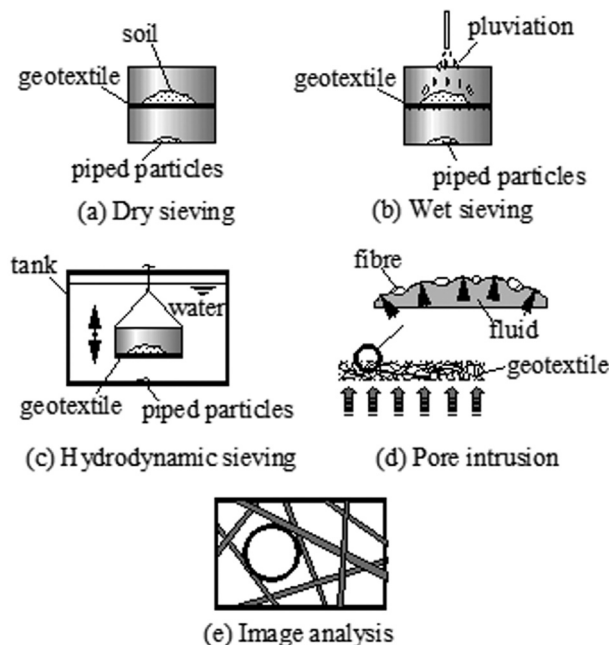


Figure 1. Techniques for the measurement of geotextile filtration opening size (modified from Palmeira, 2018).

The value of FOS can be assumed as the value of a geotextile pore equivalent diameter (O_e) for which a given percentage (commonly, $\kappa = 90\%$, 95% or 98%) of the remaining pores have diameters smaller than that value. The percentage κ chosen depends on the testing technique used and standard considered. Analytical and probabilistic solutions are also available for the estimate of FOS as a function of geotextile type, mass per unit area, thickness, porosity, fibre orientation and fibre diameter (Laflaive & Puig, 1974, Fayoux & Evon, 1982, Faure *et al.*, 1990, Giroud, 1996, Rawal, 2010, for instance).

The permeability criterion requires the geotextile coefficient of permeability (k_c) to be high enough to avoid the impairment of the water flow and pore pressure increase in the base soil. Criteria available in the literature require the geotextile permeability coefficient to be equal to or greater than that of the base soil, depending on the geotextile type, soil type, project characteristics and type of permeant (Calhoun, 1972, Schoeber & Teindl, 1979, Giroud, 1982, Christopher & Holtz, 1985, Corbet, 1993, Lafleur, 1999, for instance). Typically, the permeability criteria require k_c ranging from 1 to 100 times the soil coefficient of permeability.

The evaluation of the possibility of filter clogging is complex, and the clogging mechanisms considered for a geotextile filter are shown in Fig. 2. Blinding (Fig. 2a) is a clogging mechanism where fine particles are retained on the geotextile surface, creating a thin and low permeability layer. Special attention to this clogging mechanism must be paid for filters in contact with internally unstable soils. Blocking (Fig. 2b) is a mechanism in which the geotextile pores are blocked by soil particles. Although possible in the case of woven geotextiles, its occurrence is very unlikely in nonwoven geotextiles due to the variety of shapes, dimensions and number of pores at the surface of such geotextiles. Internal clogging can take place due to excessive impregnation of the geotextile (nonwoven) pores by base soil particles intrusion (Fig. 2c), the formation of bacterial films (bacterial clogging) or the precipitation of chemicals (chemical clogging). In case of possible geotextile blinding, the designer will have to decide whether to specify a geotextile open enough to allow the passage of fine-grained soil particles or a less porous geotextile that will retain these particles. A too open geotextile may allow excessive piping of soil particles that may cause large soil mass deformations or collapse. On the other hand, retaining too many soil particles may cause soil blinding and severe reduction of flow rate, with increase of pore pressures in the vicinity of the filter layer. Sound engineering judgement must be exercised in these situations.

Clogging criterion can be expressed as (Holtz *et al.*, 1997):

$$FOS > bD_{15} \quad (2)$$

where D_{15} is the base soil particle diameter for which 15 % of the remaining soil particles are smaller and b is a number

which depends on the criterion considered and on soil characteristics (for instance, the soil coefficient of uniformity, $CU = D_{60}/D_{10}$). For less critical/less severe applications, Holtz *et al.* (1997) suggest $b = 3$ for soils with $CU > 3$. For soils with $CU \leq 3$ the filter should have the largest filtration opening size which attends the retention criterion. For critical/severe application these authors recommend the selection of a geotextile that meets the retention and permeability criteria and the performance of filtration tests with the same soil and hydraulic conditions expected in the field.

The durability criterion aims at guaranteeing that the geotextile will endure the typical damaging mechanisms present during handling, filter installation, construction activities etc., besides resisting to potential degradation mechanism with time. The criteria available are based on minimum required values of mechanical properties and resistance to damage and degradation (Holtz *et al.*, 1997).

Several experimental techniques provide index values of properties and tests may be carried out under conditions far from those expected in the field. For instance, most experiments do not consider the influence of the vertical stress on the geotextile, geotextile tensile strains, impregnation of geotextile voids by base soil particles and type of soil underneath the geotextile layer. An example of a field situation where partial clogging of the geotextile can take place due to impregnation by fill particles is shown in Fig. 3. Intrusion of soil particles in the geotextile voids can occur during soil spreading and compaction. Soil particles carried by seepage forces can also wind up entrapped in the fibre matrix of the filter. The level of geotextile impregnation, λ , defined as the ratio between the mass of soil particles in the geotextile voids and the mass of geotextile fibres,

is greater for fine cohesionless soils, varying typically between 2 and 15 depending on soil type, compaction technique and geotextile properties (Palmeira & Gardoni, 2000b, Palmeira *et al.*, 2005). Thus, in-service conditions can be quite different from those simulated in common laboratory tests. Under the conditions shown in Fig. 3, when fluid flow starts, the filter will have different pore dimensions (if impregnation is significant) and will be compressed by the weight of soil layers and surcharges. Both conditions are not simulated in routine laboratory tests for the determination of geotextile filtration opening size.

Bearing in mind the possible influences of field conditions on the geotextile filter behaviour, this paper aims at discussing some experimental and theoretical approaches for the prediction of the behaviour of geotextile filters in geotechnical and geoenvironmental applications.

2. Some experimental techniques to evaluate geotextile filter properties and performance

2.1 The gradient ratio test

Different laboratory experimental techniques can be used to study the behaviour of geotextile filters. A simple and traditional method is the use of conventional permeameters, where the soil of interest is placed on the geotextile filter and the test is executed in a similar way as a conventional soil permeability test. One type of test which has been commonly used to assess soil-filter compatibility for soils with permeability coefficients greater than 10^{-7} m/s is the Gradient Ratio Test (GR test). This type of test is illustrated in Fig. 4 and the gradient ratio (GR) is defined as:

$$GR = \frac{i_{LG}}{i_s} \quad (3)$$

where i_{LG} is the hydraulic gradient in a region including the geotextile (Fig. 4) and i_s is the hydraulic gradient in the soil, some distance from the soil-geotextile interface.

The standard version of the test as per ASTM (2012) adopts the distance L (Fig. 4) from the closest port to the geotextile layer equal to 25 mm and i_s being measured along a 50 mm segment of soil starting 25 mm above the geotextile-

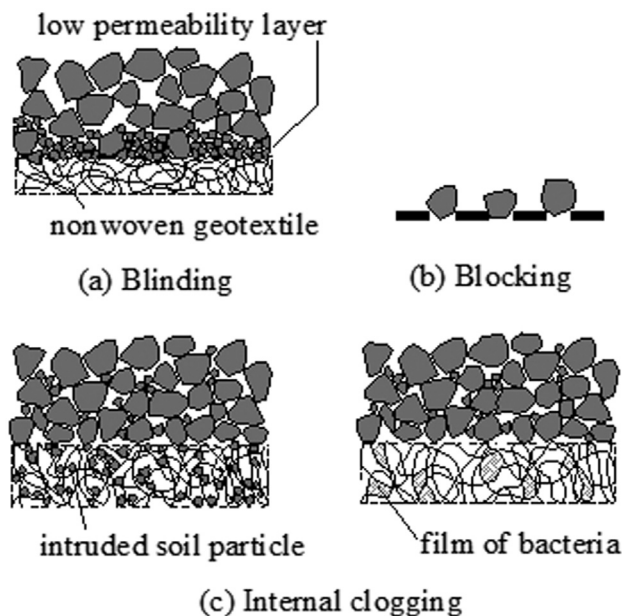


Figure 2. Clogging mechanisms in geotextile filters (modified from Palmeira 2018).

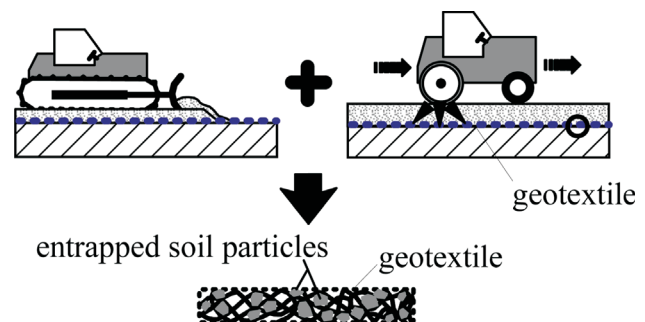


Figure 3. Geotextile impregnation by soil particles (modified from Bessa da Luz & Palmeira, 2006).

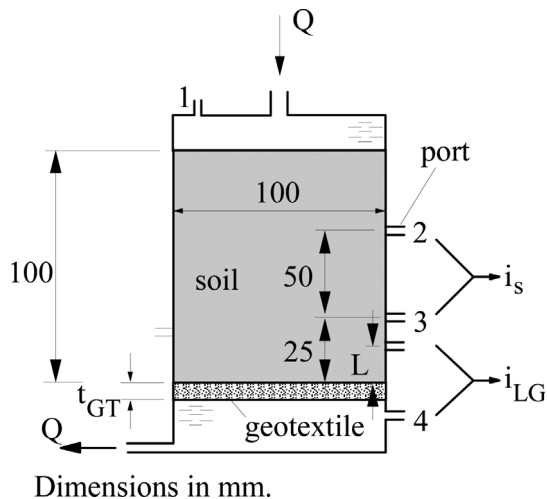


Figure 4. Typical gradient ratio test configuration (modified from Palmeira, 2018).

tile filter (Fig. 4). Other authors (Palmeira *et al.*, 1996, Gardoni, 2000) have used smaller values of L ($L = 3$ mm or 8 mm, for instance) in an attempt to capture soil-filter interaction closer to the soil-geotextile interface. In the standard procedure the test is carried out for different values of total hydraulic gradient of the system (gradient between ports 1 and 4 in Fig. 4) and without the application of vertical stress on the soil layer.

In practically all field situations the geotextile filter is buried in the soil. Therefore, a more realistic approach would be to conduct the GR test under confined conditions, with the application of vertical stress on the soil surface. Figure 5 shows an equipment developed at the University of Brasília (Gardoni, 2000), which can perform GR tests

with vertical stresses up to 2000 kPa on the soil-geotextile system.

2.2 Bubble point tests

The determination of geotextile pore sizes is of utmost importance for the design of geotextile filters. Simple sieving methods can be used, but they present some important limitation, such as influence of the test operator, vibration energy, electrostatic forces in dry sieving, different procedures depending on the standard considered etc. In addition, these tests do not simulate actual conditions of the filter in the field. A quicker, although rather more sophisticated, experimental technique consists of tests based on capillary flow and one that has gained increasing acceptance is the Bubble Point Test (*BBP*). Some of its advantages are that it is a quick and repeatable test and practically insensitive to the operator. It can also be adapted to perform tests under confinement and on partially clogged geotextile specimens. Figure 6 shows the *BBP* equipment developed at the University of Brasília, which allows the execution of tests on geotextiles subjected to confinement, partial clogging and tensile forces. The test consists in subjecting the geotextile specimen to gas flow under dry and wet conditions. The distribution of pore dimensions can be obtained from the relation between equivalent pore diameters and fluid pressures necessary to overcome the capillary forces in the pores for fluid intrusion, and from differences between flow rates under geotextile dry and saturated conditions. The results to be obtained depend on the fluid employed in the test and a capillary constant must be applied to correct the value of the equivalent pore diameter obtained. Details on test procedure can be found in ASTM (2011).

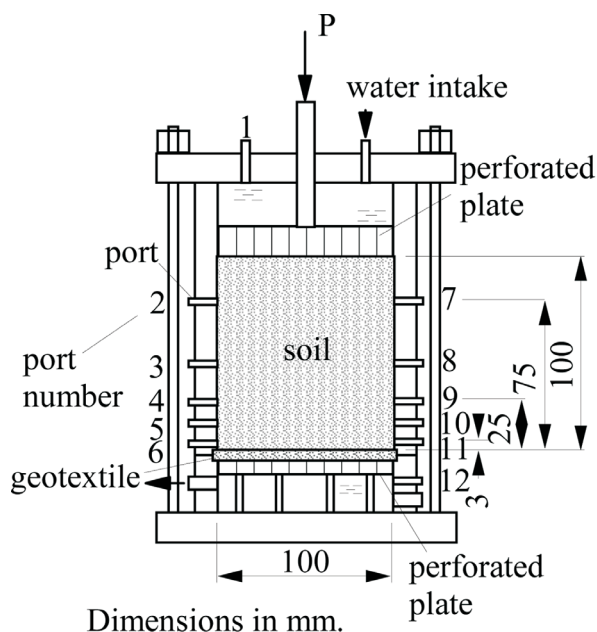
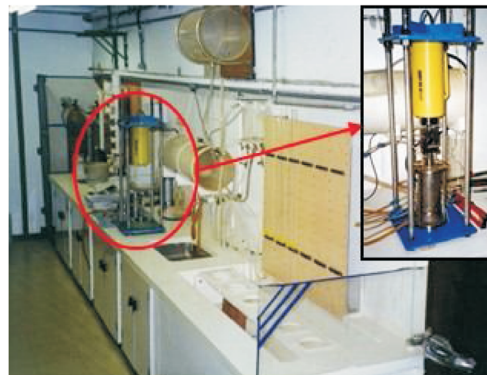


Figure 5. Gradient ratio test device for tests with confinement (modified from Palmeira *et al.*, 2005).



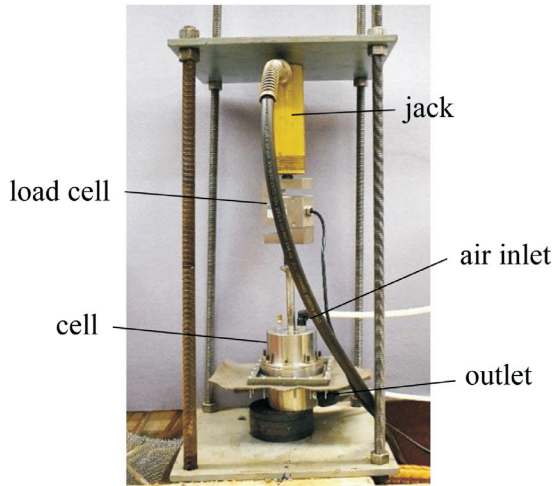


Figure 6. Bubble point test apparatus (Moraes Filho, 2018).

3. Some theoretical predictions of pore dimensions

Analytical and probabilistic solutions for the estimate of geotextile filtration opening size (*FOS*) have been proposed for nonwoven geotextiles. The first proposals were mainly based on geometrical models of varying degrees of complexity (Laflaive & Puig, 1974, Fayoux & Evon, 1982, for instance), as shown in Fig. 7, relating the filtration opening size with geotextile porosity (or thickness) and fibre diameter. One of the simplest versions of this type of approach leads to (Giroud, 1996):

$$\frac{O_F}{d_f} = \frac{\delta}{\sqrt{1-n}} - 1 \quad (4)$$

where O_F is the geotextile filtration opening size, d_f is the diameter of the fibres (assumed as cylindrical), n is the geotextile porosity and δ is a parameter which is a function of the spatial arrangement of the fibres assumed to model the geotextile, ranging from 0.89 to 1.65.

Giroud (1996) introduced an additional term in Eq. 4 dependent on the geotextile porosity, mass per unit area and fibre diameter, yielding to:

$$\frac{O_F}{d_f} = \frac{\delta}{\sqrt{1-n}} - 1 + \frac{\xi n}{\frac{M_A}{\rho_f d_f}} \quad (5)$$

where M_A is the geotextile mass per unit area, ρ_f is the density of the geotextile fibres and ξ is an empirical parameter. Giroud (1996) assumed δ equal to 1 and ξ equal to 10, the latter based on results of hydrodynamic sieving tests on unconfined nonwoven geotextiles.

Several probabilistic approaches for the estimate of geotextile filtration opening sizes can also be found in the literature (Gourc, 1982, Faure, 1988, Faure *et al.*, 1990, Lombardi *et al.*, 1989, Elsharief & Lovell, 1996, Urashima & Vidal, 1998, Rawal, 2010). Faure *et al.* (1990) presented an approach in which the nonwoven geotextile is assumed as a set of layers with a network of straight lines distributed based on the Poissonian polyhedral model, as schematically shown in Fig. 8. The geotextile is assumed as a succession of elementary layers, each layer with a thickness (T_e) equal to the fibre diameter (d_f) in Faure *et al.* (1990) original work. Based on probabilistic analysis, the following equations were derived for the determination of the probability of existing a pore smaller than an inscribed circle with a diameter equal to d in N elementary layers forming the geotextile:

$$Q(d) = 1 - [1 - G(d)]^N \quad (6)$$

with

$$N = \frac{t_{GT}}{T_e} \quad (7)$$

$$G(d) = 1 - \left(\frac{2 + \chi(d + d_f)}{2 + \chi d_f} \right)^2 e^{-\chi d} \quad (8)$$

and

$$\chi = \frac{4(1-n)}{\pi d_f} \quad (9)$$

where $Q(d)$ is the gradation of the pore conduits, d is the diameter of a circle inscribed between fibres, t_{GT} is the thick-

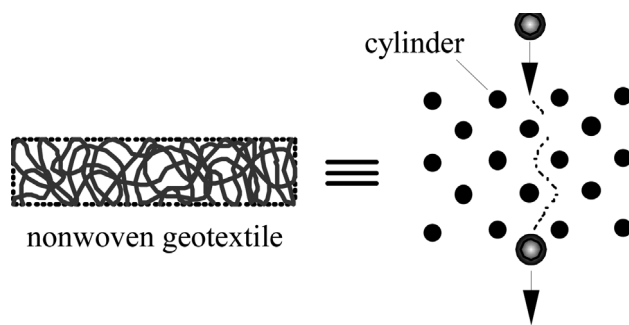


Figure 7. Nonwoven geotextiles modelled as an arrangement of cylinders.

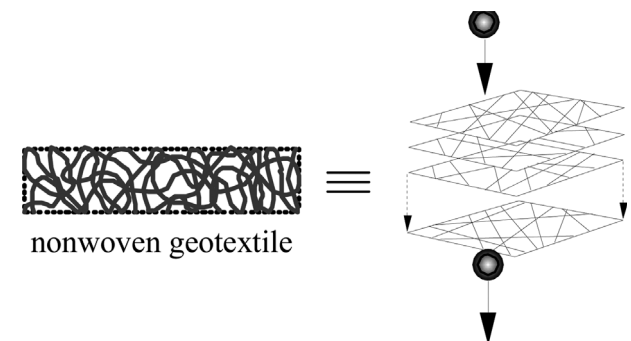


Figure 8. Nonwoven geotextile modelling approach used by Faure *et al.* (1989).

ness of the geotextile, T_e is the elementary layer thickness, $G(d)$ is the cumulative probability of obtaining an inscribed circle between the geotextile fibres of diameter equal to or less than d and d_f is the fibre diameter. The pore size distribution curve of a nonwoven geotextile can be obtained by solving Eqs. 6 to 9.

4. Behaviour of geotextile filters under different conditions

4.1 Influence of confinement

Nonwoven geotextiles are highly compressible materials which can be subjected to different levels of compres-

sive stress depending on the depth of installation of the filter, height and density of the overlying soil layer and presence of surcharges on the ground surface. Hence, confinement can significantly reduce geotextile pores and change filtration conditions. Figure 9 (Gardoni, 2000, Gardoni & Palmeira, 2002) presents microscopic views of cross-sections of a nonwoven geotextile (mass per unit area of 200 g/m^2) under vertical stresses varying from 2 kPa to 1000 kPa. A significant reduction of geotextile pores with increasing vertical stress can be observed.

Figure 10 depicts the pore size distribution curves of a nonwoven geotextile ($M_A = 200 \text{ g/m}^2$) obtained in confined Bubble Point tests, where it can also be seen that a signifi-

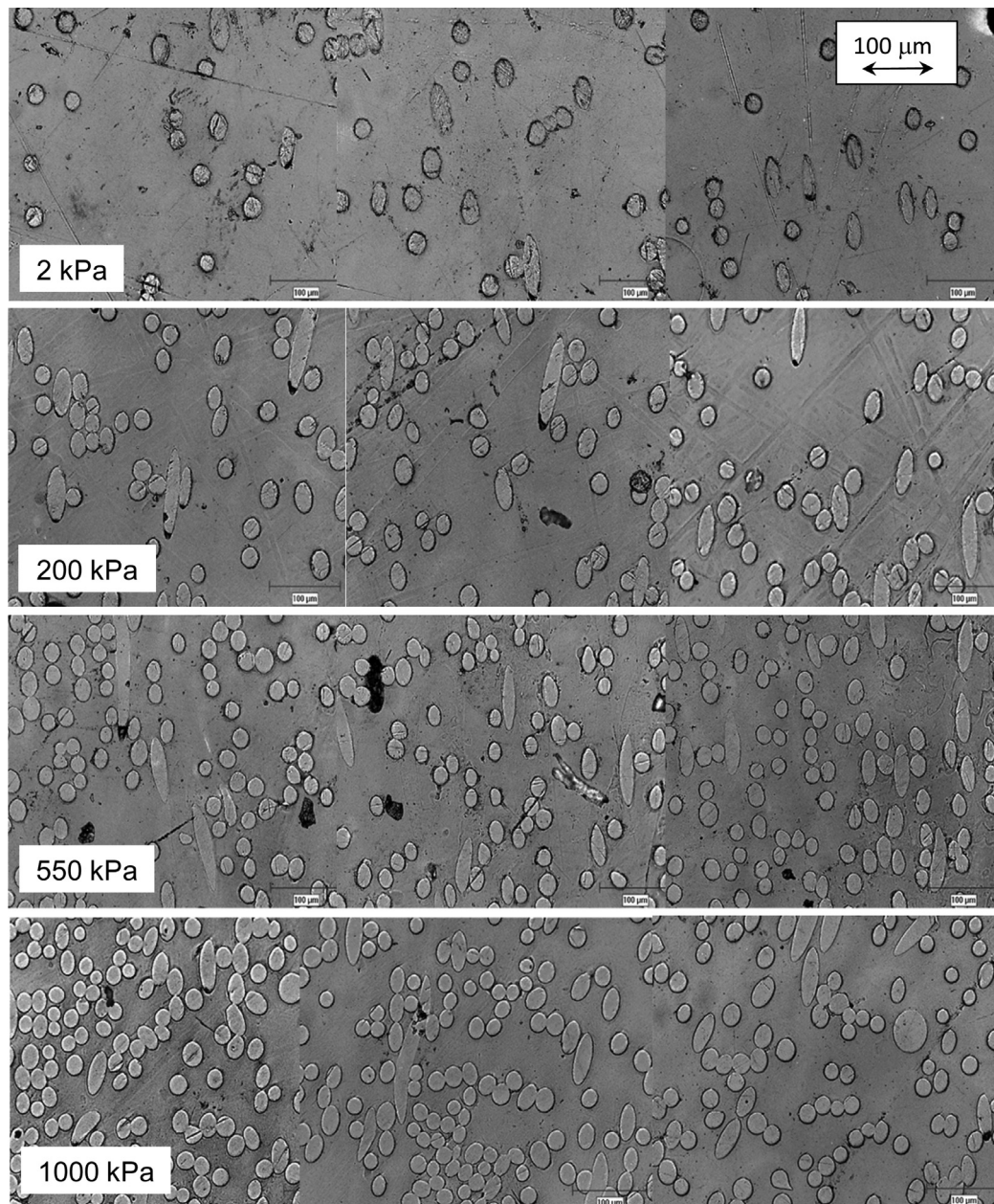


Figure 9. Images of cross-sections of a nonwoven geotextile under different normal stresses (Gardoni, 2000, Gardoni & Palmeira, 2002).

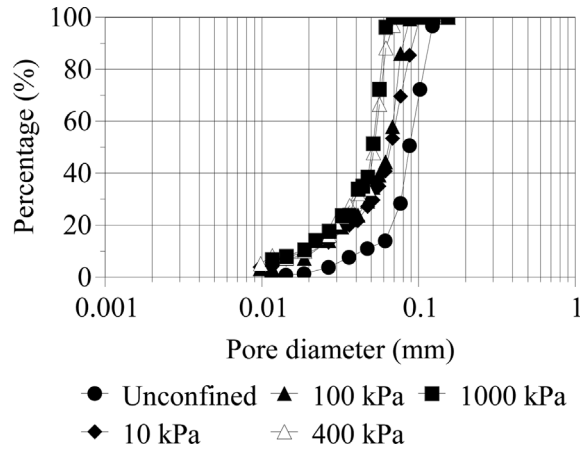


Figure 10. Pore diameter distribution curves of a nonwoven geotextile (Palmeira & Trejos-Galvis, 2017).

cant variation of pore diameters occurs, with less variation for large vertical stresses. From data like the ones presented in Fig. 10, the variation of geotextile filtration opening size (*FOS*) with confining stress can be obtained. Figure 11 shows the variation of *FOS* normalised by the geotextile fibre diameter (d_f) with vertical stresses obtained in Bubble Point Tests on a confined geotextile. In this case, *FOS* was assumed as being equal to O_{98} , which is the pore dimension for which 98 % of the remaining pores are smaller than that value. In this case, the geotextile was a nonwoven, needle-punched, geotextile, made of polyester, with a mass per unit area of 300 g/m². The reduction in O_{98} was more significant for confining stresses smaller than 400 kPa, beyond which O_{98} decreased at a smaller rate with vertical stress. The results in Figs. 10 and 11 illustrate how the filtration opening size value to be used in Eqs. 1 and 2 can be affected by geotextile filter confinement.

The variation of other values of pore dimension (κ from 5 % to 98 %) with vertical stress for a 200 g/m² nonwoven geotextile is shown in Fig. 12, where it can be

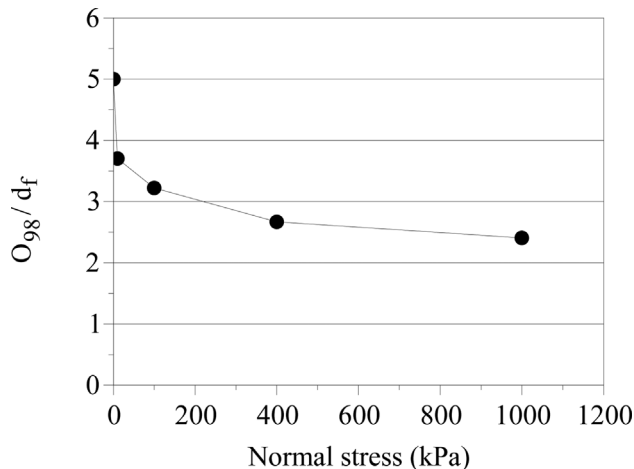


Figure 11. Typical variation of filtration opening size with vertical stress (Trejos-Galvis, 2016).

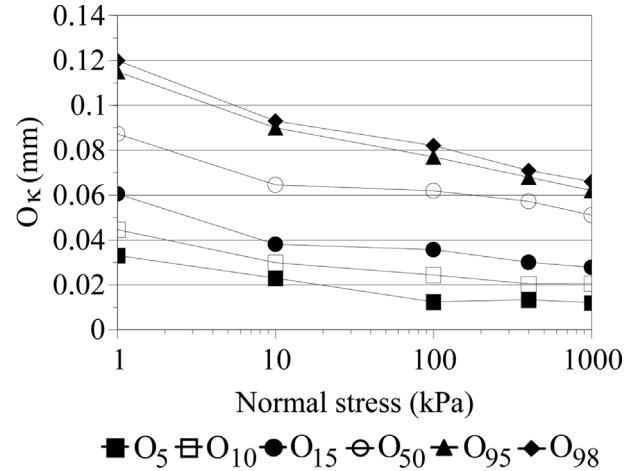


Figure 12. Variation of geotextile pore diameters with vertical stress.

seen that for a stress of 1 kPa a significant fraction of geotextile pore dimensions falls in the range of particle sizes of coarse silts to fine sands. For vertical stresses greater than 10 kPa, most of the geotextile pores fall in the range of diameters of particles of silts to very fine sands. Thus, due care must be taken when geotextile filters are used in cohesionless internally unstable silts and fine sands. In these cases, the movement of fine-grained soil particles may cause filter clogging.

It is clear from Figs. 9 to 12 that confinement changes the retention capacity and filtration properties of geotextile filters. However, in the tests reported in these figures soil is not in contact with the geotextile, which is the actual condition in the field. In this context, a useful test that can simulate conditions closer to those in the field is the Gradient Ratio test. Figure 13 shows results of compatibility tests using the Gradient Ratio test in terms of gradient ratio (*GR*) vs. normal stress (Palmeira *et al.*, 2010). The soil tested was a potentially internally unstable mining tailings with $D_{85} = 0.251$ mm, $D_{50} = 0.128$ mm, $D_{15} = 0.066$ mm, coefficient of uniformity (*CU*) of 3.7, coefficient of curvature (*C_c*) equal to 0.9 and a percentage of particles smaller than

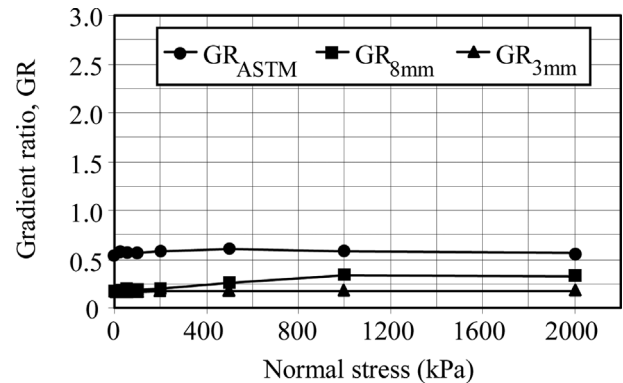


Figure 13. *GR* vs. normal stress for an internally unstable mining tailings (Palmeira *et al.*, 2010).

0.074 mm equal to 29 %. The geotextile tested was a nonwoven, needle-punched geotextile, made of polyester, with a mass per unit area of 627 g/m^2 and FOS (data from the manufacturer's catalogue from sieving tests) ranging from 0.06 mm to 0.13 mm. The total hydraulic gradient (hydraulic gradient between ports 1 and 12 in Fig. 5) applied to the system was equal to 1. Significantly low values of GR can be observed, indicating severe piping in the vicinity of the filter, particularly for measurements closer to the geotextile filter ($GR_{3 \text{ mm}}$ and $GR_{8 \text{ mm}}$, see Fig. 5). However, the values of GR kept constant with increasing vertical stress, showing a stable behaviour of the system for the conditions and duration of the test.

Figure 14 presents the variation of GR with vertical stress in a test on a confined residual soil-geotextile system (Palmeira *et al.*, 2005). In this test, a potentially internally unstable residual soil was used, with the following grain size characteristics: $D_{85} = 0.34 \text{ mm}$, $D_{50} = 0.2 \text{ mm}$, $D_{10} = 0.01 \text{ mm}$, coefficient of uniformity (CU) of 21, coefficient of curvature (C_c) equal to 12.2 and a percentage of particles smaller than 0.074 mm equal to 20 %. The geotextile filter consisted of a nonwoven, needle-punched, geotextile with M_A equal to 300 g/m^2 and unconfined value of

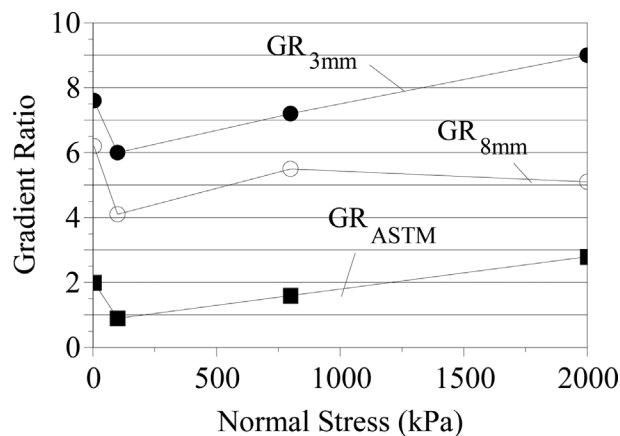


Figure 14. GR vs. normal stress for an internally unstable residual soil (Palmeira *et al.*, 2005).

FOS equal to 0.11 mm. The hydraulic gradient of the system was equal to 1. Figure 14 shows increasing values of GR with vertical stress, almost reaching the ASTM acceptance limit of 3 for 2000 kPa vertical stress. The values of GR measured closer to the soil-geotextile interface ($GR_{3 \text{ mm}}$ and $GR_{8 \text{ mm}}$) were more sensitive to the vertical stress increase. Although good performance of geotextile filters has been reported in the literature (Palmeira *et al.*, 1996, Palmeira & Gardoni, 2000a, Palmeira & Fannin, 2002, Palmeira *et al.*, 2010), the results in Figs. 13 and 14 highlight the importance of investigating the performance of geotextile filters in contact with internally unstable soils, particularly in tests with long durations.

4.2 Influence of partial clogging

Partial clogging of the geotextile filter can take place before water flow due to soil spreading and compaction over the filter layer (Fig. 3), which will cause some level of impregnation of the geotextile voids. Additional impregnation can be caused by soil particles carried by the water during operational conditions of the filter. The effect of partial clogging due to soil particles impregnation was first highlighted by Masounave *et al.* (1980) and Heerten (1982). Rather large soil particles can be forced into the geotextile voids, depending on the soil type and compaction characteristics employed in the field. Figure 15 shows examples of a large soil grain and soil particle clusters entrapped in a geotextile filter exhumed from a drain in BR-020 highway, close to Brasília, Federal District, Brazil (Gardoni & Palmeira, 1998, Gardoni, 2000). Palmeira *et al.* (2005) also observed the entrapment of large soil particles in the voids of nonwoven geotextiles.

It has been observed that impregnation of the geotextile by soil particles reduces its compressibility (Palmeira *et al.*, 1996, Palmeira & Gardoni, 2000b, Palmeira & Fannin, 2002, Palmeira *et al.*, 2005, Palmeira & Trejos-Galvis, 2017). So, the greater the impregnation level (λ) of the geotextile the less it compresses under confinement. For a given vertical stress, a clean geotextile may be even more

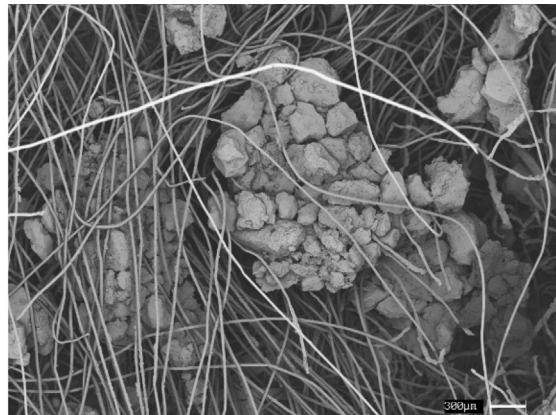


Figure 15. Entrapped soil particles in a geotextile filter exhumed from a drain in BR-020 highway (Gardoni, 2000).

compressible than an impregnated one. Figure 16 illustrates this by means of compression tests carried out on a nonwoven geotextile ($M_A = 200 \text{ g/m}^2$) under virgin (clean) and partially clogged conditions, where it can be seen the reduction of geotextile compressibility as λ increases. The presence of the soil particles inside the geotextile voids will reduce the sizes of the pores through which additional particles may pass, increasing geotextile retention capacity and modifying the conditions for further clogging of the geotextile to take place. For heavier nonwoven geotextiles, it has been noticed that impregnation tends not to be uniform along the entire geotextile thickness, with greater particle entrapment in the region closer to the geotextile surface (Palmeira & Trejos-Galvis, 2017).

Palmeira and Trejos-Galvis (2017) performed *BBP* tests to assess the influence of confinement and partial clogging on geotextile pore dimensions. Figure 17 shows the variation of *FOS* (assumed as O_{95}) normalised by the geotextile fibre diameter with the level of impregnation obtained in tests on unconfined nonwoven polypropylene and polyester geotextiles (M_A ranging from 200 g/m^2 to 1800 g/m^2). A significant influence of the level of impregnation of the geotextile on the value of O_{95} can be noticed. This shows that if the geotextile filter is impregnated before fluid flow starts, its retention capacity may be significantly increased. The combined effect of impregnation and confinement is to reduce even further the value of O_{95} , as shown in Fig. 18, for tests on a nonwoven geotextile ($M_A = 200 \text{ g/m}^2$, corresponding to G3 in Fig. 17) with varying values of λ .

Partial clogging and confinement also influence the geotextile coefficient of permeability. However, because partially clogged geotextiles are less compressible than vir-

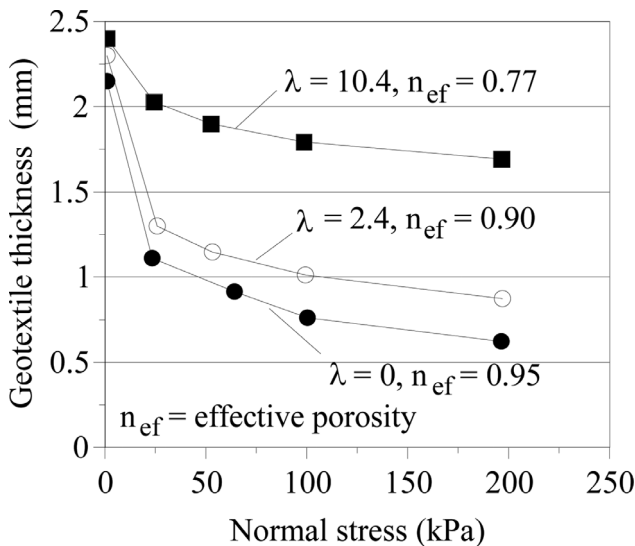


Figure 16. Compression tests on virgin and partially clogged geotextile (Palmeira *et al.*, 1996).

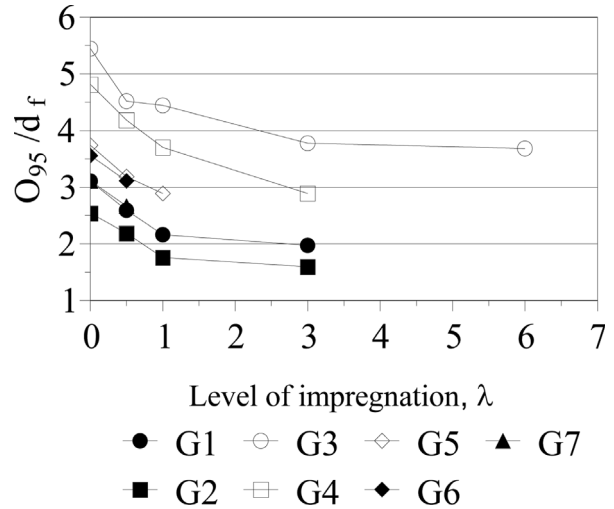


Figure 17. Filtration opening size vs. level of impregnation in unconfined *BBP* tests (Palmeira & Trejos-Galvis, 2017).

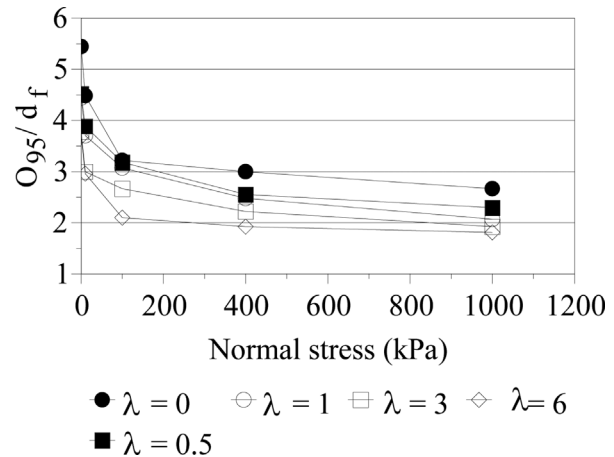


Figure 18. Influence of impregnation and confinement.

gins ones, for a given vertical stress the coefficient of permeability of a partially clogged nonwoven geotextile may be even greater than that of the same geotextile under virgin conditions, depending on the vertical stress and level of impregnation considered (Palmeira *et al.*, 2005). Palmeira *et al.* (2005) estimated reduction factors for geotextile permeability (defined as the ratio between the permeability coefficients of virgin, k_σ , and partially clogged, $k_{\sigma-pc}$, geotextiles under the same vertical stress, σ) varying between 0.3 ($k_{\sigma-pc} > k_\sigma$) and 21.7 in Gradient Ratio tests with nonwoven geotextiles and different soils, including residual soils and mining wastes. These authors also estimated ratios between the coefficients of permeability of confined and partially clogged geotextiles and those of the base soils tested, reaching ratio values varying between 1.3 and 10000, showing that the tested geotextiles attended satisfactorily permeability criteria. Figure 19 shows some of the results of $k_{\sigma-pc}/k_\sigma$ obtained in tests with some geotextile-residual soil combinations (Palmeira *et al.*, 2005).

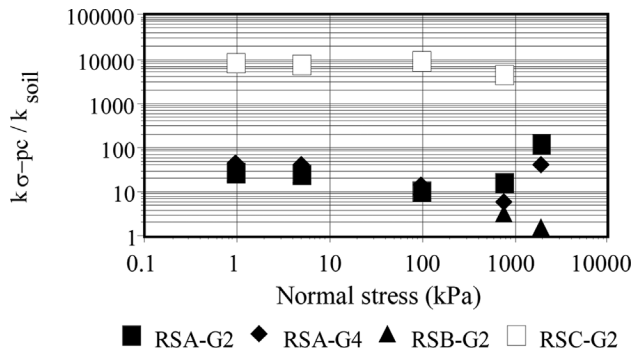


Figure 19. Permeability coefficient ratio vs. confining stress (Palmeira *et al.*, 2005).

4.3 Influence of tensile strains

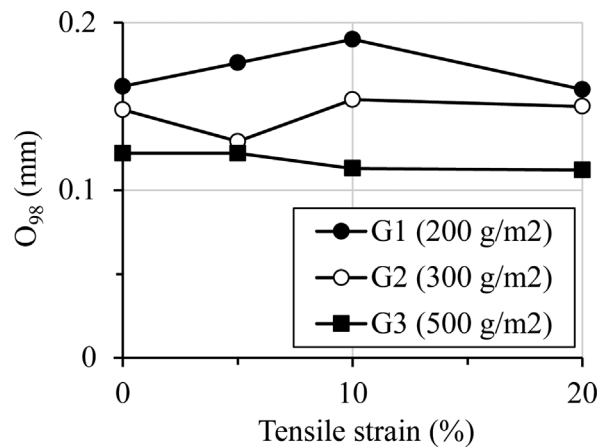
A geotextile may be subjected to tensile strains in some applications, such as in geotextile tubes, silt fences, drainage layers at the base of embankments on compressible grounds and geotextile separators in roads and railways. Thus, if the geotextile is tensioned, some changes in its pore dimensions should be expected.

Several researchers have investigated the behaviour of tensioned geotextile filters (Fourie & Kuchena, 1995, Fourie & Addis, 1997 and 1999, Moo-Young & Ochola, 1999, Wu *et al.*, 2008, Wu & Hong, 2016, Palmeira *et al.*, 2012, Melo, 2018, Moraes Filho, 2018, Palmeira *et al.*, 2019) and different trends of geotextile pore size variation with tensile strain have been reported. These differences in results may have been a consequence of different types, properties and microstructure of the geotextile products tested, different testing equipment and testing conditions.

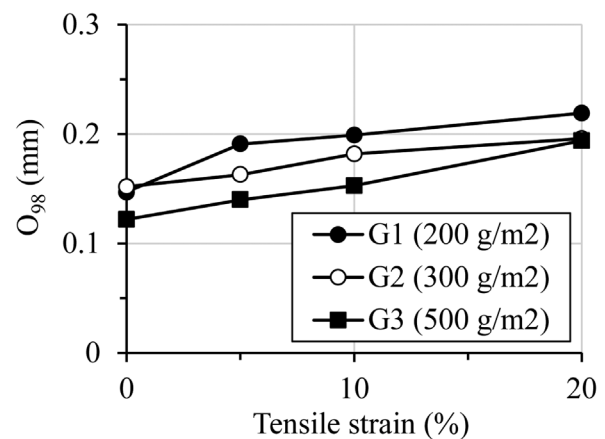
Palmeira *et al.* (2019) report results of Bubble Point Tests on nonwoven, needle-punched geotextiles, made of polyester, subjected to tension and confining stresses. The masses per unit area of the geotextiles tested varied between 200 g/m² and 500 g/m². Figure 20 shows some of the results obtained in terms of the variation of O_{98} with tensile strain obtained in tests on unconfined nonwoven (needle-punched) geotextiles tensioned under plane strain (Fig. 20a) and biaxial strain (Fig. 20b, with $\varepsilon_x = \varepsilon_y$) conditions. Figure 20(a) shows no consistent trend for the variation of O_{98} with strain under plane strain conditions. However, a consistent increase in geotextile filtration opening size can be seen in Fig. 20(b) for tests under biaxial conditions with the same strain value in both x and y directions. Palmeira *et al.* (2019) observed the latter to be the most critical situation in terms of filtration opening size increase with tensile strain. These authors also observed that confinement reduces the pore sizes of tensioned nonwoven needle-punched geotextiles.

Nonwoven, needle-punched, geotextiles are fibrous materials and tensile loads will cause their fibres to be stretched and displaced. Hence, depending on the magnitude and orientation of the tensile load, the largest pore may

have its size reduced and another pore may increase in size, eventually becoming the new filtration opening size under tension. A rather crude exemplification of this can be seen in Fig. 21, where a nonwoven geotextile was simulated by a set of intertwined strings. The set of strings was then subjected to different tensile strains. Figure 21(a) shows a situation where the set of strings was deformed under plane strain conditions to a tensile strain of 13.6 %. The largest inscribed circles in between strings are identified before and after deformation. In this case it can be noted that the tensile strain reduced the size of the largest inscribed circle. However, for the string arrangement shown in Fig. 21(b) the size of the largest inscribed circle increased after a tensile strain of 10.5 %, also under plane strain conditions, suggesting the influence of the initial fibre arrangement on the variation of pore sizes. Figure 21(c) shows a set of fibres before and after a biaxial tensile strain of 8.8 %. In this case, it is clear that the size of the maximum inscribed circle increased. Thus, despite the limitations of the experiment, the results in Fig. 21 suggest that the fibre arrangement, strain



(a) Plane strain condition



(b) Biaxial strain condition ($\varepsilon_x = \varepsilon_y$)

Figure 20. Results of Bubble Point Tests on tensioned geotextiles (modified from Palmeira *et al.*, 2019).

orientation and strain level may influence how the filtration opening size of a tensioned nonwoven geotextile will vary

and are consistent with the results of Bubble Point Tests shown in Fig. 20.

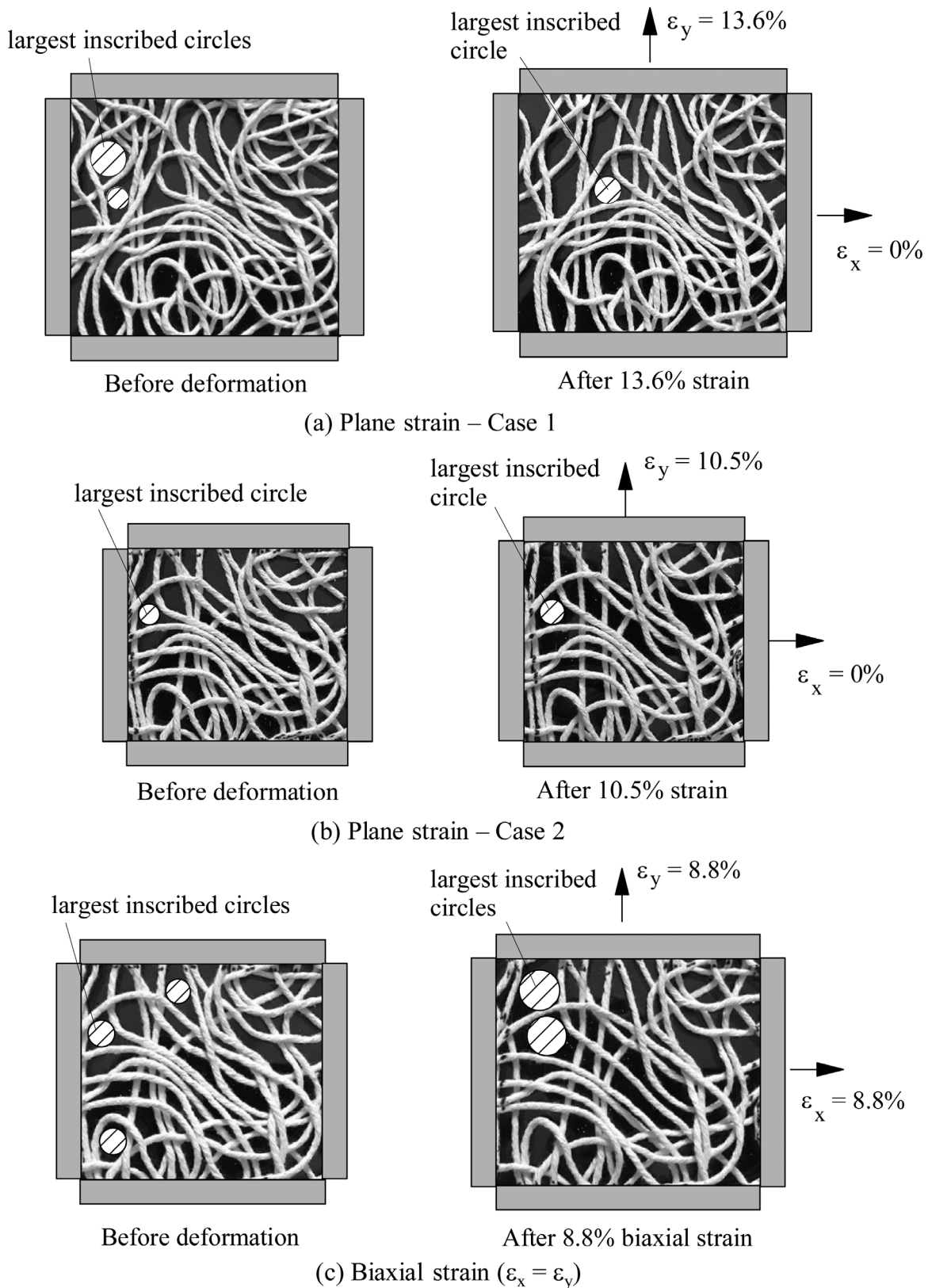


Figure 21. Deformation of model nonwoven geotextiles under tension.

The presence of a coarse granular layer underneath the geotextile may also cause significant tensile strains in the filter due to sagging in the voids between soil particles. Spreading and compaction of the base soil on the filter layer is likely to enhance filter sagging and deformation, as schematically shown in Fig. 22, particularly for fine-grained base soils, heavy compaction and thin base soil covers.

Palmeira *et al.* (2012) evaluated the retention capacity of geotextiles in tests under vertical confining stresses up to 2000 kPa with the nonwoven geotextile filter on a granular bedding material with round or angular particles distributed in plan in a triangular pattern, as shown in Fig. 23. The deformed shape of the geotextile was obtained at the end of each test, which allowed the measurement of average geotextile tensile strains. Figure 24 shows geotextile tensile strain vs. vertical stress (σ_v , Fig. 23) at the top of the base soil (50 mm thick) for varying values of the ratio between spherical particles spacing (s) and particle diameter (d) in some of the tests performed (Palmeira *et al.*, 2012). It can be noted that significant geotextile tensile strains can be mobilized, depending on the ratio s/d and ver-

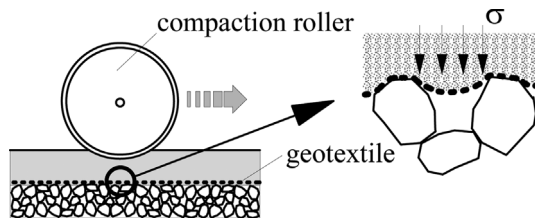


Figure 22. Sagging of geotextile filter in the voids of coarse drainage layer.

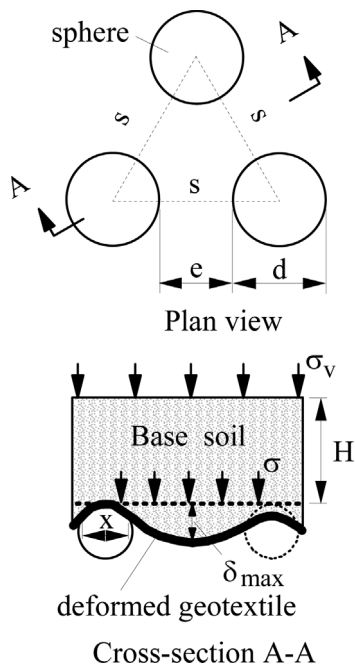


Figure 23. Distribution of underlying granular layer particles (modified from Palmeira *et al.*, 2012).

tical stress considered. Tests with the bedding material consisting of gravel showed that the strains in this case can be significantly greater than those obtained for spherical particles.

The results in Fig. 24 show that a geotextile filter on a coarse granular layer may work under tension. The greater the sagging of the geotextile in the voids of the bedding layer, the greater the tensile strain mobilised. This highlights the importance of good construction practices and careful base soil compaction. Thin soil layers associated with high compaction energies may cause significant geotextile sagging or even filter mechanical damage.

5. Accuracy of some methods to predict of geotextile pore dimensions

5.1 Analytical methods

Most analytical methods to predict filtration opening sizes are simple to use, and researchers have investigated their limitations and accuracy. Gardoni & Palmeira (2002) backanalysed values of δ in Eq. 4 from results of *BBP* tests on confined nonwoven, needle-punched, geotextiles made of polyester, with masses per unit area varying between 200 g/m² and 600 g/m². Figure 25 shows the best comparisons between predictions and measurements, which were obtained for a value of δ equal to 1.6. This figure shows a significant scatter between predicted and measured values of O_{98} .

Giroud (1996) reports good agreement between predictions by Eq. 5 and results of sieving tests on unconfined nonwoven geotextiles for a value of δ equal to 1 and ξ equal to 10. Palmeira & Trejos-Galvis (2018) backanalysed values of δ and ξ using results of *BBP* tests under confinement (vertical stresses between 0 and 1000 kPa) on five nonwoven, needle-punched, geotextiles made of polyester, with M_A values ranging from 200 g/m² to 1800 g/m². An average value (coefficient of variation of 9.84 %) of ξ equal to 4.369

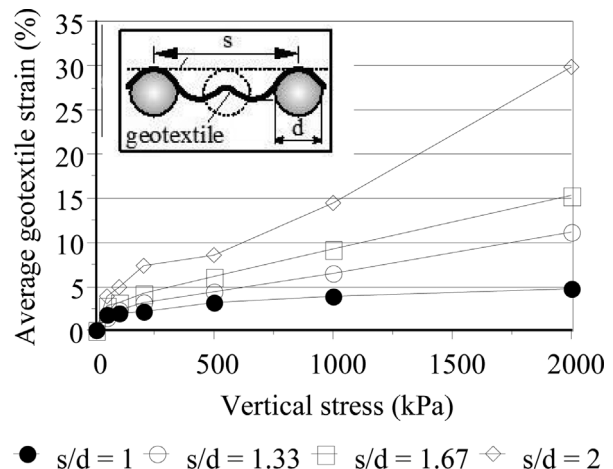


Figure 24. Average geotextile strain vs. vertical stress (Palmeira *et al.*, 2012).

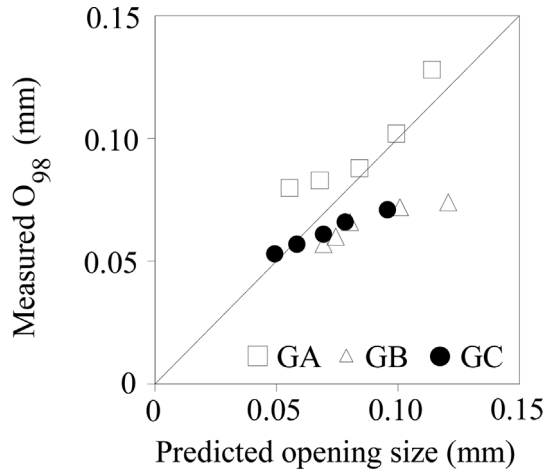


Figure 25. Comparisons between measurements and predictions by Eq. 4.

was obtained for the best fit (Fig. 26) between predicted and observed results and the following equation ($R^2 = 0.97$) was derived for the value of δ for best fit:

$$\delta = 0.6056 - 0.0093\kappa \quad (10)$$

where κ is the percentage considered for the pore opening ($10\% \leq \kappa \leq 98\%$).

From Figs. 25 and 26 it is clear that Eq. 5 can provide more accurate predictions of geotextile filtration opening sizes than Eq. 4. Palmeira & Trejos-Galvis (2017) also observed rather satisfactory comparisons between predictions by Eq. 5 and measurements in the case of tests on confined and partially clogged nonwoven, needle-punched, geotextiles (M_A between 200 g/m^2 and 1800 g/m^2). However, in this case δ for best fit varied between 1.0 and 1.38, and ξ varied between 12.5 and 15.0, depending on the geotextile and level of impregnation (λ) considered.

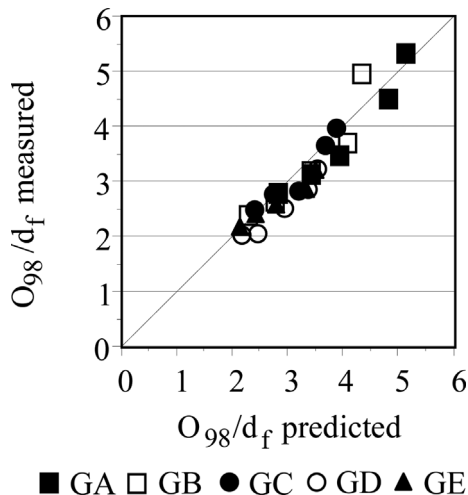


Figure 26. Comparisons between measurements and predictions by Eq. 5 (Palmeira & Trejos-Galvis, 2018).

The results presented above show that Eq. 5 (Giroud, 1996) can be a useful tool for the prediction of nonwoven geotextile filtration opening size under confined conditions. However, further studies should be carried out to check the accuracy of such predictions for other geotextile products, since polymer type, fibre characteristics and manufacturing process are factors that may certainly influence the values of δ and ξ .

5.2 Faure *et al.* method

As described earlier, Faure *et al.* (1990) presented a probabilistic method for the estimate of geotextile pore sizes. Gardoni & Palmeira (2002) and Palmeira & Trejos-Galvis (2018) observed that predictions by the method are very sensitive to the value of the thickness of the elementary layer (T_e , Eq. 7) adopted. In their original work, Faure *et al.* adopted a value of T_e equal to the geotextile fibre diameter (d_f). Palmeira & Trejos-Galvis (2018) developed an equation to estimate the value of T_e , for which the predictions best fitted the results of *BBP* tests on five nonwoven, needle-punched geotextiles, made of polyester, with M_A varying between 200 g/m^2 and 1800 g/m^2 and for vertical stresses in the range 0 kPa to 1000 kPa. The optimum value of T_e was observed to be a function of the geotextile mass per unit area, fibre diameter, fibre density and the percentage κ for which the value of O_κ is calculated. Figure 27 shows comparisons between measurements of O_{98}/d_f and predictions by Faure *et al.* (1990) when optimum values of T_e were used in Eq. 7. A good agreement between measurements and predictions can be seen. Palmeira & Trejos-

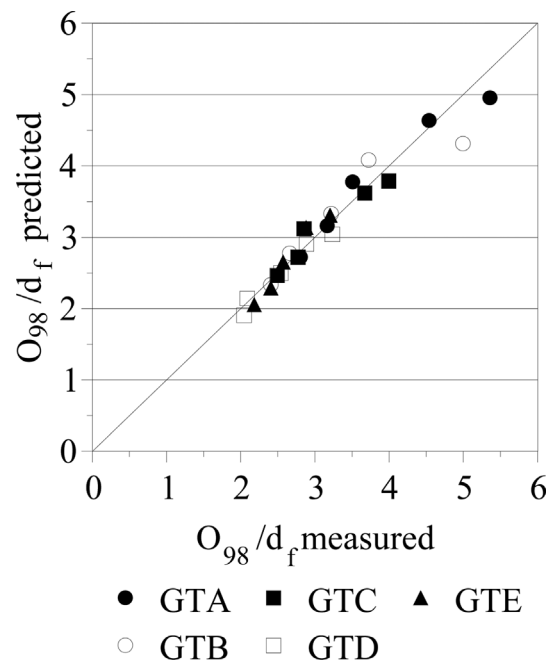


Figure 27. Comparisons between O_{98}/d_f values measured and predicted O_{98}/d_f by Faure *et al.* (1990) (modified from Trejos-Galvis, 2016).

Galvis (2018) also observed that satisfactory predictions of geotextile pore size distribution curves can be obtained by Faure *et al.*'s method if appropriate values of T_e are used in the calculations.

5.3 Upper bound for tensioned nonwoven geotextile filter

Despite satisfactory agreement between predictions and measurements can be achieved by the methods described above, they still do not truly consider actual field situations, where a base soil is in contact with the geotextile filter. In addition, they do not account for the presence of a drainage soil layer underneath the geotextile filter, as it would be the case in most geotextile filter applications. As shown earlier in this paper, the presence of a coarse granular layer underneath the geotextile may cause significant tensile strains in the filter due to its sagging in the voids between soil particles.

As an approximation, the situation in Fig. 23 can be assumed as similar to a soil layer overlying a cavity. Giroud *et al.* (1990) presented a theoretical solution for the estimate of vertical stresses on a cavity underlying a fill material reinforced with a geosynthetic layer at the fill base, as well as the average strain in the deformed geosynthetic as a function of the geotextile deflection in the void. Palmeira *et al.* (2012) extended the solution by Giroud *et al.* (1990) to the situation presented in Fig. 23. These authors observed that the solution presented by Giroud *et al.* (1990) to predict strains in a geosynthetic layer overlying a cavity yielded satisfactory predictions for the tensile strains in geotextile filters overlying granular drainage layers consisting of steel spheres when the measured geotextile deflection in the void was used in the calculations.

The influence of tensile strains and confinement on geotextile opening sizes was investigated by Palmeira *et al.* (2019) by means of Bubble Point tests (Fig. 6) for vertical

stresses in the range 0 to 1000 kPa and geotextile strains in the range 0 to 20 %. In the tests the geotextile layers were tensioned under uniaxial, plane strain and biaxial conditions. The authors also developed equations to estimate an upper bound for geotextile filtration opening sizes of tensioned geotextile filters based on the deformation of initially circular holes in a homogeneous layer subjected to large equal orthogonal tensile strains (worst case scenario, as commented earlier in this paper). Figure 28 shows upper bounds for the ratio O_e/O_o for geotextile Poisson ratios of 0.3 and 0.5, where O_e is the filtration opening size of the tensioned geotextile and O_o is the initial filtration opening size. This figure also shows results of O_e/O_o (with $O_e = O_{98}$) obtained in *BBP* tests on a tensioned nonwoven, needle-punched, geotextile made of polyester (code G3, $M_A = 500 \text{ g/m}^2$) vs. tensile strain under different strain conditions. The results in this figure show that a value of Poisson ratio (ν) of 0.3 yielded a satisfactory upper bound for the filtration opening size of the tensioned geotextile. Similar results were obtained for other geotextiles tested. Palmeira *et al.* (2019) also observed that the vertical stress had the beneficial effect of reducing the filtration opening size of the tensioned geotextile.

Figure 29 depicts a comparison between the upper bound for filtration opening sizes of tensioned geotextiles (Palmeira *et al.*, 2019) and the maximum diameter (D_{95}) of particles that actually passed through the filter (nonwoven geotextile, $M_A = 200 \text{ g/m}^2$) in Gradient Ratio tests under confinement (Palmeira *et al.*, 2012). In these tests a layer consisting of 18 mm diameter steel spheres with spacing to diameter ratios (s/d , Fig. 23) of 1 and 2 was used to simulate a granular drainage layer underneath the geotextile filter. Vibration and water flow were the mechanisms used to cause piping of soil particles through the geotextile. It should be pointed out that the vertical stress (σ) considered in Fig. 29 is that acting on the voids between bedding layer

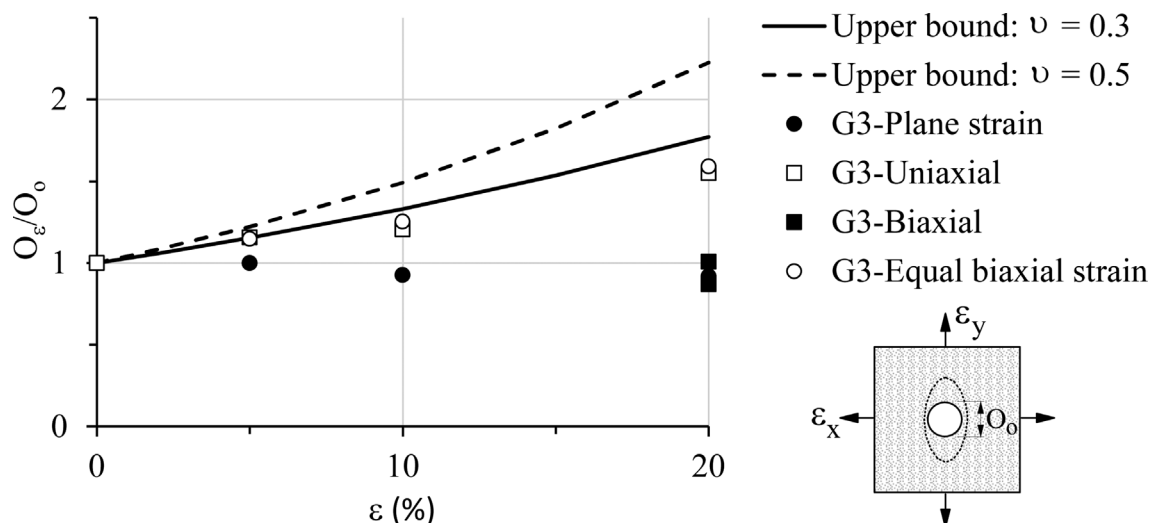


Figure 28. Upper bound for filtration opening size of tensioned geotextiles (modified from Palmeira *et al.*, 2019).

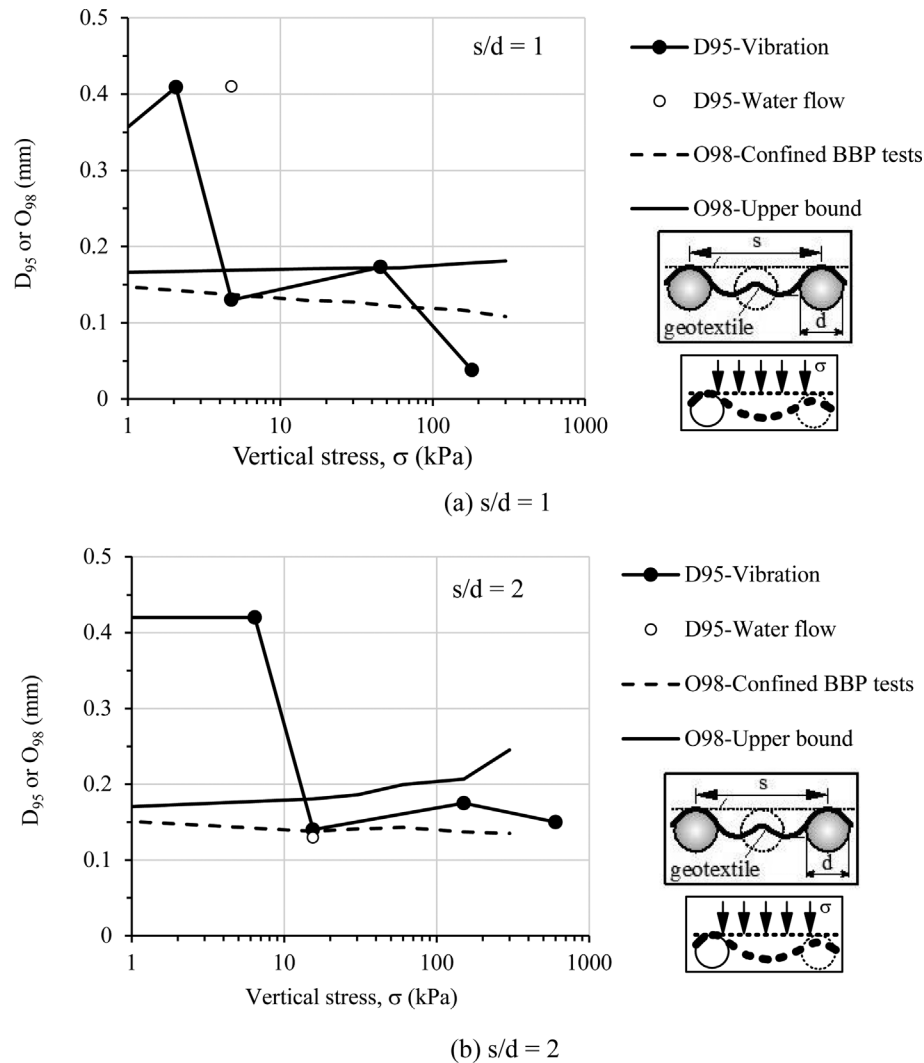


Figure 29. Maximum piped soil particle diameter for a nonwoven geotextile filter overlying a granular drainage layer.

particles and was calculated using the method presented by Giroud *et al.* (1990), as described in Palmeira *et al.* (2012). The variation of O_{98} with σ for the same geotextile, also shown in Fig. 29, was obtained from *BBP* tests on confined and tensioned geotextiles (no drainage layer underneath the filter, Moraes Filho, 2018 and Palmeira *et al.*, 2019). A geotextile Poisson ratio of 0.3 was used to obtain the upper bound for a tensioned geotextile filtration opening size shown in Fig. 29. The results in this figure show piping of large particles, considerably greater than the expected upper bound, for low vertical stresses. This can occur due to large soil particles being pushed through the voids of the geotextile (or through holes left by the needle-punching manufacturing process of the geotextile) during base soil compaction (see Fig. 15, for instance) or as a consequence of the action of high seepage forces. However, the amount of such large piped particles was observed to be very small for the conditions of the tests performed. For greater vertical stresses, the maximum diameters of piped particles

were smaller than the predicted upper bound. It is also interesting to note that for vertical stresses greater than 6 kPa the values of D_{95} of the piped particles oscillated around the curve of O_{98} from *BBP* tests on the confined and tensioned geotextile vs. vertical stress (Fig. 29a) or were a little greater (Fig. 28b). Despite the limited amount of data available, the results in Fig. 29 are encouraging regarding possible predictions of filtration opening sizes of tensioned nonwoven, needle-punched, geotextiles for retention capacity evaluation under more realistic situations.

6. Conclusions

Geotextiles have been highly successful as filters in geotechnical engineering works. Bearing in mind the enormous number of works where these filters were used so far, the number of reported failures can be considered as extremely low. In most of these failures the conditions would also be troublesome for sand filters. Unfortunately, some unsatisfactory performance of geotextile filters has still

been a consequence of lack of proper design of the system, wrong product specification or installation. Not rarely, geotextiles are still specified by their prices by inexperienced designers rather than based on sound filter criteria requirements. Besides, it is also common the lack of care during installation and construction works in the field. So, most of the reported unsatisfactory performance might have been avoided or its consequences minimized if appropriate design and specification had been exercised.

Nowadays, several filter criteria, standards, testing techniques and recommendations on geotextile filters are available. Atypical liquids and soils, such as internally unstable soils, are of concern. Thus, the possibility of base soil internal instability should be investigated, and proper filtration tests performed for such situations, as well as for any other possible atypical condition.

This paper addressed some factors that may influence geotextile filter performance, focusing on the behaviour of nonwoven, needle-punched, products. Factors such as confinement, impregnation by soil particles, tensile strains and filter intrusion in the voids of coarse drainage layers were discussed. For some of these situations there are already experimental and theoretical tools to predict the behaviour of a geotextile filter under conditions closer to those expected in the field. The results in the literature and in the present work suggest that available sound retention criteria can provide conservative designs with respect to geotextile capacity to retain base soil particles, particularly bearing in mind that under compression and partial clogging the retention capacity of the geotextile will increase. However, both compression and soil particle intrusion reduce the sizes of the geotextile pores, influencing clogging conditions. For low levels of particle intrusion in the geotextile voids, the results suggest that the dimensions of the compressed geotextile pores fall into the range of particle diameters of silts and fine sands. Therefore, due attention should be paid if particles in this diameter range may reach the geotextile filter. On the other hand, geotextile pores increase in size when subjected to equal biaxial tensile strains. A preliminary approach to predict the upper bound for geotextile filtration opening size under such conditions has been presented and discussed.

The knowledge on geotextile filter behaviour today is much better than some decades ago. Nevertheless, it should still be emphasised that the design of geotextile filters must be made based on validated filter criteria and sound engineering judgement. Proper design tools are available in the literature. For severe and critical applications, the performance of filtration tests as close as possible to the field conditions is of utmost importance. Further research is required for a better understanding on the behaviour of geotextile filters under such conditions.

Acknowledgments

The author would like to thank for the invitation to publish this paper in this special issue of *Soils & Rocks* to commemorate the 70th anniversary of the creation of the Brazilian Association of Soil Mechanics and Geotechnical Engineering (ABMS). The author is indebted to the University of Brasília and to several graduate students whose research works have been presented in this paper. The continuous support from geosynthetic manufacturers and research sponsoring agencies (particularly CNPq, CAPES and FAPDF) throughout the years is greatly appreciated.

References

- ASTM (2011). Standard Test Method for Pore Size Characteristics of Geotextiles by Capillary Flow Test - D 6767. ASTM International, West Conshohocken, PA, USA, 6 p.
- ASTM (2012). Standard Test Method for Measuring the Filtration Compatibility of Soil-Geotextile Systems. ASTM International, West Conshohocken, PA, USA, 8 p.
- Bessa da Luz, D.W. & Palmeira, E.M. (2006). Interação solo-geotêxtil em ensaios de filtração sob elevadas tensões normais. *Solos & Rochas*, 29(1):33-47.
- Bhatia, S.K. & Smith, J.L. (1996a). Geotextile characterization and pore-size distribution: Part II - A review of test methods and results. *Geosynthetics International*, 3(2):155-180.
- Bhatia, S.K. & Smith, J.L. (1996b). Geotextile characterization and pore-size distribution: part III - Comparison of methods and application to design. *Geosynthetics International*, 3(3):301-328.
- Blond, E.; Vermeersch, O. & Diederich, R. (2015). A comprehensive analysis of the measurement techniques used to determine geotextile opening size: AOS, FOS, O90, and 'Bubble Point'. *Proc. Geosynthetics' 2015*, Portland, Oregon, 10 p.
- Calhoun, C.C. (1972). Development of design criteria and acceptance specifications for plastic filter cloths. Technical Report S-72-7, Vicksburg, MS, US Army Engineer Waterways Experiment Station, 83 p.
- Carroll, R.G. (1983). Geotextile filter criteria. *Transportation Research Record*, No. 916:46-53.
- Christopher, B.R. & Holtz, R.D. (1985). Geotextile engineering manual. Report No. FHWA-TS-86/203, Washington, DC, Federal Highway Administration, 1044 p.
- Corbet, S.P. (1993). The design and specification of geotextiles and geocomposites for filtration and drainage. *Proc. Geotextile in Filtration and Drainage*. Corbet, S.P. & King, J. (eds), London, v. 1, pp. 29-40.
- Damians, I.P.; Bathurst, R.J.; Adroguer, E.G.; Josa, A. & Lloret, A. (2017). Environmental assessment of earth retaining wall structures. *Environmental Geotechnics*, 4(6):415-431. <https://doi.org/10.1680/jenge.15.00040>

- Elsharief, A.M. & Lovell, C.W. (1996). Determination and comparisons of the pore structure of nonwoven geotextiles. *Proc. Recent Developments in Geotextile Filters and Prefabricated Drainage Geocomposites*. Bhatia, S.S. & Suits, L.D. (eds) ASTM STP 1281, American Society for Testing and Materials, West Conshohocken, pp. 35-53.
- Faure, Y.-H. (1988). *Approche Structurale du Comportement Filtrant-Drainant des Geotextiles*. Ph.D. Thesis, Université Joseph Fourier, Grenoble, 352 p. (in French).
- Faure, Y.H.; Gourc, J.P. & Gendrin, P. (1990). Structural study of porometry and filtration opening size of geotextiles. *Proc. Geosynthetics: Microstructure and Performance*, ASTM STP 1076, I.D. Peggs (ed.). West Conshohocken, Pennsylvania, v. 1, pp. 102-119.
- Fayoux, D. & Evon, E. (1982). Influence of the fibre size on the filtration characteristics of needled-punched geotextiles. *Proc. 2nd International Conference on Geotextiles*, Las Vegas, v. 1, pp. 49-53.
- Fischer, G.R.; Christopher, B.R. & Holtz, R.D. (1990). Filter criteria based on pore size distribution. *Proc. 4th International Conference on Geotextiles, Geomembranes and Related Products*, The Hague, The Netherlands, v. 1, pp. 289-294.
- Fourie, A.B. & Kuchena, S.M. (1995). The influence of tensile stresses on the filtration characteristics of geotextiles. *Geosynthetics International*, 2(2):455-471. <https://doi.org/10.1680/gein.2.0018>
- Fourie, A.B. & Addis, P.C. (1997). The effect of in-plane tensile loads on the retention characteristics of geotextiles. *Geotechnical Testing Journal*, 20(2):211-217. <https://doi.org/10.1520/GTJ10740J>
- Fourie, A.B. & Addis, P.C. (1999). Changes in filtration opening size of woven geotextiles subjected to tensile loads. *Geotextiles and Geomembranes*, 17:331-340. [https://doi.org/10.1016/S0266-1144\(99\)00011-4](https://doi.org/10.1016/S0266-1144(99)00011-4)
- Frischknecht, R.; Stucki, M.; Büsser, S. & Itten, R. (2012). Comparative life cycle assessment of geosynthetics vs. conventional construction materials. *Ground Engineering*, 45(10):24-28.
- Gardoni, M.G. (2000). *Estudo do Comportamento Dreno-Filtrante de Geossintéticos sob Compressão*. D.Sc. Thesis, University of Brasília, 313 p. (in Portuguese).
- Gardoni, M.G. & Palmeira, E.M. (1998). The performance of a geotextile filter in tropical soil. *Proc. 6th International Conference on Geosynthetics*, Atlanta, v. 2, pp. 1027-1032.
- Gardoni, M.G. & Palmeira, E.M. (2002). Microstructure and pore characteristics of synthetic filters under confinement. *Géotechnique*, 52(6):405-418. <https://doi.org/10.1680/geot.2002.52.6.405>
- Giroud, J.P. (1982). Filter criteria for geotextiles. *Proc. 2nd International Conference on Geotextiles*, Las Vegas, August 1-6, v. 1, pp. 103-108.
- Giroud, J.P. (1996). Granular filters and geotextile filters. *Proc. GeoFilters'96*. Lafleur, J. & Rollin, A.L. (eds) Ecole Polytechnique de Montreal, Montreal, Canada, v. 1, pp. 565-680.
- Giroud, J.P.; Bonaparte, R.; Beech, J.F. & Gross, B.A. (1990). Design of soil layer geosynthetic systems overlying voids. *Geotextiles and Geomembranes*, 9(1):11-50. [https://doi.org/10.1016/0266-1144\(90\)90004-V](https://doi.org/10.1016/0266-1144(90)90004-V)
- Gourc, J.-P. (1982). *Quelques Aspects du Comportement des Geotextiles en Mécanique des Sols*. Ph.D. Thesis, University of Grenoble, France, 235 p. (in French).
- Heerten, G. (1982). Dimensioning the filtration properties of geotextiles considering long-term conditions. *Proc. 2nd International Conference on Geotextiles*, Las Vegas, v. 1, pp. 115-120.
- Heerten, G. (2012). Reduction of climate-damaging gases in geotechnical engineering practice using geosynthetics. *Geotextiles and Geomembranes*, 30:43-49. <https://doi.org/10.1016/j.geotextmem.2011.01.006>
- Holtz, R.D.; Christopher, B.R. & Berg, R.R. (1997). *Geosynthetic Engineering*. BiTech Publishers Ltd., Richmond, B.C., Canada, 452 p.
- Koerner, R.M. & Koerner, G.R. (2015). Lessons learned from geotextile filter failures under challenging field conditions. *Geotextiles and Geomembranes*, 43(3):272-281, [10.1016/j.geotextmem.2015.01.004](https://doi.org/10.1016/j.geotextmem.2015.01.004).
- Laflaive, E. & Puig, J. (1974). Emploi des textiles dans les travaux de terrassement et de drainage. *Bulletin de Liaison Laboratoires des Ponts et Chaussées*, 69:61-79 (in French).
- Lafleur, J. (1999). Selection of geotextiles to filter broadly graded cohesionless soils. *Geotextiles and Geomembranes*, 17(5-6):299-312. [https://doi.org/10.1016/S0266-1144\(99\)00007-2](https://doi.org/10.1016/S0266-1144(99)00007-2)
- Lawson, C.R. (1986). Geotextile filter criteria for tropical residual soils. *Proc. 3rd International Conference on Geotextiles*, Vienna, Austria, v. 2, pp. 557-562.
- Lombardi, G; Rollin, A. & Wolff, C. (1989). Theoretical and experimental opening sizes of heat-bonded geotextiles. *Textile Research Journal*, 59(4):208-217. <https://doi.org/10.1177/004051758905900404>
- Luetlich, S.M.; Giroud, J.P. & Bachus, R.C. (1992). Geotextile filter design guide. *Geotextiles and Geomembranes*, 11:355-370. [https://doi.org/10.1016/0266-1144\(92\)90019-7](https://doi.org/10.1016/0266-1144(92)90019-7)
- Masounave, J.; Denis, R. & Rollin, A.L. (1980). Prediction of hydraulic properties of synthetic fabrics used in geotechnical works. *Canadian Geotechnical Journal*, 17(4):517-525. <https://doi.org/10.1139/t80-06>
- Melo, D.L.A (2018). *Avaliação da Abertura de Filtração de Geotêxteis sob Diferentes Esforços Solicitantes*. M.Sc. Dissertation, University of Brasília, Brasília, 80 p. (in Portuguese).

- Mlynarek, J. (1985). Designing geotextiles as protective filters. *Proc. 21st IAHR Congress, Melbourne, Australia*, v. 1, pp. 154-158.
- Moo-Young, H. & Ochola, C. (1999). Strain effects on the filtration properties of geotextiles. *Proc. Geosynthetics'99*, v. 2, pp. 757-768.
- Moraes Filho, I.P. (2018). Avaliação da Abertura de Filtração de Geotêxteis sob Diferentes Condições de Solicitação Mecânica. M.Sc. Dissertation, University of Brasília, Brasília, 122 p. (in Portuguese).
- Palmeira, E.M. (2018). Geossintéticos em Geotecnia e Meio Ambiente. Editora Oficina de Textos, São Paulo, 294 p. (in Portuguese).
- Palmeira, E.M.; Beirigo, E.A. & Gardoni, M.G. (2010). Tailings-nonwoven geotextile filter compatibility in mining applications. *Geotextiles and Geomembranes*, 28:136-148.
<https://doi.org/10.1016/j.geotexmem.2009.10.004>
- Palmeira, E.M. & Fannin, R.J. (2002). Soil-geotextile compatibility in filtration. *Proc. 7th International Conference on Geosynthetics*. Nice, France, v. 3, pp. 853-872.
- Palmeira, E.M.; Fannin, R.J. & Vaid, Y.P. (1996). A study on the behaviour of soil-geotextile systems in filtration tests. *Canadian Geotechnical Journal*, 33(6):899-912.
<https://doi.org/10.1139/t96-120>
- Palmeira, E.M. & Gardoni, M.G. (2000a). Geotextiles in filtration: a state-of-the-art review and remaining challenges. *Proc. International Symposium on Geosynthetics/GeoEng 2000*, Melbourne, Australia, v. 1, pp. 85-111.
- Palmeira, E.M. & Gardoni, M.G. (2000b). The influence of partial clogging and pressure on the behaviour of geotextiles in drainage systems. *Geosynthetics International*, Special Issue on Liquid Collection Systems, 7(4-6):403-431. <https://doi.org/10.1680/gein.7.0178>
- Palmeira, E.M.; Gardoni, M.G. & Bessa da Luz, D.W. (2005). Soil-geotextile filter interaction under high stress levels in the gradient ratio test. *Geosynthetics International*, 12(4):162-175.
<https://doi.org/10.1680/gein.2005.12.4.162>
- Palmeira, E.M.; Melo, D.L.A. & Moraes-Filho, I.P. (2019). Geotextile filtration opening size under tension and confinement. *Geotextiles and Geomembranes*, 47:566-576. <https://doi.org/10.1016/j.geotexmem.2019.02.004>
- Palmeira, E.M.; Totto, J. & Araújo, G.L.S. (2012). Sagging and filtration behaviour of nonwoven geotextiles overlying different bedding materials. *Geotextiles and Geomembranes*, 31:1-14.
<https://doi.org/10.1016/j.geotexmem.2011.09.002>
- Palmeira, E.M. & Trejos-Galvis, H.L. (2017). Opening sizes and filtration behaviour of nonwoven geotextiles under confined and partial clogging conditions. *Geosynthetics International*, 24(2):125-138.
<https://dx.doi.org/10.1680/jgein.16.00021>
- Palmeira, E.M. & Trejos-Galvis, H.L. (2018). Evaluation of predictions of nonwoven geotextile pore size distribution under confinement. *Geosynthetics International*, 25(2):230-241. <https://doi.org/10.1680/jgein.18.00004>
- Rawal, A. (2010). Structural analysis of pore size distributions of nonwovens. *Journal of the Textile Institute*, 101(4):350-359.
- Schoeber, W. & Teindl, H. (1979). Filter criteria for geotextiles. *Proc. European Conference on Soil Mechanics and Foundation Engineering*, Brighton, v. 2, pp. 123-129.
- Stucki, M.; Büsser, S.; Itten, R.; Frischknecht, R. & Walbaum, H. (2011). Comparative Life Cycle Assessment of Geosynthetics vs. Conventional Construction Materials. Research Report, Swiss Federal Institute of Technology, Zurich, Switzerland, 94 p.
- Trejos-Galvis, H.L. (2016). Avaliação da Abertura de Filtração de Geotêxteis sob Confinamento e Parcialmente Colmatados. M.Sc. Dissertation, University of Brasília, 137 p. (in Portuguese).
- Urashima, D.C. & Vidal, D. (1998). Geotextiles filter design by probabilistic analysis. *Proc. 6th International Conference on Geosynthetics*, Atlanta, Georgia, v. 2, pp. 1013-1016.
- Wilson-Fahmy, R.; Koerner, G.R. & Koerner, R.M. (1996). Geotextile filter design critique. In: *Recent Developments in Geotextile Filters and Prefabricated Drainage Geocomposites*. Bhatia, S.S. & Suits L.D. (eds) American Society for Testing and Materials, ASTM STP 1281, pp. 132-161.
- Wu, C.S. & Hong, Y.S. (2016). The influence of tensile strain on the pore size and flow capability of needle-punched nonwoven geotextiles. *Geosynthetics International*, 23(6):422-434.
<https://doi.org/10.1680/jgein.16.00007>
- Wu, C.S.; Hong, Y.S. & Wang, R.H. (2008). The influence of uniaxial tensile strain on the pore size and filtration characteristics of geotextiles. *Geotextiles and Geomembranes*, 26(3):250-262.
<https://doi.org/10.1016/j.geotexmem.2007.09.004>

Guidelines and recommendations on minimum factors of safety for slope stability of tailings dams

Fernando Schnaid^{1,2#} , Luiz Guilherme F.S. de Mello^{3,4} ,
Bruno S. Dzialoszynski⁴ 

Article

Keywords

Factor of safety
Slope stability
Tailings dams

Abstract

Recent major upstream raised tailings dam failures have led to a reopening of the discussion of the validity of some of the existing routine practices within the profession. Despite its many shortcomings, deterministic slope stability limit equilibrium analysis is and will continue to be, at least for some time ahead, an important tool for tailings dams' safety assessment. Within this context, this paper presents a contribution to the postulation of minimum factors of safety required for tailings dams' slope stability analysis. A recent review and discussion of limit equilibrium analysis and the guidelines of international standards and current trends, with focus on tailings dams, are presented. Based on this review, and the authors' academic and professional experience, minimum required factors of safety recommendations are proposed. The framework of the recommendations strives to conciliate, in a simple manner, the deterministic minimum required factors of safety with concepts of consequence, uncertainties, risk and characteristics of loose tailings behaviour as a material.

1. Introduction

The recently reported failures of major tailings dams raised from an initial conventional earthwork structure, starter dam, by the upstream method, Mount Polley, Fundão, Cadia and Brumadinho, all owned by high standard mining companies and subjected to inspections and safety assessments following local standards and legislation, have led the profession to open the discussion on the validity of the existing routine practices.

Concomitantly, the legislators have rushed to update and adjust the standards and legislation to knowledge being acquired and made available through the investigations and causation reports of these failures (*e.g.* Morgenstern *et al.*, 2015, Morgenstern *et al.*, 2016; Robertson *et al.*, 2019, Morgenstern *et al.*, 2019). Morgenstern (2018) stated in the written version of his Victor de Mello Lecture: "At this time, there is a crisis associated with concern over the safety of tailings dams and lack of trust in their design and performance" as well as emphasized during the lecture itself that engineers have to consider that a tailings dam will liquefy if the material deposited is in a contractive condition: "if it can it will [liquefy]".

Few countries, like Brazil, took a radical step and legislated to banish upstream method tailings dams, postulating a time framework for all existing upstream dams to be decharacterized, with decharacterization having to follow stricter requirements than decommissioning.

High level academic research also focused on relevant topics, contributing to better understanding of the behaviour of loose saturated and contractive tailings stored in very complex structures due to the variability, both spatial and in time, of the disposed materials.

The profession is facing this enormous challenge in hundreds of abandoned or being decommissioned tailings dams, as well as in ongoing facilities. While the use of complex numerical simulations with sophisticated soil models as a tool to back decisions is becoming more frequent (*e.g.* Li and Wang, 1998; Pestana and Whittle, 1999; Taborda *et al.*, 2014; Jefferies and Been, 2016; Reid 2020), the routine of practicing engineers is still based on stability verifications and interpretation of monitoring data based on threshold limits implicitly associated to limit equilibrium analysis. Standards all over the world still refer to and/or build on the concept of compliance to safety requirements

#Corresponding author. E-mail address: fernando@ufrgs.br.

¹Universidade Federal do Rio Grande do Sul, Porto Alegre, RS, Brazil.

²Analysis Consultoria Geotécnica, Porto Alegre, RS, Brazil.

³Escola Politécnica da Universidade de São Paulo, São Paulo SP, Brazil.

⁴Vecttor Projetos Ltda, São Paulo SP, Brazil.

Submitted on May 30, 2020; Final Acceptance on June 24, 2020; Discussion open until December 31, 2020.

DOI: <https://doi.org/10.28927/SR.433369>



This is an Open Access article distributed under the terms of the Creative Commons Attribution License, which permits unrestricted use, distribution, and reproduction in any medium, provided the original work is properly cited.

to minimum values of factor of safety, and will continue to do so for some time ahead.

Definition of factors of safety result from a comparison of ultimate resistances in relation to acting loads; it can be emphasized that they really refer to safety against instability in the various verifications that a structure may require to comply with equilibrium verifications.

In order to structure the main aim of this paper, a short summary of what is believed to be the origin and/or root of this concept in applied geomechanics was sought.

In the landmark book, “Theoretical Soil Mechanics”, Terzaghi mentions in its Introduction that the working hypotheses of Soil Mechanics are as useful as the Theory of Structures in Civil engineering, with the uncertainties involved in the assumptions of computations that need to be anticipated by engineers when considering the differences between reality and his concept of the situation requiring his full attention.

The working hypothesis of the Theory of Structures is based on complying with the principles of static equilibrium. Terzaghi postulates that “the solution of a problem is rigorous if the computed stresses are strictly compatible with the conditions for equilibrium, with the boundary conditions, and with the assumed mechanical properties of the materials subject to investigation”. And, this concept on how to deal with safety of earthworks and foundations was probably originated earlier, with discussions on earth pressures on retaining walls.

When approaching discussions on the stability of slopes, Terzaghi starts by looking at the base failure of a vertical cut, and only afterwards proceeds to discuss inclined slopes. The estimation of a factor of safety against base failure, as well as the calculation of the excavation base heave, start by the calculation of the critical cohesion for the local soil, all focusing on guaranteeing equilibrium. A recommendation of a factor of safety of 1.5 is presented without detailed discussion of why this value was selected. When discussing the horizontal equilibrium of strutted excavations, a value of factor of safety of 2 is brought, mentioning “specifications”.

Taylor (1948) in his landmark book *Fundamentals of Soil Mechanics*, has a specific item discussing Factors of Safety in the chapter on Stability of Slopes. He reports that “much criticism has been levelled in the past at improper use of *factors of safety* and the incomplete definitions that have sometimes been given to such factors. However, any quantitative stability analysis must make use of some measure of the degree of safety. It must be realized that many types of failure are possible with respect to a system as a whole and also that many types are possible with respect to individual points or individual parts of the system. It thus appears that there is no such thing as *the* factor of safety and that when a factor of safety is used its meaning should be clearly defined. For this reason, considerable care will be used in defining the factors of safety used herein”. Taylor

uses the wording of a margin of safety being specified so that “the working values must be smaller than those given above”, those being related to the available shear strength of the soil in a slope. He also proposes that the margins of safety may be different for the two components of the shear strength, recommending a value of 1.5 in the cohesion component, and 1.26 in the tangent of the friction angle, and postulates that it is usually preferred that the two factors have the same value. Comparison of the value of factor of safety with respect to shear strength with that used in steel and other structural materials is made. The concern of the “low degree of dependable accuracy in shearing strength determinations in soils” is brought and discussion that the value of 1.37 that results from the equalization of the factor on the cohesion and on the friction angle on his example, should be considered too small. But Taylor concludes “it is a typical value, however, and many embankments, which according to engineering practice are safe, have safety factors smaller than this value. The fact that the usual margin of safety that can be specified in stability analyses is often no larger than the probable amount of inherent error in the procedures used is alone sufficient to show that soil mechanics is not an exact science”.

Additionally, it is worth mentioning that, according to Meyerhof (1994), the concept of factor of safety was first used in geotechnical design by Bélidor and Coulomb in the 18th Century.

This brief historical introduction highlights the fact that selecting the safety conditions and reducing the risk of failure of a structure is a controversial topic since the early works of soil mechanics, requiring continuous scrutiny and judgment. A conceptual view of required factors of safety for slope stability shared by the authors is put forward for discussion and debate, based upon academic and professional experience and recently revised guidelines of international standards on tailings dams.

2. Guidelines and recommendations from international standards

In order to better understand the status in which the profession is basing, studying and discussing the evaluation of safety conditions of existing, operating or to be decommissioned tailings dams, a critical review of the main recommendations, as provided by international standards, as well as by recognized and influencing entities, is necessary. As mentioned, the failures of Mount Polley (Morgenstern *et al.*, 2015), Fundão (Morgenstern *et al.*, 2016), Cadia (Morgenstern *et al.*, 2019) and Brumadinho (Robertson *et al.*, 2019) have, in the recent past, led to relevant changes in attitudes, propositions and requirements, trying to prevent additional catastrophes.

Minimum required factor of safety recommendations from various landmark sources are briefly presented and described herein. Priority was given to recommendations postulated specifically for mining and tailings dams, but

relevant publications for embankment and rockfill dams in general were also included.

2.1 International Council of Mining & Metals' Global Tailings Standard (ICMM, 2019, draft)

After and in the light of Brumadinho's catastrophic event, the ICMM has published a draft version for an international standard for tailings facilities. Consultation to the geotechnical community was performed in the end of 2019 and is now closed.

Even though no specific minimum required factor of safety recommendations are provided, from a conceptual standpoint some important requirements are postulated. Initially, despite requiring the Operator to study and assess the potential consequences of the tailings facility's failure and considering it for various activities and decisions, the standard also states that:

"PRINCIPLE 4: Design, construct, operate and manage the tailings facility on the presumption that the consequence of failure classification is 'Extreme', unless this presumption can be rebutted"

According to the proposed standard, design should normally assume 'Extreme' consequences of failure, and thus, would not depend on the assessment of consequence categories, unless otherwise specifically justified. The justifications for applying other consequence categories are defined as:

- "a) The knowledge base demonstrates that a lower classification can be applied for the near future, including no potential for impactful flow failures; and*
- b) A design of the upgrade of the facility to meet the requirements of an 'Extreme' consequence of failure classification in the future, if required, is prepared and the upgrade is demonstrated to be feasible; and*
- c) The consequence of failure classification is reviewed every 3 years, or sooner if there is a material change in any of the categories in the Consequence Classification Matrix, and the tailings facility is upgraded to the new classification within 3 years. This review should proceed until the facility has been safely closed and achieved a confirmed 'landform' status or similar permanent non-credible flow failure state."*

In other words, tailings facility related activities - and thus minimum factor of safety postulation - may assume lower consequence categories only if one of the abovementioned requirements is met. It is important to notice that this principle refers directly to the concept of consequence, but not to the notion of probability of failure, which is also an

important design consideration and is considered in other principles of the publication.

Regarding the decision to rebut the 'Extreme' consequence hypothesis, it is postulated that it:

"shall be taken by the Accountable Executive or the Board of Directors (the 'Board'), with input from an independent senior technical reviewer or the ITRB [Independent Tailings Review Board]. The Accountable Executive or Board shall give written reasons for their decision."

The standard states as a principle that design criteria should be adopted to minimize risk. The criteria should be clearly selected and identified and should be adequate to minimize risk of the adopted Consequence Category.

Specifically regarding factors of safety, it postulates:

"REQUIREMENT 6.2: Apply factors of safety that consider the variability and uncertainty of geologic and construction materials and of the data on their properties, the parameters selection approach, the mobilized shear strength with time and loading conditions, the sensitivity of the failure modes and the strain compatibility issues, and the quality of the implementation of risk management systems."

That is, uncertainties, loading scenarios and quality of risk management are explicitly required to influence Factor of Safety selection. Influence of the Consequence Category is not explicitly stated.

Additionally, it mentions:

"REQUIREMENT 6.3: Identify and address brittle failure mechanisms with conservative design criteria and factors of safety to minimize the likelihood of their occurrence, independent of trigger mechanisms."

This quote highlights an important point: if the behaviour of the tailings material leads to potential brittle failure liquefaction, factors of safety should be conservatively postulated, independently of the trigger mechanism for this behaviour.

Moreover, when describing Consequence Categories, the standard states that "Where the consequence of failure includes loss of life, tailings facilities must be designed, built and operated so that there is a negligible likelihood of failure". However, only a table of Consequence Category-dependent earthquake and flooding loads are prescribed, but not minimum required factors of safety.

The Consequence Category classification of tailings facilities is referred to a matrix, based on provisions by ICOLD (Bulletin 121, 2001), with the highlight that it may change with time. Table 1 reproduces the referred matrix.

As indicated in the matrix, the Consequence Category classification is evaluated based on potential population at risk (PAR), potential loss of life (PLL), and impacts related to the environment, health, society, culture, infrastructure

Table 1. ICMM's consequence category matrix (ICMM, 2019).

Dam failure consequence classification	Incremental losses (ICMM DRAFT)				
	Potential population at risk	Potential loss of life	Environment	Health, social & cultural	Infrastructure & economics
Low	None	None expected	Minimal short-term loss or deterioration of habitat or rare and endangered species.	Minimal effects and disruption of business. No measurable effect on human health. No disruption of heritage, recreation, community or cultural assets.	Low economic losses; area contains limited infrastructure or services. < US\$1 M
Significant	Temporary only	None expected	No significant loss or deterioration of habitat. Potential contamination of livestock/fauna water supply with no health effects. Process water low potential toxicity. Tailings not potentially acid generating and have low neutral leaching potential. Restoration possible within 1 to 5 years.	Significant disruption of business, service or social dislocation. Low likelihood of loss of regional heritage, recreation, community or cultural assets. Low likelihood of health effects.	Up to 10 household livelihood systems disrupted and recoverable in the longer-term; or up to 100 household livelihood systems disrupted and recoverable in the short-term. No long-term non-recoverable loss of livelihoods.
High	10-100	1 - 10	Significant loss or deterioration of critical habitat or rare and endangered species. Potential contamination of livestock/fauna water supply with no health effects. Process water moderately toxic. Low potential for acid rock drainage or metal leaching effects of released tailings. Potential area of impact 10 km ² - 20 km ² . Restoration possible but difficult and could take > 5 years	500-1 000 people affected by disruption of business, services or social dislocation. Disruption of regional heritage, recreation, community or cultural assets. Potential for short term human health effects.	Up to 10 household livelihood systems lost and non-recoverable; or up to 50 household livelihood systems disrupted and recoverable over the longer-term; or up to 200 household livelihood systems disrupted and recoverable in the short term.
Very High	100-1000	10 to 100	Major loss or deterioration of critical habitat or rare and endangered species. Process water highly toxic. High potential for acid rock drainage or metal leaching effects from released tailings. Potential area of impact > 20 km ² . Restoration or compensation possible but very difficult and requires a long time (5 years to 20 years).	> 1 000 people affected by disruption of business, services or social dislocation for more than one year. Significant loss of national heritage, community or cultural assets. Potential for significant longer-term human health effects.	Up to 50 household livelihood systems lost and non-recoverable; or up to 200 household livelihood systems disrupted and recoverable over the longer-term; or up to 500 household livelihood systems disrupted and recoverable in the short term.

Dam failure consequence classification	Incremental losses (ICMM DRAFT)				
	Potential population at risk	Potential loss of life	Environment	Health, social & cultural	Infrastructure & economics
Extreme	> 1000	More than 100	Catastrophic loss of critical habitat or rare and endangered species. Process water highly toxic. Very high potential for acid rock drainage or metal leaching effects from released tailings. Potential area of impact > 20 km ² . Restoration or compensation in kind impossible or requires a very long time (> 20 years).	> 5 000 people affected by disruption of business, services or social dislocation for years. Significant national heritage or community facilities or cultural asset destroyed. Potential for severe and/or longer-term human health effects.	Extreme economic losses affecting critical infrastructure or services, (e.g., hospital, major industrial complex, major storage facilities for dangerous substances) or the longer-term; or more than 500 household livelihood systems disrupted and recoverable in the short term.

and economics, and livelihoods. The estimation of such impacts is complex in itself and shall not be discussed in depth in the present paper. Readers may refer, for example, to ANCOLD (2012). It is interesting to notice that the matrix does not allow for combination of criteria - for example, extreme environmental impacts with minor risk to life - simply assigning, for each criterion, a correspondent description for the consequence severity.

2.2 ANCOLD's guidelines on tailings dams - Planning, design, construction, operation and closure - Revision 1 (ANCOLD, 2019)

This publication dates from after the Brumadinho's catastrophic event and provides guidelines for various aspects of tailings dams design and management.

The guidelines foresee Dam Failure Consequence Category assessment, and some aspects of design are re-

Table 2. ANCOLD's Severity Level impact assessment (ANCOLD, 2019).

Damage type	Minor	Medium	Major	Catastrophic
Infrastructure (dam, houses, commerce, farms, community)	< \$10 M	\$10 M-100 M	\$100 M-\$1 B	> \$1 B
Business importance	Some restrictions	Significant impacts	Severe to crippling	Business dissolution, bankruptcy
Public health	< 100 people affected	100-1000 people affected	< 1000 people affected for more than one month	> 10,000 people affected for over one year
Social dislocation	< 100 person or < 20 business months	100-1000 person months or 20-2000 business months	> 1000 person months or > 200 business months	> 10,000 person months or numerous business failures
Impact area	< 1 km ²	< 5 km ²	< 20 km ²	> 20 km ²
Impact duration	< 1 year	< 5 years	< 20 years	> 20 years
Impact or natural environment	Damage limited to items of low conservation value (e.g. degraded or cleared land, ephemeral streams, non-endangered flora and fauna). Remediation possible.	Significant effects on rural land and local flora & fauna. Limited effects on: (A.) Items(s) of local & state natural heritage. (B.) Native flora and fauna within forestry, aquatic and conservation reserves, or recognized habitat corridors, wetlands or fish breeding areas.	Extensive rural effects. Significant effects on river system and areas A & B. Limited effects on: (C.) Item(s) of National or World natural heritage. (D.) Native flora and fauna within national parks, recognized wilderness areas, RAMSAR wetlands and nationally protected aquatic reserves. Remediation difficult.	Extensively affects areas A & B. Significantly affects areas C & D. Remediation involves significantly altered ecosystems.

Table 3. ANCOLD's recommended consequence category. Adapted from ANCOLD (2019).

Population at risk	Severity of damage and loss			
	Minor	Medium	Major	Catastrophic
< 1	Very low	Low	Significant	High C
≥ 1 to < 10	Significant (Note 2)	Significant (Note 2)	High C	High B
≥ 10 to < 100	High C	High C	High B	High A
≥ 100 to < 1000	(Note 1)	High B	High A	Extreme
≥ 1000	(Note 1)	Extreme	Extreme	

Note 1: With PAR excess of 100, it is unlikely Damage will be minor. Similarly, with a PAR in excess of 1000 it is unlikely Damage will be classified as Medium.

Note 2: Change to "High C" where there is the potential of one or more lives being lost. The potential for loss of life is determined by the characteristics of the flood area, particularly the depth and velocity of flow.

Note: A, B and C are subdivisions within the HIGH Consequence Category level with A being highest and C being lowest.

Table 4. ANCOLD's minimum required factor of safety recommendations (ANCOLD, 2019).

Loading condition (Note 1)	Recommended minimum for tailings dams	Shear strength to be used for evaluation
Long-term drained	1.5	Effective strength
Short-term undrained (potential loss of containment)	1.5	Consolidated undrained Strength
Short term undrained (no potential loss of containment)	1.3	Consolidated undrained Strength
Post-seismic	1.0-1.2 (Note 2)	Post seismic shear strength (Note 3)

Note 1 See Section 6.1.3 [of reference publication] for description of loading conditions.

Note 2 To be related to the confidence in selection of residual shear strength. 1.0 may be adequate for use with lower bound results.

Note 3 Cyclically reduced undrained/drained shear strength and/or liquefied residual shear strength for potentially liquefiable materials.

lated to the defined Category, such as earthquake loading, freeboard and storm storage allowance. However, the prescribed minimum factors of safety are not related to consequence categories, but to loading conditions, as traditionally done for conventional embankment dams.

The Dam Failure Consequence Category definition procedure is somewhat more complex than that described previously for ICMM (2019).

- Firstly, the “Severity Level” shall be postulated - as minor, medium, major or catastrophic - based on a table (reproduced hereafter on Table 2) that takes into account estimated damage upon failure related to infrastructure, business, public health, environment, social dislocation, impact area, impact duration.
- Then, the Population at Risk (PAR) must be estimated. This metric relates to the potential damage to human life.
- Both the aforementioned metrics are then inputted to a second table, which yields the Dam Failure Consequence Category. Such table is reproduced in Table 3.

It is important to notice that this methodology for assessing Consequence Category differs from that described in ICMM (2019) in the sense that it allows for ‘decoupling’ the impact related to human life. For example, it is possible to assess the combination of low impact to human life and catastrophic impact to the environment.

It is worth noticing that in this case duration of the impact is an input parameter for the Severity Level, which

would allow, for example to consider tailings with and without potential for acid drainage in the assessment.

Table 4 presents the recommended minimum required factor of safety values. Guidance on the shear strength considerations is also provided.

Specifically for static liquefaction, which is a crucial verification for contractive tailings stability, despite not being explicitly indicated in the previous table, it is stated:

“Several trigger mechanisms are well documented, such as a rapid change in loading, change in the state of drainage or deformation of the structure. However, the assessment of trigger mechanisms for static liquefaction is very difficult. Accordingly, a conservative approach to stability assessments involving materials susceptible to static liquefaction would be to assume that triggering does occur. The Factor of Safety for static liquefaction should be considered with reference to Table 8 [the table above] of these guidelines, allowing the static-liquefaction condition to be equivalent to the post-seismic loading condition. For a stability assessment of high consequence dams, it is also considered necessary to assume undrained conditions for contractive materials regardless of whether or not the undrained behaviour is expected.”

Table 5. CDA's Screening Level target factors of safety for slope stability of mining dams - static loading - construction, operation, and transition phases (CDA, 2019).

Loading condition	Minimum factor of safety	Slope
During or at end of construction (prior to commencing of tailings deposition or impoundment of water)	1.3	Downstream and Upstream
During operation of a mining dam when impounding water and/or tailings. Also, during construction of dam raises.	1.5	Downstream and Upstream
Long term (steady state conditions with respect to the dam configuration and seepage, normal reservoir level)	1.5	Downstream and Upstream
Full or partial rapid drawdown	1.3	Upstream slope

Table 6. CDA's screening level target factors of safety for slope stability - seismic loading - construction, operation, and transition phases (CDA, 2019).

Analysis method	Minimum factor of safety	Slope
Post-seismic	1.2	Downstream and Upstream
Pseudo-static	1.0*	Downstream and Upstream

* Unless deformations due to seismic loadings are assessed and are acceptable.

Table 7. CDA's screening level target factors of safety for slope stability - post liquefaction shear strengths - construction, operation, and transition phases (CDA, 2019).

Loading condition	Minimum factor of safety	Slope
Seismic	1.1	Downstream and Upstream
Static	1.1	Downstream and Upstream

That is, for static liquefaction the downstream slope of a tailings dam should be verified with the residual post-liquefaction shear strength of the potentially liquefiable materials targeting a factor of safety of 1.0-1.2, depending on the confidence in residual strength selection. It is important to highlight that despite the table reading "Post-seismic" the recommendation for this "post liquefaction" verification is valid regardless of the liquefaction trigger being seismic or not. Moreover, contractive materials should be considered with undrained behaviour, "regardless of whether or not the undrained behaviour is expected", that is, independently of the trigger mechanism and if it allows partial or reduced drainage during the shearing process - which is in line with ICMC's Global Tailings Review, previously discussed.

It is important to point that, despite explicitly presenting recommended minimum values, the guidelines state that there are no "rules" for acceptable factors of safety, because they need to account for the consequences of failure and the uncertainties involved.

Additionally, various guidelines are postulated for stability analysis, including aspects of liquefaction, analysis / shear resistance considerations / types, earthquakes, etc.

2.3 Canadian Dam Association's application of dam safety guidelines to mining dams (CDA, 2014) and revision (CDA, 2019)

This publication by CDA complements their Dam Safety Guidelines (CDA, 2013) by providing specific guidance on tailings dams. Various provisions on safety from a broad point of view are provided. Specifically for the sec-

tion regarding slope stability and minimum required factors of safety, a revision was prepared in 2019, after the catastrophic event in Brumadinho.

The discussion presented hereafter is related to the 2019 revision.

Table 5, Table 6 and Table 7 are presented with values referred as "screening levels" of factors of safety, which "if met, are generally viewed as acceptable practice", but "if they are not met, further investigation and analyses, supplemented by analyses and comprehensive use of the observational method, can be used to reduce uncertainty and support lower targets".

Table 7 refers to analyses to be performed with post liquefaction shear strengths. The selection of the type of shear strength parameters to be applied for the analyses related to the values in Table 5 and Table 6 is further discussed in the publication, and briefly summarized hereafter.

Regarding the peak undrained shear strength assessment associated to static liquefaction, in line with the propositions of the ICMC standard (2019), the CDA 2019 revision postulated:

"The undrained shear strengths are applicable to both the dams that are under construction and dams that have reached a steady-state operating condition. The undrained failure mode describes material behaviour under shearing during which pore water pressures change and the strength changes, and so this stability check is still required for dams that may not be considered to have a "trigger" for undrained shearing."

That is, the undrained stability check is required regardless of the likelihood of an associated trigger. The document considers that the drained strength may be overestimated at the time of failure, regardless of the trigger, and "the true factor of safety calculation for dams with contractive elements should be based on undrained loading condition".

In summary, it is proposed that, for dams with contractive materials, factors of safety associated to potential triggers for static liquefaction - including creep - may be checked, but even if no trigger is expected, a verification with peak undrained strength parameters should still be performed.

Similar recommendation is proposed for stability verifications with residual post liquefaction undrained shear strength parameters, which refer to Table 7:

"A post-peak analysis should be performed independent of the results of the triggering assessment, to understand the consequences if a loss of strength occurs. Then it can be assessed if a trigger analysis can be performed with confidence and if it is appropriate given the magnitude of the risk, or if simply the precautionary approach assuming post-peak strengths should be used."

Table 8. CDA's factors of safety for slope stability - static assessment (CDA, 2013).

Loading condition	Minimum factor of safety [Note 1]	Slope
End of construction before reservoir filling	1.3	Upstream and downstream
Long term (steady-state seepage, normal reservoir level)	1.5	Downstream
Full or partial rapid drawdown	1.2-1.3 [Note 2]	Upstream

Note 1. Factor of safety is the factor required to reduce operational shear strength parameters to bring a potential sliding mass into a state of limiting equilibrium (using generally accepted methods of analysis).

Note 2. Higher factors of safety may be required if drawdown occurs relatively frequently during normal operation.

Table 9. CDA's factors of safety for slope stability - seismic assessment. (CDA, 2013).

Loading condition	Minimum factor of safety
Pseudo-static	1.0
Post-earthquake	1.2-1.3

That is, the CDA 2019 revision brought forth the explicit indication of the verification of stability residual post liquefaction shear strengths, considering that “the strengths used for the calculation are a lower bound of the post peak strengths that could be realized”. This is relatively in tune with other post-Brumadinho recommendations by ANCOLD (as previously presented) and Brazilian Legislation (as presented hereafter).

In line with most standards and guidelines, the provided factors of safety are regarded as a means to manage risk, and it is stated that they should be based on considerations of both probability and consequence.

Further commentary on the proposed “screening level” values is provided in detail in the document, such as assumed hypotheses, premises, and justifications. A relatively thorough commentary on parameter selection is also presented.

CDA's other publication, Dam Safety Guidelines (2007, 2013 Edition), on the other hand, provides safety guidelines to dams in general, and thus is not specific to mining or tailings dams. Nonetheless, regarding safety and safety factors, some relevant comments are provided. The publication states that:

“[...] the level of safety cannot easily be measured using traditional methods. Specific methods, standards and procedures have been adopted with the expectation that, in following the prescribed approach, the desired safety objective will be achieved although the level of protection is still not actually known.”

In that sense, the guidelines detail both the traditional, deterministic, minimum factor of safety approach, and the risk based approach, arguing that they complement each other to a certain degree. The publication acknowledges

that the traditional approach historically shows success and is essential to dam safe design and management.

Under the observation that the quantitative definition of minimum factors of safety is based primarily on empirical evidence, experience and engineering judgement, and that they take into account the reliability of inputs, probability of loading condition and the consequences of failure, Table 8 and Table 9 are presented. The tables refer to dams in general, and not specifically tailings dams, and are somewhat different from those presented specifically for tailings dams (Table 5, Table 6 and Table 7).

2.4 SEMAD - FEAM's term of reference for the decharacterization of upstream tailings dams (SEMAD-FEAM, 2020)

The term “decharacterization” in the title of the document refers to decommissioning a facility taking it to a condition in which it cannot be characterized as having been a tailings dams before - a more restrictive final condition.

Shortly after, and as a direct response to Brumadinho's catastrophic event, the government of the state of Minas Gerais, Brazil (state where intense mining activity exists and Brumadinho is located) legislated that all upstream tailings dams within the state have to be decharacterized in a time framework. In this context, the Minas Gerais state regulator, SEMAD-FEAM (State Secretary for Environment and Sustainable Development - State Foundation for the Environment, freely translated by the authors from Secretaria de Estado de Meio Ambiente e Desenvolvimento Sustentável - Fundação Estadual do Meio Ambiente.), issued a term of reference with minimum requirements for the design of upstream tailings dam's decharacterization. The document complements Law 23.291 of February 2019, which instituted the State's Dam Safety Policy for Minas Gerais.

The publication foresees the development of a diagnosis of the current conditions of the structure, prior to decharacterization. This diagnosis includes the potential identification of alert / emergency levels, which in turn affects features of the design requirements and activities.

However, regardless of the conclusions of the diagnosis, it is demanded that the design must comply to a minimum factor of safety for the condition at the beginning of

Table 10. ABNT's minimum required factors of safety for tailings dams (ABNT, 2017, free translation by the authors).

Stage	Failure type	Slope	Minimum factor of safety
End of construction ^a	Dam and foundations	Upstream and downstream	1.3
Operation with normal operation condition flow net, maximum reservoir level	Dam and foundations	Downstream	1.5
Operation with extreme condition flow net, maximum reservoir level	Dam and foundations	Downstream	1.3
Operation with rapid drawdown of the reservoir water level	Dam	Upstream	1.1
Operation with normal condition flow net	Dam	Downstream	1.5
		Between berms	1.3
Seismic loading, with maximum reservoir level	Dam and foundations	Upstream and downstream	1.1

^a Successive raising stages of tailings dams cannot be analysed as “end of construction”, and must adhere to the minimum factors of safety defined for the operational conditions.

the decharacterization works of (direct quotes of terms as free translation by the authors):

- 1.3 for “undrained peak conditions”, referring to limit equilibrium stability analyses applying undrained peak shear strength parameters;
- 1.1 for “undrained residual conditions”, referring to limit equilibrium stability analyses applying undrained post liquefaction residual shear strength parameters.

These provisions are somewhat more explicit and stringent than those of the current Brazilian Standard NBR 13028:2017 for the design of tailings dams, as described in the following item. Nonetheless, the Term of Reference states that decharacterization designs shall abide by the guidelines provided in the aforementioned standard.

However, once again, more explicit and stringent requirements are postulated for the minimum required factors of safety for design situations that foresee that an embankment and reservoir will remain after the decharacterization process. The minimum required values are postulated as (direct quotes of terms as free translation by the authors):

- 1.5 for “drained failures”, for values obtained for limit equilibrium stability analyses where drained shear strength parameters are applicable;
- 1.5 for “peak undrained failures”, for values obtained for limit equilibrium stability analyses where undrained peak shear strength parameters are applicable;
- 1.1 for “residual undrained failures”, for values obtained for limit equilibrium stability analyses where undrained post liquefaction residual shear strength parameters are applicable.

It should be noted that the factor of safety value required for an analysis in undrained conditions, and peak shear strength parameters, is equal to that for drained analysis, in tune with the uncertainties existing in either case. The typical consideration of undrained analysis when used for the construction of embankments over soft clayey materials, allowing for a lower value of factor of safety at the

end of construction as consolidation with time increases the shear strength properties of the clays, is not associable to the case of contractive sandy tailings. It must also be acknowledged that upon decharacterization the level of monitoring and maintenance decreases - increasing uncertainties - and the restriction of the project's limited lifetime is also eliminated - potentially increasing the overall probability of this loading condition occurring.

2.5 ABNT's NBR 13028:2017 Standard - Mining - Preparation and presentation of design of tailings, sediments and/or water dams - Requirements (ABNT, 2017)

The Brazilian standard for the design of tailings dams, along with other recommendations, presents some criteria for the analysis and verification of slope stability of its structures. This standard is referred to by Brazilian legal documentation, and, therefore, is associated to all legal requirements and discussions within the country.

A brief discussion on loading and shear strength type - drained or undrained - and analysis type - total or effective stresses based - is provided.

Table 10 with minimum required factors of safety is presented, based on loading conditions.

Some measure of ambiguity on the applicability of the presented values is introduced by the standard's text. On one hand it is stated that the values (free translation by the authors) “must be obtained, independent of the type of analysis and loading conditions”. On the other hand, shortly after, it also states that (free translation by the authors):

“For stability analyses that utilize undrained strength parameters, the minimum safety factors should be established by the designer, based on good engineering practice”

2.6 Chilean Ministry of Mining's Regulations for the approval of design, construction, operation and closure of tailings dams (Ministerio de Minería, 2007)

This publication is a Chilean government decree establishing legal requirements for tailings dams within the country.

It is worthy of note that upstream tailings dams are legally banned in Chile since the failure of El Cobre N. 1 in 1965 (Valenzuela, 2015).

Slope stability analyses are explicitly required to be presented in the design. A total of 4 “precision phases” (free translation of the term by the authors) is defined, according to the importance of the evaluation and the risks that the reservoir poses to neighbouring areas. They are:

- Phase I: static slope stability analyses (or pseudo-static) considering liquefaction of all tailings;
- Phase II: static slope stability analyses (or pseudo-static) with simplified estimation of the pore pressures;
- Phase III: dynamic analyses based on dynamic property testing of the soils, including displacement calculations;

Table 11. Hezra and Phillips' Modified minimum FoS example table. (Hezra and Phillips, 2017).

Level of uncertainties in data, assessment, loading conditions, etc.	Consequence category		
	Low	Significant	High
Low	1.3	1.5	1.5
Medium	1.4	1.5	1.7
High	1.5	1.6	Note 1

Note 1: High consequence dams with high uncertainties in the input data, assessments and loading conditions should not be designed until the level of uncertainties is reduced.

- Phase IV: analysis for closure conditions, including critical loading condition events and time-dependent effects on the properties of the dam.

Only for phases I and II a minimum required factor of safety value, of 1.2, is postulated, recalling that design of dams and large reservoirs constructed on areas with high seismicity should necessarily focus on loss of stability due to a loss of strength of the embankment and foundation material.

2.7 South African Bureau of Standards' mine residue code of practice (SABS, 1998) and South African Government's Mining Residue Regulations (South African Government Department of Environmental Affairs, 2015)

The South African Bureau of Standards' Mine Residue Code of Practice from 1998 is an important guidance document for the management of tailings facilities. The document provides objectives, principles and minimum requirements for good practice along various stages of a tailings dam life cycle, especially dam safety.

Minimum design requirements are postulated, which include design calculation for structural adequacy, including safety factors and slope stability analysis. However, the publication does not postulate specific values for minimum required factors of safety.

In 2015 the Government of South Africa established new Mining Residue Regulations regarding “the planning and management of residue stockpiles and residue deposits from a prospecting, mining, exploration or production operation”. Within SABS 0286 (SABS, 1998) “mine residue” is defined as “any waste tailings derived from any mining operation or from the processing of any material” (excluding overburden from opencast mining operations and residue used as a support medium in an underground mine) and

Table 12. Fell *et al.*'s Baseline recommended minimum acceptable factors of safety and load conditions. (Fell *et al.*, 2015).

Slope	Load condition	Reservoir characteristic	Minimum factor of safety
Upstream and Downstream	End of construction steady state seepage	Reservoir empty	1.3
Downstream	Maximum flood	Reservoir at normal maximum operating level (Full Supply Level)	1.5
Downstream	Drawdown	Reservoir at maximum flood level	1.5, free draining crest zones, 1.3 otherwise
Upstream		Rapid drawdown to critical level	1.3

Notes: (1) These factors of safety apply to design of new high consequence of failure dams, on high strength foundations, with low permeability zones constructed of soil which is not strain weakening, using reasonably conservative shear strengths and pore pressures developed from extensive geotechnical investigations of borrow areas, laboratory testing and analysis of the results and using the methods of analysis detailed above [in the reference publication]. It is assumed there will be monitoring of deformations by surface settlement points during construction and during operation of the dams.,

(2) “High permeability crest zones” means the pore pressures in zones near the crest will respond to reservoir level as it rises. For dams with a low permeability earthfill core, the pore pressures will not respond to reservoir rise and lower factors of safety may be acceptable.

Table 13. Fell *et al.*'s Factors which influence the selection of factor of safety and their effect on the baseline minimum factor of safety. (Fell *et. al.*, 2015).

Factor	Description	Recommended change to the baseline minimum factor of safety
Existing (vs. new) Dam	A lower factor of safety may be adopted for an existing dam which is well monitored and performing well	0 to -0.1
Soil or weak rock foundation	A higher factor of safety may be needed to account for the greater uncertainty of the strength	0 to +0.2 for effective stress +0.1 to +0.3 for undrained strength analyses.
Strain weakening soils in the embankment or foundation	A higher factor of safety may be needed to account for progressive failure, and greater displacements if failure occurs	0 to +0.2
Limited (little or no good quality) strength investigation and testing, particularly of soil and weak rock foundations	A higher factor of safety should be used to account for the lack of knowledge. Detailed investigations will be required to confirm conditions.	+0.1 to +0.3 for effective stress analyses, +0.3 to +0.5 for undrained strength analyses.
Contractive soils in the embankment or foundation	A higher factor of safety may be needed to account for the greater uncertainty in the undrained strength	+0.1 to +0.3 for undrained strength.

Note: These figures are given for general guidance only. Experienced Geotechnical Professionals should use their own judgment, but note the principles involved in this table.

“residue deposit” is defined as “that portion of a facility that is the temporary or final depository for mine Residue”.

Regarding design considerations for residue stockpiles and deposits, the regulations state that a factor of safety of 1.5 must be achieved. Deviation from this value is only accepted if there are valid technical reasons, in which case adequate motivation must be provided and design must be reviewed by a competent and knowledgeable person.

2.8 Hezra and Phillips' design of dams for mining industry (Hezra and Phillips, 2017)

Even though the publication of individual authors does not bear the same weight as that of associations and institutions, this publication is worthy of note because it presents recommendations for minimum factors of safety related to uncertainties and consequence categories, being specific to tailings dams.

The paper presents a discussion on the safety of tailings dams and the factor of safety (FoS). The authors present an example table for minimum required factors of safety adjusted to both consequence categories and uncertainties, reproduced hereafter in Table 11.

It is important to highlight that the authors present the table as an example, and state that “Different loading conditions would require different adjustments of the minimum FoS. Additional research will be required to define the levels of uncertainties using objectively measured indicators”.

2.9 Fell *et. al.*'s Geotechnical Engineering of Dams (Fell *et. al.*, 2015)

Once again, it must be acknowledged that this publication is due to specific authors and not an association or institution. However, it is worthy of note because it bears recommendations for factors of safety with regard to uncertainties for dams in general, that is, not specific to tailings dams.

Firstly, the authors present Table 12, with minimum required factors of safety according to loading conditions.

Even though the values themselves are fairly traditional, it is interesting to notice that the authors state that they apply specifically to dams with high consequences associated to failure, which implies a consequence category (see Note 1 of the table).

The authors also specify that the values apply to new dams, and to some required features, which imply measures of uncertainty (see Note 1 of the table). With regard to those measures of uncertainty, the authors provide another table, Table 13, with recommended changes to the baseline minimum required factor of safety values.

2.10 NRCS's technical release 210-60 - Earth dams and reservoirs (NRCS, 2019)

This publication by the United States Department of Agriculture's National Resources Conservation Service describes design procedures and provides minimum requirements for planning and designing earth dams. Thus, it does not refer specifically to tailings dams. However, it is worth mentioning that it was released on 03/2019, shortly after Brumadinho's catastrophic event.

Table 14. NRCS's Static Slope Stability Criteria. (adapted from NRCS, 2019).

Design condition	Primary assumption	Remarks	Applicable shear strength parameters	Minimum factor of safety
1. Construction Stability (upstream or downstream slope)	Zones of the embankment or layers of the foundation expected to develop significant pore pressures during construction	Low-permeability embankment soils should be tested at water contents that are as wet as likely during construction (usually wet of optimum). Saturated low permeable foundation soils not expected to consolidate fully during construction. Existing dams with additional fill placed above saturated low-permeability zones.	Unconsolidated; Total stress consistent with preconstruction stress state	1.4 for failure surfaces extending into foundation layers 1.3 for embankments on stronger foundations where the failure surface is located entirely in the embankment
	Embankment zones and/or strata not expected to develop significant pore pressures during construction	Embankment zones, foundation strata, or both comprised of material with a permeability high enough to drain as rapidly as they are loaded	Effective stress	
2. Rapid drawdown (upstream slope)	Drawdown from the highest normal pool to the lowest gated outlet	Consider failure surfaces both within the embankment and extending into the foundation Low-permeability embankment and foundation soils that will have limited drainage during reservoir drawdown	Lowest of effective stress or consolidated, total stress; consistent with pre-drawdown consolidation stresses (See Fig. 5-1 [of ref. publication])	1.2; and 1.1 for near surface (infinite slope) failure surfaces in cohesionless soils
		Embankment zones, foundation strata, or both comprised of material with a permeability high enough to drain as the reservoir is drawn down	Effective stress	
3. Steady seepage	Reservoir water surface at highest normal pool. Phreatic surface developed from the highest normal pool; typically the principal spillway crest	Consider failure surfaces within both the embankment and extending into the foundation. Foundation analysis may require separate phreatic surface evaluation, particularly in sites with confined seepage that results in uplift at the downstream toe.	Effective stress	1.5; and 1.3 for near surface (infinite slope) failure surfaces in cohesionless soils
4. Flood surcharge	Reservoir at freeboard hydrograph level. Steady seepage phreatic surface incorporating increased pore water pressure that may occur from flood detention and pore water pressure from short term seepage resulting from reservoir surface above the normal pool elevation	Consider failure surfaces within both the embankment and extending into the foundation.		1.4; and 1.2 for near surface (infinite slope) failure surfaces in cohesionless soils
		Embankment zones, foundation strata, or both comprised of material with a permeability high enough to drain rapidly with changes in reservoir elevation	Effective stress	
		Low-permeability embankment and foundation soils that will have limited drainage as the increased reservoir load is applied	Lowest of effective stress or consolidated, total stress (See Fig. 5-1 [of ref. publication])	

Table 15. USACE's minimum required factors of safety: New Earth and Rock-Fill dams (USACE, 2003).

Analysis condition ¹	Required minimum factor of safety	Slope
End-of-construction (including staged construction) ²	1.3	Upstream and Downstream
Long-term (steady seepage, maximum storage pool, spillway crest or top of gates)	1.5	Downstream
Maximum surcharge pool ³	1.4	Downstream
Rapid drawdown	1.1-1.3 ^{4,5}	Upstream

¹For earthquake loading see ER 1110-2-1806 for guidance. An Engineer Circular "Dynamic Analysis of Embankment Dams" is still in preparation.

²For embankments over 50 feet high on soft foundations and for embankments that will be subjected to pool loading during construction, a higher minimum end-of-construction factor of safety may be appropriate.

³Pool thrust from maximum surcharge level. Pore pressures are usually taken as those developed under steady-state seepage at maximum storage pool. However, for pervious foundations with no positive cutoff, steady-state seepage may develop under maximum surcharge pool.

⁴Factor of safety (FS) to be used with improved method of analysis described in Appendix G [of reference publication].

⁵FS = 1.1 applies to drawdown from maximum surcharge pool; FS = 1.3 applies to drawdown from maximum storage pool.

Specifically, on the topic of static slope stability analyses, among other recommendations, a table with minimum required factors of safety is provided, and reproduced hereafter in Table 14. Remarks and guidance on applicable shear strength parameters are also provided.

A particular feature of this publication is the prescription of specific minimum values for infinite slope analyses, when applicable for the stability of near surface failure surfaces in the exterior slope of embankments with cohesionless soils.

Another element to consider is that lower factors of safety for construction stability are allowed for cases where foundations are stronger and the potential failure surfaces are restricted to the embankment. This may be interpreted as an allowance for a lower stability margin in the light of lower uncertainties, probably associated with engineered construction materials submitted to QC/QA, which is not the case of tailings dam construction.

Guidelines are also provided for dynamic / seismic stability. Regarding specific provisions for factors of safety, the publication indicates 1.2 as the required minimum value for post-earthquake static stability, when there is potential for significant loss of strength under earthquake loading, therefore for residual or post liquefaction shear strength.

2.11 USACE's slope stability - Engineer manual (USACE, 2003)

This publication by the US Army Corps of Engineers presents recommendations for the analysis and design of slopes in general, regarding their stability. Thus, recommendations are not specific to tailings dams.

Regarding minimum required factors of safety, the manual states that the values are based on design practice developed by USACE during several decades.

Emphasis is put on the fact that appropriate factors of safety postulation should consider the uncertainties of the conditions being analysed and consequences of unacceptable performance. Likewise, it is stressed that criteria for existing dams may be different from those dams to be designed and constructed, with emphasis on investigation, observation, monitoring and performance evaluation, as uncertainties are reduced.

Indeed, the table with minimum required factors of safety presented in the manual is specifically referenced to "New Earth and Rock Fill Dams". The table is reproduced hereafter as Table 15. For existing dams and other types of slopes, the values are regarded as "advisory".

For dams used in pump storage schemes or similar applications where rapid drawdown is a routine operating condition, higher factors of safety, *e.g.*, 1.4-1.5, are appropriate. If consequences of an upstream failure are great, such as blockage of the outlet works resulting in a potential catastrophic failure, higher factors of safety should be considered.

2.12 USBR's design standards no. 13: Embankment dams - Chapter 4: Static stability analysis (USBR, 2011)

This publication by the US Bureau of Reclamation presents recommendations for the analysis and design of embankment dams in general, regarding their static stability analysis. Thus, recommendations are not specific to tailings dams.

Recommended minimum factors of safety are provided based on loading conditions. It is stated that deviations from the recommended values may be acceptable if supported with appropriate justification.

It is also stated that the minimum values need to consider the: design condition being analysed; consequences of failure; reliability of parameter estimation; presence of structures within embankment; reliability of investigations;

stress-strain compatibility of embankment and foundation materials; probable quality of construction control; embankment height and judgment based on past experience with earth and rockfill dams.

Another comment worthy of note is that the standard considers that “The factor of safety indicates a relative measure of stability for various conditions but does not precisely indicate actual margin of safety.”

Table 16 is presented, with the recommended minimum factor of safety values.

2.13 FERC’s engineering guidelines for the evaluation of hydropower projects - Chapter 4 - Embankment dams (FERC, 2006)

The USA’s Federal Energy Regulatory Commission produced various documents on risk management and risk-informed decision making for dams. The institution’s publication that provide actual guidelines on minimum required factor of safety values is the Engineering Guidelines for the Evaluation of Hydropower Projects.

As specified by the title, the guidelines refer to hydropower, and not mining projects. Still, due to the importance of FERC, the publication is considered relevant.

In line with most publications, the guidelines state that minimum required factor of safety values should depend on uncertainties - specifically the measurement of shear strength, likelihood of the assumed loading, assumptions in the method of analysis, construction quality, confidence on data, etc. - and the consequences of failure - specifically impact on human life, property damage, impairment of project functions, etc.

Despite these conceptual considerations, Table 17, with specific minimum required values “generally required by FERC” is provided.

2.14 CBdB’s guide to dam safety (CBdB, 2001)

The Guide to Dam Safety, prepared by the Brazilian Committee for Dams (CBdB) in 2001, provides guidelines on various aspects of the safety of dams in general. Regarding tailings dams, it is simply stated that they may have additional requirements, which should be specifically evaluated by specialists.

For slope stability analyses, the publication provides Table 18 with “normally acceptable” minimum factor of safety values for static slope stability assessment.

In line with other publications, it is stated that lower values may be adopted in specific cases, as long as they are

Table 16. USBR’s Minimum factors of safety based on two-dimensional limit equilibrium method using Spencer’s procedure. (USBR, 2011).

Loading condition	Shear strength parameters*	Pore pressure characteristics	Minimum factor of safety
End of construction	Effective	Generation of excess pore pressures in embankment and foundation materials with laboratory determination of pore pressure and monitoring during construction	1.3
		Generation of excess pore pressures in embankment and foundation materials and no field monitoring during construction and no laboratory determination	1.4
		Generation of excess pore pressures in embankment only with or without field monitoring during construction and no laboratory determination	1.3
	Undrained strength		1.3
Steady-state seepage	Effective	Steady-state seepage under active conservation pool	1.5
Operational conditions	Effective or undrained	Steady-state seepage under maximum reservoir level (during a probable maximum flood)	1.2
		Rapid drawdown from normal water surface to inactive water surface	1.3
	Effective or undrained	Rapid drawdown from maximum water surface to active water surface (following a probable maximum flood)	1.2
Other	Effective or undrained	Drawdown at maximum outlet capacity (Inoperable internal drainage; unusual drawdown)	1.2
	Effective or undrained	Construction modifications (applies only to temporary excavation slopes and the resulting overall embankment stability during construction)	1.3

*For selection of shear strength parameters, refer to Appendix A [of reference publication].

Table 17. FERC's minimum required factor of safety guidelines (FERC, 2006).

Loading condition	Minimum factor of safety	Slope to be analysed	Shear strength envelope
End of construction condition	1.3	Upstream and Downstream	
Sudden drawdown from maximum pool	> 1.1*	Upstream	
Sudden drawdown from spillway crest or top of gates	1.2*	Upstream	
Steady seepage with maximum storage pool	1.5	Upstream and Downstream	
Steady seepage with surcharge pool	1.4	Downstream	
Earthquake (for steady seepage conditions with seismic loading using a pseudo static lateral force coefficient)	> 1.0	Upstream and Downstream	

The values in the table are referred to analyses with peak shear strengths, and the publication considers liquefaction mainly in association to earthquakes, not in the static liquefaction perspective.

Table 18. CBdB's minimum required factors of safety for static slope stability assessment. (CBdB, 2001, free translation by the authors).

Factors of safety, static evaluation		
Loading conditions	Min. factor of safety	Slope
Steady state seepage with reservoir at the normal maximum level	1.5	Downstream
Rapid drawdown	From 1.2 to 1.3	Upstream
End of construction, before filling the reservoir	From 1.25 to 1.3	Downstream and Upstream

OBS: Higher factors of safety may be required if rapid drawdown occurs with relative frequency during normal operation.

justified, for example through demonstration of good performance with monitoring or more sophisticated analysis. Likewise, situations in which higher factor of safety values may be needed are stated.

The need to take into consideration data reliability, adequacy and limitations of analyses, failure consequences and deformation restrictions when postulating minimum required factors of safety is also highlighted.

Regarding liquefaction, the publication states that susceptible materials should be identified, but the method for their identification is not detailed. If said materials are identified, it is indicated that post-liquefaction stability analysis should be performed.

2.15 Eletrobrás' criteria for the civil design of hydro-electric plants (Eletrobrás, 2003)

The publication by Eletrobrás in 2003 presents criteria for the various design disciplines involved in the design of a hydroelectric plant's dam. Thus, the publication refers to embankment and rockfill water dams, rather than tailings dams.

Brief comments on analysis and shear strength parameter type are provided, as well as on loading scenarios and earthquake loading to be considered in the analyses.

Table 19 is presented with minimum required factors of safety depending on loading conditions. Guidance on the

Table 19. Eletrobrás' minimum required factors of safety (Eletrobrás, 2003, free translation by the authors).

Case	Factor of safety	Shear strength	Observations
End of construction	1.3 (a)	Q or S (b)	Upstream and Downstream Slopes
Rapid drawdown	1.1 to 1.3 (c)	R or S	Minimum value for dilatant soils Maximum value for soils that contract upon shearing
Steady state seepage	1.5	R or S	Downstream Slope
Seismic analysis	1.0	R or S	Upstream and Downstream Slopes

(a) For dams higher than 15m on relatively weak foundations apply minimum factor of safety of 1.4.

(b) In zones where no pore pressure is foreseen apply shear strength from S type tests.

(c) In cases where drawdown is frequent consider factor of safety of 1.3.

type of test to estimate shear strength parameters is also provided.

It is worth mentioning that Eletrobrás' recommendations for seismicity criteria have been frequently used for tailings dams in Brazil.

2.16 Summary of the recommendations

From a conceptual standpoint, traditionally recommendations from standards and guidelines state that minimum required factors of safety are a means / tool for managing risk, and thus should be defined based on elements of uncertainty / probability and consequence. However, from a practical standpoint, usually no detailed or specific guidance is provided on how to consider the impact of those elements other than that experience and sound engineering judgement must be applied.

As previously attempted in works by Hezra and Phillips (2017) and Fell *et al.* (2015), this work proposes recommendations on how to practically apply measures of uncertainty and consequence to the postulation of adequate minimum required factors of safety as obtained from limit equilibrium analysis. That is, taking the broadly philosophically accepted concepts to a practical level.

Regarding tailings dams, some rather clear important trends are noticeable in post-Brumadinho standard and guideline reviews. Mainly, they are:

- The requirement of checking for undrained behaviour considering both peak and residual (post-liquefaction) undrained shear strengths regardless of an associated triggering mechanism being expected;
- Emphasis on consequence assessment influence on design, management and analysis elements and sophistication.

For illustration, a summary table on recommended minimum required factors of safety for tailings dams is presented hereafter (Table 20). Terminologies, methodologies, hypotheses, applicability, remarks, etc. vary from publication to publication, and even though they are bundled together in the following table for the sake of simplicity, they should be considered in the light of the specifics of each publication. For those specifics, the preceding items of this work, or the publications themselves should be referred to.

Additionally, it is worth mentioning that it is expected that ICOLD will soon release a new publication with guidance on factors of safety for tailings dams, which may add to the information presented in Table 20.

It is important to highlight that most publications (except for the legislations) usually postulate the recommended values as a general base, which may be adapted by the engineer, if properly justified.

Lastly, it is known that other important institutions are in the process of discussing and, eventually, reviewing their guidelines and recommendations. For those ongoing reviews, the aforementioned general post-Brumadinho

trends usually seem to apply: the explicit recommendation or requirement of post-liquefaction analyses and minimum required factors of safety; the recommendation or requirement of undrained shear strength analyses regardless of specific trigger identification (with minimum factors of safety of 1.3, 1.5, for example); etc.

3. Limit equilibrium analysis

The most commonly adopted method for evaluating the stability of tailings dam embankments, as well as natural, cut and earthfill slopes, under static and pseudo-static conditions in both two and three dimensions is the limit equilibrium method. Several procedures are currently adopted in engineering practice, considering that they all explicitly satisfy force and moment equilibrium of the sliding mass (*e.g.* Bishop, 1955; Morgenstern and Price, 1965; Spencer, 1967, Sarma, 1973, among others). These procedures allow identification of potential failure mechanisms and derive global factors of safety for a particular geotechnical situation based on the general Mohr-Coulomb yield criterion, allowing use of drained, undrained or residual shear strength parameters. The factor of safety is calculated simply as the ratio of the shear strength to the shear stresses required for equilibrium.

Recently, more advanced numerical modelling for slope stability analysis has become common, allowing to predict deformation and pore pressure distribution fields within the soil mass, in addition to limit state conditions. In finite element calculations various schemes for strength reduction are applied to assess the equivalent factor of safety or to estimate the surplus of resistance provided by the input soil or tailings shear strength parameters with relation to what would lead to slope failure. As a result, different methods of analysis may yield different factors of safety depending on the complexity of the problem to be modelled, adding an uncertainty in the decision making process.

Design problems relating simple geometries to textbook material responses may produce similar results. Conversely, problems with complex geometries coupled to complex mechanical soil responses, especially when dealing with post-failure strain softening and progressive failure, would not necessarily yield comparable factors of safety.

In fact, from a theoretical viewpoint, it should be understood that the classical limit equilibrium method only considers the ultimate limit state of the slope and provides no assessment on the development of progressive landslide failure. Although extension of limit equilibrium principles to analyse the stability of strain-softening slopes has been proposed over the years, considering different algorithms to describe the Mohr-Coulomb elasto-plastic soil strength reduction from peak to residual (*e.g.* Law and Lumb, 1978; Miao *et al.*, 1999; Zhang and Wang, 2010), the severe limitations of the classical limit equilibrium method are only circumvented by numerical simulations with

Table 20. Summary of minimum required factors of safety for tailings dams.

Loading condition		ANCOLD (2019)	SEMAD - FEAM (2020)	CDA (2019)	ABNT (2017) ⁵	Chile (2007)	S. Africa (2015)
Long-term, normal operation / reservoir level / conditions		1.5 (drained parameters)	- / 1.5 ^{*1} (drained parameters)	1.5 ^{*2}	1.5 / 1.3 ^{*6}	-	-
Operation with extreme reservoir level / flow net		-	-	-	1.3	-	-
Short-term undrained (potential loss of containment)		1.5	-	-	-	-	-
Short-term undrained (no potential loss of containment), or during / end of construction		1.3	-	1.3	1.3	-	-
Rapid drawdown		-	-	1.3	1.1	-	-
Seismic / Pseudo-static		-	-	1.0 ^{*3}	1.1	-	-
Post-seismic		1.0-1.2	-	1.2	-	-	-
Static liquefaction (regardless of trigger)	Peak undrained shear strength	-	1.3 / 1.5 ^{*1}	-	-	-	-
Post liquefaction undrained shear strength	1.0-1.2	1.1 / 1.1 ^{*1}	1.1 ^{*4}	-	-	-	-
Unspecified		-	-	-	-	1.2 ^{*7}	1.5

Notes:

(*1) Values refer to: (prior to decharacterization) / (after decharacterization).

(*2) Also applicable during construction of dam raises.

(*3) Unless deformations due to seismic loading are assessed and acceptable.

(*4) Also applies to liquefaction associated to seismic loading.

(*5) For undrained shear strength parameters, values should be defined by the designer.

(*6) Values refer to: (downstream slope) / (between berms).

(*7) Upstream tailings dams are banned where the publication applies, pseudo-static analysis highlighted.

References:

ANCOLD (2019) - Guidelines on Tailings Dams - Planning, Design, Construction, Operation and Closure

SEMAD - FEAM (2020) - Term of Reference for the Decharacterization of Upstream Tailings Dams

CDA (2019) - Application of Dam Safety Guidelines to Mining Dams Revision (2019)

Ministerio de Minería (2007) - Chilean Ministry of Mining's Regulations for the approval of design, construction, operation and closure of tailings dams

South African Government Department of Environmental Affairs (2015) - South African Government's Mining Residue Regulations.

strain-softening models such as those proposed by Jefferies (1993); Potts *et al.* (1997), Conte *et al.* (2010), among others. The common design practices of using simple analytical methods, at the expense of more sophisticated numerical analysis, associated with low safety factors cannot guarantee a sufficient safe level of the structure for the combination or superposition of the shortcomings in mathematical modelling and the uncertainties in material properties.

Summarizing, a global factor of safety broadly defines the load-bearing capacity of a structure but the actual value depends on the calculation method, whereas the extent to which the calculated value ensures the safety and positive behaviour of a structure will depend on other factors such as the material constitutive model, the accuracy of different soils or tailings strength parameters, the assumed hydrogeological conditions, among other factors. Under

the scenario described for static downstream slope stability calculations, the general recommendation is to perform drained and undrained strength analyses and adopt a minimum static factor of safety of 1.5 for the condition that yields the coefficient against instability lower limit, called factor of safety. This general recommendation stands since the 1990s (*e.g.* Carrier, 1991; Szymansky, 1999). However, using factors of safety even greater than 1.5 for static analysis could be justified for dams in higher consequence categories as the values presented in standards and bibliography are minimum values to be pursued.

Conservatism in design and/or posterior verifications should be considered as a general rule in the design of upstream method Tailings Storage Facility (TSF) given the uncertainties in estimating the constitutive parameters, the spatial variability of tailings, and the complex geomechanical behaviour emerging from flow instability,

as well as the enormous environmental and social/civilian consequences. For this reason, probabilistic slope stability analysis and risk assessment should be used as complementary to the deterministic method, providing a tool for considering uncertainties of the soil parameters within a range and according to a probability distribution (*e.g.* Griffiths and Fenton, 2004; El-Ramly *et al.*, 2005; Espósito and Palmier, 2013).

4. Recommendations for appropriate values of factors of safety in limit equilibrium analysis

The principle of complying with minimum acceptable factors of safety when assessing the stability of embankment dams of any type or for any use has been gradually adjusted throughout the years. The recent major accidents reported from 2015 to 2019 enforced regulators and industry to question and to review international standard guidelines and the recommended minimum acceptable factors of safety for the different loading conditions that apply to these embankments. The preceding discussion has demonstrated that there is still no acceptable consensus for recommended threshold values.

Currently there are three possible alternatives to design or verify the stability of an operating or abandoned upstream method TSF structure:

- a) Adopt prescribed minimum values of factors of safety as related to different loading conditions, without explicitly linking these values to recommended values to consequence categories.

- b) Assume the conservative approach of defining factors of safety for ‘Extreme’ consequences of failure, regardless the real consequence categories of the structure as evaluated in specific additional and parallel studies.
- c) Adopt minimum values of factors of safety embracing the overall design uncertainties together with the failure consequences to population at risk downstream of the structure.

The principles of minimum values of factor of safety linked to and dependent from the overall uncertainties in design and operational management, and on dam failure consequences are calling attention and have been addressed in several recent publications (*e.g.* Fell *et al.*, 2015; Hezra and Phillips, 2017).

As far as the uncertainties are concerned, tailings storage facilities can be divided into three basic categories, as postulated in Table 21. Information summarized herein works as a basic qualitative classification approach for risk assessment, in line with ICOLD recommendations, intended to evaluate the technical requirements related to dam design, construction and operation (Bulletin 121, ICOLD, 2001). The features described within the table are further discussed in the Appendix.

In summary, the categories proposed in Table 21 may be described as:

- Category I: TSF for which design, construction and operation features lead to negligible or lower level of uncertainty for engineering decision making regarding safety;
- Category II: TSF for which design, construction and operation features lead to an intermediate level of uncertainty for engineering decision making regarding safety;

Table 21. Classification system for qualitative risk assessment of tailings dams. (ICOLD, 2001).

Category	I	II	III
Characterization	Site-specific detailed characterization Advanced lab testing	Routine field and laboratory testing of tailings and foundations	Insufficient site characterization of tailings and foundations
Analysis to back design or evaluation of safety	Numerical analysis with appropriate constitutive stress-strain models together with high quality limit equilibrium analysis	Limit equilibrium analysis	Limit equilibrium analysis
Instrumentation	State-of-the art with continuous reading, transfer of data and interpretation	Cost-effective monitoring	Limited instrumentation
Operation	Expert construction supervision and inspection	Routine construction supervision	No historical construction process.
	Controlled water management	Occasional deviation from ideal operation, leading to beach length, freeboard, water balance in non-compliance	Saturation of critical zones
	Robust long-term asset management planning process	Observation of standards and management procedures	Maintenance planning and management process not implemented

- Category III: TSF for which design, construction and operation features lead to higher or critical level of uncertainty for engineering decision making regarding safety.

High level engineering expertise and judgment is required to take full advantage of this classification system. A factor of safety of 1.3, although accepted in some countries, is not endorsed by all national standards, and in the authors view this value could only be accepted for temporary structures or short-term conditions with no potential loss of containment. A higher factor of safety should be applied even for low risk slopes on tailings dams that fully comply with the design precept that the phreatic surface is fully controlled, and should not daylight in the embankment downstream slope and should be well below the embankment face and in the tailings deposit, with maintenance of the internal drainage systems assuring the long term safety of the structure.

In addition, the authors recall that the residual (post-liquefaction) undrained shear strength (S_{ur}) of a material, soil or tailings, is a strain rate-dependent strength phenomenon in which the viscous component is a function of volumetric strain rate and void ratio (*e.g.* Schnaid *et al.*, 2014; Schnaid, 2021). The undrained residual strength has also been referred to as the undrained steady-state shear strength (Poulos, 1981), the undrained critical shear strength (Seed, 1987) or the liquefied shear strength (Olson & Stark, 2002). Estimating S_{ur} of a liquefied material, soil or tailings, which behaves as non-Newtonian fluid, whose viscosity decreases drastically with increasing shear strain rate, is still an unresolved issue. Currently, *in situ* test interpretation (CPTU, full penetrometers and FVT) gives only rough estimates of S_{ur} , which limits our ability to approach static liquefaction stability through total stress analysis, because the difficulties in measuring the very low strengths mobilized under brittle response when the material loses strength rapidly, moving from peak to residual, and the possible slip at the element boundary along the failure surface (Schnaid, 2021). For this reason, up to present, engineers have relied on back-analysis procedures (Seed & Harder, 1990; Olson & Stark, 2002; Robertson, 2010; Sadrekarimi, 2014) in which liquefied shear strength $S_{u,liq}$ is rationalized with relation to the pre-failure vertical effective stress and is related to original cone penetration resistance, prior to the liquefaction phenomena. The uncertainty in estimating this key design parameter inherently enforces a choice for factors of safety higher than 1.5 for peak undrained shear strength in static limit equilibrium analysis, which, in the view of the authors, would indirectly lead to at least marginal safety in post-liquefaction conditions.

As for the consequence-based dam safety principle, it will be increasingly used for the design of tailings dams. In undertaking a consequence category assessment, the information provided in Table 22 can be used as a guideline to estimate appropriate factors of safety (Simplified from ICMM, 2019).

Minimum required factors of safety should then be established from the assessment of the combination of management / uncertainty conditions - according to categories I, II, or III from Table 21, in line with ICOLD (2001) - and consequence category - according to categories A, B or C from Table 22, adapted from ICMM (2019).

Once both categories are defined for the TSF, they may be applied to define the recommended minimum required factors of safety as proposed in Table 23. The table also accounts for the TSF lifecycle stage, for which is important to highlight that it is assumed that new TSFs shall be designed ensuring management / uncertainty conditions of Category I.

Values listed in this table apply to both static drained and undrained loading conditions that can prevail in the short term and/or long term and are applicable to the design of new structures and during dam's operation life, as well as for decommissioning, decharacterization and closure of existing structures. Established for slope stability analysis using limit equilibrium methods, these recommended factors of safety are proposed based on some fundamental concepts.

Under the complex hydrogeological environment of tailings dams, the uncertainties in material properties and the potential loss of containment, it is unreasonable to accept design factors of safety lower than 1.5 for both long-term drained or short-term undrained conditions. As for the proposed factors of safety of existing structures, a more detailed explanation is required to fully appreciate the suggested values safety greater than 1.5.

Being a widely used term in dam engineering, decommissioning a water storage dam means completely removing or breaching the structure in such a way that it can no longer retain or store water. When applied to tailings dams, the term decommissioning is assigned to an engineering process that seeks to shut down a structure and involves activities such as reshaping the slope of downstream or upstream dikes, implementing cover and surface drainage systems, revegetating the covered areas, all of which should be implemented according to specific guidelines and procedures for environmental protection and closure plans (*e.g.* Geological Survey of Finland, 2008; ICOLD, 2011; 2013).

Similarly, dam decharacterization is also related to the closure phase of a structure, but it specifically refers to the process by which a dam ceases operating as a tailings containment structure to be used for other purposes. Introduced in Brazil by the Dam Safety Policy provisions for the State of Minas Gerais, issued on February 2019, it implies that during the physical decharacterization works the structure is removed by excavating the tailings for subsequent disposal in caves or filtered stacks, or is entirely adapted so that the remaining structure will no longer be a dam, being reincorporated into the surrounding geographical environment. Alternatively, one may consider that decharacteri-

Table 22. Consequence categories based on potential loss of life (PLL) and severity of damage and loss, adapted and simplified from ICMM (2019).

Category		Consequence
	Severity of Damage and Loss	Potential Loss of Life (PLL) / Severity of Damage and Loss
A	Relevant	<p>PLL: None expected</p> <p><i>Environment:</i> No significant loss or deterioration of habitat. Contamination of fauna with no health effects. Material has low potential hazardous characteristics. Restoration possible within 1-5 years.</p> <p><i>Health, Social & Cultural:</i> Significant disruption of business, services or social dislocation (< 500 people). Low likelihood of loss of relevant socio-cultural assets and low likelihood of health effects.</p> <p><i>Infrastructure & Economics:</i> Loss limited to less relevant / infrequently used facilities and infrastructure. Up to US\$ 10 M.</p> <p><i>Livelihoods:</i> disruption of up to 10 household livelihood systems recoverable in the longer term or up to 100 recoverable in the short term. No non-recoverable loss of livelihoods.</p>
B	High	<p>PLL: 1-50</p> <p><i>Environment:</i> Significant to important loss or deterioration of critical habitat / species. Material has moderate to high potential hazardous characteristics. Area of impact 10-20 km². Restoration possible but difficult and likely requires significant to long time.</p> <p><i>Health, Social & Cultural:</i> 500-1000 people affected by disruption of business, services or social dislocation. Disruption and/or minor loss of relevant socio-cultural assets. Potential for short term and/or minor long-term human health effects.</p> <p><i>Infrastructure & Economics:</i> High to very high losses affecting relevant to important infrastructure, facilities or employment. Significant relocation / compensation to communities. US\$ 10 M to 500 M.</p> <p><i>Livelihoods:</i> non-recoverable loss of up to 25 household livelihood systems, or; longer term recoverable disruption of up to 100 household livelihood systems or; short term recoverable disruption of up to 250 household livelihood systems.</p>
C	Catastrophic	<p>PLL: > 50</p> <p>Effects greater than those described for Category B, for example:</p> <p><i>Environment:</i> Major to catastrophic loss or deterioration of critical habitat / species. Material has high to very high potential hazardous characteristics. Area of impact > 20 km². Restoration / compensation impossible or possible but very difficult and requires a long / very long time.</p> <p><i>Health, Social & Cultural:</i> > 1000 people affected by disruption of business, services or social dislocation for > 1 year. Significant loss / destruction of relevant socio-cultural assets. Potential for severe and/or significant longer-term human health effects.</p> <p><i>Infrastructure & Economics:</i> Very high to extreme losses affecting important to critical infrastructure, services or employment. High to very high relocation / compensation to communities and or very high social readjustment costs. US\$ > 500 M.</p> <p><i>Livelihoods:</i> number of household livelihood systems impacted greater than those of Category B.</p>

zation involves transforming an upstream dam into a downstream structure.

In existing well-maintained structures, operating under expert construction supervision and inspection, decommissioning and decharacterization are performed under the specific requirement of meeting the safety regulations from updated Standards. Design for decommissioning embraces the same risk management associated with building new

dams and should, therefore, follow the same factors of safety recommended in design of new structures.

On the other hand, in decommissioning a vulnerable structure (Categories II and III on Table 21) engineers have to handle various challenges emerging from deficiencies in construction and operation, insufficient data to obtain complete and objective characterization of tailings and foundations, heterogeneity of the tailings as produced from

Table 23. Recommended factors of safety for static short term and/or long term undrained and drained analyses.

Category	Design	Operation to closure		
	New upstream or downstream structures	I - Well-maintained upstream structures	II	III
Consequence category	A	1.5	1.5	1.5
	B	1.5	1.5	1.7
	C	1.5	1.5	1.8

Note: Management / uncertainty category (I, II or III) may be defined from Table 21, in line with ICOLD (2001). Consequence category (A, B or C) may be defined from Table 22, adapted from ICM (2019).

different ore and beneficiation processes along time, malfunction and deterioration of the dam, among other factors, in order to ensure that it remains stable for all conceivable load combinations and structural reinforcement phases. These uncertainties inherently increase the probability of failure in each stage decommissioning scenario, which is partially compensated by the higher factors of safety listed in Table 23, *i.e.* factors of safety in limit equilibrium analysis, if numerical simulations cannot be performed, larger than the minimum value of 1.5 for both short and long term conditions are necessary to minimize the likelihood of accidents during the process of decommissioning or decharacterization, and avoid major human consequences if they occur.

In addition, adoption of higher factors of safety for dams under Categories II and III has major implications when considering static and cyclic liquefaction-triggered stability analysis in tailings. A critical element of liquefaction assessment is the uncertainty associated to the residual (liquefied) undrained shear strength ($S_{u,liq}$), which limits our ability to approach liquefaction stability through routine total stress analysis. Factors of safety equal or greater than 1.7 for static short term analyses using undrained peak shear strength ($S_{u,p}$) implicitly circumvent this limitation because a safer design for peak strength works as a minimum requirement to satisfy the recommended factors of safety for static liquefaction (of the order of 1.1 as has been discussed by many professionals). Under a more conservative approach, liquefaction stability assessment is still required to manage liquefaction related risk, but errors in predicting $S_{u,liq}$ when performing deterministic analysis become less critical.

A final comment refers to seismic stability assessment of tailings dams. Countries across the world rely on codes of practice to establish minimum levels of safety requirements against earthquakes in order to ensure structural performance. Over decades, there has been considerable research in this topic and a critical review of loading conditions not associated to pseudo-static or post-seismic analyses is not covered by the current discussion and proposals.

In respect to Table 23, lower factors of safety may be acceptable when geotechnical design is improved by making extensive use of finite element and finite difference

techniques coupled to appropriate constitutive modelling, and proper knowledge of the behaviour of the structure and the tailings contained is gained. This is especially relevant in cases where tailings do not sustain a constant value of deviatoric stress under undrained shearing leading to high strain softening and subsequent failure by flow liquefaction. However, it should be recognized that numerical analysis is an expert field requiring skills, judgment and experience other than mathematical expertise (see ANCOLD, 2019).

5. Conclusions

This paper explores early works on the subject and presents a proposal of guidelines that try to help select suitable minimum design factors of safety for tailings dams slope stability analysis using limit equilibrium calculations. The proposed values are more conservative than what has become standard in international practice for vulnerable structures where consequence, uncertainties, risk and characteristics of loose tailings increase engineering design challenges.

References

- ANCOLD (2012). Australian National Committee on Large Dams Guidelines on the Consequence Categories for Dams. ANCOLD, Hobart, 40 p.
- ANCOLD (2019). Australian National Committee on Large Dams Guidelines on Tailings Dams - Planning, Design, Construction, Operation and Closure - Revision 1. ANCOLD, Hobart, 70 p.
- ABNT (2017). Mining - Preparation and Presentation of Design of Tailings, Sediments and/or Water Dams - Requirements - NBR 13028:2017. ABNT, Rio de Janeiro, Brazil, 16 p.
- Bishop, A.W. (1955). The use of the slip circle in the stability analysis of slopes. *Géotechnique*, 5(1):7-17. <https://doi.org/10.1680/geot.1955.5.1.7>
- CDA (2013). Canadian Dam Association Dam Safety Guidelines 2007 (2013 Edition), CDA, Toronto, 82 p.
- CDA (2014). Canadian Dam Association Application of Dam Safety Guidelines to Mining Dams. CDA, Toronto, 41 p.

- CDA (2019). Canadian Dam Association Revision to Application of Dam Safety Guidelines to Mining Dams. CDA, Toronto, 18 p.
- Carrier, W.D. (1991). Stability of tailings dams. Proc. XV Ciclo di Conferenze di Geotecnica di Torino, Univ. of Torino, Torino.
- CBdB (2001). Guia Básico de Segurança de Barragens. CBdB, São Paulo, 77 p.
- Conte, E.; Silvestri, F. & Troncone, A. (2010). Stability analysis of slopes in soils with strain-softening behaviour. *Computers and Geotechnics*, 37(5):710-722. <https://doi.org/10.1016/j.compgeo.2010.04.010>
- Eletrobrás (2003). Critérios para Projeto Civil de Usinas Hidrelétricas. Eletrobrás, CBdB, [s.l.], 278 p.
- El-Ramly, H.; Morgenstern, N.R. & Cruden, D.M. (2005). Probabilistic assessment of stability of a cut slope in residual soil. *Géotechnique*, 55(1):77-84. <https://doi.org/10.1680/geot.55.1.77.58590>
- Espósito, T. & Palmier, L.R. (2013). Application of risk analysis methods on tailings dams. *Soils and Rocks*, 36(1):97-117.
- FERC (2006). Federal Energy Regulatory Commission Engineering Guidelines for the Evaluation of Hydropower Projects - Chapter 4 - Embankment Dams. FERC, [s.l.], 90 p.
- Fell, R.; MacGregor, P.; Stapledon, D.; Bell, G. & Foster, M. (2015) *Geotechnical Engineering of Dams*, 2nd ed. CRC Press, Boca Raton, 1338 p.
- Gama, F.F.; Paradella, W.R.; Mura, W.R. & dos Santos, A.R. (2013). Técnicas de interferometria radar na detecção de deformação superficial utilizando dados orbitais. Proc. XVI Simpósio Brasileiro de Sensoriamento Remoto, INPE, São José dos Campos, pp. 8405-8412.
- Gobierno de Chile - Ministerio de Minería (2007). *Aprueba Reglamento para la Aprobación de Proyectos de Diseño, Construcción, Operación y Cierre de los Depósitos de Relaves*. Biblioteca del Congreso Nacional de Chile available online at www.leychile.cl/N?i=259901&f=2007-04-11&p= and downloaded on 01/04/2020.
- Governo do Estado de Minas Gerais - Secretaria de Estado de Meio Ambiente e Desenvolvimento Sustentável - Fundação Estadual do Meio Ambiente (2020). *Termo de Referência para Descaracterização de Barragens Alteadas pelo Método de Montante*. SEMAD-FEAM, Belo Horizonte, 16 p.
- Griffiths, D.V. & Fenton, G.A. (2004). Probabilistic slope stability analysis by finite elements. *Journal of Geotechnical and Geoenvironmental Engineering*, 130(5):507-518. [https://doi.org/10.1061/\(ASCE\)1090-0241\(2004\)130:5\(507\)](https://doi.org/10.1061/(ASCE)1090-0241(2004)130:5(507))
- Geological Survey of Finland (2008). *Mine Closure Handbook*. Heikkinen, P.M.; Noras, P. & Salminen, R. (eds), Geological Survey of Finland, Espoo, 169 p.
- Hezra, J. & Phillips, J. (2017) Design of dams for mining industry. Proc. 85th Annual Meeting of International Commission on Large Dams, ICOLD, Prague.
- ICOLD (2013). International Commission on Large Dams Bulletin 153 - Sustainable design and post-closure performance of tailings dams, ICOLD, Paris, France, 88 p.
- ICOLD (2001). International Commission on Large Dams Bulletin 121 - Tailings Dams Risk of Dangerous Occurrences - Lessons Learnt from Practical Experiences. ICOLD, Paris, 144 p.
- ICOLD (2011). International Commission on Large Dams Bulletin 139 - Improving Tailings Dam Safety - Critical Aspects of Management, Design, Operation, and Closure. ICOLD, Paris, 171 p.
- ICOLD (2013). International Commission on Large Dams Bulletin 153 - Sustainable Design and Post-Closure Performance of Tailings Dams. ICOLD, Paris, 88 p.
- ICMM (2019). International Council of Mining & Metals Global Tailings Standard - Draft for Public Consultation. ICMM, [s.l.], 33 p.
- Jefferies, M. (1993). Nor-Sand: a simple critical state model for sand. *Géotechnique*, 43(1):91-103. <https://doi.org/10.1680/geot.1993.43.1.91>
- Jefferies M. & Been, K. (2016). *Soil Liquefaction - A Critical State Approach*, 2nd ed. CRC Press, Boca Raton, 676 p.
- Law, K.T. & Lumb, P. (1978). A limit equilibrium analysis of progressive failure in the stability of slopes. *Canadian Geotechnical Journal*, 15(1):113-122. <https://doi.org/10.1139/t78-009>
- Li, X.S. & Wang, Y. (1998) Linear representation of steady-state line for sand. *Journal of Geotechnical and Geoenvironmental Engineering*, 124(12):1215-1217. [https://doi.org/10.1061/\(ASCE\)1090-0241\(1998\)124:12\(1215\)](https://doi.org/10.1061/(ASCE)1090-0241(1998)124:12(1215))
- Meyerhof, G.G. (1994) Evolution of safety factors and geotechnical limit state design - 2nd Spencer J. Buchanan Lecture. Texas A&M University, College Station, 31 p.
- Miao, T.; Ma, C. & Wu, S. (1999). Evolution model of progressive failure of landslides. *Journal of Geotechnical and Geoenvironmental Engineering*, 125(10):827-831. [https://doi.org/10.1061/\(ASCE\)1090-0241\(2001\)127:1\(98\)](https://doi.org/10.1061/(ASCE)1090-0241(2001)127:1(98))
- Morgenstern, N.R. (2018). *Geotechnical Risk, Regulation, and Public Policy - The Sixth Victor de Mello Lecture*. *Soils and Rocks*, 41(2):107-129. <https://doi.org/10.28927/SR.412107>
- Morgenstern, N.R.; Jefferies, M.; Zyl, D.V. & Wates, J. (2019). *Report on NTSF Embankment Failure Cadia Valley Operations for Ashurst Australia*. Newcrest, [s.l.], 101 p.
- Morgenstern, N.R. & Price, V.E. (1965). The analysis of the stability of general slip surfaces. *Géotechnique*, 15(1):79-93. <https://doi.org/10.1680/geot.1965.15.1.79>

- Morgenstern, N.R.; Vick, S.G.; Viotti, C.B. & Watts, B.D. (2016). Fundão Tailings Dam Review Panel - Report on the Immediate Causes of the Failure of the Fundão Dam. Fundão Tailings Dam Review Panel, [s.l.], 66 p.
- Morgenstern, N.R.; Vick, S.G. & Zyl, D.V. (2015). Independent Expert Engineering Investigation and Review Panel - Report on Mount Polley Tailings Storage Facility Breach. Government of British Columbia, Victoria, 147 p.
- NRCS (2019). National Resources Conservation Service Technical Release 210-60 - Earth Dams and Reservoirs. NRCS, [s.l.], USA, 63 p.
- Olson, S.M. & Stark, T.D. (2002). Liquefied strength ratio from liquefaction flow failure case histories, *Canadian Geotechnical Journal*, 39(3):629-647. <https://doi.org/10.1139/t02-001>
- Pestana, J.M. & Whittle, A.J. (1999). Formulation of a unified constitutive model for clays and sands. *Proc. International Journal for Numerical and Analytical Methods in Geomechanics*, 23(12):1215-1243. [https://doi.org/10.1002/\(SICI\)1096-9853\(199910\)23:12<1215::AID-NAG29>3.0.CO;2-F](https://doi.org/10.1002/(SICI)1096-9853(199910)23:12<1215::AID-NAG29>3.0.CO;2-F)
- Potts, D.M.; Kovacevic, N. & Vaughan, P.R. (1997). Delayed collapse of cut slopes in stiff clay. *Géotechnique*, 47(5):953-982.
- Poulos, S.J. (1981) The steady state of deformation. *Journal of Geotechnical and Geoenvironmental Engineering*, 107(5):553-562. [https://doi.org/10.1016/0148-9062\(81\)90548-9](https://doi.org/10.1016/0148-9062(81)90548-9)
- Reid, D. (2020) Inherent uncertainties in numerical models to assess triggering likelihood. ABMS MG E-talk March 3rd 2020, ABMS, online presentation.
- Robertson, P.K. (2010). Evaluation of flow liquefaction and liquefied strength using the cone penetration test. *Journal of Geotechnical and Geoenvironmental Engineering*, 136(6):842-853. [https://doi.org/10.1061/\(ASCE\)GT.1943-5606.0000286](https://doi.org/10.1061/(ASCE)GT.1943-5606.0000286)
- Robertson, P.K.; de Melo, L.; Williams, D.J. & Wilson, G.W. (2019). Report of the expert panel on the technical causes of the failure of Feijão Dam I. Expert Panel, [s.l.], 71 p.
- Sadrekarami, A. (2014) Effect of soil plastic contraction on static liquefaction triggering analysis. *Géotechnique*, 64(4):325-332. <https://doi.org/10.1680/geot.13.P.139>
- Sarma, S.K. (1973). Stability analysis of embankments and slopes. *Géotechnique*, 23(3):423-433. <https://doi.org/10.1680/geot.1973.23.3.423>
- Schnaid, F. (2021). On the geomechanics and geocharacterization of tailings. *Proc. 9th J.K. Mitchell Lecture*. In print.
- Schnaid, F.; Nierwinski, H.P.; Bedin, J. & Odebrecht, E. (2014). On the characterization and classification of bauxite tailings. *Soils and Rocks*, 37(3):277-284.
- Seed, R.B. (1987). Design problems in soil liquefaction. *Journal of Geotechnical Engineering*, 113(8):827-845. [https://doi.org/10.1061/\(ASCE\)0733-9410\(1987\)113:8\(827\)](https://doi.org/10.1061/(ASCE)0733-9410(1987)113:8(827))
- Seed, R.B. & Harder Jr., L.F. (1990). SPT-based analysis of cyclic pore pressure generation and undrained residual strength. *Proc. H.B. Seed Memorial Symposium*, BiTech Publishers, Richmond, v. 2, pp. 351-376.
- SABS (1998). South African Bureau of Standards Code of Practice - Mine Residue - SABS 0286:1998. SABS, Pretoria, South Africa, 117 p.
- South African Government Department of Environmental Affairs (2015). National Environmental Management: Waste Act, 2008 (Act No. 59 of 2008) - Regulations Regarding the Planning and Management of Residue Stockpiles and Residue Deposits from a Prospecting, Mining, Exploration or Production Operation. South African Government Gazette, [s.l.], South Africa, 16 p.
- Spencer, E. (1967). A method of analysis of the stability of embankments assuming parallel inter-slice forces. *Géotechnique*, 17(1):11-26. <https://doi.org/10.1680/geot.1967.17.1.11>
- Szymansky, M.B. (1999). Evaluation of Safety of Tailings Dams. BiTech Publishers, Vancouver, 100 p.
- Taborda, D.M.G.; Zdravkovic, L.; Kotoe, S. & Potts, D. (2014) Computational study on the modification of a bounding surface plasticity model for sands. *Computers and Geotechnics*, 59:145-160. <https://doi.org/10.1016/j.compgeo.2014.03.005>
- Taylor, D.W. (1948). *Fundamentals of Soil Mechanics*. John Wiley & Sons, New York, 700 p.
- Terzaghi, K. (1943). *Theoretical Soil Mechanics*. John Wiley & Sons, New York, 510 p.
- Thomas, A.; Edwards, S.J.; Engels, J.; McCormack, H.; Hopkins, V. & Holley, R. (2019). Earth observation data and satellite InSAR for the remote monitoring of tailings storage facilities: A case study of Cadia Mine, Australia. *Proc. 22nd International Conference on Paste, Thickened and Filtered Tailings*, Australian Centre for Geomechanics, Perth, v. 22, pp. 183-196.
- USACE (2003). U.S. Army Corps of Engineers Engineer Manual - Engineering and Design - Slope Stability. USACE, Washington, 205 p.
- USBR (2011). U.S. Department of Interior Bureau of Reclamation Design Standards No. 13 - Embankment Dams - Chapter 4: Static Stability Analysis. USBR, [s.l.], 159 p.
- Valenzuela, L. (2015). Tailings Dams and Hydraulic Fills - The 2015 Casagrande Lecture. Sfriso, A.O.; Manzanal, D. & Rocca, R.J. (eds.), *Geotechnical Synergy in Buenos Aires 2015*, IOS Press, Amsterdam, pp. 5-49.
- Zhang, G. & Wang, L. (2010). Stability analysis of strain-softening slope reinforced with stabilizing piles. *Journal of Geotechnical and Geoenvironmental Engineering*

ring, 136(11):1578-1582.
10.1061/(ASCE)GT.1943-5606.0000368

DOI: *Category II*

Appendix

The authors recognize that subjectivity exists in qualitative risk assessments, leading to different interpretations from users from different backgrounds and/or technical culture. Trying to minimize the impact of this fact, a tentative, and at the same time more precise description of the Categories listed in Table 21, allowing for a more consistent qualitative risk assessment of tailings dams, is proposed herewith. These are the views of the authors and cannot be seen as a prescription without the users own judgement.

Site Characterization

Category I

- Geological complexity of the site is well-defined for soils and rock formations.
- Topographical, hydro-geological, geotechnical and geo-environmental information acquired and documented.
- Extensive and continuous ground investigation programs implemented periodically during the construction and life-time operation.
- Site-specific detailed characterization - encompassing at least but not only:
 - CPTUs, with pore-pressure dissipation curves performed at depths to full stabilization to identify perched water tables and complex flow patterns.
 - In Hole seismic geophysical tests, like Cross Hole or Down Hole, S-CPTU seismic CPTUs; S-DMT, as well as Surface Geophysical Methods.
 - Complementary tests such as DMT (Marchetti dilatometer), SBPM (self-boring pressuremeter tests) and FVT (vane tests).
- Advanced laboratory testing, with detailed analysis of constitutive parameters of tailings and foundations., comprising:
 - Undisturbed samples, preferably using stationary piston samplers and the Gel-Push sampler when recommended.
 - Reconstituted samples (problem of aging generating structure is a pending issue after the Brumadinho failure).
 - Consolidated undrained tests, isotropically and anisotropically consolidated, CIU and CAU on saturated samples as well as on partially saturated samples. Compression and extension tests.
 - Direct simple shear tests, DSS.
 - Cyclic triaxial tests.

- Basic geological topographical, hydro-geological, geotechnical and geo-environmental information, following basic standards and international specifications.
- Routine field and laboratory testing of tailings and foundations.
 - SPT, CPTUs with routine dissipation tests. Vane tests in close arrays to better interpret that data.
 - Disturbed samples from continuous soil samplers or small diameter thin-wall samplers to calculate the void ratio variation with depth from water content measurements taken below the water table.
 - Reconstituted samples to test on CIU and DSS tests.

Category III

- Insufficient site characterization of tailings and foundations, not in compliance with the standards postulated for Category I.
 - No detailed knowledge of the tailings dam foundations, the starter dam and raising dikes; their internal drainage system and the global internal drainage concept.
 - In situ SPT and CPTU with routine dissipation tests.

Analysis to back design or evaluation of safety

Category I

- Numerical analysis with appropriate constitutive stress-strain models together with well-established limit equilibrium analysis.
 - Use of critical state soil mechanics (CSSM).
 - Introduction of sensitivity analyses to understand and evaluate change of conditions, as a trigger of static liquefaction.
 - Develop limit equilibrium analysis for shear strength associated to the collapse surface of the tailings.
 - Proper alert levels defined for the interpretation of the monitoring program.

Category II

- Limit equilibrium analysis based on average constitutive parameters.
 - Conventional series of limit equilibrium analysis, both in drained and undrained analyses; circular and polygonal potential failure surfaces minimizing value of FS.
 - Difficulties in postulating alert levels for all the instruments, not only associated to displacements.

Instrumentation

Category I

- State-of-the art with continuous reading, transfer of data and interpretation.
 - Electric Piezometers and Water level indicators automated with readings at short periodicity.

- Inclinometers, either manual or vibrating wire in place inclinometers.
- Interferometric technologies for surface displacement monitoring - such as InSAR and Ground Based Radar - have seen and are seeing a significant popularization in Geotechnical Engineering practice as a whole and in mining applications.
 - These are considered to be useful tools for effective monitoring, if used correctly.
 - Nonetheless, their limitations should always be highlighted and considered for interpretation. For example, usually the displacement measurements refer only to a given orientation axis or plane related to the line of sight of the equipment, potentially implying a bias. Also, authors state that changes in surface conditions - for example, moisture, temperature, and especially vegetation - may lead to significant noise and errors in measurements (Thomas *et al.*, 2019; Robertson, *et al.*, 2019; Gama, *et al.*, 2013).
 - Thus, these tools are valuable, but should be used with due care provided that precision is within the acceptable range. In the same sense that geophysical *in situ* tests should be interpreted together with traditional borehole data in the light of a geological model, interferometric data should be interpreted together with other monitoring techniques - such as topographic monitoring, DGPS, visual inspection, etc. - and by a team of professionals that are proficient both in the measured geotechnical physical behaviours and in the interferometric technology applied.
- Flow meters in the exit/outlet of all internal drainage devices.

Category II

- Cost-effective monitoring.
 - Electric Piezometers and Water level indicators read manually.
 - Inclinometers read manually.
 - Topographic survey marks read by precision topography.
 - Flow meters in the connections of main drainage ditches and bottom exit of the drainage system.

Category III

- Limited instrumentation.
 - Mechanical instrumentation systems including standpipe Casagrande piezometers, water level indicators, flow meter at the bottom exit of the internal drainage system and topographic survey marks.

Operation

Category I

- Expert construction supervision and inspection.
 - Thorough, robust, and formal implementation of Quality Control (QC), Quality Assurance (QA) and Construction vs. Design Intent Verification (CDIV), with high standards and capacitation of involved professionals.
 - Preparation of Site Inspection Manuals, with well-established methodology and straightforward procedures, types and frequency of QA/QC test work, inspection, recording and reporting requirements.
 - Periodic (*e.g.* annual) preparation of a detailed Construction Records Report.
 - Implementation of formal change management systems to evaluate, review, approve and document all changes to design, construction, operation and monitoring.
 - Assignment and due empowerment of a qualified Engineer of Record. Conduct annual construction and performance reviews through the Engineer of Record or a senior independent technical reviewer. An independent senior technical reviewer shall also conduct periodical Dam Safety Reviews.
- Controlled water management.
 - Development and implementation of water balance and water management plans, taking into account all relevant information and criteria, and all stages of the tailings facility lifecycle.
 - Proper monitoring, recording and management of relevant parameters and phenomena (*e.g.* seepage, flow, etc.). Both dam and environmental safety should be provided for.
 - Operators properly trained and periodically retrained. For higher consequence facilities, the team includes a qualified civil or geotechnical engineer.
- Robust long-term asset management planning process.
 - Development of a “*Life of Mine Plan*”, integrating all the processes, systems, procedures and other activities required for safe and economical tailings storage facility, considering all stages of the lifecycle, according to recognized standards and guidelines. Provision of all the necessary planning data and information. Plan reviews should be periodically (*e.g.* annually) conducted.
 - Develop and formally implement a Tailings Management System (TMS) as well as an Environmental and Social Management System (ESMS), and perform periodic audits to verify those systems, considering all stages of the facility lifecycle.
 - Conduction and regular update of risk assessment with multidisciplinary team applying best practice methodologies. Provide a robust, state of the art sys-

tems for the management, communication and disclosure of such risks.

- Development, implementation and periodic (*e.g.* annual) update of an Operations, Maintenance and Surveillance Manual with context and critical controls for safe operations and proper record of inspections, findings, etc.
- Refine the design, construction and operation along the facility lifecycle through lessons learned from ongoing work and the evolving state of the art.

Category II

- Routine construction supervision.
 - Construction supervision is provided for, but inspection and the level of control, documentation, robustness, etc. do not fully meet the standards postulated for Category I.
- Occasional deviation from ideal operation, leading to beach length, freeboard, water balance in non-compliance.

- Some level of water control is provided, but standards postulated for Category I and not fully met, in a manner that allows for occasional non-compliance.
- Observation of standards and management procedures.
 - Standards and management procedures are established / recognized and observed for the current tailings storage facility operation.
 - However, a comprehensive, long term asset management planning process is not fully implemented as described for Category I.

Category III

- No historical construction processes.
 - No formal documentation or record of the construction process, supervision and inspection is available.
- Saturation of critical zones.
 - Non-existing or ineffective water management leads to identifiable saturation of critical zones within the tailings storage facility.
- Maintenance planning and management process not implemented.
 - No formal and standardized planning and management process is implemented for the tailings storage facility.

Stabilization of major soil masses using drainage tunnels

Werner Bilfinger^{1,#} , Luiz Guilherme F.S. de Mello^{1,2} , Claudio Michael Wolle^{2,3} 

Article

Keywords

Deep drainage
Drainage tunnel
Landslides
Monitoring
Stabilization

Abstract

The destabilizing effect of groundwater is one of the major causes for landslides, which represent a major hazard to human life and the environment. Groundwater lowering is often the most efficient way to stabilize large unstable ground masses. Among groundwater lowering measures, drainage tunnels have several advantages, although construction costs may be proportionally high. This paper presents the concepts involved in the design and construction of drainage tunnels. Three case histories, two in Brazil and one in Argelia are presented, including geological background and monitoring results, where large landslides were stabilized using deep drainage through tunneling solutions.

1. Introduction

Slope failures have been a major hazard to human life and the environment, with a recorded average of around 4700 fatalities per year from 2004 to 2016 (Froude & Petley, 2018) and 3270 fatalities in 2019 (Petley, 2020), excluding seismic triggered slope failures. For this reason, slope stabilization works in urban environment and along transportation routes is, and has been, a main issue in geotechnical engineering.

Traditional slope stabilization measures include changes in slope geometry, construction of active or passive retaining structures and groundwater lowering measures used by itself or in different combinations.

Undoubtedly, the destabilizing effect of water plays a major role in triggering landslides and its control is one of the most effective tools for stabilization.

This paper is structured as follows:

- In item 2 the concepts of destabilizing effects of the groundwater are discussed.
- Item 3 presents the concepts of slope stabilization using drainage tunnels.
- Item 4 presents the importance of geology and a representative geological-geomechanical model on locating the drainage tunnels.
- Item 5 discusses briefly safety approaches for slopes.
- Item 6 presents important drainage tunnel design and construction issues.

- Item 7 presents 3 case histories, where drainage tunnels were used to stabilize slope failures that were affecting important infrastructure projects.
- Conclusions are presented in Item 8.

2. Effects of groundwater on slope stability

In Brazil, slope failures are concentrated in the rainy seasons, where superficial water infiltration and rise of groundwater table generate destabilizing forces and cause different types of slope failures. Similar conditions are encountered around the globe: Popescu (2002) and Highland & Brobowski (2008), for example, describe water, seismic and volcanic activities as major triggering mechanisms of landslides. This paper focuses on failures caused by water, specifically, rising groundwater, one of the main causes of the destabilization of large soil masses. It implicitly considers that the soils involved, mainly colluvial deposits, residual soils and/or saprolites, are not very brittle, going through a large and sudden loss of their shear strength with very small displacements. In this specific failure mode, large excess pore pressures can be generated faster than their dissipation, and the soil mass can go into a flow type of landslide; additional analysis have to be performed in this case to define the stabilization concept to be used.

A simple way to show the effect of groundwater on slope stability is the so-called infinite slope model, where the soil-rock interface is considered impermeable and the flow lines are parallel to the surface.

[#]Corresponding author. E-mail address: werner@vector.com.br.

¹Vecttor Projetos Ltda, São Paulo, SP, Brazil.

²Escola Politécnica da Universidade de São Paulo, São Paulo, SP, Brazil.

³Independent Consultant, São Paulo, SP, Brazil.

Submitted on May 30, 2020; Final Acceptance on June 26, 2020; Discussion open until December 31, 2020.

DOI: <https://doi.org/10.28927/SR.433397>



This is an Open Access article distributed under the terms of the Creative Commons Attribution License, which permits unrestricted use, distribution, and reproduction in any medium, provided the original work is properly cited.

Considering the model presented in Fig. 1, with a clearly defined failure plane at the soil-rock interface, equilibrium can be evaluated by a *FoS* (Factor of Safety), defined as the ratio between the available shear strength and the acting shear stress. Groundwater reduces safety, because it reduces the effective stress along the failure plane, while the acting shear stress is almost not affected. The more frictional the soil is, the more safety is affected by the groundwater:

$$\sigma_z = \rho \times g \times z \times \cos \beta \quad (1)$$

$$\sigma_n = \rho \times g \times z \times \cos^2 \beta \quad (2)$$

$$u = \rho_w \times g \times h \times \cos^2 \beta \quad (3)$$

$$\tau_{app} = \rho \times g \times z \times \cos \beta \sin \beta \quad (4)$$

$$\tau_s = c' + (\sigma_n - u) \tan \varphi \quad (5)$$

$$FoS = \frac{\tau_s}{\tau_{app}} \quad (6)$$

where: σ_z = vertical stress; σ_n = normal stress; ρ = specific gravity of the soil; ρ_w = specific gravity of water; β = slope declivity; z = thickness of soil layer; h = water head measured from the soil rock interface; φ = friction angle of the soil; c' = cohesion of the soil.

For soils with no or negligible cohesion, the *FoS* can be written as:

$$FoS = \frac{\tan \varphi}{\tan \beta} \left(1 - \frac{\rho_w}{\rho} \frac{h}{z} \right) \quad (7)$$

For a dry slope ($h = 0$), the *FoS* becomes:

$$FoS = \frac{\tan \varphi}{\tan \beta} \quad (8)$$

If the soil has a specific gravity of around 20 kN/m³, the *FoS* of the saturated slope is approximately 0.5 of the *FoS* of the dry slope, showing the high impact of the groundwater on safety. The groundwater level at the surface means $h = z$ and the *FoS* can be approached as being:

$$FoS = \frac{1}{2} \frac{\tan \varphi}{\tan \beta} \quad (9)$$

Analogous results are obtained using limit equilibrium or continuum modeling. Intuitively and as shown by

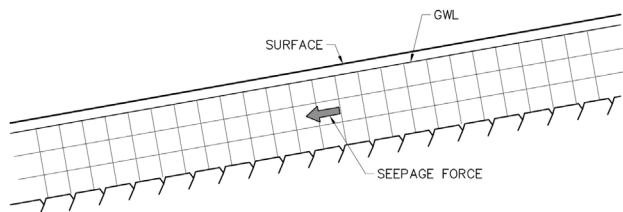


Figure 1. Simplified infinite slope model.

several authors (for example, Patton & Hendron, 1974; Borges & Lacerda, 1986; Bastos, 2006), flow conditions tend to generate even more critical conditions at the base of slopes, where water flows in the direction of the external surface and, additionally, the existence of less permeable soil covers, like talus deposits, may lead to the generation of increase of pore pressures.

Popescu (2002) describes typical remedial measures for landslide stabilization:

- Modifications in slope geometry;
- Drainage;
- Retaining structures;
- Internal slope reinforcement.

Especially for large ground masses, the control of the groundwater is one of the most efficient ways to achieve stability. Typical means to reduce the destabilizing action of the groundwater are:

- Horizontal gravity drains;
- Deep pumping wells;
- Large diameter wells, possibly associated to horizontal gravity drains;
- Drainage tunnels.

Other ways to reduce the destabilizing action of water include well points, electro-osmosis and the use of vacuum to increase pumping wells efficiency, among others. However, these solutions are normally temporary and may not be feasible for large massifs; therefore, they will not be further discussed.

It is important to mention that these groundwater lowering measures have different efficiency, considering at least three aspects:

- Influence radius of individual elements: spacing of small diameter elements must be evaluated to guarantee efficient ground water lowering. The smaller the equivalent permeability, the smaller the influence radius of each individual element;
- Influence of the position of draining elements inside the unstable mass: drainage at the upper part of the unstable soil mass may look efficient to “cut” access of water, as an interceptor of the flow. But, depending on the problem, this location may not be efficient, due to complex water flow patterns. Drainage at the bottom, on the other hand, may be optimal from a constructive point of view, but not as efficient, because of reduced influence on pore pressures in the upper part of the unstable soil mass. In most of the published case histories, drainage, by different means (wells, horizontal drains, tunnels), is installed in different positions along the unstable soil mass, to achieve broader groundwater lowering;
- Influence on the direction of the destabilizing seepage forces:
 - Sub-horizontal drains tend to lower the groundwater, but seepage forces normally continue to act in the slope direction, *i.e.*, they continue, to a certain extent, contributing to destabilization (Fig. 2);

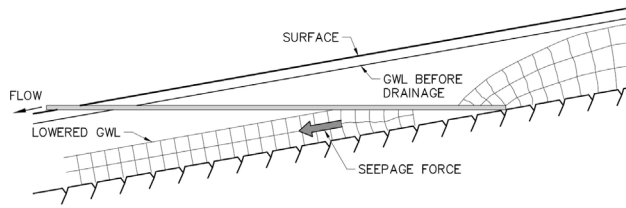


Figure 2. Schematic view of flow model for groundwater lowering using gravity drained sub-horizontal drains. Seepage force acts in the destabilizing direction.

- Deep wells when pumped often tend to invert seepage forces, *i.e.*, seepage forces may act as a stabilizing force, instead of destabilizing the soil mass (Fig. 3). The use of deep wells may be of interest to contribute as a temporary solution, helping to stabilize the soil mass while the long-term solution is implemented, as they have direct costs of electricity supply, require maintenance, backup pumps, etc.;
- Drainage tunnels may influence stability in different ways. The main goal is to obtain generalized groundwater lowering. The way the groundwater is lowered depends on the tunnel location (length, position with relation to the geological singularities), number, length and position of drains installed from the tunnel, position, among others. If vertical flow is achieved (Fig. 4), the destabilizing effect of water is practically eliminated.

In the case of vertical flow, the groundwater level cannot be interpreted as one of the boundaries of a “flow-channel”: vertical flow is gravitational, *i.e.*, the vertical gradient i equals 1 and pore pressures are zero in all points of the flow net.

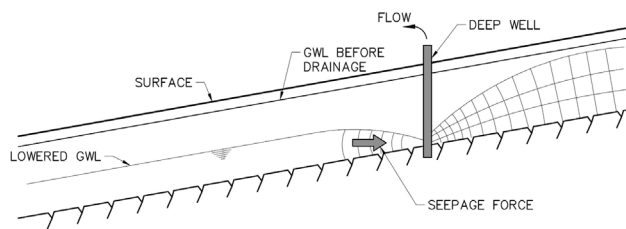


Figure 3. Schematic view of flow model for groundwater lowering using pumped deep wells. Seepage force acts partially as stabilizing force.

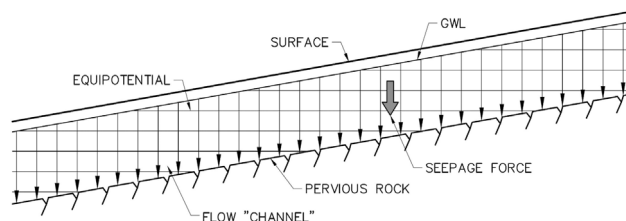


Figure 4. Simplified flow model for vertical flow, considering pervious rock.

3. Drainage tunnels

The broad concept of drainage through tunnels is to excavate them at depth, beneath the failure surface, in competent and stable material, serving as access for implementation of radial drainage, mainly upwards but also incorporating knowledge from the geological model to optimize the location of the drains. Main advantages of this drainage solution are:

- Groundwater lowering through predominantly vertical flow, conceptually eliminating / reducing significantly destabilizing seepage forces;
- Use of gravity flow, eliminating the necessity of energy supply and long-term maintenance of pumping systems;
- No need of any activity, including construction, inside the unstable soil mass;
- No impact on the surface and risk of damage to the stabilizing system through vandalism.

Stabilization of unstable or failed soil masses through drainage tunnels has been used in several locations around the world, with case histories presented, from different locations, in Europe (for example, Bardanis & Cavounidis, 2016; Bertola & Beatrizzotti, 1997; Eberhardt *et al.*, 2007; Marinos & Hoek, 2006; Futai *et al.*, 2009), in the Americas (Rico & Castillo, 1974; Vargas, 1966; Wolle *et al.*, 2004; Yassuda, 1988), Asia (JLS, 2002; Lin *et al.*, 2016; Sun *et al.*, 2009; Wang *et al.*, 2013; Wei *et al.*, 2019; Yan *et al.*, 2019), and Oceania (Gillon & Saul, 1996).

The use of drainage tunnels to reduce pore pressures is not restricted to the stabilization of landslides. Drainage galleries are often designed and built to reduce pore pressures and increase safety in the foundations and abutments of dams (de Mello, 2018).

Figure 5 presents an example of a typical drainage tunnel (Eberhardt *et al.*, 2007), installed inside the rock mass, below the landslide, with drains upwards drilled into the unstable soil, to reduce pore pressures:

The first published use of drainage tunnels to stabilize landslides in Brazil is described by Vargas (1966) and Guidicini & Nieble (1976). These authors describe a landslide that mobilized around 500.000 m³ of material, triggered by a cut, built for the construction of the powerhouse

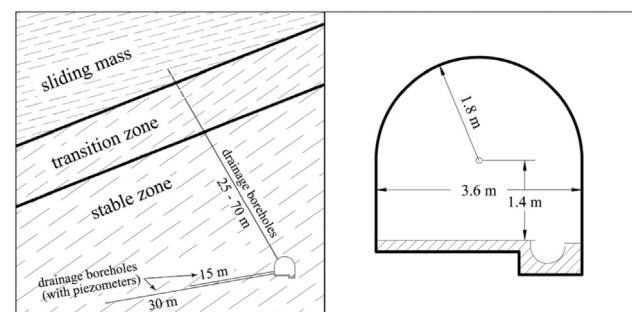


Figure 5. Typical cross section of drainage tunnel (Eberhardt *et al.*, 2007).

of Henry Borden hydro scheme in the foothill of Serra do Mar, Cubatão, Brazil in the past (around 1947). Following Terzaghi's (who acted as consultant) recommendations, drainage tunnels were excavated in the unstable soil mass and drains were drilled from inside the tunnels aiming at a specific geologic feature, said to be a quartzitic permeable high dip stratum (de Mello) that itself had a very broad influence in the slope. Drainage stabilized the soil mass completely, with a groundwater lowering of only around 3 m. Figure 6, reproduced from Vargas (1966) shows a plan view and cross section of the landslide. Figure 7 presents data published by Vargas (1966), showing the effectiveness of the groundwater lowering solution.

An important issue associated to drainage tunnels is its location under and outside the unstable soil mass. To optimize construction costs, the excavated tunnel length should be minimized. An adequate access must be found under unstable groundmass, where the tunnel portal can be located allowing gravity discharge flow, and excavation can start safely, but also minimizing tunnel length. Figure 6

above shows that for the stabilization of the landslide in Cubatão, several tunnels (galleries) were excavated and drains were drilled from these galleries. Figure 8 below shows the drainage tunnel and its adits used to stabilize the VA-19 landslide, published by Wolle *et al.* (2004). A single access tunnel was excavated from an adequately located position at the surface, under the unstable ground mass; adits were built from the tunnel alignment to optimize drainage and tunnel length.

Drainage tunnels are normally excavated in stable ground, but the drains perforated and installed from them into the unstable soil mass are often not conventional drains. Potential problems associated to the drains can be divided into installation problems and maintenance problems.

Installation of the drains in the tropical environment is often associated to drilling initially through rock, weathered rock and the rock-soil interfaces, with all its associated difficulties (Bilfinger, 2019), into soil and an unstable ground mass, often including blocky and unconsolidated

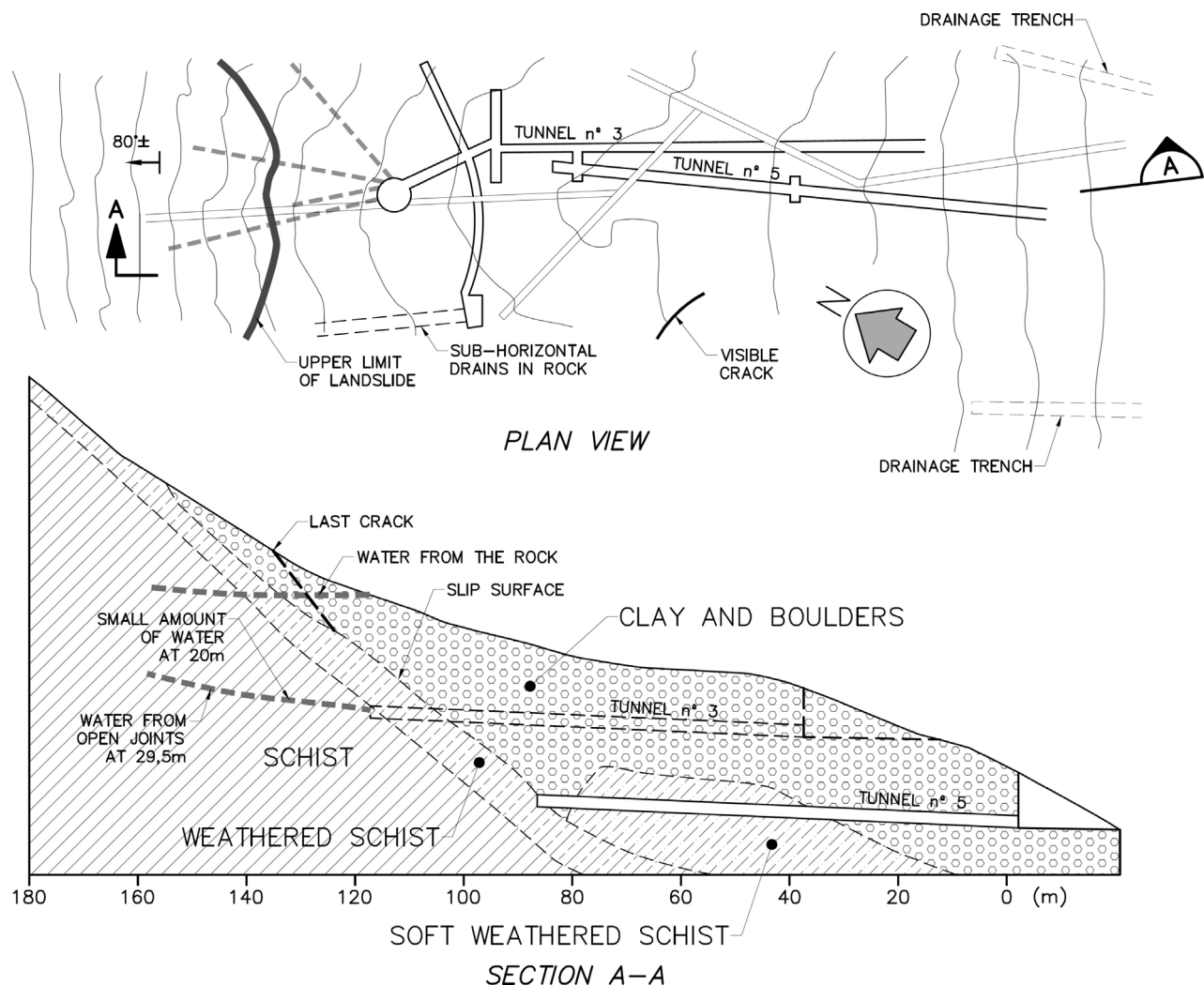


Figure 6. Landslide stabilized using drainage tunnels in Cubatão - Brazil (from Vargas, 1966).

material, with high groundwater level. Concentrated flow many times exists in the saprolite-weathered rock interface.

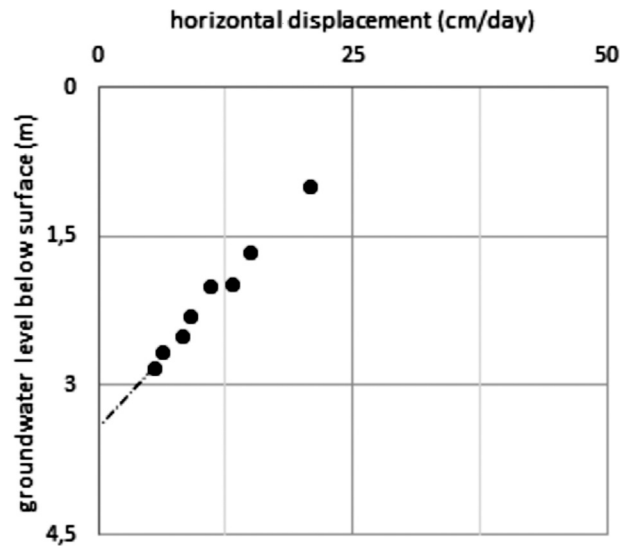


Figure 7. Ground mass movement as a function of the groundwater lowering for the stabilized landslide in Cubatão (from Vargas, 1966).

Sometimes, conventional drilling is not possible or is associated to risk of fines being washed through the drain or through the annular space between the drilled hole and the drain. In intensively fractured rock, there are concerns that in the procedure to retrieve the drilling tool and install the perforated drain, fragments of rock fall into the drilled void and the perforated drain pipe cannot be installed. Self-boring drains are often a more efficient and safe way to install drains in these situations.

Maintenance problems can be divided into short-term and long-term problems. Short-term problems are normally associated to a still non-stabilized ground mass, that may damage or shear the drains, reducing efficiency or even destroying them, sometimes releasing the water collected in the displacing massif in the shear zone. In the long-term, drains may be clogged with time by, for example, oxidation, which also reduces their efficiency. This problem is particularly relevant in tropical soils, with high iron oxide content.

Table 1 presents the main critical issues associated to the drains installed from drainage tunnels.

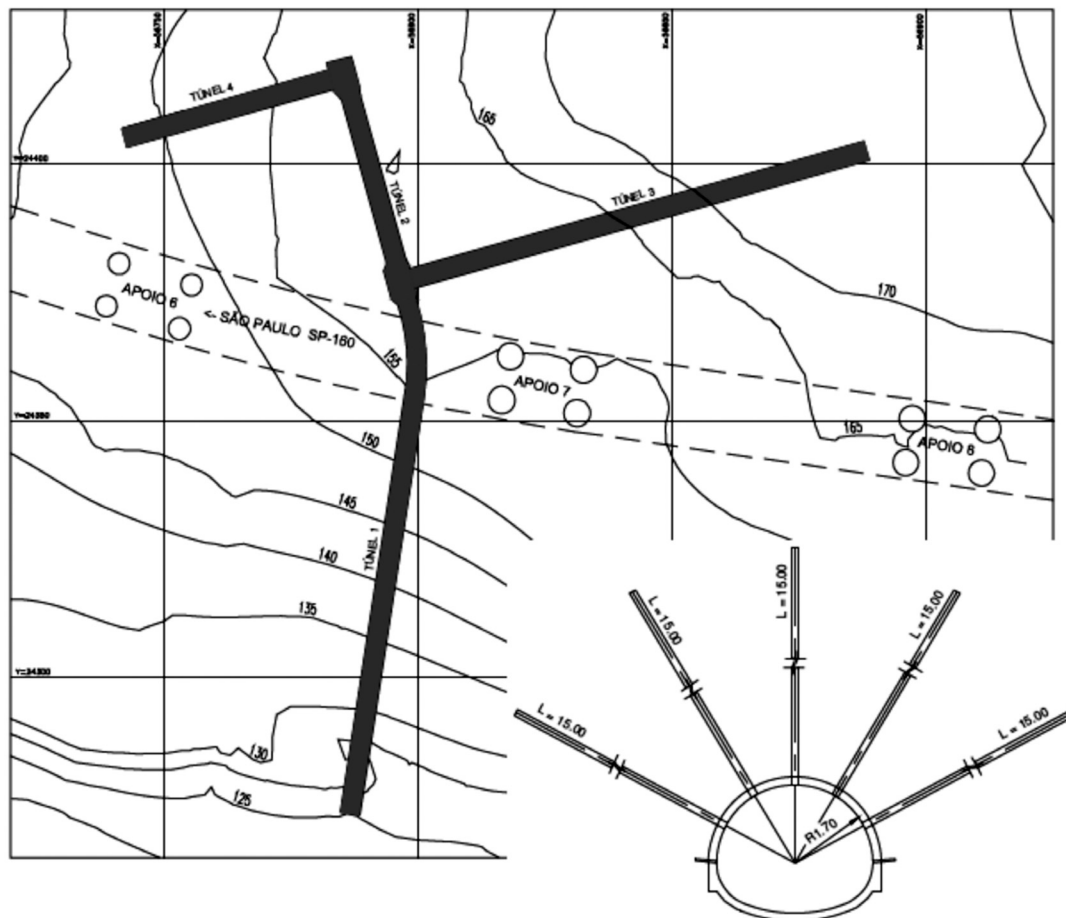


Figure 8. Plan view and tunnel cross section of the VA-19 drainage tunnel (Wolle *et al.*, 2004).

Table 1. Critical issues associated to drains installed from drainage tunnels.

Phase	Potential problem	Solution
Installation	Drilling through different materials (rock, blocky material, soil)	Cased drilling, selfboring drains
	High water table	Preventer
Maintenance	Unstable soil mass leading to shearing of drains	Water flow control and re-installation of drains
	Clogging (oxidation, fines)	Water flow control, washing and re-installation of drains

4. Importance of geology and geological-geomechanical model

Knowledge of the geology of a site and a solid and consistent geological model play a fundamental role in any engineering project. Fookes *et al.* (2000) present an interesting approach, starting from simple models, that evolve with time and help to plan the different steps of the geological and geotechnical project steps. What is particularly interesting in Fookes *et al.* (2000) approach, is its initial phase, where, to characterize a realistic model, the project site geology is identified as being one or more of the typical predefined models:

- Global scale tectonic models, based on plate tectonics;
- Local or site scale initial geological models;
- Local or site scale initial geomorphological models which characterize landforms.

Based on these models, an initial framework of the sites geological conditions can be established, reducing the risk of encountering not foreseen conditions.

A typical development of a geological model, which could include the interesting initial steps proposed by Fookes *et al.* (2000), follows the steps below:

- Desk studies, including aerial photo interpretation, bibliographic research, etc.;
- Walkover;
- Ground investigation;
- Supplementary investigation;
- Finally, during construction the model is updated with data from the site. In the case of drainage tunnel, the geological mapping of the excavation faces may be useful to

optimize drain location or even for adjustments of tunnel alignment.

In the case of landslides, a geological-geomechanical model must be complemented by information about the extent and depth of the mobilized ground mass.

A slightly different site investigation approach, directly associated to the development of the geological model, is presented for tunnels by ITA (2015), but can be generalized:

- Feasibility studies, detailed in Table 2;
- Preliminary design, detailed in Table 3;
- Detailed design, detailed in Table 4.

Independently of the references, there is consensus that the development of an adequate geological model can be divided into 3 or 4 phases, initiating with desktop studies, followed by walkovers by experienced geologist(s). After these initial phases, investigation and studies include different types of geological-geomechanical investigations (boring, geophysical evaluations) in one or more phases.

When a landslide is being investigated, these steps are normally complemented by monitoring results, including:

- Surficial displacements, using conventional topography or more recently developed remote sensing techniques; (Zhao & Lu, 2018; Mantovani *et al.*, 2019);
- Displacements inside the ground mass, mainly through inclinometers;
- Pore-pressures, using piezometers - different types are available, for different conditions and soil types. In the case of failures in rock masses, the measurement of pore pressures is often more complicated, because normally water flows through discontinuities and pressures act on

Table 2. Site Investigations for feasibility studies, based on ITA recommendations (ITA, 2015).

Expected results	Investigation means
Geological and hydrogeological maps	Regional topographic, geological, hydrogeological / groundwater, seismic hazard map
Natural risk maps, when appropriate	Information from field surveys and/or adjacent similar projects
Longitudinal geological profile	Geophysics may provide useful information
Longitudinal geotechnical and geomechanical profile and identification of major hazards	Limited site investigations to confirm extremely critical geological or groundwater conditions
Preparation of risk register	

Table 3. Site Investigations for preliminary design, based on ITA recommendations (ITA, 2015).

Expected results	Investigation means
Longitudinal geological profile (1:5000 to 1:2000)	Geophysics and boreholes at portals and shafts
Longitudinal geotechnical-geomechanical profile (1:5000 to 1:2000) with ground behavior classes	Boreholes along the alignment
Geological and geotechnical cross sections at the portals (1:500 to 1:200)	Water sources and groundwater monitoring
Geological and geotechnical cross sections at access and ventilation shafts	Laboratory tests
Preliminary characterization of the hydrogeological regime	Outcrop and surface mapping
Update of risk register	<i>In situ</i> measurements and permeability tests, when appropriate
	Exploratory galleries / shafts, if needed

Table 4. Site Investigations for detailed design, based on ITA recommendations (ITA, 2015).

Expected results	Investigation means
Longitudinal geological profile (1:2000 to 1:1000)	Additional boreholes at portals and along alignment
Longitudinal geotechnical-geomechanical profile (1:2000 to 1:1000) with ground behavior classes	Laboratory and field tests
Geological and geotechnical cross sections at the portals and shafts (1:200 to 1:100)	In specific cases / locations, geophysics may provide useful information
Definition of detailed set of design parameters and their variability	Excavation of experimental sections along tunnel alignment, if needed
Detailed characterization of the hydrogeological regime	Continue the monitoring of water sources and groundwater
Update of risk register	

discontinuities. To measure the correct pore pressures, piezometers must be positioned adequately inside the water bearing discontinuities. Previously performed special Lugeon tests, manipulating the packers to properly determine the water bearing discontinuities by pinching in until they are located, will make this possible, reducing the risk of non-representative pore pressure measurements.

In the case of drainage tunnels to stabilize large unstable soil masses, geology must focus on some aspects, which may not be all that relevant in other types of projects or situations. A detailed and adequate geological-hydrogeological-geomechanical model of the unstable soil mass has to be conceived, characterizing geo-materials, flow patterns and pore-pressures. Additionally, the stable ground under the landslide, as well as regions outside the unstable soil mass, where an access tunnel is to be built, must also be characterized, because it is in these locations and materials that the tunnel will be built.

Table 5 below presents important aspects that should be part of the geological-geomechanical model.

5. Safety concepts

Slope stability is conventionally evaluated using the static limit equilibrium *FoS* approach, where available shear strength is compared to acting shear stress.

Table 5. Important aspects associated to geological-geomechanical models for drainage tunnels.

	Important aspects
Landslide	<p>Focus on longitudinal cross sections</p> <p>Main soil and rock layers inside and immediately under the unstable mass</p> <p>Geomechanical characterization of each layer</p> <p>Geohydrological model</p> <p>Position of “slip surface(s)” / shear zones</p> <p>Tridimensional landslide model for optimal tunnel location</p>
Tunnel	<p>Evaluation of access tunnel location (outside landslide area)</p> <p>Soil and rock layers under the unstable mass and their geomechanical properties</p> <p>Permeability of material and possible naturally draining features</p>

For conventional conditions, a design *FoS* is normally defined between 1.3 and 1.5. These *FoS* are compatible with the Brazilian slope stability standard, NBR 11682 (ABNT, 2009), where the minimum *FoS* of the “safety level” is related to human life and material and environ-

mental losses. Table 6 presents the *FoS* proposed in the Brazilian Standard:

A *FoS* includes 3 types of uncertainties (Hachich, 1996):

- Intrinsic: the natural or fundamental uncertainty;
- Statistical: uncertainty associated to the parameters of the assumed model;
- Model: uncertainties associated to the model assumed to be representative of the phenomena.

When dealing with an unstable soil mass, the *FoS* can be considered as being around 1.0 prior to any intervention and some uncertainties tend to be nonexistent. Therefore, when stabilizing an unstable ground mass, the conventional approach of designing for a conventional *FoS* would be overconservative. Conceptually, a small increase in the *FoS* would be sufficient to maintain the ground mass stable. However, the limitation of the *FoS* approach should not be forgotten: in slope engineering, a *FoS* approach is associated normally to limit equilibrium calculations, whose use is often questionable, especially for large ground masses. Limit equilibrium analyses compare available shear strength with mobilized shear stresses and, theoretically, if the available shear strength is higher than the mobilized shear stress, the ground mass is stable. Ground behavior is far more complex: *FoS* close to 1 are normally associated to creep and possibly even to progressive failure.

Therefore, the authors consider adequate that stabilizing measures could be dimensioned for an increase of *FoS* of 25 to 30 %, which would be seen as lower than conventional approaches, but sufficient to obtain a stable condition.

6. Design and construction

The design of drainage tunnels can be divided in two parts:

- The tunnel itself, to be built safely and economically.
- The tunnel as part of a drainage system.

The description of the tunnel design itself is not the scope of this paper. Several approaches and methods are available in the literature, like publications from ITA (1988, 2000, 2009, 2019), BTS (2004), NGI (2015) and several others.

The design of the tunnel as part of a drainage system should focus on the following aspects.

6.1 Tunnel cross section

The tunnel cross section should be minimized, sufficiently to allow drilling from inside to install drains and tunnel excavation itself. Knowledge of dimensions of available drilling equipment is fundamental, to optimize tunnel cross section and consequent construction costs. Variable cross section may be an alternative: access to the areas where the drains will be installed may have a smaller cross section than the regions where drilling is foreseen. A minimum tunnel diameter to allow manual drilling, in the experience of the authors, is around 2 m, although a case of 1.5 m high \times 1.0 m width galleries is described by Moraes & Assis (2017). Table 7 below presents approximate equivalent tunnel diameters and corresponding constructive methods.

Tunnel length, according to available published data, is not significantly affected by tunnel dimensions: relatively small equivalent diameter tunnels (around 2 m) have been excavated with total tunnel length of more than 1 km. However, some aspects should be considered when defining the tunnel cross section:

- Construction time, as a function of equipment - conventional tunneling equipment tend to have higher production rates and probably will allow faster construction than manual excavation;
- If complex geological-geomechanical conditions are foreseen requiring special equipment, the cross section needs to be sufficiently large to allow operation and movement inside the tunnel.
- Tunnel length: movement of equipment inside the tunnel may be very complicated in narrow tunnel cross sections. This may be compensated by building enlarged tunnel sections at every 100 to 200 m;
- Ventilation during construction in future maintenance;
- Utilities to be used during construction and future maintenance.

6.2 Tunnel location

Tunnel location has to be chosen to minimize tunnel length, optimizing construction and operational costs. However, some aspects have to be considered when defining tunnel location:

- Tunnel portal in a location:
 - where gravity drainage is possible;
 - safe, not influenced by the landslide;

Table 6. *FoS* proposed in the Brazilian Standard (NBR 11682/2009).

Safety level against material and environmental damage	Safety level against human life		
	High	Intermediate	Low
High	1.5	1.5	1.4
Intermediate	1.5	1.4	1.3
Low	1.4	1.3	1.2

Table 7. Equivalent tunnel diameters and corresponding constructive methods.

Equivalent tunnel diameter	Constructive method
2 m	Manual excavation
3.5 m	Small equipment
5 m	Conventional tunneling equipment

- Vertical and horizontal alignment to:
 - excavate material that minimizes excavation cost (lining type, lining thickness, ground treatments, construction time);
 - minimize drain (drilled from inside the tunnel) length;
 - optimize geohydrological position;
 - optimize position to maximize groundwater lowering effect on the unstable ground mass.

It is often necessary to excavate more than a single tunnel to achieve efficient groundwater lowering. Landslides extend often over hundreds of meters and a single tunnel may not generate a regional groundwater lowering. Figure 9 below presents a cross section of the Hilane landslide (JLS, 2002) and it can intuitively be seen that a single tunnel would be much less efficient, than the two tunnels built to stabilize the landslide.

The plan view of the tunnel built to stabilize the VA-19 landslide (Wolle *et al.*, 2004), presented in Fig. 8, shows also that a single tunnel would be much less effective than the system of adits and tunnels built.

Some interesting details may be important during design and construction:

- Use of self-drilling drains. Self-drilling drains have the advantage to transform drain installation into a single operation;
- In some cases, preliminary stabilization must be implemented before the radial drains are perforated and installed, as ongoing displacements could shear through recently installed drains until stabilization of displacements is achieved;
- Cost-benefit analysis of the drainage tunnel solution has to consider long term costs, associated to maintenance, which with a tunnel as access can be higher as initial cost, but are minimized in the long term.

Drainage tunnels have been built using conventional tunneling method (ITA, 2009). The main advantages of this constructive methodology are:

- Excavation does not need special equipment, like TBMs, and therefore, construction can be started quickly;
- Use of variable, non-circular, cross sections;
- Flexibility during excavations, changing and adjusting tunnel alignment as a function of geological and geomechanical conditions encountered during excavation.

However, mechanized excavation method also presents important advantages:

- Excavation under difficult conditions using EPB or Slurry technology, without the need of complex and costly soil conditioning;
- High excavation velocities;
- Fixed circular cross sections, that may be used for special remotely controlled drain drilling equipment.

At least in Brazil, so far, no mechanized drainage tunnel has been built.

7. Case histories

7.1 Case 1: Stabilization of viaduct VA-19 of the Imigrantes Highway, Brazil

This case history is described in detail by Wolle *et al.* (2004) and is considered by the authors a landmark in Brazil. For this reason, in this item a summarized version is presented.

7.1.1 Description of the Landslide

Imigrantes Highway was built in the 1970's connecting São Paulo to the closely located coast, including the harbor city of Santos. The highway crosses "Serra do Mar" mountains, from the São Paulo metropolitan area at approximately elevation 750 m, to the coastline, below elevation 10 m. It includes several tunnels and viaducts, with up to 90 m support towers.

VA-19, one of the viaducts, had been suffering anomalous openings of floor slab joints in a specific stretch since the 1980's. At the end of that decade, in 1988, comprehensive geotechnical monitoring started and deep-seated movements were identified, in weathered biotite gneiss at substantial depths. Average velocity was around 10 mm/year, with higher velocities during the rainy seasons. The oblique direction of the movements generated differential movements of translation and rotation, and consequent not foreseen stresses in the viaduct structure. Monitoring showed also that the deep foundations of the viaduct were being intercepted by the interpreted failure plane. When all these conditions were clearly identified, the decision to implement stabilizing works was taken. Some unsuccessful attempts were tried previously, including the use of Jet Grouting.

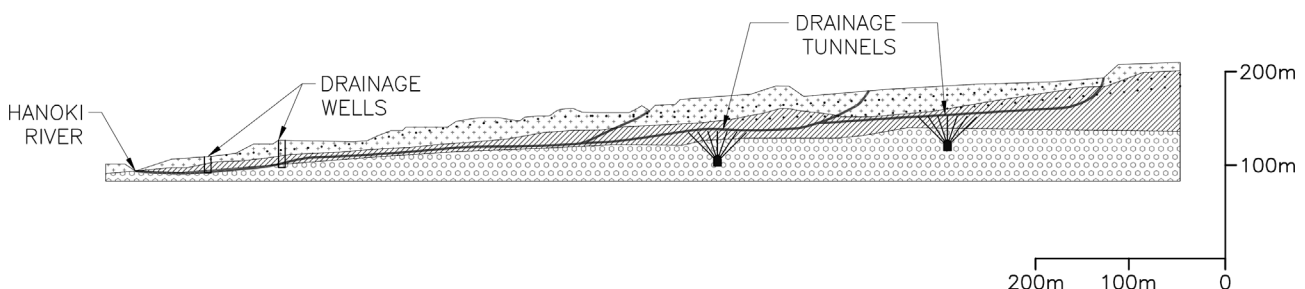


Figure 9. Cross section of the Hilane landslide (from JLS, 2002).

7.1.2 Geological model

Figure 10 presents a geological-geotechnical cross section through one of the viaducts supports. The figure includes a schematic representation of inclinometer readings, showing clear movements inside the residual soil. The residual soil - weathered rock was originated from foliated gneiss, with intercalations of quartzite and calcium silicate. The weathering profile allows a subdivision between highly weathered residual soils, with $N_{SPT} < 40$, overlaying a weathered layer (saprolite), with $N_{SPT} > 40$. At the basis, slightly weathered rock was encountered.

Groundwater level in the area was relatively high and increased even more during the rainy season.

7.1.3 Tunnel design

Several alternatives were evaluated, but, as frequently is the case with large landslides, the most effective way to improve stability was groundwater lowering. Stability analyses showed that a groundwater head reduction would be necessary to achieve an adequate safety increase. A drainage tunnel was chosen as solution. The location of the tunnel was optimized, taking into account geological and structural particularities of the ground mass.

Figure 11 and Fig. 12 present tunnel location and cross section. Total tunnel length is around 280 m and the

cross section varied from 7 to 10 m³/m, respectively in rock or soil.

Detailed geological mapping during the excavations was used to optimize drain locations: more fractured rocks or quartzitic veins concentrated water flow and the drains were concentrated, when possible, in these materials.

7.1.4 Monitoring results

Several instruments were installed during decades and, in part, lost due to vandalism or excessive horizontal displacements. This intensive monitoring led to the understanding of the mechanisms and, later, the control of the groundwater lowering measures results. Figure 13 presents the readings of one of the inclinometers, with readings between 1991 and 2002, including the tunnel construction period, that took place during the second semester of the year 2000. Accumulated horizontal displacements at approximately 30 m depth was 60 mm, but almost no further movement occurred during the next years.

Figure 14 presents water level readings of 3 piezometers, including a short period of about two years before tunnel construction, construction time and some three years of operation of the drainage tunnel. Significant groundwater lowering was measured, variable according to the position of the piezometers in respect to the tunnel location.

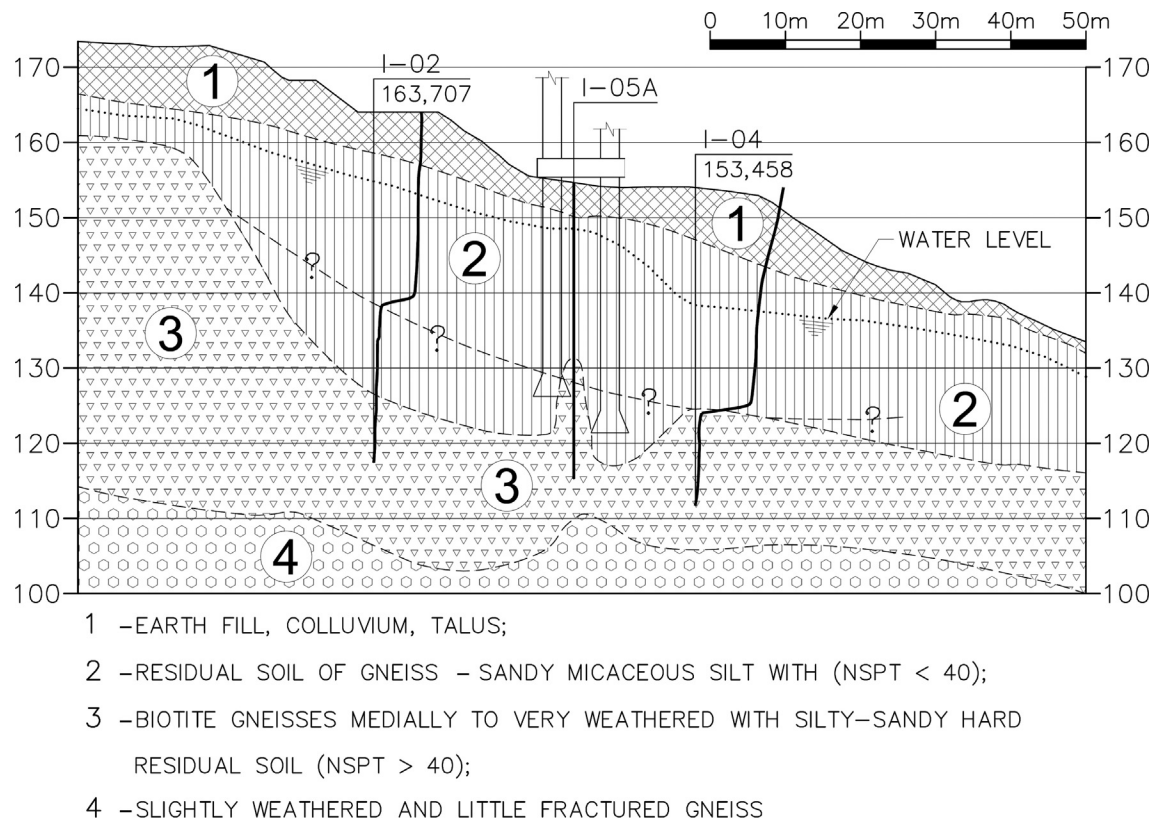


Figure 10. Transverse geological section with indication of shearing zones as detected by the inclinometers.

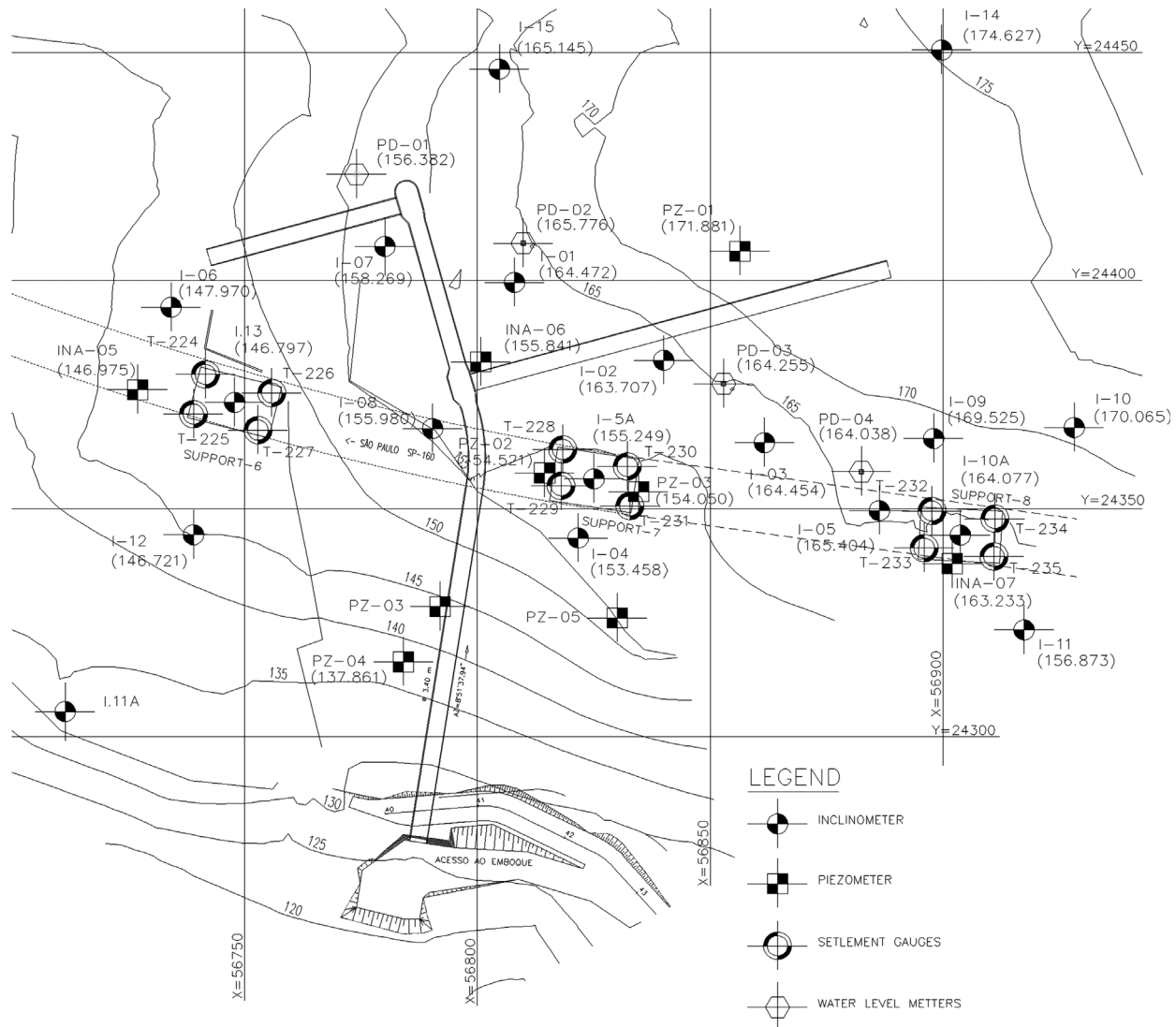


Figure 11. Plan view of tunnel, foundation of 3 pillars and monitoring instruments.

7.2 Case 2: Stabilization of km 376+400 of Candido Portinari Highway, Brazil

7.2.1 Description of the landslide

Candido Portinari Highway is in the state of São Paulo, Brazil, connecting Ribeirão Preto to Rifaina, close to the border with the state of Minas Gerais. It is a double lane highway with an average movement of around 12,800 vehicles per day (DER, 2020).

During the rainy season of 2006, at km 376+400 the north bound lanes suffered significant settlements and an emergency stabilizing berm was built, approximately at the toe of the existing embankment.

In early January 2007, during the rainy season, sudden vertical displacement of 2 to 3 m occurred, characterizing a geotechnical failure, with a mobilized ground mass of around 80.000 m³. The failure was not limited to the existing embankment, but a significant part of its foundation

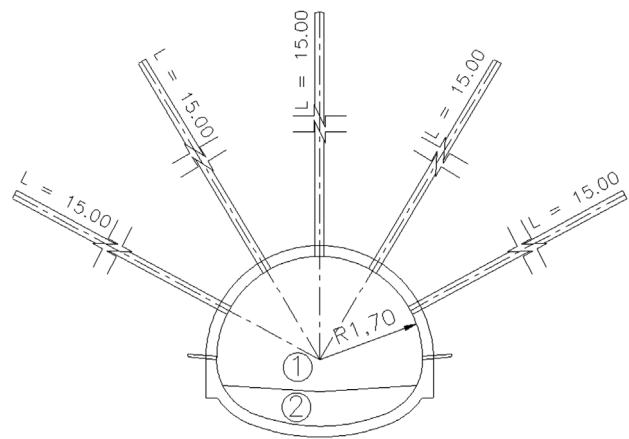


Figure 12. Tunnel cross section.

was also involved in the unstable mass. Figure 15 shows a picture of the failure.

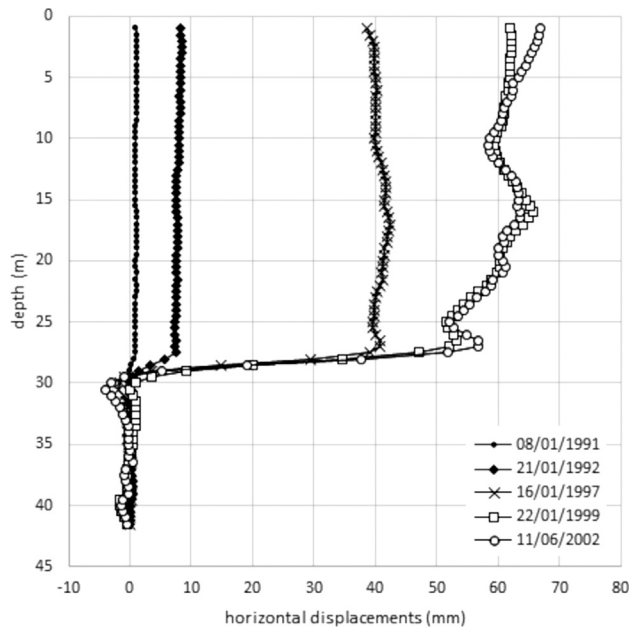


Figure 13. Inclinometer readings before and after tunnel construction.

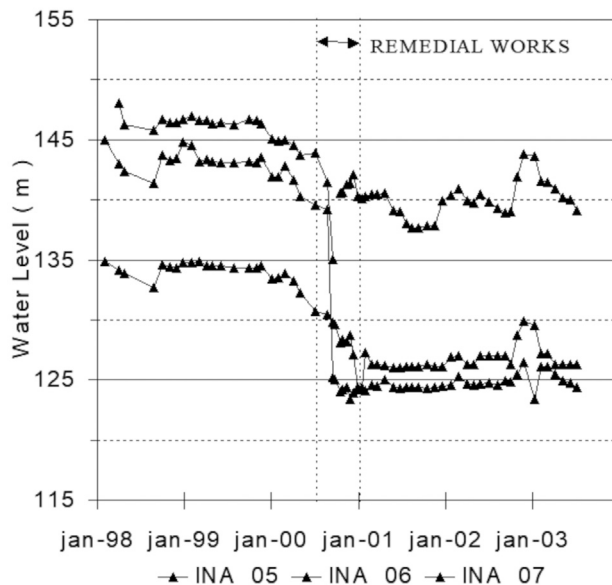


Figure 14. Piezometer readings before and after the construction of the drainage tunnel.

The average slope of the existing embankment was around 20° , and the average slope of the unstable area was around 13° to 15° .

7.2.2 Geological model

The region where the failure occurred is covered by reddish-purple soil (“terra roxa”), known in the past as excellent soil for coffee production. Geologically, the region is covered by basalts, and the products of its weathering, of



Figure 15. Geotechnical failure of the northbound lane of SP-334.

the Serra Geral Formation, over the sandstones of the Botucatu formation. Figure 16 below presents a geological cross section of the failed area.

The cross section shows relevant soil and rock layers, which explain the failure: the sound sandstone has low permeability and can be interpreted as an impermeable boundary. The fractured basalt, as shown by permeability tests, has high permeability. Borings showed also the presence of expansive clay minerals in part of the basalt fractures. The colluvial soils, as well as the road embankment, are mainly clayey soils, with low permeability. These low permeability layers generated a barrier, which led to a significant increase of pore pressure at the base of the unstable mass. The stabilizing berm built in the year prior to the main failure even increased the effectiveness of this water flow barrier. This pore pressure increase was interpreted as the main cause of the failure.

A few days after the failure, deep wells were installed between the highway lanes, immediately “upstream”, temporarily stopping the movements of the failed ground mass.

7.2.3 Tunnel design

The drainage tunnel was designed to substitute the deep wells, which proved to be efficient to stabilize the unstable ground mass, in a permanent long-term stabilizing solution: the tunnel was excavated approximately 0.5 m from the bottom of the wells. After excavation, short horizontal drains were drilled from the tunnel to the wells, allowing drainage from the wells into the tunnel. 9 m long drains were also drilled into the fractured basalt, to improve the drainage of the fractured basalt. Figure 17 presents a schematic cross section of the solution.

Figure 18 presents a plan view of the tunnel location, with relation to the highway and the failed slope. Figure 19 presents a geological longitudinal section along the tunnel, including tunnel location.

The tunnel was built using steel corrugated plates as lining, with two different diameters. The initial stretch, that

serves only as drain to allow gravitational flow, was built with a 1.2 m diameter. The stretch excavated close to the deep wells was excavated with a 2.2 m diameter, to allow

the operation of a small drilling equipment, to perforate the holes and install the pipes between the tunnel and the wells and the drains into the soil massif.

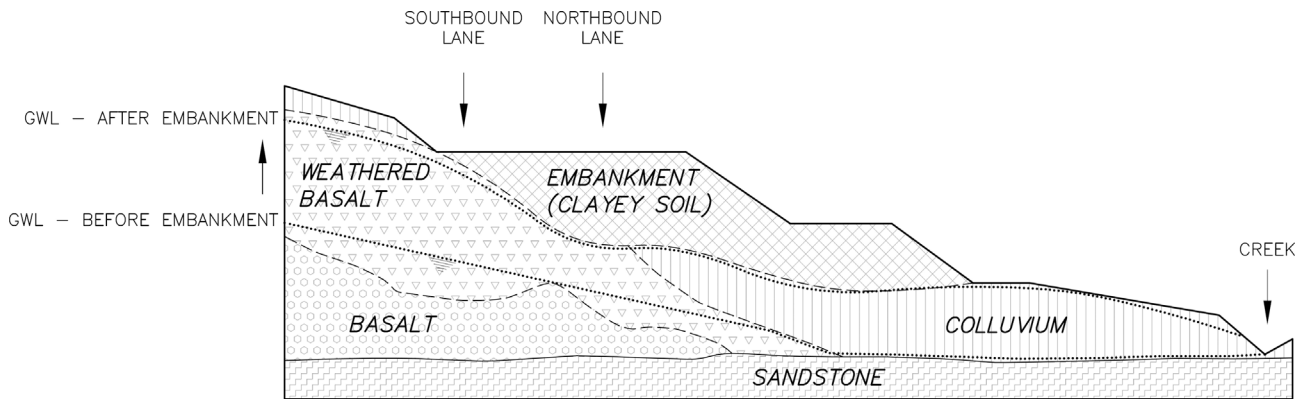


Figure 16. Cross section of the failure.

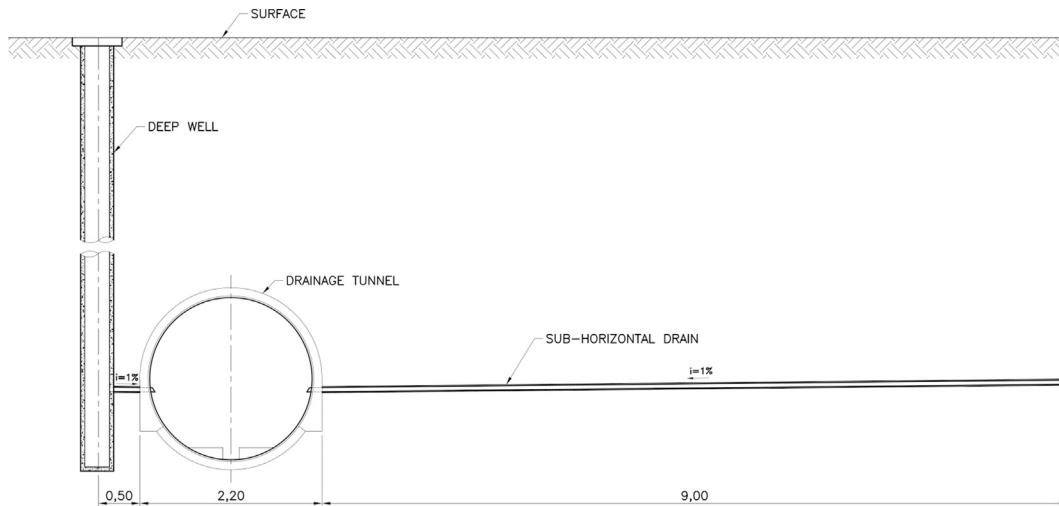


Figure 17. Schematic cross section of the tunnel and the deep wells.

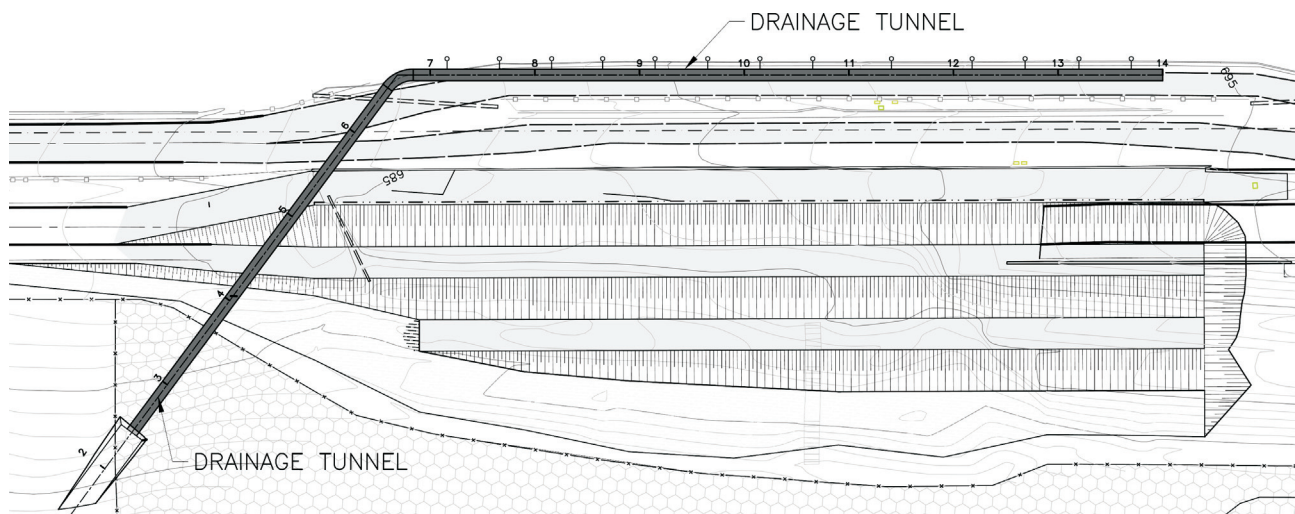


Figure 18. Plan view of the tunnel. The southern part of the tunnel was located in a position to allow gravitational drainage.

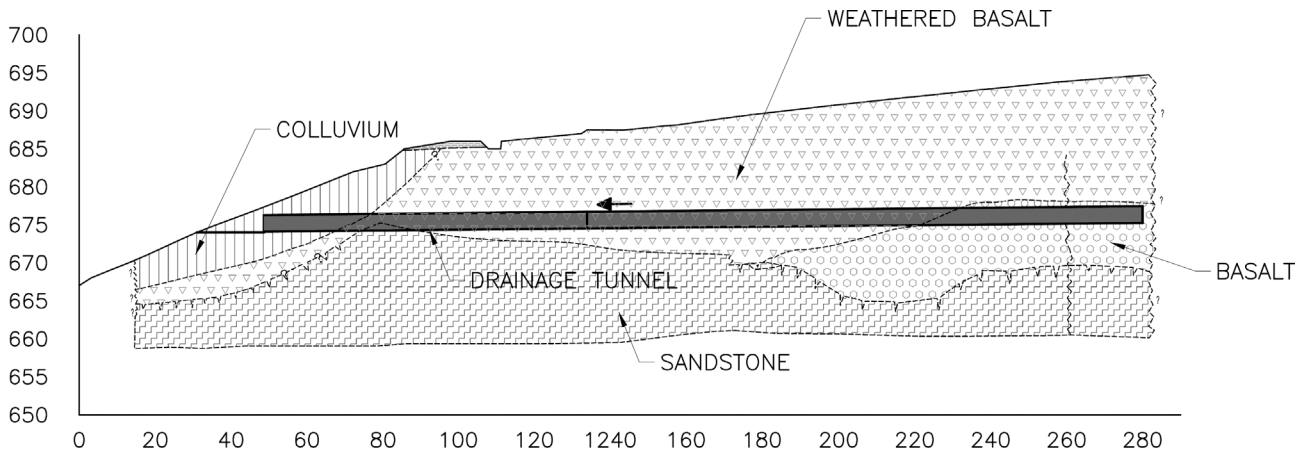


Figure 19. Longitudinal section along tunnel alignment.

7.2.4 Monitoring results

Unfortunately, displacement measurements, on the surface or inside the ground by inclinometers, were not made available until the deep wells were installed, and after their installation, movements ceased almost immediately.

The most relevant quantitative monitoring results is the information related to the groundwater level before and after the installation and operation of the deep wells. Figure 20 presents a longitudinal geological section, with highlighted position of pre and post pumping water levels.

After the groundwater lowering measures, the slope has been monitored until now and no significant movements have been registered.

7.3 Case 3: Stabilization of the Transrhmel Viaduct abutment in Constantine, Argelia

7.3.1 Description of the landslide

Constantine, in Algeria, north Africa, is known as the city of the Suspended Bridges. Founded in 300 b.C. it was

reconstructed, renamed and chosen as the capital of the Roman Empire in North Africa by Constantino in 313 a.C.

Geological faults isolate the ancient town, facilitating its defense and imposing the need of bridges, at different heights since early times; technology and different cultures built impressive bridges of different materials, engineering concepts, and spans.

To commemorate the 21st century and to be ready for the election of the city as being the Arabic Culture Capital in 2015, a new cable stayed bridge was designed and built. The bridge is 756 m long, with a central span of 259 m and 60 m high pylons.

Constantine is also known for its active geological past, with many ancient landslides conditioning today's infrastructure.

A dormant ancient landslide previously known in the bridge's right abutment was remobilized by an earthquake linked to a particularly heavy rainy/snowy season when the bridge was near completion, about to close the main span. Emergency actions were taken to preserve the integrity of all foundations in the right abutment, as well as to design

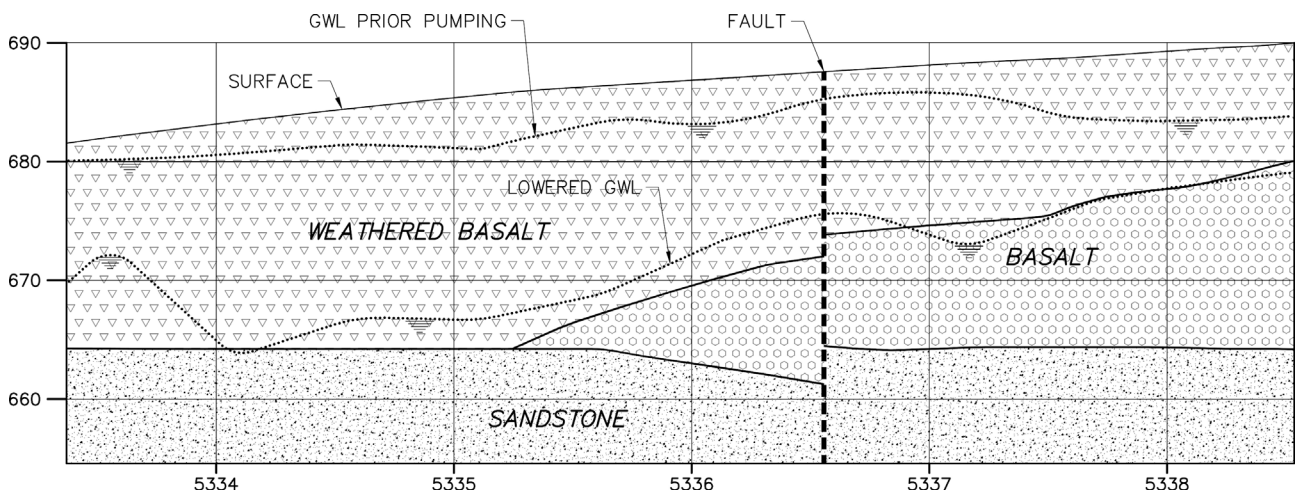


Figure 20. Longitudinal section with pre- and post-pumping water level.

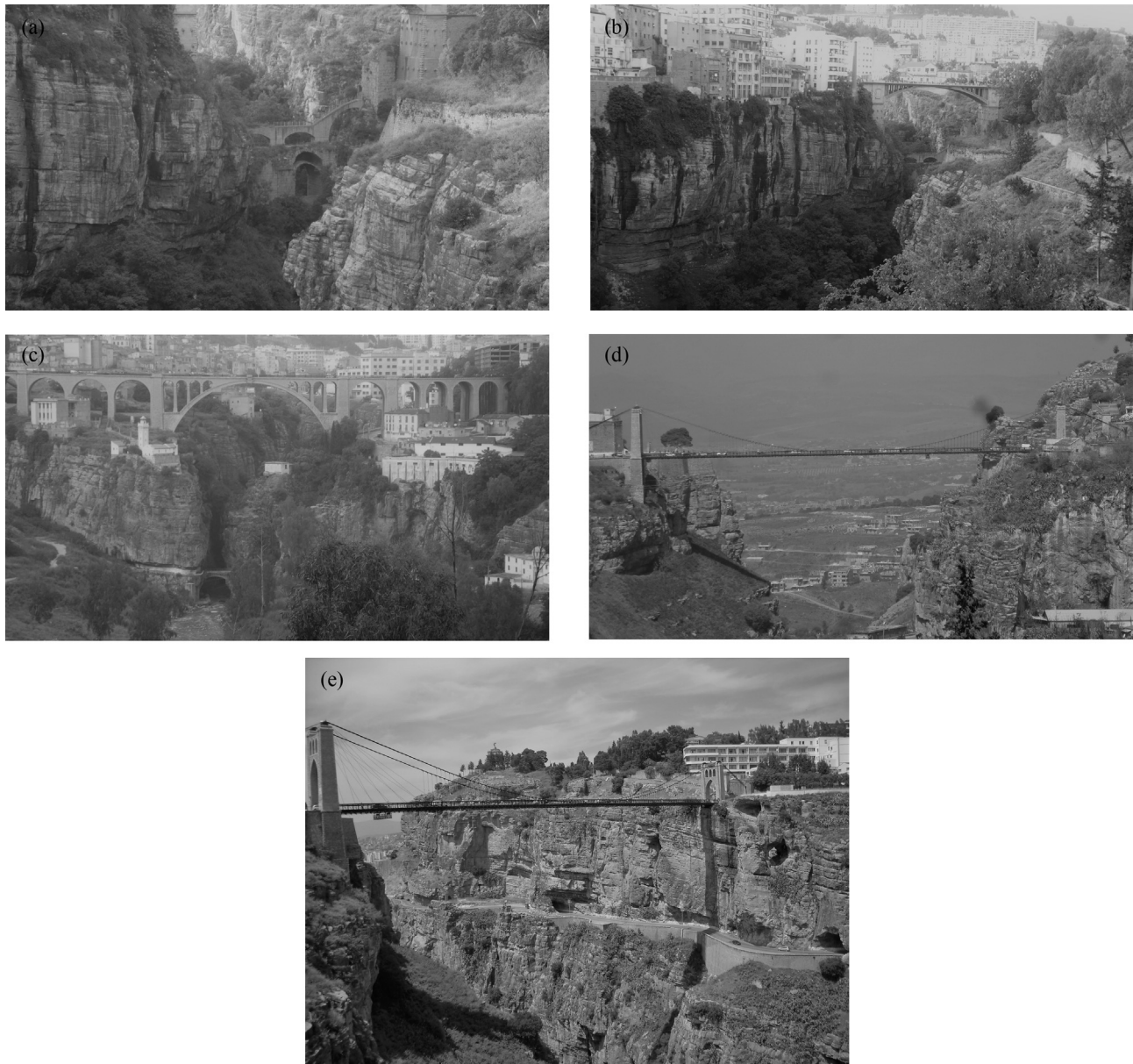


Figure 21. View of bridges built in different ages in Constantine.

and construct a definite solution to stabilize the whole slope. From the early discussions and considering the enormous mass involved, it was decided that the only solution was to lower the groundwater level through a tunnel.

7.3.2 Geological model

The Constantine region is located near the boundary between the African and Eurasian tectonic plates and the geological conditions of the region are complex with active seismicity prevalent in the area. The still ongoing collision introduces a compressional regime which is indicated by deformation of more recent Pliocene deposits. In the Constantine area outcrops range from Cretaceous, like marls and marlstones, to Quaternary deposits, like travertine con-

glomerates and top soils. The formation of the Rhumel river network and valley across which the Viaduct lies probably dates between 56 to 23 Ma.

The Constantine Viaduct is identified as being located in seismic zone IIa, with a range of peak ground acceleration from 1.6-2.4 m/s^2 . Constantine has recorded three major earthquakes ($M_s > 5$) in the past century, in 1908, 1947, and 1984. The epicenters of all these earthquakes were located within 10 km of Constantine.

Many ancient landslides have been mapped in the Constantine region. The majority of the noted landslides are located in the region west of the Rhumel valley, while the landslide affecting the right abutment of the bridge is located in the east side of the valley.



Figure 22. View of the new bridge.

For the bridge foundations design an extensive site investigation campaign was pursued with many investigation boreholes as shown in Fig. 23, associated to geophysical methods and laboratory tests. The brittle and fragile characteristics of the marls and marlstones led to difficulties in retrieving quality samples for laboratory tests. The geological longitudinal profile along the bridge alignment shows superficial marls of different weathering degrees, followed by marlstones and limestones, as shown in Fig. 24.

The site investigation extended to the east, along the access road to the bridge, allowing knowledge of the extension of the stratigraphy.

Specifically, in the region comprising the stretch of bridge in its right abutment as well as the road system extending from it, numerous inclinometers, piezometers and

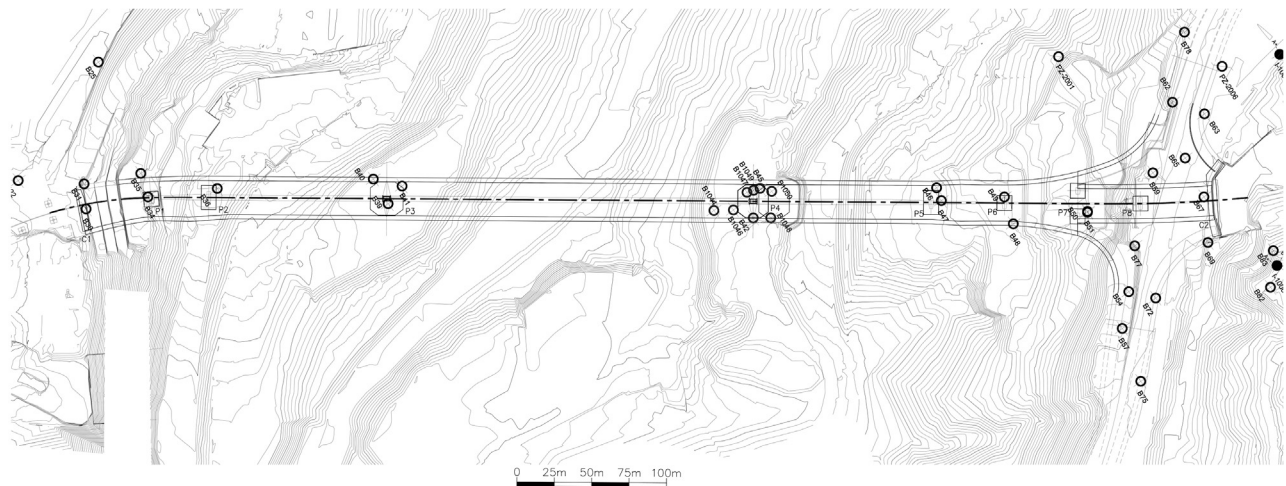


Figure 23. Location of Site Investigation boreholes.

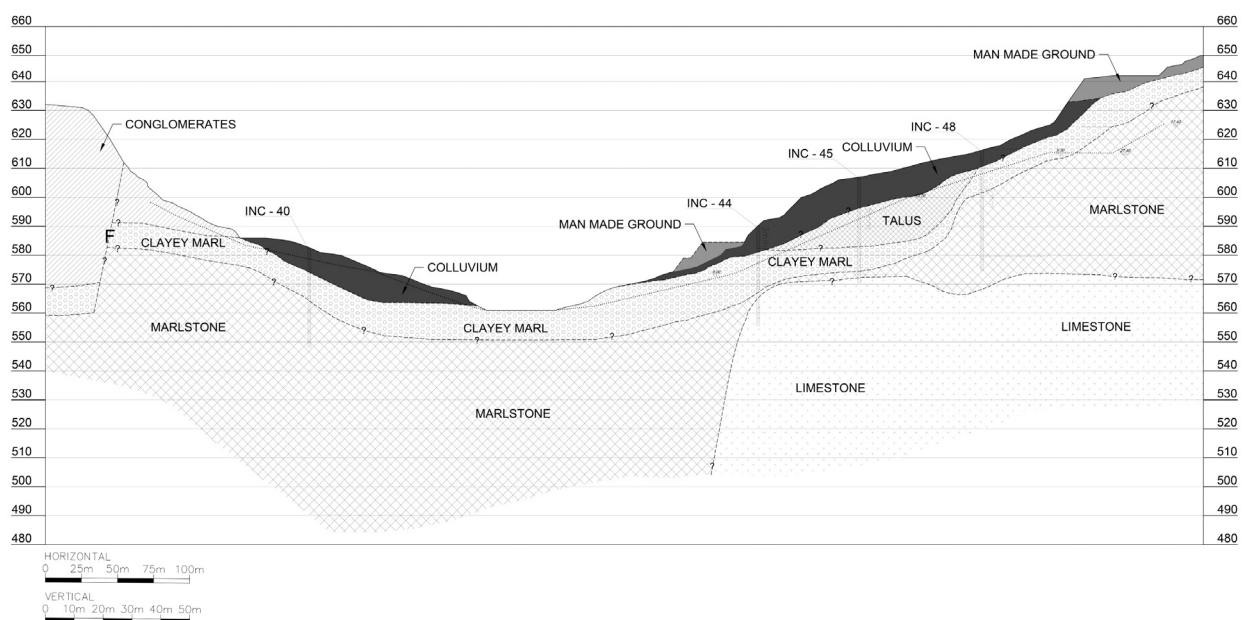


Figure 24. Geological profile along the alignment of the bridge.

drainage wells that also supply water level indication were installed. Figure 25 presents the location of the inclinometers, piezometers and wells/water level indicators used for interpretation of the slope behaviour. Deep wells and a displacement buffer were installed to temporarily stabilize the region and guarantee the structural integrity of the pylon's foundations; while the final solutions were conceived, designed and constructed, the bridge's pylons and pillars were preserved.

Inclinometer and piezometer data clearly show the existence of a slip surface at depth, and that a stable slope was reactivated by a sudden event in late January 2013, and enhanced during the spring of 2014 when melting snow generate substantial water infiltration.

The displacement pattern at different depths is seen as indicated in Fig. 26 and Fig. 27. Figure 28 shows the displacement direction as measured by several inclinometers and the effects at the ground surface is almost obvious, as Fig. 29 shows.

The Sidi Rached bridge, a masonry structure constructed in early 20th century, presented in Fig. 21c and in

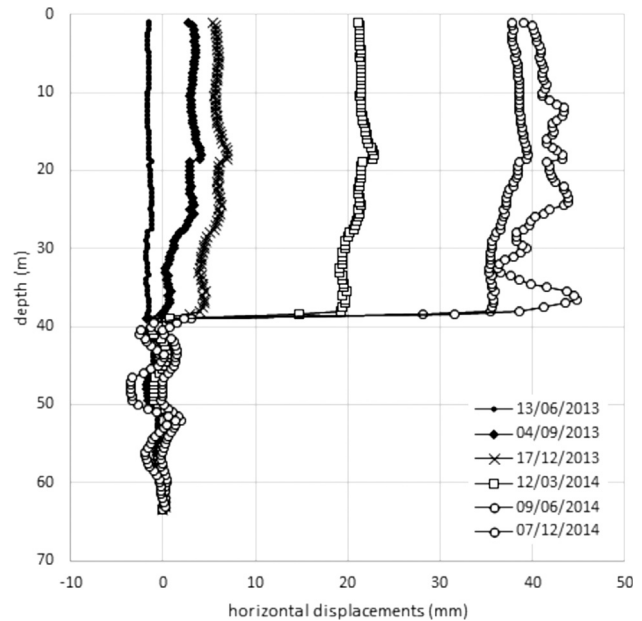


Figure 26. Typical inclinometer readings, showing clear development of slip surface at almost 40 m depth.

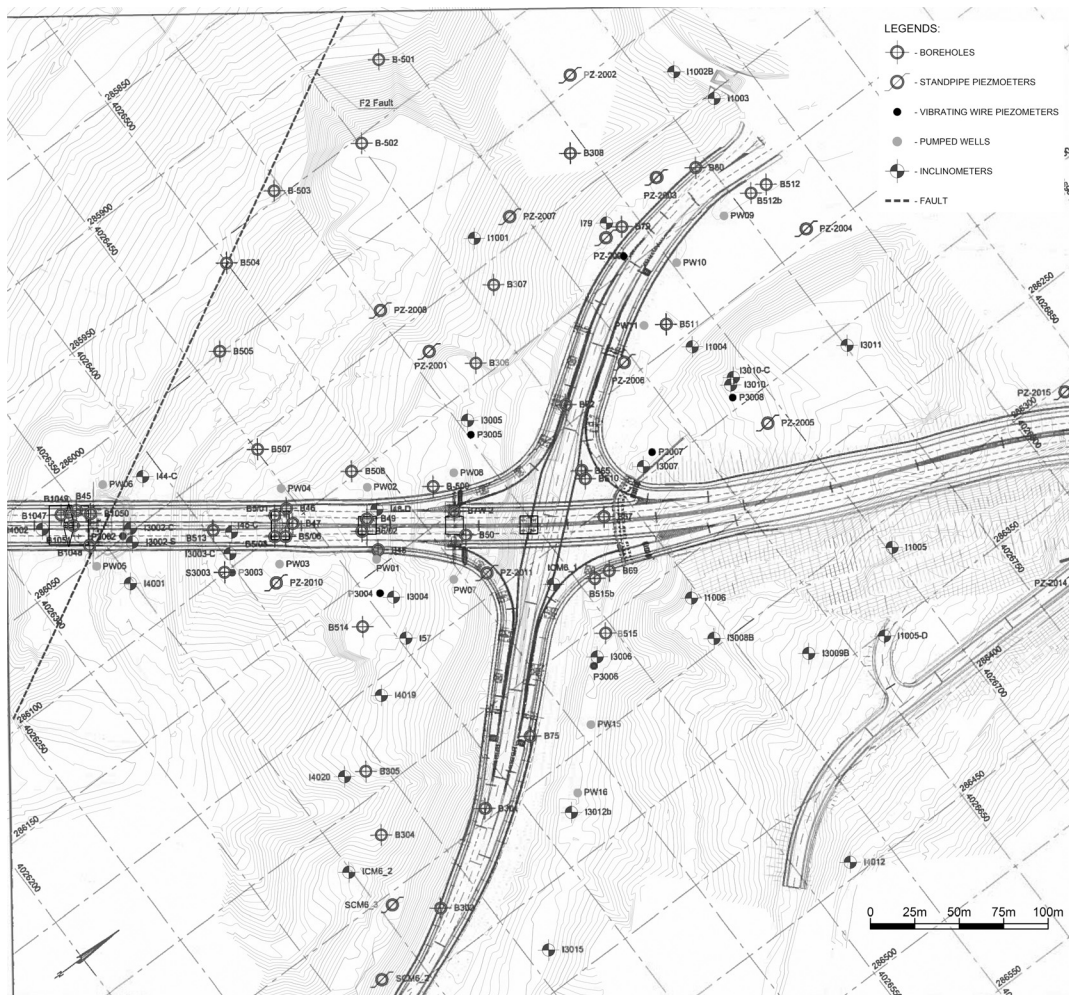


Figure 25. Location of boreholes, inclinometers, piezometers and deep wells. Data of highlighted inclinometer are presented in Fig. 26.

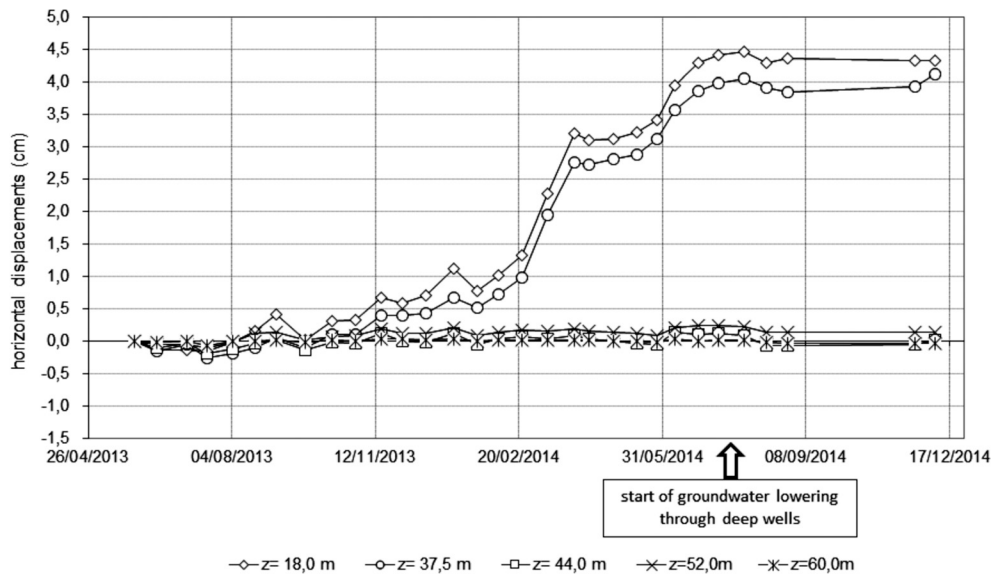


Figure 27. Shear displacements along depth for inclinometer of Fig. 26.

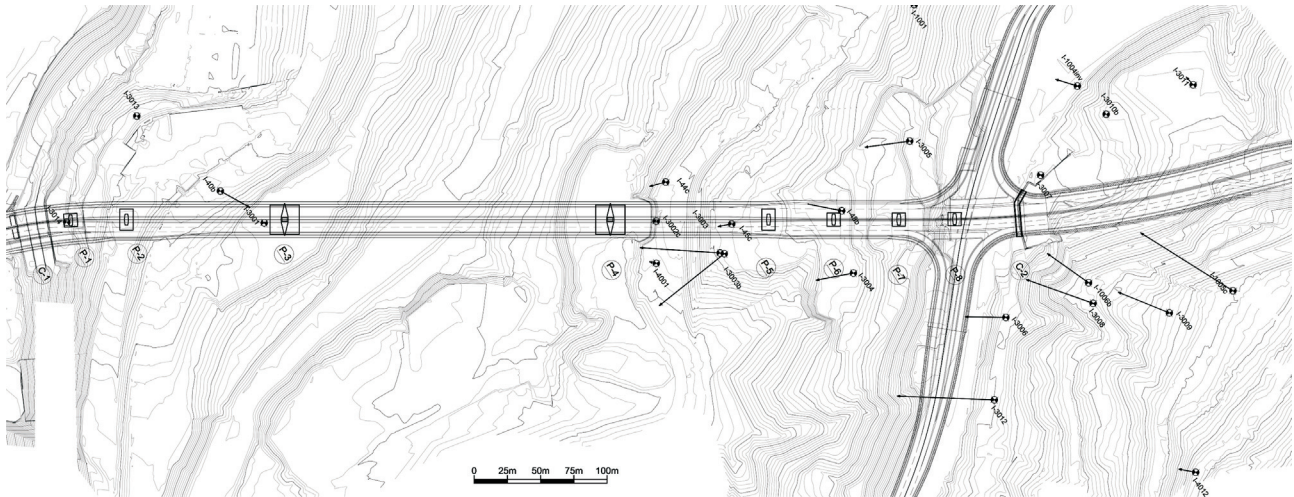


Figure 28. Displacement vectors as measured by inclinometers.

the background in Fig. 29, shows important signs of distress and is being reinforced and retrofitted so that it maintains its integrity and functionality.

The evaluation of all the inclinometer data leads to the interpretation of a deep seated landslide, retrogressing in its active part, shearing the foundations of one of the bridge's pylons while the foundations of all other pillar in this abutment would be "floating" in the sliding mass. The shear surface is located in the interface between the marls and the marlstones and limestones.

The emergency pumping to lower the groundwater showed almost immediate results, which were noticed by a significant displacement velocity reduction, as well as significant pore pressure reduction, as can be seen in Fig. 31.

A direct correlation between the rainfall data and the ground water response was also identified.

7.3.3 Tunnel design

The stabilization of the right abutment slope was conceived using an access tunnel and three adits excavated in the limestone beneath the slide surface and spreading laterally so that 3D limit equilibrium slope stability analysis numerical simulations associated to a hydrogeological model showed that the decrease of the water table would generate an increase in safety of 25 to 30 %.

Radial drains were perforated to reach and lower the pore pressures acting on the slip surface. Drains were located at constant intervals of the tunnel length; a very detailed geological mapping of the face of the excavation allowed perforation of additional drains at specific locations where geological features like open water bearing discontinuities would be intercepted and drained.

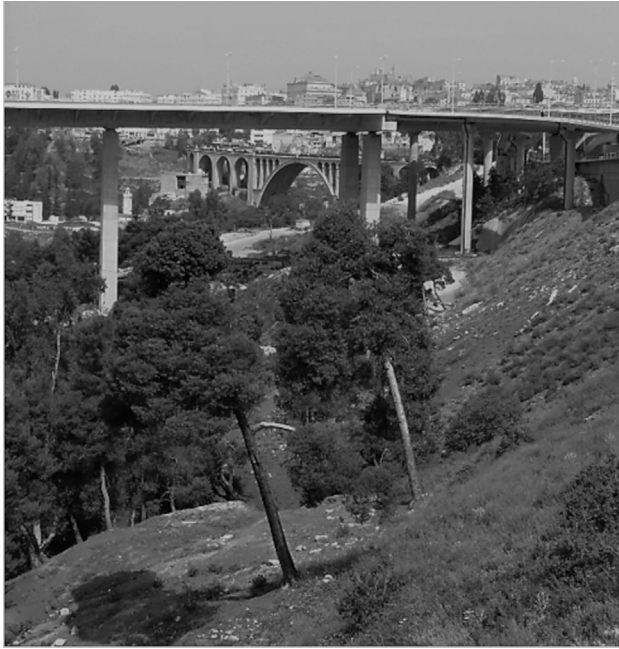


Figure 29. Signs of horizontal displacements at the surface.

A complementary monitoring program was also installed. To present date tunnelling works are finished, but not all drains were installed.

7.3.4 Monitoring results

Figure 34 below shows the target drawdown of the drainage system as well as the drawdown achieved as to May 2019. The measurements and target values presented are plotted along the reference line of Fig. 32.

Drainage achieved by the tunnel has led, so far, to groundwater drawdown of around 25 m close to the new bridge. A more generalized groundwater drawdown is expected when the originally designed drains as well as

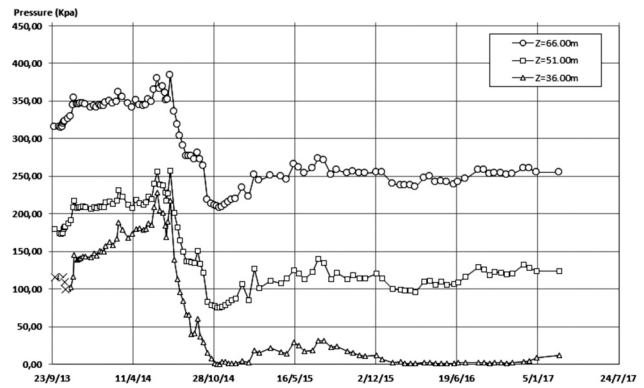


Figure 31. Pore pressure measurements of a piezometer located close to inclinometer 3003 (Fig. 26 and Fig. 27).

drains located based on the mapped geology during tunnel excavation are installed and the slope will be stabilized.

8. Concluding remarks

The most efficient way to stabilize large unstable soil and rock masses is, usually, groundwater lowering. Other types of stabilizing solutions are often almost impossible to use, because of the enormous forces involved. Depending of the topographical and geological conditions, drainage tunnels can be a very efficient and definitive solution relying on gravity drainage. Tunnels also allow access for maintenance and drainage improvements at any moment during their design life.

Several successful projects were implemented around the world, especially in Asia, according to literature. At least 3 projects were built and successfully stabilized unstable ground masses in Brazil.

The drainage tunnel solution has several advantages, including gravity drainage, staged installation of drains during tunnel construction, permanent access to the drains

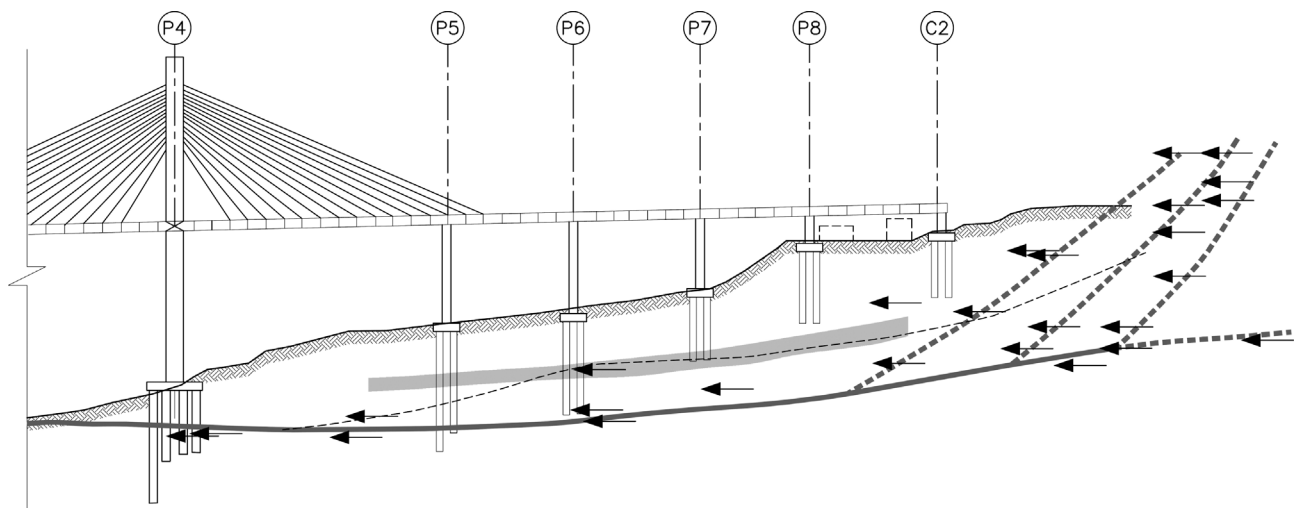


Figure 30. Cross section along the right abutment of the bridge and location of the slip surface.

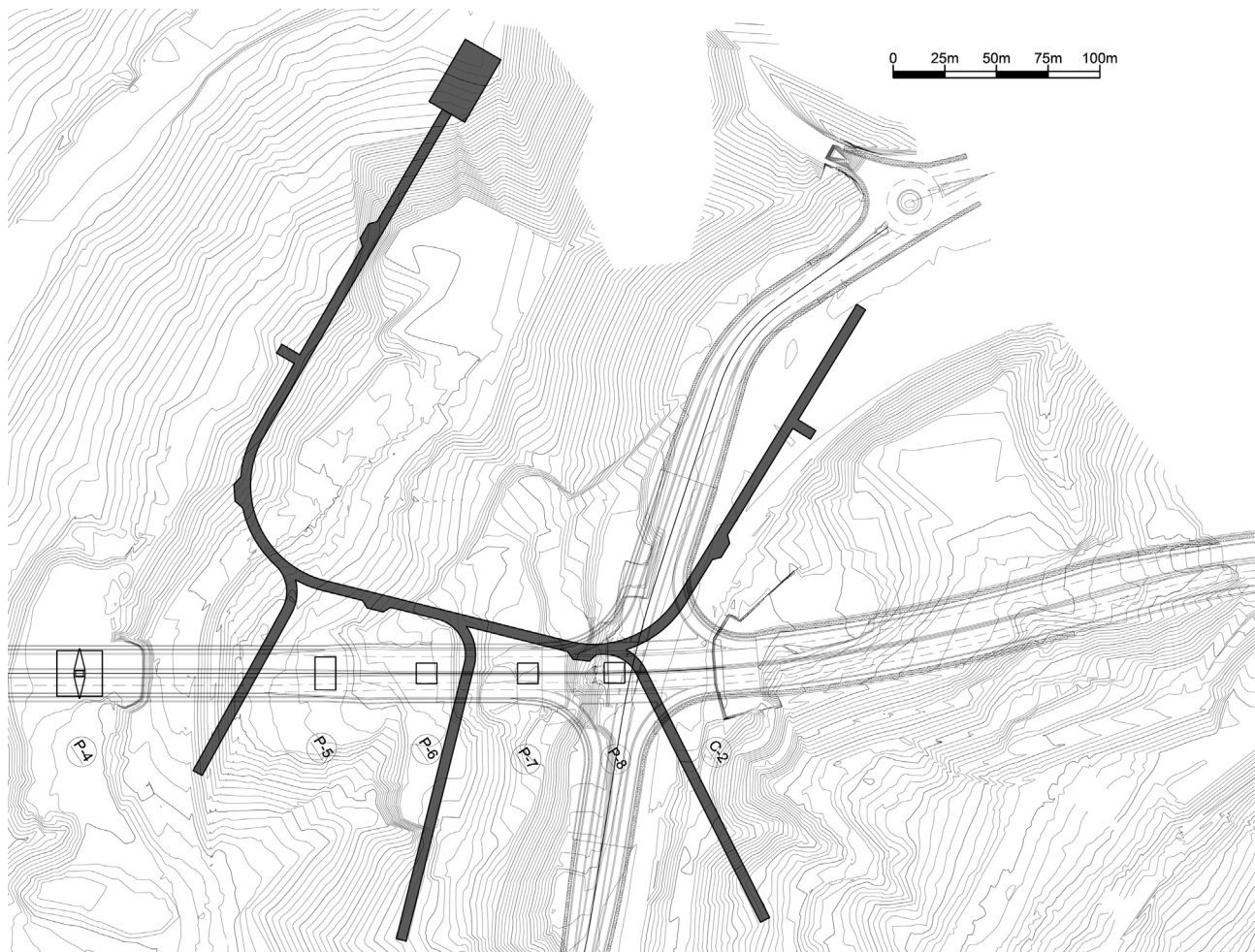


Figure 32. Plan view of main tunnel and adits, as well as location of bridge foundations.

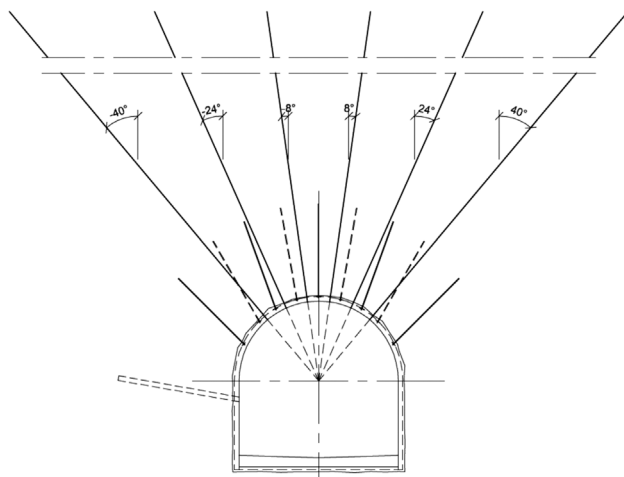


Figure 33. Tunnel cross section and drain location.

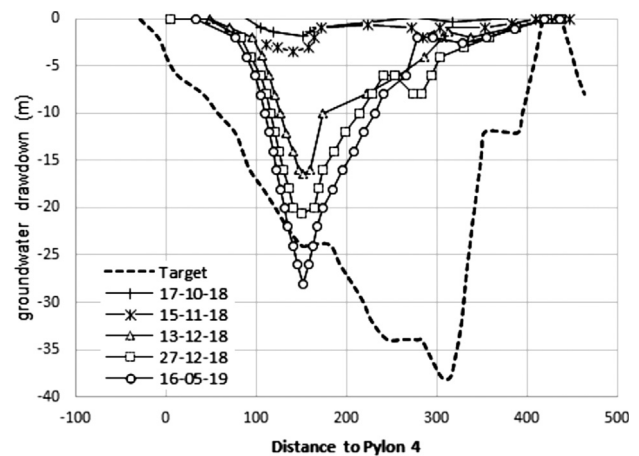


Figure 34. Groundwater drawdown monitoring results and target values.

allowing maintenance, possibility to expand drainage if necessary, among others.

The decision to build a drainage tunnel is often a long-lasting process, as well as the tunnel construction itself.

Therefore, it may be interesting to initiate stabilizing the unstable ground mass, to protect the slope and existing infrastructure, by groundwater lowering through deep wells.

Acknowledgments

The authors want thank Ecovias, Autovias, Construtora Andrade Gutierrez and COWI for the opportunity to publish the case histories, and Engineer Cristiano Yai for his valuable help with the illustrations.

References

- ABNT - Associação Brasileira de Normas Técnicas (2009). Estabilidade de Encostas - NBR 11682. ABNT - Associação Brasileira de Normas Técnicas, Rio de Janeiro, Brazil, 33 p.
- Bardanis, M., Cavounidis, S. (2016). The stabilization of the landslides in Area B, Section 2.4 of Egnatia Highway in Western Greece. Proc. 1st Int. Conf. on Natural Hazards & Infrastructure, Chania, Greece.
- Bastos, I.G. (2006). Estabilização de encostas através de drenagem profunda: Estudo de um Caso de Estabilização com Túnel de Drenagem. M.Sc. Dissertation. Escola Politécnica, Universidade de São Paulo. 204 p.
- Bertola, F.; Beatrizotti, G. & Torre, F.D. (1997). La estabilización del deslizamiento activo de Campo Vallemaggia en Suíza. Proc. 2nd Pan. Am. Symp. on Landslides, Rio de Janeiro, pp. 655-663.
- Bilfinger, W. (2019) Tunneling through the rock-soil interface. Proc. XVI PCSMG, Cancun, pp. 194-214.
- Borges, M.S.N. & Lacerda, W.A. (1986). Sobre a drenagem interna de taludes de corte e aterro. Proc. VIII COBRAMSEG - 8th Brazilian Conf. on Soil Mech. and Geot. Eng., Porto Alegre, v. 5, pp. 17-33.
- BTS - British Tunneling Society (2004). Tunnel Lining Design Guide. ICE Publishing, London, 196 p.
- de Mello, L.G.F.S. (2018). Some Case Histories with Lessons to Learn in Dam Engineering. Soils and Rocks, 41(3):267-307. <https://doi.org/10.28927/SR.413267>
- de Mello, V.F.B. (not specified). Personal communication.
- de Mello, V.F.B. (1972). Thoughts on Soil Engineering Applicable to Residual Soils. Proc. 3rd Southeast Asian Conference on Soil Engineering, Hong Kong, pp. 5-43.
- DER - Departamento de Estradas de Rodagem (2020). <http://www.der.sp.gov.br/WebSite/MalhaRodoviaria/VolumeDiario.aspx>.
- Eberhardt, E.; Bonzanigo, L. & Loew, S. (2007). Long-term investigation of a deep-seated creeping landslide in crystalline rock. Part II. Mitigation measures and numerical modelling of deep drainage at Campo Vallemaggia. Can. Geotech. J., 44(10):1181-1199. <https://doi.org/10.1139/T07-044>
- Fookes, P.G.; Baynes, F.J. & Hutchinson, J.N. (2000). Total geological history: a model approach to understanding site conditions. Proc. GEOENG 2000 - International Conference on Geotechnical and Geological Engineering, Melbourne, pp. 370-460.
- Froude, M.J. & Petley, D.N. (2018). Global fatal landslide occurrence from 2004 to 2016. Nat. Hazards Earth Syst. Sci., 18(8):2161-2181. <https://doi.org/10.5194/nhess-18-2161-2018>, 2018
- Futai, M.M.; Wolle, C.M.; Bastos, I.G. & Suzuki, S. (2009). Utilização de Túneis e Galerias de Drenagem para Estabilização de Encostas. Proc. COBRAE 2009 - 5 °Congresso Brasileiro de Estabilidade de Encostas, São Paulo, pp. 223-232.
- Gillon, M.D. & Saul, G.J. (1996). Stabilization of Cairnmuir Landslide. Proc. 7th International Symposium on Landslides, Trondheim, v. 3, pp. 1693-1698.
- Guidicini, G. & Nieble, C.N. (1976). Estabilidade de taludes naturais e de escavação. Edgard Blucher, São Paulo, 170 p.
- Hachich, W.C. (1996). Segurança das fundações e escavações. In: Fundações: Teoria e Prática. 1st Ed., Pini, São Paulo.
- Highland, L.M. & Bobrowsky, P. (2008). The Landslide Handbook: A Guide to Understanding Landslides. USGS, Reston, Virginia, 129 p.
- ITA - Working Group on General Approaches for the Design of Tunnels (1988). Guidelines for the design of tunnels. Tunneling and Underground Space Technology, 3(3):237-249.
- ITA - WG 2 (2000). Guidelines for the design of shield tunnel lining. Tunneling and Underground Space Technology, 15(3):303-331.
- ITA - WG 9 (2009). General Report on Conventional Tunneling. ITA Report n° 002. ITA, São José dos Campos.
- ITA - WG 2 (2015). Strategy for Site Investigation of Tunneling Projects. ITA Report n° 15. ITA, São José dos Campos.
- ITA - WG 2 (2019). Guidelines for the Design of Segmental Tunnel Lining. ITA Report n° 22. ITA, São José dos Campos.
- JLS - Japan Landslide Society Japan (2002). Landslides in Japan - The 6th revision. JLS - Japan Landslide Society Japan & National Conference of Landslide Control, 64 p.
- Lin, D.-G.; Hung, S.-H.; Ku, C.-Y. & Chan, H.-C. (2016). Evaluating the Efficiency of Subsurface Drainages for Li-Shan Landslide in Taiwan, Nat. Hazards Earth Syst. Sci. Discuss. <https://doi.org/10.5194/nhess-2015-309>
- Mantovani, M.; Bossi, G.; Marcato, G.; Schenato, L.; Tedesco, G.; Titti, G. & Pasuto, A. (2019). New Perspectives in Landslide Detection Using Sentinel-1 Datasets. Remote Sens., 11(18):2135. <https://doi.org/10.3390/rs11182135>
- Marinos, P. & Hoek, E. (2006). The construction of the Egnatia highway through unstable slopes in Northern Greece. Proc. XI Conf. Rock Mech., Turin.
- Moraes, L.K.C. & Assis, A.P. (2018). Efeito de túneis drenantes no comportamento de taludes. Rev. Técn. Cient. Crea-PR. Special Edition, 17 p.
- NGI - Norwegian Geotechnical Institute (2015). Handbook - Using the Q-System - Rock Mass Classification and

- Support Design. Norwegian Geotechnical Institute, Oslo, 54 p.
- Patton, F.D. & Hendron, A.J. (1974). General Report on Mass Movements. Proc. 2nd Int. Cong. Int. Ass. Eng. Geol., v. 2, pp. 1-57.
- Petley, D. (2020). Fatal Landslides in 2019. Available online: <https://blogs.agu.org/landslideblog/2020/03/25/2019-fatal-landslides/>.
- Popescu, M. (2002). Landslide Causal Factors and Landslide Remedial Options. Proc. 3rd Int. Conf. on Landslides, Slope Stability and Safety of Infrastructures, Singapore, pp. 61-81.
- Rico, A. & Castillo, H. (1974). La ingeniería de suelos en las vías terrestres. Mexico, Ed. Limusa, v. 1, 460 p.
- Sun, H.Y.; Wong, L.N.Y.; Shang, Y.Q.; Shen, Y.J. & Lü, Q. (2010). Evaluation of drainage tunnel effectiveness in landslide control. Landslides, 7:445-454. <https://doi.org/10.1007/s10346-010-0210-3>
- Vargas, M. (1966). Estabilização de taludes em encostas de gnaisses decompostos. Proc. 3º Congr. Bras. Mec. Sol. Belo Horizonte, v. 1, pp. 32-55.
- Wang, Z.L.; Shang, Y.Q. & Sun, H.Y. (2013). Optimal Location and effect judgement on drainage tunnels for landslide prevention. J. Cent. South. Univ., 20:2041-2053. <https://doi.org/10.1007/S11771-013-1706-5>
- Wei, Z.L.; Shang, Y.Q.; Sun, H.Y. & Wang, D.F. (2019). The effectiveness of a drainage tunnel in increasing the rainfall threshold of a deep-seated landslide. Landslides, 16:1731-1744. <https://doi.org/10.1007/s10346-019-01241-4>
- Wolle, C.M.; Mello, L.G.F.S.; Ribeiro, A.V.; Mori, M. & Yassuda, A. (2004). Stabilization of deep seated movement in a saprolitic massif supporting a highway viaduct. Proc. 9th International Symposium on Landslides, Rio de Janeiro, v. 2, pp. 1305-1312.
- Yan, L.; Xu, W.; Wang, H.; Wang, R.; Meng, Q.; Yu, J. & Xie, W.C. (2019). Drainage controls on the Donglingxing landslide (China) induce by rainfall and fluctuation in reservoir water levels. Landslides, 16:1583-1593. <https://doi.org/10.1007/s10346-019-01202-x>
- Yassuda, C.T. (1988). Aspectos gerais de estabilização de encosta Andina em Tablachaca - Encontro Técnico: Estabilidade de encostas. ABMS, São Paulo, pp. 3-15.
- Zhao, C. & Lu, Z. (2018). Remote sensing of landslides: A review. Remote Sensing, 10(2):279. <https://doi.org/10.3390/rs10020279>

Experimental, numerical, and analytical investigation of the effect of compaction-induced stress on the behavior of reinforced soil walls

Seyed H. Mirmoradi^{1,*} , Maurício Ehrlich¹ , Gabriel Nascimento² 

Article

Keywords

Compaction
Design method
Experimental study
Numerical analysis
Reinforced soil walls

Abstract

The influence of the compaction-induced stress (CIS) is experimentally, numerically and analytically evaluated on the behavior of reinforced soil walls (RSWs), under working stress conditions. Experimental studies have been carried out to evaluate the effect of the compaction condition at the back of the block facing on the behavior of geosynthetic-reinforced soil walls using three large-scale geosynthetic-reinforced soil walls constructed at the COPPE/UFRJ Geotechnical Laboratory. The numerical analyses have been carried out using the two-dimensional finite difference computer program FLAC to verify the influence of the compaction modelling procedure at the end of construction as well as post-construction performance of a full-scale geosynthetic-reinforced soil, GRS, segmental wall under surcharge loading. Two procedures for modelling the CIS found in the literature were employed in the analyses. Moreover, the calculated values using two design methods have been compared to the measurements and numerically calculated maximum reinforcement load, T_{max} , to evaluate the prediction accuracy of these methods when the value of the CIS is relevant.

1. Introduction

The effect of backfill compaction on the behavior of reinforced soil (RS) walls has been investigated and discussed in some studies found in the literature (*e.g.*, Ehrlich & Mitchell, 1995, Tatsuoka *et al.*, 1997, Uchimura *et al.*, 2003, Ehrlich *et al.*, 2012, Ehrlich & Mirmoradi, 2016). Depending on the magnitude of the compaction-induced stress (CIS) and the wall height, the horizontal residual stresses in the reinforced soil mass may be much greater than those from a geostatic origin, which may lead to a significant increase in the reinforcement loads. This effect is also dependent on the soil type, because higher interlocking may lead to greater induced stress due to backfill compaction. As a result, the structure becomes less sensitive to post-construction movements. The final effect of this process can be understood as a kind of over-consolidation or pre-loading of the reinforced soil mass that may significantly reduce post-construction movements (Ehrlich & Mitchell, 1995, Ehrlich *et al.*, 2012).

Depending on some controlling factors such as wall height, backfill material, facing, reinforcement and founda-

tion stiffness, CIS may significantly affect the connection load values, which may be strongly influenced by the differential settlement (Ehrlich *et al.*, 2012). A review of case studies carried out by Koerner & Koerner (2013, 2018) including 320 failed mechanically stabilized earth (MSE) walls has shown that 72 % of the failure case histories had poor or moderate compaction, which emphasized the influence of this factor on the wall performance. For the backfill soil, it is recommended to achieve 95 % standard Proctor compaction (Berg *et al.*, 2009, Collin *et al.*, 2002, Bernardi *et al.*, 2009, Koerner & Koerner, 2013).

Furthermore, regarding compaction conditions of the backfill near the facing, some recommendations have been made, such as using lightweight compaction equipment (recommended by the Federal Highway Administration, FHWA) or placing higher quality backfill in this zone to obtain the desired properties with reduced compaction effort in order to minimize the compaction-induced outward deformation and lateral stresses against the back of the facing. The application of heavy compaction equipment may also cause structural damage of the wall facing. Neverthe-

*Corresponding author. E-mail address: shm@ufrj.br.

¹Programa de Engenharia Civil, COPPE, Universidade Federal do Rio de Janeiro, Rio de Janeiro, RJ, Brazil.

²Departamento de Engenharia Agrícola e Meio Ambiente, Universidade Federal Fluminense, Niterói, RJ, Brazil.

Submitted on June 1, 2020; Final Acceptance on July 9, 2020; Discussion open until December 31, 2020.

DOI: <https://doi.org/10.28927/SR.433419>



This is an Open Access article distributed under the terms of the Creative Commons Attribution License, which permits unrestricted use, distribution, and reproduction in any medium, provided the original work is properly cited.

less, it should be noted that this zone is an important part of the backfill from a structural standpoint and may have a significant effect on the wall response, such as wall deformation and reinforcement strains (Hatami *et al.*, 2008).

Most of the current design methods, which are limit equilibrium (LE) methods or are based on the Rankine method, do not explicitly take into account the effect of the CIS on their calculations. Examples are the AASHTO (2017) method in the USA and the BS 8006 (BSI, 2010) method in the UK. This deficiency may be overcome by using the analytical method proposed by Mirmoradi & Ehrlich (2015a) that included the effect of CIS to use with any conventional design methods that do not already take into consideration the effect of CIS in calculations. Nevertheless, these methods have also some other important drawbacks. For example, these methods disregard the effects of reinforcement deformability, soil deformability, and in some cases cohesion. Working stress design methods have been developed to overcome these deficiencies and address more realistic approaches to the complex behaviour of reinforced soil structures (*e.g.*, Ehrlich & Mitchell, 1994, Ehrlich & Mirmoradi, 2016). The Ehrlich & Mitchell (1994) method and the simplified version of this method proposed by Ehrlich & Mirmoradi (2016) explicitly consider the effect of compaction in the determination of the maximum tensile force in the reinforcements, T_{\max} .

Regarding the numerical simulation, it should be noticed that if boundary conditions, geometry, constitutive models, parameters, and representative modelling procedure are correctly employed, numerical modelling may be a powerful tool to properly represent field conditions. Over the last few decades, several numerical studies have been carried out to investigate the influence of different controlling factors including the compaction effort on the behaviour of reinforced soil structures (*e.g.*, Hatami & Bathurst, 2005, Guler *et al.*, 2007, Ambauen *et al.*, 2015, Mirmoradi & Ehrlich, 2015b, Scotland *et al.*, 2016, Zheng & Fox, 2017, Zheng *et al.*, 2018, Jiang *et al.*, 2019). In the studies in which CIS was modelled, two procedures have been used (hereafter referred to as procedures type I and type II):

Type I) a uniform vertical stress applied only to the top of each backfill layer, as the wall was modelled from the bottom up (*e.g.* Hatami & Bathurst, 2005, Guler *et al.*, 2007, Ambauen *et al.*, 2015, Yu *et al.*, 2016).

Type II) an equally distributed load at the top and bottom of each soil layer (*e.g.* Mirmoradi & Ehrlich, 2015a, 2018a, Liu *et al.*, 2017, Scotland *et al.*, 2016).

Mirmoradi & Ehrlich (2014a, 2015a) stated that a model of compaction procedure type II could properly simulate the effects of compaction observed in the physical model studies. Moreover, a model of compaction procedure type I overestimated the measurements, and the discrepancy increased with depth and magnitude of the compaction effort. Nevertheless, Yu *et al.* (2016) stated that

“there is no obvious advantage of one method over the other on theoretical grounds”.

The present study experimentally, numerically and analytically investigates the influence of compaction-induced stress in the reinforced wall performance. The experimental study consists in the testing of large-scale geosynthetic-reinforced soil walls constructed at the COPPE/UFRJ Geotechnical Laboratory (Mirmoradi & Ehrlich, 2018b). The numerical analysis is carried out using the two-dimensional (2D) finite difference (FD) computer program FLAC. The numerical simulation of the compaction was performed using the two mentioned procedures found in the literature. The behaviour of the wall was studied using both compaction procedures at the end of construction as well as the post-construction (Nascimento *et al.*, 2020). Furthermore, two design methods are used to evaluate the prediction accuracy of these methods, when the induced stress due to the compaction is relevant (Mirmoradi & Ehrlich, 2015b, Ehrlich & Mirmoradi, 2016, Ehrlich *et al.*, 2017).

2. Experimental study

2.1 Test characteristics and material used

A series of well-instrumented physical model walls were constructed at the COPPE/UFRJ Laboratory of Physical Models. The results of two of these walls in addition to another recently constructed wall are used in this paper to evaluate the effect of compaction near the facing on the behavior of GRS walls. The three walls described here are identified as Walls 1, 2, and 3.

A cross-section of a physical model is shown in Fig. 1. The height of each physical model wall was 1.2 m. The length and vertical spacing of the geogrid were 2.2 and 0.4 m, respectively. A flexible polyester geogrid was used as reinforcement. Precast blocks were used for the wall with block facing. The walls were constructed with the facing having an inclination value of 6° to the vertical. The characteristics of the geogrid provided by the production company are shown in Table 1.

Moreover, regarding the reinforcement length it should be mentioned that in the laboratory test model the length of reinforcement was designed in order to guarantee no pullout of reinforcement from the resistant zone. Note that, as discussed by Ehrlich & Mirmoradi (2013) the value of maximum tension in the reinforcement may be consid-

Table 1. Mechanical and physical properties of reinforcement.

Longitudinal tensile strength (kN/m)	≥ 55
Transverse tensile strength (kN/m)	≥ 25
Elongation (%)	≤ 6
Weight (g/m ²)	240
Opening size (mm)	20 × 30

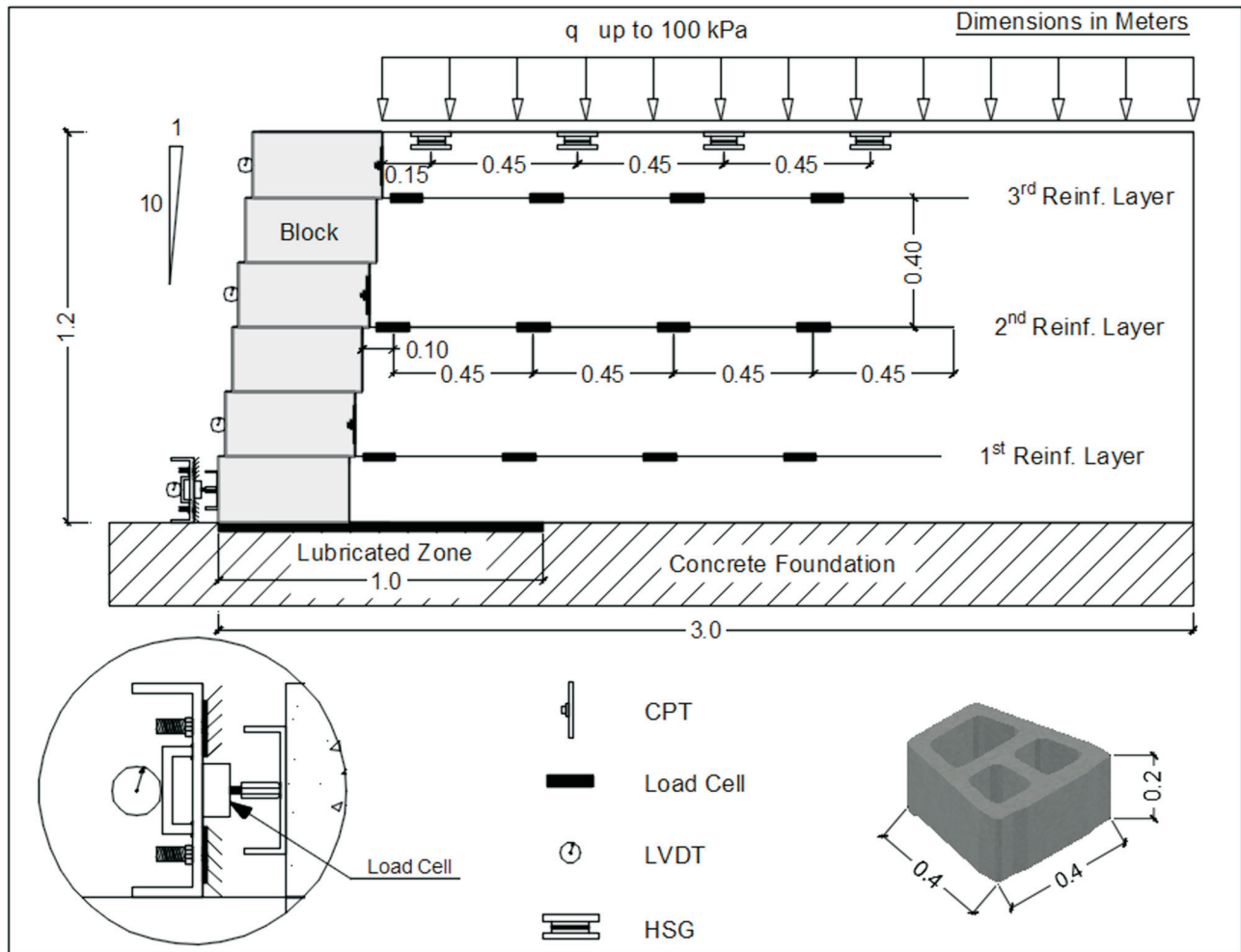


Figure 1. A cross-sectional view of a block face wall.

ered independent of the reinforcement length if there is enough length to guarantee no pullout failure. Furthermore, based on the AASHTO (2017) specification for RSWs, a minimum reinforcement length of 1.9-2.4 m, regardless of wall height, has been recommended.

The backfill material consists of well-graded sand, composed of crushed quartz powder with a significant amount of fines (19 % < #200), $D_{50} = 0.25$ mm, curvature coefficient $C_c = 1$, uniformity coefficient $C_u = 8.9$, and plasticity index PI equal to zero. Figure 2 shows the particle size distribution curve for the sand backfill.

In Wall 1, the entire surface of the backfill layers was compacted using a light vibrating plate (Dynapac LF 81) only. In Wall 2, first the entire surface of the backfill layers was compacted using a light vibrating plate, and then the backfill, except for 0.5 m from the back of the facing, was compacted using a vibratory tamper (Dynapac LC 71-ET). For Wall 3, the entire surface of the backfill layers was compacted using the vibrating plate and vibratory tamper. The equivalent static load of each compactor was determined through Kyowa accelerometers installed in the bodies of the compactors. In this case, the concept of equivalent

static weight is the one presented by Ehrlich & Mitchell (1994), rather than the classic definition related to the work carried out by a force. The mass and the contact areas of the

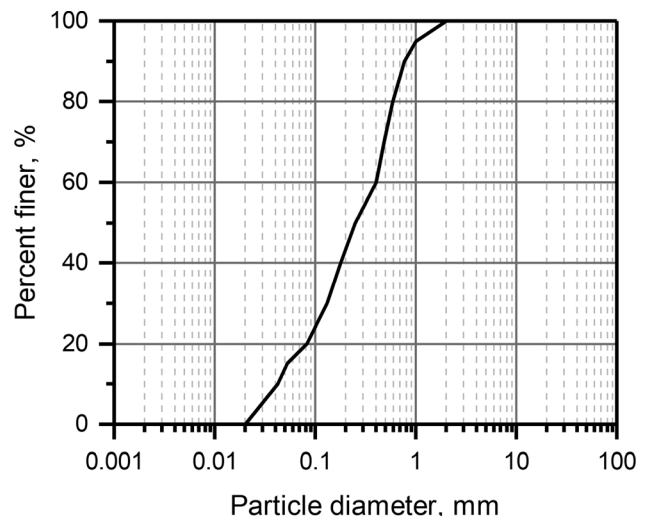


Figure 2. Grain-size curves for backfill soil.

two equipments are known and the related forces were determined through the acceleration measurements. Using this procedure, an equivalent vertical stress of 8.0 kPa was obtained by the vibrating plate (hereafter referred to as the “light compactor”), while 73 kPa was obtained by the vibratory tamper (hereafter referred to as the “heavy compactor”). Nevertheless, based on the back-analysis performed by Ehrlich *et al.* (2012), an equivalent vertical stress of 63 kPa may be obtained by the vibratory tamper.

The soil unit weights after light and heavy compactions were 19 and 20 kN/m³, respectively and the corresponding relative density (D_r) were 71 and 89 %. The soil friction angles, considering the measured unit weight, were determined by triaxial and plane strain compression tests as 42° and 50°, respectively. Additional information about properties of the backfill soil can be found in Ehrlich *et al.* (2012), Ehrlich & Mirmoradi (2013), Mirmoradi & Ehrlich (2016) and Mirmoradi *et al.* (2016).

The toes of the block facing of the walls were restricted during the construction and surcharge application. Figure 1 also shows a schematic view of the procedure used to guarantee the toe restraint of the walls. Lateral movement of the toe was restricted by a steel beam that was fixed to the concrete U-shaped wall box using two bolts in each side of the beam (see Fig. 3).

2.2 Construction sequence and surcharge loading

The construction of the model was performed in six soil layers, 0.2 m thick and placed dry. The sequence of construction of Wall 1 was developed in two stages per layer of soil: (1) soil placement and (2) compaction of the placed backfill using the vibrating plate. In Walls 2 and 3,

in addition to the two stages performed for Wall 1, a third stage was performed that entailed compaction of the back-fill layer using a vibratory tamper.

The 1 m wide zone at the bottom of the walls that included the base of the block face was lubricated (sandwich of rubber sheets and Teflon grease). To reduce the effect of the lateral friction at the interface between the backfill soil and the concrete wall, PVC sheets were installed in all lateral faces of the wall that comprise the U-shaped concrete box of the model. In addition, in order to assure a plane strain condition during the tests, a thin layer of Teflon grease covered by PVC and plastic sheets were used to minimize the friction between the soil and the model box. The friction angle between the rubber sheets and the Teflon grease was measured about 3°. Moreover, the concrete box used to perform the physical model tests was designed to make possible the assumption of no normal strain in the transversal direction of the model walls.

Three layers of reinforcement were installed along the height of the wall, placed at: 0.2 m (first layer), 0.6 m (second layer), and 1.0 m (third layer) above the bottom of the wall. Each reinforcement layer was longitudinally divided into three sections, and only the 0.5 m reinforcement placed at the center of the wall was instrumented. After the end of construction, a surcharge loading of up to 100 kPa was applied over the entire surface of the backfill soil using an air bag. The surcharge load was then kept constant at 100 kPa. In the meantime, the toes of the walls were gradually released to the free base condition at the end of the toe release (0.5 mm release in each step).

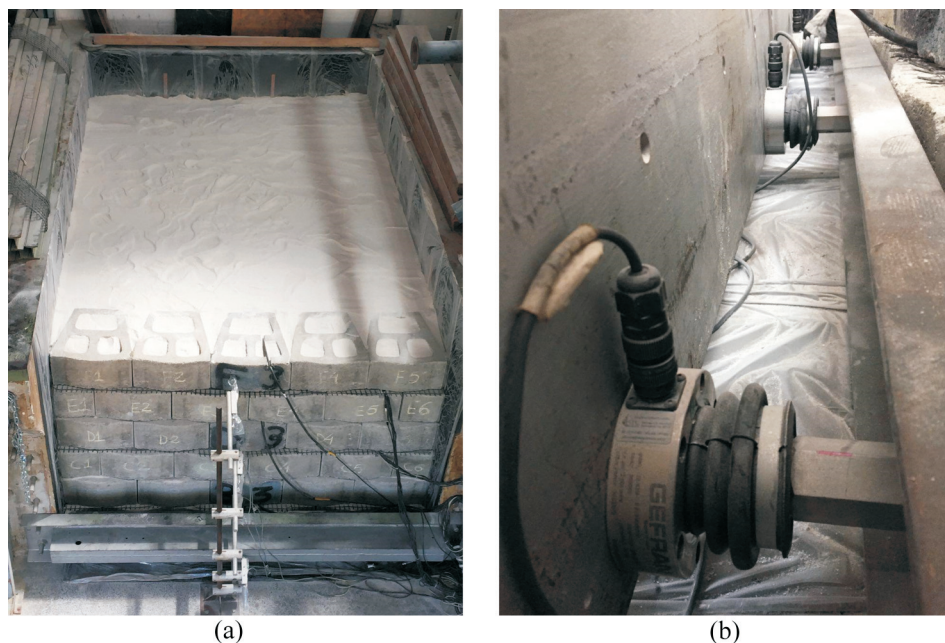


Figure 3. Views of Wall 3 at the end of construction (a) and load cells installed to measure the toe horizontal load (b).

2.3 Instrumentation

The walls were instrumented to monitor the values of the reinforcement load, toe horizontal load, horizontal facing displacement, horizontal stress on the back of the block facing, and vertical displacement at the top of the walls. Reinforcement loads were monitored using the load cells installed at four points along the reinforcement (*i.e.* two load cells at each point). The load cells allowed for reinforcement load monitoring without the need to determine the reinforcement stress-strain curves, which are time dependent. The load cells were also capable of counterbalancing the temperature effects and bending moments and were strong enough to resist the stress induced during the operation of the compaction equipment (Ehrlich *et al.*, 2012, Ehrlich & Mirmoradi, 2013, Mirmoradi & Ehrlich, 2014b, Mirmoradi *et al.*, 2016).

The horizontal displacements of the wall face were monitored by LVDTs. The horizontal facing displacements were measured at the second (0.3 m height), fourth (0.7 m height), and sixth (1.1 m height) layers. Furthermore, the horizontal stress at the back of the block facing was monitored using total stress pressure cells (TPCs). Two TPCs were installed on the back of the blocks to evaluate the horizontal stress values at the top and bottom of the back of the block face. Those blocks were placed next to the second and sixth soil layers.

The toe horizontal load was measured using the load cells installed on the steel beam fixed to the concrete U-shaped wall box. The load cells were placed between the aforementioned steel beam and another steel beam installed on the blocks of the first layer. As stated earlier, a 1-m wide zone at the bottom of the walls that included the base of the block face was lubricated. Thus, the toe was free and the re-

striction of lateral movements was guaranteed through the load cells; the toe horizontal load was measured using these load cells (see Fig. 3).

A special device was used for monitoring the vertical displacements. This hydraulic settlement gage (HSG) consists of an acrylic settlement cell filled with mercury connected to a plastic tube, also filled with mercury, which is monitored by a pressure transducer. Any settlement or heave in the settlement cell can thus be related to the readings in the pressure transducer. For all walls, the monitoring points, HSG 1, HSG 2, HSG 3, and HSG 4, were located at four different distances from the back of the face: 0.15, 0.6, 1.05, and 1.50 m, respectively. These instruments were installed at the top of the walls and monitored the settlement after the end of construction.

2.4 Test results

Figure 4 shows the comparison of the toe horizontal loads observed at the end of construction during application of the surcharge and during toe release for Walls 1, 2, and 3. The results show higher toe horizontal loads for the walls in which heavy compaction was applied (Walls 2 and 3). At the end of construction, the toe horizontal loads for Walls 2 and 3, respectively, are about 2.9 and 2.4 times higher than the value measured for Wall 1. At the end of loading, that is, at 100 kPa, the ratios decrease to about 1.5 and 1.4, respectively. Figure 4 also indicates the toe horizontal loads during toe release of the walls. As shown, the toe horizontal loads gradually decrease during toe releases of the walls. The toes of the Walls 1, 2, and 3 were completely released after 5, 7, and 8.5 mm, respectively.

Figure 5 presents the toe horizontal load increments during stage construction for the walls. It is shown that, irrespective of the type of the compaction used for construc-

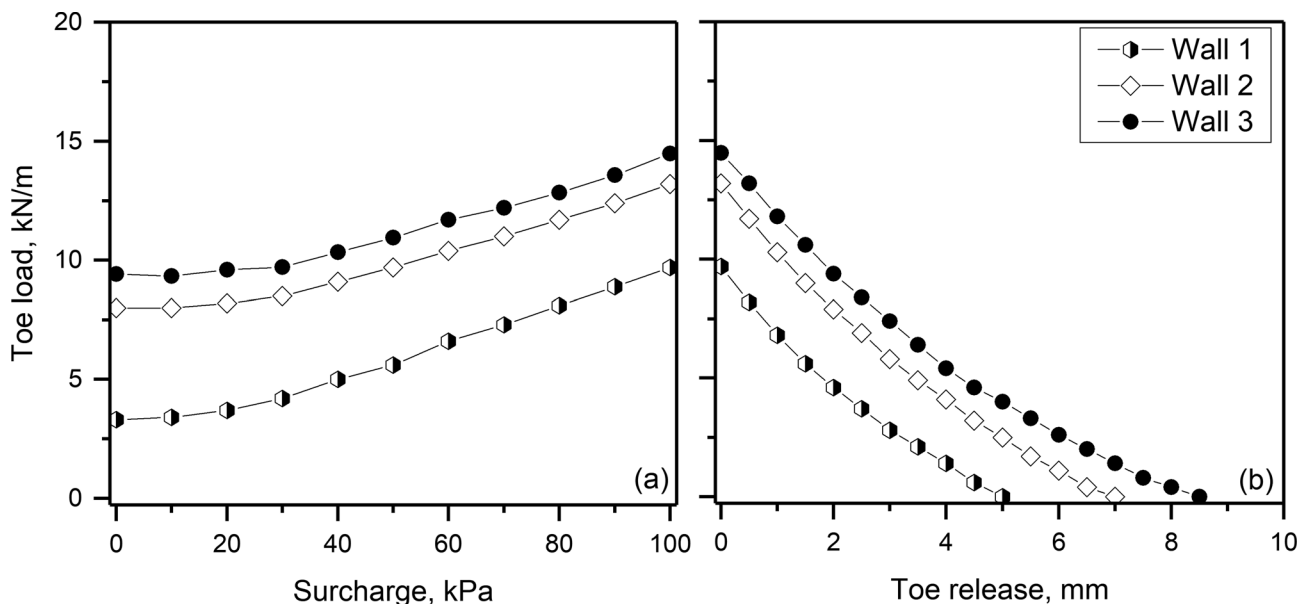


Figure 4. Toe horizontal load vs. surcharge application and toe release for Walls 1, 2, and 3.

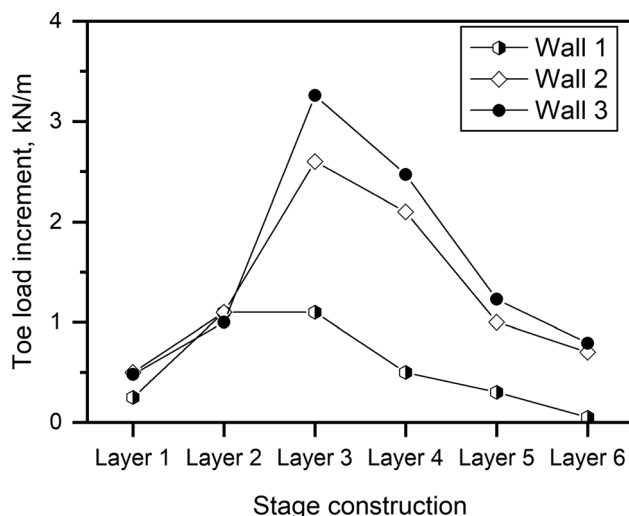


Figure 5. Toe horizontal load during construction.

tion of the walls, the maximum toe horizontal load increment occurs at the end of the construction of the third layer. Thereafter, the effect of the compaction on the toe horizontal load decreases significantly. It may be expected that after a few more layers the effect of the compaction on the increment in toe horizontal load values may disappear, in agreement with the results of the numerical analyses presented by Mirmoradi & Ehrlich (2015b).

Figure 6 shows the sum of the maximum reinforcement loads, ΣT_{\max} , at the end of construction (EOC), during surcharge application and toe release. The figure indicates that although the values of ΣT_{\max} are different at the EOC, this difference decreases as the applied surcharge increases and at the end of loading (EOL) similar values were measured for all walls irrespective of the compaction condi-

tions, which agrees with the discussion presented by Ehrlich & Mitchell (1994) and Ehrlich *et al.* (2012). They stated that compaction of backfill using heavy compaction equipment may lead to a significant increase in the reinforcement load and this increase may vanish when the surcharge value exceeds the corresponding value of the vertical stress induced by heavy compaction. Figure 6(b) also illustrates that ΣT_{\max} increases for the walls during toe release. Nevertheless, this increase is greater for the walls in which the backfills were compacted using light and heavy compactor equipment.

Figure 7 illustrates the measured values of the horizontal displacements during construction (Fig. 7a) and the average of the post-construction horizontal displacements (H_{ave}) vs. surcharge application (Fig. 7b). The figure shows that in Wall 3, in which the entire surface of the backfill was compacted using the vibratory tamper, the highest and lowest horizontal facing displacement occur during construction and post-construction, respectively. This is an expected behavior as the heavy compaction promotes displacement during the construction period and reduces post-construction horizontal displacement. This means that heavy compaction may cause the reinforced soil mass to exhibit a kind of over-consolidation that promotes a stiffer behavior after construction (Ehrlich & Mitchell, 1994, Ehrlich *et al.*, 2012, Mirmoradi & Ehrlich, 2018b). Nevertheless, this behavior is not observed for Wall 2.

Furthermore, Fig. 7 indicates that both during construction and the post-construction horizontal displacement in Wall 2 are higher than that in Wall 1. This is also observed in Fig. 8, in which the vertical displacements, measured using hydraulic settlement gage (HSG) at four positions at the end of loading and toe release, are presented.

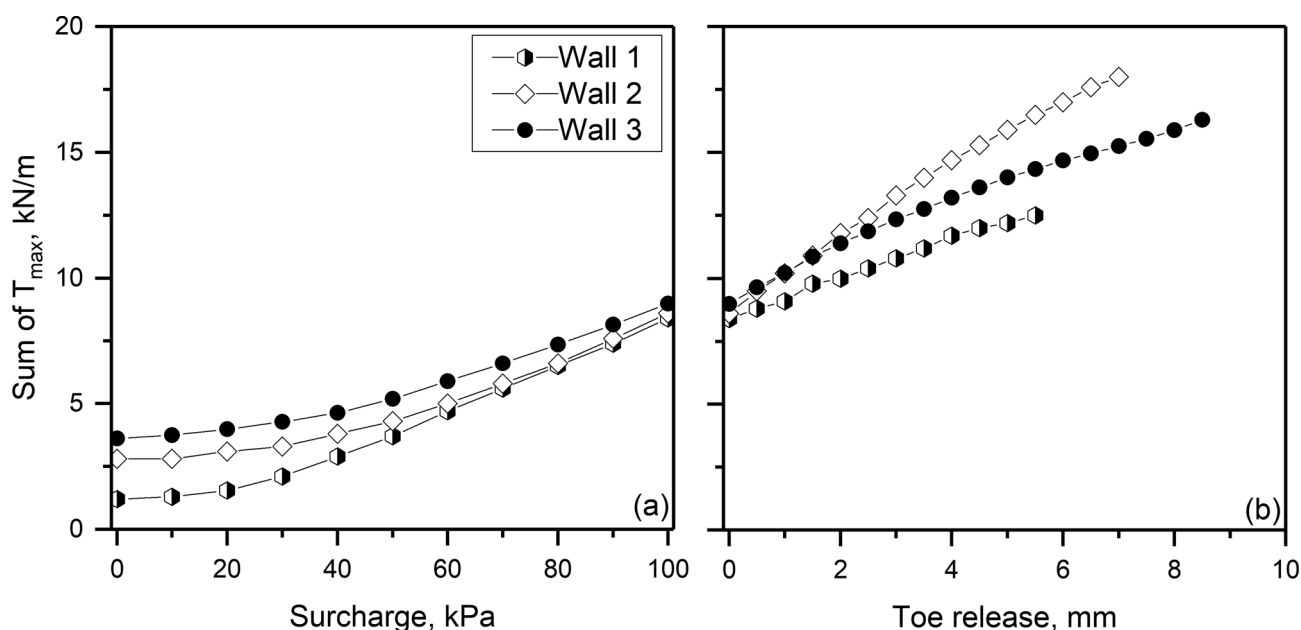


Figure 6. Sum of maximum reinforcement load (a) during surcharge application and (b) toe release.

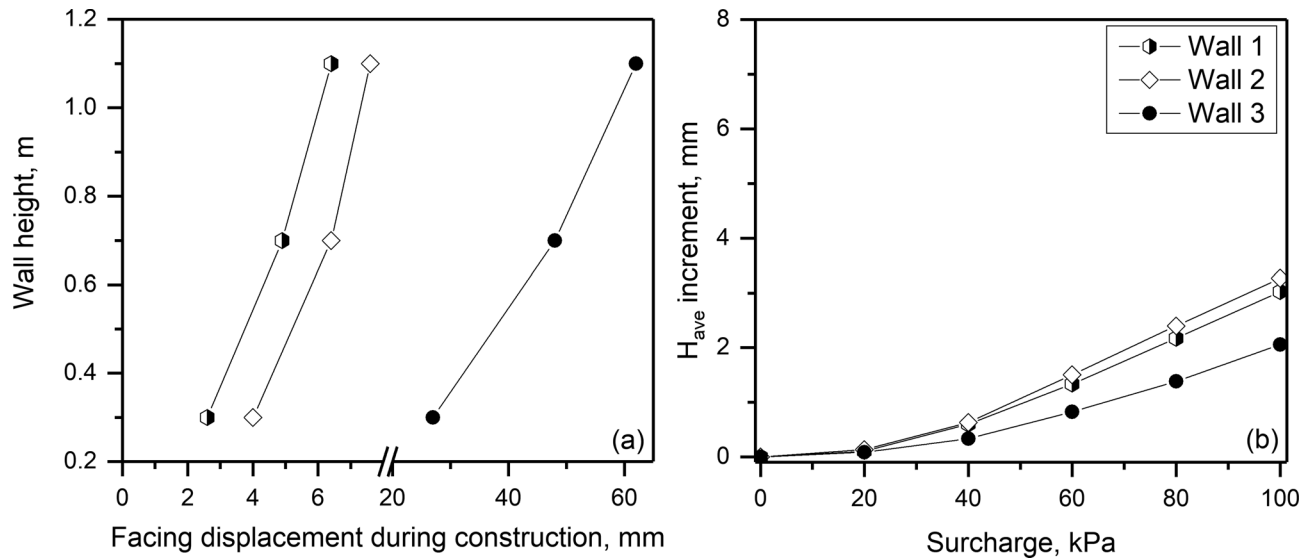


Figure 7. Horizontal facing displacement (a) during construction and (b) post construction.

The figure shows the significantly greater vertical displacements for Wall 2 in the first (0.15 m from the back of the face) and second measurement positions (0.6 m from the back of the face) compared with Walls 1 and 3. On the other hand, in the third (1.05 m from the back of the face) and fourth measurement positions (1.5 m from the back of the face), similar values were obtained for all walls. It is also indicated that the lowest vertical displacement values were measured in Wall 3 (Mirmoradi & Ehrlich, 2018b).

As stated earlier, in Wall 2, the backfill was firstly compacted with the light compactor. Then the heavy compactor was used except for the first 0.5 m of backfill directly behind the facing. The high vertical displacement of

the backfill located close to the back of the facing may be associated with an increase of the void ratio of the soil near to the face due to the vibration promoted by the operation of the tamper equipment nearby. This can be clearly seen in Fig. 8, in which, the backfill soil unit weight vs. distance from the facing is presented for the walls. As shown, in Walls 1 and 3, the average backfill unit weights of 19 kN/m³ and 20 kN/m³ were measured after the end of compaction operations, irrespective of the distance from back of facing. In Wall 2 however, the magnitude of the soil unit weight measured in the first 0.5 m zone was (~5 %) lower than those measured in Wall 1, in which the same compactor equipment (light compactor) was employed in the entire

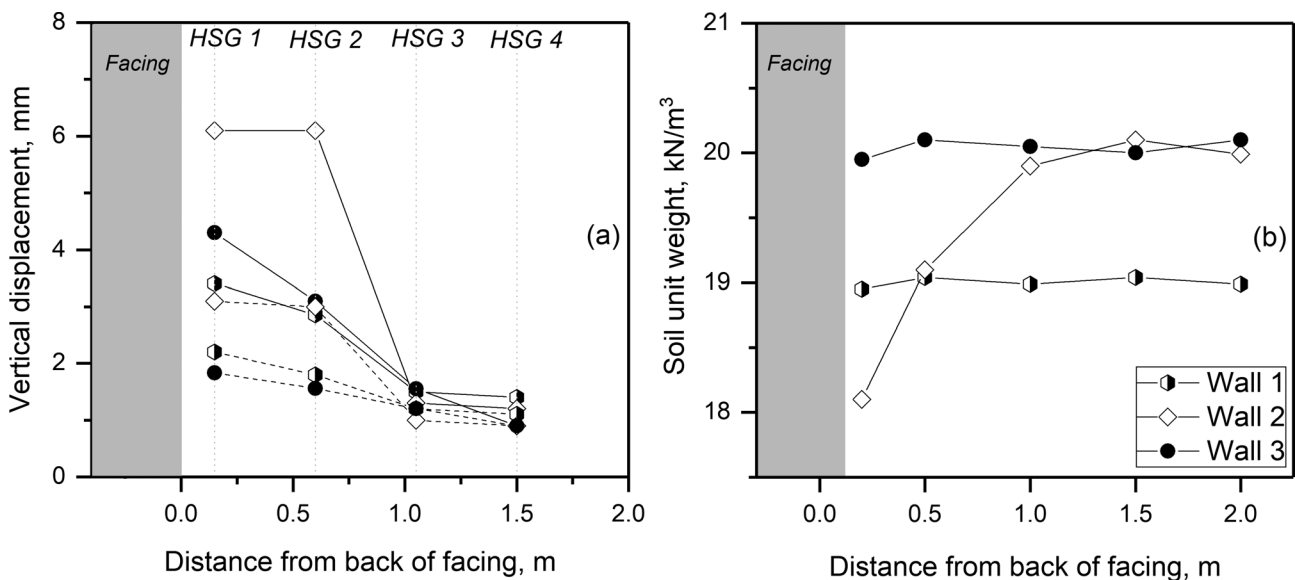


Figure 8. Vertical displacement at the end of surcharge application, EOL (dashed lines), and toe release, EOR (solid lines) and backfill soil unit weight for three walls.

surface of the soil layers. This highlights the importance of the compaction condition close to the back of the facing (Mirmoradi & Ehrlich, 2018b).

3. Numerical analysis

3.1 Compaction-induced stress

Duncan & Seed (1986) indicated that the compaction operation may be modelled by load and unload cycles that would induce high horizontal residual stresses in the soil. In the field, the soil backfill goes through a complex stress path because of the various load and unload cycles caused by the passing of compaction equipment. The roller sinks into the soil to a depth sufficient to produce a limit equilibrium condition. Note that the roller-soil contact area varies with the shear resistance and stiffness of the backfill soil that varies with the number of passes. This was simplified by Ehrlich & Mitchell (1994) by assuming only one cycle of load-unload for each layer of backfill. Note that in the modelling of compaction-induced stress-strain, soil parameters representative of the backfill soil at the end of compaction should be used, so that they represent the condition found at the last compaction cycle.

Figure 9 shows the assumed stress path due to the compaction of the backfill layer by applying a single load-unload stress cycle. In this figure, different stress states were considered, corresponding with four conditions as follows: (1) soil placement; (2) compaction equipment operation; (3) end of compaction; and (4) placement of the next soil layer. Due to the operation of the compaction equipment, the vertical stress increases to the maximum effective vertical stress induced during compaction, $\sigma'_{zc,i}$ and simultaneously the horizontal stresses would increase to their maximum values (point 2). Although after unloading (at the

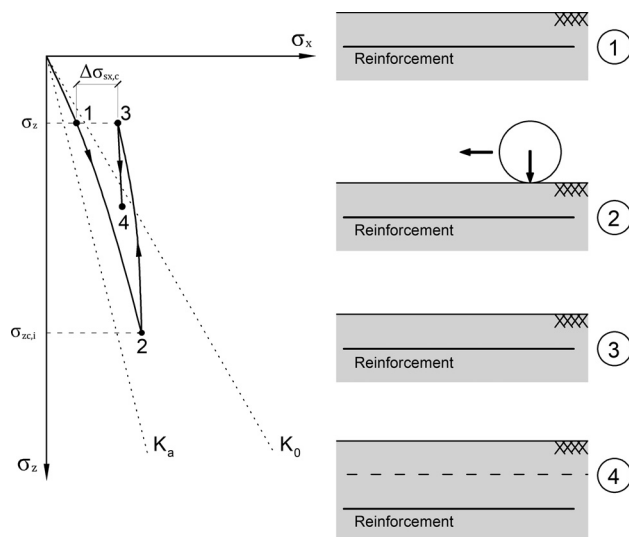


Figure 9. Assumed stress path due to compaction of soil backfill layer: (1) soil layer placement; (2) compaction equipment operation; (3) end of compaction; (4) next soil layer placement.

end of the compaction operation) the vertical stress returns to its initial value, $\sigma'_{z,i}$ (point 3), the same cannot be said to occur for the horizontal stresses, as the soil is not an elastic material. Thus, a residual horizontal stress remains in the soil due to the compaction operation ($\Delta\sigma_{sx,c}$). The placing of the next layer leads to an increase in vertical stress, and a small variation in horizontal stress (point 4). The residual horizontal stress completely disappears only when the geostatic stress at the top of the soil layer overcomes the value of the vertical stress induced during the compaction operations, $\sigma'_{zc,i}$.

Figure 10 shows a schematic view of the increase in vertical stress during a roller operation in soil backfill. The vertical stress at the top of each layer during the compaction roller operation may be represented by a strip load, and an elastic solution could be used to represent its evolution with depth. For each soil layer the maximum stress increase during the roller operation occurs at the point of soil-roller contact, and decreases with depth. This depth depends on the width of the load applied for the compaction operation, B . For roller (strip load) and tamper (rectangular load) compactors, the depths of soil in which about 10 % of the maximum stress increase would occur during the compaction operation are about six and two times the load width, B , respectively (Lambe & Whitman, 1969).

Ehrlich & Mitchell (1994) stated that “in multilayer construction, the compacted layers are relatively thin, typically 0.15-0.3 m thick, and all points in each soil layer may be assumed to have been driven to the same maximum soil stress state during compaction”. Therefore, it may be assumed that all points are driven to the same vertical induced stress, $\sigma'_{zc,i}$, due to compaction.

The lateral strain of the reinforced soil layer, in the direction perpendicular to the face of the wall, reduces the maximum horizontal stress induced by compaction when compared to the maximum stress that would exist in cases

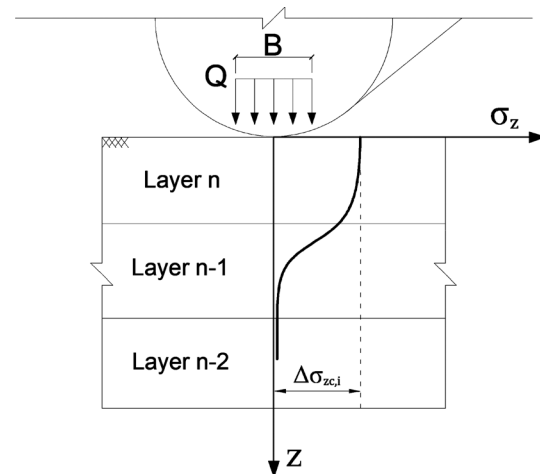


Figure 10. Vertical stress increase during a roller operation in the backfill (strip load; Boussinesq elastic solution).

where there are no lateral strains. Therefore, the actual maximum horizontal stress induced by compaction is also a function of the reinforcements and facing stiffness (point 3 in Fig. 9). However, the vertical stress induced by compaction may be assumed to be independent from the horizontal strains (Ehrlich & Mitchell, 1994).

Tables 2 and 3 show the characteristics of various vibrating rollers and vibrating tampers, respectively, which were provided by the producing companies. For plates, the vertical compaction-induced stress, $\sigma'_{zc,i}$, can be assumed to be the average contact pressure at the base of the equipment. The centrifugal forces listed are the maximum vibration amplitude of the rollers. Figure 11 shows the $\sigma'_{zc,i}$ values of compactor rollers for soil with a specific 18 kN/m^3 weight and various angles of friction, determined using equations developed by Ehrlich & Mitchell (1994). For a cohesionless soil, $\sigma'_{zc,i}$ is given by:

$$\sigma'_{zc,i} = \frac{1+K_a}{1+K_0} \left[\frac{1}{2} \gamma' Q \frac{N_\gamma}{L} \right]^{1/2} \quad (1)$$

where K_a is the Rankine active earth pressure coefficient, K_0 is the at rest earth pressure coefficient calculated using Jaky's equation (Jaky, 1944); Q is the compactor equipment equivalent static load, L is the length of the roller drum, γ' is the effective soil unit weight and N_γ is the soil-bearing capacity factor according to the Rankine wedge theory, calculated by:

$$N_\gamma = \tan(45^\circ + \phi' / 2) [\tan^4(45^\circ + \phi' / 2) - 1] \quad (2)$$

where ϕ' is the effective stress friction angle. As shown in Fig. 11, the value of the induced stress due to compaction operation significantly varies with the soil backfill friction angle. The reader is directed to the paper by Ehrlich & Mitchell (1994) for details about the derivation of the equations.

3.2 Model characteristics

The physical model used for the numerical modelling validation was built at the Royal Military College of Canada (RMC), and consisted of a 3.60 m high reinforced soil

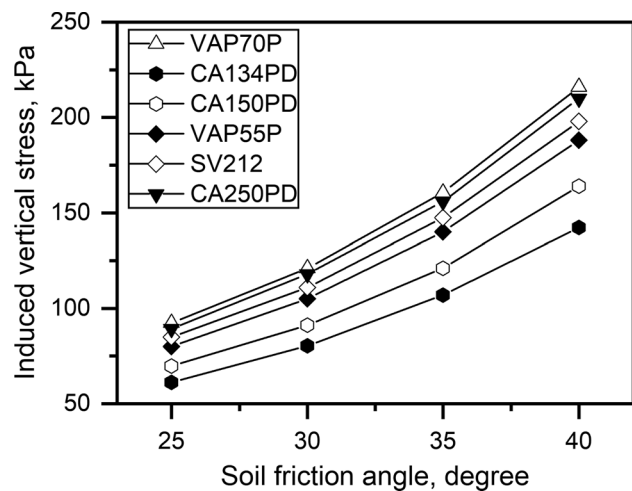


Figure 11. Vertical stress induced by several compactor rollers (after Ehrlich & Becker, 2010).

Table 2. Characteristics of various vibrating roller compactors (after Ehrlich & Becker, 2010).

Manufacturer	Model	Weight (kN)	Width (m)	Equivalent static load (kN)	Vertical stress (kPa)
Case	SV212	72.3	2.20	277	*
Müller	VAP55P	-	1.68	190	*
	VAP70P	-	2.14	320	*
Dynapac	CA134PD	19.6	1.37	89	*
	CA150PD	39.2	1.68	143	*
	CA250PD	72.6	2.13	300	*

* See Fig. 11.

Table 3. Characteristics of rammer compactors (after Ehrlich & Becker, 2010).

Manufacturer	Model	Equivalent static load (kN)	Base area (m ²)	Vertical stress (kPa)
Dynapac	LT500	10.0	0.076	132
	LT600	14.8	0.092	160
	LT700	18.6	0.092	201
Wacker	BS 50-4	14.7	0.092	159
	BS 60-4	15.6	0.092	169
	BS 70-2i	17.8	0.092	193

wall with a face inclination of 8° to the vertical. The reinforcement was provided by polypropylene (PP) geogrids with 0.60 m vertical spacing and approximately 2.20 m length (Hatami & Bathurst, 2006).

The numerical modelling was developed using the code FLAC version 8.0.455 (Itasca Consulting Group, 2016), which is based on the finite difference method (FDM). According to this method, the continuum material (e.g. soil and concrete) is discretized into zone regions (quadrilaterals) defined by grid points (GPs). Figure 12 shows the numerical grid used for the segmental retaining wall.

The bottom GPs (first row) of the soil regions were restrained to move in horizontal and vertical (x and y) directions, simulating a rigid foundation and a no-slip condition. At the backfill far-end boundary, the GPs were allowed to move only in the vertical direction and, at the first block, the bottom GPs were allowed to move only in the horizontal direction. A spring connected to a GP from the bottom left corner represented the load ring from the physical model, considering a 4 (MN/m)/m toe stiffness.

The mechanical connectors between the blocks and reinforcements of the physical model were numerically represented by two-node beam elements with large axial and bending stiffness. The master/slave pair FLAC feature made it possible to restrain the element nodes displacements to the corresponding nodes of the block (x and y di-

rection) or GPs of the soil (y direction) regions. Cable elements represented the reinforcement with a nonlinear tangent stiffness, calculated by (Hatami & Bathurst, 2006).

$$J_t = \frac{1}{J_0 \left(\frac{1}{J_0} + \frac{\eta}{T_f} \varepsilon \right)^2} \quad (3)$$

where J_t = time-dependent reinforcement tangent stiffness function; J_0 = initial tangent stiffness; η = scaling function; T_f = stress-rupture function for the reinforcement; ε = strain; and t = time. The parameters of this equation are summarized in Table 4.

The CHSoil constitutive model was adopted for the soil, based on a hardening/softening logic (Itasca Consulting Group, 2016). The elastic shear and bulk modulus are calculated by

$$G^e = G_{ref} p_{ref} \left(\frac{p'_m}{p_{ref}} \right)^n \quad (4)$$

and

$$K^e = K_{ref} p_{ref} \left(\frac{p'_m}{p_{ref}} \right)^m \quad (5)$$

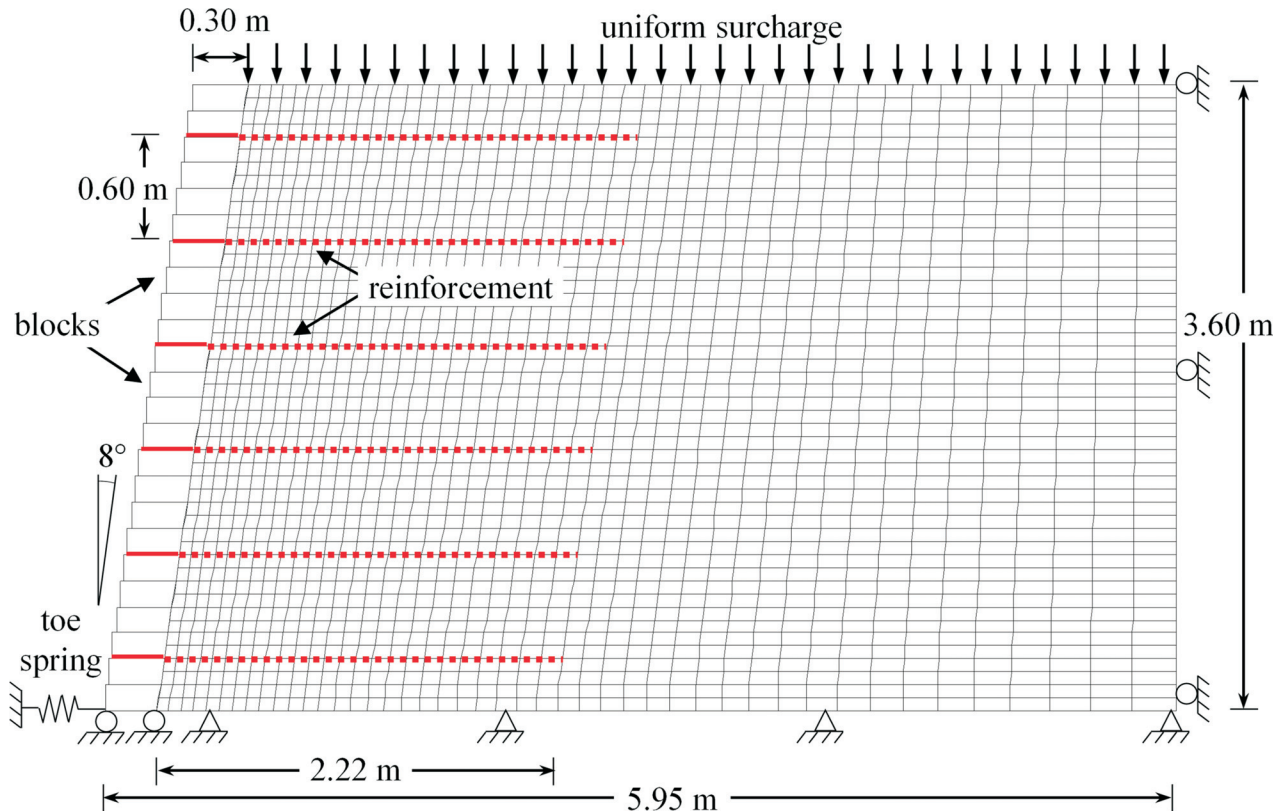


Figure 12. Numerical model grid, components and boundary conditions.

Table 4. Input parameters from the full-scale wall.

Property	Value
Soil properties	
Model	CHSoil
Friction angle, ϕ_f (°)	40 (triaxial) and 44 (plane strain)
Cohesion, c (kPa)	2.0
Ultimate dilation angle, ψ_f (°)	11.0
Unit weight, γ (kN/m ³)	16.8
Bulk modulus number, K_{ref}	575
Shear modulus number, G_{ref}	500 (triaxial) and 600 (plane strain)
Bulk modulus exponent, m	0.5
Shear modulus exponent, n	0.5
Failure ratio, R_f	0.95
Reference pressure, p_{ref} (kPa)	101.3
Min. initial mean effective pressure, p'_m (kPa)	1.0
Reinforcement	
Elastic axial stiffness (kN/m)	variable, Eq. (3)
Initial tangent stiffness, J_0 (kN/m)	115
Scaling factor, η	0.85
Rupture load, T_f (kN/m)	7.7
Modular block properties	
Model	Linear elastic
Size (m × m)	0.30 × 0.15 (length × height)
Weight (kg)	20
Stiffness modulus (GPa)	2.0
Poisson's ratio, ν	0.15
Block-block interface	
Friction angle (°)	57
Cohesion (kPa)	46
Normal stiffness, k_{nbb} (MPa/m)	1 000
Shear stiffness, k_{sbb} (MPa/m)	50
Soil-block interface	
Friction angle (°)	44
Dilation (°)	11
Normal stiffness, k_{nbb} (MPa/m)	100
Shear stiffness, k_{sbb} (MPa/m)	1
Grout (backfill-reinforcement)	
Friction angle (°)	44
Adhesive strength (kPa)	1,000
Shear stiffness [(kN/m)/m]	1,000
Toe condition	
Axial stiffness of anchor [(kN/m)/m]	4,000

respectively, where $p'_m = (\sigma'_1 + \sigma'_2 + \sigma'_3)/3$ is the initial value of the mean effective stress; G_{ref} , K_{ref} and p_{ref} are reference values; and m and n are constant exponents. In order to avoid an inconsistent Poisson equivalent value, K^e is limited by $2G^e/3 < K^e < 49.66G^e$.

The mobilized friction angle ϕ_m increases as a strain-hardening behaviour represented by

$$d(\sin \phi_m) = \frac{G^p}{p'_m} d(\gamma^p) \quad (6)$$

where γ^p is the plastic shear strain and the plastic shear modulus G^e is calculated by

$$G^p = G^e \left(1 - \frac{\sin \phi_m}{\sin \phi_f} R_f \right)^2 \quad (7)$$

where ϕ_f is the ultimate friction angle and R_f is the failure ratio, which assigns a lower bound to G^p .

To represent the typical dilation behaviour, the mobilized dilation angle is assumed as $\psi_m = 0$ for $\phi_m < \phi_{cv}$, then $\psi_m = \psi_f$ for $\phi_m > \phi_{cv}$, where ψ_f is the ultimate dilation angle and ϕ_{cv} is the mobilized friction angle at constant volume, estimated by

$$\sin \phi_{cv} = \frac{\sin \phi_f - \sin \psi_f}{1 - \sin \phi_f \sin \psi_f} \quad (8)$$

The values selected for the parameters (Table 4) produced a good match for the soil stress-strain curve under confining pressures equal to 20 kPa and 30 kPa, and for strain less than 1.5 % (Fig. 13), which corresponds to the stress levels during the analysis.

The same procedure and interface values employed by Huang *et al.* (2009) are used in this study. The contact between components (*i.e.* block-block and block-soil) was modelled with interface pairs based on Coulomb sliding and normal/shear stiffness (Table 4). The interaction between the reinforcement and soil is modelled by the grout feature, which provides a rigid attachment until the adhesive strength is overcome, then slipping is allowed and friction force is calculated by the friction angle and cohesion. High value of soil-reinforcement interface resistance employed in the analyses results in no slip between soil and reinforcement. As shown by Dyer & Milligan (1984) and Jewell (1980), perfect adherence is a reasonable assumption for a soil-reinforcement interface under working stress conditions.

3.3 Numerical modelling of compaction

Backfill soil placement and compaction were modelled during the stage construction. Two different procedures were used for modelling the CIS during the construction sequence (Mirmoradi & Ehrlich, 2018a):

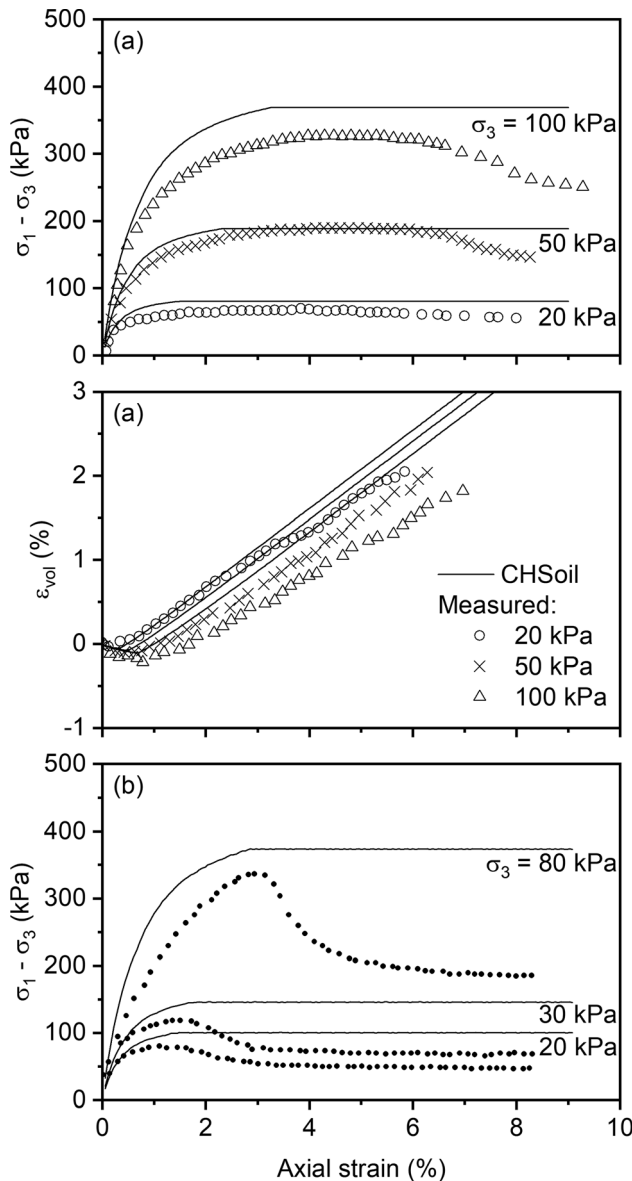


Figure 13. Soil constitutive model response compared to measured values from (a) triaxial and (b) plane strain tests presented by Hatami & Bathurst (2005).

- **Type I:** A uniform vertical stress is applied at the surface and then removed (*e.g.* Hatami & Bathurst, 2005) (referred to as procedure type I, see Fig. 14a).
- **Type II:** During the application of the vertical stress, the GPs located at the bottom of the layer are prevented from vertical displacement, which restricts the vertical stress increment to only the layer being compacted as suggested by Mirmoradi & Ehrlich (2015a) (referred to as procedure type II, see Fig. 14b). This means that during compaction of a given soil layer, no vertical stress increase takes place in the underlying layers. This approach is an adaptation of the original procedure described by the referred authors, where the

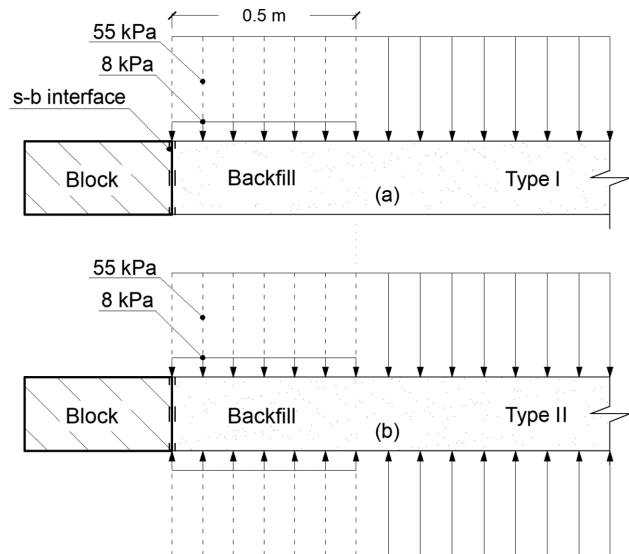


Figure 14. Compaction procedures employed in the numerical analyses.

vertical stress was applied to both sides (top and bottom) of each layer.

Regarding the compaction condition of the physical model considered in this study, it should be mentioned that the first 0.5 m directly behind the wall-facing was hand-tamped to a target 95 % of standard Proctor density, using a rigid steel plate to minimise construction-induced outward deformation and lateral stresses against the back of the facing. The backfill located beyond 0.5 m of the facing was compacted in 150 mm lifts using three passes of a walk-behind, gasoline-powered, vibrating-plate compactor (Whacker VPG-155A) with a dynamic contact pressure of 55 kPa (Bathurst *et al.*, 2009).

For the numerical modelling of compaction, two conditions were considered, as shown in Fig. 14: A) The vertical stress used to model the CIS in the first 0.5 m behind the facing was 8 kPa, and the value of 55 kPa was employed for the backfill located beyond 0.5 m of the facing; B) The value of 55 kPa was applied to the entire surface of the backfill (including the first 0.5 m behind the facing). These two conditions have been considered in all the analyses using the different procedures employed for modelling CIS, *i.e.* types I and II. Note that in the physical model, the first 0.5 m directly behind the wall-facing was hand-tamped using a rigid steel plate and beyond that was compacted using a vibrating-plate (Whacker VPG-155A) with a dynamic contact pressure of 55 kPa (Bathurst *et al.*, 2009). After the end of construction, a uniform vertical stress was applied at the entire surface of the top of the wall. The vertical stress was gradually raised by increments of 0.001 kPa to 80 kPa.

Figure 15 shows two different approaches for the simulation of the induced stress due to compaction. Figures 15a and b show a schematic view of the numerical modelling of

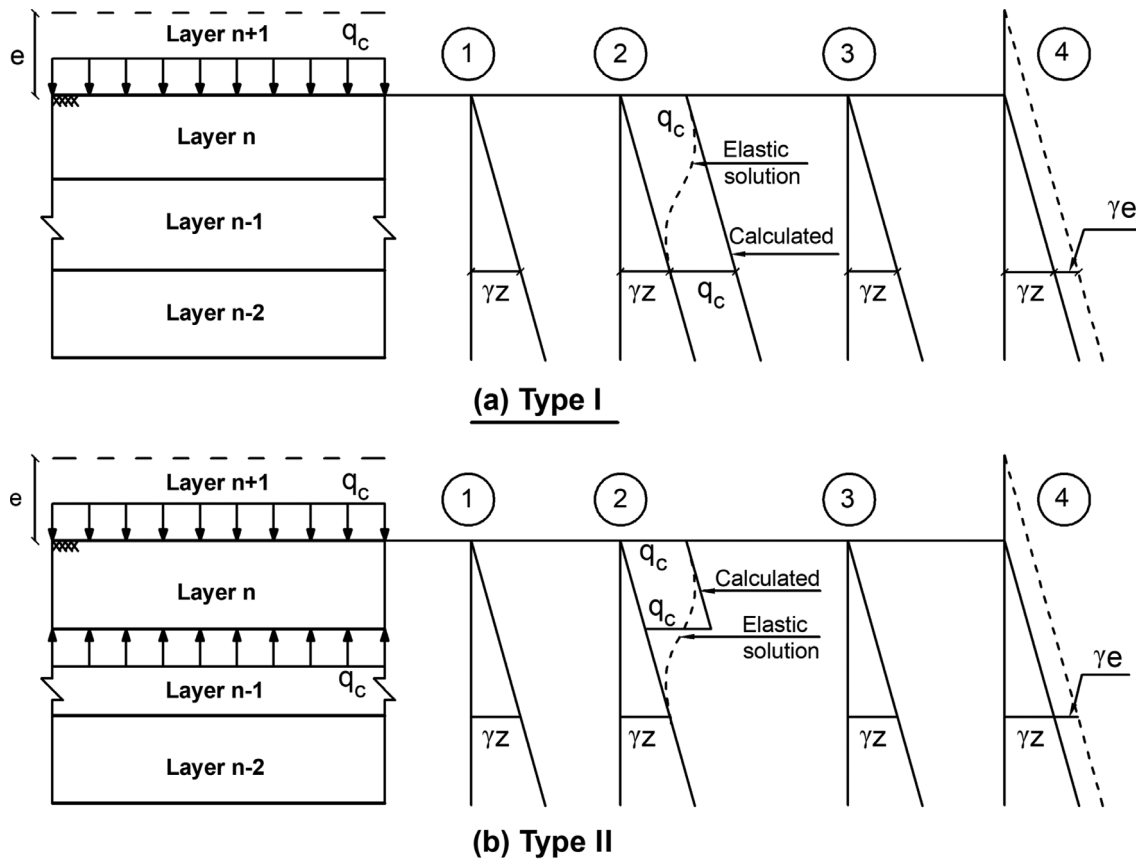


Figure 15. Modelling of the vertical stress load-unload cycles verified during the compaction of the backfill layer, using compaction procedures types I and II.

compaction-induced stress using a distributed load, q_c , at the top of each soil layer (type I); and distribution loads, q_c , at the top and bottom of each soil layer (type II), respectively. Stage construction is used in all procedures, and compaction modelling is represented by only one cycle of loading and unloading for each soil layer. In Fig. 15, four steps for backfill soil construction in a specific soil layer, n , were considered: (1) soil layer placement, (2) compaction equipment operation, (3) end of compaction, and (4) next soil layer placement (layer $n + 1$). Figure 15a, step (2) shows that when procedure type I is used for numerical modelling of the induced stresses due to compaction in soil layer n , it leads to a constant increase in the vertical stress due to compaction, q_c , in all layers below. The dashed line in this figure shows the expected vertical stress increased during the roller operation for soil layer n based on the strip load elastic solution, where its maximum value takes place at soil-roller contact and decreases significantly with depth. This figure clearly shows that using the distribution load solely at the top of each soil layer when modelling compaction cannot match the actual field conditions represented by the elastic solution.

Figure 15b shows a schematic view of procedure type II, as suggested by Ehrlich & Mirmoradi (2013) and Mirmoradi & Ehrlich (2015a) for the numerical simulation of

the induced stress due to compaction. Figure 15b, step (2) shows that when procedure type II is used for the soil layer n , all points in this soil layer would be driven to the same vertical stress increase. In addition, for the soil layers placed under this layer, only geostatic stresses occur. A comparison between the curves related to the compaction modelling using procedure type II, and the dashed line represented by the elastic solution, indicates that this procedure may be more representative of the actual induced vertical stress during roller operation.

Of note, the compaction was simulated by applying a single load-unload stress cycle, which may closely represented the actual multicycle load-unload stress path during compaction (Ehrlich & Mitchell, 1994). Campanella & Vaid (1972) through laboratory tests of multicycle loading and unloading have shown that the residual stress state of a multicycle loading and unloading can be conservatively determined by using the largest virgin hysteretic stress cycle. Thus, the one hysteretic cycle assumption may be considered to be conservative; *i.e.*, the estimated horizontal stress should be an upper-bound value for the actual one.

In the analyses performed, for both type I and II procedures, the load increments were gradually applied over 20,000 steps in order to assure numerical stability.

3.4 Results and discussion

The results obtained from the numerical analysis for the different compaction modelling approaches described

above are compared with the measured values presented by Holtz & Lee (2002) and Hatami & Bathurst (2005, 2006). Figure 16 shows the reinforcement strain at the end of con-

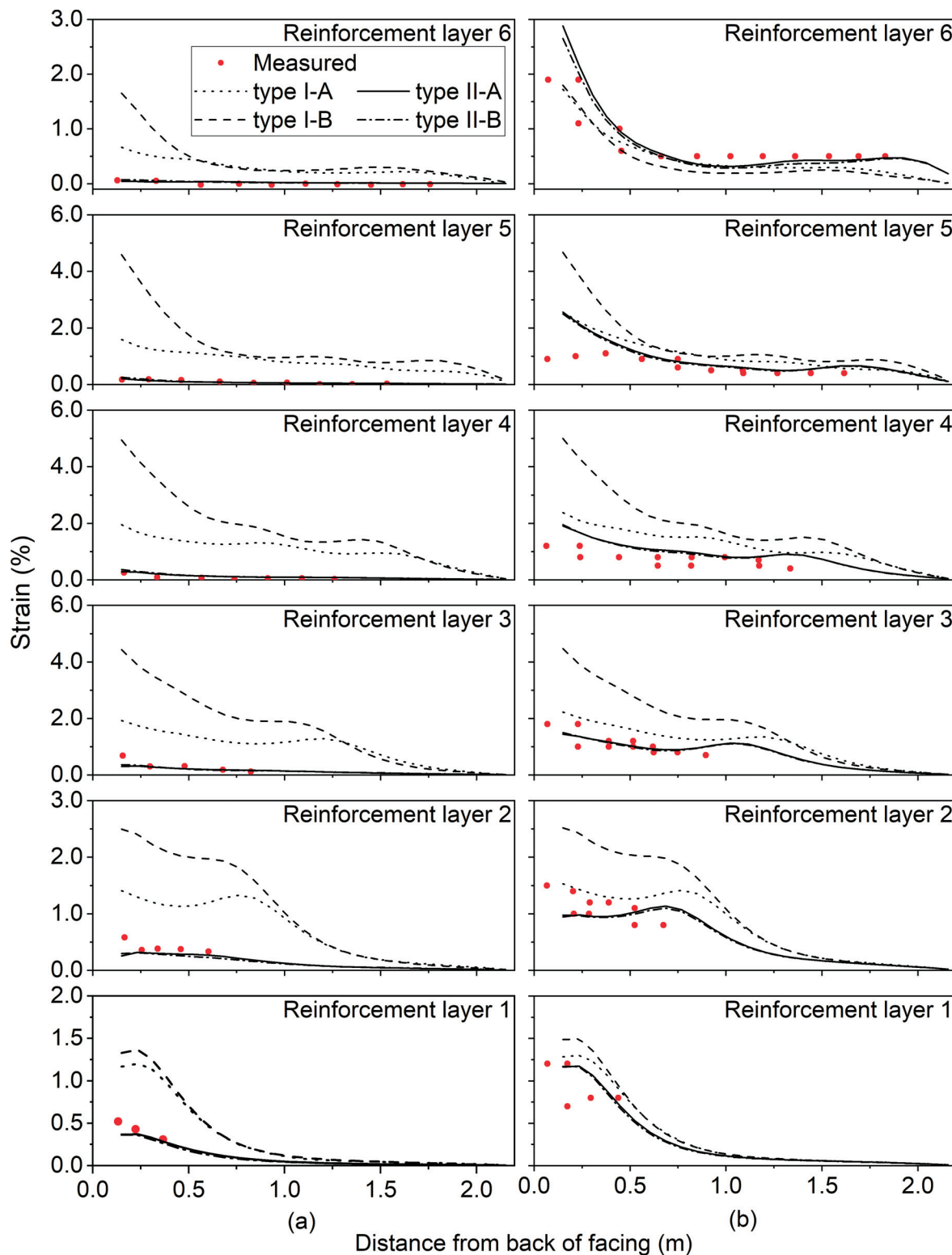


Figure 16. Measured and calculated values of reinforcement strains using different compaction modelling (a) at the end of construction and (b) under 50 kPa surcharge.

struction (EOC) and under a 50 kPa surcharge. The figure indicates that, in general, the determined values using compaction modelling type II properly represented the measurements, while the type I modelling overestimated the reinforcements strain. This agrees with the results presented by Mirmoradi & Ehrlich (2018a), who used PLAXIS 2D to simulate the same physical model wall up to the end of construction.

The connection loads calculated using type II-A and type II-B compaction modelling agree well with the measurements at EOC (Fig. 17a) and under 50 kPa surcharge (Fig. 17c). The connection loads calculated using compaction modelling type I-A & B led to overestimated values at EOC. Moreover, for 50 kPa surcharge loading and the compaction condition type I-B, the numerical model, except for the 6th reinforcement layer, over-predicted the measurements. However, when the type I-A compaction condition was considered, the results are close to the measured values. Note that the analyses performed using the type I procedure led to results that were nearly the same for EOC and during surcharge application (see Fig. 17a, b and c). On the other hand, the type II compaction modelling led to more realistic results, in which the connection load significantly increases with surcharge, as observed in the measured values obtained from the physical model wall. The discrepancy between the behaviour of the experimental models considering different compaction condition near the face and numerical analyses is related to the variation of the soil parameters. In the numerical analyses, the soil parameters

used were the same, irrespective of the compaction conditions. In the physical models, however, both soil parameters and stress conditions were changed, as discussed earlier.

Figure 18 presents the measured and calculated facing horizontal displacements at each block layer during the stage construction. The displacements calculated for the modelling of compaction type I at EOC are overestimated and remain nearly constant up to 50 kPa surcharge loading, which is close to the pressure applied to model the CIS (55 kPa). The results of the numerical analyses in which the compaction type I was employed show a larger facing displacement compared with the measurement. This overestimation is more highlighted considering the lower values of the surcharge. Moreover, the shape of the facing profile is different and the maximum facing displacement did not occur at the wall top as observed in the physical model. On the other hand, the predictions using type II modelling are in good agreement with the physical model measurements, with slightly larger values determined for the model with compaction type II-B than type II-A.

The displacement calculated at the facing at 0.3 m from the toe was larger than the measurement for all conditions and types of CIS modelling. These results may indicate that the toe stiffness assumed in the numerical analyses is smaller than the real response. The value used in the present analyses was the same as that used by Hatami & Bathurst (2006), based on measurements in the physical model (4 MN/m).

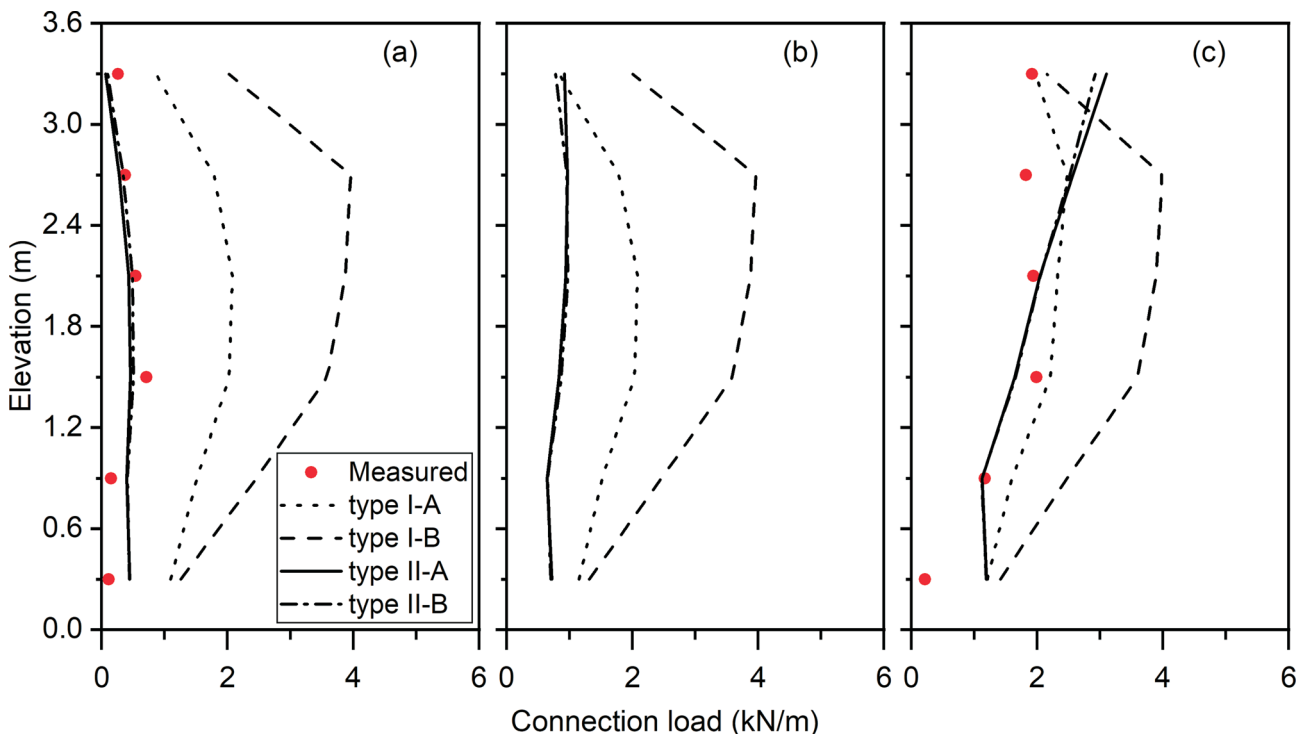


Figure 17. Measured and calculated values of connection loads using different compaction modelling (a) at the end of construction, (b) under 20 kPa and (c) 50 kPa surcharge.

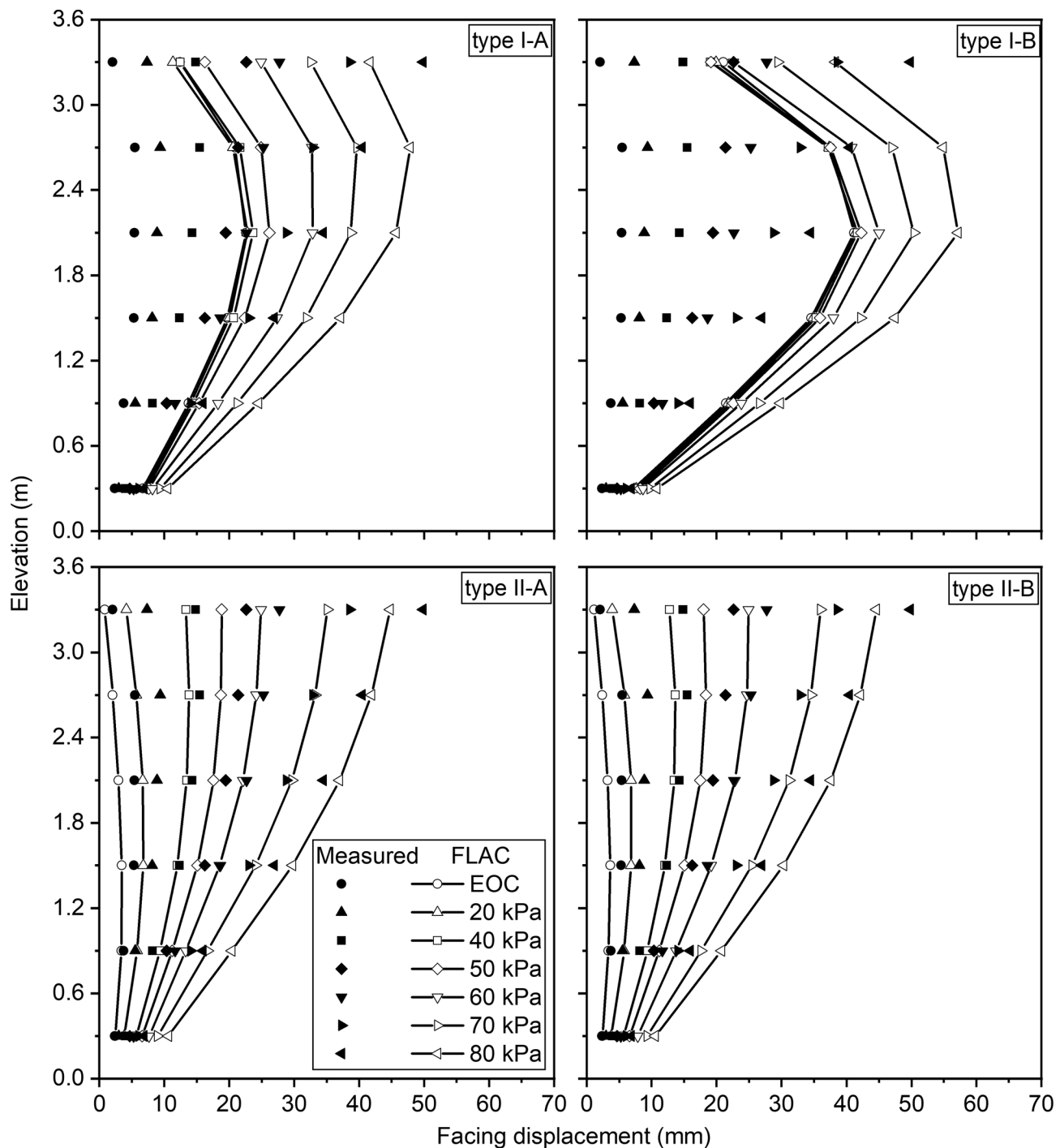


Figure 18. Measured and calculated values of the horizontal facing displacement at the end of construction (EOC) and under different surcharge loading.

Regarding the toe reaction loads during the construction, good agreement is observed between the measurements and calculated values when type II compaction modelling is used (Fig. 19a). Nevertheless, the type I modelling presented good results only for the vertical reaction and significantly overestimated the horizontal load. The determined results indicate that vertical reaction at the toe is

mainly controlled by geostatic stress and is not affected by the type of modelling of the compaction induced stress. During the surcharge application, when type II modelling is used, good agreement is observed between the measured and calculated values up to 30 kPa, and then both compaction types and conditions led to larger values than the measurements (Fig. 19b).

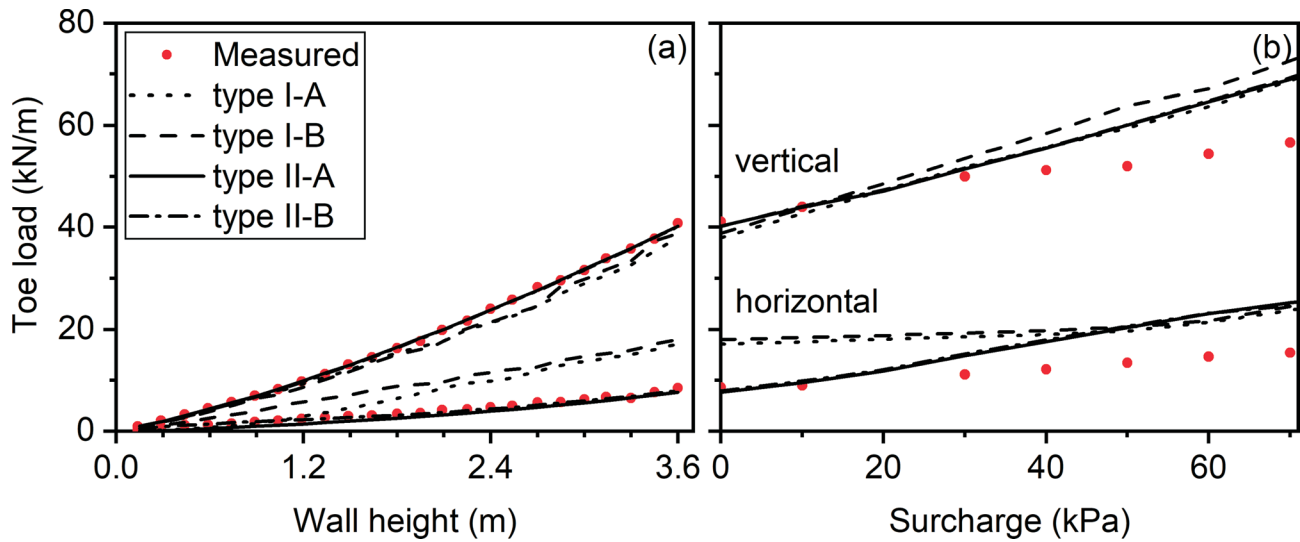


Figure 19. Measured and calculated values of the vertical and horizontal toe reactions using different compaction modelling (a) during the construction stages and (b) under different surcharge loading.

Figure 20 shows the calculated and measured values of the vertical pressure at the base of the wall. The values were normalized considering the geostatic vertical stress at that depth (soil unit weight, γ_s times wall height, H , plus surcharge, q). The results show no significant difference between the considered compaction modelling types and conditions, since, as discussed above, the geostatic stress may be the predominant controlling factor of the vertical pressure at the base of the wall.

In general, the calculated and measured normalized pressure agree and are about 1.0, except near to the face, where at 0.15 m and 0.40 m from the facing, the values were 2.2 and 0.3, and 1.6 and 0.5 for EOC and under the

surcharge of 55 kPa, respectively. This behaviour is mostly due to the arching effects related to the differential vertical movements of the facing and the base of the wall.

4. Evaluation of design methods

Ehrlich & Mirmoradi (2016) proposed an analytical procedure for the calculation of T_{\max} under working stress conditions. This method explicitly takes into account the effect of CIS, reinforcement and soil stiffness properties and facing inclination. The proposed method was based on Ehrlich & Mitchell's (1994) procedure. There are three key differences between the proposed method and Ehrlich & Mitchell's (1994) procedure: (1) the effect of the facing in-

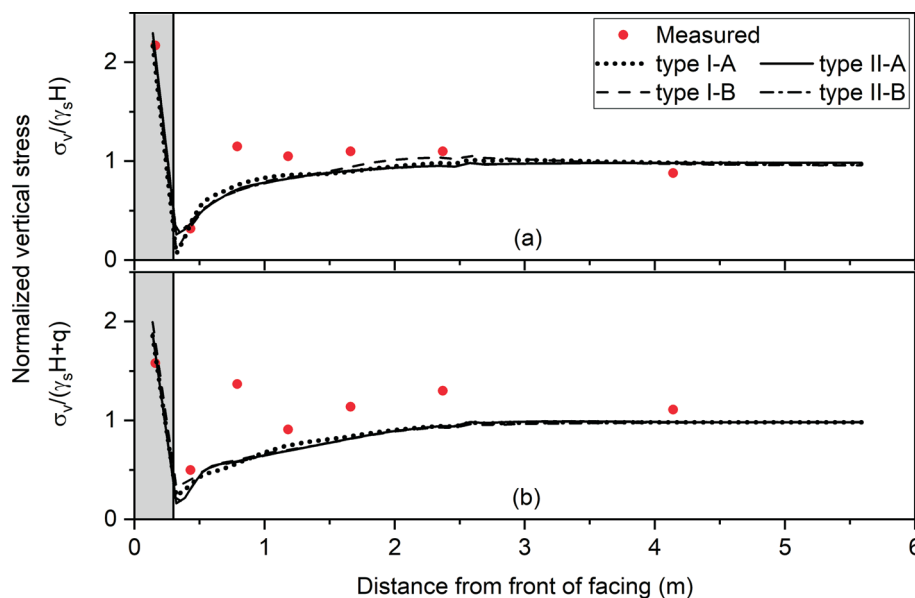


Figure 20. Measured and predicted distributions of contact pressures at the base of the wall using different compaction modelling (a) at the end of construction and (b) under 50 kPa surcharge pressure.

clination is considered in the new method, while the original method was developed for vertical walls; (2) the calculation of T_{\max} using the Ehrlich & Mirmoradi (2016) method does not need iteration, which was required by the original method; and (3) the equations are simpler to use.

Furthermore, Mirmoradi & Ehrlich (2015a) proposed a new simple analytical procedure that includes the effect of the induced stress due to backfill compaction for use with conventional design methods of GRS walls. This proposed analytical procedure may be used with any conventional design methods that do not take into consideration the effect of CIS in their calculations. Of note, the currently used design methods do not explicitly take into consideration the effect of the compaction-induced stress in the calculation [e.g., AASHTO, 2017, FHWA, 2008]. Therefore, the proposed analytical method could be used to modify the calculated T_{\max} using these methods to consider the effect of CIS in calculation.

In order to verify the prediction accuracy of the analytical procedures, in Fig. 21 the measured values of the summation of the maximum tension mobilized in the reinforcement provided by Ehrlich & Mirmoradi (2013), ΣT_{\max} , was compared with those determined by FLAC for compaction procedures type I and II, the Ehrlich & Mirmoradi (2016) method, the AASHTO simplified method, and the modified calculated values by the AASHTO method to consider the effect of CIS, called AASHTO modified. The vertical dotted line in Fig. 21 represents the compaction influence depth, Z_c . The equivalent depth of the soil layer (Z_{eq}) is defined by:

$$Z_{eq} = Z + \frac{q}{\gamma} \quad (9)$$

where Z and q are the real depth of a specific layer and the surcharge load value of the physical model, respectively. As shown in Fig. 21, the values measured from the physical

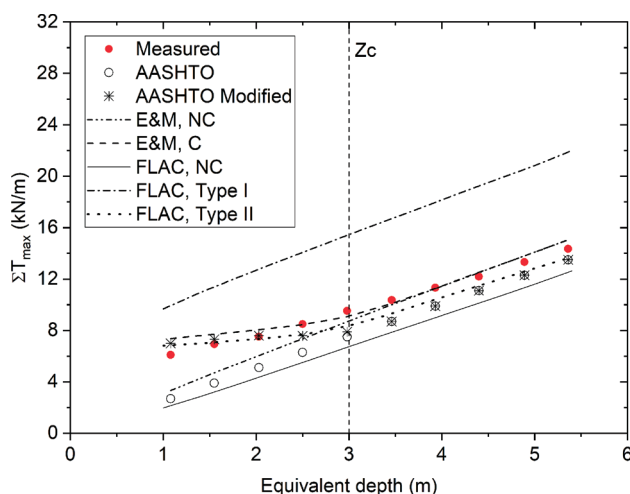


Figure 21. Comparison of measured and determined summations of the maximum reinforcement loads.

model were properly captured by the AASHTO modified method, the Ehrlich & Mirmoradi (2016) method, and the numerical analysis using compaction procedure type II. However, regardless of the value of Z_{eq} , the curve corresponding to the numerical simulation using compaction procedure type I overestimates the values of ΣT_{\max} and this discrepancy increases with equivalent depth.

Comparison of the results corresponding to the conditions with and without induced stresses due to compaction illustrates that for compacted backfill soil walls, when $Z_{eq} < Z_c$, the values of ΣT_{\max} are greater than the values obtained for the no-compaction conditions. However, for $Z_{eq} > Z_c$, the compaction-induced stress was overcome by the geostatic stress and the values determined are the same irrespective of whether or not the induced stress due to the backfill soil compaction is considered in the analysis.

In Fig. 21, the results related to the condition without compaction are also shown. These curves were obtained with the Ehrlich & Mirmoradi (2016) method, the AASHTO simplified method, and by numerical modeling with FLAC. The results show practically similar values for the no-compaction condition.

Figure 22 shows a comparison of the maximum mobilized tension in each reinforcement layer, T_{\max} , vs. depth determined with FLAC for the described numerical compaction modeling (type I and II) and calculated values using the Ehrlich & Mirmoradi (2016) method and the AASHTO methods (*i.e.*, AASHTO simplified and AASHTO modified), for the compaction-induced stresses of 63 (Fig. 22a) and 120 kPa (Fig. 22b), respectively.

In Figs. 22, for the analyses in which the compaction modeling type II was used, a consistent representation of the expected behavior is found and discussed as follows. For $Z > Z_c$, the effect of compaction vanishes because the geostatic stress overcomes the induced stress due to backfill soil compaction. Furthermore, T_{\max} is the same; regardless the induced stress due to backfill soil compaction is included ($Z > Z_c$). However, when $Z < Z_c$, T_{\max} would be greater than the corresponding values for the no-compaction condition. Nevertheless, for the analyses in which the compaction modeling was performed using procedure type I, the T_{\max} values are much larger than the previous values and this overprediction increases with depth. Good correspondence is also observed for the determined results using the AASHTO modified method and the Ehrlich & Mirmoradi (2016) method.

5. Conclusions

The present study experimentally, numerically and analytically investigated the effect of the compaction-induced stress on the behavior of GRS walls. The experimental evaluation was performed using three large-scale GRS walls with different compaction condition at the back of block facing constructed at the COPPE/UFRJ Geotechnical Laboratory. The numerical analyses were carried out using

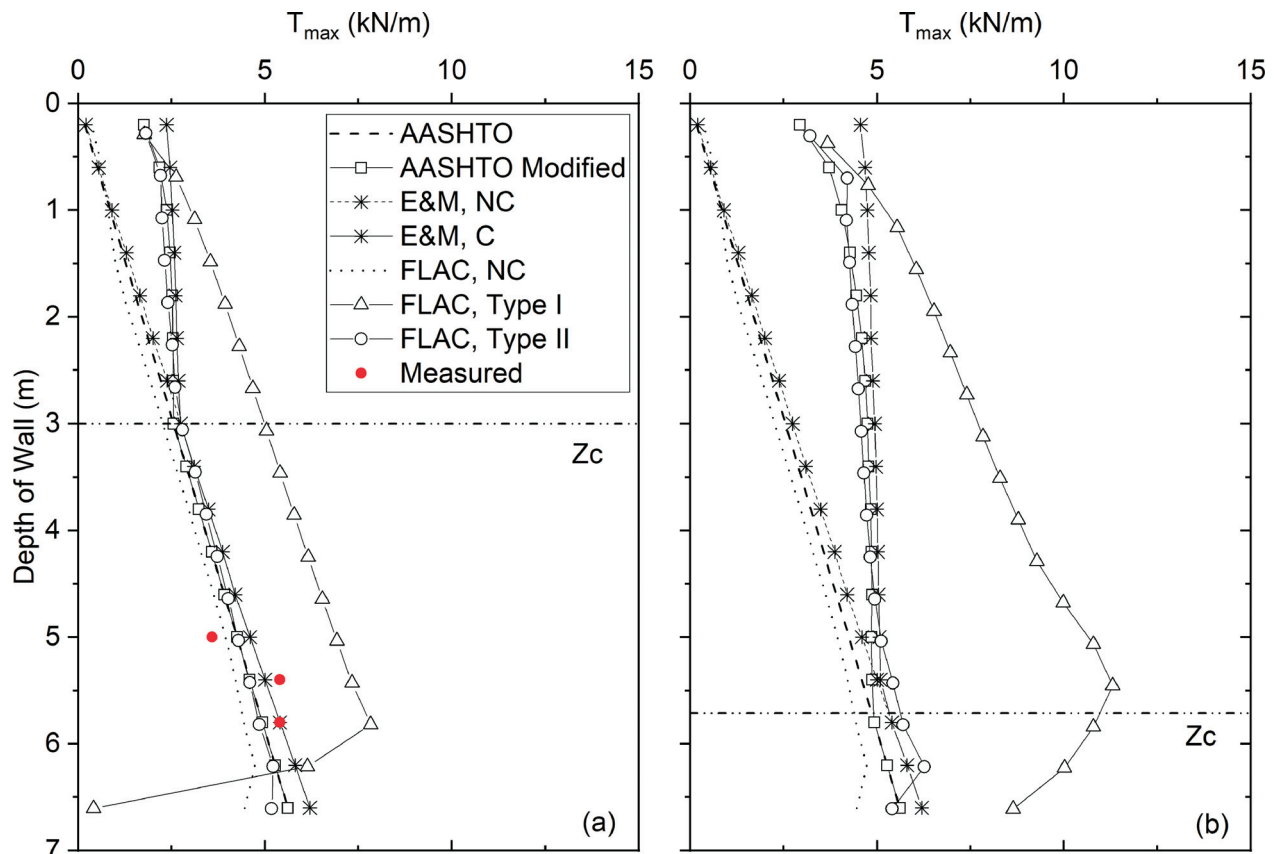


Figure 22. Depth of wall vs. individual values of T_{\max} at the end of construction; a) $\sigma'_{zc,i} = 63$ kPa, and b) $\sigma'_{zc,i} = 120$ kPa.

two different procedures to simulate the CIS and the results of the modelling during construction and post construction were compared against the data from a full-scale GRS segmental wall built at the Royal Military College of Canada. Furthermore, the calculated values of T_{\max} using two design methods have been compared to the measurements and numerically calculated T_{\max} to evaluate the prediction accuracy of these methods when the value of the CIS is relevant. The main findings of this study are summarized, as follows.

The results of the experimental study highlight the importance of the compaction conditions close to the back of the facing. It is shown that when the backfill near the back of block facing is not adequately compacted, the maximum reinforcement loads, horizontal and vertical displacements of the GRS wall increase during construction and post construction. It should be noted that in the real field-work, on one hand, it is common to prevent operation of heavy compactors behind the facing to minimize compaction-induced outward deformation and lateral stresses against the back of the facing. On the other hand, due to inadequate compaction in this zone, the wall may present unexpected behavior as observed in the performed tests. Therefore, it may be a good specification for backfill compaction to be performed using tamper compaction in the interval of 0.5–1.0 m behind the facing and roller compaction beyond that. Tamper compaction may lead to a more simi-

lar compaction induced stress found in a typical roller compaction (Ehrlich & Mirmoradi, 2016, Mirmoradi & Ehrlich, 2018b).

Considering the compaction modelling by applying a uniform vertical stress to the top of each backfill layer, the numerical analyses significantly overestimate the measured values of the reinforcement strains, connection loads and facing displacement. When the compaction was simulated by applying a distribution load at the top and bottom of each soil layer, satisfactory agreement has been generally observed between measurements and calculated values during construction (Mirmoradi and Ehrlich, 2018a) and surcharge loading (Nascimento *et al.*, 2020).

The measured and calculated T_{\max} values were compared with the AASHTO simplified, AASHTO modified and Ehrlich & Mirmoradi (2016) design methods. The Ehrlich & Mirmoradi (2016) method properly captured measured and calculated values of T_{\max} whether or not CIS is applied on the backfill. The AASHTO simplified method may properly represent T_{\max} , in which no CIS was assumed for a wrapped-face wall. However, the AASHTO method may underestimate T_{\max} for the walls, in which a high compaction-induced stress assumed. The procedure proposed by Mirmoradi & Ehrlich (2015a) may satisfactory modify the calculated values by the AASHTO method to take into consideration the effect of CIS.

Acknowledgments

The authors greatly appreciate the funding of this study by the Brazilian Research Council, CNPq, and the Brazilian Federal Agency for Support and Evaluation of Graduate Education, CAPES. We also thank Flavio Montez and Andre Estevão Ferreira da Silva from the Huesker Company for their support, as well as Cid Almeida Dieguez for his support in performing the experiments.

References

- AASHTO (2017). AASHTO LRFD bridge design specifications. 8th ed. American Association of State Highway and Transportation Officials., Washington, D.C., USA, 1780 p.
- Ambauen, S.; Leshchinsky, B.; Xie, Y. & Rayamajhi, D. (2015). Service-state behavior of reinforced soil walls supporting spread footings: a parametric study using finite element analysis. *Geosynth. Int.*, 23(3):156-170. <https://doi.org/10.1680/jgein.15.00039>
- Bathurst, R.J.; Nernheim, A.; Walters, D.L.; Allen, T.M.; Burgess, P. & Saunders, D.D. (2009). Influence of reinforcement stiffness and compaction on the performance of four geosynthetic reinforced soil walls. *Geosynth. Int.*, 16(1):43-59. <https://doi.org/10.1680/jgein.2009.16.1.43>
- Berg, R.; Christopher, B.R. & Samtani, N. (2009). Mechanically Stabilized Earth Walls and Reinforced Soil Slopes, Design and Construction Guidelines - FHWA-NH1-09-083 and FHWA GEC011. U.S. Department of Transportation, Federal Highway Administration, Washington, DC, 668 p.
- Bernardi, M.; Collin, J.G. & Leshchinsky, D. (2009). Design Manual for Segmental Retaining Walls. 3rd ed. National Concrete Masonry Association, Herndon, 281 p.
- BSI (2010). BS 8006-1: Code of Practice for Strengthened/Reinforced Soils and Other Fills. BSI, London, UK, 260 p.
- Campanella, R.G. & Vaid, Y.P. (1972). A simple Ko triaxial cell. *Can. Geotech. J.*, 9(3):249-260. <https://doi.org/10.1139/t72-029>
- Collin, J.G.; Berg, R.R. & Meyer, M.S. (2002). Segmental Retaining Wall Drainage Manual. National Concrete Masonry Association, Herndon, 96 p.
- Duncan, J.M. & Seed, R.B. (1986). Compaction-induced earth pressures under Ko-conditions. *J. Geotech. Engng.*, 112(1):1-22.
- Dyer, N.R. & Milligan, G.W.E. (1984). A photoelastic investigation of the interaction of a cohesionless soil with reinforcement placed at different orientations. *Proc. Int. Conf. on In-Situ Soil and Rock Reinforcement*, International Society of Soil Mechanics and Geotechnical Engineering (ISSMGE), London, pp. 257-262.
- Ehrlich, M. & Becker, L. (2010). Reinforced Soil Walls and Slopes: Design and Construction. Taylor & Francis, Abingdon. 118 p.
- Ehrlich, M. & Mirmoradi, S.H. (2013). Evaluation of the effects of facing stiffness and toe resistance on the behavior of GRS walls. *J. Geotextile Geomembr.*, 40(1):28-36. <https://doi.org/10.1016/j.geotexmem.2013.07.012>
- Ehrlich, M. & Mirmoradi, S.H. (2016). A simplified working stress design method for reinforced soil walls. *Géotechnique*, 66(10):854-863. <https://doi.org/10.1680/jgeot.16.P.010>
- Ehrlich, M.; Mirmoradi, S.H. & Xu D. S. (2017). A simplified working stress design method for reinforced soil walls. *Geotechnique*, 67(11):1029-1032. <https://doi.org/10.1680/jgeot.16.D.007>
- Ehrlich, M.; Mirmoradi, S.H. & Saramago, R.P. (2012). Evaluation of the effect of compaction on the behavior of geosynthetic-reinforced soil walls. *J. Geotextile Geomembr.*, 34(1):108-115. <https://doi.org/10.1016/j.geotexmem.2012.05.005>
- Ehrlich, M. & Mitchell, J.K. (1994). Working stress design method for reinforced soil walls. *J. Geot. Eng. ASCE*, 120(4):625-645. [https://doi.org/10.1061/\(ASCE\)0733-9410\(1994\)120:4\(625\)](https://doi.org/10.1061/(ASCE)0733-9410(1994)120:4(625))
- Ehrlich, M. & Mitchell, J.K. (1995). Closure to "Working Stress Design Method for Reinforced Soil Walls" by Mauricio Ehrlich and James K. Mitchell. *Journal of Geotechnical Engineering*, 121(11):820-821. [https://doi.org/10.1061/\(ASCE\)0733-9410\(1995\)121:11\(820\)](https://doi.org/10.1061/(ASCE)0733-9410(1995)121:11(820))
- FHWA (2008). Geosynthetic design and construction guidelines, FHWA-NHI-07-092. FHWA, Washington, D.C., 592 p.
- Guler, E.; Hamderi, M. & Demirkan, M.M. (2007). Numerical analysis of reinforced soil retaining wall structures with cohesive and granular backfills. *Geosynth. Int.*, 14(6):330-345. <https://doi.org/10.1680/jgein.2007.14.6.330>
- Hatami, K. & Bathurst, R.J. (2005). Development and verification of a numerical model for the analysis of geosynthetic-reinforced soil segmental walls under working stress conditions. *Canadian Geotechnical Journal*, 42(4):1066-1085. <https://doi.org/10.1139/t05-040>
- Hatami, K. & Bathurst, R.J. (2006). Numerical model for reinforced soil segmental walls under surcharge loading. *J. Geotech. Geoenviron. Eng.*, 132(6):673-684. [https://doi.org/10.1061/\(ASCE\)1090-0241\(2006\)132:6\(673\)](https://doi.org/10.1061/(ASCE)1090-0241(2006)132:6(673))
- Hatami, K.; Witthoeft, A.F. & Jenkins, L.M. (2008). Influence of inadequate compaction near the facing on the construction response of wrapped-face MSE walls. *Transpn. Res. Rec.*, 2045(1):85-94. <https://doi.org/10.3141/2045-10>
- Holtz, R.D. & Lee, W.F. (2002). WA-RD 532.1: Internal Stability Analyses of Geosynthetic Reinforced Retaining Walls. Washington State Transportation Center (TRAC), Seattle. 466 p.

- Huang, B.; Bathurst, R.J. & Hatami, K. (2009). Numerical study of reinforced soil segmental walls using three different constitutive soil models. *J. Geotech. Geoenviron. Eng.*, 135(10):1486-1498. [https://doi.org/10.1061/\(ASCE\)GT.1943-5606.0000092](https://doi.org/10.1061/(ASCE)GT.1943-5606.0000092)
- Itasca Consulting Group (2016). *FLAC - Fast Lagrangian Analysis of Continua*. Version 8.0, Minneapolis.
- Jaky, J. (1944). The coefficient of earth pressure at rest. *J. Soc. Hungarian Archits Engrs*, 78(22):355-358 (in Hungarian).
- Jewell, R.A. (1980). *Some Effects of Reinforcement on the Mechanical Behavior of Soils*. Ph.D. Dissertation, Univ. of Cambridge, Cambridge.
- Jiang, Y.; Han, J.; Zornberg, J.; Parsons, R.L.; Leshchinsky, D. & Tanyu, B. (2019). Numerical analysis of field geosynthetic-reinforced retaining walls with secondary reinforcement. *Geotechnique*, 69(2):122-132. <https://doi.org/10.1680/jgeot.17.P.118>
- Koerner, R.M. & Koerner, G.R. (2013). A data base, statistics and recommendations regarding 171 failed geosynthetic reinforced mechanically stabilized earth (MSE) walls. *J. Geotextile Geomembr.*, 40(1):20-27. <https://doi.org/10.1016/j.geotextmem.2013.06.001>
- Koerner, R.M. & Koerner, G.R. (2018). An extended data base and recommendations regarding 320 failed geosynthetic reinforced mechanically stabilized earth (MSE) walls. *J. Geotextile Geomembr.*, 46(6):904-912. <https://doi.org/10.1016/j.geotextmem.2018.07.013>
- Lambe, T.W. & Whitman, R.V. (1969). *Soil Mechanics*, Wiley, New York, 553 p.
- Liu, H.; Yang, G. & Hung, C. (2017). Analyzing reinforcement loads of vertical geosynthetic-reinforced soil walls considering toe restraint. *Int. J. Geomech.*, 17(6):04016140. [https://doi.org/10.1061/\(ASCE\)GM.1943-5622.0000840](https://doi.org/10.1061/(ASCE)GM.1943-5622.0000840)
- Mirmoradi, S.H. & Ehrlich, M. (2014a). Modeling of the compaction-induced stresses in numerical analyses of GRS walls. *Int. J. Comput. Methods (IJCM) Special Issue "Comput. Geomech."*, 11(2):13422002. <https://doi.org/10.1142/S0219876213420024>
- Mirmoradi, S.H. & Ehrlich, M. (2014b). Geosynthetic reinforced soil walls: experimental and numerical evaluation of the combined effects of facing stiffness and toe resistance on performance. *Proc. 10th Int. Conf. on Geosynthetics, International Society of Soil Mechanics and Geotechnical Engineering (ISSMGE)*, London, v. 3, pp 2645-2652.
- Mirmoradi, S.H. & Ehrlich, M. (2015a). Modeling of the compaction-induced stress on reinforced soil walls. *J. Geotextile Geomembr.*, 43(1):82-88. <https://doi.org/10.1016/j.geotextmem.2014.11.001>
- Mirmoradi, S.H. & Ehrlich, M. (2015b). Numerical evaluation of the behavior of GRS walls with segmental block facing under working stress conditions. *ASCE J. Geotech. Geoenviron. Eng.*, 141(3):04014109. [https://doi.org/10.1061/\(ASCE\)GT.1943-5606.0001235](https://doi.org/10.1061/(ASCE)GT.1943-5606.0001235)
- Mirmoradi, S.H. & Ehrlich, M. (2016). Evaluation of the effect of toe restraint on GRS walls. *Transp. Geotech. SI Geosynthetics in Tpt.*, 8(1):35-44. <https://doi.org/10.1016/j.trgeo.2016.03.002>
- Mirmoradi, S.H. & Ehrlich, M. (2018a). Numerical simulation of compaction-induced stress for the analysis of RS walls under working conditions. *J. Geotextile Geomembr.*, 46(3):354-365. <https://doi.org/10.1016/j.geotextmem.2020.02.011>
- Mirmoradi, S.H. & Ehrlich, M. (2018b). Experimental evaluation of the effect of compaction near facing on the behavior of GRS walls. *J. Geotextile Geomembr.*, 46(5):566-574. <https://doi.org/10.1016/j.geotextmem.2018.04.010>
- Mirmoradi, S.H.; Ehrlich, M. & Dieguez, C. (2016). Evaluation of the combined effect of toe resistance and facing inclination on the behavior of GRS walls. *J. Geotextile Geomembr.*, 44(1):287-294. <https://doi.org/10.1016/j.geotextmem.2015.12.003>
- Nascimento, G.; Ehrlich, M. & Mirmoradi, S.H. (2020). Numerical- simulation of compaction-induced stress for the analysis of RS walls under surcharge loading. *J. Geotextile Geomembr.*, 48(4):532-538. <https://doi.org/10.1016/j.geotextmem.2020.02.011>
- Scotland, I.; Dixon, N.; Frost, M.; Fowmes, G. & Horgan, G. (2016). Modelling deformation during the construction of wrapped geogrid-reinforced structures. *Geosynth. Int.*, 23(3):219-232. <https://doi.org/10.1680/jgein.15.00049>
- Tatsuoka, F.; Uchimura, T. & Tateyama, M. (1997). Preloaded and pre-stressed reinforced soil. *Soils Found.*, 37(3):79-94. https://doi.org/10.3208/sandf.37.3_79
- Uchimura, T.; Tateyama, M.; Tanaka, I. & Tatsuoka, F. (2003). Performance of a preloaded-prestressed geogrid-reinforced soil pier for a railway bridge. *Soils Found.*, 43(6):155-171. https://doi.org/10.3208/sandf.43.6_155
- Yu, Y.; Bathurst, R.J. & Allen, T.M. (2016). Numerical modeling of the SR-18 geogrid reinforced modular block retaining walls. *J. Geotech. Geoenviron. Eng.*, 142(5):04016003. [https://doi.org/10.1061/\(ASCE\)GT.1943-5606.0001438](https://doi.org/10.1061/(ASCE)GT.1943-5606.0001438)
- Zheng, Y. & Fox, P.J. (2017). Numerical investigation of the geosynthetic reinforced soil-integrated bridge system under static loading. *J. Geotech. Geoenviron. Eng.*, 143(6):04017008. [https://doi.org/10.1061/\(ASCE\)GT.1943-5606.0001665](https://doi.org/10.1061/(ASCE)GT.1943-5606.0001665)
- Zheng, Y.; Fox, P.J. & McCartney, J.S. (2018). Numerical simulation of deformation and failure behavior of geosynthetic reinforced soil bridge abutments. *J. Geotech. Geoenviron. Eng.*, 144(7):04018037. [https://doi.org/10.1061/\(ASCE\)GT.1943-5606.0001893](https://doi.org/10.1061/(ASCE)GT.1943-5606.0001893)

Foundation-structure interaction on high-rise buildings

Alexandre Duarte Gusmão^{1,2,#} , Augusto Costa Silva³ , Maurício Martines Sales³ 

Article

Keywords

Foundations
Global stability
Load redistribution
Soil-structure interaction
Spring coefficient

Abstract

This article addresses the importance of considering foundation-structure interaction in the design of high-rise buildings. Embedding the behavior of the foundation in the analysis of structures is fundamental to simulate the real deformability of these constructions. On the foundation design side, the addition of structure stiffness implies in the reduction of maximum settlement and angular distortions. On the structural dimensioning side, the consideration of the foundation settlement modifies the flexibility of the structure by changing internal efforts in several parts, which is against safety in many cases. The study of a building with 50 floors is presented, as well as the report of 13 cases of construction where the settlements measurements reached more than 10 times the results of the load test of the isolated element, illustrating the effect of the interaction between different foundation elements. There was a considerable increase in the loads of corner columns and an increase in the overall building's stability. The γ_z that is a parameter associated to second-order effects increased exponentially with the increase in the building's non-verticality.

1. Introduction

The structure and the foundation design of buildings are generally calculated separately, where the structure designer calculates the loads that reach the foundations of these structures without considering the soil behavior, and the foundation designer receives these loads and calculates the settlements without considering the building's stiffness.

The concern with this subject is not recent. Meyerhof (1953) evaluated the effects of absolute and differential settlement on the stresses that occur in the structural elements and in the foundation. Meyerhof's theory considered different foundation-structure relative stiffness and observed that the incorporation of differential settlement in the building design increased the stresses generated in the superstructure, mainly in the beams and columns of the first floors.

Rocha (1954), in the first Brazilian Congress of Soil Mechanics, presented a suggestion on how to calculate hyperstatic structures considering the settlement of foundations, using the traditional methods of displacement and force method. The foundation load-settlement ratio was considered linear, allowing the incorporation of propor-

tionality coefficients (spring constants) in the equations. The calculation would be made in an iterative way, and the convergence would be evaluated in terms of the loads and the settlement of the columns.

Chamecki (1954) presented a methodology to calculate foundation settlement and superstructure support reactions, incorporating rigidity of both parts. It used load transfer coefficients between adjacent columns for the entire structure, noting the transfer of the loads from the most loaded elements to the least loaded. Consideration of the superstructure's stiffness in the foundation analysis caused the reduction of differential settlement.

Gusmão (1990, 1994) proposed a methodology to evaluate the effects of soil-structure interaction from the measurement and analysis of settlement. Using this concept, the redistribution of loads in the columns and the uniformity of the settlement deformation, by means of parameters defined by the author, was evaluated.

With the current trend of constructing higher and higher buildings in Brazil, in a similar tendency to the rest of the world, the theme of foundation-structure interaction is becoming more and more relevant in the study of the behavior and stability of these high and very flexible structures. This article presents and discusses the analysis of a

[#]Corresponding author. E-mail address: alexandreduartegusmao@gmail.com.

¹Universidade de Pernambuco, Recife, PE, Brazil.

²Instituto Federal de Pernambuco, Recife, PE, Brazil.

³Escola de Engenharia Civil e Ambiental, Universidade Federal de Goiás, Goiânia, GO, Brazil.

Submitted on June 5, 2020; Final Acceptance on June 20, 2020; Discussion open until December 31, 2020.

DOI: <https://doi.org/10.28927/SR.433441>



hypothetical tall building evaluated with and without the foundation-structure interaction process, and it compares settlement measurements in real buildings, highlighting the importance of incorporating the settlement superposition effect between different foundation elements in the study of the interaction with the structure.

2. Problem analysis model

To try to solve the problem of the interaction between the superstructure behavior and that of the foundation, different methods of calculation have been employed. The main methods used are: calculation by iterative process (Rocha, 1954; Iwamoto, 2000; Araújo, 2009; Bahia *et al.*, 2016; Silva, 2018); the coupled method presented in Poulos (1975); and considering the superstructure and foundation as a unique problem in numerical models.

The iterative calculation starts from obtaining the loads on the columns considering the supports as fixed nodes. Using these loads, foundation settlements are obtained for each column, incorporating the interaction effect between different points of foundations. Considering “spring coefficient” as the ratio between load and settlement of each column, these coefficient values are assigned as the stiffness of the supports under each column, and the structure is recalculated, now supported by elastic supports, to obtain a new load set. The process is repeated iteratively, recalculating the settlement and the loads on the supports. This procedure is repeated until the result convergence of some variable, usually the settlement. The aforementioned authors (Iwamoto, 2000; Araújo, 2009; Bahia *et al.*, 2016; Silva, 2018), among others, highlight: the important load redistribution between columns located in areas of different settlements; that the lower floors are the most affected by changes of loads and moments in columns and beams; that a small number of iterations (3 to 5) are already sufficient to achieve the settlement convergence; and that the first iteration is responsible for a preponderant percentage of changes.

In the coupled calculation proposal, presented in Poulos (1975), the analysis of the soil-structure interaction (SSI) is performed by coupling the equations of the superstructure forces calculation with the foundation deformability equations. Eq. 1 describes the vector $\{V\}$ as the support reactions obtained considering the SSI; $\{V_0\}$ is the vector of the reactions calculated for the case of fixed supports; $\{\delta\}$ refers to the displacement vector of the supports considering the SSI; and $[SM]$ is the structure stiffness matrix, which relates the additional support reactions due to unitary displacements of other supports.

$$\{V\} = \{V_0\} + [SM]\{\delta\} \quad (1)$$

This formulation allows considering the structure as three-dimensional and with 6 degrees of freedom. The support reactions can be calculated considering external loads and the hypothesis of fixed supports. The stiffness matrix

can be calculated by imposing unitary displacements to the supports. The displacement vectors and support reactions are unknown when considering the SSI process.

The soil-foundation interaction is governed by Eq. 2, in which $[FM]$ is the foundation flexibility matrix that relates the displacements of the foundation supports to unit loads.

$$\{\delta\} = [FM]\{V\} \quad (2)$$

Through these equations, the following relationships are obtained to reach the final loads.

$$\{V\} = \{V_0\} + [SM][FM]\{V\} \quad (3)$$

$$\{V_0\} = [I - [SM][FM]]\{V\} \quad (4)$$

Another way to consider soil-structure interaction is to adopt a unique 3-D model that gathers the superstructure and the foundation. To solve this problem, numerical tools are used, such as the finite element method (FEM) and the boundary element method (BEM), with a very high computational effort to try to incorporate specific models to the superstructure and soil materials (Poulos, 2013).

3. Evidence of soil-structure interaction

Gusmão (1990, 1994) developed a methodology to interpret settlement measurements in order to verify the effect of SSI on building performance. The settlement distribution was evaluated by means of the coefficient of variation (CV), which is the relationship between the standard deviation (σ) and the settlement average (w_m). The author highlights that the standard deviation is influenced by the average magnitude of the settlements, so the use of the coefficient of variation is indicated (CV).

Gusmão (1990, 1994) observed that the average settlements are related to the adopted stress-strain soil model, while the distribution of the settlement (evaluated by the CV) is related to the SSI model, where there is a tendency to smooth the settlement curves. It should be noted that increasing structure stiffness decreases the dispersion of settlement curves. The methodology developed and applied by Gusmão (1990) was also employed in 7 identical buildings in Recife-PE, with 18 slabs, based on precast concrete piles, in which it was observed that the measured CVs were smaller than the CVs theoretically estimated without the SSI effect, evidencing the tendency to the settlements uniformity (Gusmão & Gusmão Filho, 1994).

Gusmão *et al.* (2000) applied Gusmão (1990) methodology to a 15-story building built in Recife, with soil improvement using compaction piles. The settlement monitoring showed that the CV began to stabilize at the time of the construction of the first floors, in about 100 days, denoting that the building reached a limit of rigidity, after which the mechanism of SSI was less significant.

Mota (2009), through the settlement monitoring of a 28-story building located in Fortaleza-CE, observed that

the average settlement increased and the CV decreased with the evolution of the construction, which reveals the tendency for settlement uniformity.

In Gusmão (1990), the absolute settlement factor (*AR*) was also defined to evaluate the effect of the SSI on load redistribution in the columns, calculated according to the following equation:

$$AR = \frac{w}{w_m} \quad (5)$$

in which w is the absolute settlement at a given support point and w_m is the average absolute settlement.

Differential settlements are responsible for the redistribution of loads among the columns when analyzing the SSI. When the estimated *AR* of a column is greater than one, it means that the estimated absolute settlement, without an SSI, is greater than the average absolute settlement. In these situations, there is a tendency for this column to suffer a load relief. Therefore, the measured *AR* value of this same column tends to decrease in relation to the estimated value. If the column has an estimated absolute settlement lower than the average (estimated *AR* less than one), there is a tendency to suffer an overload, and the measured *AR* value tends to increase and be higher than the estimated *AR*.

4. Interaction between foundation elements

4.1 Interaction between footings

The settlement of single footings can be calculated by several methods. The soil profile and the presence of the groundwater greatly interfere with the final result. In saturated clays, for example, the final settlement is composed of a short-term component (initial settlement) and another component caused by the consolidation process, which, as a rule, is the predominant one. In sandy soils or unsaturated soils in general, the settlement can be predicted using the theory of elasticity with good accuracy, since the elastic modulus of each soil layer could be estimated. Numerous elastic solutions for different loading sets and boundary conditions for the soil profile are presented in Poulos & Davis (1974). The Fadum's solution (1948) allows the easy composition of areas to represent the shape and stiffness of the footing, as shown in the equation below, already disregarding the small effect of the Poisson ratio:

$$w_i = I \sum_{j=1}^n \sum_{l=1}^n \frac{\Delta\sigma_i \Delta z_i}{E_i} \quad (6)$$

in which w_i is the settlement of an isolated footing; I refers to the stiffness factor (1 for central recalculation in flexible footing and 0.8 for rigid footing); j is the number of areas to fit the footing geometry; n is the number of layers in soil discretization; $\Delta\sigma_i$ is the vertical induced stress in the center of the layer i under the projection of the footing center; Δz_i

is the thickness of each layer; and E_i is the elastic modulus of layer i .

To consider the interaction between two footings, Eq. 6 can be used when considering $\Delta\sigma_i$ as the vertical stress induced under the center of the neighboring footing and $I = 1$. Therefore, the compression on each footing will be the sum of all interactions to its isolated compression:

$$w_{if} = \sum_{j=1}^n w_{ij} \quad (7)$$

in which w_{if} is the total settlement of the foundation I , considering all the interactions of n neighbouring footings; w_{ij} is the stress induced by footing j in footing i .

4.2 Interaction on piling foundations

Aoki & Lopes (1975) used Mindlin's equations to estimate stresses and settlements in deep foundations. The loads are transmitted to the soil by the foundation elements considering the shaft and the base loads. When the foundation is a group of piles, the effects of interaction between the piles and between piles and soil can be estimated.

Poulos (1968) analyzed the effect of settlement increase due to the interaction between two identical piles admitting the behavior of the soil as an elastic medium, defining the percentage of the increase of the settlement as a pile-pile interaction factor. Through the superposition of interaction factors of all neighboring piles, it is possible to reach the total settlement of a pile, as seen in Eq. 8. The stiffness of the pile cap joining the piles is the boundary condition necessary to find the pile group settlement.

$$w_i = \sum_{j=1}^n \alpha_{ij} \frac{P_j I_j}{ES \cdot D} \quad (8)$$

in which w_i is the foundation total settlement (pile i); α_{ij} is the interaction factor between pile j and pile i ; P_j is the load on pile j ; I_j is an influence factor of the geometry and soil conditions in the calculation of the loaded pile j ; Es is the average modulus of the soil profile along the pile; and D is the diameter of the piles.

In a similar way to that described for footings, Eq. 8 also allows evaluation of the pile-group settlement considering the interaction of all the piles in the work.

On a piled raft foundation, the superposition of stress fields implies in the interaction between the surface plate (raft) and the various piles. Several papers (Hain & Lee, 1978; Clancy & Randolph, 1993; Poulos, 1994; Russo, 1995; El-Mossalamy & Franke, 1997; Bernardes *et al.*, 2019) presented numerical solutions incorporating the four interaction processes involved in a piled raft design: soil-soil, soil-pile, soil-pile, and pile-pile.

4.3 Interaction of nearby buildings

In extreme situations of nearby constructions, the stresses induced in the soil may induce additional stresses

in neighbouring foundations. This effect is recurrent and noted when a large building is built close to old buildings, as the proximity can result in new cracks in the pre-existing building due to the suffered pressure increase. The more deformable the soil under those buildings, the more serious is the problem. The city of Santos, São Paulo, is a classic example of interaction between nearby buildings, resulting in tilt of several buildings in different directions, depending on the chronological order of construction of neighboring buildings.

5. Cases of buildings

Two real cases in Recife, Brazil, are here presented to show the effect of interactions on the overall behavior of buildings (Fig. 1). For both cases, the monitoring of settlements and the static load test (SLT) were performed.

5.1 Case 1 - Recife/PE - Brazil

The building has 30 floors and 17 columns in the main tower, with a total permanent load of 102.25 MN. The soil profile is composed of sand layers, as presented in Fig. 2. The foundation has 84 continuous flight auger piles



Figure 1. Location of Recife, Brazil.

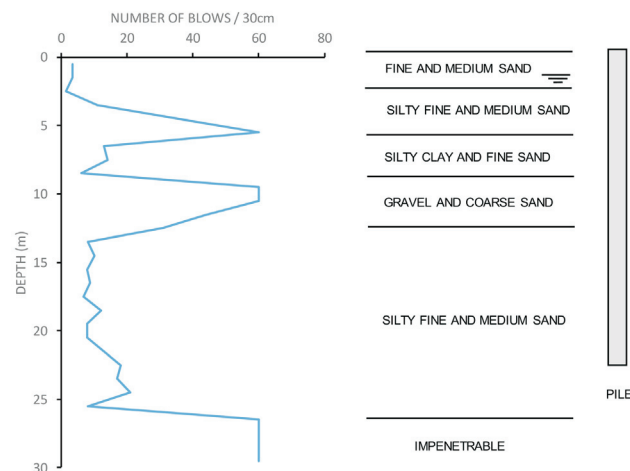


Figure 2. Soil Profile - Case 1.

with 50 and 60 cm in diameter, and length ranging from 22 m to 25 m (Fig. 3).

A static load test (SLT) was carried out in a pile with 500 mm in diameter and reached 2600 kN, which represented two times the project load. Figure 4 shows the pile test and the hyperbolic-method fit. For the value of 1300 kN (project load), the settlement was around 2 mm.

At a certain stage of settlement measurements, the total load acting on the building can be estimated, considering the construction stages completed up to that time. In this example, the last settlement measurement was carried out just after the completion but before receiving the residents. The load at this stage (only dead loads) was considered to be 85 % of the total load (dead and live loads). Figure 5 presented minimum, maximum, and average settlement with the values ranging from 9 to 19 mm, which are much higher than the 2 mm of the SLT.

The average absolute settlement of the building is independent of structure stiffness, while this last one influences only the settlements dispersion. Assuming the average load per pile as the division of the total permanent load by the number of piles, at each stage of measurements, it is possible to compare the average settlements and average pile loads. For the presented building, when 85 % of the construction was completed, the average load per pile would result in 1,034 kN. The average load per block is 5,794 kN.

Figure 6 compares the load curve of the SLT (without group effect) with the average settlement of the piles belonging to the foundations of P17 (corner column), P6 (central column); and the average of the whole building with the implicit group effect. The effect of the interaction between the foundations is clear, implying that the building settlement is much higher than that of the isolated pile.

The parameter (R_s), defined by Poulos & Davis (1980), is the relation of the pile settlement in a group compared with the pile settlement when isolated, and it represents the increase of the pile settlement as a function of the interaction of all the neighbouring piles. In this example, the value of R_s could be obtained by the ratio between the average pile settlement obtained during building monitoring and the settlement obtained in SLT, for the same load level.

Figure 7 compares calculated R_s values for piles in corner groups, central groups, and mean values across all piles. The monitoring showed a higher R_s value for the central groups of piles when compared with the corner piles. In average terms, the building showed settlements from 12 to 20 times higher than the measured SLT value for the same average load per pile. In this case, the effect of the interaction between the piles was clear. For the soil profile in question, the piles did not reach an impenetrable layer and therefore could be considered as floating piles, where the portion of lateral friction is predominant.

5.2 Case 2 - Recife/PE - Brazil

The building in Case 2 has 28 floors and 17 columns with a total permanent load of 79.58 MN. The foundation was de-

signed using steel piles driven through soft layers and reached the impenetrable stratum, thus predominating the base resistance portion in the load capacity of these piles (Fig. 8).

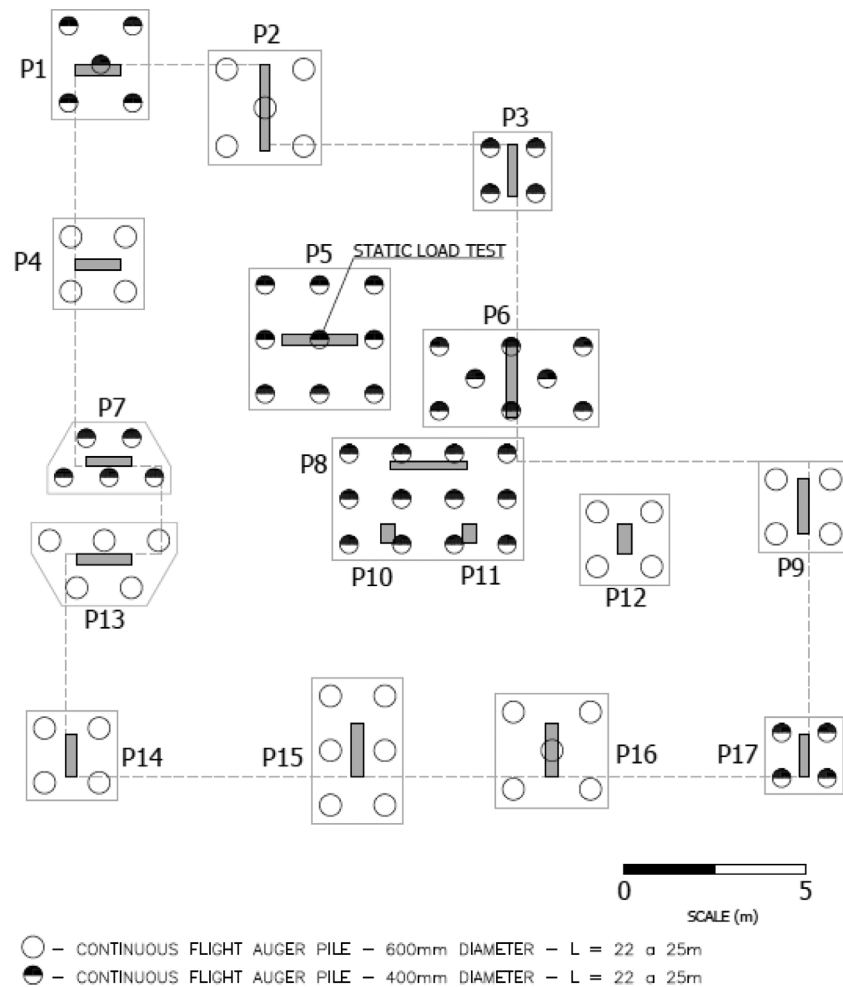


Figure 3. Foundation layout in plan - Case 1.

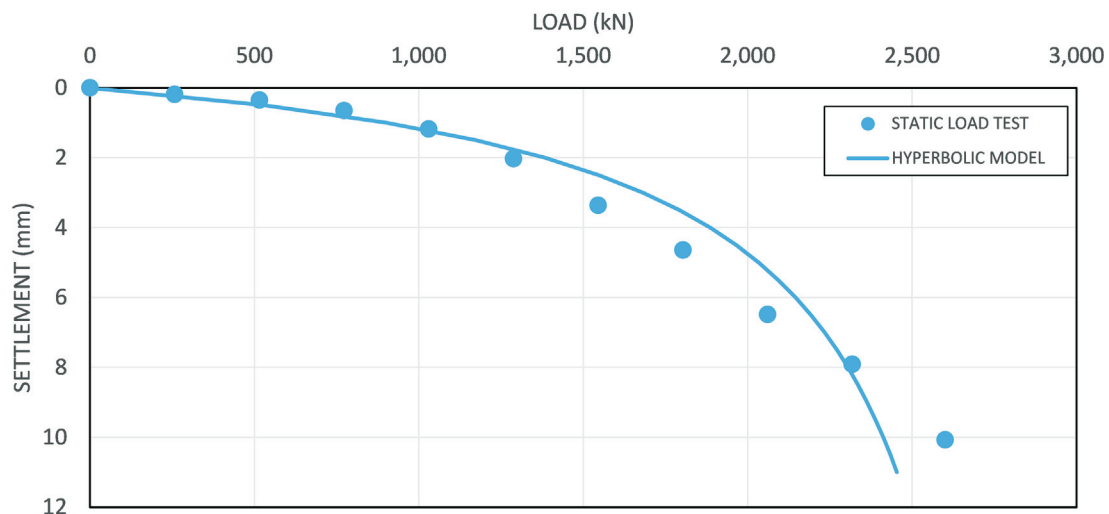


Figure 4. Pile load test and hyperbolic model fit for a pile with 500 mm diameter.

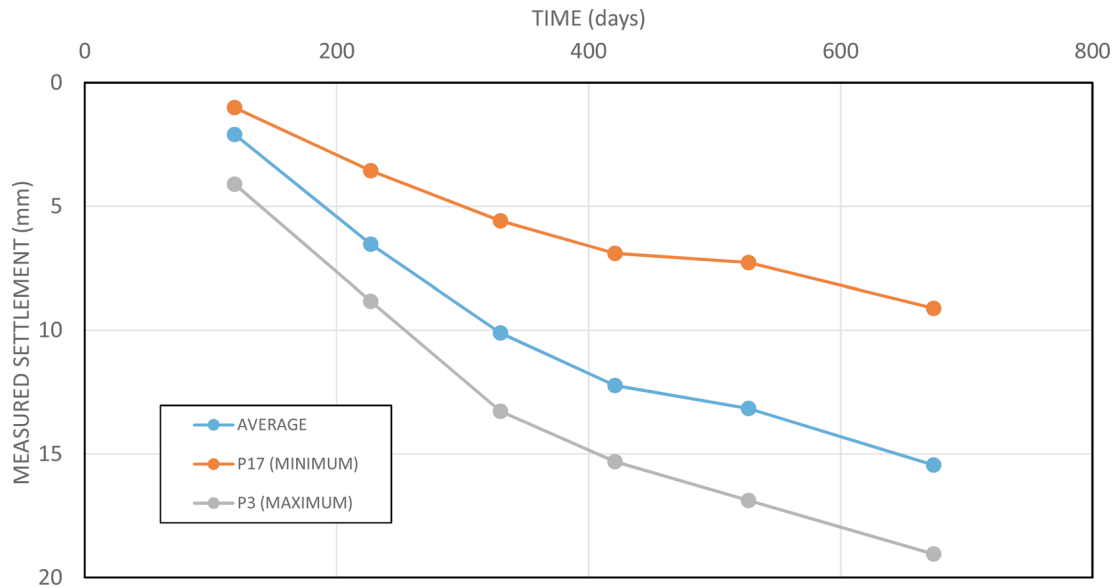


Figure 5. Settlement measurements during construction - Case 1.

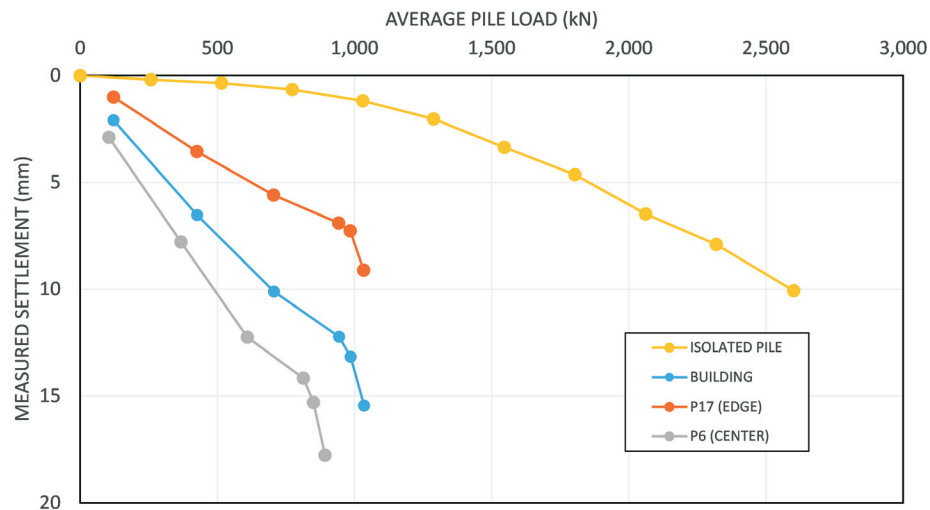


Figure 6. Comparison of SLT curve (isolated pile) and monitoring settlements of the piles - Case 1.

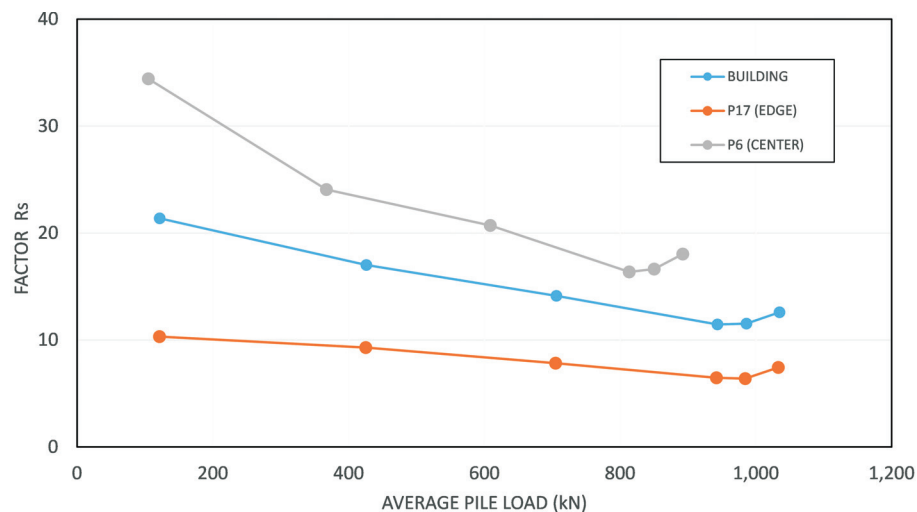


Figure 7. R_s vs. load, comparing the SLT and settlement monitoring - Case 1.

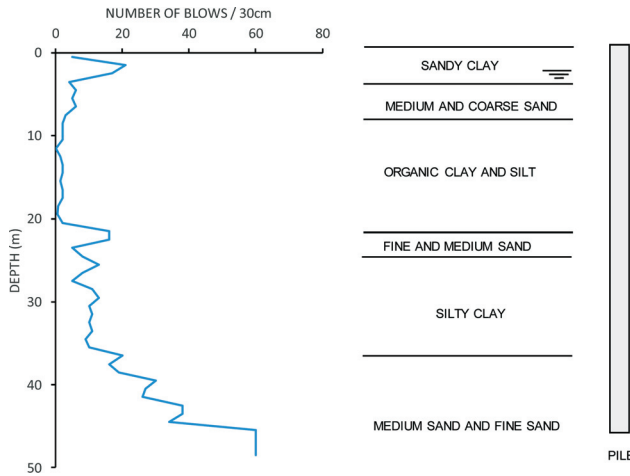


Figure 8. Soil Profile - Case 2.

The steel piles had 45 m in length and H-section of type HP310x93 and HP-310x110 (Fig. 9). Sharing the total project load for all piles would result in an average design load of 1,206 kN. A static load test was carried out at the beginning of the construction work (Fig. 10), and the piles were monitored during the construction period.

Figure 11 presents the maximum, minimum, and average settlements until building completion (around 85 % of total permanent load). In the last stage of measurements, the settlements ranged from 2 to 8 mm, close to the measured values of SLT.

In a similar way, described in Case 1, Fig. 12 compares the average pile load-average settlement behavior for one edge column (P13); one center column (P8) and for the building mean, and these curves were also compared with the static load test result for a single pile. It is observed that

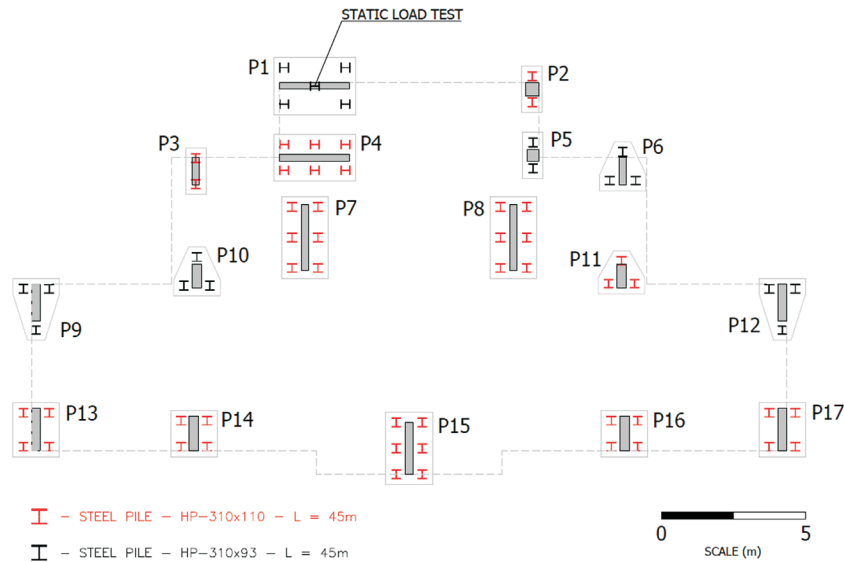


Figure 9. Foundation plan - Case 2.

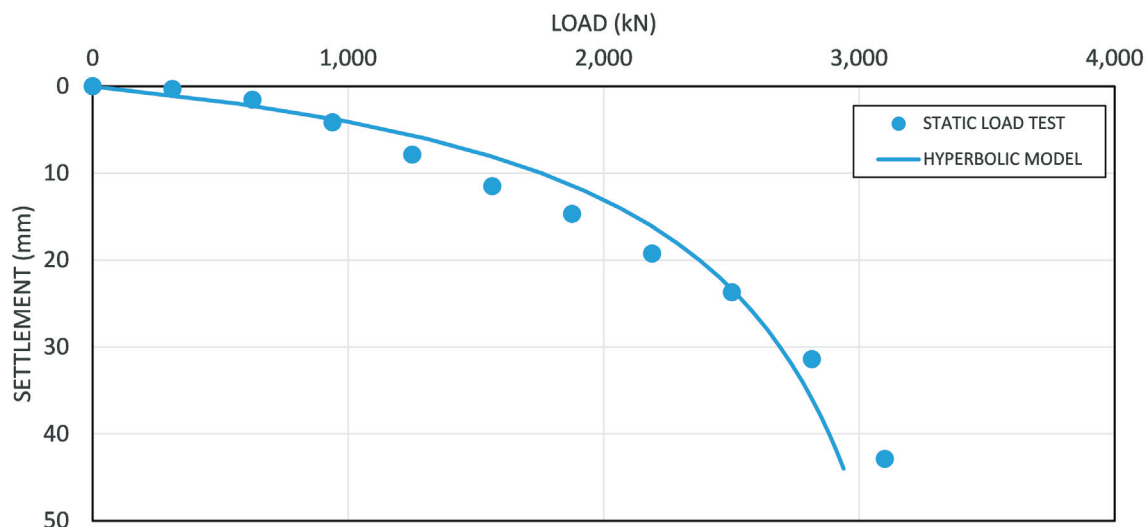


Figure 10. Static load test on a HP-310x110 pile - Case 2.

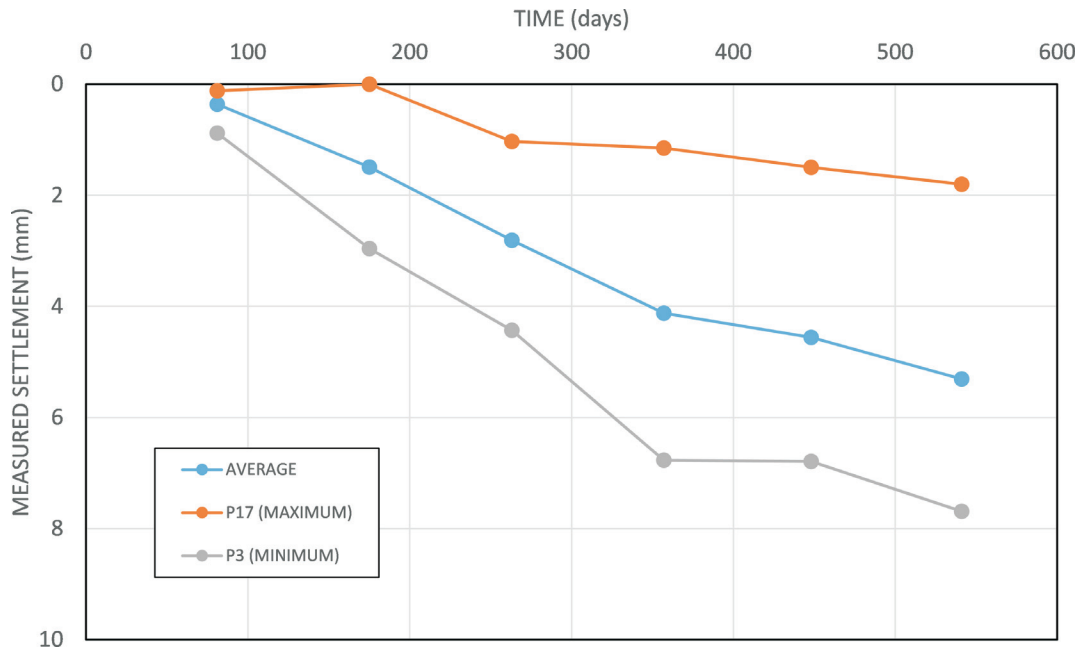


Figure 11. Evolution of measured settlements - Case 2.

the curves behaved in a very similar way, indicating that the interaction between piles was not relevant. The explanation lies in the fact that the support layer of the tip was quite rigid and did not induce relevant settlements in the neighboring piles. Adding to this fact, Sales *et al.* (2017) point out that the process of installation of pre-molded piles creates a thin layer of soil (shearband) along the pile, where the soil structure is destroyed, and cannot induce important settlements in the vicinity.

The settlement ratio (R_s) was also calculated for columns in different positions in Case 2. Figure 13 presents the

values obtained for R_s , noting that all cases are close to 1. Unlike the previous case, in this building, the behavior of tip piles indicated that the interaction effect between piles was practically negligible.

5.3 Other cases

Figure 14 presents a database of 14 buildings (represented by different letters) in the Metropolitan Region of Recife, where it can be observed that the settlement ratio (R_s) was between 1 and 22, considering different percentages of building loads (Almeida, 2018).

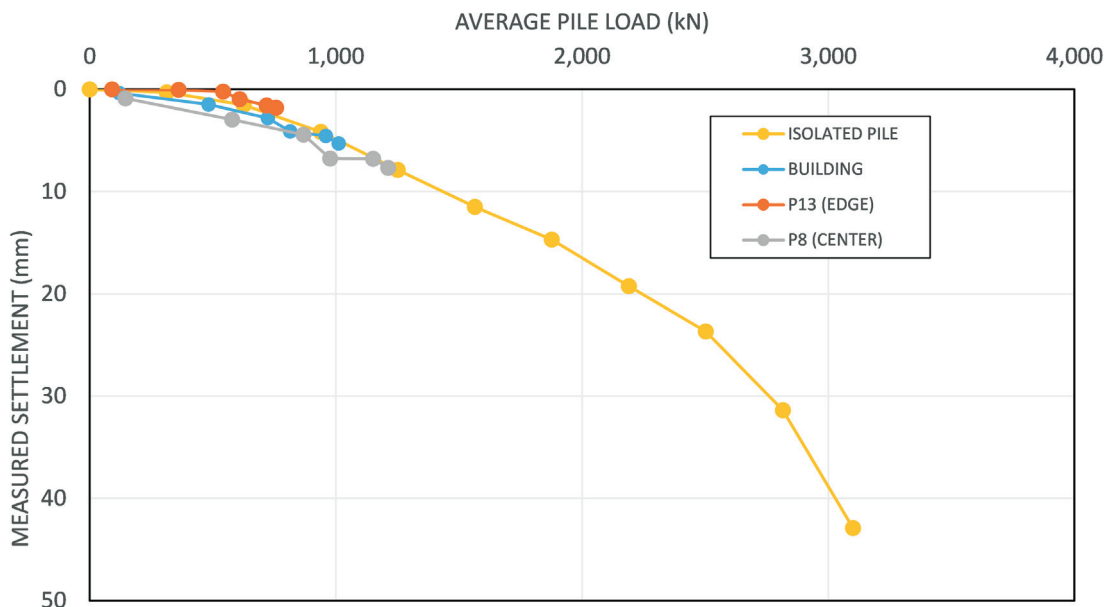


Figure 12. SLT curve (isolated pile) and monitoring pile settlements - Case 1.

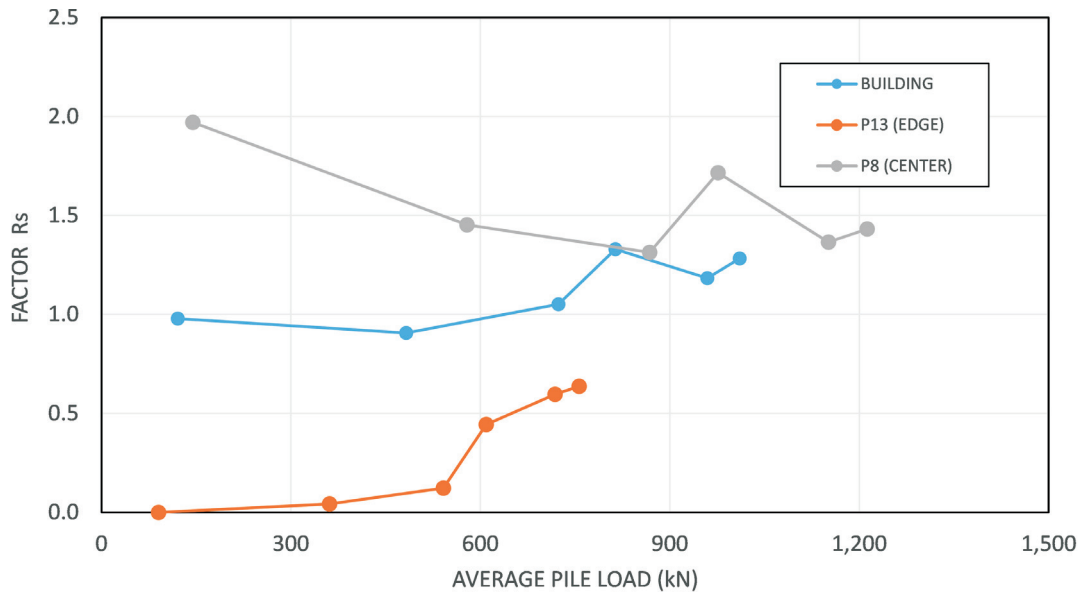


Figure 13. R_s vs average load, comparing SLT and settlement monitoring in building 2.

The value of R_s did not vary much with the stage of the work, but it can be quite different from one construction to another depending on the number of piles, proximity of columns, and soil profile.

6. High-Rise building (A theoretical study)

Silva (2018) evaluated the behavior of hypothetical high-rise buildings, considering and not considering the foundation-structure interaction by iterative process described in Section 2 of this paper. The case presented in this article simulates the behavior of a 50-story building, with rectangular geometry in plan projection, as illustrated in Fig. 15. The structure was analysed using the

software TQS (2016) and the foundation behavior was evaluated with the GARP software presented in Small & Poulos (2007).

Figure 16 presents the soil profile considered (sandy non-saturated clay from 0-5 m and sandy residual silt below this elevation). Two possibilities of foundations were taken into account: the first representing the case where the foundation is little embedded (inferior raft surface at -3 m elevation) and the second representing a 7 m excavation and thus the raft is laid at -10 m elevation. The first alternative foundation, called RFA140, resulted in the use of a 3 m thick raft resting on 220 piles with 1.4 m diameter and 21 m length under the raft. The second foundation option, case RFO140,

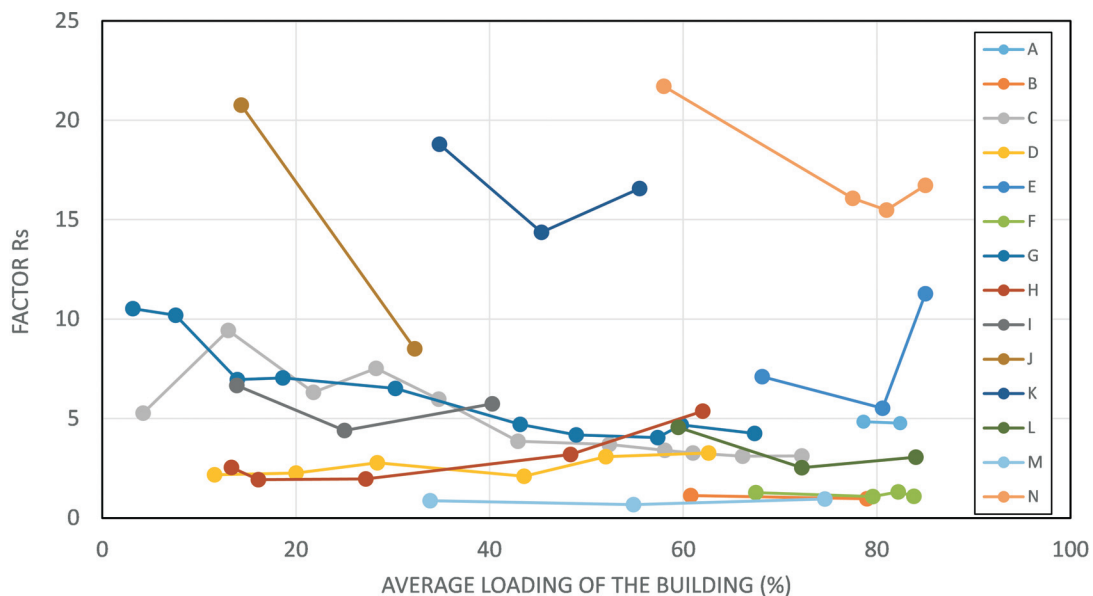


Figure 14. R_s -values vs. percentage of loading of 14 buildings (Almeida, 2018).

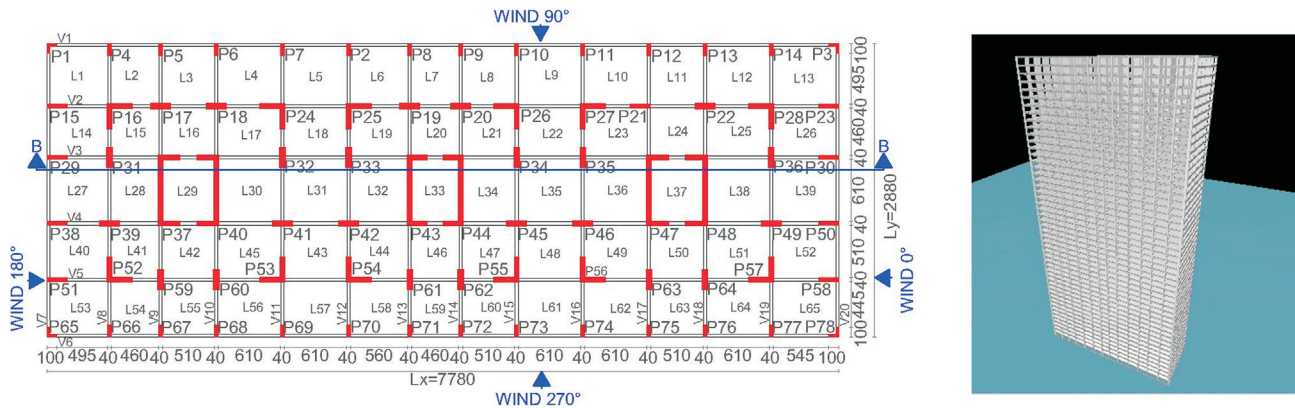


Figure 15. Modeled building - Location of the columns.

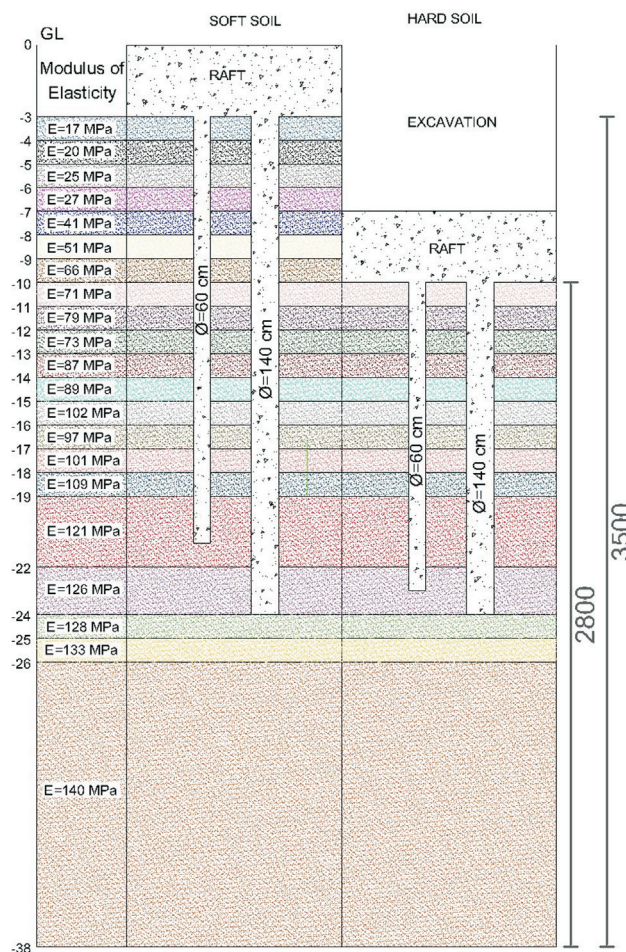


Figure 16. Soil profile and analysed foundation.

would be a raft with the same thickness supported on 27 piles (1.4 m in diameter and 14 m in length). The quantity of piles was determined by considering the contribution of the soil under the raft and satisfying a minimum Safety Factor of 2.5 for the load capacity when both raft and piles are considered, in the form of Eurocode7 (2004). Figure 17 illustrates the distribution of the piles under the raft.

The results presented by Silva (2018) revealed that after the third iteration of the calculation of the structure and foundations, the settlement values in successive interactions were very close. The following sections discuss the changes in settlement results, angular distortion, loads on the columns, bending moments in the raft when the building is calculated with or without the SSI, and spring coefficients to make the supports more flexible.

6.1 Settlements

Figures 18a and 18b show the settlement curves for the columns near the BB cross section, shown in Fig. 15, for the two alternatives of foundations: RFA140 and RFO140.

In both cases, the incorporation of the process of interaction between the foundation and the structure led to a load increase on the corner columns. The internal columns P31 and P36 did not present a defined behavior of increase or reduction of the settlements, but the other internal columns presented a reduction of the settlements with the interaction.

The corner (P1), lateral (P7), and inner (P43) columns were selected for the calculation of the relative percentage change of settlements (ΔV_j), which was obtained by means of Eq. 9, in which Δw_j is the difference between the settlement of the current iteration and the previous one, of the column j ; and $w_{0,j}$ is the settlement obtained without iteration for this column.

$$\Delta V_j = \frac{\Delta w_j}{\Delta w_{0,j}} \quad (9)$$

Figures 19a and 19b show the relationship between the percentage variation of settlements and the number of iterations for the cases RFA140 and RFO140, respectively. In both analyses, the corner column (P1) showed a settlement increase in relation to the previous iteration (positive variation) of about 10 % in the first iteration and smaller increments, but still positive variations of its value in the 2nd and 3rd iterations. The internal column (P43) presented in

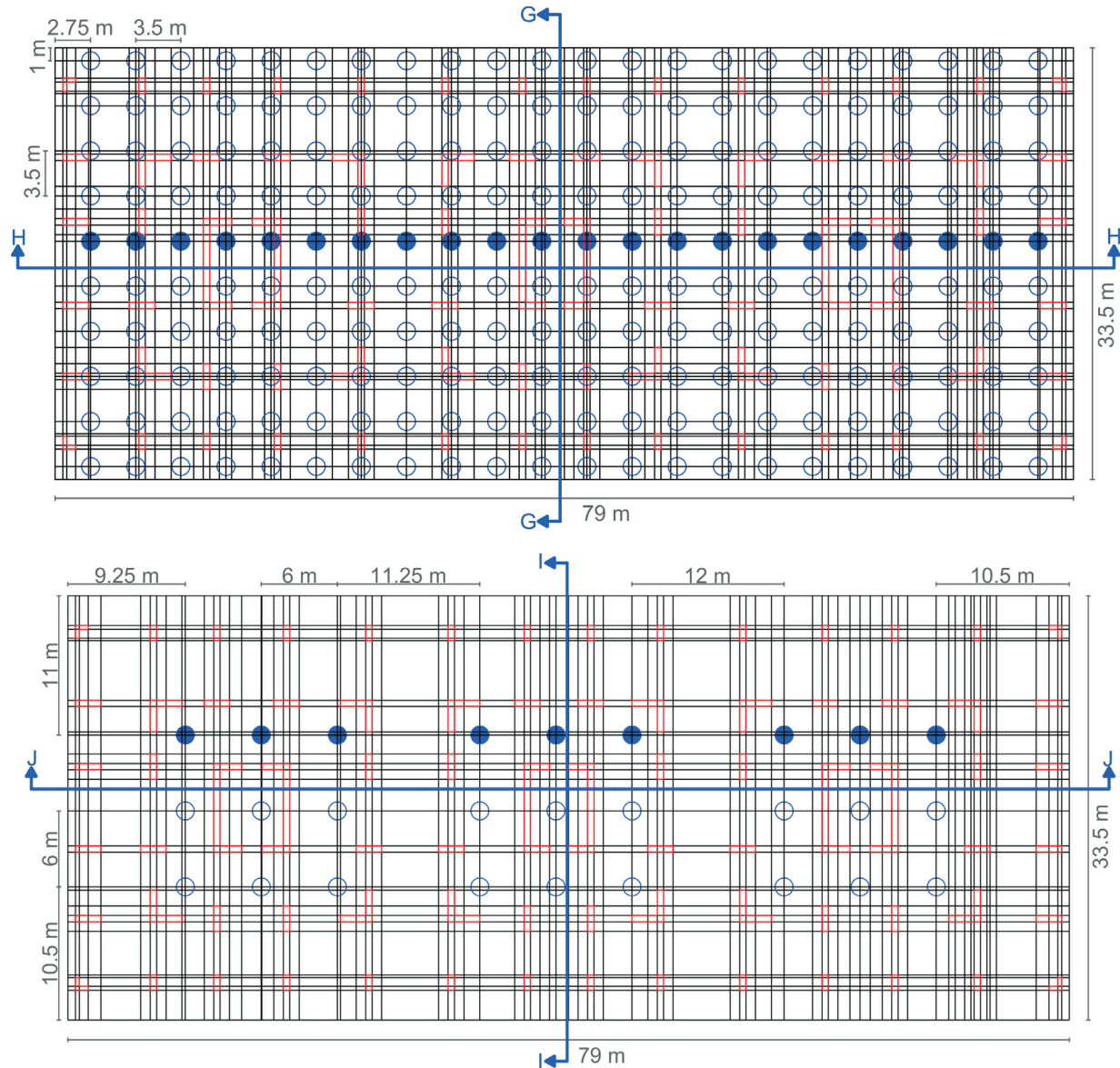


Figure 17. Modeled building - Pile location.

the first iteration a settlement reduction, around 5 %, and smaller reductions of the settlement with the following iterations. In both cases, the lateral column (P7) presented an intermediate behaviour. Increasing the number of iterations, the settlement variation curves converge to values close to zero in all columns.

Table 1 shows the average settlements (w_m), standard deviation (σ) and the coefficient of variation (CV), with (SSI-soil structure interaction) and without (FS-Fixed supports) interaction. The case RFO140 showed higher average settlements than RFA140. For both cases, the difference between the mean settlement with and without the interaction was less than 1 %, *i.e.*, the foundation-structure interaction process hardly affects the mean settlements prediction. However, with the interaction, there was a 26 %

relative reduction in the coefficient of variation in the case RFA140, and a 33 % reduction in the case RFO140. The reduction in CV indicates greater uniformity (less differential settlements) when performing the foundation-structure interaction. Thus, the soil-structure interaction had a greater influence on smoothing the settlement curve than on the reduction of the mean settlements magnitude.

6.2 Angular distortions

Disregarding the perfect building verticality or not, highest rotations or angular distortions (ratio of the settlement difference to the columns distance) of five pairs of columns were calculated after 3 iterations steps, and these results are shown in Figs. 20a and 20b.

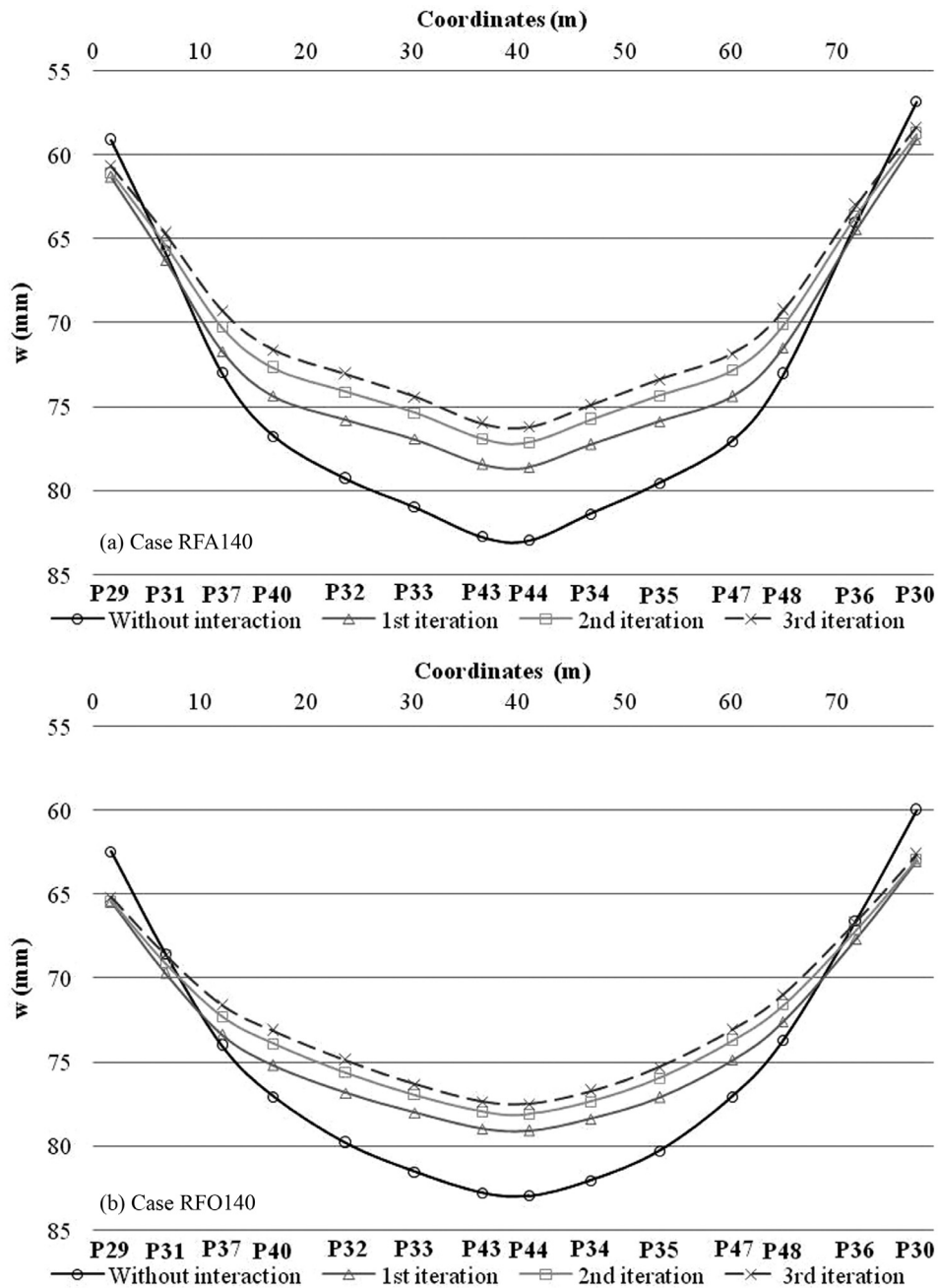


Figure 18. Settlement prediction for the BB-cross section.

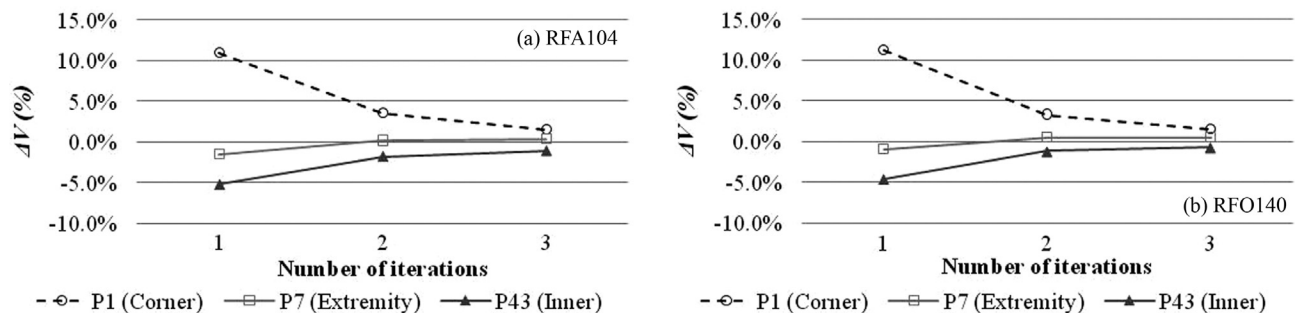


Figure 19. Relative percentage change of settlements with the number of iterations.

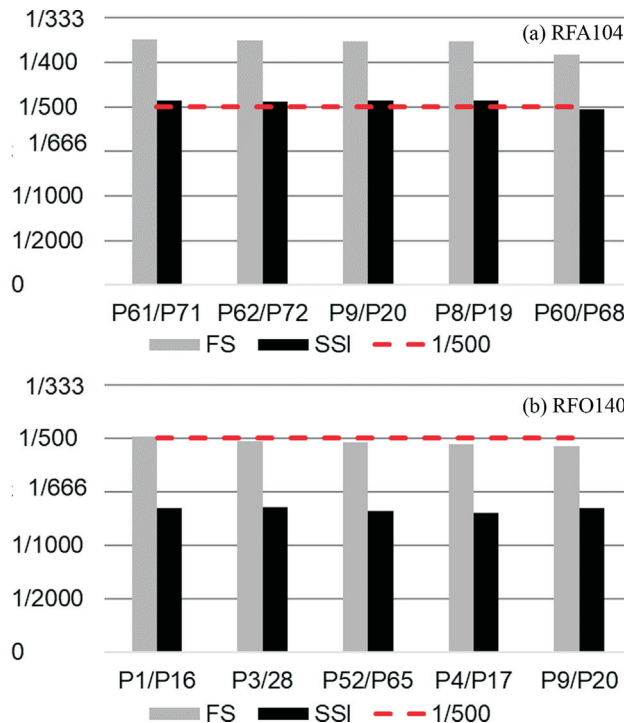
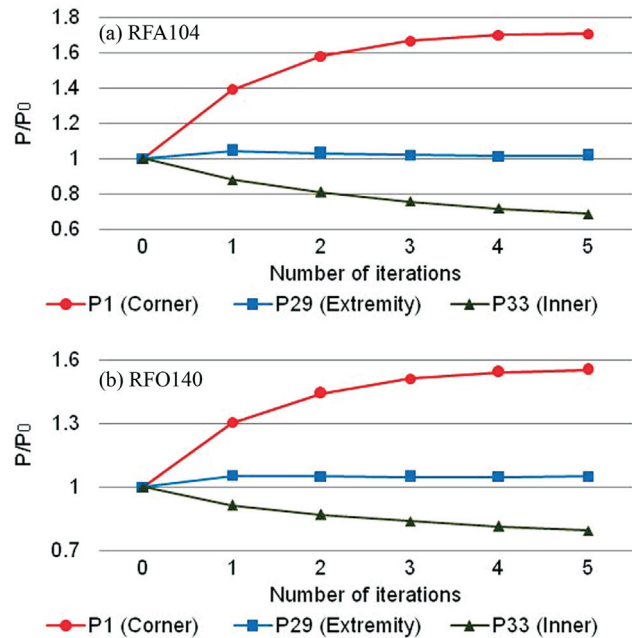
Table 1. Average settlements and coefficient of variation for the analysed cases.

Settlement	RFA140		RFO140	
	FS	SSI	FS	SSI
w_m (mm)	62.71	61.50	67.13	66.84
σ	11.76	8.50	9.65	6.40
CV	0.19	0.14	0.14	0.10

Comparing with the ratio of “1:500”, which would correspond to situations of unlikely appearance of cracks in the building, as suggested in Skempton & MacDonald (1956), and Poulos (2017), Figs. 20a and 20b show that, for both analysed foundations, the interaction process resulted in less angular distortions than the conventional project without interaction. In the case of RFA140, the results obtained without the SSI could have been discarded or altered by excessive distortion between nearby columns, but the evaluation considering the interaction pointed out that it could be accepted by the criterion mentioned above.

6.3 Column loads

Figure 21 shows the load evolution in different columns with the increase in the number of iterations, for the cases RFA140 and RFO140. The loads varied more in the first two iterations and showed the tendency of convergence for the following steps. It should be noted that the P1

**Figure 20.** Angular distortions obtained with and without interaction for both foundations options.**Figure 21.** Load changes in three different columns considering SSI for both foundations alternatives.

(corner) column now has an increased load of approximately 60 % in relation to the predicted value without foundation-structure interaction (P_0 = initial loads without interaction). Column 33, in a more central position, had its load reduced between 20-30 % for the two foundation alternatives studied. In turn, the P29, located in an intermediate position, had little change in its load over the several iteration steps. The comparison between the RFA140 and RFO140 foundations shows that the stiffness of the foundation also interferes with the load redistribution process.

Load redistribution can also be evidenced by means of the AR parameter, which is calculated using foundation settlements according to Eq. 5. In regions where AR is less than 1, the interaction generates overload, and if AR is greater than 1, the tendency will be to relieve the load on the columns. Figures 22a and 22b show the calculated AR values for the same columns shown in section BB in Fig. 15, for cases RFA140 and RFO140. It is observed in the central region that the AR values are higher than 1, *i.e.*, their settlement exceeds the mean settlement, implying a tendency of load reduction when considering SSI effect. Reverse behavior occurs in the extremities.

Figure 23 presents a relationship between AR obtained with SSI (AR_{SSI}) and without interaction (AR_{CONV}) of all the columns of the building evaluated for the two alternative foundations. It can be noted that when AR_{CONV} was greater than unity the SSI process resulted in a settlement decrease in relation to the first forecast (conventional), indicating that the region of settlement reduction will also be the region of columns that will have their loads reduced at the end of the interaction process. Conversely, the region

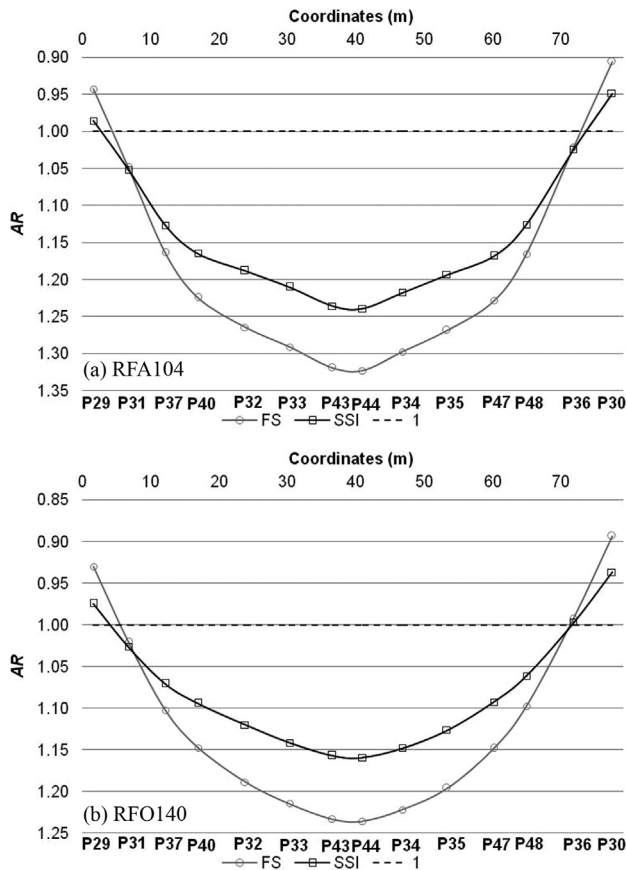


Figure 22. Values of AR 's obtained with and without SSI.

with settlements below the average ($AR_{conv} < 1$) tends to have its settlements and loads increased by the interaction process. Figure 24 illustrates the regions where relief (shaded zone) and overload occurred after the SSI process.

6.4 Bending moment in the raft

The effect of the SSI, previously described, implies lower differential settlements and a tendency to smooth out

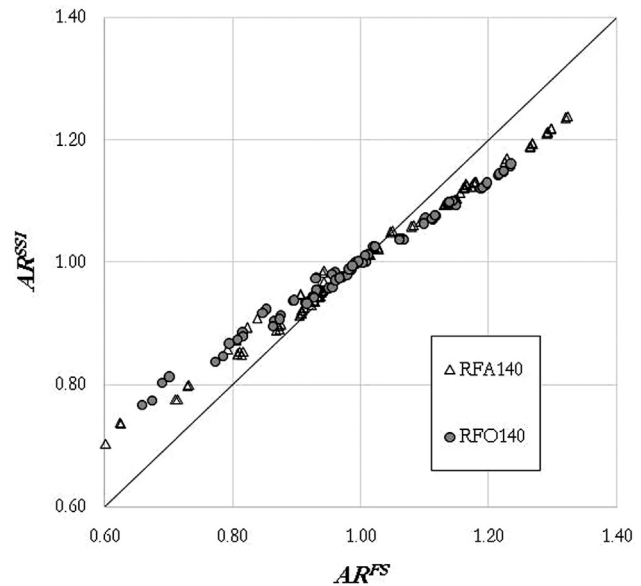


Figure 23. AR parameter relationship with and without interaction.

the “settlement basin”. When the foundation is designed as a piled raft, as in the analysed case, considering the SSI implied in a lower raft bending, thus reduced the internal moments.

Figure 25 shows that for a cross-section in the smallest dimension (Y-direction) of the building, close to the P8 column (see Fig. 15) the results were similar near the edges, but there was a clear reduction in the central part of the foundation when considering the SSI. In the greater building direction (X-direction) of the raft, the internal moments are presented in Fig. 26. Reductions between 25-50 % were found in the full extent of the raft. As the concrete reinforcement is directly proportional to the value of the bending moment, the reductions would result in considerable cost reduction when considering the SSI effect.

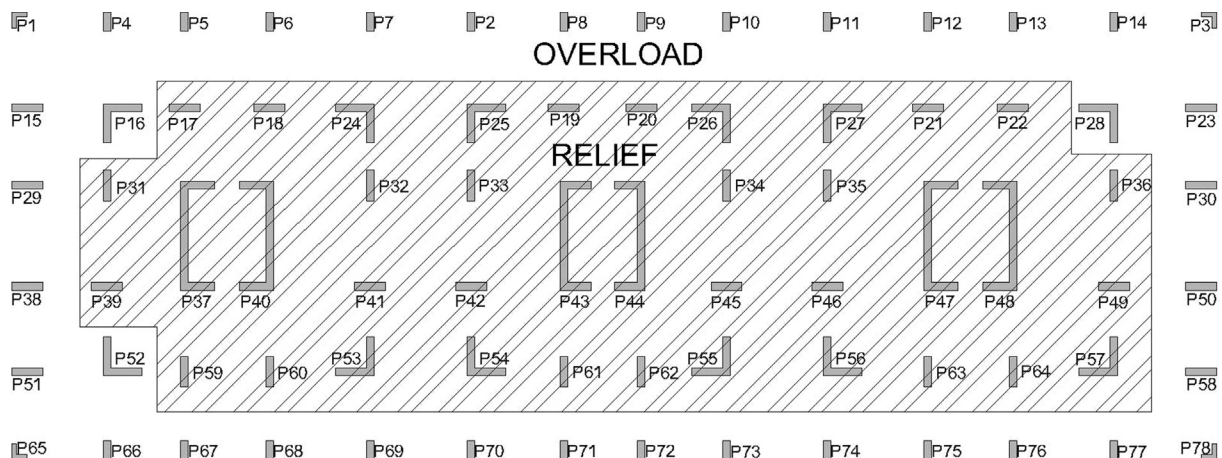


Figure 24. Relieved and overload regions due to the SSI process for the case RFA140.

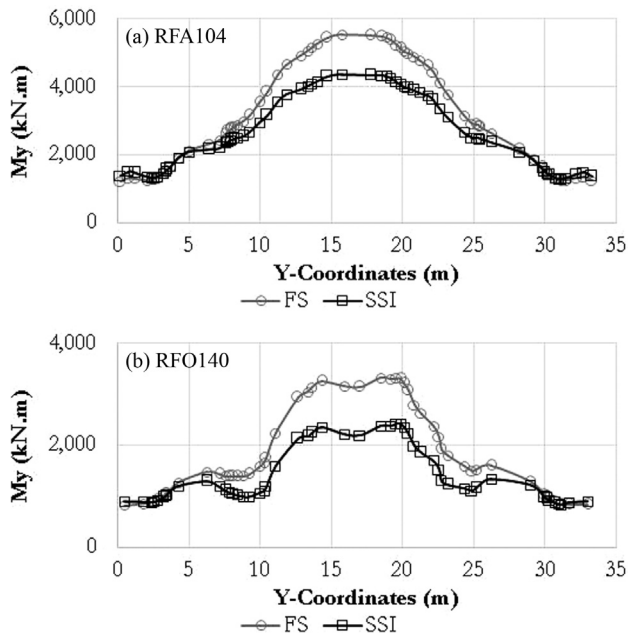


Figure 25. Bending moment on Y-direction with and without interaction for rectangular building.

6.5 Spring effect

In the search for a structural model closer to reality, structural designers replace the fixed supports under the columns by elastic ones. The parameter describing the stiffness of these supports is, by similarity, called “spring coefficient”. An attempt is made to relate the spring coefficient to the deformability of the foundations, and some geotechnical engineers have been consulted frequently about what spring coefficient they would indicate to that specific project. The most frequent choice is to try to find a spring coefficient based on the vertical subgrade modulus (k_v), defined by the ratio of the vertical stress acting on soil surface (q) and the resulting settlement (w):

$$k_v = \frac{q}{w} \quad (10)$$

The technical incoherence lies in the fact that the vertical reaction modulus is not a soil property. It depends on the scale factor, the geometry of the foundation, and the soil heterogeneity, and mainly, it does not incorporate the interaction effect between all the elements of the foundation. As in the theory of elastic beam, the spring coefficients do not reflect the continuity of the soil surrounding the foundations.

Antoniazzi (2011) used the Soil Structure Interaction System (SSIS) developed by TQS (2016), which uses a model that connects the superstructure and foundation by using vertical and horizontal reaction coefficients. In this methodology, the interaction between the foundation elements is not considered. However, the results obtained by

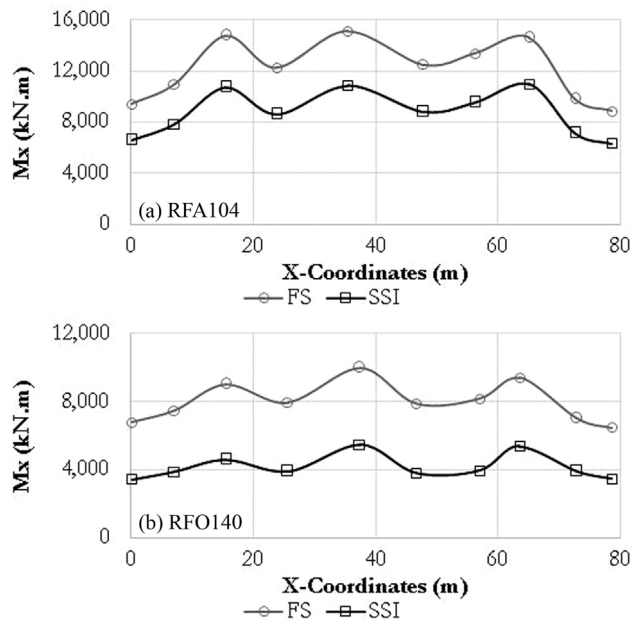


Figure 26. Bending moment on the X-direction with and without interaction for rectangular building.

that author were closer to reality when compared to the hypothesis of fixed supports.

Poulos (2018), after calling the attention to the importance of considering the process of interaction between foundations, suggests that estimating the spring coefficients as the load-settlement ratio, obtained in load tests, is more accurate than using the vertical reaction modulus.

The cases nominated as RFA140 and RFO140 are piled raft foundations, where the piles function fundamentally as settlement reducers. On the other hand, there are interactions between the piles that increase the settlements. The soil profile in question is stratified, which makes the use of spring coefficients difficult to succeed if the coefficients are estimated by means of vertical reaction moduli.

Comparisons were made between the predicted settlements for the studied building, with and without the SSI, and with the described use of spring coefficients. The values of these coefficients were estimated from vertical reaction moduli of 1 and 5 MN/m³, for the soils RFA and RFO, respectively, chosen based on tabulated values in the literature (Bowles, 1996) for the shown soil profile. Figure 27 presents only the result for 1 MN/m³, since the results for 5 MN/m³ were very similar. It can be observed that the use of the spring coefficients calculated from k_v did not practically change the results of the settlements of the initial assessment without the use of the SSI.

Figure 28 includes the results after the first interaction applying the SSI. These results were much more effective to approximate the final convergence values than the case using spring coefficients. As the format of the settlement curves is directly linked to load redistribution, it can

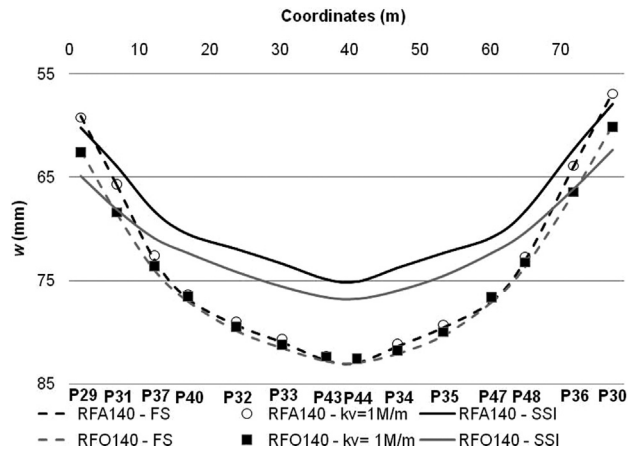


Figure 27. Comparison of settlements predictions considering (SSI) or not (FS) the SSI with the results based in the use of spring coefficients to substitute the foundations.

be concluded that the use of spring coefficients does not simulate SSI for the presented cases.

7. Effect of SSI on γ_z

Franco & Vasconcelos (1991) developed one method to evaluate the global stability of buildings, denoted by “parameter γ_z ”, mentioned by NBR 6118 (2014), which is valid for structures with 4 or more floors. This parameter is obtained from a linear analysis of the loaded structure, considering the physical nonlinearity by reducing the structural elements stiffness. The parameter γ_z is calculated by the equation:

$$\gamma_z = \frac{1}{1 - \frac{\Delta M_{1,tot,d}}{M_{1,tot,d}}} \quad (11)$$

in which $M_{1,tot,d}$ is the tipping moment, that is, the sum of the moments produced by the horizontal forces in relation to

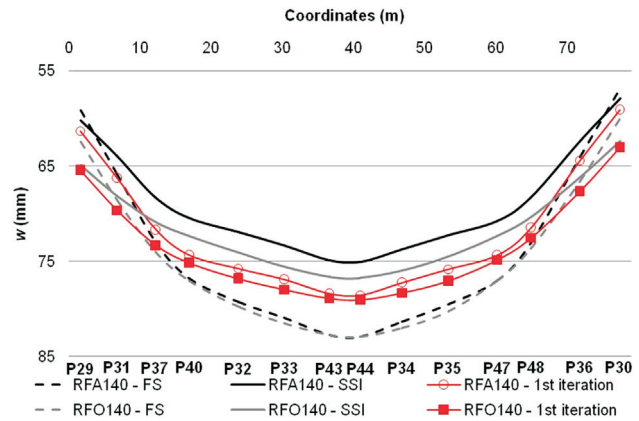


Figure 28. Comparison of the first interaction results with the simulations with (CI) and without (SI) the SSI.

the base of the structure; and $\Delta M_{tot,d}$ is the sum of the products of all vertical forces acting on the structure by the horizontal displacements of their respective points of application, obtained from the 1st order analysis, in the considered combination.

When the parameter γ_z is less than 1.1, according to NBR 6118 (2014), second order effects are not considered, and the structure is classified as having fixed nodes; otherwise, second order effects must be considered, and the structure is classified as having mobile nodes. If the value is between 1.1 and 1.3, this effect is considered approximately by multiplying the horizontal forces by a factor of $0.95\gamma_z$. Finally, when this parameter is greater than 1.3 the second order effects need to be calculated more precisely.

The value of the parameter γ_z is influenced by the tilt and geometrical imperfections of the building columns. This rotational displacement is calculated considering the perfectly fixed supports, as shown in Fig. 29. However, as already discussed, the foundation will suffer differential

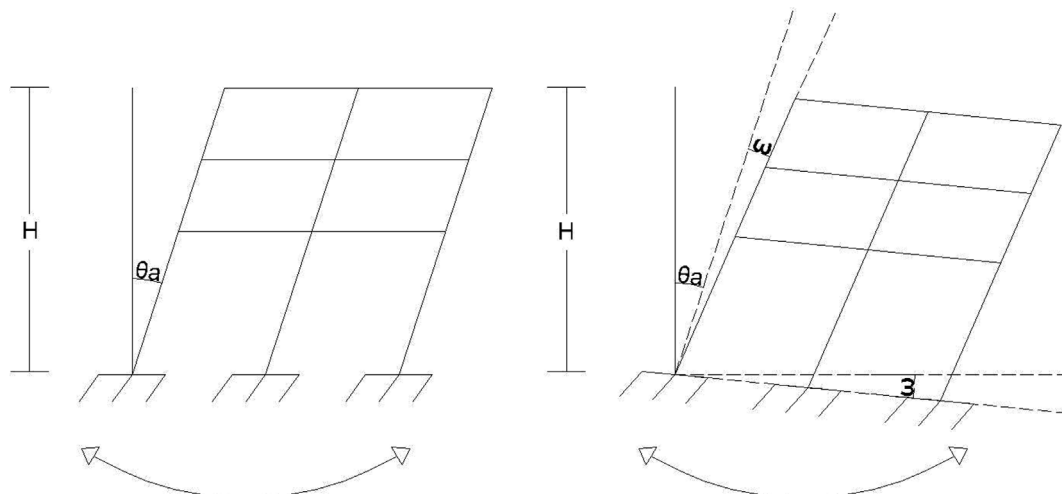


Figure 29. Superposition of the lack of verticality of the structure (θ_a) and differential foundation settlements (ω).

settlements that will affect the final verticality of the superstructure.

Borges (2009) evaluated the effect of the SSI at the value of γ_z and found that considering the interaction effect between foundation-structure as well as possible rotations of the foundations resulted in an increase of up 37 % in the values of γ_z . Silva (2018) analyzed two high-rise buildings with seven different alternative foundations and also found the magnification of the γ_z factor when incorporating the effect of foundation deformability (SSI).

Based on these results, Gusmão (2018) defined the parameter β_z , expressed by Eq. 12, as the amplification factor of the parameter γ_z due to the interaction between the foundations and the superstructure of a building.

$$\beta_z = \frac{\gamma_z^{SSI}}{\gamma_z^{FN}} \quad (12)$$

in which γ_z^{SSI} is the coefficient γ_z calculated with the SSI and γ_z^{FN} is the initial coefficient γ_z calculated without interaction and using fixed supports.

Tables 2 and 3 summarize the values calculated for β_z from the off plumb buildings (ω) obtained by Silva (2018) and Borges (2009), respectively, when considering the SSI. In all cases presented in Tables 2 and 3, the consideration of interaction increased the parameter γ_z . The greater the lack of verticality of the building, the greater is the amplification factor (β_z) due to the SSI, *i.e.*, when the SSI is considered the global stability coefficient will always be higher than the initial value of γ_z , calculated for a building over fixed

supports. The data compiled from both works are plotted in Fig. 30 and indicate an exponential growth of β_z when the tilt ratio is close to or higher than 1:1000.

8. Conclusions

This article presented the importance of considering the interaction between different elements of a foundation in predicting the building settlement, as well as the effect of including the settlements of the foundation in the performance of the structure of a high-rise building. Many examples of settlement monitoring were presented to explain the SSI process. Results of iterative process to estimate loads and settlements of buildings supports were discussed. The process concerns in repeating the structure analysis considering the stiffness of each support based in previous settlement prediction. This procedure is repeated until the convergence of the support settlement results.

The highlights are listed below:

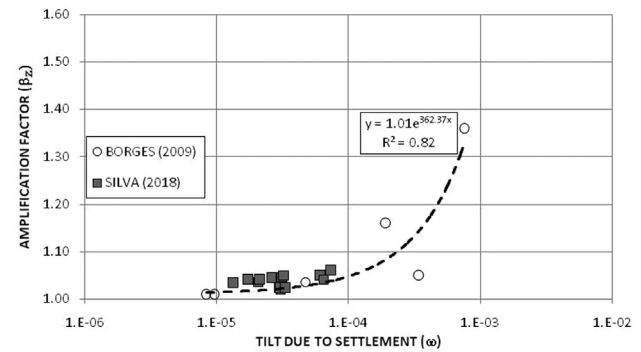


Figure 30. Tilt vs. amplification factor of parameter γ_z (β_z).

Table 2. Amplification factor (β_z) due to the SSI (Silva, 2018).

Case	X-direction				Y-direction			
	ω	γ_z^{FS}	γ_z^{SSI}	β_z	ω	γ_z^{FS}	γ_z^{SSI}	β_z
QFA60	1/16386	1.095	1.15	1.05	1/74746	1.091	1.128	1.03
QFA140	1/15357	1.095	1.161	1.06	1/57276	1.091	1.136	1.04
QFO	1/13613	1.095	1.167	1.07	1/38011	1.091	1.139	1.04
RFA60	1/32558	1.084	1.106	1.02	1/48110	1.086	1.124	1.03
RFA140	1/33476	1.084	1.109	1.02	1/47059	1.086	1.131	1.04
RFO60	1/32806	1.084	1.109	1.02	1/31724	1.086	1.135	1.05
RFO140	1/29936	1.084	1.11	1.02	1/30916	1.086	1.139	1.05

Table 3. Amplification factor (β_z) due to the SSI (Borges, 2009).

Case	X-direction				Y-direction			
	ω	γ_z^{FS}	γ_z^{SSI}	β_z	ω	γ_z^{FS}	γ_z^{SSI}	β_z
1	1/5192	1.25	1.45	1.16	1/1312	1.18	1.61	1.36
2	1/21100	1.14	1.18	1.04	1/2936	1.2	1.26	1.05
3	1/119286	1.12	1.13	1.01	1/103214	1.1	1.11	1.01

- In order to predict the building settlements, it is essential to consider the interaction effect between the different elements of its foundation;
- The result of a load test on a single element cannot be directly compared with the measured settlements during building construction. While the first represents the behaviour of an isolated foundation, the latter is the result of the entire interaction process;
- Two actual cases of tall buildings on piles were presented, and they behaved very differently. The case with floating piles resulted in a relevant process of interaction between the piles, while the case employing fixed-tip showed nearly no interaction between the piles;
- In a set of 13 monitored constructions, values of R_s factor between 1 and 22 were observed, which made clear the increase of the measured settlement in relation to that of an isolated pile. This number depends on the number of piles, their proximity, and the soil profile;
- Calculating the building superstructure, considering the supports as rigid (conventional calculation) and the subsequent isolated calculation of the foundations, does not well represent the performance of the building in terms of load distribution and loads on the columns;
- The foundation-structure interaction process, or more simply denoted by soil-structure interaction (SSI), represents the coupling of the stiffness of the building parts and is closer to the construction behavior;
- A few steps of iteration (suggestion of 3) within the process of interaction between the foundation and the structure are sufficient for commercial designs. The first iteration already points out more than 2/3 of the changes coming from SSI;
- Columns that in the conventional calculation have settlements below the average of the building, which in general are the columns of the periphery, will have the tendency to increase the load and the settlements. On the other hand, the columns with initially predicted above average settlement will lose load and settle less in a load redistribution process;
- Using SSI, the predicted settlements result in lower values of angular distortions in the foundations, which may make possible the use of an alternative foundation that would not satisfy the criterion of maximum distortions for the conventional calculation;
- In the presented examples, the foundations in rafts or piled rafts presented reductions in the maximum bending moments in the order of 20 % to 50 %, when the SSI was employed. This points to the possibility of a more economical foundation design;
- The global stability parameter, γ_z , is also affected by the calculation with or without the SSI. When considering the interaction process between the foundation and the structure, the values obtained for γ_z were higher;

- The article presents a factor β_z to represent the ratio of the increase in the value of γ_z when it is calculated with and without SSI. The increase observed depends on the building's non-verticality, with a non-linear and accelerated growth as it approaches a ratio of 1:1000.

Acknowledgments

The authors thank TQS Informática; Prof. H.G. Poulos for providing the GARP program; the Post-Graduation Program in Geotechnics, Structure and Civil Construction of UFG; the Federal Institute of Pernambuco; University of Pernambuco; CAPES (Coordination for the Improvement of Higher Level Personnel); and the CNPq (Brazilian National Council for Scientific and Technological Development) for scholarships and the support for recent researches.

References

- Almeida, A.K.L. (2018). Analysis of Group Effect of Deep Foundations. Bachelor Monography. Civil Engineering Course. Universidade Católica de Pernambuco, 139 p. (in Portuguese).
- Antoniazzi, J.P. (2011). Soil- Structure Interaction of Buildings with Shallow Foundations. M.Sc. Dissertation. Post-Graduate Program in Civil and Environmental Engineering. Universidade Federal de Santa Maria, 139 p. (in Portuguese).
- Aoki, N. & Lopes, F.R. (1975). Estimating stresses and settlements due to deep foundations by the theory of elasticity. Proc. 5th Congreso Panamericano de Mecánica de Suelos e Ingeniería de Fundaciones, Buenos Aires, pp. 378-286.
- Araújo, A.C. (2009). Analysis of Soil-Structure Interaction in High-Rise Buildings. M.Sc. Dissertation. Post-Graduate Program in Civil Engineering. Universidade Federal de Goiás. 120 p. (in Portuguese).
- Associação Brasileira de Normas Técnicas. (2014). Design of Concrete Structures - NBR-6118. Rio de Janeiro, 221 p. (in Portuguese).
- Bahia, G.A.D.; Mota, N.M.B.; Cunha, R.P. & Sales, M.M. (2016). Evaluation of foundations behavior in a building in Federal District. Proc. 18th Brazilian Congress of Soil Mechanics and Geotechnical Engineering, Belo Horizonte. (in Portuguese).
- Bernardes, H.C.; Carvalho, S.L.; Sales, M.M.; Almeida, S.R.M.; Farias, M.M. & Pinho, F.A.X.C. (2019). Hybrid numerical tool for nonlinear analysis of piled rafts. Soils and Foundations, 59(6):1659-1674. <https://doi.org/10.1016/j.sandf.2019.04.011>
- Borges, A.C.L. (2009). Methodology for Evaluation of Structural Behavior in High-Rise Concrete Buildings Considering Soil-Structure Interaction. Ph.D. Thesis, Center of Technology and Geoscience. Post-Graduate

- Program in Civil Engineering. Universidade Federal de Pernambuco, 205 p. (in Portuguese).
- Bowles, J.E. (1996). *Foundation Analysis and Design*, 5ed, New York, The McGraw-Hill Companies Inc., 1207 p.
- Chamecki, S. (1954). Consideration of structure stiffness in foundation settlement calculation. *Proc. First Brazilian Congress of Soil Mechanics*, Porto Alegre, pp. 35-80. (in Portuguese).
- Clancy, P. & Randolph, M.F. (1993). An approximate analysis procedure for piled raft foundations. *International Journal for Numerical and Analytical Methods in Geomechanics*, 17(12):849-869. <https://doi.org/10.1002/nag.1610171203>
- El-Mossalamy, Y. & Franke, E. (1997). Piled rafts - numerical modelling to simulate the behaviour of piled raft foundations. Darmstadt, Germany, 182 p.
- Eurocode 7. (2004). *Geotechnical Design - Part 1: General rules*, European Committee for Standardization.
- Fadum, R.E. (1948). Influence values for estimating stresses in elastic foundations. *Proc. Second International Conference on Soil Mechanics and Foundation Engineering*, v. 3, pp. 77-84.
- Franco, M. & Vasconcelos, A.C. (1991). Practical assessment of second order effects in tall buildings. *Proc. Colloquium on the CEB-FIP MC90*, Rio de Janeiro, pp. 307-323. (in Portuguese).
- Gusmão, A.D. (1990). *Study of Soil-Structure Interaction and its Influence on Building Settlements*. M.Sc. Dissertation. COPPE/UFRJ. Universidade Federal do Rio de Janeiro, 165 p. (in Portuguese).
- Gusmão, A.D. (1994). Relevant aspects of soil-structure interaction in buildings. *Soils and Rocks*, 17(1):47-55 (in Portuguese).
- Gusmão, A.D. (2018). *Buildings settlement measurements: Evidences of soil-structure interaction effects*. Lecture delivered at CREA/GO, Goiânia (in Portuguese).
- Gusmão, A.D. & Gusmão Filho, J.A. (1994). Evaluating the influence of soil-structure interaction in buildings. *Proc. 10th Brazilian Congress of Soil Mechanics and Foundation Engineering*, Salvador, v. 1, pp. 67-74 (in Portuguese).
- Gusmão, A.D.; Gusmão Filho, J.A. & Maia, G.B. (2000). Settlement measurements of a building in the city of Recife. *Proc. Symposium about soil-structure interaction*, São Carlos, SP. (in Portuguese).
- Hain, S.J. & Lee, I.K. (1978). The analysis of flexible raft-pile systems. *Géotechnique*, 28(1):65-83. <https://doi.org/10.1680/geot.1978.28.1.65>
- Iwamoto, R.K. (2000). *Some Aspects of the Effects of Soil-Structure Interaction in Multi-Floors Buildings with Deep Foundations*. M.Sc. Dissertation. School of Engineering of São Carlos, Universidade de São Paulo, 140 p. (in Portuguese).
- Meyerhof, G.G. (1953). Some recent foundation research and its application to design. *The Structure Engineering*, 31:151-167.
- Mota, M.M.C. (2009). *Soil-Structure Interaction in Buildings with Deep Foundations: Numerical Analysis and In-situ Measurements*. Ph.D. Thesis. School of Engineering of São Carlos, Universidade de São Paulo, 187 p. (in Portuguese).
- Poulos, H.G. (1968). Analysis of the Settlement of Pile Groups. *Géotechnique*, 18(4):449-471. <https://doi.org/10.1680/geot.1968.18.4.449>
- Poulos, H.G. (1975). Settlement analysis of structural foundation systems. *Proc. 4th South-East Asian Conference on Soil Engineering*, Kuala Lumpur, Malasia, v. 4, pp. 52-62.
- Poulos, H.G. (1994). An approximate numerical analysis of pile-raft interaction. *Inter. Journal for Numerical and Analytical Methods in Geomechanics*, 18(2):73-92. <https://doi.org/10.1002/nag.1610180202>
- Poulos, H.G. (2013). Tall building foundation design - the 151 story Incheon Tower. *Proc. 7th International Conference on Case Histories in Geotechnical Engineering*. Missouri, USA, pp. 1-13.
- Poulos, H.G. (2017). *Tall Building Foundation Design*. Taylor and Francis Group, New York, 532 p.
- Poulos, H.G. (2018). Rational Assessment of Modulus of Subgrade Reaction. *Geotechnical Engineering Journal of the SEAGS & AGSSEA*, 49(1):1-7.
- Poulos, H.G. & Davis, E.H. (1974) *Elastic Solutions for Soil and Rock Mechanics*. John Wiley & Sons, New York, 411 p.
- Poulos, H.G. & Davis, E.H. (1980). *Pile foundation analysis and design*. John Wiley and Sons, New York, 397 p.
- Rocha, A.M. (1954). Hyperstatic structure calculation taking into account foundations settlements. *Proc. First Brazilian Congress of Soil Mechanics*, Porto Alegre, pp. 162-165. (in Portuguese).
- Russo, G. (1995). *Interazione Terreno Struttura per Piastrini su Pali*. Ph.D. Thesis. University of Napoli Federico II, Napoli. (in Italian).
- Sales, M.M.; Prezzi, M.; Salgado, R.; Choi, Y.S. & Lee, J. (2017). Load-settlement behaviour of model pile groups in sand under vertical load. *Journal of Civil Engineering and Management*, 23(8):1148-1163. <https://doi.org/10.3846/13923730.2017.1396559>
- Silva, A.C. (2018). *Soil-Structure Interaction in the Design of High-Rise Buildings*. M.Sc. Dissertation. Post-Graduate Program in Geotechnical, Structure and Construction Engineering. Universidade Federal de Goiás. 188 p. (in Portuguese).
- Skempton, A.W. & MacDonald, D.H. (1956). The Allowable settlements of buildings. *Proc. Institution of Civil Engineers*, 5(6):727-768.
- Small, J.C. & Poulos, H.G. (2007). A method of analysis of piled rafts. *Proc. 10th Australia New Zealand Conference on Geomechanics*, Common Ground Proceedings, Brisbane, pp. 550-555.
- TQS Informática. (2016). *User's Manual of CAD/TQS*. TQS Informática, São Paulo.

Some topics of current practical relevance in environmental geotechnics

Maria Eugenia Gimenez Boscov¹ , Paulo Scarano Hemsí^{2, #} 

Article

Keywords

Geoenvironmental engineering
MSW landfill
Remediation
Reuse of waste

Abstract

Environmental Geotechnics has been an established branch of Geotechnical Engineering for about 40 years. The contribution from Brazilian practitioners and researchers is meaningful in the many activities in this field. This paper proposes to discuss three topics of relevance to modern sustainability in Brazil, in which Geotechnicians could have an even greater involvement: expansions in MSW landfills, geotechnical confinement and other geotechnical solutions for remediation of contaminated land, and reuse of wastes as geomaterials. First, important aspects of the environmental protection system recommended for landfill expansions are described through examples, as well as the possibility of immersing geogrids to reinforce the MSW mass and increase storage capacity. Secondly, an industrial-site case study is presented to point out the additional challenges associated with site remediation at an urban region of past industrial land use and the importance of a joint regional investigation and remediation plan. The possibility of benefiting from geotechnical confinement and *in situ* passive remediation to treat the area also is highlighted. Finally, on the third topic, preparedness to accept working with wastes in geotechnical works is encouraged, and two investigation examples on the reuse of construction and demolition waste and water treatment sludge are presented and discussed.

1. Introduction

Environmental Geotechnics is the branch of Geotechnical Engineering that deals with environmental conservation in the face of impacts from anthropic activities and natural disasters. The term environmental conservation expresses the intent to both preserve and benefit from Nature for social-economic and technological development, safeguarding natural resources for future generations. Geotechnics may help reduce the extraction of natural resources for new developments, dispose of waste, control water, soil and atmospheric contamination, and recover degraded areas of the planet. Environmental Geotechnics may provide new spaces for human use by recovering areas degraded by desertification, erosion, salinization, pollution, and neglect after termination of industrial activities. The UNEP (UN Environment Programme) estimates that 15 % to more than 30 % of the soils of the planet are degraded by human activities, and the proportion of degraded rangelands, which cover about 50 % of the global land area, is around 23 %

(Thenkabail, 2016). The recovery of degraded areas may use traditional Geotechnical techniques, such as earthwork, dredging, drainage, erosion control works, as well as techniques for remediation of contaminated land. Continuous development in Environmental Geotechnics is in great demand due to the increasing generation of waste, wastes of greater complexity, reuse of contaminated areas due to scarcity of space in urban conglomerates, ever more stringent environmental standards, and growing sustainability awareness and requirements in all human activities.

1.1 A brief historical perspective

Environmental issues have become a significant component of Geotechnical Engineering since *circa* 1980, although for long Geotechnical engineers have been involved with such themes (Shackelford, 2005). A first technical session on Environmental Geotechnics took place in the IX ICSMFE (International Conference on Soil Mechanics and Foundation Engineering) in 1977. In 1992, TC5, the Technical Committee on Environmental Geotechnics, presently

[#]Corresponding author. E-mail address: paulosh@ita.br.

¹Departamento de Engenharia de Estruturas e Geotécnica, Universidade de São Paulo, São Paulo, SP, Brazil.

²Departamento de Geotecnia, Instituto Tecnológico de Aeronáutica, São José dos Campos, SP, Brazil.

Submitted on June 23, 2020; Final Acceptance on June 25, 2020; Discussion open until December 31, 2020.

DOI: <https://doi.org/10.28927/SR.433461>



This is an Open Access article distributed under the terms of the Creative Commons Attribution License, which permits unrestricted use, distribution, and reproduction in any medium, provided the original work is properly cited.

TC215, was created in the scope of ISSMGE (International Society for Soil Mechanics and Geotechnical Engineering). In 2012, came the time for creating the Technical Committee on Sustainability in Geotechnical Engineering, TC307. The 1st International Congress on Environmental Geotechnics occurred in 1994, in Canada, and since then, the congress occurs every four years. In 2002, the ICEG took place in Brazil, and the latest congress was held in 2018 in China. Most Geotechnical journals have been covering the subject area, explicitly the prestigious ASCE's Journal of Geotechnical Engineering altered the name to Journal of Geotechnical and Geoenvironmental Engineering, in 1996, and ISSMGE TC215 launched in 2014 the journal Environmental Geotechnics.

In Brazil, a state-of-the-art report on Environmental Geotechnics was conveyed in the VIII COBRAMSEF (Brazilian Conference on Soil Mechanics and Foundations Engineering), in 1986. A Symposium on Tailings Dams and Waste Disposal, sponsored by the Brazilian Societies for Soil Mechanics and Geotechnical Engineering (ABMS) and Engineering Geology (ABGE), took place in 1987. This technical-scientific meeting turned eventually into a regular congress, the Brazilian Congress on Environmental Geotechnics, taking place every fourth year after 1991, and since 2003 occurring together with the Brazilian Congress on Geosynthetics. In 1994, the Technical Committee on Environmental Geotechnics (CTGA) was founded at ABMS. Presently, there are more than 20 research groups on Environmental Geotechnics registered at CNPq (National Research Council).

1.2 Branches of activity in Environmental Geotechnics

The main branches of activity in Environmental Geotechnics include waste disposal (site selection, design, operation and monitoring of MSW landfills, industrial landfills and other waste disposal facilities); use of soils and geosynthetics as construction materials for environmental protection works; use of geotechnical techniques for environmental protection; use of waste as geomaterial; monitoring and prevention of, and recovery from, accidents and natural disasters; prevention of contamination of superficial soil, subsoil, and surface- and groundwater; recovery of degraded areas; remediation of contaminated land; environmental impact assessment of civil works; risk analyses; investigation, instrumentation, monitoring and sampling of water and soil; environmental licensing and elaboration of environmental impact studies; environmental diagnosis and risk management of urban slopes; among others. Such applications of Environmental Geotechnics could be divided in three main groups: soils as receptors of contamination; soils as construction material in geoenvironmental works; and use of waste as geotechnical materials.

Not all of these activities are exclusive to Environmental Geotechnicians, and interaction with other fields is the key to meet the challenges with relevant solutions based

on up-to-date knowledge. Basic knowledge of other disciplines to develop a common language is required, as well as a capacity to move away from the problem to acquire a wider perspective, and then move back to contribute in the specific scope of Geotechnics. Yet, multidisciplinary is not a stranger to Geotechnics. From the rheology of polymers for injections in dam foundations or special concretes for tunnels to the survey of the geological history of a region to understand the behavior of a particular soil, Geotechnical Engineers have frequently worked together with professionals from other fields of knowledge. Nonetheless, in Environmental Geotechnics multidisciplinary is a marked characteristic; the Engineer works with colleagues from Geology, Pedology, Chemistry, Hydrology, Microbiology and, more recently, Rheology, Thermodynamics, Biology and Nanotechnology.

1.3 Objectives

The objectives of this paper are to provide firstly a brief critical overview, and then a discussion on selected topics of practical relevance, in each of the following themes:

- Municipal solid waste landfills,
- Site remediation, and
- Geotechnical reuse of waste.

2. Municipal solid waste landfills

2.1 Overview

A municipal solid waste (MSW) landfill is a facility to contain the waste collected in households, small businesses and urban public spaces (roads, streets, parks, squares, public buildings, etc.) designed and built according to well-defined environmental and engineering concepts so as to guarantee structural and environmental safety. The demand for landfill storage capacity depends on waste generation, waste management and alternatives to landfilling, societal practices, and legislation, varying from place to place. Nonetheless, increasing landfill storage capacity remains a necessity around urban areas in the majority of countries. Landfill piggyback expansions and the possibility to reinforce slopes of municipal solid waste for increasing storage capacity are exemplified and discussed.

2.1.1 Destination of MSW in Brazil

In Brazil, an estimate of the average generation of MSW is 1.039 kg/inhabitant/day: in 2018, approximately 199×10^3 tons of waste were collected daily in Brazil, 59.5 % being disposed in landfills, 23.0 % in controlled dumps and 17.5 % in uncontrolled dumps (ABRELPE, 2020). Between 2000 and 2018, the percentage of MSW destined to landfills increased significantly, from 35.4 % to 59.5 % (ABRELPE, 2020). Estimates of MSW generation growth and disposal over the years can also be found in BNDES (2014).

In terms of number of municipalities, in 2015, 40.2 % of the Brazilian municipalities disposed MSW in landfills, 31.8 % in controlled dumps and 27.9 % in uncontrolled dumps (ABRELPE, 2016). In contrast, in 2008, only 13 % of municipalities disposed waste in landfills, while 59 % still used uncontrolled dumps (IBGE, 2010). The numbers vary according to region and population; for instance, 301 out of 399 municipalities in Paraná state disposed waste in landfills in 2017 (IAP, 2017, Oliveira, 2019), whereas the proportion was only 43 out of 417 municipalities in Bahia state. According to BNDES (2014), in 2012, the northeast and southeast Brazil generated, together, 75 % of the total MSW; however, NE destined only 35.4 % of MSW to landfills that year, whereas in the SE the percentage was 72.2 %.

The Federal Law 12,305 - National Policy on Solid Waste (BRASIL, 2010) - established that by 2014 the total generated MSW in the country should be adequately disposed of and, subsequently, waste dumps should be recovered and remediated. BNDES (2014) estimated financial investments on the order of US\$ 1 billion between 2015 and 2019 to build the necessary landfills for Brazil to comply with the National Policy on Solid Waste, based on consolidated data from 2012. The requirement, however, was not met, and the deadline has been extended.

The demand for landfills continues to grow, due to the growth of cities, consortia formed among small municipalities to share the costs of implementation and operation, and implementation of large private MSW landfills to serve several neighboring municipalities. The increase in height, maintaining design concepts and construction methods, has led to slides, such as, for example, at Aterro São João, 2007, and Taiaçupeba, 2011.

A study by ABLP (2019), published in the journal *Limpeza Pública*, aimed at updating waste-disposal site numbers in Brazil. The study compared 2016 data from the National Data System on Solid Waste Management (SINIR) to a 2018-2019 survey by ABLP. The SINIR data are the official data of the Environmental Ministry, based on an annual survey on state-level environmental agencies. According to the SINIR data from 5,393 municipalities, 2,692 municipalities deposited waste in uncontrolled dumps, 427 in controlled dumps, and 2,274 in landfills. Based on these data, there were 1,803 uncontrolled dumps in Brazil, 40 controlled dumps, and 801 landfills in 2016.

The survey by ABLP, also from direct consultation to the state-level environmental agencies (ended January 2019), comprised 25 states and the Federal District, resulting in 792 landfills in the country, and 308 more landfills under licensing process. The numbers on a per-state basis are shown in Fig. 1.

Since the approval of the National Policy on Solid Waste (BRASIL, 2010), the country faces the challenge of implementing planned collection, selection, treatment and adequate disposal of MSW, domestic, commercial and industrial. Law 12,305 establishes shared responsibility for integrated management of solid wastes. The National Policy on Solid Waste rests on the principles of public-health and environmental protection, promoting non-generation, reduction, reuse, recycling, treatment and environmentally-adequate disposal of waste, as well as fostering industrial recycling, clean technologies, integrated management, and continued technical capacitation.

Decrees for the implementation of the law enforce the development of municipal-, state- and national-level management plans. Municipalities and states are enforced to

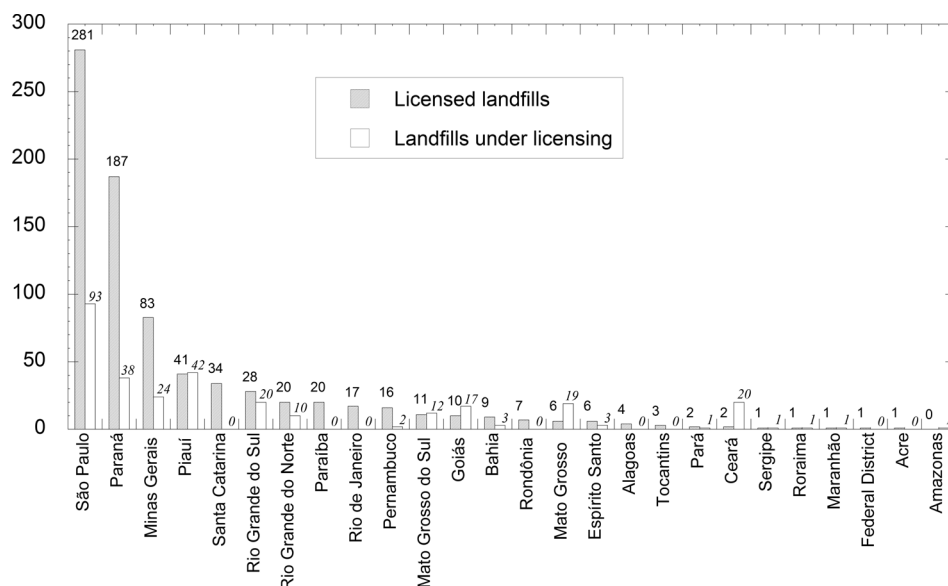


Figure 1. Number of licensed and under licensing landfills in 25 Brazilian states and the Federal District (Based on data from ABLP, 2019).

prepare a Plan for Integrated Solid Waste Management (PGIRS) as a condition for receiving federal sanitation funds. In 2011, a preliminary version of the National Plan for Solid Waste was prepared, containing the following targets (BNDES, 2014, van Elk & Boscov, 2016):

- Eradication of open uncontrolled dumps in Brazil, originally by August 2014; all such dumps should be decommissioned or converted into sanitary landfills, and the possibly contaminated area remediated;
- Reduction of the amount of waste generated, from around 1.1 kg/inhabitant/day to 0.6 kg/inhabitant/day;
- Implementation of organic matter composting (recycling), since organic matter should no longer be disposed in sanitary landfills;
- Differentiation between “solid waste” and “refuse” (the latter without any usefulness), with solid waste being selected/sorted and processed for reusable and recyclable materials, with a reduction of up to 70 % in the amount of waste going to landfills;
- Implementation of selective collection, with the insertion of 600,000 collectors;
- Implementation of energy from MSW biogas based on a viability study supported by gas monitoring, and
- Establishment of directives and responsibilities over the integrated management of solid waste, with reverse logistics and shared responsibility.

These targets, environment-friendly and up-to-date with most developed countries, are however very far from being robustly implemented, so that demand for MSW landfills is still on the agenda in the vast majority of the country.

Additionally, a Brazilian technical standard specifying the minimum requirements for location, design, implantation and operation of low volume sanitary landfills was enacted in 2010 (ABNT, 2010 - NBR 15,849). According to the coordinator of the group that developed the standard, the standard would allow the adoption of solutions adequate for the geographical reality of each municipality, making construction of landfills easier and therefore avoiding the proliferation of dump sites; else, requirements for a large city (*e.g.*, São Paulo) would be the same as for little towns. Other public managers also believed that the standard would allow the sustainability of MSW landfills for small municipalities, with lower costs of implantation and operation.

Unfortunately, the standard used very limited contribution from Geotechnical Engineers, and was prepared by a group majorly composed of public managers without an engineering background. In order to simplify licensing procedures, despite the insistence of Geotechnicians in the group, the requirements of engineered design, stability analyses, surface drainage, groundwater flow, among others, were oversimplified, regardless of the fact that the municipalities might be located over vulnerable subsoil profiles. The basis for adhering to the standard was simply

daily generation of MSW (< 20 ton/day), and not landfill geometry and height. Also, a single compacted-clay layer as bottom liner may indeed adequately protect the subsoil and groundwater from leachate release in many cases (depending on climate, subsoil and compacted clay), and is a feasible solution even for small and poor municipalities, since compaction equipment is generally available. However, in order to keep distance from the requirement for a complex environmental protection system, statements on the need for designing a case-specific bottom liner and drainage systems as the adequate engineered solution were avoided in the standard. This was a strong example of the lack of Geotechnicians involvement and participation in environmental legislation, where they would have an important contribution.

Nowadays, the design of MSW landfills, mostly in large urban areas or shared MSW landfills, is carried out by Geotechnicians, with relevant technical and scientific contributions to the understanding of MSW hydro-mechanical properties and to the design, operation, monitoring and closure of landfills. However, there is still little contribution in standardization and regulation, as well as lack of an efficient channel of communication with society.

2.1.2 Main geotechnical issues in landfills

The main geotechnical issues affecting MSW landfills are geomechanical behavior, structural stability and waste compressibility, liquid and gas pore pressures, and design of the bottom liner and cover. The stability assessment remains generally based on limit-equilibrium, with Mohr-Coulomb strength parameters. Since the first Brazilian values of 13.5 kPa for cohesion and 22° for effective friction angle, obtained from back-analyzing the Bandeirantes landfill failure (Benvenuto & Cunha, 1991), national research has been developed (Machado *et al.*, 2002; Mahler & Lamare Neto, 2003; Campi & Boscov, 2011; Norberto *et al.*, 2020; Daciolo, 2020; among others), including more advanced constitutive models (Machado *et al.*, 2002; Mahler & Lamare Neto, 2005; Malavoglia, 2016; among others). Since landfills undergo large settlements, modeling of compression time evolution remains important. From adapting Terzaghi's consolidation theory (Sowers, 1973) to creating new models including biodegradation and creep (Machado *et al.*, 2009; Simões & Catapreta, 2010; Alcântara & Jucá, 2010; among others), advances have been made. Two approaches have been developed in parallel: estimating MSW parameters for geotechnical models, and developing specific models for MSW. Pore pressures in MSW are difficult to predict, measure and interpret, and are related to composition, age, biodegradation, compaction, and drainage conditions, factors that are correlated (Benvenuto & Cipriano, 2010; Coelho, 2005; Miguel *et al.*, 2018, among others). There is also an extensive Brazilian literature on the performance of bottom liners, including hydraulic conductivity and pollutant retention capacity is-

sues. Recently, much research has focused on the release of biogas through the landfill cover (Teixeira *et al.*, 2009; Bridi *et al.*, 2015; Borba *et al.*, 2017; Costa *et al.*, 2018; among others).

2.1.3 Alternatives to landfilling

With socio-economic development, two opposite trends in terms of the quantity of MSW destined to landfills occur: increase in the generation of MSW, as an indicator of economic progress, and, on the other hand, adherence to policies of reduction, reuse, recycling and stabilization of wastes before landfilling, an indicator of social progress. In the European Union (EU), the quantities of waste sent to landfill sites are decreasing, as waste management must include differentiation and recycling, composting and waste incineration. Finland, Sweden, Denmark, Poland, Germany, the Netherlands, Belgium, Austria and Slovenia have laws banning or severely restricting the disposal of household waste in landfills (Conte & Carrubba, 2013). Figure 2 illustrates the waste disposal distribution percentages for countries in the EU based on 2018 data.

However, the use of landfills is still widespread, as nine out of 27 EU countries dispose more than 80 % of the MSW in landfills. The trend is stabilizing, as the use of recycling and pretreatment has increased (in fact, six countries dispose < 10 % of the MSW in landfills). The practice of waste incineration, involving partial recovery of energy, is widespread in the Nordic countries, such as Sweden and Denmark. Germany and Italy mainly use recycling (48 %

and 37 %, respectively), while Austria is the main user of composting and anaerobic digestion (about 40 %) (Conte & Carrubba, 2013).

Nonetheless, the ashes from waste incineration must be, at least partly, taken to landfills. As a by-product of the treatment of municipal solid waste in waste-to-energy plants, roughly 230-280 kg of ashes are generated per ton of waste incinerated, bottom ash being the major stream (ISWA, 2006). Fly ash is regarded as a hazardous material due to the high content of heavy metals, whereas incineration bottom ash (IBA) can be either landfilled or utilized. Since IBA contains toxic heavy metals, not only the geotechnical properties, but also the environmental leaching properties must be studied. In China, for example, where incineration is widely used for MSW, ashes are submitted to solidification/stabilization treatment and then landfilled (Chen *et al.*, 2019). In Japan, where 5 million tons of IBA are generated every year, and landfilling space is scarce, IBA is being considered as a construction geomaterial (Fujikawa *et al.*, 2019). Almost 500 municipal solid waste incineration plants in the EU, Norway and Switzerland generate about 17.6 Mt/year of IBA. Since there is no uniform regulation for IBA utilization at EU level, countries developed their own rules with varying requirements. Metals are mostly separated and sold to the scrap market and minerals are either disposed of in landfills or utilized in the construction sector (Blasenbauer *et al.*, 2020). In France, a dedicated national legislation for IBA exists since 1994 (which has been improved along the years), which provides a detailed regu-

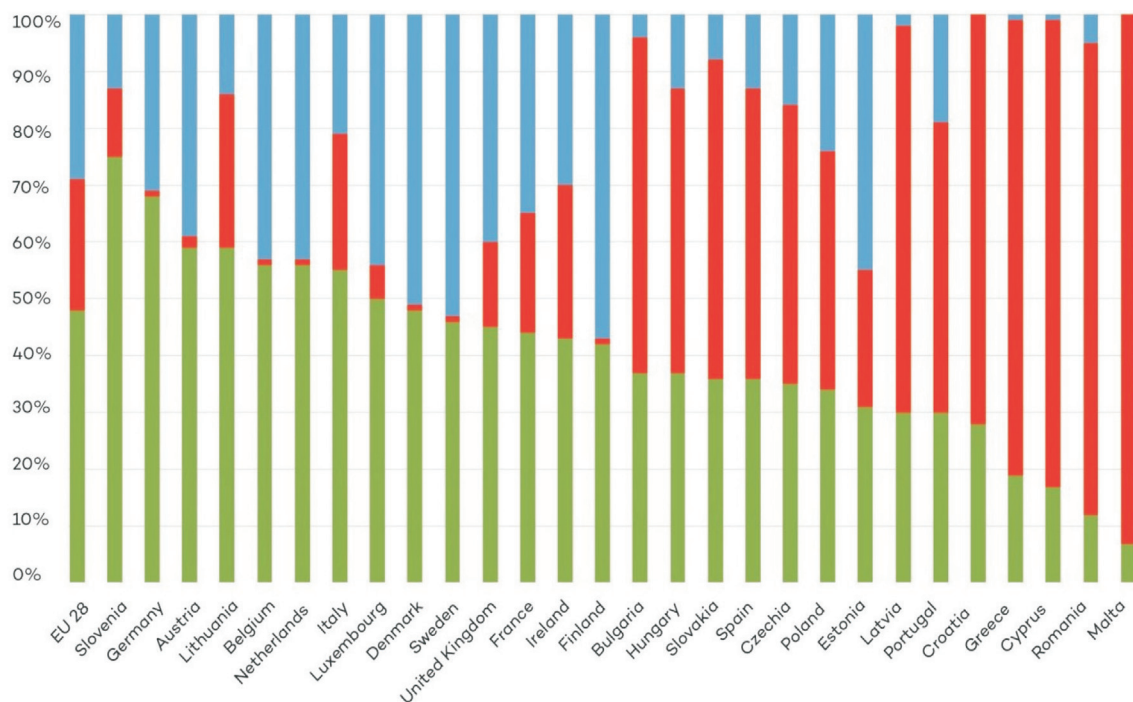


Figure 2. Percentages of MSW disposal practices in the European Union, including recycling (green), waste-to-energy (blue), and landfilling (red). Waste-to-energy includes incineration, composting and anaerobic digestion (Eurostat, 2018).

latory framework to facilitate management, with a view to reuse in road construction (ISWA, 2006).

It is important to mention that when waste-to-energy alternatives are implemented in Brazil, a trend to be expected for metropolitan regions with high MSW generation and lack of space for landfilling, Geotechnicians will have two new challenges and opportunities: design and operation of IBA landfills, and reuse of IBA in geotechnical works.

2.2 Landfill expansions

Due to the increased difficulty in finding and licensing new areas for landfills near cities, the option of expanding existing landfills becomes most attractive. The capacity increase in existing facilities may involve Geotechnical Engineering solutions such as the construction of a high peripheral reinforced-soil dike for verticalization of the landfill, rising of the landfill with geogrid-reinforcement of MSW slopes, or the so-called piggyback expansions. The two latter cases will be further discussed.

In Brazil, vertical and/or lateral expansions in landfills near urban areas, generally called amplifications, are much frequent. Brazilian landfill designers point out that layers for leachate drainage and impermeable barriers are applied in landfill expansions, but there is, however, a lack of technical guidance on the issue. The burden of the project rests entirely with the designer since there are no specific technical standards or recommendations. Geotechnicians are aware of the technical challenges imposed by the expansion foundations being constituted of a highly compressible and heterogeneous waste mass, where gas and leachate are still being generated, but most feel technically prepared to deal with this challenge.

The use of geogrid-reinforcement at the contact between the old and new landfills is generally never adopted. As shown by experience in other countries, there is a possi-

bility for damage of the emplaced environmental protection systems, caused by large and differential settlements occurring in the old underlying landfill, indicating the need for additional measures aimed at reducing strains on the mineral and geosynthetic components.

Possibly, some mistrust relative to the maintenance of the geogrid properties for a long time inside the waste mass is sensed amongst Brazilian landfill designers. However, there is strong evidence of PVA-geogrid compatibility in caustic environment (Huesker, 2017; Nishiyama *et al.*, 2006) and HPDE geomembrane compatibility in acidic environment (Renken *et al.*, 2007). On this subject, the academia could collaborate with designers, investigating geogrid performance specifically under MSW-leachate conditions: the pH range of MSW leachate in Brazil is reported as 5.7-8.6 (Souto & Povinelli, 2007, based on data from 25 Brazilian landfills; more recent papers corroborate this range), whereas temperatures may easily reach 60 °C (Carvalho, 1999).

2.2.1 Piggyback expansions

The terminology “piggyback” is used in the international literature to describe a new landfill (expansion) constructed on top of an existing one that has been either closed or scheduled to be closed, or when the new landfill uses the side slope of an old landfill as part of the support. Figure 3 illustrates some examples of possible geometries.

The reasons for adopting a piggyback expansion are maximizing the landfill utilization factor, economy in construction, sharing infrastructure, rationalizing use of equipment and facilitating authorization processes, among others. The main concerns involve safeguarding the integrity and maintenance of an adequate geometry for the environmental protection systems of both the extension and the old landfill amidst large differential settlements, enabling

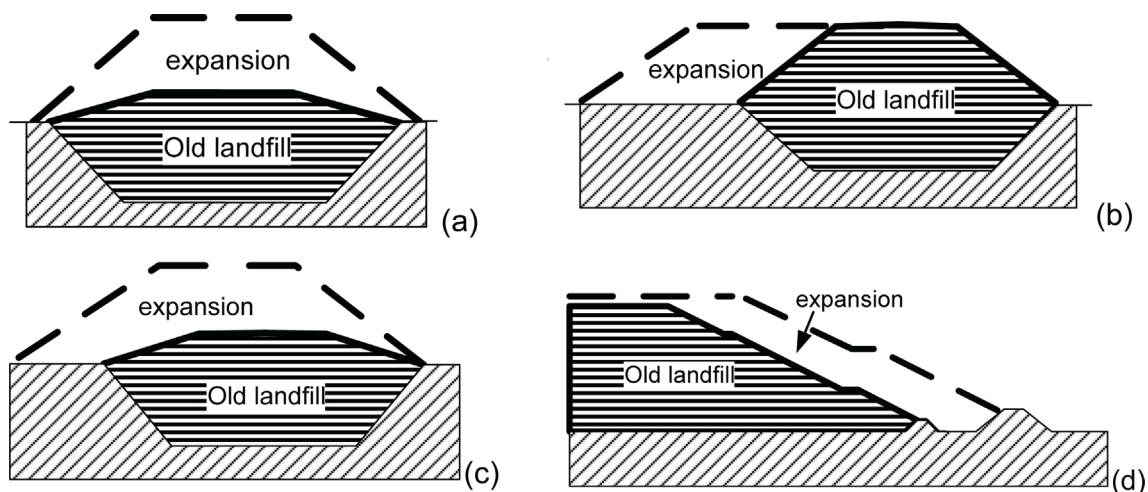


Figure 3. Geometric configurations in piggyback expansions: (a) vertical, (b) lateral, (c) mixed, and (d) veneer (Based on Qian *et al.*, 2001, Tano & Olivier, 2014, Bonaparte, 2018).

gas drainage from the old landfill and leachate drainage from the new one, and ensuring local and overall stability.

The least-desirable solution is the placement of the new landfill directly over the closed one, *i.e.*, without any new environmental protection layers. Bonaparte (2018) describes, in the 54th ASCE Karl Terzaghi Lecture, the forensic investigation carried out for a veneer piggyback sliding failure that occurred in 2011 at a MSW landfill located in the Eastern USA, designed by a third party. In this case, the slide was found to have occurred along the interface between the intermediate cover soil of the old landfill and the expansion, when the expansion achieved a height of 55 m supported on a lateral slope of the old landfill. The investigation also revealed that, at the time of failure, the waste placed in the expansion was very wet, due to leachate recirculation, introduction of municipal sludge, and rain-fall. In addition, the intermediate cover soil layer of the old landfill was found to have low hydraulic conductivity, thus, causing leachate to accumulate in the expansion. With leachate accumulation in an excessively wet landfill, gas drainage efficiency was greatly reduced. Liquid accumulation and high pore-water and gas pressures were the main factors leading to the expansion failure; ultimately, failure was due to the lack of a leachate drainage system that should have been installed between the new and old landfills, after, at least, partial removal of the intermediate cover soil.

The design considerations are well presented in Qian *et al.* (2001), and have been adequately addressed decades ago, as shown in Tieman *et al.* (1990), who described the first piggyback extension (mixed configuration) in 1987 at the Blydenburgh landfill in New York state. The knowledgeable design already included environmental protection layers and geogrid reinforcement equivalent to the current paradigm (*e.g.*, Tano *et al.*, 2015) (Figs. 4a and b). The role of the geogrid is to limit the deformation of other components, such as drainage system and the geomembrane,

amidst overall and differential settlements of the old cell. At Blydenburgh, for instance, the reinforcement was dimensioned for ensuring the integrity of the geomembrane liner under the conservative assumption of bridging a 2.4-m diameter cavity in the refuse beneath the expansion.

An additional concern with landfill expansions relates to the fact that often the new landfill is placed over an old unlined controlled dump. Contaminant hydrogeology studies are required to investigate the presence of underground contamination, as well as enable differentiating future contamination coming from the old or new landfills (*e.g.*, Brome-Missisquoi Landfill in Canada, Bouthot *et al.*, 2003).

2.2.2 Reinforcement of MSW

The concept of using high tensile strength, high stiffness geosynthetics, such as geogrids, to reinforce MSW slopes in landfills allowing higher and steeper MSW slopes appears natural given the accumulated experience with reinforced earth walls. Even though geogrids are used in veneer reinforcement of landfill cover soils, geogrids embedded directly in the MSW mass are not commonplace (Hettiarachchi & Ge, 2009).

In Brazil, landfills often receive high-organic content MSW, which may have lower shear strength than low organic MSW. Thus, reinforcement may help safely attain steeper slopes. A similar consideration applies to bioreactor landfills and landfills disposing shredded MSW, which exhibits lower interlocking, as a result of the shredding of the original MSW. Also, in the context of landfill mining, when re-landfilling the remaining waste after removing the usable MSW fractions, use of reinforcement may be interesting.

The embedment of geogrids in the waste mass requires consideration of durability issues, in particular the long-term environmental damage factor, which depends on the waste characteristics and the geosynthetic polymer. In

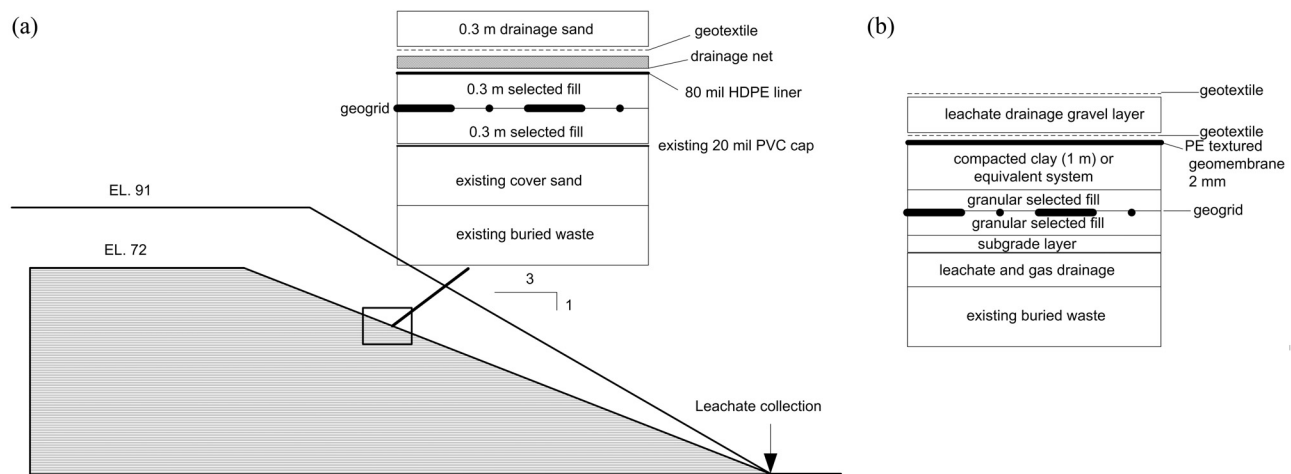


Figure 4. Geosynthetic and mineral layers to use for a piggyback expansion, (a) based on Tieman *et al.* (1990), and (b) based on Tano *et al.* (2015).

fresh MSW, temperatures may reach 50 to 70 °C, and leachate pH and chemicals may be aggressive. Other relevant concerns related to reinforcing MSW may include strain compatibility between geogrid and surrounding MSW, long-term interface strength amidst MSW degradation, effect of creep phenomena of both geogrid and MSW, mechanical damage during installation, and the aforementioned environmental concerns.

Carieri *et al.* (1999) describe one of the first times MSW reinforcement with geogrids was used, at the hillside landfill in Sesti Levante, Italy. The solution allowed the landfill storage capacity to be more than doubled, since the MSW slope increased, from gentler than 2H:1V to 1H:1V. The primary geogrids were horizontal layers spaced every 1.0 m in the vertical direction and with ultimate tensile strength of 400 kN/m (design strength = 157 kN/m). Lighter geogrids were placed near the face of the MSW slope. The selected geogrid materials were made of composite geosynthetic strips, with a core of high tenacity polyester (PET) tendons encased in a polyethylene (PE) sheath. The face of the reinforced-MSW slope was finished with a wrap-around method (Fig. 5), which included segments of 1-mm HDPE geomembrane.

Alexiew *et al.* (2015) discuss design concepts for reinforcing a 50-m rising of a hillside landfill receiving construction waste and IBA. The horizontal geogrids were considered for preventing a critical polygonal slip surface



Figure 5. Photograph from the hillside landfill in Sesti Levante, Italy (From Carieri *et al.*, 1999).

crossing the waste and emerging at the toe. The geogrids were made of high tenacity PET of ultimate tensile strength 1,600 kN/m at approximately 9 % strain.

Ma *et al.* (2019) present an approach allowing a 20-m vertical expansion at Xingfeng landfill in China (Fig. 6). The approach consisted of reinforcing an entire existing critical MSW slope before the expansion. The reinforcement was based on 33-m long HDPE geogrids at a vertical spacing of 1.0 m from the toe to the top of the slope. Thus, the project involved excavating the old MSW, and re-constructing the slope with the geogrid inclusions. At the face of the slope, geogrids were wrapped around geotextile gravel bags.

Bosco *et al.* (2020) performed limit-equilibrium and stress-strain analyses to verify the possibility of raising a landfill geometry based on reinforced soil dikes built in successive steps and geogrid reinforcement inside the MSW mass (Fig. 7), with the total landfill height reaching 48 m, after a number of successive stages of waste placement, each stage with 6.0 m in height. The soil dikes had a crest width of 5.0 m, slopes of 1H:1V, and were reinforced with geogrids; the mean slope of the landfill resulted equal to 1.8H:1V. The waste mass was reinforced with geogrids every 6.0 m (vertical distance), *i.e.*, every construction stage.

The analyses were performed considering adopted soil and MSW parameters, both for limit-equilibrium and stress-strain analyses. Also, ranges for the pore pressures due to leachate and gas generation within the MSW were varied. The geogrids in the soil dikes were assumed to have a tensile strength of 100 kN/m. The geogrids in the MSW were assumed to have 400 kN/m of maximum tensile strength, placed every 6.0 m, and anchored at both ends. Considering a safety factor of 1.5 and the geometry and parameters adopted in the study, the use of geogrid reinforcement allowed the landfill height to be increased from 10-15 m to 30-45 m, these ranges depending on the pore-pressure ratios, r_u , considered. The concept of reinforcing the MSW with geogrids in landfills may be considered relevant in the future, due to the need to increase capacity. However, impact on the operation of the landfill is expected. Not only technical, but also operational aspects must be taken into consideration, such as interference of the geogrids on the geometry of the landfill cells.

3. Site remediation

3.1 Overview

Remediation is generally defined as the process of restoring land that has been contaminated. Shackelford & Jefferis (2000) point out that, although the words 'remediation' and 'reclamation' often are used interchangeably in terms of environmental contamination, arguably the words have slightly different meanings: the goal of reclamation may be inferred as reuse of the land, whereas the

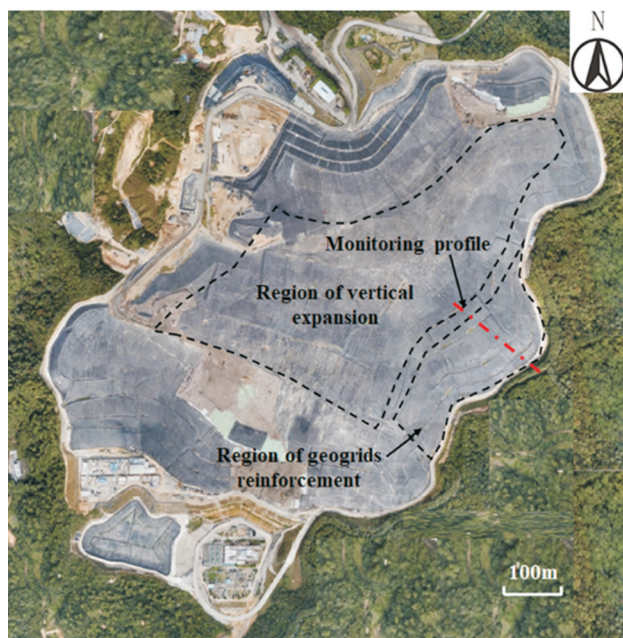


Figure 6. Region of vertical expansion and reinforced slope at Xingfeng landfill (From Ma *et al.*, 2019).

goal of remediation may be inferred as a process to prevent or minimize a real or perceived risk of harm to humans. However, there are many situations where reclamation involves remediation, and remediation is often related to new uses of the land.

Site remediation engineering knowingly must be based on a sound site conceptual model, which includes characterization of pollutants, source zones, spatial distributions and phases (solids, water, gas) involved, hydrogeological and geochemical characterization of the physical medium, flow and transport modeling, and risk analyses defining pollutant target concentrations. Not so conspicuous, on the other hand, is the need for geotechnical characterization of the site, which must be added to all this knowledge, to properly select and dimension the remediation system. Site monitoring, finally, allows adjustments to be made to remediation operation, as well as site closure.

3.1.1 Management of contaminated sites (CETESB)

The Environmental Agency of São Paulo state (CETESB), which is a reference for the whole country, classifies registered contaminated sites, according to Decree 59,263/2013, as contaminated site under investigation, contaminated site with confirmed risk, contaminated site under remediation, contaminated site under process of reutilization (new use for the site after elimination or reduction of risk to acceptable levels), site under monitoring for closure (site where risk was not confirmed, or site where remediation targets were achieved but are still under monitoring to verify maintenance of concentrations at acceptable levels), and site rehabilitated for declared use. Last

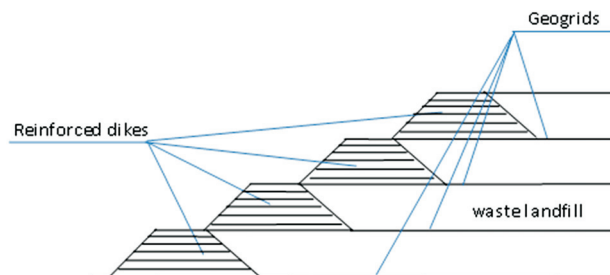


Figure 7. First four stages of construction in the reinforced landfill configuration proposed in Bosco *et al.* (2020).

year, the number of rehabilitated sites (1,775) increased remarkably (23 %) as compared to 2018 (1,441) (Fig. 8). Adding the sites under monitoring for closure (1,375), half of the registered sites are no longer classified as contaminated (Table 1).

Considering sites under remediation and sites where remediation was completed (3,710), the mostly employed remediation techniques for the treatment of subterranean water (saturated zone) were multiphase extraction, pump-and-treat and free phase recovery, while removal (excavation) and vapor extraction were mostly used for soils (unsaturated zone), as shown in Fig. 9.

In addition, among the rehabilitated sites, a total of 942 sites are being reused, or reutilization is planned. This information is relevant to show the trend of changing the use of industrial sites, now usually destined to the construction of commercial and residential real estate developments, or even construction of parks and leisure areas. This trend is bringing forth the revitalization of former industrial areas, mainly in the metropolitan region of São Paulo. Decree 59,263/2013, that regulated Law 13,577/2009, established that reutilization of rehabilitated sites, as well as the revitalization of regions, must be encouraged by government.

The main groups of contaminants in the registered sites reflect the influence of the activity of distribution of automotive fuels: aromatic solvents (benzene, toluene, ethylbenzene and xylene), Polycyclic Aromatic Hydrocarbons (PAHs) and total petroleum hydrocarbons (TPH). Following, metals and halogenated organic compounds are also frequently found, according to Fig. 10.

Automotive fuels and halogenated organic compounds are scarcely water-miscible liquids, or non-aqueous phase liquids (NAPLs). The higher solubility compounds, also toxic, and often carcinogenic (*e.g.*, in automotive fuels: benzene, toluene, ethylbenzene, xylene, naphthalene) form a considerable groundwater plume that can migrate in the direction of groundwater flow. Halogenated organic compounds are some of the most recalcitrant pollutants in sites and present low to moderate solubilities, high volatilities, low to moderate soil partition coefficients, high mobility, and densities greater than water.

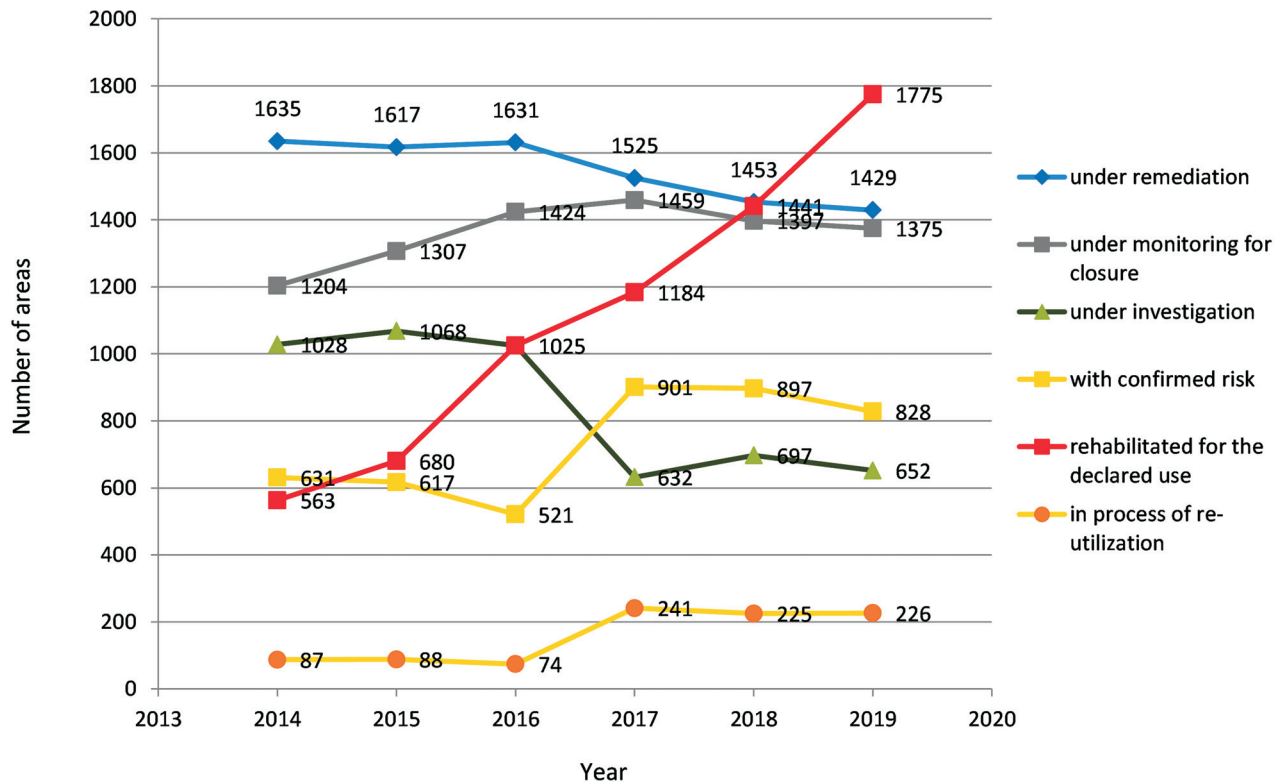


Figure 8. Time evolution of registered contaminated sites in São Paulo state by category (Based on CETESB, 2019).

3.1.2 Geotechnical confinement

Interestingly, in Brazil, differently from many other countries (*e.g.*, USA, Canada, Japan and EU countries), geotechnical confinement is practically never used as a rehabilitation solution. Geotechnical confinement may be achieved by impermeable vertical barriers (trenches or diaphragm walls with different fillings such as soil-bentonite and cement-bentonite, geomembrane panels, jet-grouting, sheet pile curtains), impermeable covers and, in some cases, also a bottom impermeabilization. The goal is to isolate

the contaminated soil or buried waste, avoiding release of contaminants to the environment and contact with living beings. The solution is acceptable when the extension or volume of soil to be treated is very large, when there is a mixture of different pollutants that would require an association of different remediation techniques (this is not rare in remediation projects, but there is a practical limitation to the number of concurrent techniques in the field), or the current available techniques are still not efficient for the pollutants found at the site.

The risk is minimized by limiting the release of contaminants (liquids and/or gases) to groundwater, surrounding subsoil or the atmosphere to acceptable levels. However, there still is in Brazil the perception that pollution is being “buried” or “hidden from the public”. Also, passive reactive barriers are seldom used (excavated permeable curtains through which groundwater flows and is treated by the filling material). There is still much more reliance on pump-and-treat or injection of reagents, even when these techniques are inadequate for subsoils with low permeability, preferential flow channeling and specific adsorption of contaminants, which are not uncommon in tropical subsoil profiles. These techniques may not deliver the reagent to the desired targets or demand a long time for remediation, and may not be environmentally sustainable when operational (*e.g.*, energy for pumping or injecting) and social (hindrance of use of the area) costs are taken into consideration.

Table 1. Occurrence numbers and percentages by category of registered contaminated sites in São Paulo state (CETESB, 2019).

Classification	Number of areas	Percentage (%)
Area under investigation	652	10
Contaminated area with confirmed risk	828	13
Contaminated area under remediation	1,429	23
Contaminated area under monitoring for closure	1,375	22
Contaminated area rehabilitated for declared use	1,775	28
Contaminated area under process of reutilization	226	4

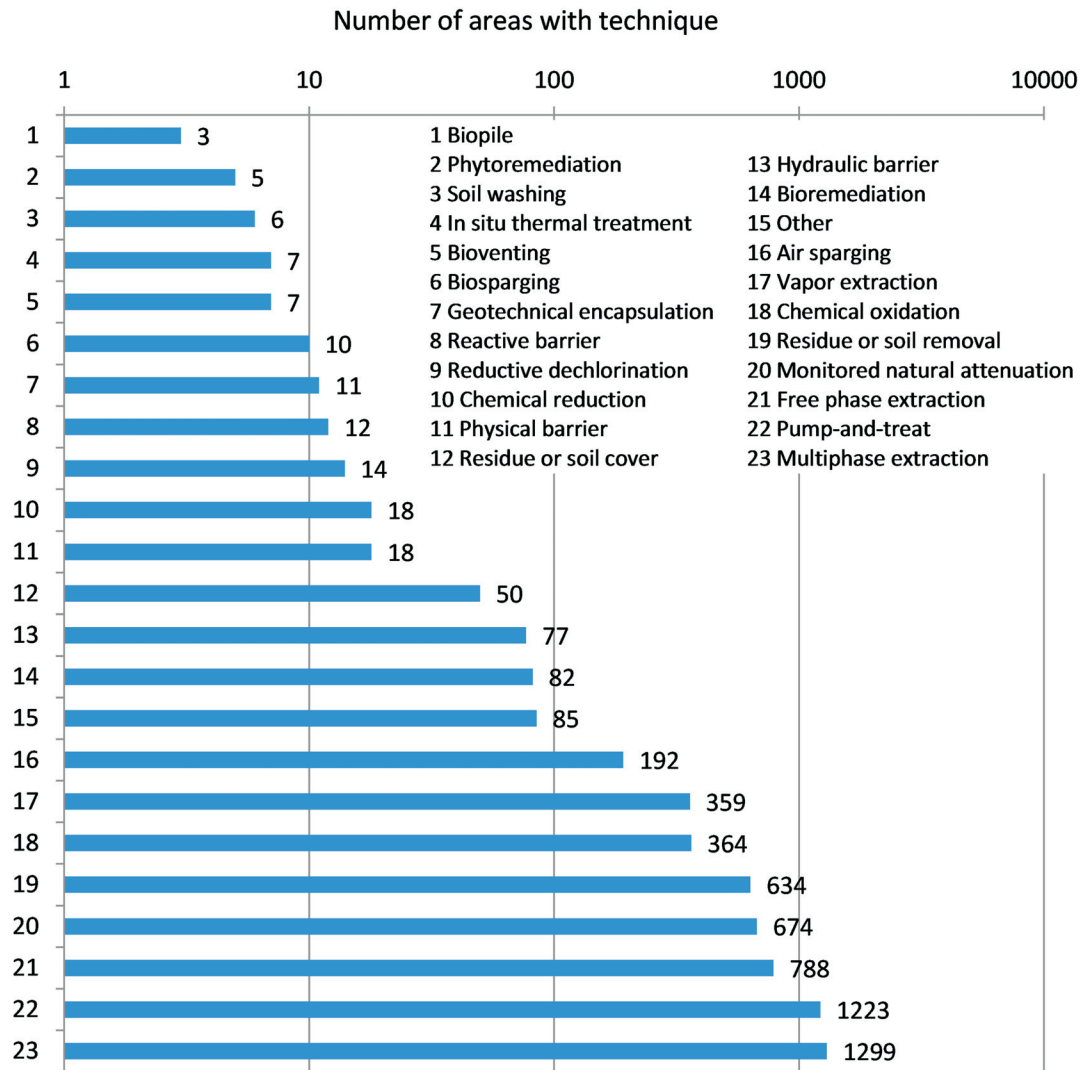


Figure 9. Occurrence (number of implementations) of each remediation technique (Based on CETESB, 2019).

Remediation time can be long and usually measured in decades (Stroo & Ward, 2010). This finding should stimulate the use and improvement of confinement techniques and monitored natural attenuation. While the former has not been internalized as a trustworthy rehabilitation technique by Brazilian professionals, the latter has been increasingly used (674 out of 3,710 sites, Fig. 9). Conferences on Environmental Geotechnics usually bring new research and practical aspects of geotechnical confinement, while CETESB's list of contaminated sites shows only 11 cases of geotechnical confinement out of 3,710 treated areas.

Another particularity of remediation of contaminated sites in Brazil, which probably helps understand the aforementioned trends, is that remediation design often underutilizes Geotechnical knowledge on local soils. Also, improvement or development of techniques for the unsaturated zone, which may be thick in tropical climates and

tain a significant portion of the contamination, is very restricted except for gas-phase pollutants.

Technical developments are necessary and constantly under way in the area of remediation, although other aspects also have to be addressed, such as public perception (as mentioned) and problems related to complex urban areas, as will be exemplified by the case study.

3.2 Complex urban areas

Contaminated areas under investigation and remediation become more complex when located in urban regions with industrial past and recent change of land use. The conceptual model for site contamination must consider the regional scale, rather than be restricted to the study area. However, the involvement of all stakeholders for a joint regional plan for investigation and remediation is rarely brought about by the environmental agencies.

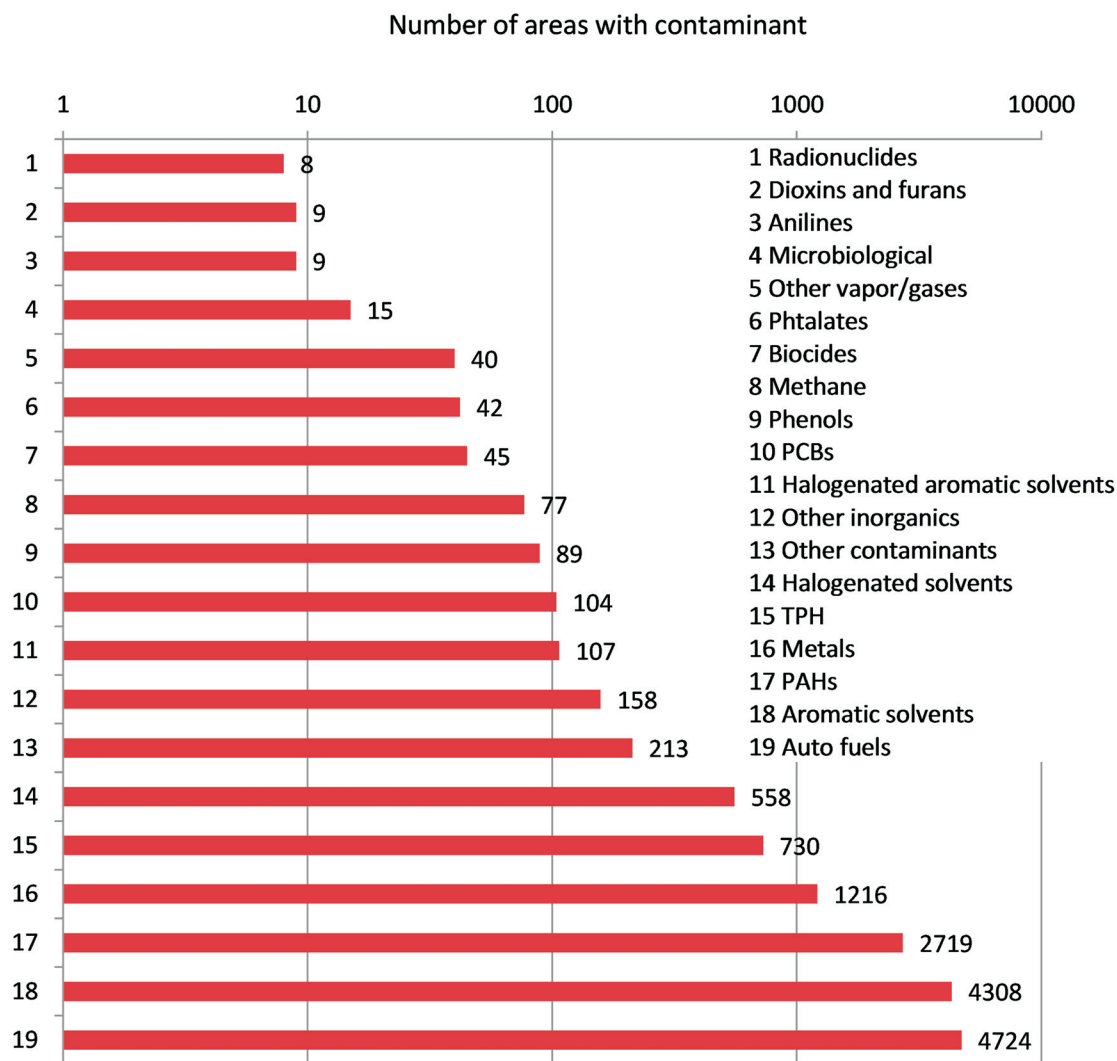


Figure 10. Occurrence of contaminant groups in contaminated areas (Based on CETESB, 2019).

3.2.1 Industrial site case study in São Paulo (Caram, 2019; Caram & Boscov, 2019)

The case study refers to an old industrial area in the north part of the city of São Paulo, where an automobile industry operated in the 1950s and 1960s (before the existence of CETESB, created in 1968), and a construction deposit from 2001 to 2008. The area is located in a district historically marked by hosting a number of heavy industries.

At the site, the main groundwater contaminant was VC (vinyl chloride). Collected soil samples showed that halogenated organic compounds were not present in the soil matrix. During excavation works, two masonry oil tanks were discovered near the northwest boundary of the area. The tanks were removed in 2009, and the whole area was covered with a compacted-soil layer. Subsequently, investigation of groundwater plumes started. Hot spots detected upstream of the area could not be related to the oil tanks. Since the CETESB process began, five study cam-

paigns were carried out, the area has been investigated with 86 monitoring wells reaching different depths (4 to 30 m), however still the plumes could not be totally defined.

The region is located over the Tertiary sediments of the São Paulo Basin and modern alluvial deposits. The stratigraphic profile indicated a top layer of 3 to 5 m of a clayey fill overlying alternating plastic clay, sandy clay and fine sand layers down to the depth of 15 m. The water table was found at a depth of 4 m. Groundwater flow directions are mainly northwest, north and northeast in shallow (6-m deep) and intermediate (9-m deep) monitoring wells. The potentiometric levels in the area agree with the regional groundwater flow pattern, which was oriented to northwest, discharging into River Tamanduateí. Slug tests, based on U.S. EPA standard, were performed in seven multilevel monitoring wells, to yield hydraulic conductivity values. The geometric means of conductivity values were 6.6×10^{-5} m/s (shallow range), 1.2×10^{-3} m/s (intermediate range,

from 7 to 9 m) and 2.6×10^{-5} m/s (deep range). Thus, the more conductive layer was located between 7 and 9 m.

3.2.1.1 The contaminant

Vinyl Chloride (VC) poses high human toxicity and is known to be a human carcinogen. VC does not occur naturally, and anthropogenic sources are related to PVC production or formation by degradation of organochlorides (WHO, 1999). In this case, there was no nearby production of PVC. Under anaerobic conditions, VC is formed by the reduction of chloroethylenes - PCE, TCE and dichloroethylene isomers (cis-1,2-DCE, trans-1,2-DCE and 1,1-DCE) - and under aerobic conditions by a direct or co-metabolic oxidation of DCE. Since PCE and TCE are the chlorinated solvents used in industry, and VC is a product of the slow natural degradation of PCE and TCE, the predominance of VC at the site indicates that the contamination is old. VC can be released to the environment through air, water or soil, however VC is most commonly found in air and groundwater. VC solubility in water is relatively low but can be raised by the presence of salts. When released to air, VC is expected to exist almost exclusively in the vapor phase, but VC half-life in air is limited by reaction with OH radicals photochemically produced (WHO, 1999). Volatilization is a significant transport mechanism and the risk assessment indicated vapor inhalation as the major exposure pathway.

3.2.1.2 Remediation technique

The remediation system adopted for the area was installed in early 2015 and operated continuously for 2.5 years. The system comprised 31 vapor extraction wells (in the vadose zone, above the water table) and 33 ozone injection wells in the saturated zone, in a technique known as ozone sparging. Also, several monitoring wells were included for control.

Ozone sparging attacks VC through oxidation and volatilization, and the vapor extraction system recuperates the volatilized contaminant mass. Ozone can also dissolve in the aqueous phase and react with the organic compounds in water (Henry & Warner, 2002). Therefore, ozone would also oxidize VC in the dissolved phase.

The selection of ozone sparging for remediating the VC plume may be justified by the combined effects of gas-phase extraction and *in situ* oxidation by ozone. In particular, vapor extraction is applicable when the contaminant has vapor pressure higher than 1.0 mmHg (20 °C) and

Henry's law constant higher than $0.001 \text{ atm} \times \text{m}^3/\text{mol}$. As revealed by the parameters for VC in Table 2, favorable strippability and volatility are expected. In terms of oxidation-reduction state, VC is the most reduced compound amongst the chlorinated compounds, thus prone to oxidation. Also, VC has a low adsorption coefficient, indicating a small tendency to remain retained in the soil. Comparing the parameters for VC with the general guidelines in Table 3 (U.S. EPA), the contaminant may be considered very weakly sorbed (water-soil organic carbon partitioning coefficient, $K_{oc} < 10$), with high mobility in the aqueous phase, and high volatility (Table 3).

Ideal conditions for the application of gas sparging in the field occur when the soil layer is a homogenous coarse-grained material, with a saturated hydraulic conductivity on the order of 10^{-5} m/s. The injection of gas beneath the water table inevitably causes mounding of the phreatic level and may laterally spread contaminated groundwater. Complex hydrogeologic and contaminant-distribution settings may be challenging; the occurrence of low-permeability clay lenses, or very high permeability layers, above the point of gas injection may further spread the contamination plume. The subsoil heterogeneity causes preferential gas flow, such that the contaminant outside the preferential flow is poorly exposed to the reagent gas. Air channeling may occur, short circuiting the path of gas between the injection point and a monitoring well, as shown in Fig. 11.

In addition, as for any contaminant-extraction technique, gas sparging is challenged by the existence of contaminant mass stored in the free phase and in immobile compartments, such as the residual pure liquid phase, the adsorbed phase and contaminant diffused into low-permeability layers, prone to reverse matrix diffusion. The complexity of mass transfer among vapor, aqueous, free (NAPL) and sorbed phases in a subsoil composed of transmissive and low permeability zones has been discussed by Vanderkooy *et al.* (2014), which presented a compartment model of mass transfer of organochlorides.

3.2.1.3 Monitoring and plumes

Several monitoring wells reaching different depths were used for the investigation of contaminant levels in groundwater and for measuring geochemical parameters. The physical-chemical parameters indicate whether the oxidant was reaching the subsoil layers in the whole area, while VC concentrations showed whether ozone degraded VC in the subsoil. Before the remediation, the following

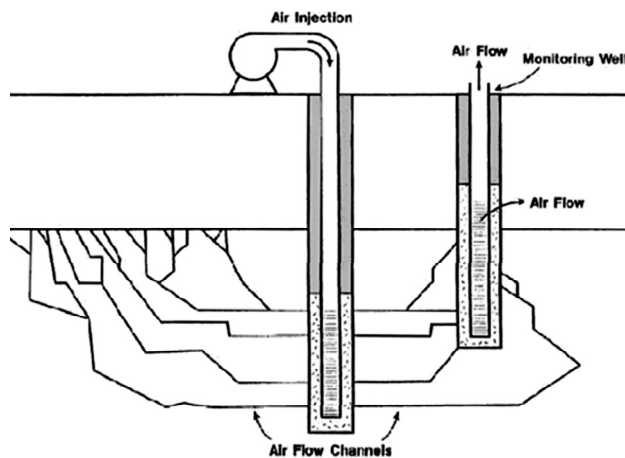
Table 2. Phase-partitioning and other parameters for vinyl chloride (Based on Suthersam, 1999; CETESB, 2016).

	Molecular weight (g/mol)	Henry's law constant ($\text{atm} \times \text{m}^3/\text{mol}$)	Vapor pressure (mmHg)	Solubility (mg/L) (25 °C)	K_{oc} (mL/g)	U.S. MCL /CETESB 2016 (mg/L)
VC	62.5	2.78	2,660 (25 °C)	1,100	2.5	0.002/0.002

K_{oc} = organic carbon partitioning coefficient; MCL = maximum contaminant level.

Table 3. Physical-chemical parameter ranges and classification according to sorption, mobility and volatility for organic compounds (U.S. EPA, 1997).

Property	Range	Description
Sorption Soil adsorption coefficient, K_{oc} (mL/g)	< 10	Very weakly sorbed
	10-100	Weakly sorbed
	100-1,000	Moderately sorbed
	1,000-10,000	Moderately to strongly sorbed
	10,000-100,000	Strongly sorbed
	$> 100,000$	Very strongly sorbed
Mobility Based on a combination of solubility (S) (mg/L) and soil adsorption (K_{oc})	$S > 3,500$ and $K_{oc} < 50$	Very high mobility
	$850 < S < 3,500$, and $50 < K_{oc} < 500$	High mobility
	$150 < S < 850$, and $150 < K_{oc} < 2,000$	Moderate mobility
	$15 < S < 150$, and $500 < K_{oc} < 20,000$	Low mobility
	$0.2 < S < 15$, and $2,000 < K_{oc} < 20,000$	Slight mobility
	$S < 0.2$, and $K_{oc} > 20,000$	Immobile
Volatility Henry's law constant (H), atm m ³ /mol	$H < 3 \times 10^{-7}$	Nonvolatile
	$3 \times 10^{-7} < H < 10^{-5}$	Low volatility
	$10^{-6} < H < 10^{-3}$	Moderate volatility
	$H > 10^{-3}$	High volatility

**Figure 11.** Illustration of gas channeling to a monitoring well (U.S. EPA, 1997).

were the average geochemical parameters for the intermediate level: *ORP* (oxidation/reduction potential) = -110 mV, *DO* (dissolved oxygen) = 0.48 mg/L, and *EC* (electrical conductivity) = 577 μ S/cm. After 16 months of remediation, the parameters were measured, respectively, as 103.5 mV, 0.63 mg/L and 326.4 μ S/cm. The variation of parameters along time and the final values indicate that the oxidant (ozone) reached subsurface in desired depths, since there was a general increase in *ORP* and *DO*, and a reduction in *EC* in the groundwater. As expected, the intermediate level presented the highest VC concentrations, which can be explained based on hydraulic conductivity.

The VC plumes obtained before remediation and for the five campaigns at the intermediate level are shown in Fig. 12a to f. Also, Fig. 13 presents the dissolved-phase mass of VC, calculated based on the monitored plumes, as a function of the monitoring time.

Figure 12 shows an initial decrease in VC concentrations and plume width (Aug. and Nov. 2015), probably in response to remediation, followed by a substantial increase in VC concentrations (Feb. and May 2016) with new hot-spots, and again a decrease of VC concentrations with time (Aug. 2016). However, there was no guarantee that concentrations would not rise again. Additional VC mass, originated from the upstream area or VC transfer among subsoil phases, apparently is being carried by water flow in the downstream direction. Before remediation, the VC plume showed high concentrations (*i.e.*, average of 5.3 mg/L, maximum of 37.3 mg/L) and was located near the SE border and outside the study area. The location and behavior of the plume raised important concerns. Large portions of the VC plume located outside the area of interest, and the contaminant possibly migrating from upstream adjacent areas, indicated the need to study groundwater contamination at the regional scale. For instance, the original industrial plant may have been divided, such that the location of the source is outside the study area.

3.2.1.4 Discussion

The results from the case study bring some points to be considered:

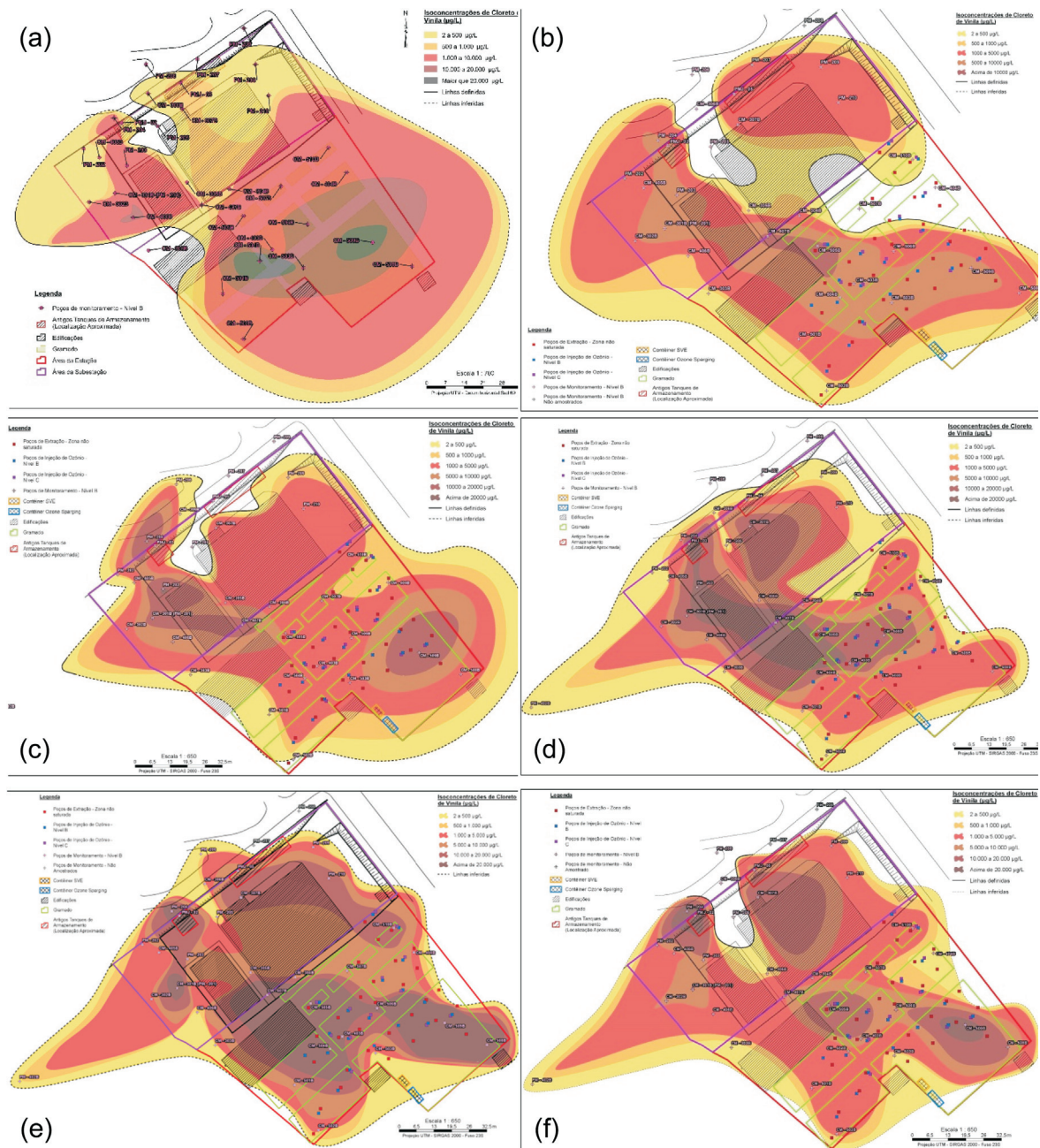


Figure 12. VC plumes at the intermediate level wells: a) 2014; b) Aug/2015; c) Nov/2015; d) Feb/2016; e) May/2016; and f) Aug/2016 (Caram & Boscov, 2019).

(1) The physical-chemical parameters at the control points indicated that ozone reached the depths where the contaminant was present throughout the area, however VC concentrations did not decrease effectively along time. Two explanations are more likely: continuous contribution of upstream contamination and mass transfer between phases. Ozone sparging can volatilize VC dissolved in the pore water and induce back diffusion from the low permeability layers, so that additional VC mass is brought to the dissolved plume. The conceptual site model did not primarily consider

the importance of the presence of alternating soil layers with different hydraulic conductivities and should be reviewed. Unintentional VC mass transfer from groundwater to the vadose zone by the ozone sparging into the subsurface should also be considered (Chong & Mayer, 2017). VC concentrations in the vapor phase in the vadose zone should also be investigated. VC contribution from neighboring areas is also a plausible hypothesis. The primary sources may be located upstream, external to the studied area, but still feeding and contributing to the dissolved phase plumes.

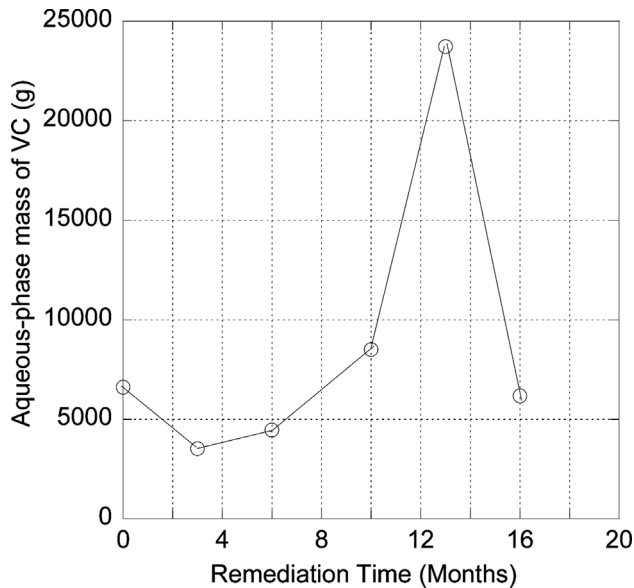


Figure 13. VC dissolved mass vs. time (Based on Caram & Boscov, 2019).

- (2) The results and consideration lead to the conclusion that a joint regional plan for investigation and remediation is essential for urban complex regions with past industrial land use and recent change of land use. The difficulties to assess a conceptual model for site contamination based on a restricted part of the potentially contaminated region often result in long-term disputes or legal action between relevant stakeholders. Remediation/containment actions at individual areas can be expensive and long-term, representing a cost to society in energy, inputs, and land use itself.
- (3) The risk assessment is based on receptors. In this case, similarly to other central and densely built urban areas with complete sanitary infrastructure, the contact of living beings with subterranean water is not a hy-

pothesis. However, contaminated groundwater not susceptible to reach or be used by human beings may still contaminate water bodies. The very polluted and unusable rivers in the city of São Paulo are expected to undergo clean-up and rehabilitation in the coming decade, therefore remediation targets will have to be reviewed. This calls for remediation techniques that confine contamination or treat contamination in a new scenario.

- (4) The three former points would benefit from Geotechnical expertise that should be ever more used in this field. An example of alternative or complementary measures in this case study follows to make this point.

3.2.2 Other possible techniques at the industrial site

The location of the original plume relative to the groundwater flow pattern indicated that contamination was likely to come from outside the study area. Also, monitoring results, *i.e.*, dissolved-phase VC concentrations vs. time, indicated concentration increase with time since the start of remediation.

An important measure to be implemented at the site is the construction of containment barriers to isolate the area from the inflow of pollutants from upstream neighbors. A viable option would be to build a soil-bentonite cut-off wall along the southeast boundary, also extending to the sides, provided that local soils are adequate for backfilling. As shown in Fig. 14, this classic cut-off wall is built by excavating a trench with a backhoe (maximum depth ~ 10 m) or clamshell (maximum depth ~30 m), using bentonite or polymer slurry for temporary support and to form a filter cake, and backfilling the trench with a mixture of local soils and bentonite (~3-5 % dry weight). Soil-cement, soil-bentonite or soil-cement-bentonite mixtures are possible backfilling alternatives. An important consideration is the resulting hydraulic conductivity of the soil-bentonite back-

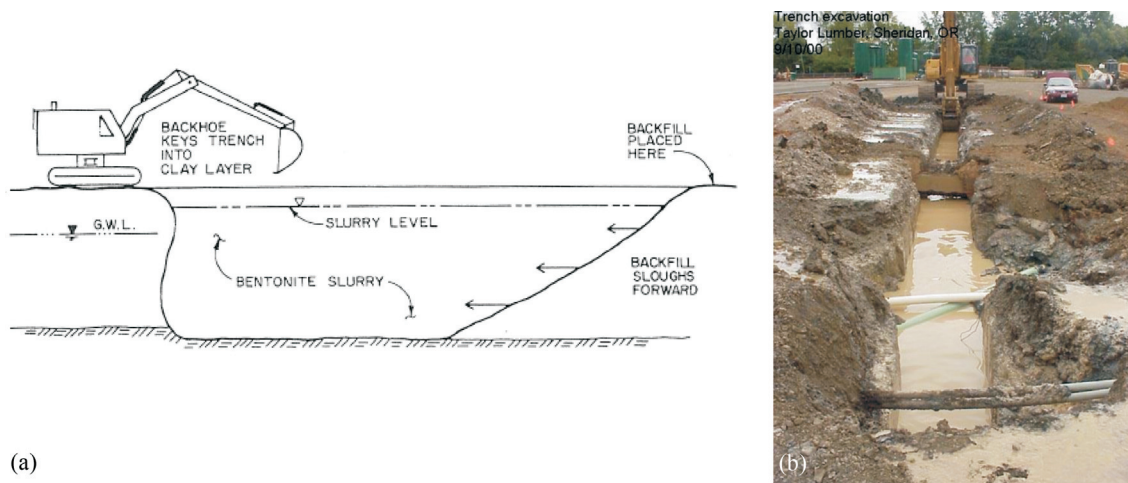


Figure 14. Soil-bentonite cut-off wall, (a) construction method schematic (Ryan, 1987), and (b) photograph during construction (From McKnight & Owaidat, 2001).

fill, which must be lower than 1×10^{-9} m/s, requiring the testing of mixtures of the available soils with different dosages of bentonite, to choose an adequate backfill, as shown in the classical work by D'Appolonia (1980), and described in Benson & Dwyer (2006). This is a low-permeability curtain to physically block the inflow of contaminated groundwater into the site.

The performance of the soil-bentonite barrier is due to the high swelling ability of the bentonite in water, which results in low hydraulic conductivity. Saline solutions and organic compounds cause a permeability increase due to chemical incompatibility with bentonite, as extensively studied for geosynthetic clay liners (*e.g.*, Shackelford *et al.*, 2000). Different polymer modified bentonites, multiswellable bentonite and HYPER clay have been developed to improve the chemical resistance in aggressive environments (*e.g.*, De Camillis *et al.*, 2019).

Another possibility would be to build one or more permeable reactive barriers (PRBs) in the area, to intercept the outside contaminant inflow, as well as promote chemical and/or biological destruction of contaminants within the site. PRBs are critically affected by (1) hydraulic performance (contaminants are routed through the reactive medium with an appropriate residence time, and should not bypass the medium), and (2) chemical/biological performance (contaminants are involved in reactions when in contact with the medium, and concentration goals must be achieved downgradient from the barrier) (Naidu & Birke, 2015). The classical continuous-trench PRB is built by the supported excavation of a trench (without bentonite), filled with a mixture of gravel, sand and reactive materials (Fig. 15).

The performance of a continuous-trench PRB may be significantly affected by flow channeling due to aquifer heterogeneity and complexity in the hydraulic conductivity (*k*) structure of the medium (*e.g.*, Hemsí & Shackelford,



Figure 15. Filling of a supported trench with a mixture containing ZVI (zero-valent iron) for building a continuous-trench PRB (From ITRC, 2011).

2006). Preferential pathways of flow and contaminant transport expose the PRB to spatially variable groundwater seepage velocities (*v*). Where contaminant residence times are shorter, the PRB effluent concentrations may locally surpass the prescribed limit. Results from numerical modeling of reactive multi-component transport in heterogeneous aquifers generated with geostatistical methods are exemplified in Fig. 16.

A classical alternative to the continuous-trench configuration is the so-called funnel-and-gate. The groundwater flow is directed to the permeable reactive “gate” by insertion of impermeable barriers in the subsoil (Gavaskar *et al.*, 1998, Naidu & Birke, 2015). An interesting case of a funnel-and-gate PRB in Brazil to treat mercury contaminated water was designed by Nobre *et al.* (2006), presented in Fig. 17.

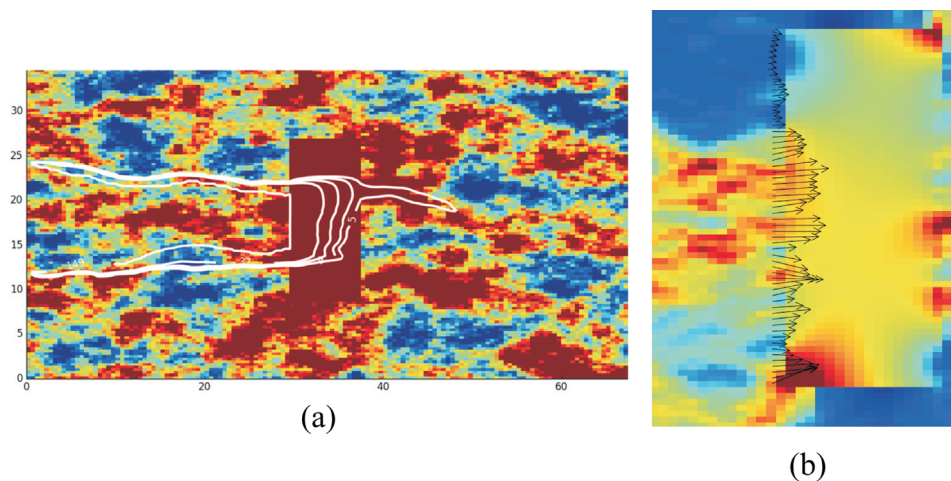


Figure 16. Plan views of (a) contaminant transport through a PRB with a formed effluent plume (5 mg/L) due to flow channeling (red: high *k* and blue: low *k*), and (b) seepage velocities map and vector representation of seepage velocities at the influent side of a PRB (red: high *v* and blue: low *v*) (Machado & Hemsí, 2016).

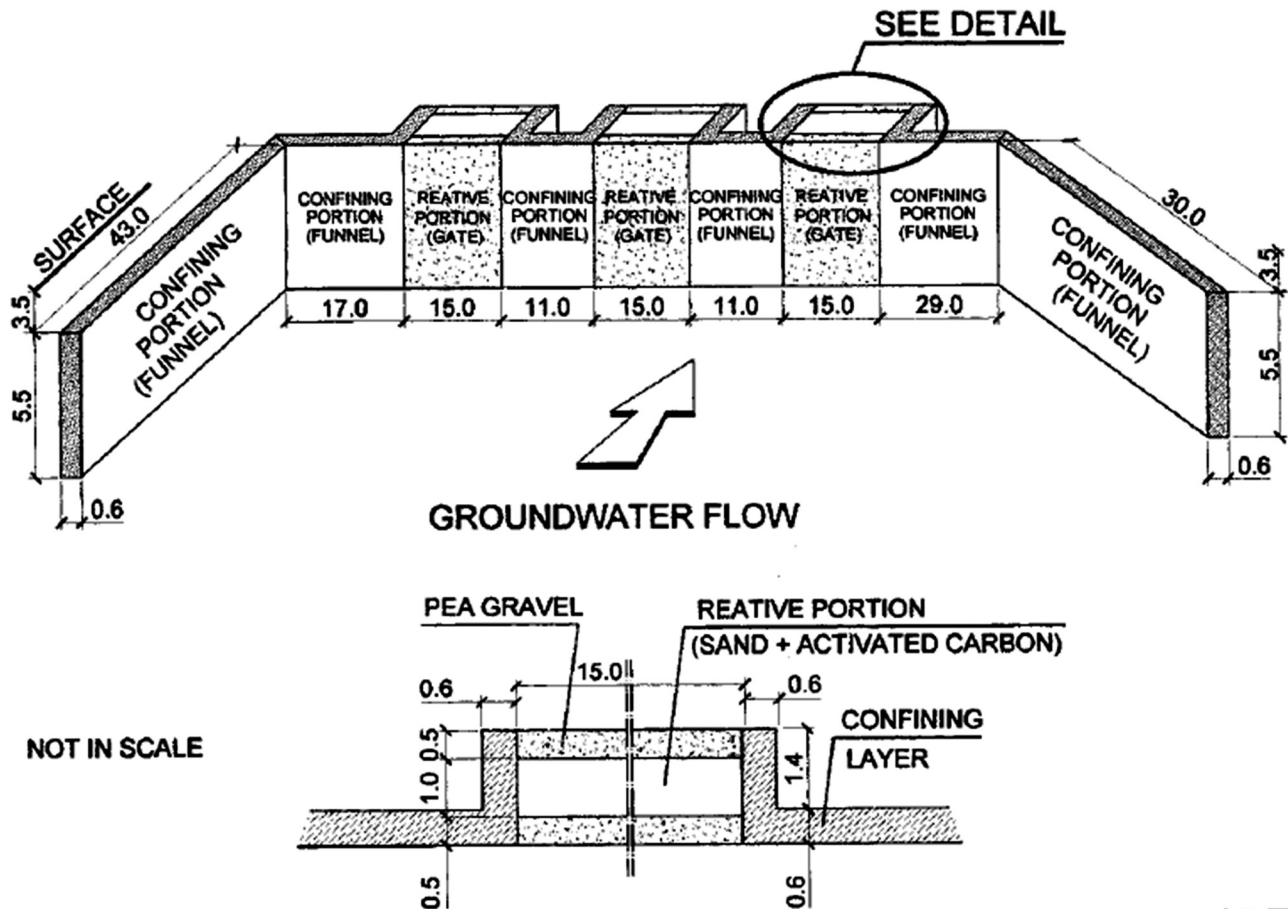


Figure 17. Funnel-and-gate PRB to treat mercury contaminated groundwater (Nobre *et al.*, 2006).

Several classes of reactive materials have been tested, as well as used in full-scale implementations, aiming at different groundwater contaminants (Table 4). From the first PRBs used for dechlorination of halogenated compounds by zero-valent iron (ZVI) (Gillham & O'Hannesin, 1994, Di Molfetta & Sethi, 2003), there has been significant innovation in the reactive materials used, including biobarriers, combination of organic materials and ZVI, and nano-scale ZVI, among others. Biobarriers contain organic materials as the major reactive component. Several organic materials have been tested, both for organic contaminant compounds and metals in acid mine drainage. For example, Mattos *et al.* (2014) and Trindade *et al.* (2018) performed tests on the use of sugarcane bagasse for removing metals and sulfate from synthetic acid mine drainage solutions. Trindade *et al.* (2018) performed column tests (triplicate) for precipitating nickel and zinc under the anaerobic (sulfate reducing) conditions that may occur in an organic PRB. The organic reactive medium used was sugarcane bagasse. The results indicated satisfactory rates of sulfate reduction and metals precipitation. Assumpção *et al.* (2020) performed batch-equilibrium tests to remove dissolved nickel using a biogenic-apatite char. The results for the fine-grained char were very satisfactory and suggested the Ni removal mechanism

to be Ni substitution for Ca in the structure of the hydroxy-apatite.

Alternative configurations include vertical-flow reactors that can be filled with different reactive media, such as adsorbents, organic materials, ZVI, etc. Such configuration was used in two PRBs in the UK. The Belfast PRB described by Birke *et al.* (2007) used a reactor consisting of a 12-m height by 1.2-m diameter steel reactor filled with ZVI (Fig. 18). Cox *et al.* (2009) describe the funnel-and-gate

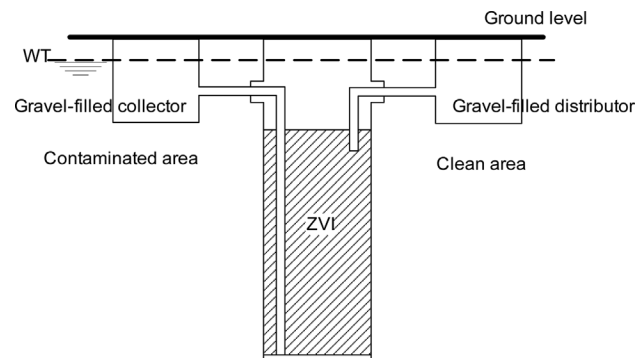


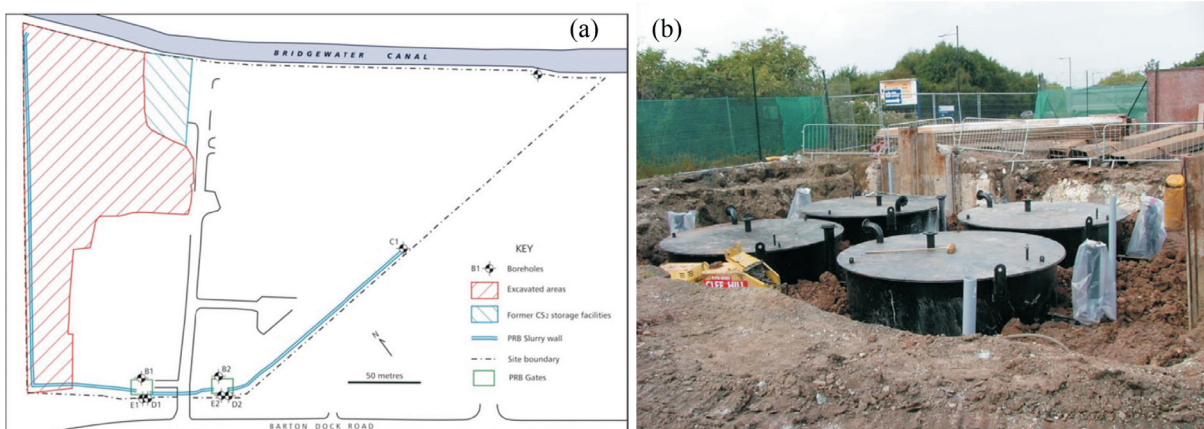
Figure 18. Passive treatment achieved by groundwater flow through steel reactor filled with ZVI (Birke *et al.*, 2007).

Table 4. Classes of contaminants treated and types of reactive media used in PRBs. Symbols: F: full-scale application, L: laboratory evaluation, and P: pilot-scale application (From ITRC, 2011).

Contaminant	ZVI	Biobarriers	Apatite	Zeolite	Slag	ZVI-carbon combinations	Organophilic clay
Chlorinated ethenes, ethanes	F	F			L	F	
Chlorinated methanes, propanes						F	
Chlorinated pesticides						P	
Freons						L	
Nitrobenzene	P						
Benzene, toluene, ethylbenzene, xylenes (BTEX)		F					
Polycyclic aromatic hydrocarbons (PAH)							L
Energetics	P	F				P	
Perchlorate		F	F	L		L	
NAPL							F
Creosote							F
Cation Metals (<i>e.g.</i> , Cu, Ni, Zn)	L	F	F		L	F	
Arsenic	F			L	F	F	
Chromium VI	F			L	L	F	
Uranium	F	P	F			T	
Strontium-90			F	F			
Selenium	L					L	
Phosphate					P		
Nitrate		F	F			F	
Ammonium				L			
Sulfate		F				L	
Methyl tertiary butyl ether (MTBE)		F					

adopted at a site in Manchester, comprising long cement bentonite slurry walls and two reactive gates, as indicated in Fig. 19a. Each individual gate consisted of two parallel treatment trains. Each treatment train consisted of two in-line reactor vessels (Fig. 19b), with the inlet reactor vessel having

downward flow and the outlet reactor vessel having upward flow. The reactors were prefabricated steel vessels of 5 m height by 3 m diameter. Since one treatment train could be taken off-line for maintenance, this allowed for future exchange of the reactive medium, when necessary.

**Figure 19.** Reactor PRB described in Cox *et al.* (2009), (a) location of the slurry walls and gates, and (b) photograph of reactors.

4. Geotechnical reuse of waste

4.1 Overview

The use of waste and recycled materials in Geotechnical Engineering, differently from pavement and buildings construction, is still mostly limited to academic studies. Examples of reuse of shredded tires, foundry sand and fly ash are described in Aydilek & Wartman (2005). The suitability of different types of wastes as geomaterials has also been investigated: construction and demolition waste, mine tailings (sand, red mud, phosphogypsum), sewage and water treatment sludge, tires, sugarcane bagasse, coconut fibers, rice husk, coal ash, MSW IBA, fly ash, rock powder, PET bottles, crushed glass, etc.

The main technical challenges facing waste reuse for geotechnical purposes are dealing with variability and obtaining representative samples, and adapting the geomechanical models of behavior to the new materials. Once the waste is considered suitable as a geomaterial, additional tests must be conducted, in accordance with the foreseen application, in order to ensure environmental safety. Statistics and probability, as well as chemistry, are mandatory knowledge. Such extension of technical-scientific scope is welcome, anyway, since the need for probabilistic approaches in Geotechnics has been long underscored. However, the problem is not confined to solving the technical aspects. In order for waste to be used as a geomaterial, acceptance and preparedness from the part of environmental agencies, designers, contractors, and society as a whole must be achieved.

Environmental agencies are ultimately responsible for environmental damage upon official permission. The society must be convinced that earthworks built with waste will not display poor performance, neither be hazardous. Designers must learn to design with unknown materials with different properties, and contractors also must adapt long established procedures. Therefore, to move from laboratory to the full scale, much work remains to be done, concerning public policies, standardization, and networking. These are fields for which engineering courses do not prepare professionals yet. Without the incorporation of such perspectives into the Geotechnical mindset, however, reuse of wastes will never become widespread. Two research studies on waste-to-geomaterial perspectives are presented next.

4.2 Examples of waste-to-geomaterial research

4.2.1 Construction and demolition waste

In Brazil, construction and demolition waste (CDW) has been largely employed in civil and pavement construction. Regulations and standardization involve, among others, technical standards ABNT (2004a, 2004b, 2004c and 2004d) and ABNT (2011), and federal environmental regulations CONAMA Resolutions n. 307/2002, n. 420/2009

and n. 431/2011. States and municipalities also have regulations such as DD CETESB 045/2014/E/C/I for São Paulo state, and Decree n. 48,075/2006 for São Paulo city. This decree, for instance, declares mandatory the utilization of recycled aggregates generated from solid waste of civil construction in paving services and works for public roads in the São Paulo municipality.

CONAMA Resolution n. 307/2002 divides CDW into four categories: Class A - waste reusable or recyclable as aggregate for construction, renovation and repair of buildings, pavements and other infrastructure: bricks, blocks, roof tiles, cladding plates, mortar, concrete, pipes, curbs and soils from earthworks; Class B - waste recyclable for other destinations: plastics, paper, cardboard, metals, glass, wood, and others; Class C - waste for which technologies or feasible economic applications that permit recycling/recuperation have not yet been developed (*e.g.*, plaster products), and Class D - hazardous waste generated during construction processes: paints, solvents, oils and others, or contaminated waste generated during demolition, renovation and repair of radiology clinics, industrial installations and others.

It is important to remember that in Brazil the amount of CDW generated is high, according to ABRELPE (2020), 0.585 kg/inhabitant/day of CDW were collected in Brazilian municipalities in 2019. Despite the generated volume of CDW being significantly lower than that of MSW, the weight of CDW is very significant.

CDW could well be used as backfilling for geosynthetic-reinforced soil retaining walls (Santos, 2011). Other options could be for drains (drainage of natural water courses before landfill implantation, leachate drains, gas recovery drains) and pavements (access roads, storage platforms, parking areas) in landfills, where there could be greater acceptance of the use of waste by the environmental agency.

In addition, the use of recovered soils and CDW fines in geotechnical works should be promoted. Table 5 shows the percentages of excavated soils present in CDW (by weight) in different countries, demonstrating that excavated soils are an important portion of CDW and should be specifically studied.

In densely urbanized areas, large quantities of excavation soils can be generated due to the construction of underground garages of multi-story buildings and urban infrastructure such as subway lines, flood prevention reservoirs, and energy, gas, and water supply networks. Katagiri *et al.* (2019), based on studies carried out in many countries, reported that excavation soils are generally disposed of in landfills, or dumped illegally, which is also the case in the Metropolitan Area of São Paulo.

When not segregated at the source, excavated soils turn into waste and must be dealt with as such. Generation of CDW increases 3-5 times when excavated soils are included (Monier *et al.*, 2011), and only around 6 % of excavated soils are recycled worldwide. Since excavated soils

Table 5. Excavated soils relative to total CDW in several countries (Kataguirí *et al.*, 2019).

Country	Excavated soils % total CDW (by weight)	Reference year
Austria	50	2011
Australia	65	2012
Brazil	32	2011
Denmark	53	2012
Finland	75	2011
France	69	2012
Germany	55	2011
Hong Kong	70	2013
Italy	24	2012
Norway	44	2008
United Kingdom	40	2012

are mixed with other types of waste, these soils have to meet construction and environmental requirements to be used in earthworks. Such soils could be used on site or redirected as daily or final covers for landfills, for backfilling of trenches or walls, for earth dams, for pavement sub-bases or bases, and for vegetation replacement.

Besides segregation of excavated soils at the source, the potential use of CDW fines should also be highlighted. The use of the coarse fraction of recycled CDW is regulated for road construction and for non-structural concrete. However, the current processes of CDW recycling mostly produce fine-grained recycled aggregates (< 4.8 mm) (Ulsen *et al.*, 2013), for which reuse strategies are still required (Magnusson *et al.*, 2015). These materials are mostly composed of mineral grains and cementitious materials (cement and lime), with good potential for earthworks. Stankevicius *et al.* (2019) reported promising results from own investigations and those of Kataguirí *et al.* (2019), Nomachi & Boskov (2016), Sharma & Hymavathi (2016), Amorim (2013), and Santos (2007) aiming at the geotechnical reuse of CDW recycled fine aggregates.

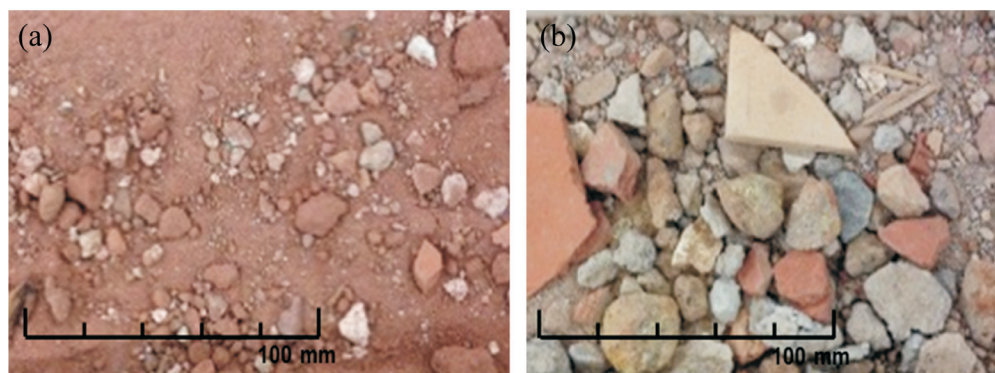
4.2.1.1 Reuse of excavated soils (Kataguirí, 2017; Kataguirí *et al.*, 2019; Nomachi & Boskov, 2016)

The investigation on the reuse of excavated soils aimed at delineating a flowchart to support screening excavated materials for different reuse options, based on current geotechnical and environmental characterization. To appeal to the end users, CDW recycling facilities and local municipalities, the flowchart was based on very simple tests and parameters. As excavated soils are still rarely segregated at the source (construction site), potential materials are assumed to be found in CDW landfills and recycling plants. Thus, the methodology includes procedures for adequate sampling of materials at these locations.

From thirty-five representative samples collected at a CDW landfill in São Paulo city, following Sampling Theory (Petersen *et al.*, 2005), eight samples were randomly selected and visually separated as either “CDW” (mixtures of excavation soils and other types of CDW) or “soil” (predominantly excavation soil). Three samples (B-5, B-19 and B-22) were defined as “CDW” and five as “soil” (B-4, B-7, B-12, B-15 and B-23), as illustrated in Figs. 20a and b. The grain-size distributions of the samples are presented in Fig. 21 and the geotechnical characterization in Table 6.

The samples were separated by sieving (0.1-0.4, 0.4-0.6, 0.6-1.2 and 1.2-2.0 mm), to estimate the percentages of cementitious and mineral grains in each fraction using image resources. The results indicated that soil grains and cementitious material are present in all fractions of all samples. “Soil” samples had higher contents of kaolinite, gibbsite, hematite, and goethite than the “CDW” samples. “CDW” samples, on the other hand, had a higher content of CaO and SO₃ than soil, due to the presence of cement, mortars, and gypsum. Calcite (CaO) is related to calcareous and cementitious materials, and the higher the content of cementitious materials, the higher the content of calcite.

The three “soil” samples were also classified according to the MCT Classification system (Nogami & Villibor, 1995). The fines of the five “CDW” samples were mixed and treated as a single sample, “CDW-composite”, as would be the case in a recycling plant, where collected

**Figure 20.** Visual classification of samples: (a) “soil”; (b) “CDW” (From Kataguirí, 2017).

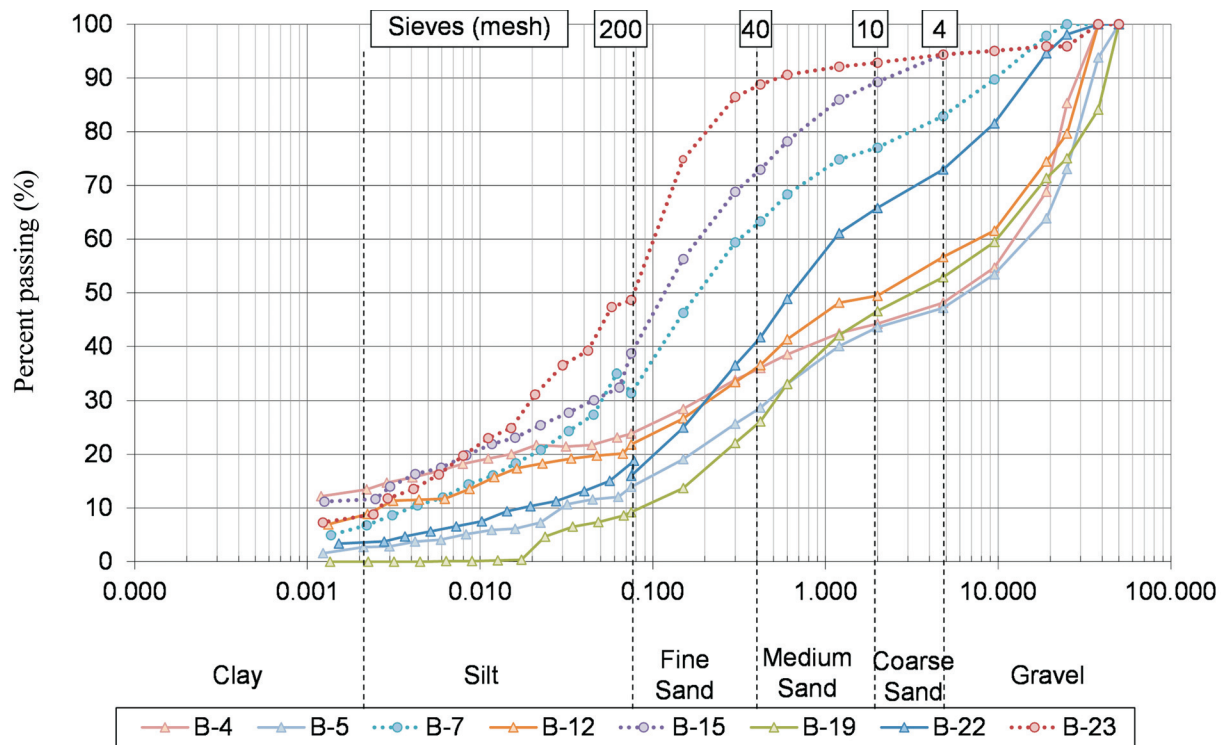


Figure 21. Grain-size distributions of the samples, including “soil” and “CDW” (From Kataguir, 2017).

Table 6. Geotechnical characterization of “soil” and “CDW” samples (From Kataguir, 2017).

Sample	Visual classification	Grain size distribution			Specific gravity	Atterberg limits			USCS classification
		Fines (%)	Sand (%)	Gravel (%)		Liquid limit (%)	Plastic limit (%)	Plasticity index (%)	
B-7	Soil	31.4	51.5	17.1	2.692	*	*	*	SM
B-15	Soil	38.7	55.6	5.7	2.703	30	22	8	SC
B-23	Soil	48.6	45.7	5.7	2.852	33	27	6	SM
B-4	CDW	23.9	24.3	51.8	2.637	28	25	3	GC
B-5	CDW	13.9	33.2	52.9	2.784	29	21	8	GM
B-12	CDW	21.8	34.8	43.4	2.567	32	19	13	GC
B-19	CDW	9.2	43.7	47.1	2.709	*	*	*	GP-GM
B-22	CDW	16.0	56.9	27.1	2.222	27	18	9	GC

*fine fraction with no plasticity.

“CDW” usually would be disposed and managed in heaps without segregation. The results from compaction, direct shear, and mini-CBR tests are presented in Table 7. Comparisons between mini-CBR results before and after immersion in water would provide an estimate of the loss of bearing capacity due to saturation. However, due to material scarcity, tests were carried out on saturated samples without surcharge in order to investigate the most unfavorable condition.

The classification and parameters of the “soil” samples are in accordance with typical soils from the outskirts

of São Paulo city, saprolitic or young tropical soils derived from granite, gneiss, phyllite and other acidic rocks. These soils swell and lose strength remarkably when saturated; however, usually they show a low swelling pressure. On the other hand, “CDW-composite”, *i.e.*, the fines from CDW samples, composed of soil and cementitious materials, were non plastic and not sensitive to water, and presented a high friction angle.

Environmental characterization showed that all samples, except for B-23, presented at least one of the contaminants sulfate and nitrate at a concentration above the re-

Table 7. Mechanical properties of soil and “CDW” samples (From Kataguirí, 2017).

Test Parameter	Compaction		MCT		Direct shear strength		Mini-CBR	
	Optimum water content (%)	Maximum dry density (g/cm ³)	Mass loss PI ** (%)	Class	Cohesion (kPa)	Friction angle (°)	Swelling* (%)	CBR (%)
B-7 (“soil”)	18.5	1.66	290	NS*	9.6	29	1.1	4
B-15 (“soil”)	18.3	1.72	110	NA*	0	34	0.4	11
B-23 (“soil”)	17.8	1.69	285	NS*	0	30	2.5	2
CDW-composite	19.5	1.67	-	-	0	38	0.0	16

MCT: miniature, compacted, tropical classification; CBR: California Bearing Ratio.

*The presented values refer to the optimum moisture content.

**Mass Loss PI: mass loss after immersion, relative to the dry mass of 20-cm³ compacted soil.

spective maximum allowable value established by waste regulations (ABNT 2004a, 2004b) and drinking water standards (CONAMA n. 357/2005). The presence of nitrate and sulfate may be related to the degradation of organic matter, from sulfide oxidation in soils and rocks, and from crushed concrete and gypsum materials. The highest sulfate concentrations were found in the “CDW” samples and in “soil” sample B-7, which had a higher fraction of cementitious materials than the other “soil” samples, while nitrate correlated to organic matter content.

Kataguirí *et al.* (2019) point out that pH values measured for the eight tested samples were higher than 7.0 (pH range = 7.3-9.4). Alkalinity decreases leaching of nitrate and sulfate by infiltration or water seepage. Nitrate in water supply has been associated with the “blue-baby syndrome”, a gastrointestinal disturbance and infant poisoning related to high levels of methemoglobin in infants, not reported in areas where nitrate concentration in drinking water is consistently lower than 50 mg /L (WHO, 2017). All studied samples had concentrations of dissolved nitrate below 50 mg/L. Sulfate concentrations in the studied samples, except for “CDW” samples B-4 and B-19, were below 1,000 mg/L, which is adequate for human health; for higher sulfate concentrations, site-specific risk assessment must be carried out. However, sulfate in water or soil may attack concrete foundation structures (Neville, 2004; WHO, 2017), requiring concrete with characteristic strength above 40 MPa for nearby foundations. The segregation of gypsum panels at the source (construction site) may reduce the concentration of dissolved sulfate in CDW. Finally, the flowchart considering visual classification as “soil” or “CDW”, fines content (diameter < 0.075 mm), swelling at optimum water content, mini-CBR, and strength parameters was proposed, allowing to select the destination alternative as reuse as backfill for trenches and retaining walls, reuse in paving, or landfill disposal.

4.2.2 Water treatment sludge

Water treatment sludge (WTS) is the residue generated during the production of potable water from raw water. In Brazil, water treatment plants (WTPs) usually employ the conventional treatment method, which comprises coagulation, flocculation, sedimentation, filtration, and disinfection processes. Chemicals are added to the water for coagulation (coagulants, such as aluminum and ferric sulfate, ferric chloride, lime and polymers), disinfection (chlorine), dental protection (fluorosilicic acid) and pH correction (lime). WTS is generated during the periodic washings of the sedimentation tanks and filters, which generate, respectively, 60-95 % and 5-40 % of the total WTS by weight (Yuzhu, 1996).

WTS is composed of water (approximately 96-99 % by weight), suspended solids and chemical compounds (chlorine, aluminum sulfate, and/or ferric chloride, lime and fluorine). Sludge solids include organic (organic mat-

ter, algae, bacteria and viruses) and inorganic substances (colloids, sand, silt, clay, calcium, magnesium, iron, manganese, aluminum hydroxides and polymers).

In Brazil, WTS ends being predominantly discharged irregularly into rivers, or disposed of in landfills or sent to sewage treatment plants (STPs). WTS discharged in rivers results in serious environmental impacts, mainly silting and degradation of water quality and the aquatic environment. WTS landfilling may cause instability of the waste mass, besides increasing the demand for landfill space. WTS sent to STPs may clog the sewer-system pipelines and overload the STP system (which is insufficient in Brazil, and in most countries, as 80 % of the global wastewater is released without treatment), with a material of composition very different from sewage sludge.

The search for alternatives for the reuse of WTS is an important environmental concern for the sustainability of the life cycle of water production. Different uses have been investigated, such as replacement for raw materials in the production of precast concrete elements, cement, asphalt, ceramics and steel, as well as applications such as composting, coagulant recovery, phosphorous removal from residual waters, and citrus production (Tsugawa *et al.*, 2017, Montalvan & Boscov, 2018). Geotechnical investigations also are being conducted. Despite promising results, case studies of practical applications are almost inexistent in the literature.

Even after dewatering by centrifuging, or on drying beds, at the WTP, WTS presents a solids content of only 20-25 %, being still inadequate for geotechnical applications. When air-dried or oven-dried, WTS usually turns into a granular material that can be useful as a construction aggregate. However, considerable amounts of time and energy are demanded. Two approaches can be considered for the geotechnical use of fresh dewatered WTS (at the “as-

collected” or *in natura* water content at the WTP) as a material for embankments, filling of trenches and retaining walls, or as landfill covers and bottom liners: mixing with soils and mixing with additives. The reuse allows a beneficial destination of WTS as opposed to release to the environment, as well as economy of mineral resources by partially substituting soils in earthworks. These two approaches were investigated for a WTS collected at one of the largest WTPs of São Paulo state, Cubatão WTP.

A remarkable characteristic of WTS is the great variation in composition and properties associated with source and seasonality, *i.e.*, the WTP location, climate, season, raw water composition, treatment process and introduced chemicals, and dewatering process. Thus, the reuse of WTS requires a thorough case-specific investigation, until adequate indicators of geomechanical behavior of WTS and mixtures based on simpler tests are available. During the investigations with Cubatão WTS, a method to obtain representative monthly samples was developed using the Theory of Sampling (Tsugawa *et al.*, 2019).

Silva (2017) determined some geotechnical properties for different mixtures of Cubatão WTS with lime. For a batch sample of the Cubatão WTS, Silva (2017) determined grain-size distribution, Atterberg limits, compaction parameters and undrained shear strength, based on unconfined compression. For the fresh WTS, the liquid limit (w_L) and plastic limit (w_p) values resulted 228 % and 75 %, respectively. For determining the undrained shear strength of fresh WTS, the material was tested at different solids content ($S_c = 1/(1 + w)$, where S_c is the solids content and w is the gravimetric water content). As shown in Fig. 22a, the S_u of the pure WTS was found to increase exponentially with solids content, as previously shown for other WTS, including a ferric-chloride sludge tested by Wang *et al.* (1992). The S_u values near the w_L and w_p were found to be 1.13 kPa

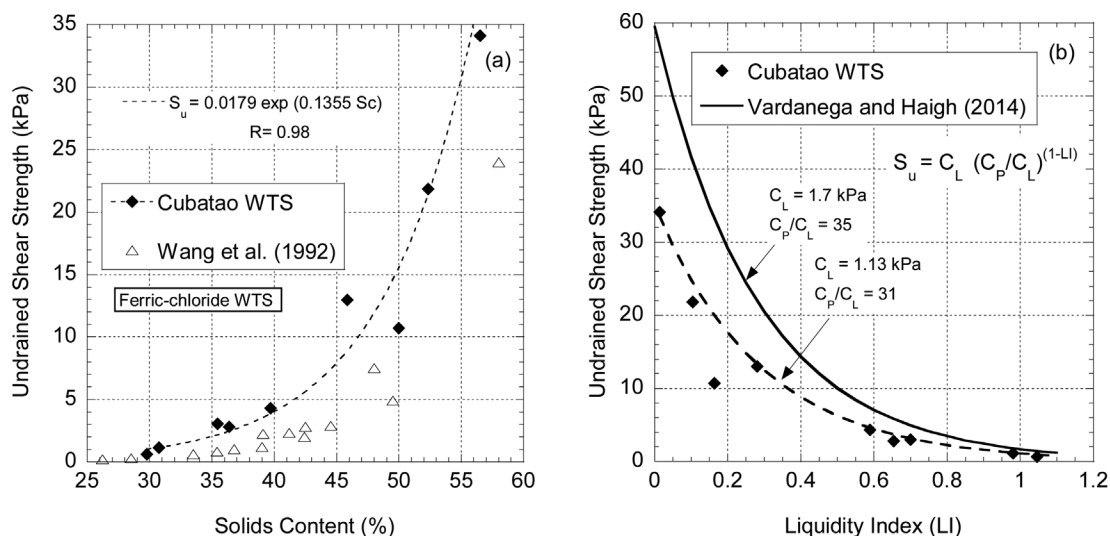


Figure 22. Undrained shear strength of the pure WTS as a function of: (a) the solids content, and (b) liquidity index, with comparison to the literature (From Silva, 2017).

and 35 kPa, respectively. Plotting the S_u values against the liquidity index (LI), defined as the ratio $(w - w_p)/(w_L - w_p)$, the obtained trend followed approximately the power (exponential) function proposed for soft clays by Vardanega & Haigh (2014). For soft clays, Vardanega & Haigh (2014) indicate C_L (defined as the S_u value at the w_L) to be equal to 1.7 kPa, and $C_p/C_L = 35$ (ratio between the strengths at the w_p and w_L). Based on the undrained shear strength experimental results for the WTS, C_L was 1.13 kPa, and $C_p/C_L = 31$ (Fig. 22b).

Montalvan & Bosco (2018) characterized and tested mixtures of Cubatão WTS with a lateritic clayey sand, representative of significant areas of São Paulo state and largely used as base material for low-traffic roads. The objective was to define the maximum WTS content that could be added without impairing the good geotechnical properties of the tropical soil.

WTS is similar to clayey soils, except for the high concentration of chemicals in the pore fluid, which displays an important role in geotechnical behavior (particles dispersion-agglomeration, water retention, among others). The pore liquid of Cubatão WTS has pH 7 and the grains contain a large amount of ferric chloride from the treatment process (iron concentration of 47.5 %, XRF). Major components of Cubatão WTS are quartz, goethite, muscovite, kaolinite, and amorphous phases. The particle size distribution by sedimentation indicated that about 70 %, by weight, of the solid particles were smaller than 0.005 mm. Specific gravity of grains varied from 2.9 to 3.2, the w_L was high (170–240 %), the specific surface area 52 m²/g, the cation exchange capacity was 252 mmolc/kg, organic content 2.6 % and the organic carbon content was equal to 1.5 %.

Grain-size distribution (GSD) curves of the soil, WTS and soil-WTS mixtures are presented in Fig. 23. The mixtures present GSD curves similar to the soil, since the added percentage of solids is very small, due to the high water content of WTS. The difference in the percentage of fines with and without dispersing agent indicates flocculation caused by the ferric chloride in the WTS. Table 8 displays the geotechnical characterization and USCS classification of the materials.

Compaction curves of the soil and the mixtures are presented in Fig. 24. WTS at the *in natura* water content is impossible to compact. The maximum dry unit weight (γ_{dmax}) for the soil compacted under standard effort resulted equal to 19.1 kN/m³ and the optimum water content (w_{opt}), 12.4 %. Mixtures of soil at $w = 1$ % (hygroscopic water content) with WTS (at the *in natura* water content of ~ 350 %) presented water contents of 15.3, 19.2 and 24.5 % for the proportions 5:1, 4:1 and 3:1, respectively. These mixtures were air-dried to a certain water content w_i to initiate the compaction tests. The tests were conducted at different values of w_i for each mixture, since the wet preparation method was a tentative trial to bracket the estimated w_{opt} , and also to investigate the influence of air-drying on the compaction parameters. When feasible, w_i was used as the first point of the compaction curve; otherwise, water was added to reach the first point of the compaction curve.

WTS addition decreased γ_{dmax} and increased w_{opt} . On the other hand, air-drying of the mixtures caused increase of γ_{dmax} and decrease of w_{opt} , and the lower w_i , the more markedly the effect was. Figure 25 shows that the compaction parameters resulted linearly correlated to the initial water content w_i for the three mixtures. The change in behavior, from that of a soft clay to a coarse-grained material

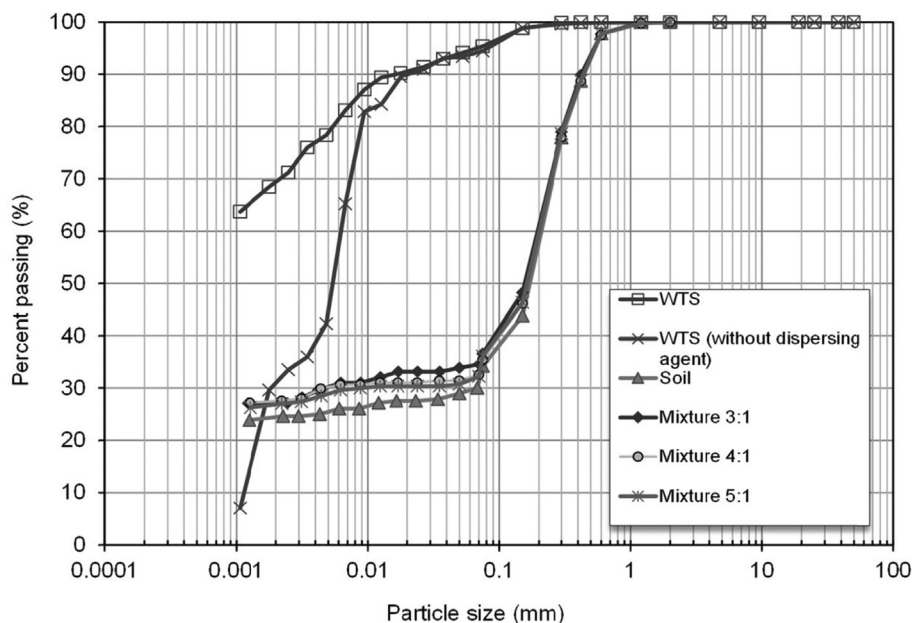
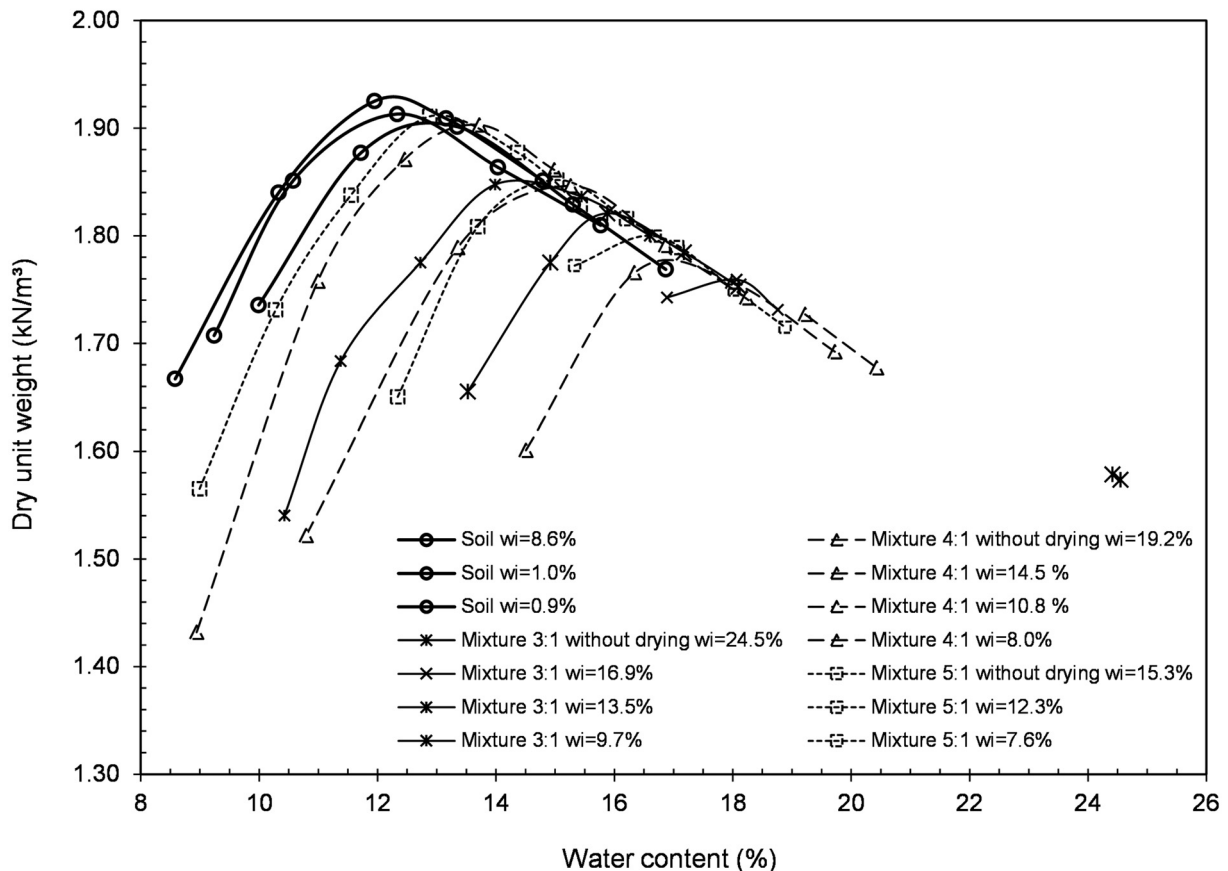


Figure 23. Grain-size distributions of the soil and soil-WTS mixtures (From Montalvan & Bosco, 2018).

Table 8. Geotechnical characterization of the materials (From Montalvan & Boscov, 2018).

Parameter	Soil	WTS	Mixture 5:1	Mixture 4:1	Mixture 3:1
Fine fraction (%)	34	95	36	36	37
Sand fraction (%)	66	5	64	64	63
Liquid limit (%)	25	239	32	29	33
Plasticity index (%)	11	158	14	12	16
Specific gravity of solids	2.69	2.85-2.95	2.69	2.70	2.71
Soil classification (USCS)	SC	MH	SC	SC	SC

**Figure 24.** Compaction curves of the soil and soil-WTS mixtures (From Montalvan & Boscov, 2018).

may be attributed to WTS and the effect of coagulants, since the compaction curve of the soil did not change substantially with air-drying.

One-dimensional consolidation tests were carried out to examine whether WTS addition would increase prohibitively the compressibility of the soil. The compression indexes C_c for the 5:1, 4:1 and 3:1 soil-WTS mixtures, of 0.14, 0.13, and 0.19, respectively, were higher than that for the soil, 0.07, but mixtures 5:1 and 4:1 could be considered as still acceptable for geotechnical works. The expansion and recompression indexes of soil and mixtures were practically equal ($C_e = C_r = 0.02$). Note that the soil was compacted at w_{opt} , whereas the mixtures were compacted with-

out drying (w_i equal to the water content after mixing the materials). Mixtures 5:1, 4:1 and 3:1 were compacted, respectively, dry of optimum, slightly wet of optimum and wet of optimum.

The results from permeability tests are shown in Table 9. The hydraulic conductivity (k) values of soil and mixture 5:1, for confining pressures of 30 and 60 kPa and hydraulic gradients of 5 and 10, were similar, despite the soil being compacted at w_{opt} and the mixture dry of optimum (flocculated structure). Values of k for mixture 4:1 were lower, possibly due to the greater addition of fine-grained WTS and wet-of-optimum compaction. For mixture 3:1, the k value decreased with time due to clogging of the test

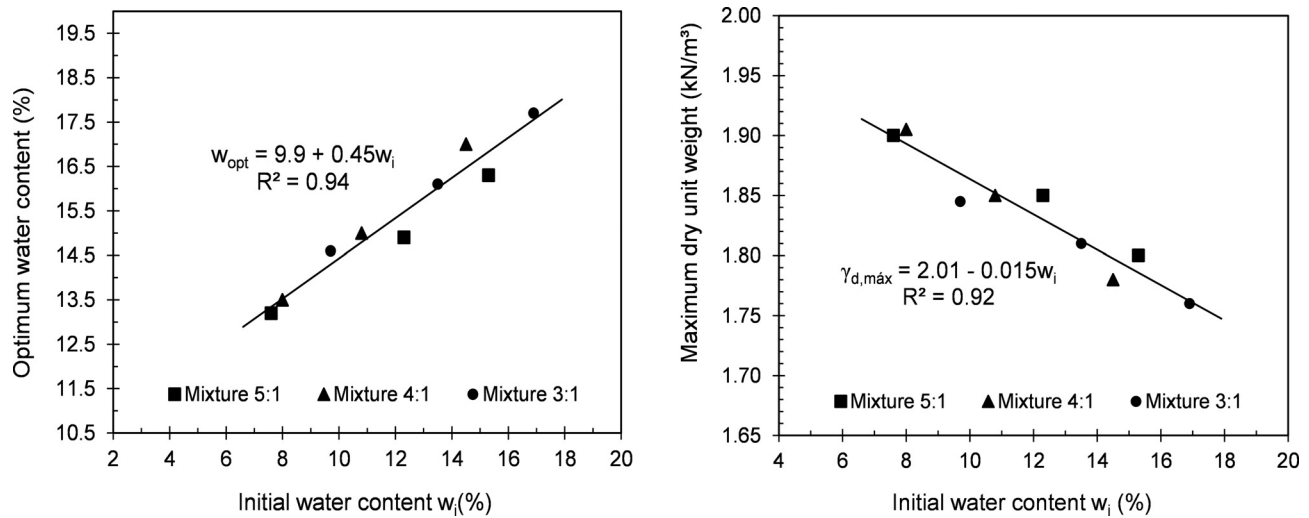


Figure 25. Variation of w_{opt} and $\gamma_{d,max}$ of the mixtures as a function of initial water content (From Montalvan & Bosco, 2018).

Table 9. Hydraulic conductivity of the soil and the soil-WTS mixtures (From Montalvan & Bosco, 2018).

Confining pressure (kPa)	Hydraulic gradient	Hydraulic conductivity (m/s)			
		Soil	Mixture 5:1	Mixture 4:1	Mixture 3:1
30	5	1.3×10^{-6}	1.4×10^{-6}	4.3×10^{-7}	7.0×10^{-9}
30	10	6.9×10^{-6}	2.0×10^{-6}	3.0×10^{-8}	-
60	5	4.3×10^{-7}	1.6×10^{-7}	8.7×10^{-8}	-
60	10	3.9×10^{-7}	1.6×10^{-7}	1.3×10^{-7}	-

specimen, practically ceasing seepage after 47 days, probably due to chemical compounds reacting with the soil grains (the mixtures with lower WTS contents did not exhibit this behavior).

The stress paths obtained from CIU triaxial testing of the soil and soil-WTS mixtures are shown in Fig. 26. The effective strength parameters for the soil and the mixtures were calculated from the effective stress paths. The obtained internal friction angles for the soil and mixtures 5:1, 4:1, and 3:1 were equal to 34, 34, 35, and 37°, respectively. The increase in ϕ' with increasing the WTS content has been observed by other authors. The effective cohesion decreased with WTS content, from 22 kPa for the soil, to 17, 15 and 10 kPa for mixtures 5:1, 4:1 and 3:1, respectively.

Soil-WTS mixtures 5:1 and 4:1, therefore, could be considered as feasible materials for geotechnical applications, given the slight variations in geotechnical parameters caused by WTS addition. Mixtures of other soils with WTS are under study, with similar promising results, but indicating different thresholds for WTS incorporation. As already mentioned, before simple indicative tests are developed, the geotechnical behavior of soil-WTS mixtures must be extensively investigated case-by-case, since results from specific materials should not be generalized.

Ongoing research aims at confirming the environmental safety of employing soil-WTS mixtures in earthworks. This beneficial application of WTS should be stimulated by environmental policies to overcome prejudice against use. The perspective of financial compensation should also be considered, to account for the additional time and cost required for proper mixing.

Another possibility for WTS reuse as a geomaterial could be incorporating additives, such as lime and fillers, to improve WTS workability and geomechanical properties. The mechanical characteristics of fresh WTS before treatment must be known, to orient the selection and dosage of additives. However, most geotechnical tests were conceived for soils and not for fresh or *in natura* WTS, a fine-grained material with very high water content. Obtaining strength parameters for fresh WTS using standard geotechnical equipment and experimental procedures often results impracticable, even with the laboratory vane shear and fall-cone tests. For this reason, rheometry tests were explored for assessing the stress-strain behavior of fresh WTS. Samples of Cubatão WTS ($w = 240\%$), WTS-lime mixtures and WTS-rock powder mixtures were submitted to rotational rheometry tests. On the other hand, mixtures

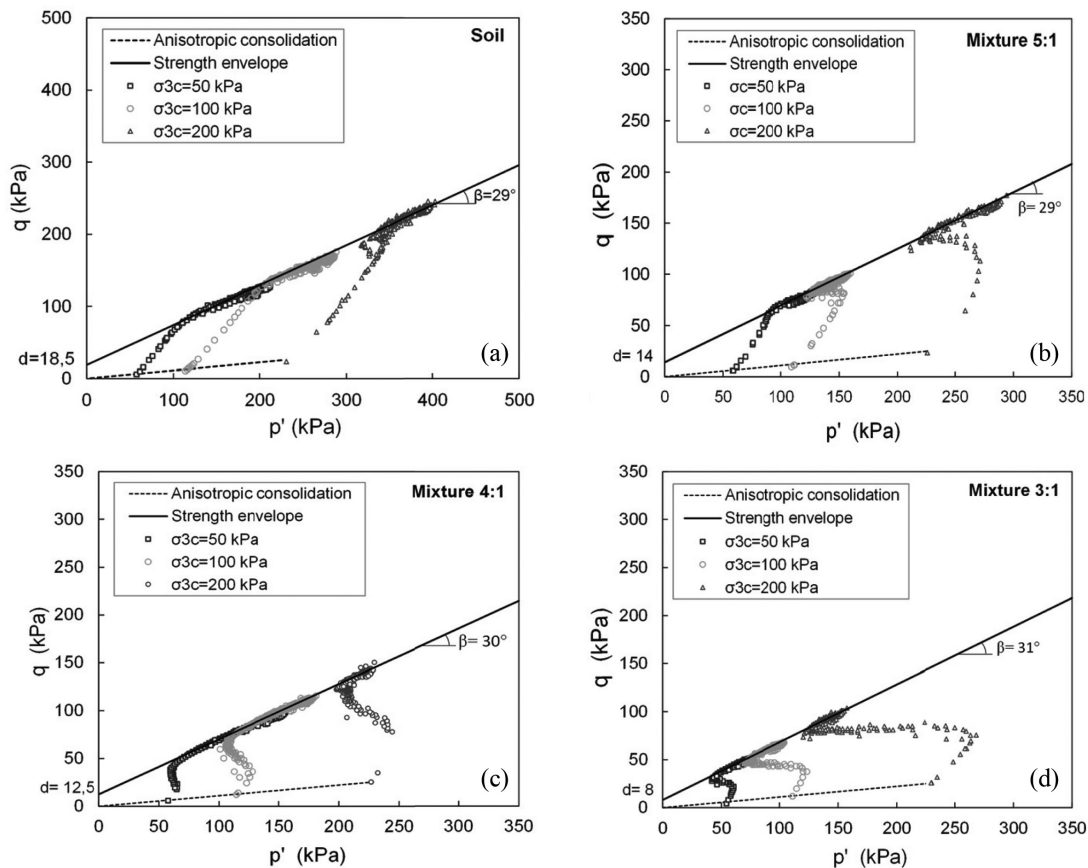


Figure 26. Effective stress paths of the soil and three different soil-WTS mixtures (From Montalvan & Boscov, 2018).

with very high additive content and, therefore, soil-like behavior were submitted to traditional geotechnical tests.

Figure 27 compares the well-known laboratory vane test with a rotational rheometry test. The vane test has a constant shear rate, while rheometry tests allow different geometries and the programmed shear rate to vary (Table 10). Measurements of rotational velocity, torque, defor-

mation and time of response can be related to shear stress and shear strain.

Stepped flow tests were performed using a steel parallel plate geometry (diameter of 35 mm, gap of 1.0 mm). Shear rate was increased (acceleration) twice and decreased (deceleration) stepwise from 0 to 50 s^{-1} ($1,080,000^\circ/\text{min}$ or 3,000 rpm), *i.e.*, two cycles of shear rate acceleration-deceleration were performed, totalizing 400 s of test (Fig. 28).

The output of the tests can be exemplified in Fig. 29, where results of a flow test for both cycles of acceleration-deceleration are presented. The first cycle is related to a “very early age” behavior of WTS, while the second cycle is the condition where test steady state has been reached. Results are discussed in Tsugawa *et al.* (2018) and can be summarized by the parameters in Table 11. The flow test also allowed to observe that Cubatão WTS may present thixotropic or rheopectic behaviors, depending on the applied shear rate: Cubatão WTS is thixotropic for shear rates lower than 180 rpm and rheopectic for higher shear rates, a fact that has implications in efficiency of field processes such as pumping, homogenizing using concrete mixers, removal from storage tanks, among others.

Besides mapping the stress-strain behavior of very moist WTS and WTS-additive mixtures, the results were compared to laboratory vane shear tests to characterize

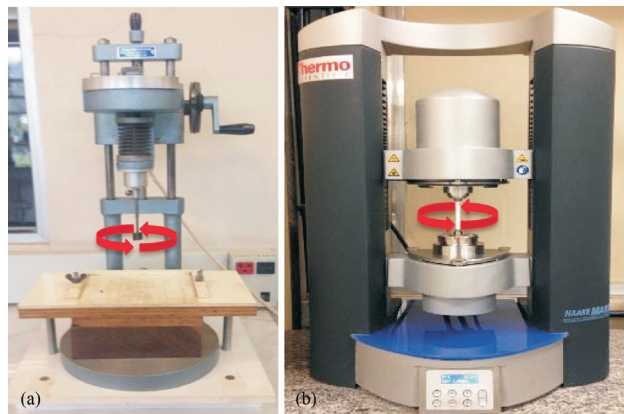
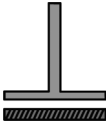

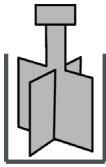


Figure 27. Comparison between experimental arrangements for: (a) laboratory vane shear test; (b) rotational rheometry test (Tsugawa *et al.*, 2018).

Table 10. Rheometry tests: shear stress and shear rate calculations for different geometries.

Geometry	Configuration	Shear stress	Shear rate
Plate-to-plate		$\sigma = \frac{2\Gamma}{\pi R^3}$	$\dot{\gamma} = \frac{\Omega R}{h}$
Cone-plate		$\sigma = \frac{3\Gamma}{2\pi R^3 \sin^2\left(\frac{\pi}{2} - \theta\right)}$	$\dot{\gamma} = \frac{\Omega}{\tan \theta}$
Vane		$\sigma = \frac{\Gamma(R_1^2 + R_2^2)}{4\pi h R_1^2 \cdot R_2^2}$	$\dot{\gamma} = \frac{\Omega(R_2^2 + R_1^2)}{(R_2^2 \cdot R_1^2)}$

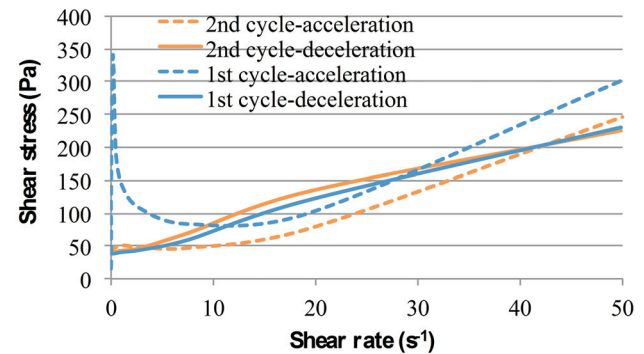
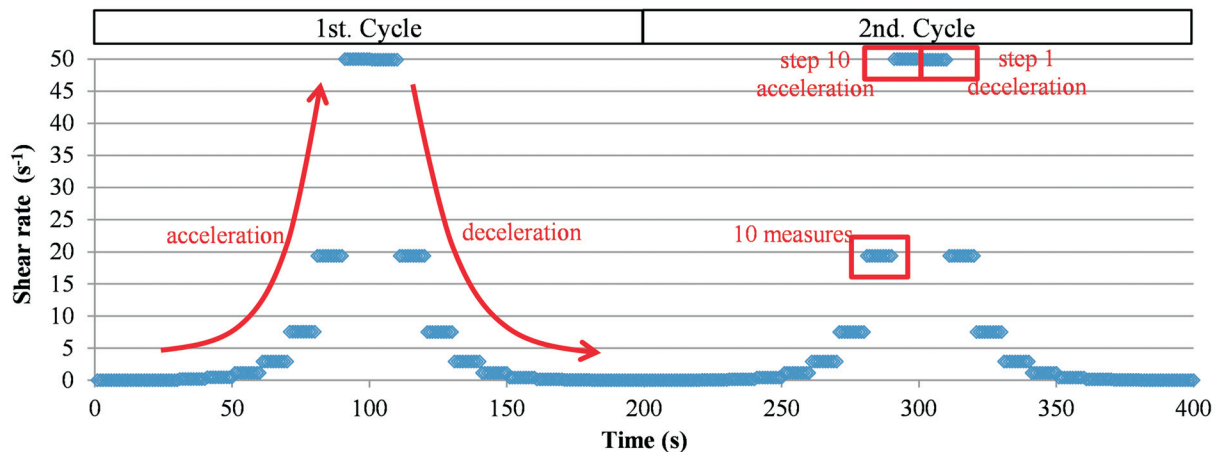
σ = shear stress (equivalent to τ in Soil Mechanics); $\dot{\gamma}$ = shear rate; Γ = torque, Ω = rotation velocity; R , h , θ , R_1 and R_2 = geometric characteristics.

thixotropy using different methodologies. Results are presented, and advantages and disadvantages of both methods are discussed in Tsugawa *et al.* (2018). The parameters of the laboratory miniature vane test were: constant shear rate of 50°/min (0.0024 s⁻¹), and vane blade of 12.7 × 12.7 mm. WTS at a water content of 240 % was remolded by hand, tested immediately after remolding ($t = 0$), and after different storage times (1, 3, 7, 14, 28, 84 and 168 days). Vane

tests measured thixotropy for longer periods of time (storage times), whereas stepped flow tests indicated thixotropy

Table 11. Rheological parameters of Cubatão WTS (From Tsugawa *et al.*, 2018).

	Yield stress (Pa)	Apparent viscosity (Pa.s)	Hysteresis loop (Pa/s)
First cycle	43.4	4.53	1337.8
Second cycle	43.0	4.92	-1074.8

**Figure 29.** Example of a flow test output for fresh Cubatão WTS ($w = 240\%$) (From Tsugawa *et al.*, 2018).**Figure 28.** Applied shear rate history in rheometry tests (stepped flow type test) (From Tsugawa *et al.*, 2018).

at very early times after WTS being placed in the equipment. Thus, the results are related to different types of mobilizations and must be applied to measure thixotropy depending on the practical objective.

Once fresh WTS was characterized, geomechanical behavior of mixtures of WTS with lime and rock dust were investigated. The strength limit separating the use of rheometry and geotechnical tests is still under debate. Even though rheometry tests are quick and consume small quantities of materials, they are limited to materials with low shear strength compared to typical geomaterials. Such tests may be considered useful to define a threshold of additive content for applications such as coulis for diaphragm walls or for minimum workability in the field for spreading daily landfill covers with compaction equipment. However, to screen ranges of additive contents for road construction, backfilling of trenches or reinforced walls, and compacted embankments in general, traditional geotechnical tests remain required.

5. Conclusions

The field of Environmental Geotechnics has matured over the past decades, developing and advancing a broad repertoire of theoretical knowledge and applied techniques to deal with the challenge of building and maintaining infrastructure while safeguarding environmental conservation. This paper aimed at focusing on three topics of significant relevance to modern sustainability in Brazil in which Geotechnical Engineers contribute, but could have an even greater participation: expansions in MSW landfills, site remediation benefiting from geotechnical solutions, and reuse of wastes in geotechnical works. First, the issues associated with designing an appropriate environmental protection system at the base of new landfill expansions are highlighted, as well as the possibility of immersing geogrids to reinforce the mass of MSW, allowing increased storage capacity. Secondly, dealing with the additional challenges of site remediation at a complex urban region of past industrial land use, the importance of a joint regional plan for investigation and remediation is discussed, as well as the possibility of using geotechnical confinement and *in situ* passive remediation to treat the area. Finally, preparedness to accept working with wastes as geomaterials is pointed out, and two examples of investigation on the reuse of construction and demolition waste and water treatment sludge are discussed. Construction and demolition waste is shown to contain a significant amount of excavation soils, for which reuse options are still not in place. Water treatment sludge is a challenging material, but could be useful when mixed with local soils or stabilized with additives. The topics discussed in this paper are three examples of the many interesting challenges posed to Geotechnical Engineers facing environmental conservation. Environmental Geotechnics is permanently undergoing significant advancements, at the same time new demands require innovative

solutions, making this science and engineering continuously stimulating.

Acknowledgments

The authors acknowledge CAPES, CNPq and FAPESP for scholarships granted to researchers, and project SABESP-FAPESP 2013/50448-8 for supporting the water treatment sludge research.

References

- ABLP (2019). Data update: Sanitary landfills - Technical or economical solution. *Limpeza Pública*, 101(1):32-33 (in Portuguese).
- ABNT (2004a). Solid Waste - Classification. NBR 10,004. ABNT, Rio de Janeiro, Brazil, 71 p.
- ABNT (2004b). Sampling of Solid Waste. NBR-10,007. ABNT, Rio de Janeiro, Brazil, 21 p.
- ABNT (2004c). Construction and Demolition Wastes - Selection Areas - Lines of Direction for Project, Implantation and Operation. NBR 15,112. ABNT, Rio de Janeiro, Brazil, 7 p.
- ABNT (2004d). Recycled Aggregate of Solid Residue of Building Constructions - Requirements and Methodologies. NBR-15,116. ABNT, Rio de Janeiro, Brazil, 12 p.
- ABNT (2010). Urban Solid Wastes - Small Sanitary Landfills - Guidelines for Location, Design, Implantation, Operation and Closure. NBR 15,849. ABNT, Rio de Janeiro, Brazil, 24 p.
- ABNT (2011). Environmental Passive in Soil and Groundwater Part 2: Confirmatory Assessment. NBR 15,515-2. ABNT, Rio de Janeiro, Brazil, 19 p.
- ABRELPE (2016). Solid Residue Panorama in Brazil 2016. Associação Brasileira de Empresas de Limpeza Pública e Resíduos Especiais, available at <http://abrelpe.org.br/panorama/>.
- ABRELPE (2020). Solid Residue Panorama in Brazil 2018/2019. Associação Brasileira de Empresas de Limpeza Pública e Resíduos Especiais, available at <http://abrelpe.org.br/download-panorama-2018-2019/>.
- Alcântara, P.B. & Jucá, J.F. (2010). Landfill settlements: influence of composition, climate and biodegradation. *Geotecnia*, 118(1):1-28 (in Portuguese).
- Alexiew, D.; Plankel, A.; Widerin, M. & Jaramillo, J. (2015). A landfill with innovative reinforcing solutions: history, experience, solution flexibility. *Proc. XVI Geot. Eng. for Infrastructure and Development*, Edinburgh, v. 1, pp. 2679-2685.
- Amorim, E.F. (2013). Technical and Economic Viability of Mixtures Soil-CDW in Base Layers for Urban Pavements. Case Study: Campo Verde (MT) Municipality. Ph.D. Thesis, University of Brasília, 173 p. (in Portuguese).
- Assumpção, L.; Hems, P.S. & Machado, J.P.B. (2020). Removal of nickel from aqueous solution using a bone-

- meal char and monetite. *Journal of Environmental Engineering*, in review.
- Aydilek, A.H. & Wartman, J. (2005). Recycled materials in geotechnics: Proc. ASCE Civil Engineering Conference and Exposition, Baltimore, Maryland. American Society of Civil Engineers. Geo-Institute, Reston, 233 p.
- Benson, C.H. & Dwyer, S.F. (2006). Material Stability and Applications. Chien, C.; Inyang, H. & Everett, L.G. (eds) *Barrier Systems for Environmental Contaminant Containment and Treatment*. Taylor & Francis, Boca Raton, pp 143-201.
- Benvenuto, C. & Cipriano, M.A. (2010). Rheology model for the behavior of waste and sanitary landfills according to design and operation criteria in Brazil. *Limpeza Pública*, 74(1):42-47 (in Portuguese).
- Benvenuto, C. & Cunha, M.A. (1991). Sliding of the waste mass at Bandeirantes landfill in São Paulo. Proc. REGEO-91, Symposium on Tailings Dams and Waste Disposal, Rio de Janeiro, RJ, v. 2, pp. 55-66 (in Portuguese).
- Birke, V.; Burmeier, H.; Jefferis, S.; Gaboriau, H.; Touzé, S. & Chartier, R. (2007). Permeable Reactive Barriers (PRBs) in Europe: Potentials and Expectations. *Italian Journal Engineering Geology and Environment*, Special Issue 1(1):1-8. <https://doi.org/10.4408/IJEGE.2007-01.S-04>
- Blasenbauer, D.; Huber, F.; Lederer, J.; Quina, M.; Blanc-Biscarat, D.; Bogush, A.; Bontempi, E.; Blondeau, J.; Chimenos, J.; Dahlbo, H.; Fagerqvist, J.; Giro-Paloma, J.; Hjelm, O.; Hyks, J.; Keaney, J.; Lupsea-Toader, M.; O'Caollai, C.; Orupöld, K.; Pajak, T.; Simon, F.; Svecova, L.; Syc, M.; Ulvang, R.; Vaajasaari, K.; Caneghem, J.; Zomeren, A.; Vasarevicius, S.; Wégner, K. & Fellner, J. (2020). Legal situation and current practice of waste incineration bottom ash utilization in Europe. *Waste Management*, 102:868-883. <https://doi.org/10.1016/j.wasman.2019.11.031>
- BNDES (2014). Estimate of Investments in Sanitary Landfills for Complying with the Targets Established by the National Policy on Solid Waste between 2015 and 2019. BNDES Sectorial 40, 51 p. (in Portuguese).
- Bonaparte, R. (2018). Geotechnical stability of waste fills - Lessons learned and continuing challenges. Proc. 54th ASCE Karl Terzaghi Lecture, Geo-Institute of ASCE, Reston, VA.
- Borba, P.F.; Martins, E.M.; Ritter, E. & Correa, S.M. (2017). BTEX emissions from the largest landfill in operation in Rio de Janeiro, Brazil. *Bulletin of Environmental Contamination and Toxicology*, 98(1):624-631. <https://doi.org/10.1007/s00128-017-2050-5>
- Boskov, M.E.G.; Schiavon, J.A.; Hemsí, P.S.; Suzuki, D.K. & Schmidt, C.S. (2020). Modeling the rising of a MSW landfill with dikes and geogrid reinforcement. Proc. XX Congresso Brasileiro de Mecânica dos Solos e Engenharia Geotécnica, Campinas, SP. In Press.
- Bouthot, M.; Blond, E.; Fortin, A.; Vermeersch, O.G.; Quesnel, P. & Davidson, S. (2003). Landfill extension using geogrids as reinforcement: Discussion and case study in Quebec, Canada. Proc. Sardinia 2003, 9th International Waste Management and Landfill Symposium, Cagliari, Italy.
- BRASIL (2010). Law 12,305/10. National Policy on Solid Waste. Ministry of the Environment, Federal Government (in Portuguese).
- Bridi, E.; Ritter, E. & Bressani, L.A. (2015). Evaluation of biogas emissions in a landfill. Proc. VIII Congresso Brasileiro de Geotecnica Ambiental, Brasília, v. 1, pp. 109-115. (in Portuguese).
- Campi, T. & Boskov, M.E.G. (2011). Determination of shear strength parameters of Municipal Solid Waste (MSW) by means of static plate load tests. Proc. Geo-Frontiers 2011, Advances of Geotechnical Engineering, Dallas, v. 1, pp. 1227-1236.
- Caram, E.K.K. (2019). Use of a Remediation Technique by Ozone Injection in the Dissolved Phase: a Case Study at a Former Industrial Area Contaminated with Vinyl Chloride. M.Sc. Dissertation, Polytechnic School, University of São Paulo, 100 p. (in Portuguese).
- Caram, E.K.K. & Boskov, M.E.G. (2019). Effects of chemical oxidation in-situ by ozone sparging on groundwater physical-chemical parameters at a contaminated area. Proc. X Seminário de Engenharia Geotécnica do Rio Grande do Sul, GEORS 2019, Santa Maria, RS, v. 1, pp. 183-193. (in Portuguese).
- Carieri, F.; Nebbia, G. & Scotto, M. (1999). The construction of a "soil reinforced structure" by using waste. Proc. Sardinia 99, 7th International Waste Management and Landfill Symposium, Cagliari, Italy, v. 1, pp. 261-269.
- Carvalho, M.F. (1999). Mechanical Behavior of Urban Solid Waste. Ph.D. Thesis, São Carlos Engineering School. University of São Paulo, 330 p. (in Portuguese).
- CETESB (2016). Orienting Values for Soil and Ground Water in the State of São Paulo, available at <https://cetesb.sp.gov.br/aguas-subterraneas/valores-orientadores-para-solo-e-agua-subterranea/>.
- CETESB (2019). List of Contaminated and Rehabilitated Areas in the State of São Paulo - Updated until December 2019, available at <https://cetesb.sp.gov.br/areas-contaminadas/relacao-de-areas-contaminadas/>.
- Chen, Y.; Zhan, L. & Gao, W. (2019). Waste mechanics and sustainable landfilling technology: Comparison between HFWC and LFWC MSWs. Proc. 8th Int. Congress on Environmental Geotechnics, Hangzhou, China, v. 1, pp. 3-37.
- Chong, A.D. & Mayer, K.U. (2017). Unintentional contaminant transfer from groundwater to the vadose zone during source zone remediation of volatile organic com-

- pounds. *Journal of Contaminant Hydrology*, 204(1):1-10.
<https://doi.org/10.1016/j.jconhyd.2017.08.004>.
- Coelho, M.G. (2005). Behavior of Piezometers in a Landfill. M.Sc. Dissertation, Polytechnic School, University of São Paulo, 150 p. (in Portuguese).
- Conte, M. & Carrubba, P. (2013). Geotechnical implications in the construction of landfills. *Rivista Italiana di Geotecnica*, 1/2013:32-41.
- Costa, M.D.; Mariano, M.O.; Araújo, L.B. & Jucá, J.F. (2018). Laboratory studies to evaluate the performance of landfill cover layers for the reduction of gases emissions and infiltrations. *Engenharia Sanitária e Ambiental*, 23(1):77-90 (in Portuguese).
<https://doi.org/10.1590/S1413-41522018160393>
- Cox, R.; Campbell, M.; Thurgood, R. & Morgan, P. (2009). Design and Installation of a Permeable Reactive Barrier to Treat Carbon Disulphide Contaminated Groundwater. CLAIRE Technology Demonstration Project Report: TDP20, 118 p.
- Daciolo, L.V.P. (2020). Strength Parameters for MSW: Probabilistic Approach for Stability Analysis. M.Sc. Dissertation, Federal University of São Carlos, 100 p. (in Portuguese).
- D'Appolonia, D.J. (1980). Soil-bentonite slurry trench cut-offs. *Journal of Geotechnical Engineering*, 106(4):399-417.
- De Camillis, M.; Di Emidio, G.; Bezuijen, A. & Verastegui-Flores, R.D. (2019). Hydraulic conductivity and swelling ability of a polymer modified bentonite subjected to wet-dry cycles in seawater. *Geotextiles and Geomembranes*, 44(5):739-747.
<https://doi.org/10.1016/j.geotexmem.2016.05.007>
- Mattos, R.C.; Hems, P.S.; Kawachi, E.Y. & Silva, F.T. (2014). Use of sugarcane bagasse as carbon substrate in permeable reactive barriers: Laboratory batch tests and mathematical modeling. *Soils and Rocks*, 38(3):219-229.
- Di Molfetta, A. & Sethi, R. (2003). Permeable reactive barriers. Contaminated sites: Remediation technologies. Proc. 57th Corso di aggiornamento in Ingegneria Sanitaria Ambientale. Milan, Italy (in Italian).
- EUROSTAT (2018). Waste Statistics 2018, available at http://ec.europa.eu/eurostat/statistics-explained/index.php/Waste_statistics.
- Fujikawa, T.; Sato, K.; Koga, C. & Sakanakura, H. (2019). Evaluation of environmental safety on municipal solid waste incineration bottom ash using aging method. Proc. 8th Int. Congress on Environmental Geotechnics, Hangzhou, China, v. 1, pp. 320-327.
- Gavaskar, A.R.; Gupta, N.; Sass, B.M.; Janosy, R.J. & O'Sullivan, D. (1998). Permeable Barriers for Groundwater Remediation: Design, Construction and Monitoring. Battelle Press, Columbus, 176 p.
- Gillham, R.W. & O'Hannesin, S.F. (1994). Enhanced degradation of halogenated aliphatics by zero-valent iron. *Groundwater*, 32(6):958-967.
<https://doi.org/10.1111/j.1745-6584.1994.tb00935>
- Hemsi, P.S. & Shackelford, C.D. (2006). An evaluation of the influence of aquifer heterogeneity on permeable reactive barrier design. *Water Resources Research*, 42:W03402. <https://doi.org/10.1029/2005WR004629>
- Henry, S.M. & Warner, S.D. (2002). Chlorinated Solvent and DNAPL Remediation - Innovative Strategies for Subsurface Cleanup. American Chemical Society, Washington, DC, 346 p.
- Hettiarachchi, H. & Ge, L. (2009). Use of geogrids to enhance stability of slope in bioreactor landfills: A conceptual method. Proc. Int. Foundation Congress and Equipment Expo 2009, Orlando, v. 1, pp. 520-526.
- Huesker (2017). Recommendations for the use of PET and PVA geosynthetic reinforcements in an alkaline environment. Huesker Technical Report 2017-02-19.
- IAP (2017). "75 % of municipalities dispose residues at licensed landfills". Instituto Ambiental do Paraná, available at <http://www.iap.pr.gov.br/2017/07/1243/75>.
- IBGE (2010). National Research on Basic Sanitation. Instituto Brasileiro de Geografia e Estatística, available at <http://www.sidra.ibge.gov.br/bda/pesquisas/pnsb/default.asp>.
- ISWA (2006). Management of Bottom Ash from WTE Plants - An Overview of Management Options and Treatment Methods. ISWA, Working Group on Thermal Treatment. Rotterdam, Netherlands, 86 p.
- ITRC (2011). Permeable Reactive Barrier: Technology Update. Interstate Technology & Regulatory Council. PRB: Technology Update Team. Washington, D.C., 234 p.
- Kataguir, K. (2017). Proposition of Technical and Environmental Criteria for Creating a Soils Bank for the Metropolitan Region of São Paulo. M.Sc. Dissertation, Polytechnic School. University of São Paulo, 123 p. (in Portuguese).
- Kataguir, K.; Boscov, M.E.G.; Teixeira, C.E. & Angulo, S.C. (2019). Characterization flowchart for assessing the potential reuse of excavation soils in São Paulo city. *Journal of Cleaner Production*, 240:118215.
<https://doi.org/10.1016/j.jclepro.2019.118215>
- Ma, P.; Lan, J. & Ke, H. (2019). Field monitoring of a geogrid reinforced MSW slope. Proc. 8th Int. Congress on Environmental Geotechnics, Hangzhou, China, v. 2, pp. 724-731.
- Machado, M.R.V. & Hemsi, P.S. (2016). Continued development of a software for the probabilistic simulation of contaminant transport in aquifers. Proc. XXII Meeting of Scientific Undergraduate and Graduated Research, XXII ENCITA, Aeronautics Institute of Technology, São José dos Campos.

- Machado, S.L.; Carvalho, M.F. & Vilar, O.M. (2002). Constitutive model for municipal solid waste. *Journal of Geotechnical and Geoenvironmental Engineering*, 128(11):940-951.
<https://doi.org/10.1016/j.wasman.2009.09.005>
- Machado, S.L.; Carvalho, M.F. & Vilar, O.M. (2009). Modeling the influence of biodegradation on sanitary landfill settlements. *Soils and Rocks*, 32(3):123-134.
- Magnusson, S.; Lundberg, K.; Svedberg, B. & Knutsson, S. (2015). Sustainable management of excavated soil and rock in urban areas - A literature review. *Journal of Cleaner Production*, 93(1):18-25.
<https://doi.org/10.1016/j.jclepro.2015.01.010>
- Mahler, C.F. & Lamare Neto, A. (2003). Shear resistance of mechanical biological pretreated domestic urban waste. *Proc. 9th International Waste Management and Landfill Symposium, Sardinia 2003, Cagliari*, v. 1, pp. 6-10.
- Mahler, C.F. & Lamare Neto, A. (2005). Fiber influence on shear strength of mechanically and biologically pretreated waste. *Proc. XXIII Congresso Bras. Engenharia Sanitária e Ambiental, Campo Grande*, v.1, pp. 1-8. (in Portuguese).
- Malavoglia, G.C. (2016). Viscoelastic models applied to compression of MSW. M.Sc. Dissertation, University of São Paulo, São Paulo, 110 p. (in Portuguese).
- McKnight, J.T. & Owaidat, L.M. (2001). Quality control and performance of a cut-off wall for containment of a DNAPL plume. *Proc. Int. Conference on Containment & Remediation Technology, Orlando*, v. 1, pp. 1-5.
- Miguel, M.G.; Mortatti, B.C.; Paixão Filho, J.L. & Pereira, S.Y. (2018). Saturated hydraulic conductivity of municipal solid waste considering the influence of biodegradation. *Journal of Environmental Engineering*, 144(9):10.1061.
[https://doi.org/10.1061/\(ASCE\)EE.1943-7870.0001432](https://doi.org/10.1061/(ASCE)EE.1943-7870.0001432)
- Monier, V.; Mudgal, S.; Hestin, M.; Trarieux, M. & Mimid, S. (2011). Service Contract on Management of Construction and Demolition Waste (Final Report for Commission DG Environment). Contract 07.0307/2009/540836/SER/G2. Bio Intelligence Service, Paris, 240 p.
- Montalvan, E.L.T. & Boscov, M.E.G. (2018). Geotechnical parameters of mixtures of a tropical soil with water treatment sludge. *Proc. 8th Int. Congress on Environmental Geotechnics. Hangzhou, China*, v. 1, pp. 235-241.
- Naidu, R. & Birke, V. (eds.) (2015). *Permeable Reactive Barriers - Sustainable Groundwater Remediation*. Taylor & Francis. Boca Raton, 333 p.
- Neville, A. (2004). The confused world of sulfate attack on concrete. *Cement and Concrete Research*, 34(8):1275-1296.
<https://doi.org/10.1016/j.cemconres.2004.04.004>
- Nishiyama, M.; Yamamoto, R. & Hoshiro, H. (2006). Long-term durability of Kuralon (PVA fiber) in alkaline condition. *Proc. 10th Int. Bonded Fiber Composites Conference, IIBCC 2006, São Paulo*, v. 1, pp. 120-134.
- Nobre, R.C.M.; Nobre, M.M.M. & Galvão, A.S.S. (2006). A remediation strategy for mercury contaminated groundwater using a permeable reactive barrier. *Proc. 5th Int. Congress on Environmental Geotechnics, Cardiff*, v. 1. p. 213-220.
- Nogami, J.S. & Villibor, D.F. (1995). *Low-Cost Paving using Lateritic Soils*. Villibor, São Paulo, 213 p. (in Portuguese).
- Nomachi, R.Y.G. & Boscov, M.E.G. (2016). Characterization of the scalped material of recycled construction residues for geotechnical use. Technical Report: University of São Paulo and CNPq (in Portuguese).
- Norberto, A.S.; Mariano, M.O.; Corrêa, C.L. & Jucá, J.F. (2020). Statistical analysis of shear strength parameter variability in landfills. *Journal of Environmental Analysis and Progress*, 5(1):108-116 (in Portuguese).
<https://doi.org/10.24221/jeap.5.1.2020.2840.108-116>
- Oliveira, E. (2019). "Out of 417 municipalities of BA state, only 43 have a sanitary landfill to destine daily waste, reveals research", available at <https://g1.globo.com/ba/bahia/noticia>. (In Portuguese).
- Petersen, L.; Minkinen, P. & Esbensen, K.H. (2005). Representative sampling for reliable data analysis: Theory of sampling. *Chemometrics and Intelligent Laboratory Systems*, 77(1-2):261-277.
<https://doi.org/10.1016/j.chemolab.2004.09.013>
- Qian, X.; Koerner, R.M. & Gray, D.H. (2001). *Geotechnical Aspects of Landfill Design and Construction*. Prentice Hall. Upper Saddle River, 717 p.
- Renken, K.; Mchaina, D. & Yanful, E. (2007). Use of geosynthetics in the mining and mineral processing industry. *Geosynthetics*, 25(4):38-42.
- Ryan, C.R. (1987). Vertical barriers for pollution control. *Geotechnical Practice for Waste Disposal* 87. ASCE Geotechnical Special Publication, 1(13):182-204.
- Santos, E.C.G. (2007). Use of Recycled Construction and Demolition Waste in Structures of Reinforced Soil. M.Sc. Dissertation, University of São Paulo, 168 p. (in Portuguese).
- Santos, E.C.G. (2011). Experimental Evaluation of Reinforced Walls Built with Recycled Construction and Demolition Waste and Fine Soil. Ph.D. Thesis, University of Brasília, 248 p. (in Portuguese).
- Shackelford, C.D. (2005). Environmental issues in Geotechnical Engineering. *Proc. 16th Int. Conference on Soil Mechanics and Geotechnical Engineering, Osaka, Japan*, v. 1, pp. 95-122.
- Shackelford, C.D. & Jefferis, S.A. (2000). Geo-environmental engineering for in situ remediation. *Proc. Geo-Eng2000, International Conference on Geotechnical & Geological Engineering, Melbourne*, v. 1, pp. 121-185.

- Shackelford, C.D.; Benson, C.H.; Katsumi, T.; Edil, T.B. & Lin, L. (2000). Evaluating the hydraulic conductivity of GCLs permeated with non-standard liquids. *Geotextiles and Geomembranes*, 18(1):133-161. [https://doi.org/10.1016/S0266-1144\(99\)00024-2](https://doi.org/10.1016/S0266-1144(99)00024-2)
- Sharma, R.K. & Hymavathi, J. (2016). Effect of fly ash, construction demolition waste and lime on geotechnical characteristics of a clayey soil: a comparative study. *Environmental Earth Sciences*, 75(5):1-11. <https://doi.org/10.1007/s12665-015-4796-6>
- Silva, A.S. (2017). Evaluation of mixtures of WTS and lime aiming the application as daily cover in sanitary landfills. M.Sc. Dissertation, Civil Engineering, Aeronautics Institute of Technology, 93 p. (in Portuguese).
- Simões, G.F. & Catapreta, C.A. (2010). Assessment of long-term settlement prediction models for municipal solid wastes disposed in an experimental landfill. *Soils and Rocks*, 33(2):55-67.
- Souto, G.D.B. & Povinelli, J. (2007). Characteristics of the leachate from sanitary landfills in Brazil. *Proc. 24th Brazilian Congress on Sanitary and Environmental Engineering*. Belo Horizonte, v. 1, pp. 1-7 (in Portuguese).
- Sowers, G.F. (1973). Settlement of waste disposal fills. *Proc. 8th Int. Conference on Soil Mechanics and Foundation Engineering*, Moscow, v. 22, pp. 207-210.
- Stankevicius, P.M.; Benevides, B.N.; Ângulo, S.C. & Boscov, M.E.G. (2019). Stabilization of expansive soil with scalped material of civil construction waste. *Proc. GEOSUL 2019, XII Simpósio de Práticas de Engenharia Geotécnica da Região Sul*, Joinville, v. 1, pp. 1-10. (in Portuguese).
- Stroo, H. F. & Ward, C. H. (2010). *In situ Remediation of Chlorinated Solvent Plumes*. SERDP, ESTCP, Springer Science, New York, 725 p.
- Suthersam, S.S. (1999). *Remediation Engineering Design Concepts*. CRC Lewis Publishers, New York, 627 p.
- Tano, F. & Olivier, F. (2014). Use of geosynthetics in piggy-back landfills: development of an iterative methodology for the design of the lining system over old unlined waste. *Proc. 10th Int. Conference on Geosynthetics*, Berlin, v. 3, pp. 2111-2118.
- Tano, F.; Olivier, F.; Touze-Foltz, N. & Dias, D. (2015). State-of-the-art of Piggy-Back landfills worldwide: Comparison of containment barrier technical designs and performance analysis in terms of geosynthetics stability. *Proc. Geosynthetics Conference*, Portland, v. 1, pp. 1210-1220.
- Teixeira, C.E.; Torves, J.C.; Finotti, A.R.; Fedrizzi, F.; Marinho, F.A.M. & Teixeira, P.F. (2009). Studies on the aerobic methane oxidation at three sanitary landfills covers in Brazil. *Engenharia Sanitária e Ambiental*, 14(1):99-108.
- Thenkabail, P.S. (2016). *Land Resources Monitoring, Modeling, and Mapping with Remote Sensing*. CRC Press, New York, 885 p.
- Tieman, G.E.; Druback, G.W.; Davis, K.A. & Weidner, C.H. (1990). Stability of vertical piggyback landfill expansions. In: *Geotechnics of Waste Fills - Theory and Practice*. Philadelphia, ASTM STP 1070, pp. 285-297.
- Trindade, G.B.; Hems, P.S.; Buzzi, D.C.; Tenório, J.A.S. & Boscov, M.E.G. (2018). Rates of sulfate reduction achieved in columns based on untreated sugarcane bagasse for metals removal. *Journal of Environmental Engineering*, 144(7):04018046. [https://doi.org/10.1061/\(ASCE\)EE.1943-7870.0001382](https://doi.org/10.1061/(ASCE)EE.1943-7870.0001382)
- Tsugawa, J.K.; Pereira, K.F.S. & Boscov, M.E.G. (2017). Thixotropy of sludge from the Cubatão water treatment plant, Brazil. *Proc. Geotechnical Frontiers 2017*, Orlando, v. 1, pp. 842-851.
- Tsugawa, J.K.; Romano, R.C.O.; Pileggi, R.G. & Boscov, M.E.G. (2018). A rheological approach for the evaluation of geotechnical use of water treatment sludge. *Proc. 8th Int. Congress on Environmental Geotechnics*. Hangzhou, China, v. 1, pp. 264-272.
- Tsugawa, J.K.; Sabino, E.F.; Monte, R. & Boscov, M.E.G. (2019). Importance of composing representative samples according to the Theory of Sampling (TOS) for the reuse of water treatment sludge. *Proc. XVI Pan-American Conference on Soil Mechanics and Geotechnical Engineering*, Cancun, Mexico, v. 1., pp. 2450-2457.
- Ulsen, C.; Kahn, H.; Hawlitschek, G.; Masini, E.A. & Ângulo, S.C. (2013). Separability studies of construction and demolition waste recycled sand. *Waste Management*, 33(3):656-662. <https://doi.org/10.1016/j.wasman.2012.06.018>
- U.S. EPA (1997). *Report on the North Belmont PCE Site Remedial Investigation*, North Belmont, Gaston County, 143 p., SESD Project No. 96S-058/June, 1997.
- van Elk, A.G.H.P. & Boscov, M.E.G. (2016). Geotechnical challenges resulting from the National Policy on Solid Waste. *Proc. XVIII Congresso Brasileiro de Mecânica dos Solos e Engenharia Geotécnica*, Belo Horizonte, MG (in Portuguese).
- Vanderkooy, M.; McMaster, M.; Wealthall, G.; Seyedabbasi, M.A.; Sale, T.C. & Newell, C.J. (2014). *User's Guide for 14-Compartment Model*, Prepared for the Strategic Environmental Research and Development (SERDP) Program, 53 p.
- Vardanega, P.J. & Haigh, S.K. (2014). The undrained strength-liquidity index relationship. *Canadian Geotechnical Journal*, 51(9):1073-1086. <https://doi.org/10.1139/cgj-2013-0169>
- Wang, M.C.; Hull, J.Q.; Jao, M.; Dempsey, B.A. & Cornwell, D.A. (1992). Engineering behavior of water treatment sludge. *Journal of Environmental Engineering*, 118(6):848-864. [https://doi.org/10.1061/\(ASCE\)0733-9372\(1992\)118:6\(848\)](https://doi.org/10.1061/(ASCE)0733-9372(1992)118:6(848))

- WHO (1999). Environmental Health Criteria 215 - Vinyl Chloride. United Nations Environment Programme, International Labour Organization, World Health Organization and Inter-Organization Programme for the Sound Management of Chemicals, Geneva, 382 p.
- WHO (2017). Guidelines for Drinking-Water Quality, 4th edition incorporating the first addendum. World Health Organization, available at http://www.who.int/water_sanitation_health/publications/drinking-water-quality-guidelines-4-including-1st-addendum/en/.
- Yuzhu, W. (1996). Conditioning Water Treatment Sludge: Case Study. M.Sc. Dissertation, Polytechnic School. University of São Paulo, 190 p. (in Portuguese).

Requiem for risk classification matrices

Waldemar C. Hachich^{1, #} 

Article

Keywords

Decision analysis
Reliability
Risk analysis
Utility theory

Abstract

Classification matrices are scrutinized for inconsistencies, errors and deficiencies in meaning. Proper definition, measurement and ranking of risks are demonstrated as compelling arguments whenever risk and reliability analyses of geotechnical structures, such as dams, are required.

1. Introduction: measurement scales

Classification is a most fundamental organizational activity. It may involve, for example, grouping, in classes or categories, objects which exhibit similar characteristics that distinguish them from others. For such a purpose, a nominal scale is enough. Figure 1 presents the example of a classification of a group of tailings dams exclusively in accordance with the construction procedure.

It should be quite clear that, even when numbers are used to identify different categories, none of the usual mathematical operations are valid on those numbers, because they just serve the purpose of nominating classes (thus *nominal* scale).

One could also *sort, order or rank* objects in accordance with a chosen criterion. Using a similar example, a relevant sort might be in order of increasing vulnerability (Fig. 2). The term risk is being purposely avoided at this point, while vulnerability is being temporarily proposed as a rather intuitive concept associated with the adopted construction procedure.

Figures 2 and 3 provide evidence of statements by Ackoff (1962) and other theoreticians of measurement (bold not in original paper):

*“The use of a letter or a word is no less measurement than is the use of a number, **provided that we make explicit, as we must in the case of numbers as well, what operations may be performed on the symbols.**”*

Measurement is a way of obtaining symbols to represent the properties of objects, events, or states, which symbols have the same relevant relationship to each other as do the things which are represented.”

It is indeed indifferent to name a certain dam either H or 4. No mathematical operation can or should be per-

formed on those symbols. It will be shown, however, that those dams are sorted according to a measure of decreasing risk.

In its strict sense, measurement involves the use of a constant measurement unit. This unit can be arbitrarily es-

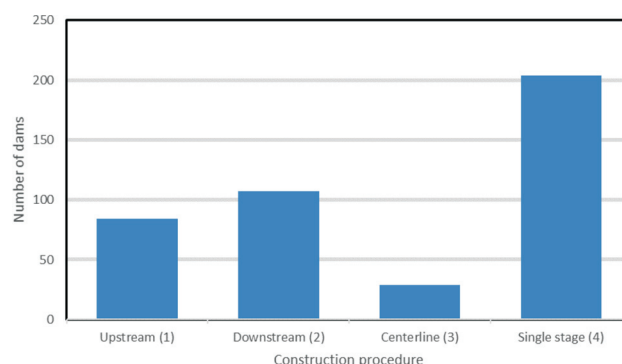


Figure 1. Example of classification of a group of tailings dams according to construction procedure.

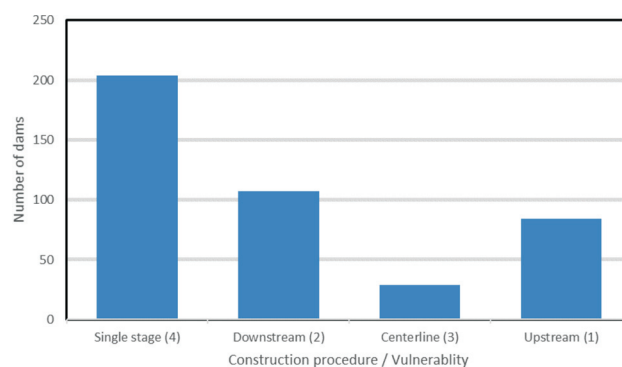


Figure 2. Example of classification of a group of tailings dams according to vulnerability derived from construction procedure.

[#]Corresponding author. E-mail address: whachich@usp.br.

¹Universidade de São Paulo, São Paulo, SP, Brazil.

Submitted on July 4, 2020; Final Acceptance on August 3, 2020; Discussion open until December 31, 2020.

DOI: <https://doi.org/10.28927/SR.433497>



This is an Open Access article distributed under the terms of the Creative Commons Attribution License, which permits unrestricted use, distribution, and reproduction in any medium, provided the original work is properly cited.

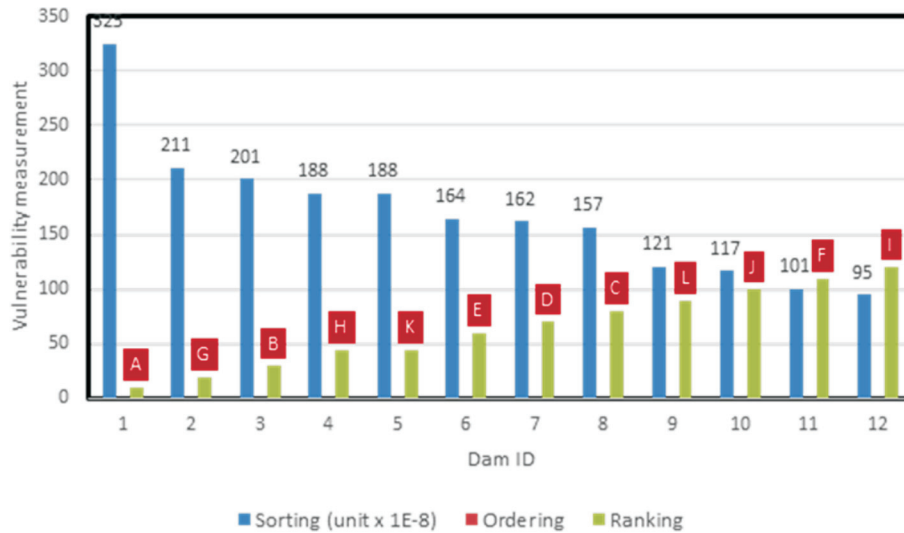


Figure 3. Example of sorting, ordering and ranking of a group of dams according to vulnerability.

tablished when there is no natural zero, such as in the case of the Celsius and Fahrenheit scales. In such cases mathematical operations can be performed on intervals, but not directly on the values themselves. Those are called *interval scales*.

When there is a natural zero, such as in the scales of length, weight, and so on, all usual mathematical operations are valid for the numbers that express the measurements and those scales are called *ratio or proportional scales*. 40 cm, for example, is twice 20 cm. One cannot say, however, that 40 degrees Celsius is twice 20 °C, while it is possible to say that the difference in temperature between 20 and 40 is equal to the difference between 40 and 60 °C.

A ratio scale is usually preferred over any of the others because it is more informative about the measured quantity. Given our interest in the risk associated with geotechnical structures such as fills, slopes, dams, the question is obvious: can a ratio scale be devised to appropriately measure risk?

2. Measurement scale for risk

The answer to that question must be based upon the definition of risk itself, as firmly established in the field of *Risk Analysis*: risk involves a combination (product) of probability of a certain action (or hazard) and the consequences thereof (it is worth noting that the insurance industry uses a different definition of risk).

Thus, Risk Analysis defines risk as the probability of an event, p , multiplied by its consequences, C^* (Fig. 4, Hachich, 2002). Consequences are seldom just economic. For the sake of conciseness, other types of consequences, such as social and environmental, which are obviously equally relevant from a practical standpoint, are not going to be explored in this paper, given that the fundamental flaw of risk matrices can be demonstrated on the basis of just one type of consequence (Pratt *et al.*, 1965).

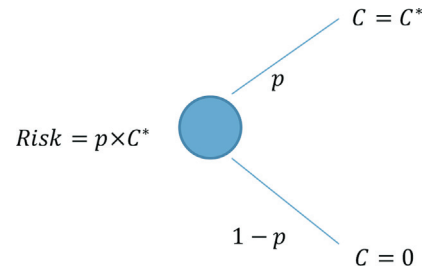


Figure 4. Risk as the product of uncertainty and consequences (Hachich, 2002).

As a matter of fact, the proper definition of risk and its use for classification of geotechnical structures is the crucial point of this paper.

When hazards present themselves at several levels, each of them associated with a certain probability and consequence, risk is computed as a weighted average of the consequences, having probabilities as weights (Fig. 5, Hachich, 2002). Risk is, therefore, the *expected value* of consequences. The risk associated with the circumstances represented by Fig. 6, for example, is quantified by the area below the dotted line.

The unduly and conceptually wrong use of matrices for risk classification has been criticized for almost 20

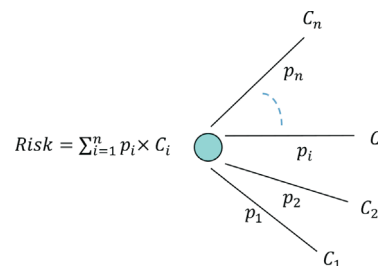


Figure 5. Risk as the expected consequence (Hachich, 2002).

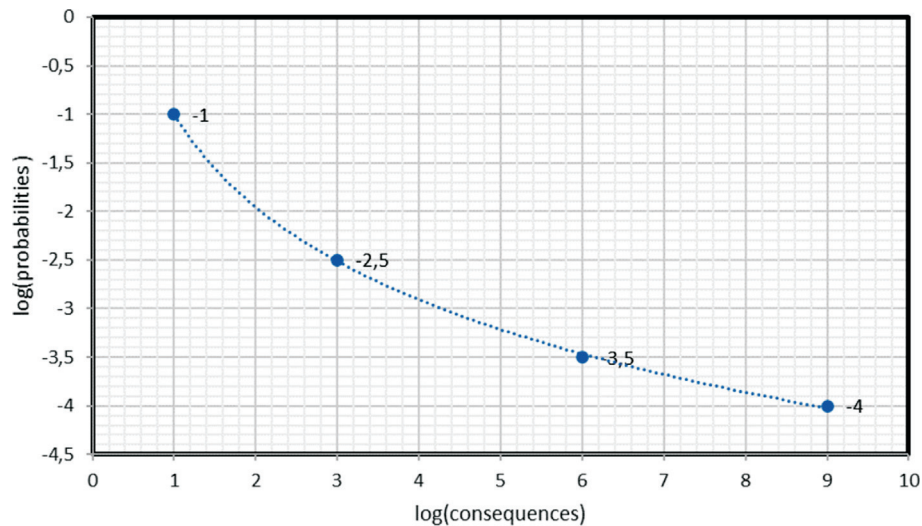


Figure 6. Example of graphical representation of risk on the probability-consequence space (adapted from Oboni, 1998).

years (Hachich, 2002). The final objective of risk evaluation is to provide guidance as to decisions that have to be made. It is therefore natural that risk be interpreted within the context of Decision Analysis (Raiffa, 1968) and *Utility Theory*.

As previously pointed out, the definition in Fig. 5 corresponds to the application of the expected value operator to the consequences. If one considers several different sets of circumstances, each with a graphical representation similar to that in Fig. 6, the values of the areas below the curves may be interpreted as a mapping on a scale of preferences, the case of smallest area being preferred over any of the others. As previously pointed out, those areas need not (or perhaps should not) be restricted to economic values: as a matter of fact, if *Utility Theory* is invoked to assign values of *utilities* to different combinations of economic, social and environmental consequences, Decision Analysis can be applied to more general situations (Keeney & Raiffa, 1976).

The preference for ratio scales has been previously stated. Probabilities are measured between zero and one in a ratio scale. Consequences are also measured in a ratio scale, and utilities can also be defined between zero and one. Given the definition of risk, there is no reason whatsoever why it should not be measured in a ratio scale.

Figure 3 presented the classification of a set of dams on the basis of risks posed by them. Classification must start, of course, with the evaluation of risks, and that is the only way of doing it correctly.

3. “Risk” classification matrices

Our interest is focused, of course, in those dams that pose higher risks: they should be the priority of mitigating actions. Given the definition of risk, its evaluation requires studies of some complexity performed by a team of engineers capable of evaluating probabilities of geotechnical,

hydrological, hydraulic and many other engineering-related events, in addition to their consequences (and possibly utilities as well).

In some cases, it is known beforehand that risks are not small because of the construction procedure, the lack of information and contingency plans, faulty conservation and many other reasons. In such cases it is usual to see published tables such as Table 1, often based on a wrong definition of risk. The scale adopted for the table is obviously nominal, even if someone decides to exchange symbols for numbers in the cells, such as in Table 2. It follows that mathematical operations performed on those numbers are not acceptable.

The inconsistencies of such an approach are further explored in Hachich (2002). Re-stating Ackoff (1962): “used symbols, such as numbers, must have the same rele-

Table 1. Example of “risk” matrix with the usual type of symbol-based nominal scale (*ad hoc* chosen characters).

“Risk”	Potential damage		
	High	Medium	Low
High	A	B	C
Medium	B	C	D
Low	B	C	E

Table 2. Example of “risk” matrix with the usual type of symbol-based nominal scale (*ad hoc* chosen digits).

“Risk”	Potential damage		
	> 1000	1 to 1000	< 1
> 0.01	5	4	3
0.0001 to 0.01	4	3	2
< 0.0001	4	3	1

Table 3. Example of “risk” matrix with the usual type of symbol-based nominal scale (arbitrarily chosen description/classification and “corresponding” digits).

Seepage (e)	Displacements (f)	Flood return period (g)
Perfectly controlled (0)	No significant displacements (0)	< 500 (0)
Some small areas of leakage downstream but abutments in good condition (3)	Small cracks and settlements undergoing corrective measures (2)	500 (2)
Areas of leakage downstream, slopes and abutments lacking proper corrective measures (6)	Small cracks and settlements lacking proper corrective measures (5)	1000 (5)
Areas of leakage downstream, with increasing flow and material (10)	Cracks, settlements and local instabilities (10)	10000 (10)
EC = Σ (e to g)		

vant relationship to each other as do the things which are represented”. In the present case, our interest in risks would require such numbers to be values measured in a ratio scale, so as to represent actually computed risks.

The possibility of “risk” scales such as those in Table 2 leading to decisions that reflect the decision maker’s preferences is never demonstrated, while Decision Analysis and Utility Theory offer mathematical proof (Keeney & Raiffa, 1976). Surprisingly, however, arbitrarily chosen nominal scales are one of the most ubiquitous features of published papers on “risk” assessment. Table 3 is just one such example, borrowed from a real-world situation.

The scales in Table 3 are obviously nominal scales. It is indifferent to identify seepage control as “perfect” or to assign the symbol “0” to it. For this reason, the summation presented in the last line of the table has no meaning whatsoever. But supposing, just for the sake of the argument, that the numbers that appear in the cells of Table 3 would have been arrived at by correctly engineered evaluations, the summation would still be completely wrong: Probability Theory (e.g. Benjamin & Cornell, 1970) teaches us that the probability of a joint event is the **product** (not sum) of the individual probabilities, whenever the events can be as-

sumed to be independent from each other, which is not necessarily true for some of the failure modes.

In the original source, however, Table 3 is presented as a table of “risk” classification. As previously discussed, those cell contents cannot be called risks for at least two reasons: their scale is just nominal, and consequences are not taken into account. As far as the latter, Table 4 presents an attempt at classification of at least part of the information that is relevant for the evaluation of the consequences of failure.

Once again, and for similar reasons, the summation presented in the last line of Table 4 is meaningless.

Table 4 naturally implies 4⁵ categories (or classes), so that a number between one and 1024 can be assigned to technically classify a given dam. If two dams fall in the same class, they may be considered as “equal” from a technical point of view. When they fall in different classes, however, Table 4 is of no help for deciding which one poses the higher risk.

It is also possible to use just the cell positions to create a 5-digit code number (with a fixed digit position for each property) to identify each technical class. Code 23442, for example, would identify a dam with height between 15 m and 30 m, crest length between 200 m and 600 m, design flow lower than 500, upstream construction and monitoring

Table 4. Classification matrix with part of the information that is relevant for the evaluation of the consequences of failure (symbol-based nominal scale with arbitrarily chosen description/classification and “corresponding” digits).

Design criteria and maintenance				
Height (a)	Length (b)	Design flow PMF (c)	Construction procedure (d)	Monitoring (e)
≤ 15 m (0)	≤ 50 m (0)	10000 (0)	Single stage (0)	Monitoring instruments installed according to design (0)
15 to 30 m (1)	50 to 200 m (1)	1000 (2)	Downstream (2)	Monitoring instruments in the process of being installed (2)
30 to 60 m (4)	200 to 600 m (2)	500 (5)	Centerline (5)	Monitoring instruments do not follow the design (6)
> 60 m (7)	> 600 m (3)	< 500 (10)	Upstream (10)	No monitoring instruments (8)
CT = Σ (a to e)				

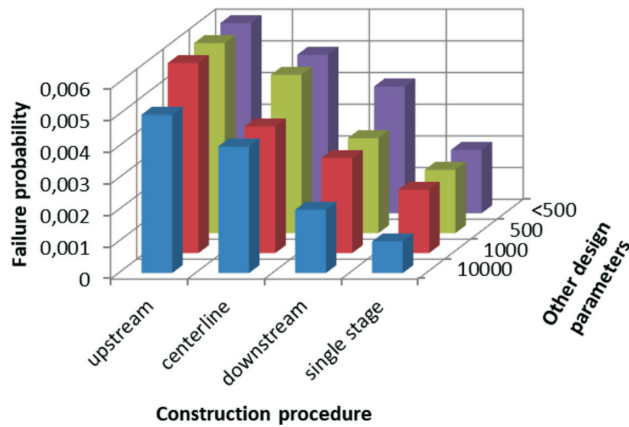


Figure 7. Example of quantitative results obtained from the elicitation of probabilities of failure of dams.

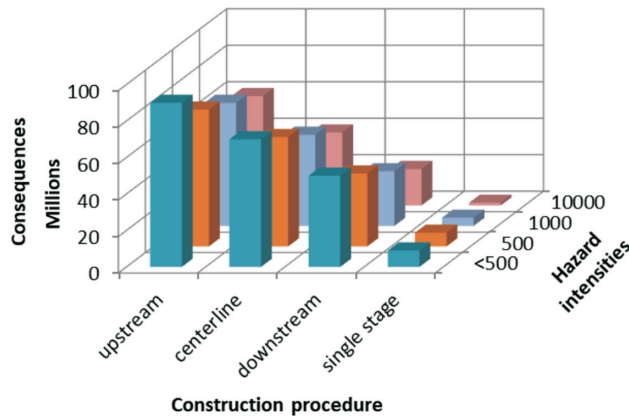


Figure 8. Example of quantitative results obtained from the evaluation of failure scenarios and their consequences.

instruments being installed. Neither this classification nor the approach based on the numeric symbols assigned to cells of Table 4 (the summation formula in particular) would support any decision regarding the relative risks of class 23442 versus, for example, class 32341.

4. Sorting a group of dams according to risk

The need to rank a group of dams according to the risks they pose is obviously desirable.

Despite having been often and extensively attempted, for the aforementioned conceptual reasons this objective cannot be correctly achieved by means of classification matrices such as Tables 3 and 4, let alone by their summaries of summation points.

Again Ackoff (1953) warns that:

“We must be careful not to impute automatically to numbers obtained by any process of assigning numbers to objects, events, or properties, the properties which these numbers have as numbers. We can add the numbers of two houses or of

two car registrations, but the question is whether or not the sum has any meaning, and if so what.”

The desired result would be Fig. 3, with the y-axis representing risks associated to the series of blue columns, and risks computed according to the proper engineering definition (Fig. 5). Two activities are therefore required:

- Engineering analysis for the quantitative elicitation of probabilities of failure of dams, usually complemented by extensive historical research in order to generate results which include and extend those in Fig. 7;
- Preview and evaluate failure scenarios and their consequences, in order to generate quantitative results which include and extend those in Fig. 8.

5. Conclusions

Decision Analysis and Utility Theory (Pratt *et al.*, 1965) provide a sound theoretical basis for the definition, evaluation and ranking of risks. Results of risks measured in a ratio scale also conform with Measurement Theory.

None of above holds for “risk” classification matrices, which usually ignore or violate well established theoretical principles. Consequently, there is no place for such arbitrary matrices in serious safety and reliability studies.

Acknowledgments

The author is deeply indebted and grateful to Bruno Szpigel Dzialoszynski, Luiz Guilherme de Mello and Werner Bilfinger. Their support and help have been essential to the very existence of this paper.

References

- Ackoff, R.L. (1962). *Scientific Method: Optimizing Applied Research Decisions*. John Wiley & Sons, New York.
- Ackoff, R.L. (1953). *The Design of Social Research*. University of Chicago Press, Chicago.
- Benjamin, J.R. & Cornell, C.A. (1970.). *Probability, Statistics and Decision For Civil Engineers*. McGraw-Hill Book Company, New York.
- Hachich, W.C. (2002). Risk assessment: some views on current practice as evidenced by papers presented to conferences and symposia. Proc. Fourth International Congress on Environmental Geotechnics, ICEG4, Rio de Janeiro, August 11-15, Balkema.
- Keeney, R.L. & Raiffa, H. (1976). *Decisions With Multiple Objectives*. John Wiley & Sons, New York.
- Oboni, F. (1998). *Geo-environmental risk: Assessment, analysis, management and planning*. Simpósio Brasileiro de Geotecnia Ambiental, SIGA98, São Paulo, September 29-30, ABMS, (CD-ROM).
- Pratt, J.W.; Raiffa, H. & Schlaiffer, (1965). *R.O. Introduction to Statistical Decision Theory*. McGraw-Hill Book Company, New York.
- Raiffa, H. (1968). *Decision Analysis*. Addison-Wesley, Reading.

SOILS and ROCKS

An International Journal of Geotechnical and Geoenvironmental Engineering

Publication of

ABMS - Brazilian Association for Soil Mechanics and Geotechnical Engineering

SPG - Portuguese Geotechnical Society

Volume 43, N. 3, July-September 2020

Author index

Abreu, A.V.	287	Leão, M.F.	297
Almeida, M.C.F.	219	Lima, C.A.	57
Almeida, M.S.S.	287	Lima, D.C.	271
Arêdes, A.C.N.B.	85	Liu, J.L.	43
Assis, A.P.	171, 311	Lopes, Ma.B.	171
Assis, L.E.	57	Luo, Y.S.	43
Augusto Filho, O.	71	Marques, E.A.G.	57, 85, 297
Bicalho, K.V.	103	Melchior Filho, J.	11
Bilfinger, Werner	397	Mello, L.G.F.S.	369
Bobet, A.	123	Mello, Luiz Guilherme de	397
Bonan, V.H.F.	11	Menezes, S.J.M.C.	57
Borges, J.L.	199	Messad, A.	181
Borges, R.G.	219	Miguel, G.D.	151, 339
Boscov, Maria Eugenia Gimenez	461	Mirmoradi, S.H.	419
Boufarh, R.	247	Moreira, Eciesielter Batista	339
Bragagnolo, L.	159, 279	Moura, A.S.	11
Braun, A.B.	97	Moussai, B.	181
Bressani, L.A.	31	Nascimento, G.	419
Carvalho, T.R.R.	297	Oliveira Filho, A.G.	103
Celestino, T.B.	123	Oliveira, A.H.C.	85
Consoli, N.C.	159, 339	Palmeira, Ennio M.	351
Craig, A.M.L.	71	Pitanga, H.N.	271
Cui, Y.X.	43	Prestes, E.	279
da Silva, J. Lins	231	Prietto, P.D.M.	159, 279
de Freitas, A.C.	3, 141	Roque, L.A.	57
Debbab, O.Y.	181	Saadi, D.	247
Dias Neto, S.L.S.	271	Sales, Maurício Martines	441
Domiciano, M.L.	231	Santos Junior, O.F.	263
Donato, M.	151	Santos, E.C.G.	231
Dong, J.G.	21	Santos, R.M.	199
dos Santos, L. F.	3, 141	Saraiva, A.	141
Dzialoszyński, B.S.	369	Schnaid, F.	369
Ehrlich, M.	419	Silva, A.C.	191, 441
Favretto, J.	151	Silva, T.O.	271
Ferrazzo, S.T.	279	Silva, W.G.	271
Ferreira, S.R.M.	191	Silveira, A.A.	159
Festugato, Lucas	339	Soares de Almeida, M.S.	219
Flores, J.A.	31	Souza Junior, L.O.	219
Floss, M.F.	151	Souza Junior, P.L.	263
Fontoura, T.B.	263	Thomé, A.	97
Freitas Neto, O.	263	Tímbola, R.S.	279
Fucale, S.	191	Totola, L.B.	103
Gusmão, Alexandre Duarte	441	Trentin, A.W.S.	97
Hachich, W.C.	497	Trindade, T.P.	271
Heidemann, M.	31	Ulsen, C.	159
Hemsi, Paulo Scarano	461	Vargas, G.D.L.P.	279
Hisatugu, W.H.	103	Visentin, C.	97
Hou, T.S.	43	Vitali, O.P.M.	123
Korf, E.P.	159, 279	Wei, G.F.	21
Laouar, M.S.	247	Wolle, Claudio Michael	397



- > **Prospecção Geotécnica**
Site Investigation
- > **Consultoria Geotécnica**
Geotechnical Consultancy
- > **Obras Geotécnicas**
Ground Treatment-Construction Services
- > **Controlo e Observação**
Field Instrumentation Services and Monitoring Services
- > **Laboratório de Mecânica de Solos**
Soil and Rock Mechanics Laboratory

Certificada ISO 9001 por

BVQI



Geocontrole



Parque Oriente, Bloco 4, EN10
2699-501 Bobadela LRS
Tel. 21 995 80 00
Fax. 21 995 80 01
e.mail: mail@geocontrole.pt
www.geocontrole.pt


Geocontrole
Geotecnia e Estruturas de Fundação SA



COBA



GEOLOGY AND GEOTECHNICS

Hydrogeology • Engineering Geology • Rock Mechanics • Soil Mechanics • Foundations and Retaining Structures • Underground Works • Embankments and Slope Stability
Environmental Geotechnics • Geotechnical Mapping



- Water Resources Planning and Management
- Hydraulic Undertakings
- Electrical Power Generation and Transmission
- Water Supply Systems and Pluvial and Wastewater Systems
- Agriculture and Rural Development
- Road, Railway and Airway Infrastructures
- Environment
- Geotechnical Structures
- Cartography and Cadastre
- Safety Control and Work Rehabilitation
- Project Management and Construction Supervision



PORTUGAL

CENTER AND SOUTH REGION
Av. 5 de Outubro, 323
1649-011 LISBOA
Tel.: (351) 210125000, (351) 217925000
Fax: (351) 217970348
E-mail: coba@coba.pt
www.coba.pt

Av. Marquês de Tomar, 9, 6º.
1050-152 LISBOA
Tel.: (351) 217925000
Fax: (351) 213537492

NORTH REGION

Rua Mouzinho de Albuquerque, 744, 1º.
4450-203 MATOSINHOS
Tel.: (351) 229380421
Fax: (351) 229373648
E-mail: engico@engico.pt

ANGOLA

Praceta Farinha Leitão, edifício nº 27, 27-A - 2º Dto
Bairro do Maculusso, LUANDA
Tel./Fax: (244) 222338 513
Cell: (244) 923317541
E-mail: coba-angola@netcabo.co.ao

MOZAMBIQUE

Pestana Rovuma Hotel. Centro de Escritórios.
Rua da Sé nº 114. Piso 3, MAPUTO
Tel./Fax: (258) 21 328 813
Cell: (258) 82 409 9605
E-mail: coba.mz@tdm.co.mz

ALGERIA

09, Rue des Frères Hocine
El Biar - 16606, ARGEL
Tel.: (213) 21 922802
Fax: (213) 21 922802
E-mail: coba.alger@gmail.com

BRAZIL

Rio de Janeiro
COBA Ltd. - Rua Bela 1128
São Cristóvão
20930-380 Rio de Janeiro RJ
Tel.: (55 21) 351 50 101
Fax: (55 21) 258 01 026

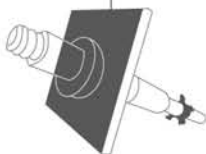
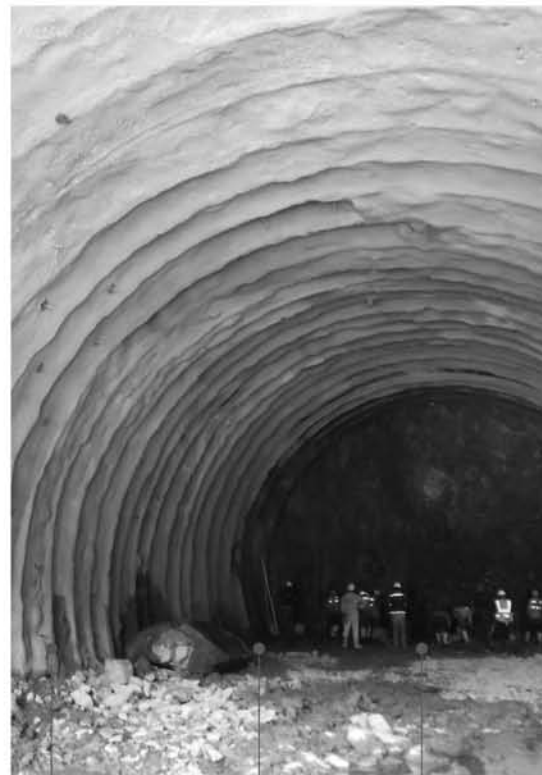
Fortaleza

Av. Senador Virgílio Távora 1701, Sala 403
Aldeota - Fortaleza CEP 60170 - 251
Tel.: (55 85) 3261 17 38
Fax: (55 85) 3261 50 83
E-mail: coba@esc-te.com.br

UNITED ARAB EMIRATES

Corniche Road - Corniche Tower - 5th Floor - 5B
P. O. Box 38360 ABU DHABI
Tel.: (971) 2 627 0088
Fax: (971) 2 627 0087

Much more support to your business.



Incotep - Anchoring Systems

Incotep anchoring Systems is a division of Açotubo Group, which engaged in the development of Anchoring Systems, used in geotechnical and structural applications where high quality prestressing systems are designed to meet diverse needs.

Know our solutions for your processes

- Self Drilling Injection Hollow Bar
- Cold Rolled Thread Bars and Micropiles
- Hot Rolled Thread Bars
- Incotep Tie Rods (Port and Dike Construction)

- Umbrella Tubes Drilling System
- Pipes for Root Piles, among others

www.incotep.com.br
+55 11 2413-2000

Incotep
Sistemas de Ancoragem

A company Açotubo Group





Conheça mais:

www.geobrugg.com/pt/taludes



Safety is our nature

TECCO® SYSTEM³ com fio de aço de alta resistência

**SISTEMA ECOLOGICAMENTE
CORRETO PARA ESTABILIZAÇÃO
DE TALUDES**

Reliable solutions with **technology, quality,** and **innovation** for Civil Engineering proposes



MACCAFERRI POLIMAC

New polymeric coating
with high performance
PoliMac™



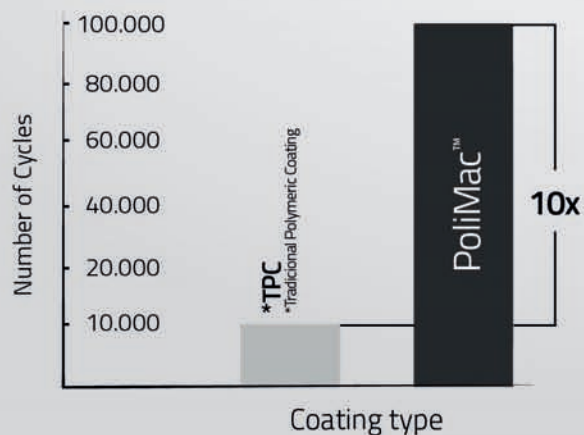
Long-life galvanising
GalMac® 4R

Intermetallic coating

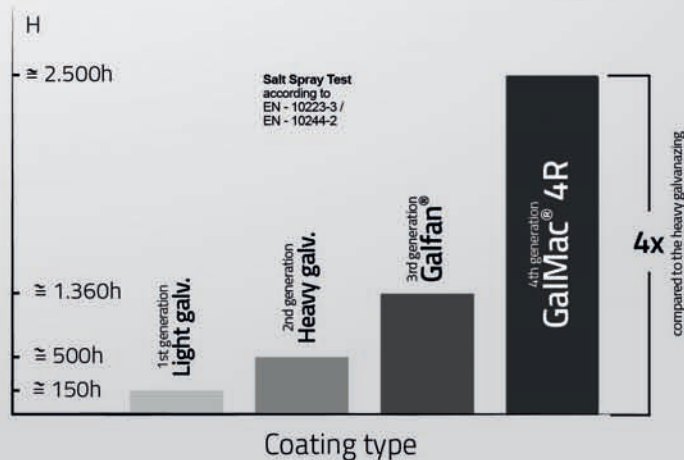
Steel wire LCC*
*Low Carbon Content



The **PoliMac™** in controlled abrasion resistance tests, it showed its excellent performance by resisting up to 100,000 cycles in the standard tests **ABNT NBR 7577** and **EN 10223-3**; about **10x more** than the traditional coating.



The **GalMac® 4R** coating complies with the main national and international standards such as: **EN 10223-3: 2013, ASTM B860** and **NBR 8964**.



Follow us on our **social media**



/maccaferri



/maccaferrimatriz



@Maccaferri_BR



+MaccaferriWorld



/maccaferriworld



MACCAFERRI

www.maccaferri.com/br

GEOTECHNICAL SERVICES (onshore and offshore)

■ **IN-SITU TESTS**

Seismic CPT
Cone Penetration Testing Undrained-CPTu (cordless system)
Vane Shear Testing (electrical apparatus)
Pressuremeter Testing (Menard)
Flat Dilatometer Test-DMT (Machetti)
Standard Penetration Test-SPT-T

■ **INSTRUMENTATION**

Instrumentation, installation and direct import
Routine Monitoring
Operation and Maintenance
Engineering analyses
Consultancy, design & geotechnical engineering services

■ **SAMPLING**

Soil sampling and monitoring
Groundwater sampling and monitoring
Field and laboratory testing

■ **ENVIRONMENTAL**

Environmental Services
Soil and groundwater sampling and monitoring
Field and laboratory testing



0800 979 3436

São Paulo: +55 11 8133 6030

Minas Gerais: +55 31 8563 2520 / 8619 6469

www.deltageo.com.br deltageo@deltageo.com.br



A strong, lasting connection.

With a history of over 150 years of pioneering in geosynthetics, we strive to create solutions for the most diverse engineering challenges.

Our business areas:



**Earthworks and
Foundations**



**Environmental
Engineering**



Roads and Pavements



Hydraulic Engineering

Talk to HUESKER Brasil:
www.HUESKER.com.br
HUESKER@HUESKER.com.br
+55 (12) 3903 9300

Follow HUESKER Brasil in social media:



HUESKER
Ideen. Ingenieure. Innovationen.

PIONEERING AND INNOVATION

SINCE 1921

 **TEIXEIRA DUARTE**
ENGENHARIA E CONSTRUÇÕES, S.A.

PORT FACILITY CONSTRUCTION
NACALA - MOZAMBIQUE



Building a better world.
teixiraduarteconstruction.com

BUILDING THE WORLD, BETTER



TPF



Engineering and Architectural Consultancy

Geology, Geotechnics, Supervision of Geotechnical Works
Embankment Dams, Underground Works, Retaining Structures
Special Foundations, Soil Improvement, Geomaterials



MEMBER OF

TPF

TPF - CONSULTORES DE ENGENHARIA E ARQUITETURA, S.A.
www.tpf.pt

40
years
celebrating

Guide for Authors

Soils and Rocks is an international scientific journal published by the Brazilian Association for Soil Mechanics and Geotechnical Engineering (ABMS) and by the Portuguese Geotechnical Society (SPG). The aim of the journal is to publish original papers on all branches of Geotechnical Engineering. Each manuscript is subjected to a single-blind peer-review process. The journal's policy of screening for plagiarism includes the use of a plagiarism checker on all submitted manuscripts.

1. Category of papers

Submissions are classified into one of the following categories:

- Article – an extensive and conclusive dissertation about a geotechnical topic, presenting original findings.
- Technical Note – presents a study of smaller scope or results of ongoing studies, comprising partial results and/or particular aspects of the investigation.
- Case Study – report innovative ways to solve problems associated with design and construction of geotechnical projects. It also presents studies of the performance of existing structures.
- Review Article – a summary of the State-of-the-Art or State-of-the-Practice on a particular subject or issue and represents an overview of recent developments.
- Discussion – specific discussions about published papers.

Authors are responsible for selecting the correct category when submitting their manuscript. However, the manuscript category may be altered based on the recommendation of the Editorial Board. Authors are also requested to state the category of paper in their Cover Letter and in the Author's Checklist.

2. Paper length

Full-length manuscripts (Article, Case Study) should be between 4,000 and 8,000 words. Review articles should have up to 10,000 words. Technical Notes have a word count limit of 2,000 words. Discussions have a word count limit of 500 words. These word count limits exclude the title page, notation list (*e.g.*, symbols, abbreviations), captions of tables and figures, Acknowledgments and references. Each single column and double column figure or table is considered as equivalent to 150 and 300 words, respectively.

3. Scientific style

The manuscripts should be written in UK or US English, in the third person and all spelling should be checked in accordance with a major English Dictionary. The manuscript should be able to be readily understood by a Civil Engineer and avoid colloquialisms. Unless essential to the comprehension of the manuscript, direct reference to the names of persons, organizations, products or services is not allowed. Flattery or derogatory remarks about any person or organization should not be included.

The author(s) of Discussion Papers should refer to himself (herself/themselves) as the reader(s) and to the author(s) of the paper as the author(s).

The International System (SI) units must be used. The symbols are recommended to be in accordance with Lexicon in 14 Languages, ISSMFE (2013) and the ISRM List of Symbols. Use italic for single letters that denote mathematical constants, variables, and unknown quantities.

4. Submission requirements and contents

A submission implies that the following conditions are met:

- the authors assume full responsibility for the contents and accuracy of the information presented in the paper;
- the manuscript contents have not been published previously, except as a lecture or academic thesis;
- the manuscript is not under consideration for publication elsewhere;
- the manuscript is approved by all authors;
- the manuscript is approved by the necessary authorities, when applicable, such as ethics committees and institutions that may hold intellectual property on contents presented in the manuscript;
- the authors have obtained authorization from the copyright holder for any reproduced material;
- the authors are aware that the manuscript will be subjected to plagiarism check.

The author(s) must upload a single digital file of the manuscript to the Soils and Rocks submission system. The size limit for submission file is 50 MB. The manuscript should be submitted in docx format (Word 2007 or higher) or doc format (for older Word versions). Currently, the journal is not accepting manuscripts prepared using LaTeX. Manuscripts submitted in PDF format are also not acceptable.

The single submission file must combine the following documents, in this order:

- cover letter;
- Author's checklist;
- permission of the use of previously published material when applicable;
- title page;
- manuscript.

4.1 Cover letter

The cover letter should include: manuscript title, submission type, authorship information, statement of key findings and work novelty, and related previous publications if applicable.

4.2 Author's checklist

Fill the checklist available in the journal's website before submitting the manuscript. The Author's Checklist must be submitted after the cover letter. Submissions that

fail to follow this Guide for Authors are automatically rejected.

4.3 Title page

The title page is the first page of the manuscript and must include:

- A concise and informative title of the paper. Avoid abbreviations, acronyms or formulae. Discussion Papers should contain the title of the paper under discussion. Only the first letter of the first word should be capitalized.
- Full name(s) of the author(s). The first name(s) should not be abbreviated. The authors are allowed to abbreviate middle name(s).
- The corresponding author should be identified by a pound sign # beside his/her and in a footnote.
- The affiliation(s) of the author(s), should follow the format: Institution, (Department), City, (State), Country.
- Affiliation address and e-mail must appear below each author's name.
- The 16-digit ORCID of the author(s) – mandatory
- Main text word count (excluding abstract and references) and the number of figures and tables

4.4 Permissions

Figures, tables or text passages previously published elsewhere may be reproduced under permission from the copyright owner(s) for both the print and online format. The authors are required to provide evidence that such permission has been granted at the moment of paper submission.

4.5 Declaration of interest

Authors are required to disclose conflicting interests that could inappropriately bias their work. For that end, a section entitled “Declaration of interest” should be included following any Acknowledgments and prior to the reference section. In case of the absence of conflicting interests, the authors should still include a declaration of interest.

5. Plagiarism checking

Submitted papers are expected to contain at least 50 % new content and the remaining 50% should not be verbatim to previously published work.

All manuscripts are screened for similarities. Currently, the Editorial Board uses the plagiarism checker Plagius (www.plagius.com) to compare submitted papers to already published works. Manuscripts will be rejected if more than 20% of content matches previously published work, including self-plagiarism. The decision to reject will be under the Editors' discretion if the percentage is between 10% and 20%.

6. Formatting instructions

The text must be presented in a single column, using ISO A4 page size, left, right, top, and bottom margins of 25 mm, Times New Roman 12 font, and line spacing of 1.5. All lines and pages should be numbered.

Figures, tables and equations should be numbered in the sequence that they are mentioned in the text.

Abstract

Please provide an abstract between 150 and 250 words in length. Abbreviations or acronyms should be avoided. The abstract should state briefly the purpose of the work, the main results and major conclusions or key findings.

Keywords

A list with up to six keywords at the end of the abstract that represent the content of the manuscript is required. Authors should preferably use keywords that do not appear in the manuscript title. To maximize visibility of the published paper, choose words that are specific to the field of study.

Examples:

Poor keywords – piles; dams; numerical modeling; laboratory testing

Better keywords – friction piles; concrete-faced rockfill dams; material point method; bender element test

List of symbols

A list of symbols and definitions used in the text must be included after the keywords.

6.1 Citations

References to other published sources must be made in the text by the last name(s) of the author(s), followed by the year of publication. Examples:

Narrative citation: [...] while Silva & Pereira (1987) observed that resistance depended on soil density

Parenthetical citation: It was observed that resistance depended on soil density (Silva & Pereira, 1987).

In the case of three or more authors, the reduced format must be used, e.g.: Silva *et al.* (1982) or (Silva *et al.*, 1982). Do not italicize “et al.”

Two or more citations belonging to the same author(s) and published in the same year are to be distinguished with small letters, e.g.: (Silva, 1975a, b, c.).

Standards must be cited in the text by the initials of the entity and the year of publication, e.g.: ABNT (1996), ASTM (2003).

6.2 References

A customized style for the [Mendeley](#) software is available and may be downloaded from [this link](#).

Full references must be listed alphabetically at the end of the text by the first author's last name. Several references belonging to the same author must be cited chronologically.

Some formatting examples are presented here:

Journal papers:

Bishop, A.W., & Blight, G.E. (1963). Some aspects of effective stress in saturated and partly saturated soils. *Geotechnique*, 13(2), 177-197. <https://doi.org/10.1680/geot.1963.13.3.177>

Books:

Lambe, T.W., & Whitman, R.V. (1979). *Soil Mechanics, SI version*. John Wiley & Sons.

Chapters in edited books:

Sharma, H.D., Dukes, M.T., & Olsen, D.M. (1990). Field measurements of dynamic moduli and Poissons ratios of refuse and underlying soils at a landfill site. In *Geotechnics of Waste Fills – Theory and Practice* (pp. 57-70). ASTM International. <https://doi.org/10.1520/STP1070-EB>

Proceedings:

Jamiolkowski, M.; Ladd, C.C.; Germaine, J.T., & Landellotta, R. (1985). New developments in field and laboratory testing of soils. *Proc. 11th International Conference on Soil Mechanics and Foundation Engineering, San Francisco, August 1985*. Vol. 1, Balkema, 57-153.

Theses and dissertations:

Lee, K.L. (1965). *Triaxial compressive strength of saturated sands under seismic loading conditions* [Unpublished doctoral dissertation]. University of California at Berkeley.

Chow, F.C. (1997). *Investigations into the behaviour of displacement pile for offshore foundations* [Doctoral thesis, Imperial College London]. Imperial College London's repository. <https://spiral.imperial.ac.uk/handle/10044/1/7894>

Standards:

ASTM D7928-17. (2017). Standard Test Method for Particle-Size Distribution (Gradation) of Fine-Grained Soils Using the Sedimentation (Hydrometer) Analysis. *ASTM International*, West Conshohocken, PA. <https://doi.org/10.1520/D7928-17>

Internet references:

Soils and Rocks. (2020). *Electronic version of issues*. Soils and Rocks. Retrieved in September 16, 2020, from <http://www.soilsandrocks.com.br/electronic-versions-of-issues/>

6.3 Artworks and illustrations

Each figure should be submitted as a high-resolution image, according to the following mandatory requirements:

Figures must be created as a TIFF file format using LZW compression with minimum resolution of 500 dpi.

Size the figures according to their final intended size. Single-column figures should have a width of up to 82 mm. Double-column figures should have a maximum width of 170 mm.

Use Times New Roman for figure lettering. Use lettering sized 8-10 pt. for the final figure size.

Lines should have 0.5 pt. minimum width in drawings.

Titles or captions should not be included inside the figure itself.

Figures must be embedded in the text near the position where they are first cited. Cite figures in the manuscript in consecutive numerical order. Denote figure parts by lowercase letters (a, b, c, etc.). Please include a reference citation at the end of the figure caption for previously published material.

Figure captions must be placed below the figure and start with the term "Figure" followed by the figure number and a period. Example:

Figure 1. Shear strength envelope.

Do not abbreviate "Figure" when making cross-references to figures.

All figures are published in color for the electronic version of the journal; however, the print version uses grayscale. Please format figures so that they are adequate even when printed in grayscale.

Accessibility: Please make sure that all figures have descriptive captions (text-to-speech software or a text-to-Braille hardware could be used by blind users). Prefer using patterns (e.g., different symbols for dispersion plot) rather than (or in addition to) colors for conveying information (then the visual elements can be distinguished by colorblind users). Any figure lettering should have a contrast ratio of at least 4.5:1

Improving the color accessibility for the printed version and for colorblind readers: Authors are encouraged to use color figures because they will be published in their original form in the online version. However, authors must consider the need to make their color figures accessible for reviewers and readers that are colorblind. As a general rule of thumb, authors should avoid using red and green simultaneously. Red should be replaced by magenta, vermillion, or orange. Green should be replaced by an off-green color, such as blue-green. Authors should prioritize the use of black, gray, and varying tones of blue and yellow.

These rules of thumb serve as general orientations, but authors must consider that there are multiple types of color blindness, affecting the perception of different colors. Ideally, authors should make use of the following resources: 1) for more information on how to prepare color figures, visit <https://jfly.uni-koeln.de/>; 2) a freeware software available at <http://www.vischeck.com/> is offered by Vischeck, to show how your figures would be perceived by the colorblind.

6.4 Tables

Tables should be presented as a MS Word table with data inserted consistently in separate cells. Place tables in the text near the position where they are first cited. Tables should be numbered consecutively using Arabic numerals and have a caption consisting of the table number and a brief title. Tables should always be cited in the text. Any

previously published material should be identified by giving the original source as a reference at the end of the table caption. Additional comments can be placed as footnotes, indicated by superscript lower-case letters.

When applicable, the units should come right below the corresponding column heading. Horizontal lines should be used at the top and bottom of the table and to separate the headings row. Vertical lines should not be used.

Table captions must be placed above the table and start with the term “Table” followed by the table number and a period. Example:

Table 1. Soil properties.

Do not abbreviate “Table” when making a cross-references to tables.

6.5 Mathematical equations

Equations must be submitted as editable text, created using MathType or the built-in equation editor in MS Word. All variables must be presented in italics.

Equations must appear isolated in a single line of the text. Numbers identifying equations must be flushed with the right margin. International System (SI) units must be used. The definitions of the symbols used in the equations must appear in the List of Symbols.

SOILS and ROCKS
An International Journal of Geotechnical and Geoenvironmental Engineering

Volume 43, N. 3, July-September 2020

EDITORIAL

A Journal is born...	i
Willy A. Lacerda	
A message from the President of the SPG	ii
Manuel de Matos Fernandes	
A message from the Editorial Board	iii
Renato P. da Cunha, Gilson de F. N. Gitirana Jr., José A. Schiavon	
Preface from the invited editor	iv
Waldemar C. Hachich	

LECTURE

Risk management for geotechnical structures: consolidating theory into practice	311
André P. Assis	

ARTICLES

Spread footings bearing on circular and square cement-stabilized sand layers above weakly bonded residual soil	339
Nilo Cesar Consoli, Eclesielter Batista Moreira, Lucas Festugato, Gustavo Dias Miguel	
A review on some factors influencing the behaviour of nonwoven geotextile filters	351
Ennio M. Palmeira	
Guidelines and recommendations on minimum factors of safety for slope stability of tailings dams	369
Fernando Schnaid, Luiz Guilherme F.S. de Mello, Bruno S. Dzialoszynski	
Stabilization of major soil masses using drainage tunnels	397
Werner Bilfinger, Luiz Guilherme F.S. de Mello, Claudio Michael Wolle	
Experimental, numerical, and analytical investigation of the effect of compaction-induced stress on the behavior of reinforced soil walls	419
Seyed H. Mirmoradi, Maurício Ehrlich, Gabriel Nascimento	
Foundation-structure interaction on high-rise buildings	441
Alexandre Duarte Gusmão, Augusto Costa Silva, Maurício Martines Sales	
Some topics of current practical relevance in environmental geotechnics	461
Maria Eugenia Gimenez Boscov, Paulo Scarano Hemsí	
Requiem for risk classification matrices	497
Waldemar C. Hachich	